H2 Technology Consulting, LLC
kgross@h2techconsulting.com
tel: (510) 468-7515

Recommended Best Practices for the Characterization of Storage Properties of Hydrogen Storage Materials

Karl J. Gross, H2 Technology Consulting LLC, and
K. Russell Carrington, University of California Berkeley
Steven Barcelo, University of California Berkeley
Abhi Karkamkar, Pacific Northwest National Laboratory
Justin Purewal, Ford Motor Company
Shengqian Ma and Hong-Cai Zhou, Texas A&M University
Pierre Dantzer, Université Paris-Sud
Kevin Ott, Tony Burrell and Troy Semeslberger, Los Alamos National Laboratory
Yevheniy Pivak and Bernard Dam, VU University Amsterdam and the Delft University of Technology
Dhanesh Chandra, University of Nevada Reno

We gratefully acknowledge assistance and financial support from the U.S. Department of Energy Office of Energy Efficiency and Renewable Energy Hydrogen Storage Program.

National Renewable Energy Laboratory Contract No. 147388
Contract Technical Monitor: Dr. Philip Parilla

LIST OF FIGURES **10**

LIST OF TABLES **22**

SUMMARY OF DOCUMENT STRUCTURE **23**

CITATION INFORMATION **23**

PREFACE **24**

1 MISSION 24
1.1 Objective *24*
1.2 Benefit to the DOE *24*
2 RECOMMENDED READING 25
2.1 Hydrogen Storage *25*
2.2 Hydrides *25*
2.3 Metal Hydrides *25*
2.4 Off-board Regenerable Hydrogen Storage Materials *25*
2.5 Physisorption Storage *26*
2.6 Kinetics *26*
2.7 Thermodynamics *26*
3 THE INTERNATIONAL SYSTEM OF UNITS (SI) 27
3.1 Symbols for the Seven Base Units *27*
3.2 SI Derived Units *27*
3.3 Derived Units Expressed in Terms of Base Units *28*
3.4 Units with Special Names and Symbols; Units that Incorporate Special Names and Symbols *28*
3.5 Concentrations and Related Quantities *31*
3.6 Recommended (SI) Units for Hydrogen Storage *32*
4 DEFINITIONS 34
4.1 Terminology *34*
4.2 Sorption and Desorption *34*
4.3 Adsorption and Absorption *34*
4.4 Chemisorption and Physisorption *34*
4.4.1 Physisorption 37
4.5 Spillover *38*
5 MATERIALS 39
5.1 Hydrogen Storage Materials Based on Physisorption of Molecular Hydrogen *40*
5.1.1 Nano-Structured Materials 40
5.1.2 Porous Materials 40
5.2 Hydrogen Storage Materials Based on Hydride or Covalent Bond Formation *40*
5.2.1 Types of Hydrides 41
5.2.2 Ionic Hydrides 42
5.2.3 Covalent Hydrides 42
5.2.4 Interstitial Hydrides 43
5.2.4.1 Metal Alloy - Hydrides 43
5.2.4.2 Metal Hydride Intermetallic Compounds 44
5.2.5 Transition Metal Hydrido Complexes 45
5.2.6 Dihydrogen Complexes 45
6 CLASSIFICATION OF MATERIALS FOR HYDROGEN STORAGE MATERIALS APPLICATIONS 46
7 SUMMARY 47

SECTION 1: INTRODUCTION **48**

1 PURPOSE OF MEASUREMENTS 48
1.1 Purpose: System Performance *48*
1.2 Purpose: Materials Development *49*

1.3 Purpose: Fundamental Science *50*
2 HYDROGEN STORAGE PROPERTIES 51
2.1 Property: Capacity *51*
2.2 Property: Kinetics *51*
2.3 Property: Thermodynamics *52*
2.4 Property: Cycle-Life *52*
3 TYPES OF MEASUREMENT 53
3.1 Measurement Type: Kinetics *53*
3.2 Measurement Type: Pressure-Composition Isotherm *54*
4 HYDROGEN STORAGE VARIABLES 57
4.1 Measureable Direct Variables *58*
4.1.1 Variable: Weight 58
4.1.2 Variable: Pressure 59
4.1.3 Variable: Temperature 61
4.1.4 Variable: Cycle 63
4.1.5 Variable: Time 63
4.2 Accuracy and Precision of Measurements *65*
4.2.1 Significant Digits 66
4.2.2 Error Bars in Data Representation 67
4.2.3 Error Analysis 68
4.2.4 Analog to Digital Conversion Error 69
4.2.5 Testing For Accuracy 70
4.3 Calibrations *72*
4.3.1 Weight 72
4.3.2 Volume 72
4.3.3 Pressure 74
4.3.4 Temperature 75
4.3.5 Time 75
4.3.6 Other Calibrations 75
5 METHODS OF MEASUREMENT 76
5.1 Static and Dynamic Measurements *76*
5.2 dC and dP Dosing Methods *78*
5.3 Volumetric Method *80*
5.3.1 Differential Pressure Method 81
5.3.2 Data Corrections 83
5.3.3 Temperature Correction 84
5.3.4 Volume Correction 86
5.3.5 Compressibility Factor 88
5.3.6 Gas Impurities 89
5.3.7 Instrument Temperature 90
5.3.8 Leaks 90
5.3.9 Reference Point 91
5.3.10 Gas Heating and Cooling effects 91
5.3.11 Sample Size 92
5.3.12 Skeletal Density 93
5.3.13 Calibration Volume Changes 93
5.3.14 Volume Dilatation of Sample 94
5.4 Gravimetric Method *94*
5.5 Thermal Gravimetric Analysis Method *95*
5.5.1 Buoyancy 97
5.5.2 Gas Impurities 99
5.5.3 Heat Transfer 100
5.5.4 Leaks 100
5.5.5 Sample Transfer 100
5.5.6 Volume Dilatation 101
5.5.7 Thermal Gradients and Gas Flow Forces 101

5.6 Temperature-Programmed Desorption Method *101*
5.7 Differential Scanning Calorimetry Method *104*
5.8 Differential Thermal Analysis Method *105*
5.9 TGA/Calorimetry Vital Measurement Practices: *106*
5.10 Important Consideration: Gas Composition *108*
5.11 Important Calibration Consideration: Helium Adsorption *109*
5.11.1 Background For The Issue Of Helium Adsorption 109
5.11.2 Best Practices For The Issue Of Helium Adsorption 112
5.11.2.1 Gibbsian Excess Lower Bound 112
5.11.2.2 Engineering Excess 112
5.11.2.3 Independent Skeletal Density 113
5.11.2.4 Independent Helium Adsorption 113
5.11.2.5 Recommendation for Low Temperature 113
5.12 Reporting Measurement Results: *114*
6 SUMMARY 117

SECTION 2: KINETICS MEASUREMENTS 118

1 INTRODUCTION AND DEFINITIONS 118
1.1 Chemical Kinetics *118*
1.1.1 Nature of the Reactants 119
1.1.2 Heterogeneous vs. Homogeneous Reactions 119
1.1.3 Concentration 119
1.1.4 Temperature 120
1.1.5 Catalysts 120
1.1.6 Equilibrium 121
1.1.7 Free Energy 122
1.2 Kinetics in Hydrogen Storage *123*
1.3 Impact of Heat Transfer *124*
2 KINETIC THEORY 125
2.1 Fundamental Mechanisms of Reactions *125*
2.1.1 Binding Mechanisms 126
2.1.1.1 Storage by Physisorption of H_2 on Surfaces 126
2.1.1.2 Storage of Hydrogen by Forming Hydrides 127
2.1.2 Mass Transport 127
2.1.2.1 Physisorption 127
2.1.2.2 Hydrogen Diffusion in Metal Hydrides 128
2.1.3 The Impact of Surface Interactions on Kinetics 129
2.1.3.1 Surface Energetics 130
2.1.3.2 Surface Contamination 131
2.1.3.3 Surface Hydriding 133
2.1.4 Heat Transfer 134
2.2 Kinetics Modeling *135*
2.2.1 Temperature Dependence 136
2.2.2 Concentration Dependence 137
2.2.2.1 Diffusion Models 138
2.2.2.2 Reaction Models 138
2.2.3 Pressure Dependence 140
3 EXPERIMENTAL AND ANALYSIS CONSIDERATIONS 142
3.1 The Limitations of Kinetics Measurements *143*
3.2 Discrete Kinetics Measurements *147*
3.3 Kinetics from TGA Measurements *149*
3.3.1 Single Run Methods for Kinetics Analyses 149
3.3.2 Isoconversional Methods for Kinetic Analyses 150
3.3.3 Peak Methods for Kinetic Analyses 151
3.4 Matching Experimental Setup with Purpose *152*
3.4.1 Experiments for System Performance 152

3.4.2 Experiments for Materials Development 156
3.4.3 Experiments for Fundamental Studies 157
3.5 Efficient Testing *160*
3.5.1 Kinetics and Capacity 161
3.5.2 Active Capacity 161
3.6 Activation Effects *164*
3.7 Gas Impurities *167*
3.7.1 Retardation 167
3.7.2 Gas Impurity Effects on Kinetic Performance 168
3.8 Leaks *169*
3.9 Pressure Effects *170*
3.9.1 Reservoir Selection 170
3.10 Thermal Effects *173*
3.10.1 Thermal Ballast 174
3.10.2 Heat Transfer-Maximizing Cell 175
3.10.3 Effect of Sample Thickness 176
4 APPROACHES TO IMPROVE KINETICS 177
4.1 Alloying *178*
4.2 Grain Boundaries *179*
4.3 Decrepitation *180*
4.4 Nano-Structuring *181*
4.5 Example of Improvements *181*
5 KINETIC VERSUS THERMODYNAMIC ISSUES 183

SECTION 3: CAPACITY MEASUREMENTS 185

1 INTRODUCTION AND DEFINITIONS 185
1.1 Hydrogen Storage Materials Classifications *185*
1.1.1 Physisorbed Hydrogen Storage Materials 186
1.1.2 On-Board Reversible Hydrogen Storage Materials 188
1.1.3 Off-board Regenerable Hydrogen Storage Materials 192
1.2 Definitions of Capacity With Respect to Hydrogen Storage *194*
1.2.1 Synopsis of Capacity Terminology 195
1.2.2 Capacity vs. Concentration 197
1.2.3 Reversible vs. Usable Hydrogen Capacity 199
1.2.4 Hydrogen Content vs. Reversible Capacity 199
1.2.5 Active Capacity (All Materials) 201
1.3 Units of Measured Hydrogen Capacity *202*
1.4 Physisorption Materials *203*
1.4.1 Density of Porous Solids 208
1.4.2 Material Gibbs Surface Excess Adsorption Capacity 211
1.4.3 Material Maximum Excess Adsorption Capacity 212
1.4.4 Excess Hydrogen Adsorption Capacity and Surface Area 215
1.4.5 Material Absolute Hydrogen Adsorption Capacity 216
1.4.6 Material Total Hydrogen Adsorption Capacity 222
1.4.7 Physisorption Materials: Usable Hydrogen Capacity 226
1.4.8 Material Gravimetric and Volumetric Hydrogen Densities 226
1.4.9 Reversible Physisorption 227
1.4.10 Kinetically Limited Physisorption 227
1.4.11 System-Level Hydrogen Storage Capacity 227
1.5 On-board Reversible Hydride Materials *237*
1.5.1 Reversible and Usable Hydrogen Capacity 237
1.5.2 System-Level Hydrogen Capacity 240
1.6 Off-board Regenerable Hydride Materials *242*
1.7 US DOE Hydrogen Storage Capacity Targets *243*
2 EXPERIMENTAL AND ANALYSIS CONSIDERATIONS 245

2.1 Matching an Experiment to the Purpose of a Measurement *246*
2.1.1 Experiments for System Performance 246
2.1.2 Experiments for Materials Development 252
2.1.3 Experiments for Fundamental Studies 256
2.2 Material Properties that Affect Capacity Measurements *257*
2.2.1 Materials Preparation and Handling 257
2.2.2 Impurity Effects and Capacity Testing Protocols 261
2.2.3 Surface Conditions 266
2.2.3.1 Surface Passivation 266
2.2.3.2 Poisoning 269
2.2.4 Capacity and Kinetics 272
2.2.5 Capacity and Thermodynamics 273
2.2.6 Impact of Hysteresis on Capacity 278
2.2.7 Activation Effects 284
2.3 Special Method Dependent Considerations *287*
2.3.1 Volumetric 287
2.3.1.1 Volumetric Physisorption Measurements 287
2.3.1.2 Volumetric Measurements of On-board Reversible Hydrides 289
2.3.1.3 Volumetric Sorption Dose 291
2.3.1.4 Gas Density Gradients 292
2.3.1.5 Temperature Control 293
2.3.1.6 Real gas behavior 295
2.3.1.7 Blank Sample Measurements 296
2.3.2 Gravimetric Methods 297
2.3.2.1 Gravimetric Physisorption Measurements 298
2.3.2.2 Issues Involving Impurities 304
2.3.2.3 Instrumental Stability 306
2.3.2.4 Instrumental Effects on Buoyancy Corrections 306
2.3.2.5 Thermal Errors in Buoyancy Corrections 309
2.3.2.6 Sample Density Errors in Buoyancy Corrections 310
2.3.3 Sources of Errors in Volumetric and Gravimetric Measurements 312
2.3.4 Thermal Gravimetric Analysis 314
2.3.5 Temperature Programmed Desorption 318
2.3.6 Differential Scanning Calorimetry 319
2.4 Experimental Considerations *322*
2.4.1 Desorption vs. Sorption Testing 322
2.4.2 Gas Composition 323
2.4.3 Leaks 326
2.4.4 Discrete Compositions 327
2.4.5 Effect of Sample Size 330
2.4.6 Efficient Testing 333
2.4.7 Thermal Effects 334
2.5 Potential Materials Improvements *335*
2.5.1 Doping 335
2.5.2 Grain/particle Size Effects 335
2.5.3 Alloying 335
2.5.4 Capping Layers 336
2.5.5 Chemical Hydrides Materials Improvements 336
2.5.6 Physisorption Materials Improvements 340

SECTION 4: THERMODYNAMIC MEASUREMENTS 342

1 INTRODUCTION AND DEFINITIONS 342
1.1 Basics of Thermodynamics *342*
1.1.1 Laws of Thermodynamics 343
1.1.2 First Law of Thermodynamics 343
1.1.3 Classical Thermodynamics 345
1.1.4 Statistical Thermodynamics 345

1.1.5 State Variables 345
1.1.6 Thermodynamic Systems 347
1.1.6.1 Isolated System 347
1.1.6.2 Closed System 347
1.1.6.3 Open System 348
1.1.7 Equilibrium 348
1.1.8 Reversibility 349
1.1.9 Practical Use and Limitations of the First Law 350
1.1.10 Heat Capacity 351
1.1.11 Joule-Thomson Effect 354
1.1.12 Enthalpy of Formation 359
1.1.13 Entropy of Formation 361
1.1.14 Free Energy 361
1.2 Thermodynamics of On-board Reversible Hydride Materials *363*
1.2.1 Metal Hydride Phase Diagrams 363
1.2.2 Free Energy of Formation 365
1.2.3 Reversible Phase Transformations 366
1.2.4 Van 't Hoff Plots 371
1.2.5 Irreversibility Associated with Phase Transformations 376
1.2.6 Entropy Analysis 382
1.2.7 Intrinsic Hysteresis - Potential Causes 384
1.2.8 Mechanical Strain energy 384
1.2.9 Dislocations 385
1.2.10 Interfacial Energy/Particle Size Effects 387
1.3 Thermodynamics of On-board Rechargeable Physisorption Materials *388*
1.3.1 Isosteric Heat of Adsorption 388
1.3.2 Determination of Isosteric Heats of Adsorption from Isotherm Measurements 388
1.3.3 Determination of Isosteric Heats by Modeling of Adsorption Isotherms 392
1.3.3.1 The Virial Method 1 395
1.3.3.2 The Virial Method 2 396
1.3.3.3 The Langmuir-Freundlich Equation 396
1.3.3.4 The Dubinin-Astakhov Model 397
1.3.3.5 The Modified Dubinin-Astakhov (MDA) Analytical Model 400
1.3.4 Variable-Temperature Infrared Spectroscopy 406
1.3.5 Optimal Value of Adsorption Enthalpy 408
1.3.6 Recommended Best Practices for Presenting Isosteric Heats of Adsorption 409
1.4 Thermodynamics of Off-board Regenerable Hydride Materials *410*
1.5 Hydrogen Storage System Energy Considerations *413*
1.5.1 On-board Reversible Hydride Storage Systems 413
1.5.2 Off-board Regenerable Hydrides Storage Systems 415
1.5.3 Physisorption storage systems 418
2 EXPERIMENTAL AND ANALYSIS CONSIDERATIONS 419
2.1 PCT Measurements *420*
2.1.1 Equilibrium PCT Measurements 420
2.1.2 Volumetric Method 422
2.1.2.1 Temperature Correction 422
2.1.2.2 Temperature Measurement 423
2.1.2.3 Free space measurement 423
2.1.2.4 Sample Quantity 424
2.1.2.5 Sample Handling 424
2.1.2.6 Leak Checks 424
2.1.2.7 Full Isotherm Van 't Hoff Measurements 424
2.1.2.8 Micro-Volumetric Full Isotherm Measurements 426
2.1.2.9 Direct Van 't Hoff Measurement Technique 430
2.1.2.10 Micro-Volumetric Direct Van 't Hoff Measurements 434
2.1.2.11 Physisorption Measurement Systems 438
2.1.3 Gravimetric Method 441

2.1.3.1 Hysteresis in Reversible Hydrides 441
2.1.3.2 Temperature Measurements 441
2.1.3.3 Buoyancy 442
2.1.3.4 Other Considerations 444
2.1.3.5 Gravimetric Thermodynamic Measurements 445
2.1.4 Capacity and Thermodynamic Measurements 445
2.1.5 Thermodynamic Measurements Using Hydrogenography 446
2.2 Calorimetry *454*
2.2.1 Bomb Calorimetry: Measuring Heats of combustion 454
2.2.2 Examples: 455
2.2.3 Combined Calorimetry and Gas Sorption measurements 460
2.3 Calorimetry vs. Van 't Hoff Measurements *465*
2.4 Heat Capacity Measurement *467*
2.4.1 Continuous Heat Capacity Measurements 467
2.4.2 Continuous Heat Capacity Measurements without Reference 467
2.4.3 Continuous Heat Capacity Measurements with Reference 468
2.4.4 Heat Capacity Measurements by the Step Method 469
2.4.5 Heat Capacity Measurements by the Step Method without Reference 470
2.4.6 Heat Capacity Measurements by the Step Method with Reference 470
2.5 Thermal Gravimetry (TG) or Thermal Gravimetric Analysis (TGA) *471*
2.6 Temperature Programmed Desorption (TPD) *472*
3 MATCHING EXPERIMENTAL SETUP TO MEASUREMENT GOAL 474
3.1 Experiments for Systems Performance *476*
3.1.1 On-board Reversible Hydride Storage Systems 476
3.1.2 Off-board Regenerable Hydrides Storage Systems 479
3.1.3 Physisorption Storage Systems 480
3.2 Experiments for Materials Development *481*
3.2.1 On-board Reversible Hydride Storage Materials 481
3.2.2 Off-board Regenerable Hydride Storage Materials 485
3.2.3 Physisorption Storage Materials 488
3.3 Experiments for Fundamental Studies *491*
3.3.1 On-board Reversible Hydride Storage Materials 491
3.3.1.1 Annealing 491
3.3.1.2 Hydrogenography of Thin Films 493
3.3.2 Off-board Regenerable Hydrides Storage Materials 497
3.3.3 Physisorption Storage Materials 498
4 EXAMPLE APPROACHES TO IMPROVE THERMODYNAMICS 501
4.1 Materials Improvements *501*
4.1.1 Alloys with Destabilizing Elements 501
4.1.2 Mixtures of Destabilizing Hydrides 501
4.1.3 Size Effects 502
4.1.3.1 Increased Surface Area 503
4.1.3.2 Grain Boundaries 503
4.1.4 Thermodynamic Improvements of On-board Reversible Hydride Materials 504
4.1.5 Thermodynamic Improvements of Off-board Regenerable Hydride Materials 504
4.1.6 Thermodynamic Improvements of Physisorption Materials 507

SECTION 5: CYCLE-LIFE MEASUREMENTS 508

5 INTRODUCTION AND DEFINITIONS 508
5.1 Basics of Cycle-Life Measurements *508*
5.2 Cycle-Life Properties of On-board Reversible Hydrides *509*
5.2.1 Introduction: Long-Term Stability of Metal Hydrides 509
5.2.2 Decrepitation of Hydrides 512
5.2.3 Degradation by Disproportionation of Hydrides 514
5.2.4 Gaseous Impurity Effects on Classic Hydrides 515
5.3 Cycle-Life Properties of Physisorption Storage Materials *518*

6 CYCLE-LIFE MEASUREMENTS METHODS 519
6.1 Pressure Cycling Tests *521*
6.2 Pressure-Temperature Cycling Tests *521*
6.3 Thermal Cycling Tests *522*
6.4 Closed System vs. Fresh Gas Tests *523*
6.5 Aging Testing *524*
6.6 Intrinsic Testing of Intermetallic Hydrides (Thermal, Pressure and P-T Cycling Tests) *528*
7 MATCHING EXPERIMENTAL SETUP TO THE MEASUREMENT PURPOSE 528
8 EXPERIMENTAL AND ANALYSIS CONSIDERATIONS 529
8.1 Pretreatment / Activation *530*
8.2 Preferred Experimental Procedures *531*
8.2.1 Pressure-Temperature Cycling 532
8.2.2 Thermal Aging 533
8.3 Impact of Cycle Testing Parameters *533*
9 EXAMPLES CYCLE-LIFE MEASUREMENTS 538
9.1 Examples of Intrinsic Cycling Measurements *538*
9.1.1 Pressure Cycling of Classic Hydrides 538
9.1.2 Pressure Cycling of Physisorption Materials 540
9.1.3 Thermal Cycling of Classic Hydrides 541
9.1.4 Thermal Aging Tests on Classic Hydrides 544
9.2 Examples of Extrinsic Cycling Measurements *546*
9.2.1 Pressure Cycling with Impurities on Classic Hydrides 547
9.2.2 Pressure Cycling with Impurities on Complex Hydrides 548
9.2.3 Pressure Cycling with Impurities on Imide/Amides 549
10 SUMMARY OF CYCLE-LIFE MEASUREMENTS 550

SUMMARY 551

ACKNOWLEDGEMENTS 551

DISCLAIMER 551

REFERENCES 552

List of Figures

Figure 1. Illustration of the components of a physisorption system. 37

Figure 2. Conceptual diagram of Strategy for storage by spillover: (A) Supported metal catalyst for H_2 dissociation; (B) Sorbent as receptor for H; (C) Building carbon bridges (by carbonization of a precursor) for spillover, resulting in a composite sorbent. 38

Figure 3. Family tree of hydriding alloys and complexes. 45

Figure 4. Formation and equilibrium structures of metal dihydrogen and dihydride complexes (L = ligand). 46

Figure 5. Van't Hoff diagram representing the hydriding thermodynamic properties of several different $LaNi_5$-based materials. 50

Figure 6. Representative kinetics measurement of an individual hydrogen dose to a porous material. 54

Figure 7. Representative measurement of a porous material. The last point in each 'row' of points is taken as representative of the equilibrium concentration of hydrogen in the sample at the pressure and temperature of experimentation. 55

Figure 8. Representative pressure / time measurement and the resulting PCT plot of hydrogen absorption to form a metal hydride. The last point of each gas sorption dose provides the concentration of hydrogen in the sample at the equilibrium pressure and temperature of each dose. 56

Figure 9. The relationship between pressure drop on absorption and the concentration associated with this pressure drop that is used to create each point on the equilibrium PCT diagram. 56

Figure 10. Depiction of the two types of error bands in pressure transducers. 60

Figure 11. Schematic of a typical hardware/software set-up and the flow of information in a hydrogen storage testing system. 64

Figure 12. Example of constant and step data collection artifacts during desorption. The ordinate is measured pressure. 65

Figure 13. The target analogy for accuracy and precision. The proximity of the marks to the center of the target is the accuracy and the size of the mark luster is the precision. a) Accurate and precise, b) accurate but not precise, c) precise but not accurate, d) not accurate and not precise. 66

Figure 14. Graphical representation of collection of data points in mean/error bar format. 68

Figure 15. Hydrogen absorption and desorption volumetric PCT isotherm measurements of palladium powder at 167°C. 71

Figure 16. Pressure Method calibration system. 73

Figure 17. Comparison of static and dynamic pressure-composition isotherms for $LaNi_5$ and FeTi at 298K. Results are after about 200 test cycles. 78

Figure 18. PCT of classic metal hydride material with plateau. dC (squares) and dP (red circles) dosing provide different information in solid solution (vertical) versus hydride formation (horizontal) portions of the PCT phase diagram. 79

Figure 19. Example of PCT with missing plateau information due to inherent limitation in dP dosing. 79

Figure 20. Multipurpose Gas Sorption/Desorption Apparatus. The pressure gauge on the right is only required when using the flow controller. 80

Figure 21. Schematic of the Differential Pressure Adsorption Unit. 82

Figure 22. Schematic of temperature regimes in a volumetric instrument. The volume of gas at instrument temperature and at sample holder temperature varies depending on the system design and the type of sample holder used. 83

Figure 23. PCT data for an inert material. The linear relationship between pressure and concentration is due to the temperature difference between the reservoir (302 K) and the sample holder (77 K). 85

Figure 24 Excess capacity PCT. 86

Figure 25. PCT for a physisorbing material at 77 K showing the raw data, temperature corrected, and volume corrected data. This is the same raw data that is used in Figure 24. 88

Figure 26. Compressibility factor z for hydrogen as a function of temperature and pressure. 89

Figure 27 Adiabatic gas expansion in dosing from high to low pressure can cause an increase in temperature (and pressure) of the gas. 92

Figure 28. Schematic of counterbalanced gravimetric method system for hydrogen storage testing. 94

Figure 29. Schematic of typical Temperature-Programmed Desorption experimental set-up. 102

Figure 30. Typical data representation of single-component TPD experiment with CO. 103

Figure 31. Residual gas analysis of alanate-amide sample discussed in the Kinetics section. 109

Figure 32. Generic potential energy diagram showing the effect of a catalyst in a hypothetical endothermic chemical reaction. The presence of the catalyst opens a lower energy reaction pathway (shown in red) with a lower activation energy. The final result is an increase in the rate of the reaction while the overall thermodynamics remain the same. 121

Figure 33. Hypothetical concentration versus time curves showing three different kinetic behaviors that have the same average rate at $t_{95\%}$. 124

Figure 34. Left: Dipole-induced dipole van der Waals interactions. Right: Induced dipole-induced dipole van der Waals interactions. 126

Figure 35. Schematic representation of the interaction of hydrogen with a clean crystalline surface. 129

Figure 36. Potential energy curves for activated or non-activated dissociation and chemisorption of hydrogen on a metal surface, followed by the endothermic or exothermic solution of atomic hydrogen into the bulk. 131

Figure 37. A schematic representation of surface passivation hindering the hydrogen dissociation reaction. Light-colored spheres represent oxygen occluding the surface of the material. 132

Figure 38. Surface segregation in the $LaNi_5$ system. a) fresh surface, b) surface enrichment of La lowering the surface energy, and c) selective oxidation of La and formation of Ni precipitates at the surface. 132

Figure 39. A schematic representation of the formation of a surface hydride which creates a diffusion barrier blocking the transport of atomic hydrogen into the bulk. 134

Figure 40. Arrhenius plot of rate coefficients K versus 1/T, for hydrogen absorption by La_2Mg_{17}. 137

Figure 41. Various solid-state kinetics models. 1) One-dimensional diffusion, 2) diffusion in a cylinder, 3+4) diffusion in a sphere, 5) 1st-order phase transformation, 6) constant velocity phase-boundary propagation in a cylinder, 7) constant velocity phase-boundary propagation in a sphere, 8+9) nucleation and growth. 140

Figure 42. Linear fit to the rate dC/dt versus F(C,P) for hydrogen absorption of La_2Mg_{17} at 300°C. The rate coefficient K is found from the slope of the fit. 142

Figure 43. Kinetics measurement of $LaNi_5$ Intermetallic compound with a single phase transition. The experiment was conducted at room temperature. Units in H per formula unit released. 143

Figure 44. PCT measurements of $LaNi_5$, a classic metal hydride. The transition pressure at various temperatures illustrates the thermodynamic dependence of transition between the solid solution and intermetallic hydride phases. 145

Figure 45. TPD measurement of the alanate-amide mixture described above. 146

Figure 46. PCT diagram of the alanate-amide mixture described above. 147

Figure 47. Pressure versus time plot of data used to create the PCT diagram of alanate-amide mixture in the preceding figure. 148

Figure 48. Scale up (100 g) reactor with end cap removed in Ar-glovebox to show catalyzed alanate. 154

Figure 49. Exothermic temperature excursion during scale up bed charge half-cycle (P_i=172 atm, T_i=155˚C). 154

Figure 50. Image of scaled up Alanate test bed with series of internal and external thermocouples. 155

Figure 51. Investigation of different additives for improvement of kinetics of $NaAlH_4$. Dopants are transition metals and rare earth ions. 157

Figure 52. Log desorption rates versus inverse temperature plotted for $NaAlH_4$ with no $TiCl_3$ and 4 mol% added $TiCl_3$ [Original plot modified for simplicity, Na_3AlH_6 removed from figure]. 158

Figure 53. Activation energies Q (= E_A) for $NaAlH_4$ decompositions as a function of added $TiCl_3$ [modified for simplicity, Na_3AlH_6 removed from figure]. 159

Figure 54. Example of efficient testing in determining the activation energy of a sample with slow intrinsic kinetics. The figure itself is a kinetics measurement used to relate the rate constant to temperature. 160

Figure 55. Arrhenius plot comparing desorption rates of $NaAlH_4$ Generation II, III-D, and III-E alanates (rates: II on a material weight basis, III-D and III-E on a NaH + Al weight basis). Red arrows indicate change in data points on converting from a material to an active weight basis. 163

Figure 56. The kinetic activation effects of pre-reacted sodium alanate. The marked increase in desorbed hydrogen indicates increasing kinetic rates. 165

Figure 57. The reaction follows the equilibrium pressure (darkest line) from bottom left to top right for absorption and top right to bottom left for desorption. The horizontal section of the equilibrium pressure line represent phase transitions (reactions), the vertical lines represent the alanate compounds as indicated. 166

Figure 58. Concentration offset caused by incomplete desorption. Due to thermodynamic limitations, the sample cannot be fully desorbed during the experiment, which causes the concentration to offset. 167

Figure 59. Effects of retardation of NH_3 on isobaric sorption curve of $LaNi_5$ during repeated cycling. 168

Figure 60. Example of a leak on kinetics measurement. A little after an hour in to the experiment, the leak was eliminated. 169

Figure 61. Diagram of the pressure in sorption/desorption system during hydriding reaction. The dashed line represents a test using a reservoir that is too small and the solid red line represents a test using a sufficiently large reservoir. 172

Figure 62. Calculated formation rates of $NaAlH_4$ at several temperatures and applied pressures. 173

Figure 63. Dependence of the change in the adiabatic temperature during hydriding on the fraction of thermal ballast for the $LaNi_5$-H system. 174

Figure 64. Schematic diagram of the Supper heat-pipe-cooled fast reactor specially designed cell to eliminate heat transfer effects during kinetics testing. 175

Figure 65. Measurements taken with the Supper Cell on $LaNi_{4.7}Al_{0.3}$ to investigate the effects of temperature and sample thickness on kinetics. Sample bed thickness of 1 mm. 176

Figure 66. Measurements taken with the Supper Cell on $LaNi_{4.7}Al_{0.3}$ to investigate the effects of temperature and sample thickness on kinetics. Sample bed thickness of 6 mm. 177

Figure 67. The presence of a second element, either in solution or as a compound, can improve kinetics by providing active sites for dissociation and creating a diffusion path through the lattice. 178

Figure 68. Intimate contact between two different phases may allow atomic hydrogen to diffuse through an active phase and cross the phase boundary into the passivated phase. 179

Figure 69. Lattice expansion and crack formation along phase boundaries create clean metal surfaces for dissociation and diffusion. 180

Figure 70. Poor kinetics due to a surface hydride diffusion barrier can be overcome by increasing the material's surface area to bulk ratio (i.e. decreasing the particle size). 181

Figure 71. SEM-BSE image of the cross-section of a composite particle formed by mechanically milling La_2Mg_{17} together with $LaNi_5$. The lighter phase is the $LaNi_5$. 182

Figure 72. SEM-BSE image of the cross-section of a composite particle after cycling under hydrogen at 300°C. The lightest phase is La, the medium-grey phase is Mg_2Ni, and the dark matrix is the Mg phase. 182

Figure 73. Equilibrium thermodynamics of some commonly researched hydrogen storage materials. The boxed area represents the range of practical operating conditions for a PEM Fuel Cell. 184

Figure 74. Schematic illustration of (a) physisorbed hydrogen and (b) the distinction between excess and bulk gas phase hydrogen. 187

Figure 75. Potential energy curves for the activated or non-activated dissociation and chemisorption of hydrogen on a clean metal surface, followed by the endothermic or exothermic solution of atomic hydrogen into the bulk. 189

Figure 76. Illustration of a PCT Pressure Composition Temperature phase diagram for hydrogen-metal solid solution α-phase and metal hydride formation β-phase. Temperature isotherms are shown for increasing temperatures T1, T2 and T3. 190

Figure 77. PCT measurements at different temperatures for the decomposition and rehydriding of $NaAlH_4$ and Na_3AlH_6. 191

Figure 78. Schematic representation of nature of differences in binding and density of hydrogen ranging from surface adsorption to chemical hydrides. Chemical hydrides can show significantly higher density of deliverable hydrogen as compared to other hydrogen storage materials. 193

Figure 79. Illustration of the relationship between concentration and capacity for a flat plateau hydride. 198

Figure 80. Hydrogen content of different hydrogen storage materials. 200

Figure 81. Illustration of physisorption hydrogen storage material capacity terminology. 204

Figure 82. Illustration of the Gibbs surface excess mass for a physisorption material in a storage vessel or measurement volume Vv. 205

Figure 83. Illustration of the effect of error in the free volume determination on surface excess hydrogen adsorption capacity measurements. 207

Figure 84. Volume and Density Definitions: Illustration of volume and density definitions relevant to hydrogen storage capacities at a materials and systems level. 211

Figure 85. High pressure H_2 adsorption isotherms on the superactivated carbon AX-21TM. 213

Figure 86. Illustration of the shape of excess capacity curve and the point of maximum excess capacity for physisorption material at 77K. 214

Figure 87. Data demonstrating the "Chahine Rule"; the excess H_2 adsorption capacity is linearly proportional to micropore volume. 215

Figure 88. Illustration of physisorption hydrogen storage material capacity terminology. 217

Figure 89. Illustration of the conversion of adsorbed gas density to an equivalent "Adsorption Volume" or equivalent boundary layer thickness. 219

Figure 90. Illustration of the dependence of physisorbed hydrogen. 221

Figure 91. Porous Materials Capacity Definitions: Illustration of the "Excess H_2 Storage Capacity", "Absolute H_2 Storage Capacity" and "Total H_2 Storage Capacity" at a materials level. 222

Figure 92. H2 adsorption isotherms (a) below 1.2 bar and (b) up to 90 bar within the MOFs 1' (red) and 1m' (blue) at 77 K, and within 1m' at 298 K (green). Triangles and circles represent excess and total material H2 adsorption, respectively, while filled and open symbols represent adsorption and desorption data, respectively. 225

Figure 93. Illustration of the "usable capacity" above 3 atm pressure. 226

Figure 94. Simplified representation a physisorption material hydrogen storage system. 228

Figure 95. Simplified diagram of a porous material. The outermost boundary represents the free gas volume of the hydrogen storage system; the central pore volume represents the collective accessible pore network. 229

Figure 96. A breakdown of the separate components of the hydrogen storage system capacity for physisorption materials. 230

Figure 97. Schematic plot of different components of adsorbed gas as a function of pressure (N=moles gas, Blue N_{ad} = absolute adsorbed gas (e.g. Langmuir model), Red N_f = gas in the free volume of the material storage system, Green N_{ex} = excess adsorbed gas). 232

Figure 98. Isothermal net H_2 storage capacity of a 150 L tank filled with Maxsorb MSC-30TM activated carbon (heating up to initial temperature for discharge, outlet pressure 0.25 MPa). The "break even curve" (where a cryogenic compressed gas at the specified pressure and temperature would result in the same

storage capacity) and the amount of gas stored by compression at 35 and 70 MPa at room temperature is also presented. 234

Figure 99. Calculated Net H_2 storage capacity of same 150 L tank as in Figure 98 heating to 298 K for discharge, with an outlet pressure 0.25 MPa. The heating advantage with respect to the "break even curve" can be seen. Room temperature compressed gas at 35 and 70 MPa also noted. 235

Figure 100. Representation of different physisorption system hydrogen storage capacity scenarios. 236

Figure 101. Pressure versus concentration isotherms (PCT plots) for a) an idealized material with a flat plateau, commonly seen in AB_5 materials and b) a real material with a largely sloping plateau, as is often seen in AB2 materials. The reversible and usable capacity is shown on each plot to demonstrate the potential effects of a sloping plateau. 238

Figure 102. Desorption isotherms of the Mg-Co-H system demonstrating multiple plateaus, each representing a different dissociation reaction. 239

Figure 103. Simplified representation of a Hydride Hydrogen Storage System 240

Figure 104. Representation of different hydride systems hydrogen storage capacity scenarios 241

Figure 105. Current state of the art, material hydrogen capacity vs. temperature. 244

Figure 106. Current state of the art, system gravimetric vs. system volumetric capacities and target. 245

Figure 107. Image of scaled up Alanate test bed with a series of internal and external thermocouples. 248

Figure 108. Third hydrogen desorption from scaled-up test bed (capacity on a materials only basis). 249

Figure 109. Volumetric density of H_2 in (1) an empty sample cell, (2) a sample cell filled with superactivated carbon powder, and (3) a sample cell filled with superactivated carbon granules. 250

Figure 110. 10kW scale hydrogen generator using $NaBH_4$ hydrolysis. 251

Figure 111. High pressure methane adsorption isotherms of steam-activated coconut char, with varied activation times. The traces H_2O-O through H_2O-6 correspond to activation times between 0 and 140 hours. 253

Figure 112. Variation of the maximum H_2 adsorption amount versus the oxygen/carbon ratio: (□) steam-activated coconut shell carbons (■) polyacrylonitrile-derived activated carbons. 254

Figure 113. Kinetics of hydrogen desorption from alkali amidoboranes and post-milled BH_3NH_3 samples at about 91°C (left); the right panel indicates the DSC trace, as well as the mass spectrometer traces of hydrogen and borazine from these three materials. The metal amidoboranes release significantly less borazine than the parent ammonia borane. 255

Figure 114. Excess hydrogen adsorption isotherms performed on copper-based MOFs near saturation. Notably the extrapolated excess curves down to Nex=0 are shown. At this point the adsorbed phase density equals that of the gas phase (about 50g/L); revealing the ultimate hydrogen packing density under such conditions. 257

Figure 115. Cycle life behavior of $LaNi_{5-X}Ge_X$. alloys with comparison to a good commercial mischmetal-based, multi-component alloy also evaluated at JPL. 259

Figure 116. Achievable vacuum for a roughing pump and turbo pump for various tube diameters. 263

Figure 117. Hydrogen yield as a function of temperature in the steam hydrolysis of $NaBH_4$ At higher temperatures the surface composition changes to borate hence preventing interaction of steam with the hydride ultimately decreasing the hydrogen delivery capacity. 266

Figure 118. Cycling measurements on $LaNi_5$. 267

Figure 119. Photo of incompletely hydrided LaNi5. 268

Figure 120. PCT measurements of $LaNi_5$ after heating under hydrogen. 269

Figure 121. Illustration of the effects of different types of alloy-impurity interactions on absorption-time profiles during repeated cycling: (a) poisoning; (b) retardation; (c) retardation-recovery; (d) reaction. The curves are for LaNi5 tested at 25°C and 345 kPa; only the first 4 min of 15 min absorption is shown. 270

Figure 122. Effect of the purity of ammonia borane on the onset of H_2 release. 271

Figure 123. Arrhenius plots of the temperature-dependent rate data yields a straight line. The slope is proportional to the apparent activation energy for hydrogen loss from neat ammonia borane (neat AB; Ea = -184 kJ/mol H2) and ammonia borane in the scaffold (AB:SBA-15; Ea = -67 kJ/mol H2). 273

Figure 124. Kinetics measurement of $LaNi_5$ Intermetallic compound with a single phase transition. The experiment was conducted under isothermal conditions at room temperature. Units in H per formula unit released. 274

Figure 125. Equilibrium PCT measurements of $LaNi_5$, a classic metal hydride at two different sample temperatures. 275

Figure 126. TPD measurement of the alanate-amide mixture. 276

Figure 127. PCT diagram of the alanate-amide mixture. 277

Figure 128. Example of capacity as a function of temperature and pressure for MOF-177 physisorption materials (Left: 77K , Right: 298K). 278

Figure 129. PCT measurement of lithium hydride destabilized by silicon. The first plateau (0.5 wt.% - 1.5 wt.%) corresponds to the transition from $Li_{2.35}Si$ to $Li_{1.71}Si$ + 0.64LiH. The second plateau corresponds to the transition from $Li_{1.71}Si$ to Si + 1.71LiH. 279

Figure 130. Hysteresis effects on the plateau pressure of PCT curves of Mg mechanically milled with $FeTi_{1.2}$. 280

Figure 131. Depiction of absorption (red) and desorption (blue) pressure concentration profiles for a material at one temperature. Open (blue) circles represent the effective desorption curve were the material only charged with hydrogen at a maximum pressure of 4 bar. 281

Figure 132. Depiction of absorption (red) and desorption (blue) PCT measurements made over increasingly long (1,2,3) periods of time. 283

Figure 133. Effect of FeTi Oxygen-content on second stage activation. Initial particle size -30 mesh +50 mesh. Rome temperature P ~ 67 atm. Each data point represents a dehydriding cycle. Arrows indicate sample cycled but no data taken. 285

Figure 134. The activation effects of pre-reacted sodium alanate. 286

Figure 135. Depiction of the excess adsorption as determined by the volumetric method. 1) A step by step description of the volumetric measurement process as it actually occurs. 2) Depicts the equivalent gas expansion process, which is how the excess adsorbed gas is measured. 3) A graphic representation showing how as the excess capacity is measured as a function of final measured pressure (C) by subtracting the expected (no sorption) quantity of hydrogen stored in the total volume from the measured amount of hydrogen in the total volume. 288

Figure 136. Depiction of hydrogen capacity measurements as determined by the volumetric method. 1) A step by step description of the volumetric measurement process as it actually occurs. 2) Depicts the equivalent gas expansion process, which is how the total sorption of hydrogen is measured. 3) A graphic representation showing how as the capacity is measured as a function of final measured pressure (C) by subtracting the expected (no absorption) quantity of hydrogen stored in the total volume from the measured amount of hydrogen in the total volume. 290

Figure 137. Diagram of the pressure in sorption/desorption system during hydriding reaction. The dashed line represents a test using a reservoir that is too small and the solid red line represents a test using a sufficiently large reservoir. 292

Figure 138. Schematic view of a cryostat designed for H_2 physisorption measurements. 293

Figure 139. Volumetric hydrogen evolution during the decomposition reaction of ammonia borane. 294

Figure 140. Blank tests performed at several temperatures in the 0–50 atm range. 295

Figure 141. Hydrogen density as a function of pressure at room temperature. 296

Figure 142. Depiction of the measured weight change of a sample caused by physisorption and buoyancy of the surrounding gas using the gravimetric method. a) The physical process of adsorption. b) Adsorbed molecules contribute to the weight of the sample (blue + purple), while the hydrogen molecules (red) displaced by the sample (and physisorbed gas) contribute to a buoyancy force opposing gravity. 299

Figure 143. Depiction of the excess capacity as measured by the gravimetric method. a) The physical process of adsorption. b) The buoyancy force caused by hydrogen molecules (red + purple) displaced by the

sample only (skeletal volume) is subtracted from the total measured weight change to give the "Excess" hydrogen storage capacity of the material. 300

Figure 144. Depiction of the absolute storage capacity of a sample as measured by the gravimetric method. a) The physical process of adsorption. b) The buoyancy force of hydrogen molecules (red) displaced by the sample and the adsorbed hydrogen is subtracted from the total measured weight change to give the "Absolute" hydrogen storage capacity of the material. c) In a porous sample, it can be difficult to determine the thickness and volume of the adsorption boundary layer, which leads to difficulty in evaluating the "Absolute" hydrogen storage capacity. 302

Figure 145. Gravimetric record of the activation and zeroing process of a sorbent sample of 1 g activated carbon, counterbalanced by quartz glass, in vacuum and in a helium atmosphere. 307

Figure 146. Buoyancy corrections for different sample skeletal densities at 77K and 298K. 311

Figure 147. Error in capacity by gravimetric and volumetric measurements due to a 50% error in estimating the skeletal density of a sample (50% lower than actual). Sample 23 mg activated carbon at 77K. 314

Figure 148. TGA desorption trace for a spillover sample that was dosed first with H_2 followed by D_2. 315

Figure 149. a) Mass loss on the thermal decomposition of polymeric aminoborane (H2BNH2)X versus temperature b) Experimental data for the mass loss (TG, line) in comparison with the mass loss data calculated from the released amount of hydrogen (volumetric measurements, points), (heating rates 1 and 10 °C/min). 316

Figure 150. Comparison between mass loss data detected thermogravimetrically (line) and calculated from volumetric results (points) (heating rate 1 K/min (a), 5 K/min (b)) 317

Figure 151. Thermal-programmed desorption (28°C/min) of hydrogen from 319

Figure 152. DSC curves of isothermal decomposition of BH_3NH_3 at temperatures between 343 and 363 K. 321

Figure 153. Residual Gas Analyzer set-up. 323

Figure 154. Residual gas analysis of alanate-amide sample discussed in the Kinetics section. 324

Figure 155. TPD/MS (1 °C/min) of volatile products generated by heating neat ammonia borane (solid line) and AB:SBA-15 (dashed line); m/e=2 (H_2) and m/e=80 (borazine, c-(NHBH)3). 326

Figure 156. Example of a leak on kinetics measurement. A little after two hours in to the experiment, the leak was eliminated. 327

Figure 157. Pressure-time plot of data used to create the PCT diagram of the alanate-amide mixture in the figure below. 328

Figure 158. PCT diagram of the alanate-amide mixture. 328

Figure 159. Pressure-composition-isotherm of LaMgNi4 - H system during absorption at 100°C and approximate upper phase limits (α, β, γ). 329

Figure160. Example of volumetric measurements on very small quantities of physisorption materials. Room temperature PCT isotherms from 2 mg PE CVD SWNT and HW CVD MWNT. 331

Figure161. Example of effect of sample size on the accuracy of measurements for physisorption materials. (a) Hydrogen uptake PCT isotherm of 39 mg of activated carbon sample and a stainless steel blank with the same gas displacement volume, and (b) comparison of measurements using the MicroDoser (39 and 6 mg) with those obtained using the standard sample holder setup with a 251 mg activated carbon 331

Figure 162. Schematic of a automated burette system used for Capacity and Kinetics measurements. 334

Figure 163. 1) The three step autothermal cycle demonstrated by Cooper et al (preceding page). 2) The block diagram indicating of a potential reactor scheme to transfer the heat of the onboard oxidation reaction (step 3) to the endothermic onboard dehydrogenation reaction (step 2). The spent fuel 'B' is then rehydrogenated in an off board catalytic regeneration process. 338

Figure 164. Benzene, borazine and hybrid materials 1,2-dihydro-1,2-azaborine. 339

Figure 165. Fused ring systems. 340

Figure 166. The pore size of microporous Metal-Organic Frameworks materials can be tuned during the synthesis to optimize the adsorption properties of the material. In this case, different linker sizes were used to vary the pore width. 341

Figure 167. Image depicting the distinction between path dependent and independent variables. 346

Figure 168. Diagrams of a) isolated system, no exchange with surroundings, b) closed system, only exchanges heat with surroundings, and c) open system exchanging both heat and mass with surroundings. 348

Figure 169. Joule-Thomson coefficients for various gases at atmospheric pressure. 356

Figure 170. Thermal effect of gas expansion to and from a Sievert's instrument's sample holder for various gases at room temperature. 358

Figure 171. Example of a phase diagram for the Pd-H system determined from PCT measurements. 364

Figure 172. Ideal case, reversible conditions. Top-Left) isotherm in which hydrogen induces a structural change, Middle-Left) isotherms in which the structure is maintained. Right: van 't Hoff plot. The line must stop at Tc. Bottom-left) Heat evolved during the abs/des processes. 367

Figure 173. Example Van 't Hoff Plot 372

Figure 174. Example of the construction of a van 't Hoff plot from a series of PCT measurements. 373

Figure 175. PCT plots for amorphous and crystalline $Zr_{50}Ni_{50}$. The amorphous measurements do not show a pressure plateau.[99] 374

Figure 176. Hysteresis cycle (where x is an independent variable). 378

Figure 177. Ideal hysteresis in an isothermal plot of lnP = f(composition). 379

Figure 178. Absorption and Desorption van 't Hoff plots. 380

Figure 179. Hydrogen adsorption hysteresis observed in the flexible MOF materials Co(1,4-benzenedipyrazolate). 381

Figure 180. Representative image of an unstrained (left) and a strained (right) lattice. Excess energy is stored in the stretched bonds in the right-hand image. 385

Figure 181. Representative image of an edge dislocation in a lattice. Excess energy is stored in the bonds stretched by the dislocation. 385

Figure 182. Schematic representation of the effect of plastic deformation, which accompanies hydride formation and hydride decomposition, on the integral free energy (per mole of metal). The tangent slopes $(dG/dr)_{T,p}$ give the chemical potential of hydrogen. Solid line: hypothetical equilibrium tangent slope; Dashed line: - - -, slope obtaining during hydride formation; Dotted line: · · · · · · slope obtaining during hydride decomposition. 386

Figure 183. Representative image of strain in a lattice at the interface between two grains or particles. 387

Figure 184. (a) Excess adsorption isotherm data of H_2 in MOF-5, used in the heat of adsorption calculation. Dotted lines indicate P-T data at fixed hydrogen concentrations. (b) The ln P vs. 1/T plot of H_2 in MOF-5 at various wt.%. According to the Clausius-Clapeyron equation, the isosteric heat of adsorption Q_{st} = -slope × R. (c) Q_{st} plot for H_2 adsorption in MOF-5, as derived from (b).[143] 390

Figure 185. The isosteric heat values calculated from different number of adsorption isotherms. 390

Figure 186. (Left) Measured "excess" adsorption isotherms. (Right) Calculated isosteric heat of adsorption from "excess" adsorption isotherms. 393

Figure 187. (Left) Actual ("absolute") adsorbed hydrogen vs. (Right) measured "excess" adsorbed hydrogen, the difference (red rectangle) being equal to AtP/kT. 393

Figure 188. (Left) Calculated "absolute" adsorption isotherms. (Right) Calculated isosteric heat of adsorption from "absolute" adsorption isotherms. 394

Figure 189. Comparison of isosteric enthalpies of adsorption (Q_{st}) calculated using virial methods and Langmuir-Freundlich methods for H_2 and D_2 adsorption on a MOF material. 397

Figure 190. Experimental surface excess hydrogen adsorption data (circles) of the physisorption material Maxsorb® over a temperature range of 30 to 273 K. Solid lines are the best fit made using Equation 198. 401

Figure 191. Absolute hydrogen adsorption results of Maxsorb® over a temperature range of 30 to 273 K constructed using Equation 199. 402

Figure 192. Adsorption isosteres at different absolute adsorptions. 403

Figure 193. Solid symbols give the isosteric heat of adsorption obtained by using Clausius-Clapeyron equation on the absolute adsorption. Solid line gives the isosteric heat of adsorption calculated using the modified DA model. 404

Figure 194. Solid symbols give the isosteric heat of adsorption obtained by using Clausius-Clapeyron equation on excess (black) and absolute (red) adsorption results. Solid red line gives the isosteric heat of adsorption calculated using the modified DA model. 405

Figure 195. Heat of adsorption for AX-21_33 (closed symbols) and MOF-177 (open symbols). 409

Figure 196. Design principles of metal hydride storage tanks. 414

Figure 197. Schematic diagram showing some of the balance of plant components required for a hydride based hydrogen storage / fuel cell system. 415

Figure 198. Demonstrated off-board regeneration scheme for spent ammonia borane[278]. 417

Figure 199. Typical cryogenic adsorption-based vessel. 418

Figure 200. Experimental isotherms for the system yttrium-hydrogen (O, absorption points; ● desorption points) showing the wide compositional range of the solid solution phase. 421

Figure 201. Standard method of making a Van 't Hoff plot from a series of desorption PCT measurements at different temperatures $LaNi_5$. 425

Figure 202. Illustration of detailed volumetric desorption PCT measurements at different temperatures for $LaNi_5$ (left) and different possible van 't Hoff plot derived from these isotherms (right). 426

Figure 203. A series of absorption and desorption PCT measurements at 38°C, 110°C and 200°C on a thin-film Pd/Ni sample removed from the substrate. 427

Figure 204. Portion of pressure vs. time data for a sequence of doses of hydrogen during an absorption PCT measurement at 38°C. 428

Figure 205. Pressure vs. time data for the plateau region of the desorption PCT measurement at 200°C. 429

Figure 206. Pressure vs. time data of a single desorption dose in the PCT measurement at 200°C. 429

Figure 207. A desorption PCT measurement on $LaNi_5$ at 50°C in which dosing is stopped at a hydrogen concentration of 1/2 the total sample content (i.e. ½ $LaNi_5H_6$ or 3 H/f.u.). 431

Figure 208. The pressure / time profile for the same desorption PCT on $LaNi_5$ in which dosing is stopped at 3 H/f.u. and the temperature of the sample is first reduced to room temperature then increased in steps of 10°C. 432

Figure 209. The Concentration / time profile for the same desorption PCT on $LaNi_5$ zooming in on the portion of concentration change as the sample's temperature is increased in steps of 10°C. 433

Figure 210. Van 't Hoff plot of equilibrium desorption plateau pressures from a series of PCT measurements (red) and a single "Direct van 't Hoff" measurement on $LaNi_5$ from 30°C to 80°C. The enthalpy and entropy of hydrogen desorption determined from the slope and intercept of the direct measured data are given in the inset of the figure. 434

Figure 211. Pressure vs. concentration diagram of the "Direct van 't Hoff" measurement. The initial dosing reached a concentration of 0.3 H/M. This was followed by increasing the temperature in two steps with a separate series of doses at each step to return to mid-plateau concentrations. "Direct van 't Hoff" measurements were taken at the points indicated by the red circles. 435

Figure 212. The temperature stepping process of the "Direct van 't Hoff" measurement on a Pd/Ni thin film sample with the associated changes in pressure (log scale) and concentration. 436

Figure 213. Van 't Hoff plot of equilibrium desorption plateau pressures from a series of PCT measurements (red: absorption, blue: desorption) and a single "Direct van 't Hoff" measurement on a 91 mg Pd/Ni thin film sample from 38°C to 250°C. The enthalpy and entropy of hydrogen desorption determined from the slope and intercept of the direct measured data are given in the inset of the figure. 437

Figure 214. Schematic view of a volumetric system. 438

Figure 215. Schematic view of the cryostat (details). 440

Figure 216. Adsorption enthalpy ΔH^0 plotted as function of fractional filling for different samples where w_0 is the maximum uptake at 77K. 440

Figure 217. Metal hydride thin film in the metallic (left) and in the hydrided (right) state during electrochemical loading. 446

Figure 218. Optical transmission change in the metallic thin film during hydrogenation (left) and dehydrogenation (right). 447

Figure 219. Ternary composition diagram (left) showing the final optical transmission state and the enthalpy map (right) of the Mg-Ni-Ti system, estimated using the optically determined hydrogenation plateaus. Black region on the right-hand picture represents chemical compositions that do not have a well defined plateau on the PTIs. 449

Figure 220. Schematic representation of the Hydrogenography setup. 451

Figure 221. Transmission measurements (black line) of a 65 nm PdHx thin film as a function of hydrogen pressure during absorption and desorption step scans at 294 K after cycling. Each pressure step (blue line) is maintained one hour to ensure relaxation of the film and equilibrium with the hydrogen environment. The transmission T is normalized by the transmission in the as-deposited metallic state T_0. 453

Figure 222. Diagram of a basic DSC instrument. 456

Figure 223. Diagram detailing the major chemical and physical transformations of the decomposition of ammonia borane. 459

Figure 224. PCTPro-2000 Sievert's apparatus coupled with a C80 calorimeter permitting simultaneous measurements of gas adsorption/desorption and heats of sorption. 461

Figure 225. Cycling kinetics data showing activation of $LaNi_5$. Note lower initial capacity of the sample. 462

Figure 226. Calorimetric curves showing exothermic and endothermic peaks for hydrogen absorption and desorption cycles. 463

Figure 227. After 32 cycles $LaNi_5$ sample still contains 5/6 of a course un-reacted material. 464

Figure 228. Isotherms and enthalpies corresponding to the formation ($\Delta H_{\beta\rightarrow\gamma}$), decomposition ($\Delta H_{\gamma\rightarrow\beta}$) of the nonstoichiometric γ-trihydride, and $ZrNiH_{3-\gamma}$ from the monohydride. 465

Figure 229. Isotherms and enthalpies corresponding to the formation ($\Delta H_{\beta\rightarrow\gamma}$), decomposition ($\Delta H_{\gamma\rightarrow\beta}$) of the nonstoichiometric γ trihydride, and $ZrNiH_{3-\gamma}$ from the monohydride. 466

Figure 230. Low-temperature H_2-TPD profiles of Ni-MOF material depending on dehydration temperatures. Ramping rate: 5 K/min. 473

Figure 231. Hydrogen desorption PCT measurements at 40°C for the substitution of Ni in $LaNi_5$ by the elements M=Pd, Ag, Cu, Co, Fe, Cr: $LaNi_4M$ and Pt (5%). 475

Figure 232. Sensitivity plots for gravimetric and volumetric energy density. 476

Figure 233. Scale up (100 g) reactor with end cap removed in Ar-glovebox to show catalyzed alanate.[121] 477

Figure 234. Exothermic temperature excursion during scale up bed charge half-cycle (P_i=174 bar, T_i=155˚C).[121] 478

Figure 235. Synopsis of results for the release of hydrogen from a variety of materials as a function of temperature. 480

Figure 236. Hydrogen desorption PCT measurements at 40°C for the changes in the nickel content of $LaNi_5$. Alloys were annealed at 1400°C for approximately one week before testing. 482

Figure 237. Hydrogen desorption plateau pressures at 40°C plotted as a function of nickel content in $LaNi_X$. 482

Figure 238. A van 't Hoff plot showing the expected equilibrium pressures for the dehydrogenation of $LiBH_4$ in both its orthorhombic and molten states (-o and -l suffix used to identify the respective state), MgH_2 and the destabilized system $LiBH_4$-MgH_2 with a 2:1 molar ratio. The experimental data reported by Vajo et al. (2005) are also plotted with a line of best fit for comparison. 484

Figure 239. Scaled exotherms (solid lines) from isothermal calorimetry experiments that show the time-dependent release of H_2 from AB and AB:SBA-15 (1:1 wt/wt). 486

Figure 240. Calorimetric measured heat release normalized by the ammonia borane sample amount (solid lines) and the integrated equivalents of H_2 released (mol H_2/mol AB; dashed lines) assuming a constant heat of reaction of -21.7 kJ/mol AB. 487

Figure 241. Global isothermal kinetic model results (solid lines) up to 0.80 H_2 equivalents released (the fit region) compared to the experimental data (dashed lines). 488

Figure 242. Thermal desorption temperatures of hydrogen in MOFs versus the diameter of their pores. 489

Figure 243. Excess hydrogen adsorption isotherms measured (data points) on the Cu_2(tptc) material (left) and Cu_2(bptc) material (right) over the 50–100 K range and modeled with the DA equation (dashed lines).[163] 490

Figure 244. Plot of the measured excess hydrogen adsorption as a function of the gas density up to the near-saturation region at 50 K (left) and 55 K (right). 490

Figure 245. Isotherms for ZrNi at 473K for samples annealed at (○) 473 K, (●) 673 K, (△) 773 K, (◢) 873 K and (▽) 1000 K. 491

Figure 246. PCT measurements of $LaNi_5$ after heating under hydrogen. 492

Figure 247. Schematic representation of the forces acting on a thin film during hydrogen absorption. 493

Figure 248. Schematic representation of stress release models in the metal hydride thin films with weak (left) and strong (right) adhesion to the substrate during (de)/hydrogenation. 494

Figure 249. Van 't Hoff graph of the bulk Pd and clamped Pd films (red triangles) measured by the Hydrogenography; the enthalpy is calculated from regression analysis. Literature data on Pd films (black circles) and bulk Pd (blue diamonds) are presented for comparison. Filled and opened symbols represent absorption and desorption, respectively. 495

Figure 250. (a) Differential scanning calorimetry plot of α-AlH3 in the temperature range of 35–300 ◦C ramped at a rate of 10 ◦C/min; (b) ex situ diffraction patterns acquired at room temperature before thermal treatment (I) and after a temperature ramp to 300 ◦C (II).[238] 497

Figure 251. INS spectra of H_2 in HKUST-1 at 0.2, 0.5, 1.0, 1.5, 2.0 H_2:Cu. The background spectrum has been subtracted from the H_2 spectra. 499

Figure 252. Dependence of the adsorption enthalpy (ΔH_{ads}, black circle) and of the temperature at which the H_2 complexes are observed (T onset, gray squares) on the corresponding shift of the H-H stretching frequency for the three MOFs under investigation. Para-H_2 has been used as reference. The red line corresponds to the linear regression of the T_{onset} data: y = mx + q where m = -0.90436 K cm and q = 61.15506 K (r^2 = 0.9694 and max. dev. = 8.57425). For CPO-27-Ni, the barycenter of the 4028 and 4035 cm^{-1} bands has been considered. 500

Figure 253. Thermodynamics of hydrogen release from (1) AB, (2) Ethane, and (3) potential CBN hydrogen storage materials. 505

Figure 254. Calculated Thermodynamic Properties of CBN Heterocycles. 506

Figure 255. The empirical transition metal ion radius, the calculated M-H_2 distance, the experimental Q_{st} (along with error bar), and the calculated E_B(GGA) of M_2(dhtp). 507

Figure 256. Hydrogen storage capacities of $LaNi_5$ samples from various suppliers during absorption cycling: (A) Research Chemicals sample, dry H_2; (B) Ergenics; (C) Research Chemicals; (D) Molycorp. Samples are cycled in 12 atm with about 10 Torr H_2O. 510

Figure 257. Hydrogen concentration changes Δx for $LaNi_{5-y}Sn_yH_x$ obtained from the maximum and minimum pressures for each cycle. 511

Figure 258. Reversible portions of the pressure–composition isotherms obtained at 298 K on thermal cycled $V_{0.995}C_{0.005}H_X$. 513

Figure 259. (a) Comparison of hydrogen capacity loss as function number of pressure cycles for $LaNi_{4.7}Al_{0.3}$, $LaNi_{5.2}$, and $CaNi_5$, before and after pressure cycling at 85°C between 0 and 2068 kPa (300psi). This shows a significant loss in $CaNi_5$ but this loss is recovered after reproportionation. (b) A reference isotherm of $CaNi_5$ (taken at 25°C) showing three different plateaus due to the three distinct $CaNiH_x$ phase compositions. 515

Figure 260. Effects of different types of impurity interactions with $LaNi_5$ on the absorption H/M vs. time profiles during repeated cycling. (a) Poisoning, (b) Retardation, (c) Retardation-Recovery, (d) Reaction. Curves measured at 25°C and 3.4 atm H_2 pressure.[59] 517

Figure 261. Chart of hydrogen storage materials stability testing methods. 520

Figure 262. Thermal Cycling Apparatus: Heating cooling apparatus for long-term thermal cycling. 523

Figure 263. High pressure thermal aging apparatus. 525

Figure 264. Thermal aging method is shown in the schematic. (Left) An isotherm is generated at a temperature T_1 until fully saturated in the β phase (above the plateau pressure). The sample holder is sealed and the sample heated to the aging temperature T_2. Once the temperature is stabilized, then sample is allowed to age for a certain period of time (Right). If there is disproportionation, then the pressure rises and H/M decreases as function of time. 526

Figure 265. Isotherms of $LaNi_5$ taken at 25°C after subjecting to aging at high and low hydrogen pressures. Note that the isotherm for vacuum aged sample at 180°C is nearly (but not exactly) the same as the isotherm before aging indicating full reproportionation of the $LaNi_5$ hydride with a flat plateau after vacuum aging. 527

Figure 266. Hydrogen cycling of $NaAlH_4$ (NaH + Al starting material) doped with 10 mol% of TiO_2 nanoparticles. An activation process is observed in the first 20 cycles. Red: hydrogen desorption capacity, Gray: hydrogen charging pressure at each cycle. 531

Figure 267. PCT measurement of 11th hydrogen desorption cycle of $LiNH_2$ with LiH after partial absorption. 534

Figure 268. Approach to equilibrium during PCT measurements (previous figure) of hydrogen desorption from the reaction of $LiNH_2$ with LiH. 534

Figure 269. Reversible hydrogen desorption capacity with cycling of Li-Mg-N-H (charging constant pressure 69-83 bar, discharge to 0.5 bar, 200°C). 535

Figure 270. Hydrogen desorption cycle no. 20 for the Li-Mg-N-H system (charging constant pressure ~100 bar, discharge to 0.5 bar , 200°C). 536

Figure 271. Average hydrogen desorption rate to 3.0 and 3.5 wt.% for the Li-Mg-N-H system (charging constant pressure ~100 bar, discharge to 0.5 bar , 200°C). 536

Figure 272. ($2LiNH_2 + MgH_2$) cycle test at 200 ◦C. The duration of sorption cycles and capacity loss for each cycle are marked. 537

Figure 273. (a) Room temperature isotherm of the classic $LaNi_5$, (b) van 't Hoff plot of $LaNi_5$ obtained from the isotherms taken at many temperatures (a-bottom) Hexagonal Structure of $LaNi_5H_6$. 539

Figure 274. High pressure hydrogen physisorption capacity on MOF $Zn(bdc)(ted)_{0.5}$ at 77 K as a function of the number of adsorption/desorption cycles. Each cycle is a set of adsorption-desorption isotherm. Each point represent maximum uptake (% of full capacity) of the associated adsorption isotherm. 540

Figure 275. A typical cycle for $LaNi_{4.8}Sn_{0.2}$ by heating in closed system from room temperature to 125°C and cycled between saturated conditions to depleted conditions. This is shown as high pressures below equilibrium (saturated) and low pressures above equilibrium (depleted) where lines A and B are the absorption – desorption equilibrium pressures respectively. 542

Figure 276. Isotherm of $LaNi_{5.2}$ taken at 25°C after intrinsic P-T cycling for 10 (activation), 1500, 10,000 times showing severe degradation of this hydride. 543

Figure 277. Isotherms of (a) $LaNi_{0.8}Sn_{0.2}$ and (b) $La_{0.9}Gd_{0.1}Ni_5$ taken at 25°C, before and after P-T intrinsic cycling for 1500 and 10,000 times showing virtually no loss in hydrogen capacity in the case of $LaNi_{0.8}Sn_{0.2}$, and extensive loss for $La_{0.9}Gd_{0.1}Ni_5$ after prolonged cycling. 544

Figure 278. Comparison of $LaNi_{0.8}Sn_{0.2}$ isotherms after: (a) thermal cycling and (b) thermal aging (180°C at 29.6 atm) experiments. Comparison of $La_{0.9}Gd_{0.1}Ni_5$ isotherms after: (c) thermal cycling and (d) thermal aging (180°C at 190.7 atm) experiments. The time taken for cycling several months, where as time taken for aging is ~2 weeks), yet the results are nearly the same. Note that the cycling/aging apparatuses are different form the Sievert's apparatus used to obtain the isotherms. 545

Figure 279. (a) Example plot of pressure cycling; partial view of the pressure vs. time is shown. (b) One dehydriding and one hydriding cycle is shown; (c) details of the dehydriding cycle from A to B. 546

Figure 280. High temperature and Pressure isothermal cycling using impure hydrogen: Extrinsic cyclic response of (a) $Fe_{0.85}Mn_{0.15}Ti_{0.5}$ (hydrogen cycle at 25°C, 69 → 634 → 69 kPa) and (b) $LaNi_5$, (0.5 hour cycle at 25°C, 69 → 276 → 69 kPa). 548

Figure 281. (a). Absorption isotherms of Li-amide obtained after non-equilibrium pressure cycling for 1, 56, 163, 501, 1100 times with impure hydrogen (ppm levels of O_2, H_2O and others). (b) Corresponding ex-situ X-ray diffraction taken from the sample after each isotherm was obtained in desorbed condition. 549

List of Tables

Table 1. SI base units.	27
Table 2. Examples of coherent derived units in the SI expressed in terms of base units.	28
Table 3. Coherent derived units in the SI with special names and symbols.	30
Table 4. Examples of SI coherent derived units whose names and symbols include SI coherent derived units with special names and symbols.	31
Table 5. Table of concentrations and related quantities.	32
Table 6. Recommended units for the presentation of hydrogen storage materials properties.	33
Table 7. Qualitative overview of metal hydride types as to attributes.	44
Table 8. The variance of mathematical functions of the variables A and B, having standard deviations σ_A and σ_B, correlation coefficient ρ_{AB}, and precisely-known real-valued constants a and b.	69
Table 9. Summary of the original US Department of Energy capacity targets. The material capacities are assumed to be 2 times larger than the system capacities.	243
Table 10. Summary of revised US Department of Energy capacity targets.	243
Table 11. Typical degassing conditions for different sorption materials.	265
Table 12. Maximum error due to volume expansion during hydrogen loading at various temperatures and pressures.	312
Table 13. Spectroscopic and thermodynamic data for hydrogen adsorbed on several zeolites. Error limits for ΔH^0 and ΔS^0 are ±1 kJmol^{-1} and ±10 Jmol^{-1}K^{-1}, respectively.	407

Summary of Document Structure

This Recommended Practices for the Characterization of Hydrogen Storage Materials document provides an introduction to and overview of the recommended best practices in making measurements of the hydrogen storage properties of materials. Due to the breadth of the subjects covered, material will be presented in its most concise and accessible form. The authors will use examples from literature to add clarity to key topics and to provide the reader with avenues for further detailed inquiry into a specific subject. The Recommended Practices document is divided into an introductory section and will be followed by four or more chapters that cover the topic areas of: concentration and capacity, kinetics, thermodynamics and cycle life measurements of hydrogen storage materials as well as other important hydrogen storage materials properties.

The introductory section provides the reader with the background information needed for making hydrogen storage measurements. The introduction covers the following main topics: 1) evaluating the experimental setup and procedures with respect to the ultimate purpose for making a set of measurements, 2) the relationships between direct and indirect (measureable vs. derived) quantities (which we will refer to as variables) used to describe hydrogen storage materials properties, and 3) an overview of common methods used to measure these hydrogen storage properties.

The introduction will be followed by separate chapters covering the recommended practices associated with the measurement of concentration and capacity, kinetics, thermodynamics and cycle-life properties among others. These chapters will each include: a review of theory, an evaluation of the purpose of measurements for the selection of appropriate methods, and detailed experimental considerations that are of particular importance to each property being measured.

Citation Information

It is requested that the following information be used when referencing this document in publications: Gross, K.J., Carrington, R.K., Barcelo, S., Karkamkar, A., Purewal, Ma, S., Zhou, H-C., Dantzer, P., Ott, K., Burrell, T., Semeslberger, T., Pivak, Y., Dam, B., Chandra, D., and Parilla, P., "Recommended Best Practices for the Characterization of Storage Properties of Hydrogen Storage Materials", (2011) V3-5 U.S. D.O.E. Hydrogen Program document, available online at:

http://www1.eere.energy.gov/hydrogenandfuelcells/pdfs/best_practices_hydrogen_storage.pdf

Preface

1 Mission

The ultimate goal of the United States Department of Energy's Hydrogen Storage Program is the development of hydrogen storage materials that meet or exceed the DOE's targets for onboard hydrogen storage in a hydrogen-powered vehicle. The recent rapid expansion of research efforts in this field has brought the talents of a wide range of researchers to bear in solving the grand challenge of hydrogen storage. There is a need for common metrics and recommended practices for measuring the practical hydrogen storage properties of new materials that are being developed within the US DOE Hydrogen Storage Program as well as at an international level. A clear and comprehensive resource that will provide guidelines to common metrics and recommended practices in the measurements of hydrogen storage properties is critical to the success of the Hydrogen Storage Program.

1.1 Objective

The objective of this Recommended Practices for the Characterization of Hydrogen Storage Materials Project is to create a reference guide of common methodologies and protocols for measuring critical performance properties of advanced hydrogen storage materials. This document is designed to serve as a resource to the hydrogen storage materials development community to aid in clearly communicating the relevant performance properties of new materials as they are discovered and tested.

1.2 Benefit to the DOE

The benefit of this series of Recommended Practices reference guides to the DOE is to facilitate the transfer of knowledge and experience in making these critical measurements from some of the world's experts in this field to the entire DOE and world-wide hydrogen storage community. The short-term benefit will be to provide a clear knowledge base in the form of a published resource to aid those just entering this rapidly expanding field. The long-term benefit will be to create strong ties between government, university, and small and large business entities that will lead to more open communications and ideally the establishment of uniform measurement practices and reporting.

2 Recommended Reading

This document is not meant to be a thorough review of the leading work in this field, but rather an overview and series of instructive examples of important issues concerning the measurement of the kinetic properties of hydrogen storage materials. The following resources are a good place to find more detailed information on the key topics.

2.1 Hydrogen Storage

- The book "Solid-state hydrogen storage: materials and chemistry", edited by Walker.[1]
- The book "Hydrogen Storage Materials (Materials Science Forum)" edited by Barnes.[2]
- The review article "Hydrogen-storage materials for mobile applications" by Schlapbach and Züttel.[3]
- European Commission Joint Research Centre Institute for Energy (JRC) Scientific and Technical Reports by D. P. Broom, "Hydrogen Sorption Measurements on Potential Storage Materials".[4]

2.2 Hydrides

- The book "Hydrides" by Wiberg and Amberger.[5]

2.3 Metal Hydrides

- The book "Metal Hydrides" edited by Muller, Blackledge, and Libowitz.[6]
- The book "Transition Metal Hydrides" edited by Dedieu.[7]
- The review article "A panoramic overview of hydrogen storage alloys from a gas reaction point of view" by Sandrock.[47,59]

2.4 Off-board Regenerable Hydrogen Storage Materials

- The article "Ammonia–borane: the hydrogen source par excellence?" by Frances H. Stephens, Vincent Pons and R. Tom Baker.[8]

- The chapter “Aluminum Hydride” by Ragaiy Zidan in the book, “Handbook of hydrogen storage: New Materials for Future Energy Storage”.[9]

2.5 Physisorption Storage

- The review article “Hydrogen adsorption and storage on porous materials” by K.M. Thomas.[10]
- The review article “Review of hydrogen storage by adsorption in carbon nanotubes” by Darkrim, Malbrunot and Tartaglia.[11]
- The journal article “Hydrogen Storage in Microporous Metal-Organic Frameworks” by Rosi et al.[12]

2.6 Kinetics

- The book “Basic Chemical Kinetics” by Eyring, Lin and Lin.[13]
- The book “Chemical Kinetics and Reaction Mechanisms” by Espenson.[14]
- The book “Chemical Kinetics and Catalysis.” By, Richard I. Masel.[15]
- The book “Chemical Kinetics.” by J. E.Nicholas.[16]

2.7 Thermodynamics

- The review article “Materials for hydrogen storage: current research trends and perspectives” by A.W.C. van den Berg and C.O. Arean.[17]
- The article “Heat of Adsorption for Hydrogen in Microporous High-Surface-Area
- Materials” by B. Schmitz, U. Muller, N. Trukhan, M. Schubert, G. Ferey, and M. Hirscher.[18]
- “Perry's Chemical Engineers' Handbook” by R. H. Perry and D. W. Green.[19]
- B. N. Roy (2002). Fundamentals of Classical and Statistical Thermodynamics. John Wiley & Sons. ISBN 0-470-84313-6.[20]
- F. Reif (1965). "Chapter 5 – Simple applications of macroscopic thermodynamics". Fundamentals of Statistical and Thermal Physics. McGraw-Hill. ISBN 0070518009.[21]

3 The International System of Units (SI)

In this document SI (System International) units will be used wherever possible. In some cases, example data is presented in its original form (for example: atm for pressure rather than kPa or bar). It is the recommendation of this Best Practices document that SI units be used to present results in the field of Hydrogen Storage. The following is a brief introduction to SI unit conventions. [22]

3.1 Symbols for the Seven Base Units

The base units of the International System are listed in Table 1, which relates the base quantity to the unit name and unit symbol for each of the seven base units.

Base quantity		SI base unit	
Name	Symbol	Name	Symbol
length	*l, x, r*, etc.	metre	m
mass	*m*	kilogram	kg
time, duration	*t*	second	s
electric current	*I, i*	ampere	A
thermodynamic temperature	*T*	kelvin	K
amount of substance	*n*	mole	mol
luminous intensity	I_v	candela	cd

The symbols for quantities are generally single letters of the Latin or Greek alphabets, printed in an italic font, and are recommendations. The symbols for units are mandatory

Table 1. SI base units.[22,23]

3.2 SI Derived Units

Derived units are products of powers of base units. Coherent derived units are products of powers of base units that include no numerical factor other than 1. The base and coherent derived units of the SI form a coherent set, designated the set of coherent SI units.

3.3 Derived Units Expressed in Terms of Base Units

The number of quantities in science is without limit, and it is not possible to provide a complete list of derived quantities and derived units. However, Table 2 lists some examples of derived quantities, and the corresponding coherent derived units expressed directly in terms of base units.

Derived quantity		SI coherent derived unit	
Name	Symbol	Name	Symbol
area	A	square metre	m^2
volume	V	cubic metre	m^3
speed, velocity	v	metre per second	m/s
acceleration	a	metre per second squared	m/s^2
wavenumber	σ, $\tilde{\nu}$	reciprocal metre	m^{-1}
density, mass density	ρ	kilogram per cubic metre	kg/m^3
surface density	ρ_A	kilogram per square metre	kg/m^2
specific volume	v	cubic metre per kilogram	m^3/kg
current density	j	ampere per square metre	A/m^2
magnetic field strength	H	ampere per metre	A/m
amount concentration [(a)], concentration	c	mole per cubic metre	mol/m^3
mass concentration	ρ, γ	kilogram per cubic metre	kg/m^3
luminance	L_v	candela per square metre	cd/m^2
refractive index [(b)]	n	one	1
relative permeability [(b)]	μ_r	one	1

(*a*) In the field of clinical chemistry this quantity is also called substance concentration.

(*b*) These are dimensionless quantities, or quantities of dimension one, and the symbol "1" for the unit (the number "one") is generally omitted in specifying the values of dimensionless quantities.

Table 2. Examples of coherent derived units in the SI expressed in terms of base units.[22]

3.4 Units with Special Names and Symbols; Units that Incorporate Special Names and Symbols

For convenience, certain coherent derived units have been given special names and symbols. There are 22 such units, as listed in Table 3. These special names and symbols may

themselves be used in combination with the names and symbols for base units and for other derived units to express the units of other derived quantities.

	SI coherent derived unit [a]			
Derived quantity	Name	Symbol	Expressed in terms of other SI units	Expressed in terms of SI base units
plane angle	radian [b]	rad	1 [b]	m/m
solid angle	steradian [b]	sr [c]	1 [b]	m^2/m^2
frequency	hertz [d]	Hz		s^{-1}
force	newton	N		m kg s^{-2}
pressure, stress	pascal	Pa	N/m^2	m^{-1} kg s^{-2}
energy, work, amount of heat	joule	J	N m	m^2 kg s^{-2}
power, radiant flux	watt	W	J/s	m^2 kg s^{-3}
electric charge, amount of electricity	coulomb	C		s A
electric potential difference, electromotive force	volt	V	W/A	m^2 kg s^{-3} A^{-1}
capacitance	farad	F	C/V	m^{-2} kg^{-1} s^4 A^2
electric resistance	ohm	Ω	V/A	m^2 kg s^{-3} A^{-2}
electric conductance	siemens	S	A/V	m^{-2} kg^{-1} s^3 A^2
magnetic flux	weber	Wb	V s	m^2 kg s^{-2} A^{-1}
magnetic flux density	tesla	T	Wb/m^2	kg s^{-2} A^{-1}
inductance	henry	H	Wb/A	m^2 kg s^{-2} A^{-2}
Celsius temperature	degree Celsius [e]	°C		K
luminous flux	lumen	lm	cd sr [c]	cd
illuminance	lux	lx	lm/m^2	m^{-2} cd
activity referred to a radionuclide [f]	becquerel [d]	Bq		s^{-1}
absorbed dose, specific energy (imparted), kerma	gray	Gy	J/kg	m^2 s^{-2}
dose equivalent, ambient dose equivalent, directional dose equivalent, personal dose equivalent	sievert [g]	Sv	J/kg	m^2 s^{-2}
catalytic activity	katal	kat		s^{-1} mol

(*a*) The SI prefixes may be used with any of the special names and symbols, but when this is done the resulting unit will no longer be coherent.

(*b*) The radian and steradian are special names for the number one that may be used to convey information about the quantity concerned. In practice the symbols rad and sr are used where appropriate, but the symbol for the derived unit one is generally omitted in specifying the values of dimensionless quantities.

(*c*) In photometry the name steradian and the symbol sr are usually retained in expressions for units.

(*d*) The hertz is used only for periodic phenomena, and the becquerel is used only for stochastic processes in activity referred to a radionuclide.

(*e*) The degree Celsius is the special name for the kelvin used to express Celsius temperatures. The degree Celsius and the kelvin are equal in size, so that the numerical value of a temperature difference or temperature interval is the same when expressed in either degrees Celsius or in kelvins.

(*f*) Activity referred to a radionuclide is sometimes incorrectly called radioactivity.

(*g*) See CIPM Recommendation 2 (CI-2002), p. 168, on the use of the sievert (PV, 2002, **70**, 205).

Table 3. Coherent derived units in the SI with special names and symbols.[22]

Some examples are given in Table 4. The special names and symbols are simply a compact form for the expression of combinations of base units that are used frequently, but in many cases they also serve to remind the reader of the quantity involved. The SI prefixes may be used with any of the special names and symbols, but when this is done the resulting unit will no longer be coherent.

	SI coherent derived unit		
Derived quantity	Name	Symbol	Expressed in terms of SI base units
dynamic viscosity	pascal second	Pa s	m^{-1} kg s^{-1}
moment of force	newton metre	N m	m^2 kg s^{-2}
surface tension	newton per metre	N/m	kg s^{-2}
angular velocity	radian per second	rad/s	m m^{-1} s^{-1} = s^{-1}
angular acceleration	radian per second squared	rad/s^2	m m^{-1} s^{-2} = s^{-2}
heat flux density, irradiance	watt per square metre	W/m^2	kg s^{-3}
heat capacity, entropy	joule per kelvin	J/K	m^2 kg s^{-2} K^{-1}
specific heat capacity, specific entropy	joule per kilogram kelvin	J/(kg K)	m^2 s^{-2} K^{-1}
specific energy	joule per kilogram	J/kg	m^2 s^{-2}
thermal conductivity	watt per metre kelvin	W/(m K)	m kg s^{-3} K^{-1}
energy density	joule per cubic metre	J/m^3	m^{-1} kg s^{-2}
electric field strength	volt per metre	V/m	m kg s^{-3} A^{-1}
electric charge density	coulomb per cubic metre	C/m^3	m^{-3} s A
surface charge density	coulomb per square metre	C/m^2	m^{-2} s A
electric flux density, electric displacement	coulomb per square metre	C/m^2	m^{-2} s A
permittivity	farad per metre	F/m	m^{-3} kg^{-1} s^4 A^2
permeability	henry per metre	H/m	m kg s^{-2} A^{-2}
molar energy	joule per mole	J/mol	m^2 kg s^{-2} mol^{-1}
molar entropy, molar heat capacity	joule per mole kelvin	J/(mol K)	m^2 kg s^{-2} $K^{-1}$$mol^{-1}$
exposure (x- and γ-rays)	coulomb per kilogram	C/kg	kg^{-1} s A
absorbed dose rate	gray per second	Gy/s	m^2 s^{-3}
radiant intensity	watt per steradian	W/sr	m^4 m^{-2} kg s^{-3} = m^2 kg s^{-3}
radiance	watt per square metre steradian	$W/(m^2$ sr)	m^2 m^{-2} kg s^{-3} = kg s^{-3}
catalytic activity concentration	katal per cubic metre	kat/m^3	m^{-3} s^{-1} mol

Table 4. Examples of SI coherent derived units whose names and symbols include SI coherent derived units with special names and symbols.[22]

The values of several different quantities may be expressed using the same name and symbol for the SI unit. Thus for the quantity heat capacity as well as the quantity entropy, the SI unit is the Joule per Kelvin. It is therefore important not to use the unit alone to specify the quantity. This applies not only to scientific and technical texts, but also, for example, to measuring instruments (i.e. an instrument read-out should indicate both the unit and the quantity measured).

A derived unit can often be expressed in different ways by combining base units with derived units having special names. Joule, for example, may formally be written newton meter, or kilogram meter squared per second squared. This, however, is an algebraic freedom to be governed by common sense physical considerations; in a given situation some forms may be more helpful than others.

In practice, with certain quantities, preference is given to the use of certain special unit names, or combinations of unit names, to facilitate the distinction between different quantities having the same dimension. When using this freedom, one may recall the process by which the quantity is defined. For example, the quantity torque may be thought of as the cross product of force and distance, suggesting the unit newton meter, or it may be thought of as energy per angle, suggesting the unit joule per radian. The SI unit of frequency is given as the hertz, implying the unit cycles per second; the SI unit of angular velocity is given as the radian per second; and the SI unit of activity is designated the becquerel, implying the unit counts per second. Although it would be formally correct to write all three of these units as the reciprocal second, the use of the different names emphasizes the different nature of the quantities concerned. Using the unit radian per second for angular velocity, and hertz for frequency, also emphasizes that the numerical value of the angular velocity in radian per second is 2π times the numerical value of the corresponding frequency in hertz.

3.5 Concentrations and Related Quantities

In chemistry, concentration is defined as the quantity of a constituent divided by the total volume of a mixture. Concentration can be expressed in terms of: mass concentration, molar concentration, number concentration, and volume concentration.[24] The term concentration can be applied to any kind of chemical mixture, but most frequently it refers to solutes in homogeneous solutions.

Concentration type	Symbol	Definition	SI-unit	other unit(s)
mass concentration	ρ_i or γ_i	m_i / V	kg/m^3	g/100mL (=g/dL)
molar concentration	c_i	n_i / V	mol/m^3	M (=mol/L)
number concentration	C_i	N_i / V	$1/m^3$	$1/cm^3$
volume concentration	ϕ_i	V_i / V	m^3/m^3	
Related quantities	**Symbol**	**Definition**	**SI-unit**	**other unit(s)**
normality		c_i / f_{eq}	mol/m^3	M (=mol/L)
molality	m_i	$n_i / m_{solvent}$	mol/kg	
mole fraction	x_i	n_i / n_{tot}	mol/mol	ppm, ppb, ppt
mole ratio	r_i	$n_i / (n_{tot} - n_i)$	mol/mol	ppm, ppb, ppt
mass fraction	w_i	m_i / m_{tot}	kg/kg	ppm, ppb, ppt
mass ratio	ζ_i	$m_i / (m_{tot} - m_i)$	kg/kg	ppm, ppb, ppt

Table 5. Table of concentrations and related quantities.

While hydrogen storage capacity is often expressed as mass fraction (g H_2/ g sample) it is more appropriate for comparing different hydrogen storage materials and systems to express hydrogen storage capacity in terms of weight percent [wt.%] (g H_2/ (g H_2 + g sample)).

3.6 Recommended (SI) Units for Hydrogen Storage

Many different units (SI and otherwise)[25] have been used in hydrogen storage materials research and development literature over the years. To facilitate direct comparison of measured results, the following units are recommended for all publications and presentations in this field. Note that Quantities indicated with and asterisk (*) are modified SI units that are recommended because of a more direct physical relationship with the quantities generally measured in hydrogen storage materials research and development. These quantities typically are a decimal fraction (1/1000) of the base SI unit.

Quantity	**Unit**	**Symbol**	**Expressed in terms of SI base Units**
length	centimeter	*l, x, r, etc.*	cm
area	square centimeter	*A*	cm^2
volume	milliliter	*V*	ml or cm^3
mass	gram	*m*	g
density	Gram/cubic cm	ρ	gm cm^{-3}
pressure	bar	*P*	bar
temperature*	Celsius	*T*	°C
temperature*	Kelvin	*T*	K
capacity	wt. %		g H_2 (g sample + g H_2)$^{-1}$
Gravimetric System capacity	specific energy		kW hr kg^{-1}
Volumetric System capacity	energy density		kW hr L^{-1}
rate	wt.%/minute		g H_2 $minute^{-1}$ (g sample + g H_2) $^{-1}$
heat	kilojoules	*Q*	kJ (mol H_2) $^{-1}$
enthalpy†	kilojoules/mole	ΔH	kJ (mol H_2) $^{-1}$
activation energy†	kilojoules/mole	E_A	kJ (mol H_2) $^{-1}$
entropy†	joules/ K mole	ΔS	J K^{-1} (mol H_2) $^{-1}$
heat capacity	joules/ K	C, C_p, C_v	J K^{-1}
specific heat capacity	joules/ K gram	[*C*]	J K^{-1} g^{-1}
Gas Constant	83.14472	*R*	cm^3bar/Kmol H_2

* Celsius for ambient and elevated temperatures Kelvin for cryogenic temperatures

† of formation, reaction, decomposition….

Table 6. Recommended units for the presentation of hydrogen storage materials properties.

4 Definitions

A recommended reference for detailed materials, chemistry and measurement definitions can be found in publications by IUPAC the International Union of Pure and Applied Chemistry.[26]

4.1 Terminology

For all sorption mechanisms, the suffix -ate (sorbate) refers to the substance taken up while -ent (sorbent) refers to the sorbing substance. The suffix -tive (sorptive) refers to the sorbate substance in its natural state, i.e. the bulk gas state. The coupled terms are generally considered counterparts.[27]

4.2 Sorption and Desorption

Sorption is the non-specific term that describes both adsorption and absorption. It is most often used when it is difficult or impossible to differentiate between adsorption and absorption or when both processes occur simultaneously. Desorption is the inverse process of sorption. It is important to note that the sorption and desorption of the sorbate by the sorbent is a dynamic process.

4.3 Adsorption and Absorption

Adsorption is the enrichment or depletion of one or more components in an interfacial layer. Absorption occurs when the adsorbates are incorporated into the internal structure of the adsorbent. In absorption, the structure and/or the chemical nature of the absorbate and absorbent may be modified. It is important to keep in mind that adsorption and absorption refer to the location of the sorbed species with respect to the sorbent, i.e. surface or bulk respectively.

4.4 Chemisorption and Physisorption

Chemisorption or chemical sorption is a surface specific phenomenon, and occurs when the interaction forces between a surface and an adsorbate are of the same general strength as found in chemical bonding in bulk compounds. Physisorption, or physical sorption, is restricted to adsorption and occurs when the forces involved are weak intermolecular forces of the same kind as those responsible for the non-ideality of gases and the

condensation of vapors. Weak intermolecular forces are also known as van der Waals forces. Physisorption does not involve a significant change in the electronic structure of the species involved. For a molecular adsorbate where no bond dissociation occurs, it is often difficult to draw a boundary in the energy landscape between strong physisorption and weak chemisorption. It is useful to make a distinction between molecular physisorption, in which the H-H bond in the gas phase is preserved in the sorbed state, and chemisorption, in which the H-H bond is broken during the sorption process. Also, as described in more detail below, chemisorption may occur only in a monolayer on a surface, whereas physisorption is usually accompanied by multilayer adsorption depending upon the temperature.

The following excerpt from D.H. Everett's IUPAC publication; "Manual of Symbols and Terminology for Physicochemical Quantities and Units" provides a short synopsis on differentiating chemisorption from physisorption.[28]

> "Chemisorption (or chemical adsorption) is adsorption in which the forces involved are valence forces of the same kind as those operating in the formation of chemical compounds. The problem of distinguishing between chemisorption and physisorption (see below) is basically the same as that of distinguishing between chemical and physical interaction in general. No absolutely sharp distinction can be made and intermediate cases exist, for example, adsorption involving strong hydrogen bonds or weak charge transfer.
>
> Some features which are useful in recognizing chemisorption include:
>
> (a) the phenomenon is characterized by chemical specificity;
> (b) changes in the electronic state may be detectable by suitable physical means (e.g. u.v., infrared or microwave spectroscopy, electrical conductivity, magnetic susceptibility);
> (c) the chemical nature of the adsorptive(s) may be altered by surface dissociation or reaction in such a way that on desorption the original species cannot be recovered; in this sense chemisorption may not be reversible;
> (d) the energy of chemisorption is of the same order of magnitude as the energy change in a chemical reaction between a solid and a fluid: thus chemisorption, like chemical reactions in general, may be exothermic or endothermic and the magnitudes of the energy changes may range from very small to very large;
> (e) the elementary step in chemisorption often involves an activation energy;
> (f) where the activation energy for adsorption is large (activated adsorption), true equilibrium may be achieved slowly or in practice not at all. For example in the adsorption of gases by solids the observed extent of adsorption, at a constant gas pressure after a fixed time, may in certain ranges of temperature increase with rise in temperature. In addition, where the activation energy for desorption is large, removal of the chemisorbed species from the surface may be possible only under

extreme conditions of temperature or high vacuum, or by some suitable chemical treatment of the surface;
(g) since the adsorbed molecules are linked to the surface by valence bonds, they will usually occupy certain adsorption sites on the surface and only one layer of chemisorbed molecules is formed (monolayer adsorption, see §1.1.7).
Physisorption (or physical adsorption) is adsorption in which the forces involved are intermolecular forces (van der Waals forces) of the same kind as those responsible for the imperfection of real gases and the condensation of vapors, and which do not involve a significant change in the electronic orbital patterns of the species involved. The term van der Waals adsorption is synonymous with physical adsorption, but its use is not recommended.

Some features which are useful in recognizing physisorption include:

(a') the phenomenon is a general one and occurs in any solid/fluid system, although certain specific molecular interactions may occur, arising from particular geometrical or electronic properties of the adsorbent and/or adsorptive;
(b') evidence for the perturbation of the electronic states of adsorbent and adsorbate is minimal;
(c') the adsorbed species are chemically identical with those in the fluid phase, so that the chemical nature of the fluid is not altered by adsorption and subsequent desorption;
(d') the energy of interaction between the molecules of adsorbate and the adsorbent is of the same order of magnitude as, but is usually greater than, the energy of condensation of the adsorptive;
(e') the elementary step in physical adsorption from a gas phase does not involve an activation energy. Slow, temperature dependent, equilibration may however result from rate-determining transport processes;
(f') in physical adsorption, equilibrium is established between the adsorbate and the fluid phase. In solid/gas systems at not too high pressures the extent of physical adsorption increases with increase in gas pressure and usually decreases with increasing temperature. In the case of systems showing hysteresis the equilibrium may be metastable;
(g') under appropriate conditions of pressure and temperature, molecules from the gas phase can be adsorbed in excess of those in direct contact with the surface."

The terminology "adsorbate" in f' above refers to the adsorbed molecules of gas. However, in general "adsorbate" refers generally to the gas that has been or is capable of being adsorbed, so it may include non-adsorbed species. Line g' above points out the important issue that the gas may experience attractive adsorptive interaction while not being in direct contact with the surface. Thus, the adsorption layer may be thicker than a monolayer of gas. For more details, the reader is encouraged to review the related publications by Everett.[27,28]

4.4.1 Physisorption

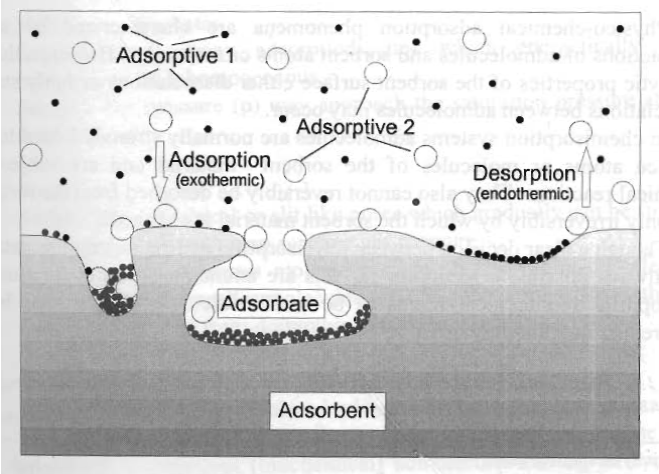

Figure 1. Illustration of the components of a physisorption system.[29]

Physisorption is a universal interaction between a gas and an adsorbent surface (Figure 1). The origins of H_2 physisorption are attractive dispersion interactions (i.e. London interactions) and short-range repulsion. The dispersion forces arise from spontaneous resonant fluctuations of electron density in one atom which induce a transient dipole moment in a neighboring atom. Since H_2 contains only two electrons, the dispersion interactions are weak. Therefore, the energy minimum of the total interaction pair potential is small, and is on the same order as the thermal energies of the adsorptive particles at ambient conditions. Physisorption is, therefore, only observed in significant amounts at cryogenic temperatures. Frequently, the adsorbent sample is kept at 77 K (N_2 boiling point) or 87 K (Ar boiling point) in experiments. Liquid N_2-based cryostats are often used to obtain a greater temperature range above 77 K. Adsorption is exothermic, and enthalpies between 4 and 10 $kJmol^{-1}$ are typically reported for H_2 physisorption.

The critical temperature (T_c) is the temperature above which a *bulk* gas cannot be liquefied by increasing the pressure. The critical temperature of H_2 is 33 K. In almost all studies of hydrogen physisorption, the sample is kept at temperatures well above T_c and therefore hydrogen is supercritical. The saturation pressure (P°) for supercritical H_2 adsorption does not exist, although empirical values are sometimes utilized for the purpose of modeling the isotherms. As a result, hydrogen adsorption isotherms can extend up to high pressures and are often denoted "high-pressure isotherms." Supercritical isotherms are generally characterized by a decrease of the saturation adsorption amount (n_{sat}) with temperature.[30] The decrease in the maximum adsorption amount (n_{sat}) is not predicted by standard monolayer adsorption models (e.g. the Langmuir model) likely because they do not take into account the energy heterogeneity of sorption sites and the expansivity of the adsorbed

layer. On the other hand, supercritical adsorption in several MOFs near saturation was found to lead to the entire filling of the porous structure with hydrogen exhibiting essentially liquid state properties.[31,32] The isotherms could be modeled with the Dubinin-Astakhov equation which accounts for decrease of n_{sat} with temperature by a coefficient of thermal expansion associated to the adsorbed phase.[33] In this model, heterogeneity is considered pore distribution. Finally, supercritical adsorption, when reported as an excess quantity, exhibits a characteristic maximum. The subsequent decrease can be explained in terms of mass of gas displaced by the adsorbed phase volume, which becomes significant near saturation.[31,32]

4.5 Spillover

Hydrogen spillover is dissociative chemisorption of dihydrogen onto a metal particle followed by migration of hydrogen atoms onto the surface of the bulk material and subsequent diffusion away from the receptor site.[34,35,36] Spillover is highly dependent on the metal, the support and the interaction between the two. Typically graphitic or nano-structured carbon is used as support because of its high specific surface area that enhances capacity. It has been illustrated in the literature that the generation of "bridges" between the metal and the support can further enhance spillover capacity.[37] One example conceptual diagram is shown in Figure 2.

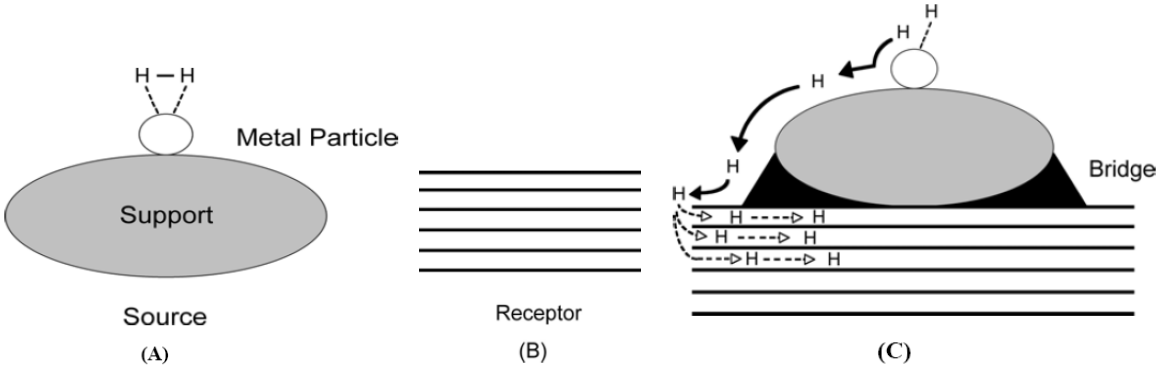

Figure 2. Conceptual diagram of Strategy for storage by spillover: (A) Supported metal catalyst for H_2 dissociation; (B) Sorbent as receptor for H; (C) Building carbon bridges (by carbonization of a precursor) for spillover, resulting in a composite sorbent.[38]

This 'bridge' concept is a useful to visualize spillover, however there is still considerable discussion and research into the mechanism and extent of spillover at this time.[37,39,40,41,42,43,44,45,46] However, this discussion in the literature illustrates the importance and need of a uniform ***Best Practices*** procedure for the evaluation of the

hydrogen sorption on carbon substrates especially when one has a need to contrast and compare “apples to apples” in the literature.

Spillover materials are an excellent example, where an especially high level of care must be exercised in the measurement to correctly ascertain the amount of hydrogen uptake. The very high surface area and presence of highly reactive catalysts in the matrix are known to be prone to side reactions or impurity effects that can be easily misinterpreted as excessive or minimized hydrogen uptake or release. For example, significant weight increase may be observed due to the reaction of hydrogen with weakly bound oxygen to form water or carbon atoms to form hydrocarbons. Similarly, impurities in the gas steam, even at ppm levels, can react with active components of the sample material and be detected as an increase in the sample mass. Conversely, the desorption of impurities (water, hydrocarbons, nitrogen compounds…) would be observed in gravimetric measurements as a sample weight loss. Without direct measurements of the sample and/or gas composition, gravimetric measurements of weight change may be mistaken as hydrogen uptake or release leading to ‘false positive’ measurements. Typically, these reactive processes will disappear after one or more hydrogen sorption cycles and this should provide a strong indication that weight changes are the result of secondary effects. Volumetric measurements are not as prone to such ‘false positive’ errors as these secondary reactions or impurity effects generally do not cause a significant change in the surrounding gas pressure. On the contrary, impurities may deactivate (or passivate) the sample, impeding hydrogen uptake, and result in a ‘false negative’ hydrogen capacity result when performing volumetric measurements. Another important difference between measuring spillover sorption versus the high surface area physisorption is in the tolerance in system leakage. Since the kinetics of spillover are slow compared to the nearly instantaneous physisorption process, the tolerance in leakage for measuring spillover needs to be substantially lower, or false results may occur. Ultimately, as in any sorption process, significant differences observed in a material’s hydrogen storage capacity that is dependent on the method of measurement is a strong indication of systematic error within a system and/or secondary reactions and/or impurity effects. Spillover demonstrates the importance and complexity of sorption measurements and how they are not “turn key” procedures.

5 Materials

Materials for hydrogen storage can be divided into two families: hydrides (atomic hydrogen resides mainly in the bulk of the material)[47], (this includes hydriding alloys, molecular hydride complexes, and other molecular covalent compounds such as amine complexes, and hydrocarbons) and physisorbed high-surface-area materials (hydrogen resides mainly as molecular hydrogen on the surface of the material)[48] (this includes carbon fullerenes, nano-tubes and highly porous media like metal-organic frameworks and aerogels).

5.1 Hydrogen Storage Materials Based on Physisorption of Molecular Hydrogen

5.1.1 Nano-Structured Materials

Nano-structured materials have much higher surface area to volume ratios than bulk materials, enabling increased adsorption. Nano-structuring of materials also improves reaction kinetics by increasing the diffusivity, reducing the reaction distance and increasing the reaction surface area. Metal hydrides and hydride complexes can be nano-structured by a variety of different processes including sputtering, pulsed laser deposition, and mechanical milling.

Nano-structured carbons, such as nanotubes, fullerenes and graphitic sheets are examples of nano-structured materials that have been extensively studied for hydrogen storage.

5.1.2 Porous Materials

Porous materials are being studied for use as hydrogen storage media due to their high surface area to volume ratio and the ability of hydrogen to adsorb to these internal and external surfaces. Moreover, for microporous materials, (pore width <2 nm), attractive physical potentials from opposite walls can overlap leading to a fully active space for the gas to adsorb. Therefore, such nanoscale pores can offer interesting gains over compression comparatively to macro pores, where such overlap is virtually absent and gas is stored mainly under a compressed state into the larger voids. Although adsorption via physisorption is significant for porous media, absorption may also contribute to the overall hydrogen storage capacity of advanced materials. Examples of porous materials being investigated for hydrogen storage are various forms of aerogels, clathrates, carbon-based materials and metal-organic frameworks (MOFs). The advantage of using an adsorbent over simple compression is temperature and pressure dependent as shown in the Capacity section 1.4.11 .

5.2 Hydrogen Storage Materials Based on Hydride or Covalent Bond Formation

Hydride is the name given to the negative ion of hydrogen, H−. Practically, the term hydride has two distinct but overlapping meanings. In the chemical vernacular the term hydride refers to a hydrogen atom that formally reacts as a hydrogen anion under common conditions as well as hydrogen atoms directly bonded to metal atoms regardless of their reactivity. The second older meaning of hydride refers to any compounds hydrogen forms with other elements, ranging over most of the periodic table, groups 1–16. This second

meaning is dealt with only in terms of formal nomenclature at the end of the article; the rest of the article concerns the popular meaning.[49,50]

Hydrides bonds range from very covalent to very ionic as well as multi-centered bonds and metallic bonding. Hydrides can be components of discrete molecules, oligomers or polymers, ionic solids, chemisorbed monolayers, bulk metals, and other materials. While hydrides traditionally react as Lewis bases or reducing agents it is also common for some metal hydrides to react as hydrogen radicals or as protonic acids.

Various metal hydrides are currently being studied for use as a means of hydrogen storage in fuel cell-powered electric cars and in batteries. The group 14 hydrides are already of vast importance in storage battery technologies. They also have important uses in organic chemistry as powerful reducing agents, and many promising uses in a hydrogen economy.

Free hydride anions exist only under extreme conditions similar to the way that free protons also exist only under extreme conditions. Still there are many examples of hydrogen atoms that formally react as hydrides.

Aside from electride, the hydride ion is the simplest possible anion, consisting of two electrons and a proton. Hydrogen has a relatively low electron affinity, 72.77 kJ/mol and reacts exothermically with protons a powerful Lewis base.

$$H^- + H^+ \rightarrow H_2;\ \Delta H = -1676\ \text{kJ/mol}$$

The low electron affinity of hydrogen and the strength of the H–H bond (ΔH_{BE} = 436 kJ/mol) means that the hydride ion is a strong reducing agent:

$$H_2 + 2e^- \rightarrow 2H^-;\ E^o = -2.25\ \text{V}$$

5.2.1 Types of Hydrides

According to the former definition every element of the periodic table (except some noble gases) forms one or more hydrides.[50] These compounds have been classified into three main types according to the nature of their bonding:

Ionic hydrides; which have significant ionic character, ***Covalent hydrides***; which include the hydrocarbons and many other compounds, and ***Interstitial hydrides***; which may be described as having metallic bonding. While these divisions have not been used universally, they are still useful to understand differences in hydrides. Please refer to the IUPAC provisional recommendations of Parent Hydride Names and Substitutive Nomenclature for an in-depth description of hydride nomenclature.[51]

5.2.2 Ionic Hydrides

Ionic hydrides are the true salts like sodium hydride, etc where there is little covalency, and a high degree of ionic character in the M-H bonding. Ionic or saline hydride, consist of a hydrogen atom bound to an extremely electropositive metal, generally an alkali metals or alkaline earth metals. In these materials the hydrogen atom is viewed as a pseudo-halide i.e. similar to halide anions such as Cl^-. Saline hydrides are insoluble in conventional solvents. Most ionic hydrides exist as "binary" materials involving only two elements including hydrogen. Ionic hydrides are used as heterogeneous bases or as reducing reagents in organic synthesis.

Typical solvents for such reactions are ethers. Water and other protic solvents cannot serve as a medium for pure ionic hydrides because the hydride ion is a stronger base than the deprotonated solvent anion. Hydrogen gas is liberated in a typical acid-base reaction.

$$NaH + H_2O \rightarrow H_2\ (gas) + NaOH\ \Delta H = -83.6\ kJ/mol,\ \Delta G = -109.0\ kJ/mol$$

Often alkali metal hydrides react with metal halides. Lithium aluminum hydride (often abbreviated as LAH) arises from reactions of lithium hydride with aluminum chloride.

$$4\ LiH + AlCl_3 \rightarrow LiAlH_4 + 3\ LiCl$$

5.2.3 Covalent Hydrides

Covalent hydrides encompass compounds such as AlH_3, the boranes and borohydrides and related derivatives, hydrocarbons, amines, amides, and ammonia complexes, etc. where the bonding is highly localized and strong between the two centers, or in the case of the boranes and borohydrides, there is often 3 center, two electron bonds formed, e.g. in bridging B-H-B compounds. Non-stoichiometry is unlikely. According to the older definition of hydride, covalent hydrides cover all other compounds containing hydrogen. The more contemporary definition limits hydrides to hydrogen atoms that formally react as hydrides and hydrogen atoms bound to metal centers. In these substances the hydride bond is formally a covalent bond much like the bond made by a proton in a weak acid. This category includes hydrides that exist as discrete molecules, polymers or oligomers, and hydrogen that has been chemisorbed to a surface. A particularly import segment of covalent hydrides are the so-called complex metal hydrides which often contain discreet cation-anion pairs. The anions include borohydride or alanate, among other hydridic anions. Hydrogen may be released thermally, or in the case of sodium borohydride, by hydrolysis to form sodium borate and hydrogen.[52] Another important class of covalent hydrides are the so-called chemical hydrogen storage materials, which are discreet molecular species, usually that do not contain cation-anion pairs such as found in the complex metal hydrides. Chemical hydrogen storage materials encompass molecules such as ammonia borane, alane, and the

hydrocarbons, among many others. These molecular hydrides often involve additional ligands such as in TMEDA-AlH_3 where the tetramethylethylenediamine ligand is ligated to the aluminum center through its two nitrogen atoms, thus helping to stabilize AlH_3.

Hydride complexes occur when combinations of ligands, metal ions and hydrogen form molecules. Hydride complexes are differentiated by whether they contain transition metals; those that do are called TM hydride complexes, those that do not are called non-TM hydride complexes. The main difference between hydride complexes and ICs (Intermetallic Compounds, to be described below) is that the bonding in hydride complexes is quite covalent, strong, and localized, whereas in intermetallic compound hydrides, hydrogen atoms reside in interstitial sites and the multi-center bonding may be relatively weak. Complexes release hydrogen through a series of decomposition and recombination reactions. Some combinations of elements, for example Mg and Fe, form hydride complexes but cannot form ICs; hydrogen is required for these two elements to form a stable compound (Mg_2FeH_6).

5.2.4 Interstitial Hydrides

Interstitial hydrides can exist as discrete molecules or metal clusters in which they are atomic centers in a defined multi-centered multi-electron bonds. Interstitial hydrides can also exist within bulk materials such as bulk metals or alloys at which point their bonding is generally considered metallic.

The interstitial hydrides are distinct from ionic or covalent hydrides, in that they may form where H atoms reside in tetrahedral or octahedral interstices within the metal or alloy framework; solid solution formation is common. The bonding between the metal(s) and the hydrogen atom is highly delocalized, with multi-center, multi-electron bonding similar to that in metals occurring.

Many bulk transition metals form interstitial binary hydrides when exposed to hydrogen. Interstitial hydrides can be further separated into subclasses of metal alloy hydrides and intermetallic hydrides.

5.2.4.1 Metal Alloy - Hydrides

The host hydrogen storage materials may consist of a solid solution alloy. These are characterized by varying composition and disordered substitution of one element for another on crystal lattice sites; they are formed by dissolving one or more minor elements into a primary element. Solid solutions based on Pd, Ti, Zr, Nb and V form hydrogen storage materials with some attractive features such as moderate reversible storage capacities near ambient conditions but cost and the heat released on hydrogen absorption deter the use of these materials for transportation applications. For example, $(V_{0.9}Ti_{0.1})_{0.95}Fe_{0.05}$ has a

reversible storage capacity of $(\Delta wt.\%)_r = 1.8$ at T = 36°C and atmospheric pressure but costs are relatively expensive for hydrogen storage.[47] Vanadium-based solid solutions (V-SS) are compared to other metal hydrides in Table 7.

5.2.4.2 Metal Hydride Intermetallic Compounds

Intermetallic compounds (ICs) are characterized by homogenous composition and crystal structure. ICs for hydrogen storage combine a strong hydriding element A with a weak hydriding element B to create a compound with the desired intermediate thermodynamic affinities for hydrogen. Hydrogen absorbs atomically into the host metal lattice as a solid solution at low concentrations and via hydride-forming metal/hydrogen bonds at higher concentrations. The host intermetallic compound elements A and B are typically present in an integer or near-integer stochiometric relationship. Element type A and/or B may be an ordered or disordered mixture of several metal elements. The total compositional variation has a strong impact on hydriding properties. This ability to form A_xB_y ICs containing up to 10 or more elements has been extensively studied and exploited in the commercialization of metal hydrides for hydrogen storage and Nickel-Metal Hydride battery applications. Common classifications of ICs for hydrogen storage are AB_5, AB_2, AB and A_2B; $LaNi_5$, $TiCr_2$, TiFe and Mg_2Ni being representative examples. Table 7 provides an overview of the relative attributes of these different classes of hydride forming Intermetallic compounds. This includes versatility (meaning the ability to tune the alloy to operate over a wide range of pressures and temperatures) and PCT meaning the ability to reversibly provide hydrogen gas over a narrow range of pressures (relatively flat plateau pressure) at room temperature conditions.

Attribute	AB_5	AB_2	AB	A_2B	V–SS
Versatility	+	+	+	−/0	0
H-Capacity	0	0/+	0/+	+	+
PCT	+	+	+	−	+
Activation	+	0	−/0	0	0
Impurity effects	+	0	−	0	−/?
Cyclic stability	−/0/+	−/0/?	−/0	0/?	?
Ease of manufacture	+	0	+	0	?
Pyrophoricity	0	−	+	+	+/0
Cost	0	+	+	+	−/0

[a] Attribute key: − = problem; 0 = neutral; + = good; ? = uncertain.

Table 7. Qualitative overview of metal hydride types as to attributes.[47]

5.2.5 Transition Metal Hydrido Complexes

Transition metal hydrides include what can be called covalent hydrides as well as interstitial hydrides and other bridging hydrides. Within the covalent transition metal hydrides there are two additional types of hydrides. The classical hydride also known as terminal hydrides involves a single bond between the hydrogen atom and a transition metal atom. Non-classical, hydrides often referred to as dihydrogen complexes, is when a dihydrogen molecule forms a sigma bonded complex with a metal center. Transition metal complexes span a range of bonding from pure dihydrogen complex to a pure dihydride complex where the dihydrogen molecules bond has been fully broken.

In the case of hydrides for hydrogen storage, the family tree in Figure 3 illustrates the relationships between different types of hydriding alloys and complexes.

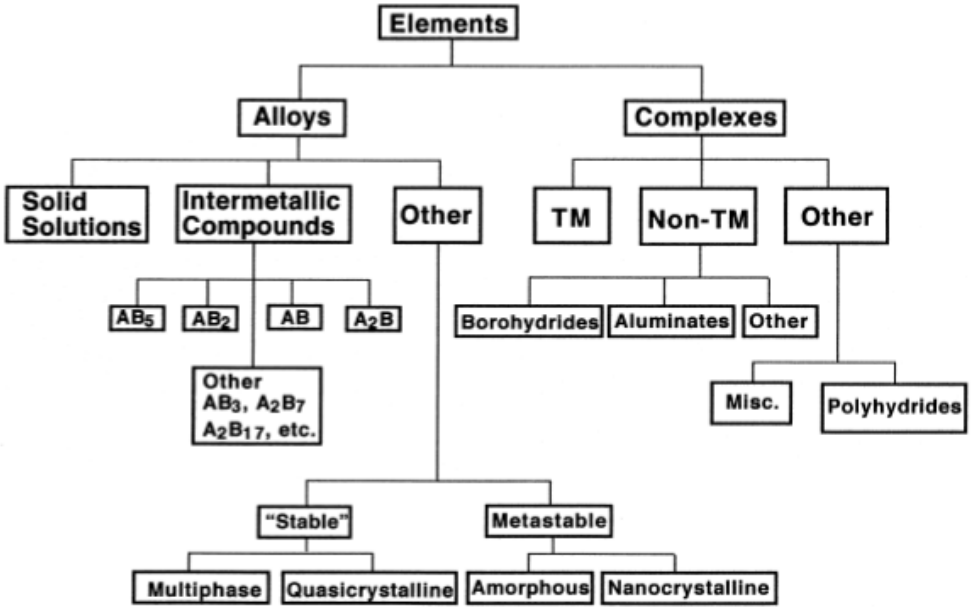

Figure 3. Family tree of hydriding alloys and complexes.[47]

5.2.6 Dihydrogen Complexes

Hydrides are capable of forming a unique form of bonding called dihydrogen bond. A dihydrogen bond exists between a negatively polarized hydride and a positively polarized hydrogen atom (hydron or proton). This is similar to the hydrogen bonding which exists between positively polarized protons and electronegative atoms with open lone pairs.

Dihydrogen complexes are coordination complexes containing intact H_2 as a ligand. This class of compounds represents intermediates in metal-catalyzed reactions involving hydrogen. The first metal complex of an H_2 molecule was discovered in 1984, when Kubas and co-workers reported the now famous "Kubas complex" $[W(CO)_3(PiPr_3)(H_2)]$ (iPr=isopropyl).[53] Since then, hundreds of dihydrogen complexes have been reported.[54] Most examples are cationic transition metals complexes with octahedral geometry.

Upon complexation, the H-H bond is extended to 0.81-0.82 Å as indicated by neutron diffraction, about a 10% extension relative to the H-H bond in free H_2. Some complexes containing multiple hydrogen ligands, i.e. polyhydrides, also exhibit short H---H contacts. It has been suggested that distances < 1.00 Å indicates significant dihydrogen character, where separations > 1 Å are better described as dihydrido complexes (see Figure 4).

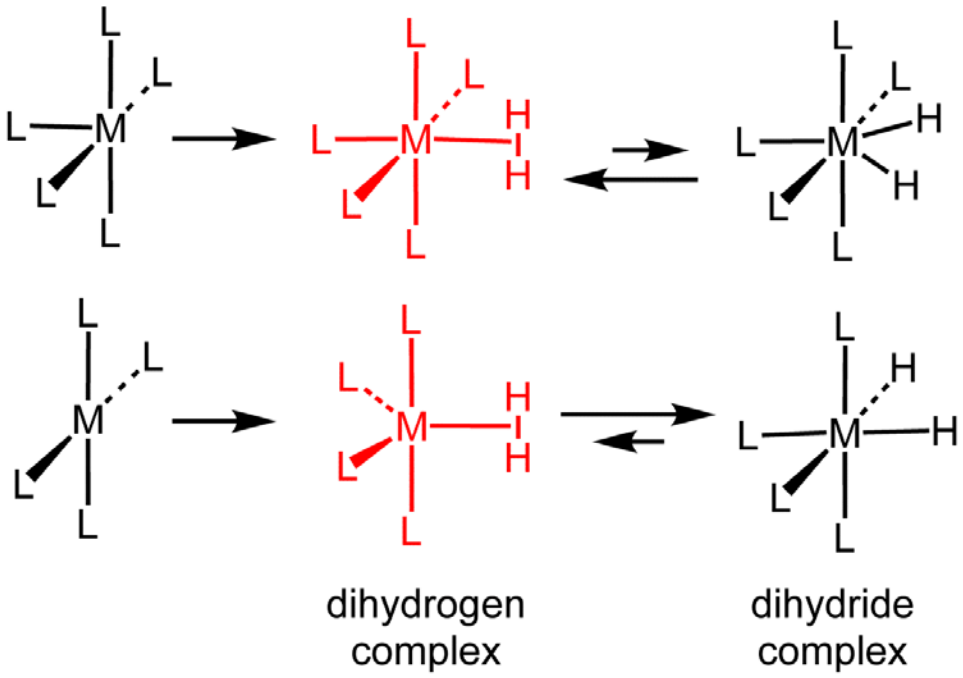

Figure 4. Formation and equilibrium structures of metal dihydrogen and dihydride complexes (L = ligand).[55]

6 Classification of Materials for Hydrogen Storage Materials Applications

The relative strength of the interaction of hydrogen with a storage material greatly influences the kinetics and thermodynamics of the hydrogen uptake and release. Hydrogen binding mechanisms differ for physisorption storage and hydride storage materials, and the

strength of the hydrogen binding affects the overall manner in which a hydrogen storage material will be used in a real application.

Materials for hydrogen storage can be separated into different classes based on how they will be used in applications. In this sense there are three categories generally based on the energetics of storing hydrogen which we will designate as "**Physisorption**", "**On-board Reversible Hydrides**", and "**Off-board Regenerable Hydrides**" materials. While not completely correct these are generically referred to as "**Sorption**", "**Metal Hydride**", and "**Chemical Hydrogen**" storage materials respectively.

The basic distinction these three classes of hydrogen storage materials are:

1) **Physisorption** materials involve weakly bound molecular hydrogen that is on-board reversible but generally require operating at liquid nitrogen temperatures (room-temperature atomic adsorption in the form of spill-over may be an exception).

2) **On-board Reversible Hydride** materials include the various metal hydrides described above, and some of the complex metal hydrides and amides…) that release hydrogen endothermically. Endothermic release allows for thermodynamically favorable, exothermic rehydrogenation during on-board recharging of the hydrogen storage materials under reasonable temperature (< 300°C) and pressure (< 200 bar) conditions.

3) **Off-board Regenerable Hydride** materials either release hydrogen exothermically, and/or involve complex chemical regeneration schemes that cannot be performed on board a vehicle. Examples in this class are the hydrocarbons, ammonia borane, and alane. The hydrocarbons and alane release hydrogen endothermically, but high hydrogen pressures or the complexity of their rehydrogenation most likely will require an off board process. Ammonia borane and other materials that release hydrogen rather exothermically cannot be rehydrogenated readily at common pressures and temperatures. This holds for compounds that release hydrogen with a free energy of greater than about 1kcal/mole exergonic.

7 Summary

The intent of the preface has been to introduce terminology commonly used in hydrogen storage materials research and to provide an overview of the fundamental processes and measurement considerations. We hope that this information proves useful and ultimately contributes to progress in the research and development of new and better hydrogen storage materials.

Section 1: Introduction

This introductory section is intended to provide the reader with the basic information necessary for productive and accurate hydrogen storage measurements. Introductory topics include: 1) evaluating the experimental setup and procedures with respect to the ultimate purpose for making a set of measurements, 2) the relationships between direct and indirect (measureable vs. derived) quantities (which we will refer to as variables) used to describe hydrogen storage materials properties, and 3) an overview of common methods used to measure these hydrogen storage properties. A variety of apparatus have been developed in the past to measure sorption properties [56]; this manuscript will focus on some instruments *typically* used for hydrogen storage measurements (namely volumetric and gravimetric systems).

1 Purpose of Measurements

For simplicity, hydrogen storage properties measurements can be broken down into three basic categories: storage system level performance measurements, materials development measurements, and fundamental science measurements. It is important to understand the purpose of a particular experimental investigation before making measurements because the experimental setup and procedures can vary greatly depending on the purpose of the measurements and results and conclusions can be misleading if they are not presented in the proper context. Of course, these categories overlap and support each other. Testing the design and performance of a storage system, comparing storage properties across new or improved materials, and gaining insight into the underlying phenomena of hydrogen storage require experimental apparatuses and procedures that may be significantly different. Care should be taken to match the experiment well to the purpose of the study to avoid misleading results.

1.1 Purpose: System Performance

System level measurements are concerned with the performance of materials at an operational scale. The primary difference between experimentation at the system level versus other levels is the importance of application-specific considerations. Depending on the utilization of the hydrogen storage system, any combination of properties may be most important for performance optimization. Properties such as energy density, reversibility and safety at standard operating conditions are some of the primary 'real world' considerations. For example, one consideration central to portable hydrogen storage systems like those envisioned for transportation is energy density because the system must be transported. Stationary applications, in contrast, may be more concerned with total energy than energy density, and cost.

To gain useful system performance information, enough material should be tested to provide results representative of the material's behavior in a full-sized operating storage system. In general, this means between 10 grams and 1 kilogram of storage material. The authors believe 100 grams is a good tradeoff between the practical issues of synthesis and handling of the materials and a characteristic, uninterrupted volume of material that would be found in a large-scale system. It is recommended to take samples from different portions of larger batch to get a good average material representation.

An example of an experimental setup that may be appropriate at a system performance level but not for other purposes, is the use of flow meters to study rates of hydrogen uptake or release. This requires that the material performance has already been well characterized at a smaller scale. This is because conventional thermal mass flow meters generally have fairly narrow dynamic measurement ranges (often less than one decade). Thus, some prior knowledge of the material's performance is needed to select flow meters with the appropriate flow range. This can be a severe limitation when a material's hydrogen sorption/desorption rates may vary over several orders of magnitude depending on state of charge, temperature and pressure. An alternative is Coriolis flow meters, which have a robust dynamic measurement range, maintaining accuracy over several decades.

1.2 Purpose: Materials Development

The purpose of experimentation at the analytical level (typically tens of milligrams to a few grams) is to guide the development of advanced materials with desirable hydrogen storage properties. It is important to realize that hydrogen storage properties of a material can be strongly influenced by any number of individual sample characteristics including total chemical composition and distribution, microscopic and macroscopic structure, etc. In the realm of materials development, parametric and comparative studies are generally the best approach to producing reliable and productive studies. There is an extremely wide range of material characteristics (including such things as doping and nano-structuring) that can be modified and manipulated to produce profound changes in hydrogen storage properties. For example, the effect of elemental substitution in the $LaNi_5$ family of Intermetallic compounds ($LaNi_{5-x}A_x$) is demonstrated in Figure 5.[47] In this case Ni has been substituted with tin or aluminum to form materials with decidedly different hydrogen storage properties, including changing the thermodynamic stability of the hydride that is formed.

In order to conduct instructive parametric studies, it is especially important that measurements are conducted under identical conditions (pressure, temperature, sample size, etc.) using identical measuring equipment. This minimizes the number of free variables associated with the experiment and allows for the accurate determination

of the effect of a specific material property. The effect of some material properties on hydrogen storage can be quite small and easily masked by variation in testing conditions and measuring equipment if the proper precautions are not taken.

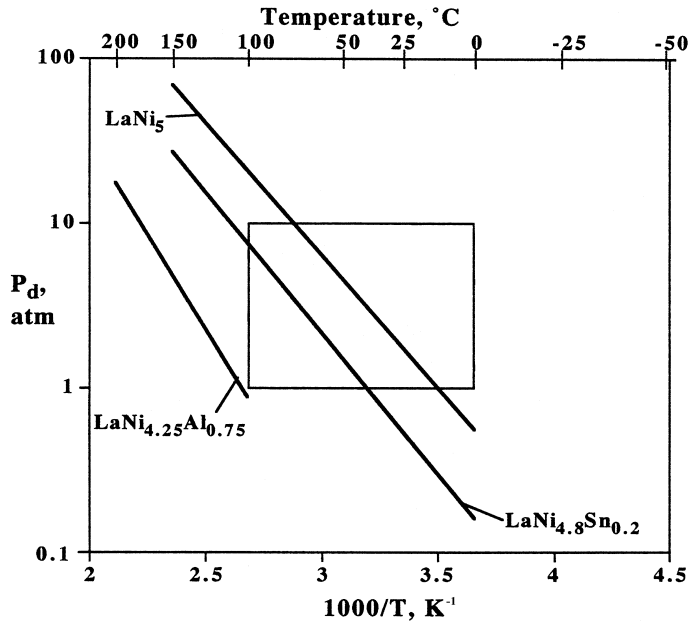

Figure 5. Van't Hoff diagram representing the hydriding thermodynamic properties of several different $LaNi_5$-based materials.[47]

1.3 Purpose: Fundamental Science

As the title suggests, fundamental science research is concerned with identifying and understanding the physics and chemistry that governs a material's hydrogen storage properties. This fundamental knowledge can be used in research at the materials development and system performance levels. It may help to validate models that describe hydrogen-material interactions or aid in making enlightened decisions on new directions in improving materials. Without some level of fundamental understanding, system and materials development measurements would be conducted solely through intuition or painstaking systematic studies. By using knowledge gained from fundamental science, researchers can eliminate much of the trial and error and more efficiently conduct measurements for material development. With regard to fundamental science, samples may be small (gram quantities) and indeed very small (milligram powders, liquids and thin films) as synthesis is achieved on lab-scales. As a consequence, very sensitive instruments will be needed to perform measurement on sample weighing as low as tens of milligrams. Also, fundamental science implies the modeling of the measurements and hence, intrinsic behavior should be clearly separated from instrumental effects to match a particular model.

2 Hydrogen Storage Properties

Measurements at all three of the levels investigation described above, probe similar hydrogen storage properties of both systems and materials. The relative importance of each property may depend on the application or the purpose of investigation. The following is a very brief summary of the principal measured properties of hydrogen storage materials and systems. Each property is investigated in more detail in the individual chapters of the Recommended Practices Documents.

2.1 Property: Capacity

Capacity is the maximum steady-state hydrogen content of a storage material. Capacity can have several different definitions that reflect the application or material considerations including reversible capacity, usable capacity and excess material capacity. These definitions in turn may depend on the material's stability, composition, temperature, pressure and number of cycles. Each of these variables has the potential to change the capacity of a material. Additionally, there is a very important distinction between concentration and capacity: capacity is a material property that does not vary at a set state (after an extended period of time). In this text, a material's capacity will be referred to as its maximum steady-state hydrogen content and concentration as its temporal hydrogen content. For a more detailed discussion of capacity definitions and theory, please see the chapter on capacity measurements Capacity sections 1.2 .

2.2 Property: Kinetics

Kinetics is a measure of the rate of hydrogen sorption or desorption of a material and may not be exclusively dependent on intrinsic material properties. Sample size, heat transfer effects and other parameters that are highly dependent on the experimental method can affect kinetic measurements and conclusions. Minimizing the effects of external influences on kinetics is very difficult and requires a great deal of knowledge and preparation. Thus, extreme caution should be used in ascribing measured kinetics to fundamental sorption mechanisms or an intrinsic property of a given material. Sample preparation, catalyst and additives, particle size, heat transfer capabilities, among other things can strongly influence the kinetics. As one example, degassing at high temperature can remove or diffuse oxide layer from metals and increase subsequent hydrogen absorption kinetics. For a more detailed discussion of experimental considerations for kinetics, please see the chapter on kinetics.

2.3 Property: Thermodynamics

The intrinsic thermodynamic properties of hydrogen storage materials influence a number of other parameters, most notably the hydrogen capacity based on temperature and pressure. Unfortunately, the relationship between measured temperature and pressure conditions and intrinsic thermodynamic properties may be complicated by kinetics considerations. In many of today's materials, the temperature and pressure conditions required for hydrogen uptake and release are dictated by kinetic considerations, not necessarily the intrinsic thermodynamics of hydrogen bonding. The ability to distinguish between the two material properties is especially important because the techniques used to improve one property are often ineffective or not available for the other.

In addition, we refer in this document to thermodynamic properties with respect to thermal equilibrium (the measure equilibrium state of hydrogen concentration in the material, hydrogen pressure and temperature). Thermal equilibrium may be dictated not only by the chemical interaction thermodynamics, but other terms as well such as strain energy, dislocation production and interfacial energy. In many metal-hydrogen systems these terms lead to differences in the absorption versus desorption equilibrium pressures at a given concentration and temperature. This is generally observed as hysteresis in the Pressure Concentration Temperature (PCT) isotherms. For a more detailed discussion on the thermodynamics of hydrogen storage, please see the chapter on thermodynamics.

2.4 Property: Cycle-Life

Cycle-life testing is restricted to reversible hydrogen storage materials such as metal and complex hydrides, amides and physisorbing materials. Materials that store hydrogen irreversibly (i.e. not reversible under practical conditions), like chemical slurries of elemental hydrides (e.g. LiH, $NaBH_4$), cannot be cycled. Cycle-life measurements are typically performed to characterize the effect of cycling on capacity that stems from activation effects, grain growth, structural degradation or chemical degradation due to gas impurities. However, kinetics may also be impacted by cycling and some of the observed change in capacity may in fact be due to changing kinetics during cycling. For example, if measurement time intervals during a cycle-life experiment do not reflect the changing kinetic properties of the material, the measured capacity will not be representative of capacity at quasi-equilibrium. Impurities in the hydrogen gas supply may have a profound effect on the cycle-life behavior of a storage material (see section 5.3.6). For a more detailed discussion of cycle-life considerations, please see the chapter on cycle-life measurements that will follow in a later version.

3 Types of Measurement

With respect to characterizing a material's hydrogen storage performance there are two principal types of measurements, kinetics measurements and pressure-composition-temperature (PCT) measurements. Kinetics measurements can be considered the fundamental measurement of hydrogen storage because other types of measurement, including PCTs, are collections of several individual kinetics measurements. The relationship between kinetics and PCT measurements will be discussed further at the end of this chapter. Beyond these two main characterization measurements, there is a host of other measurements such as scanning temperature measurements that have value in rough screening for potential new hydrogen storage materials.

3.1 Measurement Type: Kinetics

Kinetics measurements track the rate of change of hydrogen concentration in a sample after the sample has been perturbed from quasi-equilibrium. Because hydrogen storage measurements can only approximate thermodynamic equilibrium due to experimental limitations, equilibrium will be used synonymously with quasi-equilibrium throughout the rest of this manuscript. Perturbation from equilibrium is accomplished by changing the thermodynamic state of the sample's environment, which causes the sample to sorb/desorb hydrogen in the attempt to restore equilibrium. For the gravimetric and volumetric methods, kinetics measurements are generally conducted under isothermal conditions, with changes in pressure used to perturb equilibrium. This is done partly for compatibility with PCTs and partly because of the profound effect of temperature on the kinetics character of almost all materials. The profiles and interpretations of kinetics curves and the considerations for kinetics measurements are the subject of the kinetics chapter of the Recommended Practices Document.

It is instructive to introduce a few fundamental features common to almost all kinetics measurements for reversible systems. The degree of perturbation from equilibrium is the driving force behind sorption/desorption in hydrogen storage materials: large perturbations cause relatively large rates of change in concentration while smaller perturbations cause relatively small rates of change. The rate of change of hydrogen concentration in a sample is largest at the beginning of a kinetics measurement, when the sample is furthest from equilibrium with its environment. The distance from equilibrium diminishes as hydrogen is sorbed by the sample, slowing the sorption rate as the sample reaches a time independent equilibrium concentration. These effects are illustrated in the sorption kinetics measurement in Figure 6. At the beginning of the experiment, the concentration changes quickly because the sample is furthest from equilibrium and with time the rate of change of concentration decreases until it becomes effectively zero.

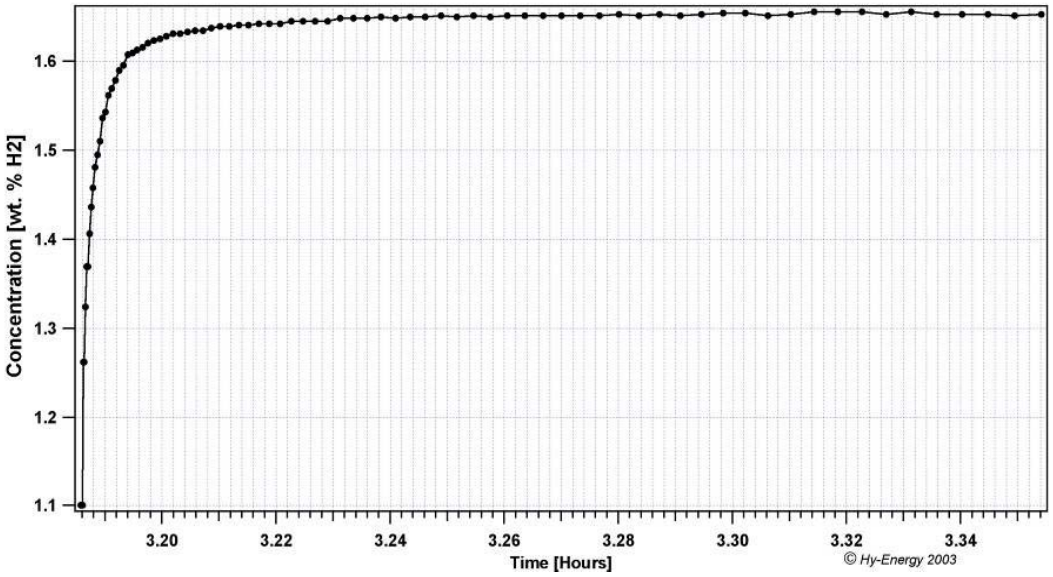

Figure 6. Representative kinetics measurement of an individual hydrogen dose to a porous material.

3.2 Measurement Type: Pressure-Composition Isotherm

Pressure-composition-temperature measurements (PCTs) are the most reported hydrogen storage measurement type in academic literature (composition in this context is synonymous with the concentration of hydrogen in a sample). A PCT measurement is a collection of data points that represents the pressure, concentration and temperature of a sample in equilibrium and relates the influence of the thermodynamic variables on concentration. PCTs are also commonly referred to as PCI (Pressure-Composition Isotherms) because they are taken at isothermal conditions. This minimizes the number of free variables and allows the relationship between concentration and pressure to be presented via two-dimensional graphics. The effect of temperature on hydrogen storage properties can be determined by comparing PCT isotherms at various temperatures. Because PCTs represent a sample in equilibrium, they can also be used to determine the thermodynamic properties of a hydrogen storage material. Unfortunately, the absolute interpretation of PCT data must be kept in perspective because it is difficult to make true equilibrium measurements. This is because as the pressure approaches the true equilibrium pressure, the driving force (or potential) becomes diminishingly small and therefore, kinetics becomes increasingly slower. In other words, it would take an infinitely long time to reach equilibrium. For more information on thermodynamics as they relate to hydrogen storage properties, please review the thermodynamics chapter in the Recommended Practices Document.

It is instructive to conceptualize the relationship between PCT measurements and kinetics measurements in the volumetric method as follows: a sample is perturbed from equilibrium by a change in the pressure of the system and is allowed to reach equilibrium through the dynamic process represented by a kinetics measurement. The last data point of each kinetics measurement, which most closely represents equilibrium, provides a single point of hydrogen concentration, pressure and temperature at equilibrium. In the volumetric method, this dosing process is performed repeatedly at one temperature until there are enough equilibrium data points are collected to construct a full PCT diagram. In this sense the PCT measurement can be thought of as a cumulative series of mini-kinetics measurements. Figure 7 demonstrates the PCT diagram of a porous material using the volumetric method by conducting a series of small dose kinetics measurements. In each kinetics measurement (separated by recharging the dosing volume which appears as discontinuities), the final pressure at the last data point represents the equilibrium pressure at a given concentration. In the volumetric method, the concentration is determined from the change in pressure with each dose (refer to the volumetric section 5.3 for details). Therefore the equilibrium pressure of the sample corresponding to each equilibrium concentration point is also known and a full PCT can be constructed from the series of kinetics measurements.

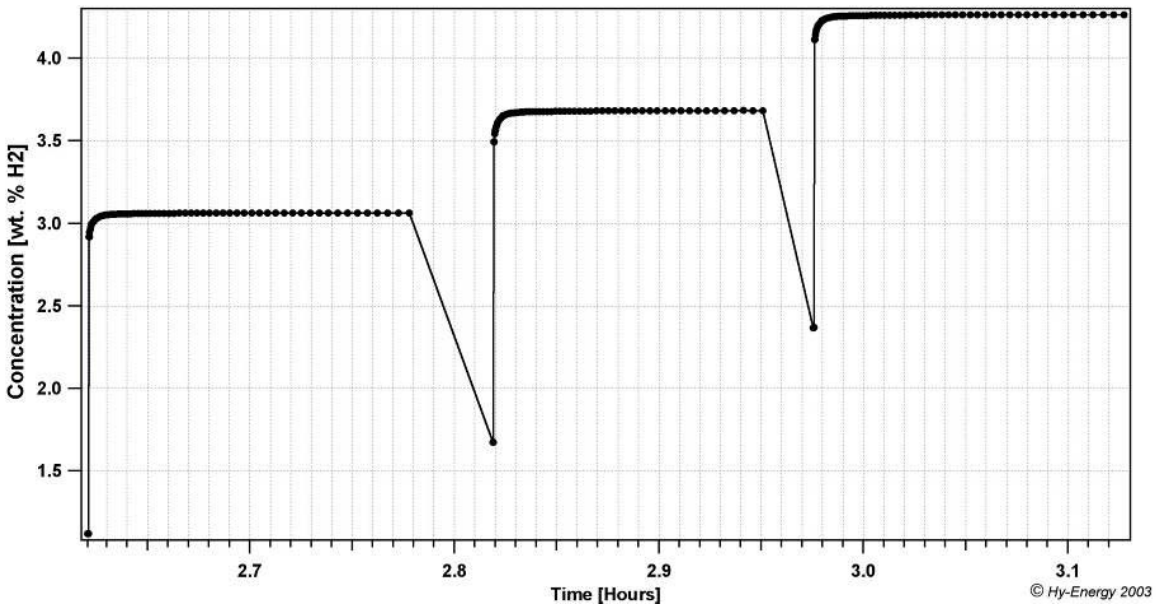

Figure 7. Representative measurement of a porous material. The last point in each 'row' of points is taken as representative of the equilibrium concentration of hydrogen in the sample at the pressure and temperature of experimentation.

This is shown in

Figure 8 where the Pressure / Time data is translated to Pressure / Concentration data to form a PCT diagram. The relationship between pressure drop due to absorption (rise on desorption) and concentration is depicted in Figure 9.

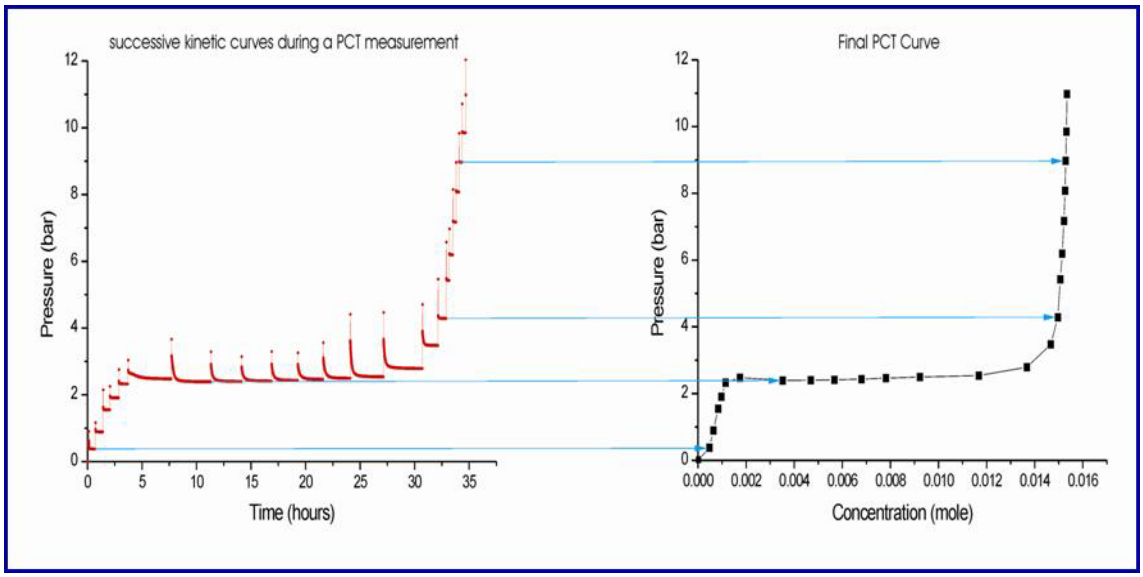

Figure 8. Representative pressure / time measurement and the resulting PCT plot of hydrogen absorption to form a metal hydride. The last point of each gas sorption dose provides the concentration of hydrogen in the sample at the equilibrium pressure and temperature of each dose.

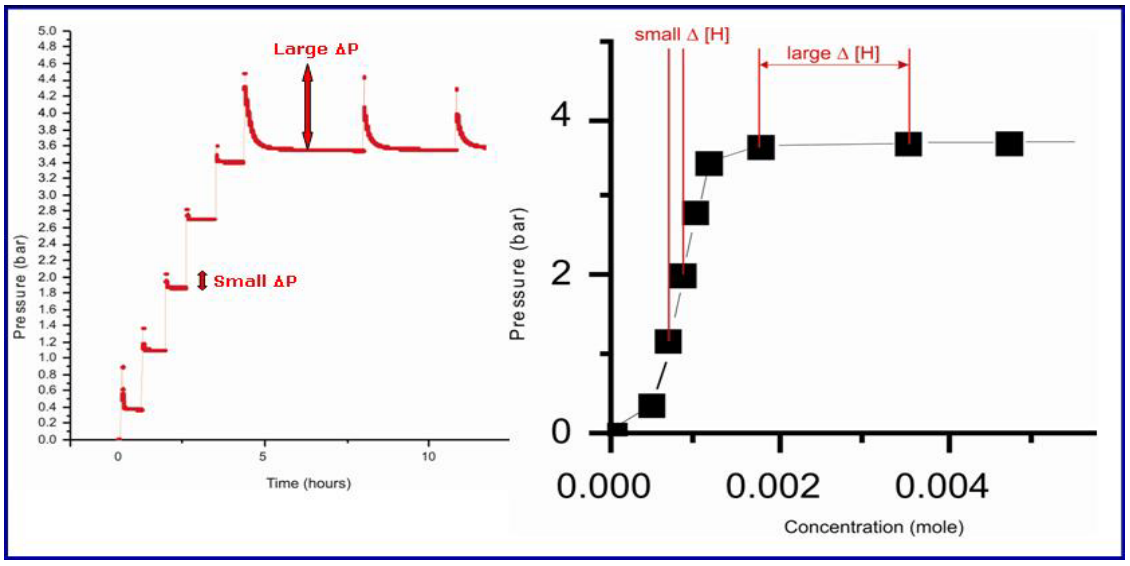

Figure 9. The relationship between pressure drop on absorption and the concentration associated with this pressure drop that is used to create each point on the equilibrium PCT diagram.

4 Hydrogen Storage Variables

Because the concentration of hydrogen in a sample is not measured directly, this important parameter necessarily relies on indirect determination from directly measured variables. Accurate measurement of direct variables is important for all hydrogen storage properties and perhaps more so for the determination of concentration than any other.

All storage properties are determined by the relationships between the variables: concentration, sample weight, temperature, pressure, cycle and time. The important distinction between direct (weight, temperature, pressure, time, cycle) and indirect (concentration) variables is made to differentiate between variables that can be measured directly from those that cannot. The last five (mass, temperature, pressure, cycle and time) are termed direct variables because they can be directly measured with traditional measuring devices such as balances, thermocouples and transducers. Concentration is considered an indirect variable because it cannot be directly measured and must be determined by correlating a direct (measurable) variable with concentration through the use of an empirical relation. Because of its dependence on measurable variables and its explicit ties to capacity, concentration will be addressed in detail in the Concentration and Capacity chapter.

The direct variables present problems in accurately collecting and interpreting data. Weight, temperature and pressure are difficult to accurately measure in all testing methods because errors can be introduced by testing equipment, sample holder design and secondary effects such as buoyancy. Errors associated with measuring the direct variables affect all property investigations and therefore the sources of these errors will be reviewed in the introductory chapter. Measurement errors specific to a particular testing method will be addressed in the associated methods section 5 . In addition to this section on the direct variables, the effects of testing and variable collecting methods unique to a particular storage property (e.g. capacity, kinetics) will be addressed in the property chapters that follow.

At this point, the reader is encouraged to briefly review the section 5 on Methods of Measurement to become familiar with the nomenclature and general principles of each testing method. Material in the sections on variables (4) and also static and dynamic measurements (5.1) will refer to basic concepts associated with the measurement methods. Familiarity with the material in these sections will aid in gaining an overall understanding of the subject.

4.1 Measureable Direct Variables

Measureable or "direct" variables (weight, temperature, pressure, time, cycle) affect the intrinsic adsorption/absorption behavior of a material:

Equation 1 $$N_a = f(P, T, solid - gas\ system)$$

Where Na is the number of moles adsorbed. In addition, the measurement of direct variables is needed to determine "indirect" variables such as capacity. The following are the direct variables that are typically measured to determine the hydrogen storage properties of a material. While the means and accuracies by which these variables are measured may vary (e.g., volumetric, gravimetric, electrochemical….) the influence on the intrinsic properties and performance of the materials should be the same.

4.1.1 Variable: Weight

The weight variable measured in the gravimetric method is often considered a direct measurement of hydrogen concentration; unfortunately, this is not the case. The balance in the gravimetric method (used to measure sample weight) actually measures the resultant force of a number of discrete forces: the weight of the sample, the buoyancy force caused by the displaced gas and the forces associated with mechanical disturbances and gas convection. The resultant force is often referred to as the *apparent* weight of the sample in order to differentiate between the measured weight and the actual weight of the sample. In order to determine the actual weight of the sample (from which concentration can be determined), it is necessary to account for and minimize the extraneous forces acting on the balance. The buoyancy force can be determined by an understanding of the skeletal density of the material while proper vibration damping can minimize mechanical forces. Forced and free convective forces are caused by pressure changes during charging/discharging and thermal gradients, respectively, and are transient in nature; patience is essential to minimize convective forces. Gravimetric measurements often use constant gas flow past the sample. In these cases, the flow drag forces must also be known and taken into account. Generally the flow drag force changes with the gas density, and therefore is a function of both temperature and pressure. Proper calibration of gas flow forces is necessary if the flow forces are significant in the particular apparatus or experimental arrangement.

In addition to the significant measurement considerations discussed above, the accuracy and precision of measuring weight depends on the type of balance used. A common weight-measuring system is an electronic strain gauge attached to a cantilever or balance (see gravimetric method section 5.4). The accuracy and precision of the strain gauge and cantilever/balance system are based on the properties of the strain gauge

and the cantilever/balance material. The deflection varies with the modulus of elasticity of the material and the weight of the sample; a low modulus of elasticity leads to greater deflection and a more sensitive instrument but the instrument is more susceptible to noise due to external forces. The modulus of elasticity will vary with temperature and this must be taken into account when making measurements at different temperatures or when ramping temperatures. The sensitivity of the balance must be considered along with other trade-offs when choosing gravimetric instruments.
With respect to hydrogen storage materials, the hydrogen storage capacity is usually given on a weight basis. Therefore accurate measurement of a samples weight is critical. Both chemisorption and physisorption materials may be highly air and water reactive, therefore samples are usually prepared and weighed in an inert atmosphere such as an argon glove-box. In addition, both types of material may require significant out-gassing of residual solvents, or adsorb impurities such as water before hydrogen testing. Thus for correct hydrogen capacity measurements it is vital that the sample is weighed after degassing. This can be performed either before or after hydrogen testing and preferably in an inert gas atmosphere.

4.1.2 Variable: Pressure

The pressure variable is intimately associated with hydrogen storage research and influences several important properties including concentration correlations, capacity and the kinetics of charging and discharging. Pressure is a commonly used measurable variable in concentration correlations and is therefore of practical interest to the measurement of all hydrogen storage properties. For example, the volumetric method measures changes in equilibrium pressure, along with volume and temperature information, to determine concentration. Changes in pressure are often used to control sorption/desorption reactions during both testing and practical operation. Isothermal measurements such as PCTs, one of the most common representations of capacity, use pressure variation to drive charging and discharging during storage property characterization. Pressure variation can also be used to control sorption and desorption in functioning storage systems, depending on the application. In fuel cell (FC) applications, hydrogen supplied at initially isothermal conditions (ambient) and elevated pressure is used to charge the storage system at the fueling station. The elevated pressure causes the reversible storage material to charge with hydrogen for future consumption by the fuel cell.

In addition to its obvious effect on reaction kinetics, pressure profoundly affects capacity measurements and practical capacities. Among the many capacity definitions are two based on thermodynamic considerations, reversible and usable capacity. Reversible capacity is of concern at the materials development level and is the measure of capacity available under feasible conditions. Reversible capacity is of particular importance to chemisorbing materials. Usable capacity is the capacity defined by the

thermodynamic restrictions placed on the storage system by the environment and the end application. Once again, fuel cells present an excellent example of the importance of the thermodynamic variables on practical storage. The range of temperatures and pressures accessible to charge and discharge a storage system are restricted by availability; in classic PEMFC applications, this translates to operating temperatures from ambient to (~353K) and roughly ambient to a few bar pressures (assuming no external pressurizing or regulating equipment is used). It is highly probable that maximum capacity of a given storage system does not occur within these limited ranges; therefore it is important to quantify usable capacity.

Electronic pressure transducers are the most common means of measuring pressure in hydrogen storage testing equipment. The accuracy limitations of transducers are generally described by two different types of error bands, those based on a percent of the actual reading (Capacitance Manometers) and those based on a percent of the full scale (Strain Gauge Transducers) (see Figure 10). For this reason, percent reading error bands are more accurate at low pressures while percent full-scale error bands may be more accurate at high pressures depending on the total error rating of the transducer. For hydrogen storage testing, particularly volumetric methods, the low-pressure range (0-15 bar) is often the most critical range for investigating storage properties. This makes the percent reading error bands the preferred error band for hydrogen storage.

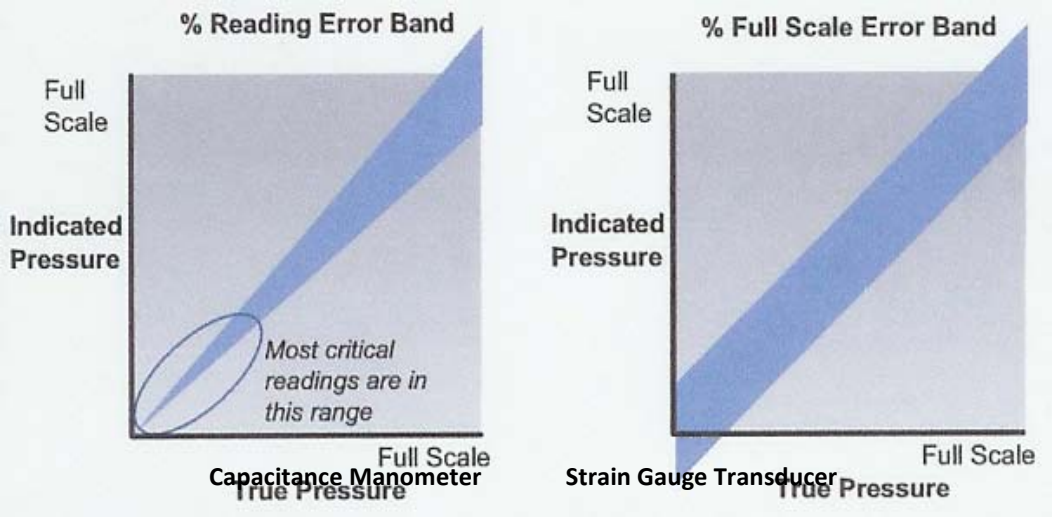

Figure 10. Depiction of the two types of error bands in pressure transducers.[57]

A simple calculation demonstrates the percent reading advantage at low pressures. Take two pressure transducers rated to 300 bar, one has a 1 % reading error band while the other has a 0.1 % full-scale error band; the 'break even' pressure for these two transducers is 30 bar. The percent reading transducer is more accurate for pressures

below 30 bar, the range of pressures most often encountered in hydrogen storage experiments. For optimum accuracy, several percent reading transducers rated to different pressures should be used.

The sensitivity of pressure transducers requires that the pressure signal change from all other sources, ΔP_0, is minimized. It is conceivable to potentially account for these other pressure signal changes and correct the data for their influence, but in practice it is more fruitful to minimize erroneous ΔP_0 signals. Background pressure signal change can be caused by a number of factors including transducer sensitivity, zero drift, miss-calibration and hysteresis effects.

With a near instantaneous change in pressure, there may be some error introduced into the immediate response of the pressure transducer, especially with respect to pressure measurements made by measuring the strain or deflection of a gauge's diaphragm. There are a couple of 'tricks' that can help determine the true measurement signal from a pressure transducer. After the transient from gas introduction has decayed, the measurement signal becomes pseudo-differential in the sense that the current signal can be compared to the measurements that came before and will come after. The signal curve is expected to show a smooth behavior and therefore noise superimposed on the curve can be "reduced" through standard procedures such as smoothing. If the sample shows marginal sorption/desorption during the transient, the pressure vs. time curve contains both the calibration data and the sorption/desorption data. In other words, since very little absorption occurred during the transient, the transient can be ignored and the pressure reading at t = 0 is the pressure with "no absorption". Thus the ideal sample, ideal in the sense that it is easy to measure, would have no sorption/desorption signal until after the transient but would come to equilibrium before other longer-term error signals such as temperature fluctuations have a chance to impact the data.

4.1.3 Variable: Temperature

Temperature is the second thermodynamic variable with important implications to hydrogen storage properties. It has many of the same hydrogen storage effects as pressure; it can be used to determine the binding energy of hydrogen in a sample (as in Differential Scanning Calorimetry), drive the sorption/desorption reactions in several testing methods and applications, and temperature influences a number of different definitions of capacity. To continue with the fuel cell example, temperature variation is the primary mechanism used to release hydrogen after initial charging because of the relatively limited pressures available due to FC structural considerations. Temperature affects practical capacity in much the same way as pressure. The two capacity definitions derived from thermodynamic considerations are based on temperature considerations as well as pressure considerations. Although, in hydrogen storage

research, pressure and temperature are intimately linked, their measurements have their own, unique considerations.

Temperature-related measurement error is one of the most common errors associated with hydrogen storage measurements, particularly kinetics measurements. The accuracy of temperature measurements is typically limited to the accuracy of the thermocouples used and the heat transfer characteristics of the sample material and sample cell. Like pressure transducers, the accuracy of a thermocouple measurement depends on what type of thermocouple is used and the temperature regime of the measurement. Some thermocouple types have a wide temperature range but are less accurate compared to those with limited temperature ranges. Because most hydrogen storage experiments are conducted under isothermal conditions, the authors advise the use of limited-range durable thermocouples that offer greater accuracy in measurement.

An important consideration is that thermocouples of all types generally present nearly the same voltage at room temperature. It is only at elevated temperatures that the deviation in the type (J, K, and N for example) will become apparent. As most modern temperature measuring devices offer many thermocouple options, it is important not only to validate the devices thermocouple type settings but also to validate by using separate secondary temperature measuring devices and to run calibrations on measurement devices on a regular basis.

Note that most thermocouples (if not all) are at the limit of their operating ranges under cryogenic temperatures and can have large errors when within a few degrees of 77K. The temperature is preferably measured with Pt resistance or silicon diode at around or below 77K.

Heat transfer between the sample material, sample cell and thermocouple is one of the primary sources of error in hydrogen storage measurements.[58] Sorption and desorption reactions can be highly exothermic and endothermic and the energy loads must be transported efficiently to maintain isothermal conditions during testing. Insufficient heat transfer can lead to pockets of sample at higher temperature than the temperature read by the thermocouple, effectively invalidating the isothermal assumption and conclusions based on that assumption. Thermocouples that are not in intimate contact with the sample, or perhaps not even in contact with the sample holder, can produce very large in-accuracies with respect to the actual sample temperature. On a system level where kilograms of storage material may be used, excellent heat transfer characteristics are required to supply and dissipate the significant amounts of energy necessary to charge and discharge a sample. The importance of heat transfer considerations will be discussed on several occasions throughout the course of the Recommended Practices Document.

4.1.4 Variable: Cycle

The desire for reusable hydrogen storage systems necessitates the ability to charge and discharge (cycle) repeatedly without loss of performance. Nearly all storage properties, particularly capacity and kinetics, vary with cycling and the variation can have a profound impact on system efficacy. Cycling phenomena include activation effects and poisoning (capacity) and retardation (kinetics) due to the gettering of impurities during cycling. In general a sample should be cycled until the capacity is stable; usually 10 cycles are sufficient for that purpose

Some important considerations for the cycle variable are primarily aimed at minimizing activation and gas stream impurity effects on measurements and are not testing method-specific. For activation effects for both capacity and kinetics, the authors advise cycling the sample at least ten times in order to measure the intrinsic properties of the material. It is also critical to evaluate the effects of poisoning and retardation on performance, especially in metal hydrides; for practical application, storage systems will commonly be charged with hydrogen gas that contains impurities like CO_2, H_2O and NH_3. The impurities adsorb to the material, occluding catalytic sites and diffusion pathways, and can be difficult to desorb because of their high thermodynamic affinity. As cycling increases with impure hydrogen gas, the impurities build to levels that poison capacity and retard kinetics.[59] Therefore, it is important to develop materials that can withstand the effects of gas stream impurities in order to avoid performance deterioration.

Several other phenomena occur when cycling a hydrogen storage material. In intermetallic compounds, decrepitation, self-pulverization due to stresses caused by lattice expansion upon hydriding, and disproportionation[60], dissociation of a compound into its fundamental components during repeated cycling (e.g. $LaNi_5 + La_2Mg_{17} \rightarrow 3La + 5Mg_2Ni + 7Mg$), cause variation in storage properties and system performance. Decrepitation and disproportionation are generally considered activation phenomena and initial cycling mitigates their effects.

Note: UHP Ultra-High purity (99.999% purity) hydrogen gas is recommended. It is also highly recommended that the source hydrogen gas is always tested for purity, especially for oxygen and water contaminants. A good solution is to have a hydrogen purifier system just before the gas enters the testing system.

4.1.5 Variable: Time

The effect of time on hydrogen storage measurements is manifested by the rate at which measurements are taken. However, some confusion surrounds how measurement rates affect data representation. Measurement data is collected in two distinct steps: the data acquisition hardware converts the continuous analog output

from the measuring device (e.g. thermocouple, pressure transducer) to a digital value at a certain rate R_1 and the computer software samples the digital value from the data acquisition hardware at another rate R_2.

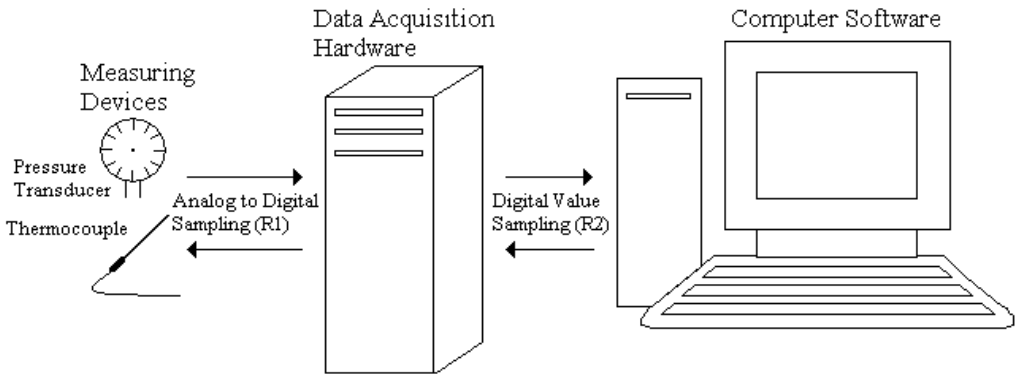

Figure 11. Schematic of a typical hardware/software set-up and the flow of information in a hydrogen storage testing system.

As Figure 11 illustrates, information is exchanged between two interfaces but not necessarily at the same rate. The sampling rate of the data acquisition hardware can be faster or slower than the sampling rate of the computer software. The difference between the rates may lead to the collection of multiple data points at the same value of the measured parameter and/or a step-wise rather than continuous change in the measured parameter. Both of these effects are most pronounced at small time steps that approach the limits of the sampling rates and are an artifact of data collection. The average results of the measured parameters are still representative of the homogeneous change in the properties being measured.

Figure 12 illustrates a number of data collection artifacts. At the beginning of the experiment, the R_2 sampling rate of the computer software is faster than the analog to digital conversion rate R_1 of the data acquisition hardware. Therefore, the computer software samples the data acquisition hardware several times before the hardware updates. This leads to several consecutive data points collected at the same pressure, an artifact that disappears as the R_2 sampling rate decreases (by design) below the data conversion rate R_1 as the experiment progress. The step-wise rather than continuous change in the data at the beginning of the experiment is caused by the difference between the sampling rates and the initial gradient in the measured parameter. Figure 12 shows the measured pressure directly after the sample is dosed with hydrogen; the pressure gradient is initially large but slowly levels off as the sample approaches equilibrium. This is reflected in the data as the pressure step size becomes less and less and the data eventually appears continuous. These kinds of data collection artifacts

demonstrate the resolution limits of the instrumentation but generally do not have a significant impact on the accuracy of the measurement and the conclusions that can be drawn. However, without understanding what causes them, they may be misinterpreted as a problem with data acquisition or instrument operation when first observed.

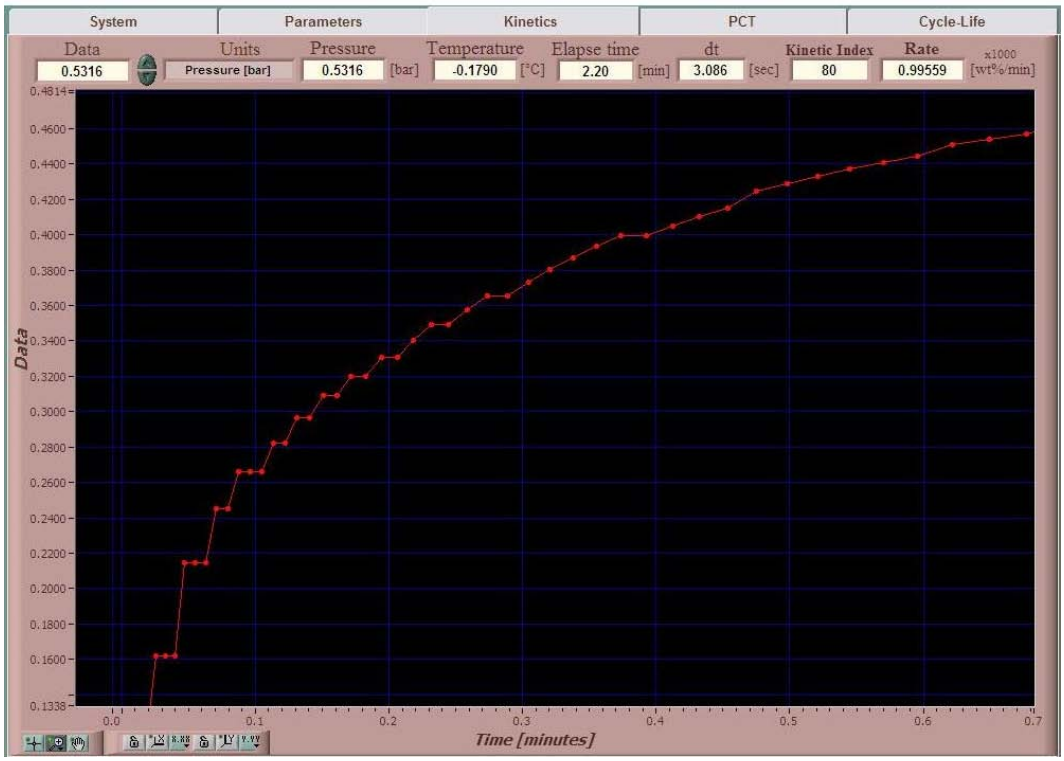

Figure 12. Example of constant and step data collection artifacts during desorption. The ordinate is measured pressure.[61]

4.2 Accuracy and Precision of Measurements

In measuring direct variables, it is important to understand the distinction between the accuracy and precision of testing equipment and convey pertinent accuracy and precision information to the reader. Accuracy is the degree of conformity of the measured variable to the actual value while precision is the degree of reproducibility of the measurement. A measurement can be accurate and precise, one or the other, or neither. An excellent and frequently used parallel to explain the relationship between accuracy and precision is the target analogy. The distance from the marks to the center of the target is the measure of accuracy and the size of the mark cluster is the precision. Figure 13 illustrates the possible combinations of accuracy and precision in the target analogy. As a thought exercise, consider the limiting cases of perfect accuracy and

perfect precision. In the case of perfect accuracy, precision must also be perfect. The reverse however, is not necessarily true: perfect precision does not ensure perfect accuracy. These cases can be easily shown in the target analogy. The limiting case of perfect accuracy necessitates that all of the marks lay one on top of another at the center of the target; obviously this ensures perfect precision because the spacing between the marks is zero. Perfectly precise marks lay one on top of another but can be located anywhere on the target, hence perfect precision does not ensure perfect accuracy.

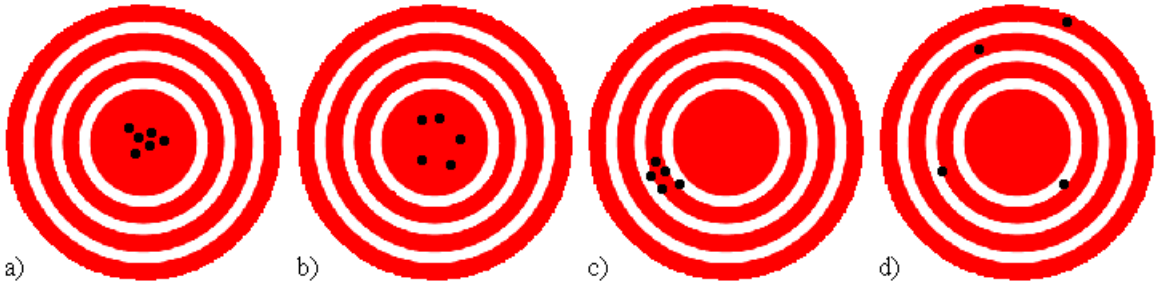

Figure 13. The target analogy for accuracy and precision. The proximity of the marks to the center of the target is the accuracy and the size of the mark luster is the precision. a) Accurate and precise, b) accurate but not precise, c) precise but not accurate, d) not accurate and not precise.

4.2.1 Significant Digits

The precision of an experimental measurement is implied in the presentation of the numerical results by the number of significant digits. This can be misleading or misinterpreted. It is therefore, the recommended best practice to always quote the precision of a numerical result. When it comes to presenting results only the number of significant figures given should be given. The following rules apply to implied precision in published data:[62]

1. The leftmost nonzero digit is the most significant digit.
2. If there is no decimal point, the rightmost nonzero digit is the least significant digit.
3. If there is a decimal point, the rightmost digit is the least significant digit, even if it is a 0.
4. All digits between the least and most significant digits are counted as significant digits.

As an example, the following numbers each have four significant digits: 1,111; 111,100; 111.1; 1,0001; 1,000.; 10.00; 0.0001010; and 1000.0. If there is no decimal point, there is an ambiguity if the rightmost digit is a 0. Thus, it is better to present results with decimal points or in exponent form with the appropriate number of significant digits.

In calculating results, approximately one more than that dictated by the experimental precision. The reason for including the extra digit is that in computation one significant figure is sometimes lost. If an extra digit is specified for all numbers used in a computation, the original precision will be retained to a greater extent.

4.2.2 Error Bars in Data Representation

Error bars are used in experimental science to serve a number of important functions in relating the precision of an experimental measurement to the reader. An error bar indicates the range of one standard deviation of the measured variable and can be used to visually compare the precision of two measurements, determine whether differences are statistically significant and determine the statistical fit of experimental data to a given function. It is important to include error bars in graphics in literature when reporting hydrogen storage properties to both reflect the experimental nature of hydrogen storage testing and aid in comparing the performance of materials and the precision of testing methods.

Experimental data is often a collection of dependent variable measurements at a given independent variable value. The collection of measurements is presented as their mean value and standard error, which is based on the standard deviation of the collection. Standard error of a collection of measurements is determined by dividing the standard deviation of the collection by the square root of the number of measurements in the collection. Standard error is represented in mathematical form by Equation 2 (M is a vector of measurements with m entries):

Equation 2

$$SE = \frac{std(M)}{\sqrt{m}}$$

For example, a (24.30, 24.68, 25.73, 26.08) collection of molar specific volume (L/mol) measurements at standard temperature and pressure would be summarized as v = 25.2 +/- .38 L/mol and presented graphically as in Figure 14.

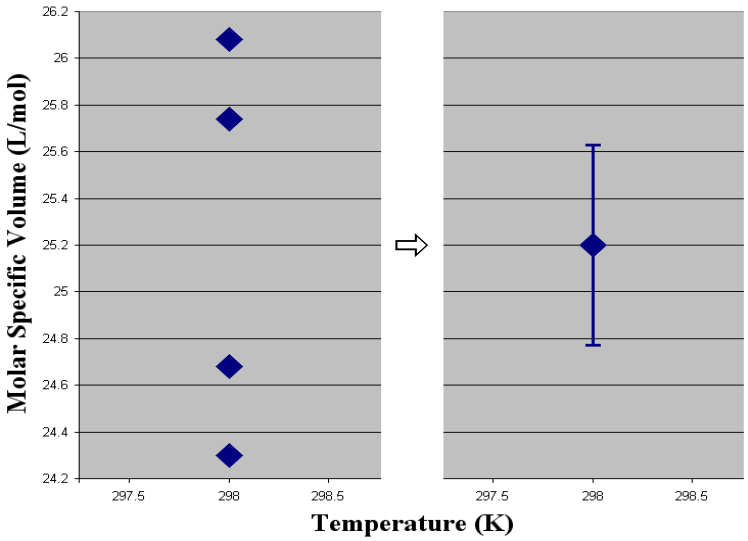

Figure 14. Graphical representation of collection of data points in mean/error bar format.

Error bars should be included on figures and error ranges on values whenever possible or at least stated in the experimental section. The value of these error limits can be determined from the known (or rated) errors of each measuring device (balance, pressure transducer, thermocouple, timing device….) and standard error analysis.[63]

4.2.3 Error Analysis

It is vitally important to understand the degree to which measurements are precise. In other words, the level of certainty of reported results based on the known error limits of the experimental data. The propagation of error (or propagation of uncertainty) is the effect of each variable's uncertainties (or errors) on the uncertainty of a function based on them (i.e. the results). When the variables are the values of experimental measurements they have uncertainties due to measurement limitations (e.g., instrument precision) which propagate to the combination of the variables in the function used to determine the results.

Uncertainty is usually defined by the absolute error. Uncertainties can also be defined by relative errors ($\Delta x/x$), which are usually written as a percentage.

Most commonly the error on a quantity, Δx, is given as the standard deviation; σ. Standard deviation is the positive square root of variance, σ^2. The value of a quantity and its error are usually expressed as $x \pm \Delta x$. If the variables are correlated, then covariance must be taken into account. For uncorrelated variables the covariance terms are zero. Table 8 shows the variances of basic mathematic equations for involving two measured variables *A* and *B*.

Function	Variance
$f = aA$	$\sigma_f^2 = a^2\sigma_A^2$
$f = aA \pm bB$	$\sigma_f^2 = a^2\sigma_A^2 + b^2\sigma_B^2 \pm 2ab\,\mathrm{cov}_{AB}$
$f = AB$	$\left(\frac{\sigma_f}{f}\right)^2 = \left(\frac{\sigma_A}{A}\right)^2 + \left(\frac{\sigma_B}{B}\right)^2 + 2\frac{\sigma_A\sigma_B}{AB}\rho_{AB}$
$f = \frac{A}{B}$	$\left(\frac{\sigma_f}{f}\right)^2 = \left(\frac{\sigma_A}{A}\right)^2 + \left(\frac{\sigma_B}{B}\right)^2 - 2\frac{\sigma_A\sigma_B}{AB}\rho_{AB}$
$f = aA^{\pm b}$	$\frac{\sigma_f}{f} = b\frac{\sigma_A}{A}$
$f = a\ln(\pm bA)$	$\sigma_f = a\frac{\sigma_A}{A}$
$f = ae^{\pm bA}$	$\frac{\sigma_f}{f} = b\sigma_A$
$f = a^{\pm bA}$	$\frac{\sigma_f}{f} = b\ln(a)\sigma_A$

Table 8. The variance of mathematical functions of the variables *A* and *B*, having standard deviations σ_A and σ_B, correlation coefficient ρ_{AB}, and precisely-known real-valued constants a and b.[64]

4.2.4 Analog to Digital Conversion Error

The accuracy and precision of all direct variable measurements are influenced by analog to digital conversion effects. Traditional analog measuring devices such as thermocouples and pressure transducers output continuous signals that must be converted into discreet digital values. The analog to digital conversion process (ADC) has three principal sources or error: quantization, non-linearity and aperture error. Quantization error is caused by the finite resolution of converting a continuous analog signal to discreet digital values, non-linearity error is caused by physical imperfections in the conversion device itself (but can be mitigated by proper calibration) and aperture error arises from uncertainty in the ADC sampling rate. In addition to errors caused by ADC, measuring devices for some direct variables have unique considerations for accuracy and precision. These considerations will be reviewed in detail in the following variable sections 4.1 .

4.2.5 Testing For Accuracy

A very important and common standard practice that should always be carried out before experimental measurements and on a regular and documented basis is blank runs under identical experimental conditions with a non-absorbing material (example: glass beads or low surface area, silica or stainless steel). It is important for both gravimetric and volumetric techniques that the blank sample has essentially the same mass and x-ray (bulk) density as that of the sample that will be measured. This criterion helps to emulate, to some degree, both buoyancy effects and corrections in gravimetric measurements and gas displacement volumes in making temperature corrections in volumetric measurements. The results of such "blank" measurements should show zero hydrogen absorption and desorption within the expected range of errors. This is an important step in identifying instrumental and/or procedural errors.

Ultimately, blank tests following a rigorous calibration procedure will produce a total experimental error that encompass all the uncertainties associated with the various variables, calibrations, calculations, corrections and uncertainties.

In addition, it is recommended that measurements on standard samples be performed on a regular basis on experimental equipment to validate the reliable operation and calibrations.

$LaNi_5$ is a convenient alloy that has a hydrogen absorption plateau pressure close to 1 bar at room temperature. However, it is generally recommended as a standard for several reasons. 1) On first hydriding it often proves difficult to hydride and usually requires activation at elevated temperatures (100°C). 2) Activation may also produce the meta-stable gamma-hydride phase which may cause a second plateau at much higher pressures than the beta-hydride phase. This change in plateau (pressure and concentration) may lead to misinterpretation of the data as having instrument related problems. 3) Doing ambient (PCT) testing of an instrument (typical for $LaNi_5$) does not test the capabilities or accuracy of the experimental equipment at non-ambient temperatures. It is important to ensure that sample and instrument temperatures are being correctly recorded. 4) $LaNi_5$ is sensitive to air contamination, cycling degradation, and inhomogeneities or impurities in the alloy composition, all of which will affect the ultimate hydrogen capacity of the material. All of these issues combined make $LaNi_5$ less than ideal for use as a standard.

For most equipment used for hydrogen storage properties measurements, high-purity (99.9%) Pd samples are recommended. A recommended measurement would be to perform one adsorption and one desorption PCT isotherm on a 1-5 gram sample at approximately 170° prior to every important series of measurements. The advantage of

palladium is that it can be handled on air prior to the measurement. It also has an ambient pressure plateau at elevated temperature which will test the ability of the equipment and data analysis software to perform accurate measurements and data reduction at non-ambient (elevated) temperatures. In addition, the hydrogen capacity of palladium is rather low on a weight basis (~0.6 wt.%) which means that errors in hydrogen storage capacity measurements will be more pronounced.

This measurement should produce a capacity of 0.63 H/f.u. at 10 bar and a desorption plateau pressure 1.8 bar. Measurements at other temperatures can be compared to published data.[65,66]

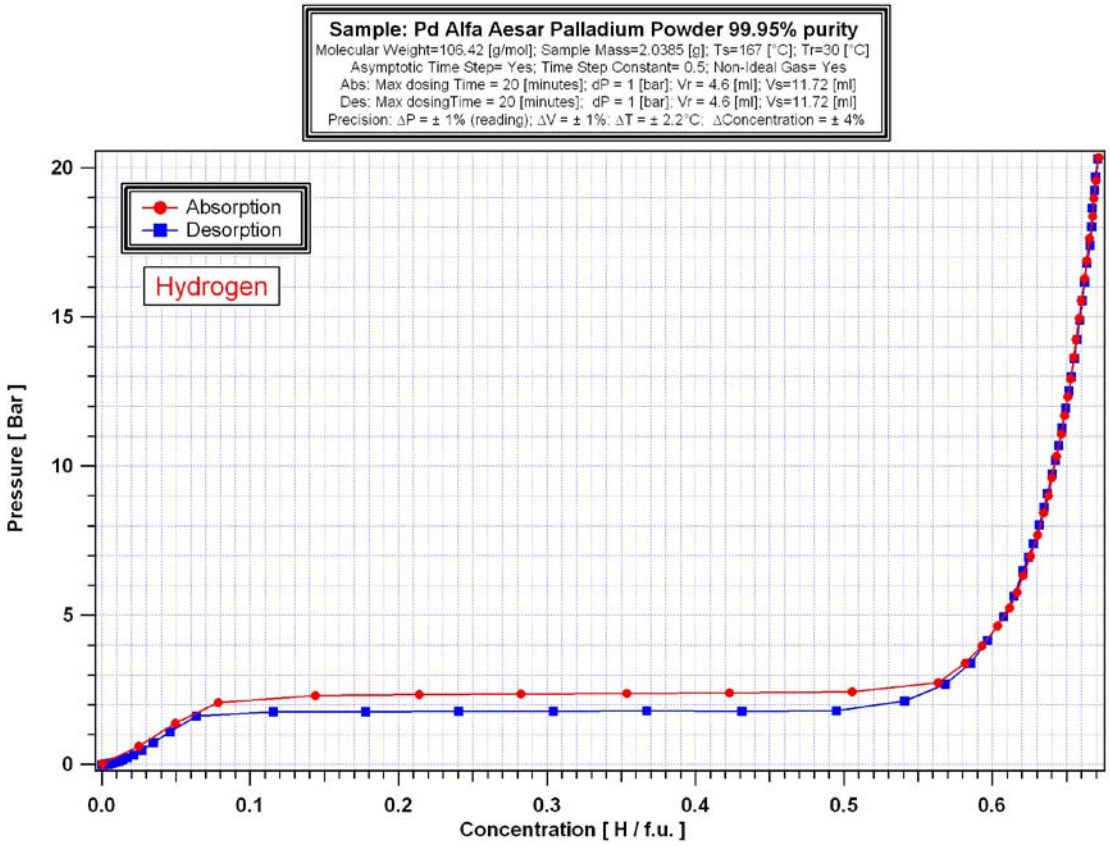

Figure 15. Hydrogen absorption and desorption volumetric PCT isotherm measurements of palladium powder at 167°C.[61]

For volumetric instruments, a hydrogen capacity significantly (5%) different that reported values would indicate a calibration or calculation error most likely associated with the volumes (reference volume, sample holder volume or sample gas displacement volume). For a gravimetric instrument, this would indicate calibration problems of the balance or errors in buoyancy corrections. For both types of equipment, plateau

pressures significantly different from reported values would indicate a calibration problem with either the pressure or temperature sensors. Decreasing capacity or radically increasing capacity at pressures above the plateau would be an indication that the effect of the elevated temperature of the gas surrounding the sample is not being adequately accounted for in the data analysis.

Finally, cross-checking or validation by performing both multiple measurements on the same sample and on different samples from the same batch of material should be performed not only on one instrument but, when available, on different types of instruments potentially at different institutions with different equipment operators. While it is often very difficult to perform measurements under exactly the same conditions and also difficult to ensure identical sample preparations or loading, the intrinsic hydrogen storage properties of a materials should be essentially the same. Thus, differences in capacity, kinetics, thermodynamics, etc. significantly larger than the total experimental error should be taken seriously. In this field, there are many instrumental and procedural issues that can lead to highly incorrect results including both false positives and negatives (usually the former). When in doubt, it would seem prudent to assume the worst.

4.3 Calibrations

Measurement instruments should be recalibrated on a regular basis. Most institutions have standard calibration protocols that should be followed. An important part of such protocols is a rigorous documenting of such calibrations so that if significant errors are discovered, previously recorded data can be corrected appropriately. The following are common methods for calibrating devices that measure important dependent variables.

4.3.1 Weight

It is recommended that NIST standard procedure be followed for making weight measurements. Documents detailing these procedures and calibrations can be downloaded from the NIST Weights and Measures website.[67]

4.3.2 Volume

The standard procedure for calibrating a volume is:

1) Liquid method
2) Gravimetric method
3) Pressure method
4) Known displacement volume calibration sample

A summary of the Liquid and Gravimetric methods can be found at NIST Handbook 143: State Weights and Measures Laboratories Program Handbook. Specifically the section: 7.3 Technical Criteria for Volume Laboratories (NVLAP Calibration Laboratories Technical Guide with OWM modifications).[68]

The Pressure method is commonly used in this field and requires a well calibrated pressure transducer connected to a standard volume (as measured through the Liquid or Gravimetric methods). The Pressure method is a secondary calibration technique that is generally used for convenience as no liquids are required. It is essentially the Sievert's method without a sample. The setup consists of a the calibration volume connected to the calibration pressure transducer with a low-displacement volume valve between the two and a rigid coupling fitting to connect the calibration system to the instrument or volume to be calibrated.

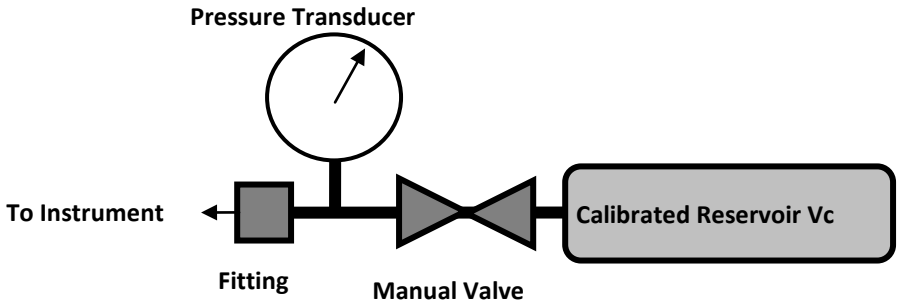

Figure 16. Pressure Method calibration system.

Gas (typically dry Nitrogen, Argon or Helium) is charged at a high pressure (0.1 to 5 bar, and at the upper 10% of the pressure transducers full scale range) into the calibration volume the valve is closed and the pressure is measured (P_1). Sufficient time (5-30 minutes) should be allowed for the gas to come to thermal equilibrium with the tubing and vessels before any pressure reading is taken. The pressure in the volume to be measured is then reduced (0.1 to 1 bar, and at the lower 10% of the pressure transducers full scale range) and the second pressure is measured (P_2). The valve is then opened gas is dosed into the unknown volume from the calibration volume. After enough time has passed for the gas to come to thermal equilibrium (5 to 10 minutes) the resulting equilibrium pressure is measured (P_3). Thus, the volume to be calibrated can be determined from the gas mass balance:

Equation 3

$$Vx = Vc \times \left(\frac{P3}{T3} - \frac{P1}{T1}\right) \div \left(\frac{P2}{T2} - \frac{P3}{T3}\right)$$

Where Vx is the unknown volume and Vc is the calibration volume. Here the ideal gas law is assumed to be sufficiently correct. The process should be repeated several times and should also be done in the opposite sense, where high pressure gas is dosed from the unknown volume into the calibration volume.

Ideally, the temperature of the entire calibration and unknown volume system are being held at exactly the same temperature (T1=T2=T3). If not the temperatures should be measured carefully at the calibration volume (T1) and the unknown volume (T2) and an assumption that the final equilibrium temperature (T3) is a weighted average of the two:

Equation 4

$$T3 = \frac{(T1 \times Vc) + (T2 \times Vx)}{Vc + Vx}$$

Where some initial approximations for Vx can be made or Equation 3 and Equation 4 can be solved uniquely for Vx as a function of Vc, P1, P2, P3, T1 and T2. Note this method of taking temperature differences into account is not very accurate because there is a temperature gradient in the gas that is not generally well represented by simply the weighted average of the two temperatures. A better approach is to take several temperature measurements along the portions of the temperature gradient and assign weighted temperature values based on the local relative volume associated with each local temperature measurement.[69] Note that if there are valves and sections of tubing between the unknown volume to be calibrated and the calibration system, then each section must be isolated and calibrated in a step-wise manner. The displacement volume associated with a closed valve is automatically included in the calibration of the volume behind such a valve.

The known displacement volume calibration sample method is similar to the pressure calibration method except that instead of using a secondary calibrated volume as in Figure 16, a cell of unknown volume is used. A sample of known density (and when weighed, thus yielding volume) is placed in the cell. The same measurements are performed as described above once with the sample in the cell and once without the sample in the cell. Then Vx is solved for using the two measurements and the difference in Vc being equal to the volume of the standard sample. An example of such a standard sample would be a large single crystal of silicon.

4.3.3 Pressure

Most of today's modern pressure transducers have associated electronics that linearize the transducers output to the applied pressure. This generally only requires span

(voltage, current or resistivity output versus pressure) and zero adjustments. Typically both will vary with temperature, time, and use. Spans can be determined from the comparative testing described below. The standard procedure for calibrating a mass balance is:

1) Perform a series of pressure transducer readings (5 minimum) over the transducer's full range of pressure with simultaneous measurements of the same gas pressure against a NIST traceable (or national equivalent) standard pressure transducers.
2) Perform a series of pressure transducer readings (5 minimum) over the transducer's full range of pressure with simultaneous measurements of the same gas pressure against a NIST traceable (or national equivalent) dead weight pressure calibrator.
3) Zeros are usually adjusted under vacuum by setting the transducer's final output (post electronics and post software) to zero (0.000… to within appropriate significant digits).

4.3.4 Temperature

It is recommended that NIST standard procedure be followed for making temperature measurements and calibrations. A document detailing thermocouple calibrations can be downloaded from the NIST Weights and Measures website. [70] Checking temperature measurement accuracy against boiling (distilled) water and ice (corrected for barometric pressure) is a recommended interim test.

4.3.5 Time

It is recommended that NIST standard procedure be followed for making time measurements. Documents detailing these procedures and calibrations can be downloaded from the NIST Weights and Measures website.[71]

4.3.6 Other Calibrations

A variety of other devices may be employed for measuring gas sorption or other properties of hydrogen storage materials. Most devices or instruments will come with appropriate calibration instructions. Detailed information concerning calibration theory, regulations, and procedures can be found though most scientific societies and national standards institutions.[71]

5 Methods of Measurement

There are a number of measurement methods that can be used to investigate hydrogen storage materials and systems. Gravimetric and volumetric methods are the two primary methods and the most robust in terms of depth of analysis; temperature-programmed desorption, differential scanning calorimetry, and thermal gravimetric analysis are also used. All measurement methods quantify a change in a measurable property to indirectly calculate the hydrogen storage capacity of a material. It is important to keep in mind that all methods indirectly calculate hydrogen concentration and each have complications associated with indirect methods. For example, characterizing the hydrogen storage capacity of highly porous media has proven difficult using gravimetric and volumetric methods because both require an understanding of the amount of gas displaced, calculated from the skeletal density of the material, and the corresponding buoyancy (gravimetric) and volume calibration (volumetric) effects on measurements.

This section will summarize these most commonly used measurement methods and provides detailed techniques for measuring hydrogen storage properties. The section also provides a series of detailed consideration that may have a significant impact on the performance and accuracy of a measurement. These range from general sample preparation considerations to issues unique to specific types of measurements and instruments.

One clear consideration is that the measurement equipment should be constructed of materials that are both hydrogen compatible and do not have significant hydrogen permeation. Obviously metal that react with hydrogen at low pressures and temperature such as Titanium, Magnesium, Palladium and Vanadium to name a few should not be used. Common copper tubing and brass components are prone to out-gassing impurities that may have an impact on measurements. 316L stainless steel is commonly used in many hydrogen applications. Teflon and many polymer sealing materials have high hydrogen gas permeation rates and are not generally recommended for these measurement applications.

5.1 Static and Dynamic Measurements

Hydrogen storage testing can be divided into static and dynamic testing based on whether or not the sorption/desorption reaction is allowed to reach equilibrium at any point during the experiment. In volumetric and gravimetric methods for example, hydrogen gas can be introduced or removed either by aliquots (static) or through a variable flow or pressure regulator (dynamic). In thermally driven methods such as TPD and TGA, the temperature of the sample can be raised in steps (static) or continuously (dynamic).

In static testing, a sample in equilibrium at a certain temperature, pressure and composition is perturbed by a sudden change in pressure (volumetric and gravimetric methods) or temperature (TPD and TGA). The sample is allowed to reach equilibrium at some new temperature, pressure and composition before it is perturbed again. This process continues until the sample is fully sorbed or desorbed. This step-by-step, or equilibrium state-by-equilibrium state process allows static testing to be used to determine the thermodynamic properties of a material by van't Hoff diagram analysis. Static testing is the most frequently reported testing method in literature when using volumetric and gravimetric methods.

Dynamic measurements are characterized by continuous changes in pressure and temperature and do not allow for equilibrium. Although they are not ideal for investigating purely thermodynamic properties, they can provide information on the kinetic activity of a material. When hydrogen flows at a constant rate into an evacuated hydrogen storage system, the pressure in the system increases linearly until the material begins to sorb. After this point, the pressure in the system is a function of the material's ability to sorb hydrogen; if the system is to remain at constant pressure across the pressure plateau in Figure 17, the rate of hydrogen flowing into the system must be equal to the rate of hydrogen sorbed by the material.

Dynamic measurements are more useful for evaluating a material's hydrogen storage performance during application than static measurements. For example, fuel cells require hydrogen at a specified constant pressure to operate efficiently and safely. In order to supply hydrogen at constant pressure, a regulator is connected between the FC and the hydrogen storage system through which the flow rate varies. Dynamic measurements allow testing of storage materials at flow rates representative of the flow through the pressure regulator in the fuel cell/storage system and the dynamic pressure limits associated with such flow rates. These results are highly dependent on the impact of heat transfer on sorption/desorption kinetics.

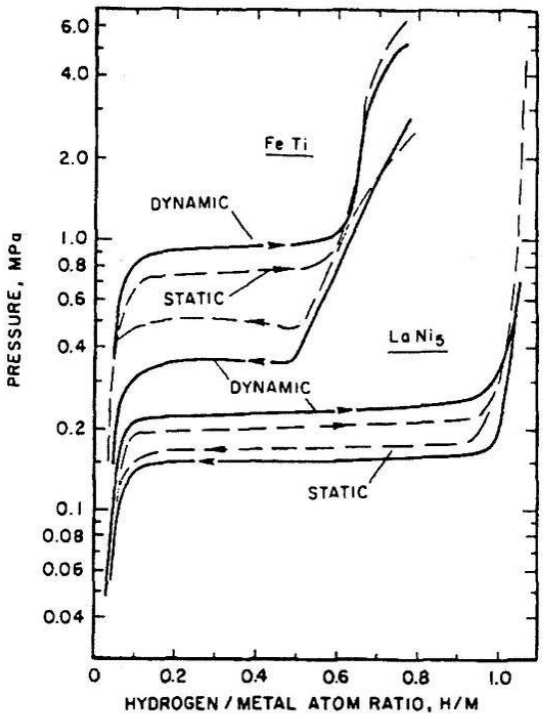

Figure 17. Comparison of static and dynamic pressure-composition isotherms for $LaNi_5$ and FeTi at 298K. Results are after about 200 test cycles.[72]

5.2 dC and dP Dosing Methods

In isothermal testing, the sample is charged and discharged by changes in hydrogen pressure in the sample holder. Hydrogen can be added step-by-step in aliquots or continuously through flow or pressure regulators. These techniques are used to provide static and dynamic methods of storage testing. Static and dynamic dosing can also be referred to as dC (differential concentration) and dP (differential pressure) dosing, respectively. In dC dosing, a specific amount of hydrogen calculated from the temperature, pressure and volume of the aliquot is dosed to the sample. In dP dosing, a flow or pressure regulator is used to increase the pressure in the sample cell a specific amount per dose. The terms dC and dP originate from the relationship between the different types of dosing and PCTs; dC dosing steps along the PCT concentration axis and dP dosing steps along the PCT pressure axis.

Volumetric instruments typically take steps in concentration (dC dosing) whereas Gravimetric instruments generally take steps in pressure (dP dosing).

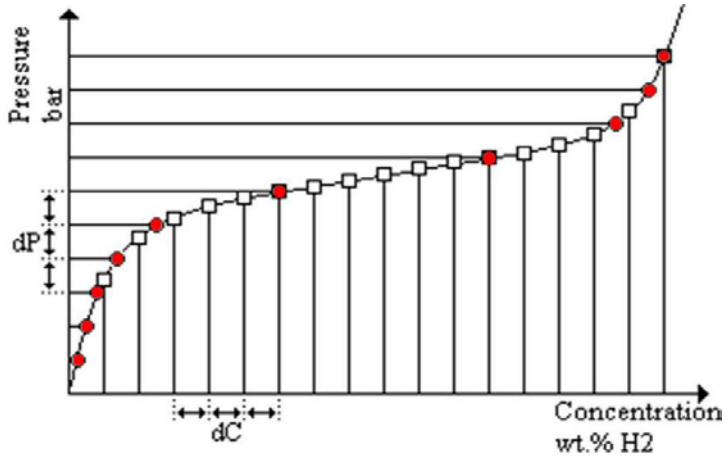

Figure 18. PCT of classic metal hydride material with plateau. dC (squares) and dP (red circles) dosing provide different information in solid solution (vertical) versus hydride formation (horizontal) portions of the PCT phase diagram.

Figure 18 shows the relationship between dC and dP dosing and PCTs for a metal hydride. dC dosing (squares) enables limited investigation of the solid solution phases, represented by the regimes with greater slope at low and high concentrations, compared to dP dosing (circles). However, the reverse is true for the investigation of transitional regimes at intermediate concentrations. dC dosing can provide much greater information across plateaus in metal hydrides and the saturation regimes of physisorbing materials. A common complaint in hydrogen storage testing is incomplete or uninformative investigation of metal hydride plateau regimes due to dP testing. In some cases where the plateau slope is very small, the plateau may be missed altogether.

An advantage of the dC stepping of the volumetric method is that samples can be prepared to specific hydrogen concentrations. This may be very useful for ex-situ examination of the materials using other analytical techniques.

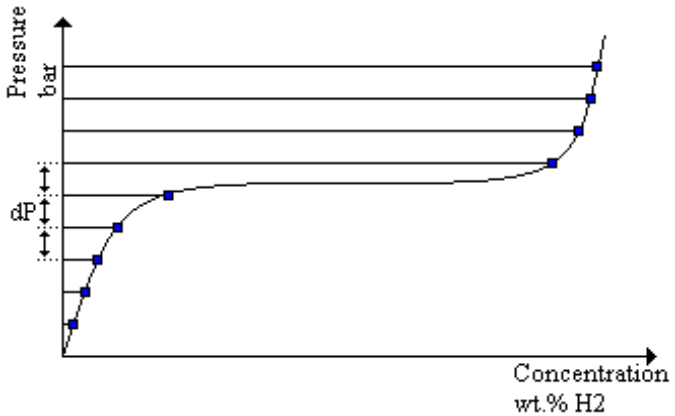

Figure 19. Example of PCT with missing plateau information due to inherent limitation in dP dosing.

5.3 Volumetric Method [73] [74]

The volumetric method of hydrogen storage measurement, also known as the manometric method, or as Sievert's method in honor of the German chemist of the same name, uses temperature-pressure-volume correlations to determine hydrogen concentration and the storage properties of a material. A generalized volumetric system with commonly employed components is shown in Figure 20.

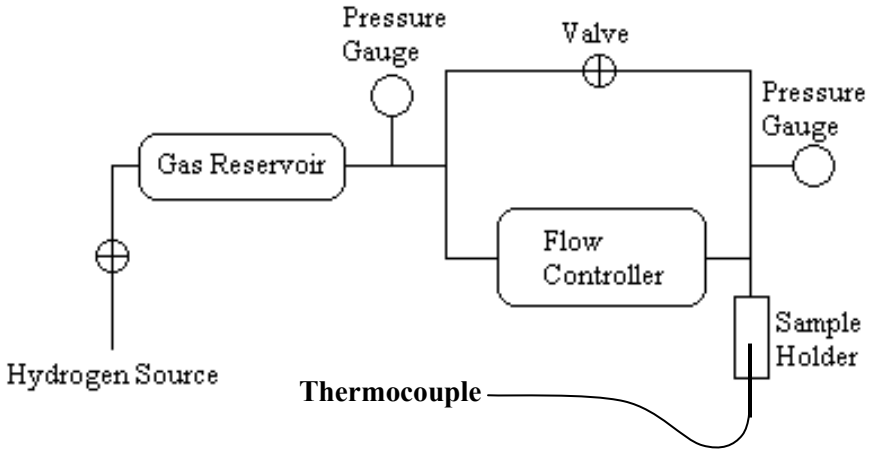

Figure 20. Multipurpose Gas Sorption/Desorption Apparatus. The pressure gauge on the right is only required when using the flow controller.

The apparatus consists of a gas reservoir connected to a specimen reactor. Because the volumetric method measures concentration indirectly through temperature-pressure-volume correlations, the volumes and temperatures of the reservoirs and sample holder (system) must be known in advance. A thermocouple should always be positioned in as close a contact as possible with the sample. The system volumes are carefully pre-calibrated and the reservoir and sample holder are maintained at constant (but not necessarily equal) temperatures using an external temperature controller. By fixing volume and temperature, reservoir and sample holder pressures can be measured using pressure transducers to provide isothermal pressure-concentration data.

The volume of the sample holder must be calibrated while filled with sample in order to get an accurate measurement of the free gas volume in the system. Although a generally straightforward procedure for chemisorbing media, calibration can be tricky for highly porous and nano-structured media at low temperatures due to inaccurate or incomplete skeletal density information and the possible physisorption of helium used to perform the calibration. Note however, that it is unlikely that most materials will have significant helium adsorption below 5 bar and at 77K, and certainly not at significantly higher temperatures. It can be verified that helium does not adsorb by

measuring the sample holder volume with the sample (free volume) as function of the helium expansion pressure at temperature. Materials that do not adsorb helium will likely show a constant free volume as function of pressure. Similarly, in a gravimetric measurement, such material would also exhibit a linearly decreasing mass response (buoyancy) as function of helium pressure. More on the issue of potential helium adsorption is presented in section 5.11 .

Volumetric testing requires accurate measurement and control of the instrument and sample holder temperatures and the associated temperature gradients. The temperature of the instrument should be controlled in order to minimize temperature fluctuations due to external sources such as room heating, ventilation and air-conditioning. The temperature of the sample can be precisely controlled below room temperature by cryogenic cooling accompanied by PID (Proportional Integral Differential control) heating or above room temperature by PID heating and appropriate insulation.

To test a sample using the static method, the gas reservoir is filled with H_2 to a pressure P and then allowed to react with the specimen reactor by opening the top valve. When filling the gas reservoir, sufficient time should be allowed for the gas to come to thermal equilibrium with the tubing and vessels before a pressure reading is taken. An equilibrium pressure P' is reached between the gas reservoir and the specimen reactor that, once paired with temperature, initial pressure and volume information, can be used to precisely determine the amount of hydrogen sorbed by the material. Dynamic testing allows the slow and continuous introduction of hydrogen to the specimen reactor. Hydrogen gas from the gas reservoir flows into the specimen reactor via the electronic flow controller while continuous pressure readings are taken by the pressure gauges attached to the reservoir and reactor. The pressure, temperature and volume data are analyzed to generate dynamic (non-equilibrium) pressure-composition isotherms.

One intrinsic advantage of the volumetric method is that, unlike gravimetric methods, the quantity of gas dosed to or from the sample can be small compared to the total capacity of the sample. Thus, the method allows the direct preparation of sample of known hydrogen contents. This may be useful for doing *in-situ* or ex-situ secondary measurements such as X-ray or neutron diffraction, NRM, IR, Raman, etc.

5.3.1 Differential Pressure Method [75]

The differential pressure method is a modification of the standard volumetric testing method and is designed to increase the accuracy of Sievert's measurements. An example of a differential pressure method apparatus is shown in Figure 21.

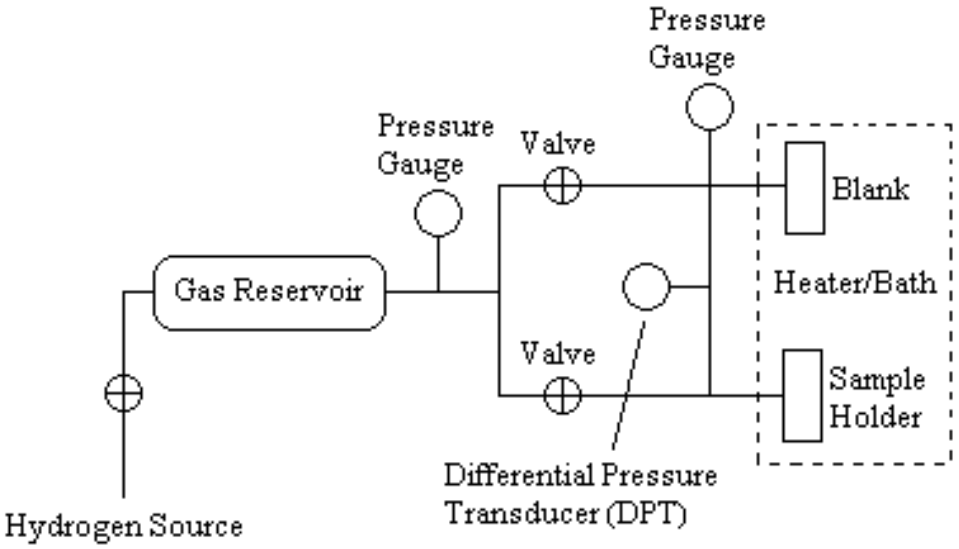

Figure 21. Schematic of the Differential Pressure Adsorption Unit.

The sample holder and a blank are maintained at the same temperature and are initially under the same pressure with the two valves in Figure 21 open. Immediately after dosing, the valves are closed, isolating the two volumes (sample holder, blank and associated tubing) from each other except for the differential pressure transducer connecting them. The differential pressure transducer measures the pressure change between the two volumes caused by the sorption/desorption of hydrogen by the sample. While adding significant complications, by measuring pressure with a differential pressure transducer instead of an absolute pressure transducer (gauge), the differential pressure method can take some advantage of the higher accuracy afforded to percent reading pressure transducers at low pressures (see section 4.1.2).

The most important consideration when testing with the differential pressure method is thermal equilibrium; the sample holder and the blank must be maintained at exactly the same temperature for the duration of the experiment for accurate isothermal data. This is often accomplished by placing the two volumes together in a heater or bath. Unfortunately, even small temperature variations like those caused by endothermic or exothermic reactions can lead to pressure fluctuations that can impair the accuracy of the differential pressure method. Excellent heat transfer and thermal management capabilities are essential to accurate testing using the differential pressure method.

5.3.2 Data Corrections

Volumetric systems determine the concentration of hydrogen in a material from changes in the concentration of hydrogen gas in the reservoir/sample holder system. The concentration of hydrogen gas in the system is determined by knowledge of the pressure, temperature and volume of the reservoir and sample holder. Pressure changes are measured on a pressure transducer inside the volumetric equipment that is at the same temperature as the instrument. Ideally, the system volumes are calibrated and the temperature is known and constant throughout so that the measured pressure is directly related to the concentration of hydrogen gas in the system. Unfortunately, temperature can vary both spatially and temporally and can be difficult to monitor because it requires many sensors to map the true temperature gradients. A common approach is to divide the instrument into isothermal regions, but care must be taken to validate this assumption to avoid the contribution of thermal effects on kinetics (see Figure 22). For example, if a sample is held at 77 K, the pressure is the same throughout the system. However, the hydrogen gas density is greater in the fraction of the system at 77 K. The volume fraction at 77 K depends on the system design, the type of sample holder used and the skeletal density of the sample.

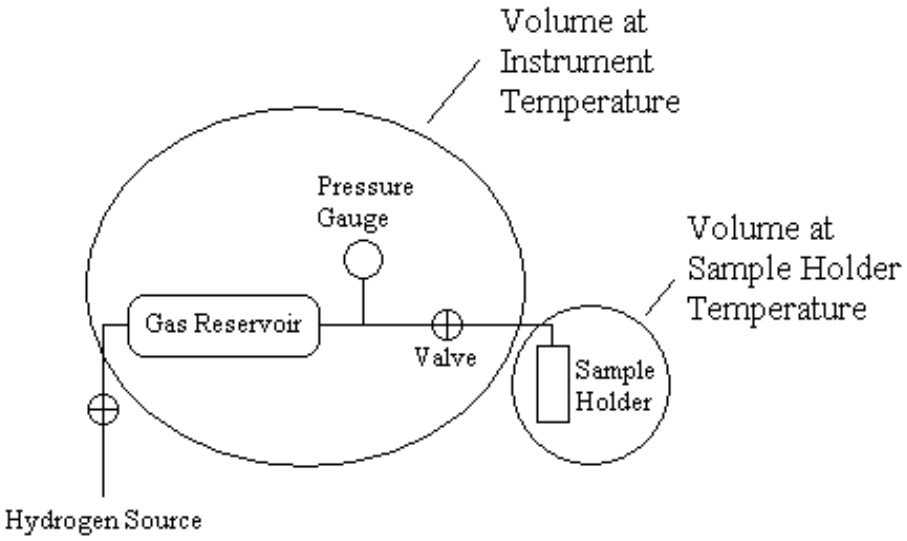

Figure 22. Schematic of temperature regimes in a volumetric instrument. The volume of gas at instrument temperature and at sample holder temperature varies depending on the system design and the type of sample holder used.

There are two data correction methods that can be used to account for temperature and hydrogen (gas) concentration variation in the reservoir/sample holder system; both involve calculating 'apparent' volumes that more closely represent the actual concentration of gas in the system. The apparent volume corrections can be applied to raw data after experimentation.

5.3.3 Temperature Correction

When the gas in a volumetric instrument is not all at one constant temperature, there will be a density gradient in the gas which must be accounted for in the measurement of hydrogen uptake or release. This is known as the "Temperature Correction" or "Apparent Volume Correction". This typically occurs because the sample is held at a temperature which is different than the gas dosing reservoir. Below we describe two methods for compensating for this gas temperature gradient. It is important to note that the temperature and the volume of the sample cell has a large impact on this correction and should be considered in the whole design of the system. While the corrections are generally small terms, in the present context, the volume and temperature differences can be substantial.

The method referred to here as the temperature correction method uses an empirically determined correction factor C_f to calculate the true hydrogen gas content in the system. In practice, the temperature correction factor does not affect the temperatures used in the concentration equation (equation of state) but rather the volume used. It is determined from the volume fraction of the system at non-ambient temperatures and is used to define an apparent volume (Equation 5). In this analytical approach the "Apparent volume" of the sample holder $V_{SH,App}$ is determined for a given sample temperature T_{SH} and reservoir temperature T_R using the room temperature volume calibration of the sample holder (with sample) V_{SH}. The apparent volume corrects for the temperature differences between the reservoir and sample holder (see section 4.3.2).

Equation 5 $$V_{SH,App} = C_f \bullet V_{SH}$$

This apparent volume is then applied to the equation of state to determine the hydrogen content in the total volume of the system.

The process for applying a temperature correction is straightforward. An inert (non-sorbing) material of similar physical properties as the sample (density, size and thermal conductivity) is tested at identical conditions to the actual sample experiment. As an example, for the hydrogen uptake measurements of a high-surface area activated carbon sample, solid (non-porous) graphite pellets of the same mass could be used as the blank or control sample for determining the temperature correction factor that will be applied to the actual adsorption and desorption data. To minimize the number of free variables associated with the temperature correction factor the sorption testing on the blank sample should be performed under identical conditions as the sorption measurements on the material of interest. Using the same example, if one is investigating the hydrogen storage properties of a sample at 77 K, the inert material should be tested at 77 K with the exact same reservoir volume, tubing and sample holder. It is important the inert material have the *same* skeletal (gas displacement)

volume as the sample, as well. Because the temperature correction factor reflects the volume fraction of the system at non-ambient temperatures, it is necessary that the volumes of gas at sample and reservoir temperatures are identical in the inert material and sample experiments. Once volumetric equivalency has been ensured, the inert sample is tested in order to establish a baseline with which to compare the performance of the sample. Theoretically, capacity (n=moles of gas sorbed) should be zero at all pressures for the inert material (Equation 6):

Equation 6 $$nRT_R = P_F(V_{SH,App} + V_R) - P_{SH}V_{SH,App} - P_RV_R = 0$$

Where P_F is the resulting pressure after sorption, P_R is the pressure in the reservoir volume V_R before dosing the sample, and P_{SH} is the pressure in the sample holder of apparent volume $V_{SH,App}$ before dosing. A correction factor is adjusted to determine an apparent volume $V_{SH,App}$ (Equation 5) that produces no sorption (i.e. Moles of sorbed gas n=0). In practice, this first-order approximation may be sufficient for the temperature correction, however, there will be a non-zero effect of pressure on the temperature (gas density) gradient (Figure 23).

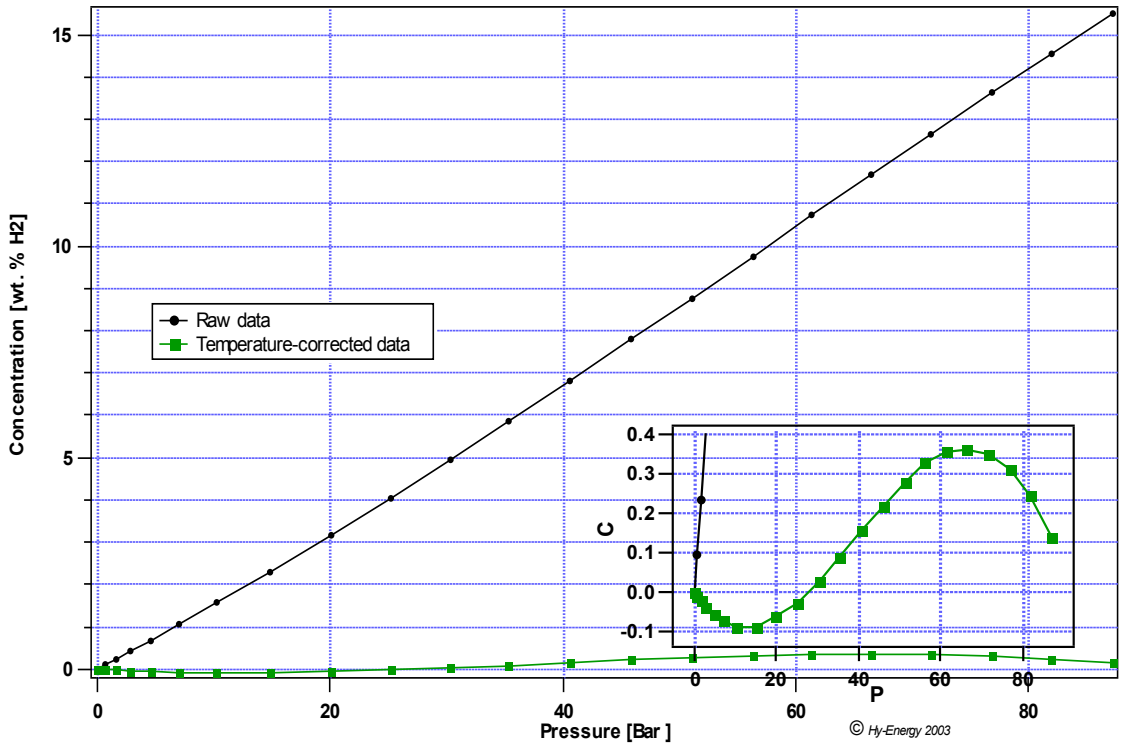

Figure 23. PCT data for an inert material. The linear relationship between pressure and concentration is due to the temperature difference between the reservoir (302 K) and the sample holder (77 K).

A temperature correction factor is applied to the raw data of the inert material and varied until the associated apparent volume yields zero sorption at over the pressure range of interest. The temperature correction factor that yields zero sorption for the inert sample is then applied to the raw data of the actual sample.

Figure 24 presents an extreme example (most difficult scenario) of a low capacity, very low density material (0.1 g/ml) showing raw and temperature corrected data for a physisorption at 77 K. The temperature correction was taken from the data in Figure 23 and applied to the raw data of the physisorbing material to give the temperature corrected results.[61]

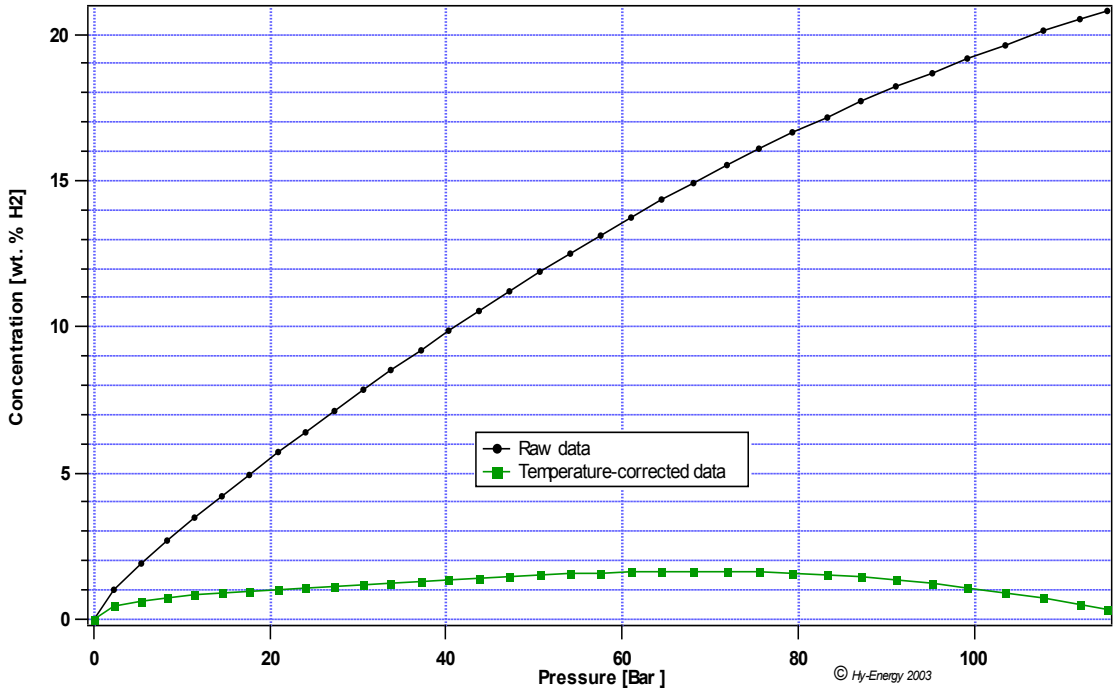

Figure 24 Excess capacity PCT.

5.3.4 Volume Correction

A volume correction is an empirical correction for the temperature based gas density gradient based on performing an inert gas (usually helium) volume calibration measurement of the sample holder (with sample) at the testing temperature. This calibrated volume is the volume at room temperature required to contain the same amount of hydrogen gas as the volume of the sample holder at testing temperature. It

provides a direct method to determine the "Apparent Volume". If there were a discrete change in temperature at the valve between the sample volume and reservoir volume (i.e. T_{SH} to T_R), the relationship between the "Apparent volume" of the sample holder $V_{SH,App}$ and the volume of the sample holder V_{SH} (measured at the same temperature as the reservoir) would be given by the simple relationship:

Equation 7

$$n_{SH} = \frac{PV_{SH}}{RT_{SH}} = \frac{PV_{SH,App}}{RT_R} \rightarrow V_{SH,App} = \frac{T_R}{T_{SH}} V_{SH}$$

Where n_{SH} is moles of gas in the sample holder, R is the gas constant, P is the measured pressure. However, this is not a realistic representation of the temperature distribution of the gas in a real system. There will be a gradient in the gas temperature (and density) in going from the sample holder to the reservoir. In addition, non-ideal behavior of the gas (compressibility, see section 5.3.5 below) would have to be taken into consideration at high pressures or low temperatures.

In practice, the "Apparent volume" is determined by calibrating the free gas (dead) volume of the sample holder using an inert gas (usually helium) with the sample holder at the temperature that the hydrogen sorption measurements will be made. The pressure change measured on dosing the inert gas from the known reservoir volume into the sample holder volume (at temperature) will compensate for the temperature gradient effect. It is critical that enough time is take in these calibration dosing measurements for the gas to come into thermal equilibrium with the heated (or cooled) sample holder. It is also very important to note that, while this method is more direct and easier to perform that the Temperature Correction method described above, it may be inappropriate to use with microporous materials that exhibit significant helium adsorption at low temperatures. More on the issue of potential helium adsorption is presented in section 5.11 .

To apply the empirical volume correction, one must use the inert gas "Apparent volume" determined at the testing temperature and reservoir temperature in the calculating the concentration of hydrogen uptake or release from a sample. Note that the reservoir temperature data must be used exclusively because the temperature variation in the system is accounted for in the apparent volume correction.

Figure 25 shows the same data as that of Figure 24 with both the Temperature Correction method and the Volume Correction method applied to the data. Note that the very low density of the sample in this example (0.1 g/ml) combined with the extreme temperature difference (sample holder 77K and reservoir 302K) causes a very large correction to the data. The difference in the corrected results demonstrates the limits of accuracy of these two different correction approaches under the most extreme conditions.

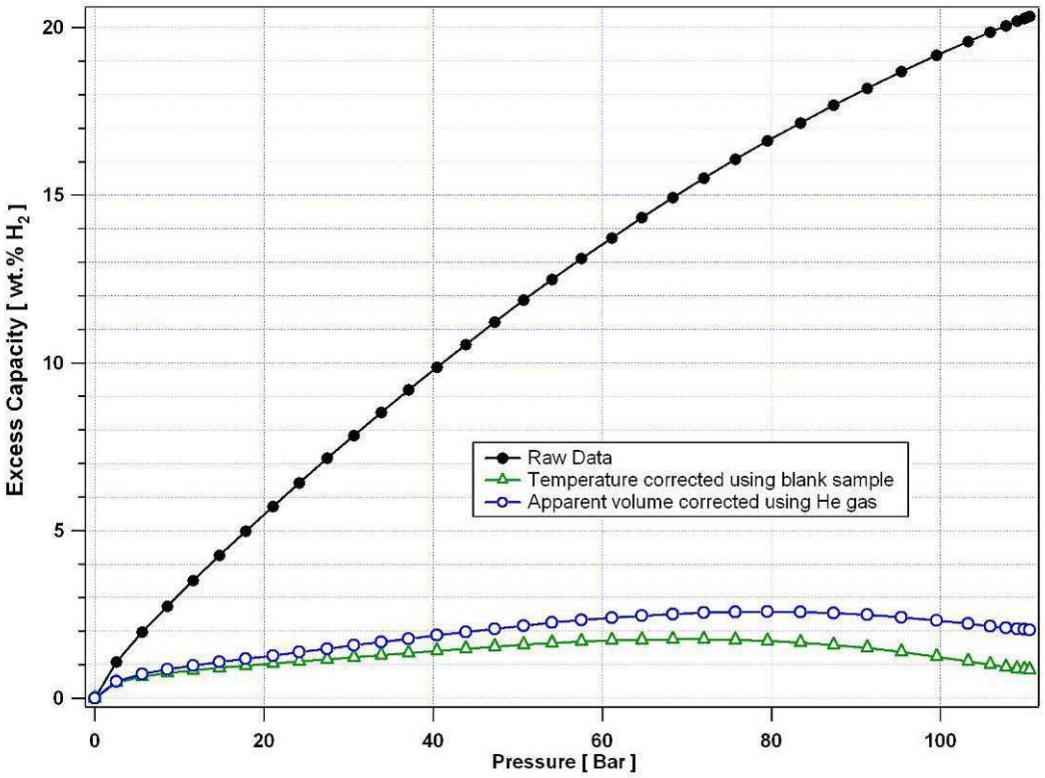

Figure 25. PCT for a physisorbing material at 77 K showing the raw data, temperature corrected, and volume corrected data. This is the same raw data that is used in Figure 24.

5.3.5 Compressibility Factor

The volumetric method uses gas laws to determine the number of moles of hydrogen in the system based on pressure, temperature and volume measurements. A gas law can be written in general form as

Equation 8

$$PV = nRTz(P,T)$$

The measurement and sources of error for pressure, temperature and volume are discussed in the variables section 4.1 . The compressibility factor, z, accounts for the non-ideality of the gas at a given temperature and pressure. For an ideal gas, the compressibility factor is unity and Equation 8 collapses into the familiar ideal gas law. The compressibility factor for hydrogen is taken from compressibility data and applied as a function of the measured pressure and temperature (Figure 26). It is recommended to determine compressibility factors using a standard reference database such as the NIST12 database for fluid properties.[76]

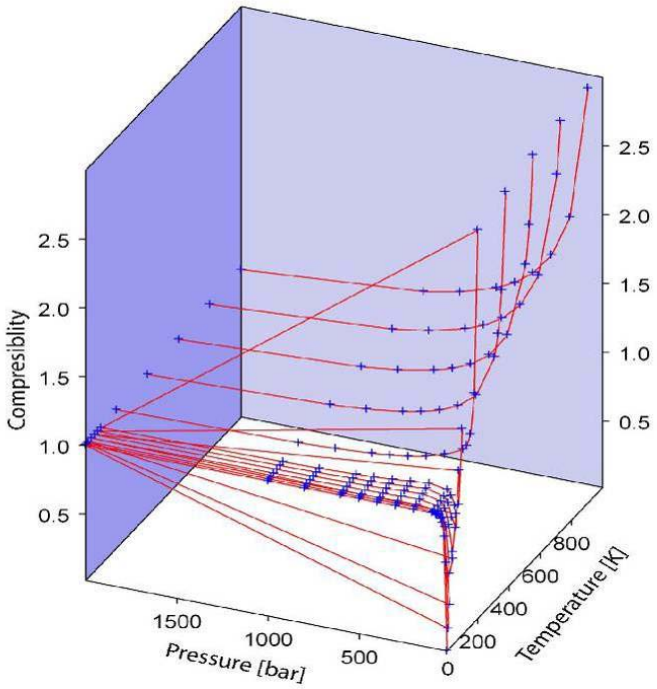

Figure 26. Compressibility factor z for hydrogen as a function of temperature and pressure.

5.3.6 Gas Impurities

Gas impurities can be introduced into a volumetric system through the use of impure hydrogen gas and leaks during desorption experiments, or can be introduced by decomposition and byproduct formation from the storage material. In volumetric measurements the sample's hydrogen storage capacity is determined by measuring pressure drop/increase due to sorption/desorption. Since the partial pressures of any low level impurities are a minute fraction (parts per million to perhaps parts per thousand) of the measured hydrogen pressure, the impact on the total capacity caused by impurities is essentially negligible. In the volumetric method, the impurities may still impact capacity and kinetics through surface effects such as poisoning and retardation; however, the measurement will be truly representative of the material's performance in the presence of impurities. In contrast, for the gravimetric method, the presence of impurities in the hydrogen can cause significant experimental errors as due to their larger masses they can mimic important hydrogen uptakes. Moreover, such error may be more important on porous materials at cryogenics temperatures as the sample may act as a getter for some vapors. Therefore, using very high purity gases and purging thoroughly the measurement system under very high vacuum is strongly recommended in such case.

Poisoning and retardation (see Capacity and Kinetics chapters) occur when gas impurities react with the sample to inhibit the total hydrogen sorbed/desorbed and/or the rates of reaction, respectively. These effects cause decreases in the measured storage capacity and kinetic activity of the sample material and may incorrectly indicate the sample material is not suitable for hydrogen storage applications. It is important to not eliminate a sample from consideration until gas impurity effects are mitigated. Impurities may simply cause "gas blanketing" which reduces sorption rates but does not necessarily impact capacity or desorption rates.

5.3.7 Instrument Temperature

The temperature of the instrument is an often-overlooked factor in taking accurate measurements. In most volumetric equipment, the dosing volume is inside the body of the instrument and is not in thermal equilibrium with the sample and sample holder. Therefore, knowledge of the instrument temperature and the temperature gradient between the instrument and the sample holder is necessary to accurately relate the pressure reading on the pressure transducer (inside the instrument) and the equilibrium pressure in the sample holder. Instrument temperature management is most often performed by a temperature control system inside the instrument housing.

5.3.8 Leaks

Hydrogen can be leaked to the environment (external leak) and across valves inside equipment (internal leak) during hydrogen storage testing. Both types of leaks during volumetric testing cause unexpectedly high capacities and strange kinetic behavior. During sorption testing above ambient pressures, gas leaked to the environment is assumed to be sorbed to the sample. Leaks during sub-ambient desorption also affect the capacity by increasing the reading of the amount of gas desorbed. In kinetic testing, leaking sorption/desorption profiles appear linear in time, as opposed to true sorption profiles that have a curved profile and eventually reach an equilibrium pressure. An equilibrium pressure of exactly 1 atmosphere and extraordinarily large hydrogen storage capacities are highly unlikely and should be double checked. Leaks also expose the sample and system to gas impurities that can affect property measurements and compromise samples.

It is advisable to check hydrogen storage testing systems for external and internal leaks every 20-40 experiments by running an empty sample holder. It is also good practice to check for external leaks on exposed tubing and joints using helium leak detection or a hand-held flammable gas detection instruments. These leak precautions apply to both volumetric and gravimetric testing methods.

An important note is that certain types of gas fittings may have "virtual leaks" that can not be picked up by external leak checking. Therefore, conical gas fittings are not recommended.

5.3.9 Reference Point

The volumetric method measures relative changes in hydrogen concentration calculated from changes in pressure in the reservoir/sample holder system. Because only changes in hydrogen concentration can be calculated, volumetric methods require a reference point with which to calculate absolute concentrations. The most obvious and most commonly used reference point is an uncharged sample under vacuum, which corresponds to (0 bar, 0 wt.% H_2). From this reference point, absolute concentration with respect to an indirect variable can be determined. Note that the quantity of hydrogen absorbed and desorbed in a closed set of isothermal cycles should be consistent. Thus, a second absorption would commence at a capacity that is the end point of the previous desorption.
Using mass balance of the gas by knowing the total gas volume, and measuring pressure and temperature, the exact concentration of hydrogen in a sample can be determined. In some cases, where the uptake (or release) of hydrogen from the sample is slow enough, it may be possible to adjust the concentration vs. time measurement to a concentration of zero (or fully charged) at time = 0.0 (the point at which the valve between the reservoir and sample holder was opened). With accurate volume calibration and pressure and temperature measurements the calculated concentration at time = 0.0 should likewise be zero (or fully charged).

5.3.10 Gas Heating and Cooling effects

An important temperature effect is the adiabatic gas expansion effect. While, hydrogen is unusual in that it has a range that exhibits reverse Joule-Thompson behavior the overriding thermal effect will be cooling of the gas on expansion and heating on compression. This effect can often be seen in the initial part of a kinetics measurement when hydrogen is dosed at high pressure from a calibrated volume to the sample held at low pressure or vacuum. There is a small temperature drop in the gas that is seen as a pressure drop and consequently what appears to be initial sorption. The gas expansion effect impacts desorption kinetics measurements in a similar manner: as the hydrogen desorbs from the sample and expands into the vacated volume, the temperature and pressure spike can be mistaken as increased desorption. These transient effects usually last only a few seconds or less depending on the thermal mass and internal surface area of the gas handling system and sample holder (see Figure 27). However, with large quantities of gas and large pressure differentials, it may take the gas, vessels and tubing several tens of minutes to return to thermal equilibrium. This effect disappears as the

gas comes into thermal equilibrium with its surroundings. One should be careful to not misinterpret this temperature relaxation behavior as gas sorption by the sample. This is one good reason why it may be quite important to have a temperature sensor in close proximity if not intimate contact with the sample. To be able to determine when transient temperature related effects have subsided, one should ideally monitor the gases return to return to isothermal conditions.

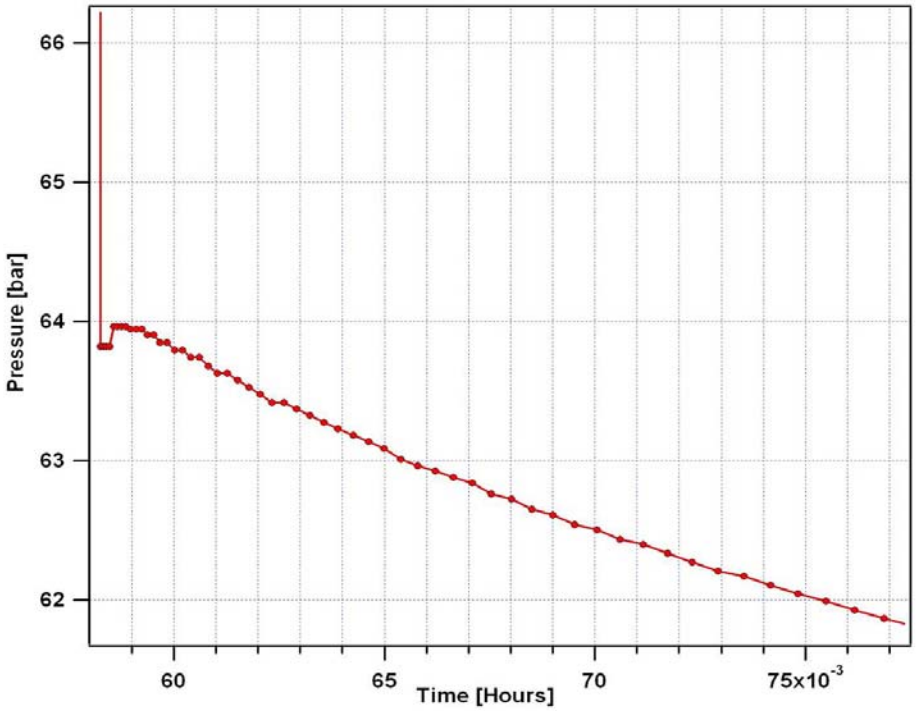

Figure 27 Adiabatic gas expansion in dosing from high to low pressure can cause an increase in temperature (and pressure) of the gas.

5.3.11 Sample Size

During single-dose measurements, the largest practical calibrated volume available limits the amount of material that can be tested. At a more sophisticated level an automatic volumetric doser with multiple volumes can be used to perform such kinetic measurements on wide range of sample sizes.

Small samples (less than 100 mg) exhibit small pressure changes due to sorption/desorption. It is therefore important to minimize the background pressure noise in order to measure the small pressure changes associated with small sample sorption/desorption. Also, small samples require that the instrument must be capable of high sensitivity both in the pressure sensor itself and the volume size. In particular, volumes should be match in size relative to the sample volume.

5.3.12 Skeletal Density

The low skeletal density of highly-porous materials can cause difficulties in accurately determining hydrogen storage properties. This is primarily due to two factors: first, knowledge of the amount of gas displaced by the sample is required to determine the free volume in the sample holder. This can be difficult to quantify for samples of low skeletal density that have the potential to adsorb helium, the gas commonly used to calibrate volume in a volumetric system. Helium adsorption during volume calibration may lead to unexpectedly large volume calibrations, an effect that becomes especially pronounced at cryogenic temperatures. Second, low skeletal density means that the volume a typical sample cell will be filled with only a small mass of sample. Insufficient sample quantity (mass) leads to small relative pressure changes on absorption or desorption. Small pressure changes in a standard volumetric instrument are less accuracy due to pressure transducer sensitivity. It is important to have enough sample mass that pressure changes are significantly above the level of resolution of the pressure transducers. This second issue is somewhat mitigated with instruments that use very high accuracy pressure transducers or differential pressure transducers. However, it is best addressed by using as much sample as possible for the volumes of the system.

When the skeletal density of the sample is very low and unknown or difficult to determine, the two factors discussed above lead to opposing considerations regarding the amount of sample necessary for accurate testing. On the one hand, the error associated with gas displacement volume of the sample in the sample holder is reduced by using a smaller amount of sample. This might be the only solution if skeletal volume (gas-displacement density) of the sample is completely unknown and the instrument has highly sensitive pressure transducers. Recent literature from Gray et al. supports this view and finds that the volume calibration error associated with skeletal density is proportional to the square of the volume of the sample.[73] On the other hand, the need for relatively significant changes in pressure to provide an accurate quantification of the amount of gas ad/absorbed or desorbed means larger samples will give more accurate results. Note that this is mostly a concern form high-surface area physisorption materials. For all other materials, and even physisorption materials given that the methods for determining the skeletal density of materials are generally commonly accessible and reliable, it is recommended to use the largest quantity of material possible for the experimental equipment (i.e. filling the isothermal portion of the instruments sample cell).

5.3.13 Calibration Volume Changes

The effects of miss-calibration of the reference volume and a possible volume change with pressure can contribute error through the volume term; the latter effect is only

considered significant in the sensor head, the valves with their accompanying diaphragm or bellows components and changes in the sample volume itself. Pressure-induced volume changes in the tubing, calibration volumes, and gas component are generally considered negligible.

5.3.14 Volume Dilatation of Sample

Some hydrogen storage materials, especially metal hydrides, undergo volume dilatation and contraction during hydrogen sorption and desorption. The volume of a system (sample, sample holder and appropriate tubing) is typically calibrated using helium before or after experiments are conducted when the sample is in the uncharged state. Because volumetric methods require knowledge of the volume of a system in order to calculate concentration, changes in the volume of the sample during testing are not accounted for in the calculations and have the potential to cause errors in measurement. Volume dilatation and contraction of a sample is often negligible when compared to the overall volume of the system. However, dilatation effects should be considered when testing large quantities of materials that exhibit large volume expansion coefficients.

5.4 Gravimetric Method

The gravimetric method of measurement uses weight changes measured on a balance to determine concentration and the storage properties of a material.[74] A schematic of a simple symmetrical microbalance gravimetric system is presented in Figure 28. Note additionally, that gravimetric systems are also often configured as flow-through systems, in which case there is also a gas exit port attached to the chamber through a pressure control device.

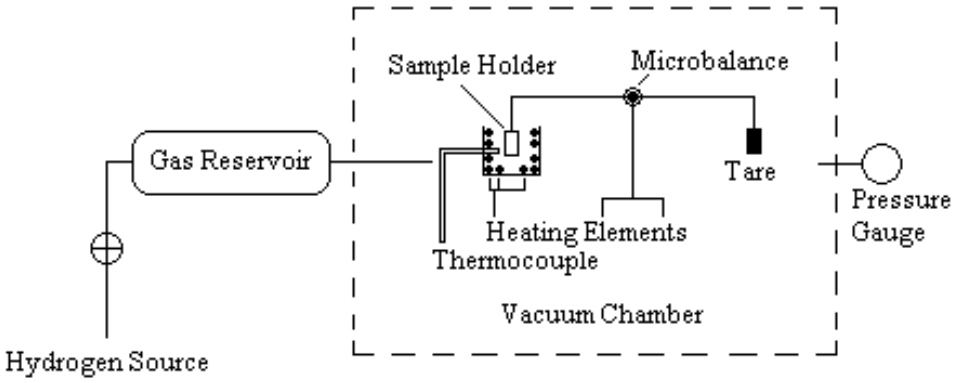

Figure 28. Schematic of counterbalanced gravimetric method system for hydrogen storage testing.

Before gravimetric testing, the weight of the sample is measured and the sample is placed on one end of a symmetric microbalance in a sample holder. In symmetrical microbalance gravimetric instruments, an inert tare with the same weight and comparable density to the sample is placed on the other end of the microbalance to provide a counterbalance. The tare is designed to minimize the effects of buoyancy caused by the hydrogen gas displaced by the sample volume and must be inert in a hydrogen atmosphere. Note that at relatively high pressures, buoyancy measurements (see the Introduction section 2.1.3.3) should be considered as an intrinsic part of the gravimetric method, basically on the same standing and care as the free (dead) space volume calibration in the volumetric method.

After the chamber containing the gravimetric equipment is evacuated, hydrogen from an external hydrogen source enters the chamber and is generally increase in incremental pressure steps as it is sorbed by the sample in the sample holder. The microbalance is typically equipped with an electronic circuit that measures the strain on the balance material that is directly related to the change in weight of the sample. This information combined with pressure and temperature readings provided by a pressure gauge connected to the chamber and a thermocouple located next to the sample holder are needed to measure hydrogen storage properties.

Measurements can generally be made under isobaric conditions with no loss of sensitivity and modification of the thermodynamic driving force or altering the kinetics by significant pressure changes. This can be accomplished even in static experiments by providing makeup gas during absorption or bleeding the evolved gas during desorption. Finally, as explained below (Introduction 5.3.6), special care must be taken to avoid contamination gases in the hydrogen using this method.

5.5 Thermal Gravimetric Analysis Method [77]

We make a distinction here between the Gravimetric instruments described above and Thermal Gravimetric Analysis (TGA) in that Gravimetric instruments generally operate under isothermal conditions with a controlled over pressure of gas. Whereas, TGAs typically operate under vacuum or low-pressure flowing gas conditions and ramping temperatures. Some equipment, however, may be setup to operate in all of these modes. TGA is a thermal analysis technique often used in conjunction with DSC to determine the hydrogen storage properties of a sample. The first documented use of TGA was in the study of the efflorescence of hydrated salts in 1912 but it is now traditionally used in the quantitative investigation of decomposition reactions. TGA is experimentally similar to DSC but instead of measuring the heat flow as function of temperature, TGA measures sample weight as a function of time or temperature. This is

accomplished by placing the sample in an environment that is heated or cooled at a controlled rate and measuring the weight change.

The equipment necessary to perform TGA consists of an accurate balance, a programmable furnace, a reaction chamber and a data collection system. As the temperature inside the furnace and reaction chamber changes, the balance measures the variation in weight due to various chemical reactions including dehydriding. TGA is affected by many of the same issues as the gravimetric testing method such as buoyancy and mechanical disturbances. The buoyancy force exerted on the sample by the displaced fluid varies with temperature and must be taken into account either during the experiment, e.g. the tare technique in the gravimetric method, or during data analysis; mechanical disturbances must be minimized through leveling and anti-vibration supports. Another complication TGA shares with the gravimetric method is how to determine the sample temperature. Using a thermocouple to directly measure the temperature affects the weight reading of the sample. Consequently, care must be taken to place the thermocouple in such a way that it accurately reads the sample temperature but does not affect weight readings.

Thermal gravimetric instruments require calibration on both temperature and mass. Temperature calibration for DTA-TG (Differential Thermal Analysis – Thermal Gravimetric) instruments is performed using the extrapolated onset temperature of the DTA peak of the melting points of standard materials. For TG instruments, temperature is calibrated by the Curie point method or the standard wire melting method.

Mass calibration is performed at room temperature by using standard masses—removal of a standard weight on the sample holder, where the recorded change in mass is calibrated to the mass of the standard weight. The drift in baseline upon heating should be checked by a measurement using a blank sample pan. Following the measurement with a blank, a standard sample which decomposes quantitatively by several well-separated reaction steps is subjected to the same measurement (i.e., heating rate, sweep or carrier gas flow rate and type, final temperature). The corrected mass change is constructed by subtracting the apparent mass change as a function of temperature from the sample under study. The experimentally corrected mass loss should be confirmed and in good agreement with the calculated mass loss from the reaction stoichiometry.

As with DSC (Differential Scanning Calorimetry) measurements, the sample (solid or liquid) is weighed into a small crucible/sample pan. Typical sample pans are made of carbon, aluminum, silica, platinum, stainless steel, or inconel. The sample pan is selected based on material compatibility with the sample and products. Sample size should be kept to a minimum, but large enough to observe the necessary mass changes. With respect to solid samples, the particle size is a critical parameter that will influence the shape and position of the TG curve. Typical TG experiments are performed under

either a constant heating ramp or under isothermal conditions. In the isothermal runs, mass change is recorded as a function of time while at a constant temperature. For the case of non-isothermal runs, the mass change of the sample is recorded as a function of temperature while being subjected to a prescribed linear heating rate. A means to reduce the temperature gradients present within the sample is to impose slower heating rates (typical heating rates rarely exceed 10 k/min).

Scanned temperature experiments (TGA) are often done using flowing inert gas, such as argon. Although useful for comparing different materials (catalyzed vs. uncatalyzed, for example), desorption occurs into an essentially H_2-free environment, and thus it does not reflect the actual conditions encountered in a real storage system application, where there is always H_2 gas present at pressures at or exceeding 1 bar. Interpretation of desorption temperatures thus must be done carefully. For this reason TGA may be used as a screening tool, but not as a technique to rely on for realistic system desorption temperatures. When one really wants to know practical desorption temperatures, the experiment must be conducted by flowing H_2 gas into the TGA at the particular pressure of interest (say, 1-8 bar).

As mentioned above, in most cases the TG experiments are performed under either an inert carrier gas or a reactive gas. The flow rates and type of gas will affect the apparent mass change. Consequently, buoyancy calibration runs need to be made with an empty pan for a given gas composition, heating rate, and purge/sweep gas flow rate. Buoyancy calibrations need to be performed on a regular basis, ideally every time a sample is performed.

5.5.1 Buoyancy

The weight of the fluid displaced by the sample exerts an upward force on the sample holder that can affect the measured weight change appreciably. The degree of the buoyancy effect is proportional to the volume displaced by the sample and the density of the surrounding gas. The upward force due to buoyancy on a symmetric microbalance like that in Figure 28 is:

Equation 9

$$F_b = g\rho\Delta V = g\rho\left(\frac{m_s}{\rho_s} - \frac{m_t}{\rho_t}\right)$$

where ρ is the density of the hydrogen gas, m_s and ρ_s are the mass and density of the sample and m_t and ρ_t are the mass and density of the tare which may include terms representing the mass and density of the sample holder (bucket, pan, beam, and the hang-down wires). At elevated pressures ρ is not only a function of pressure and temperature but must also include corrections for non-ideal gas behavior. This

calculation is may be complicated by the fact that at sample temperatures far from room temperature there will most probably be a temperature gradient (and thus hydrogen gas density gradient) in the gas surrounding the components of the balance (pan, hang-down wires, balance beam). In a symmetrical microbalance instrument, it is generally assumed that both sides of the balance experience the same gradients and are zeroed accordingly. However, with very small samples, any minute difference in the instrumental buoyancy may present large apparent mass changes in the sample.

For asymmetric balances (spring balances or magnetic suspension balances), the influence of buoyancy on the sample and instrument components must be corrected computationally, taking into account that the buoyancy of the balance parts occurs at temperatures different from that of the sample. Thus, the upward force due to buoyancy on an asymmetric microbalance is:

Equation 10

$$F_b = g\rho\Delta V = g\rho\left(P_s, T_s\right)\left(\frac{m_s}{\rho_s}\right) + g\rho\left(P, T_x\right)\left(\frac{m_B}{\rho_B}\right)$$

where $\rho(P_s,T_s)$ is the density of the hydrogen gas at the sample, $\rho(P,T_x)$ is the density of the hydrogen gas at various points along the components of the balance (P is constant, but T_x will vary), m_s and ρ_s are the mass and density of the sample and m_B and ρ_B are the mass and density of the balance components (bucket, pan, beam, and the hang-down wires).

When the density of the materials is ill-defined (e.g. for many microporous materials) helium displacement curves can be used to calculate the buoyancy effect. In this case, the essence of the buoyancy measurement lies in the extraction of the skeletal volume ($V_s=m_s/\rho_s$) from the helium displacement curve. This can be performed directly using a microbalance to determine the skeletal volume of the adsorbent. This measurement is quite straightforward when a sample is tested on a symmetrical *instrument* with no tare weight. This approach is basically the gravimetric [method] equivalent of the free (dead) space volume measurement in the volumetric [method]. In fact, there might be no need for separate pycnometry measurements although it can constitute as excellent verification.

Note that there is some concern that the helium may interact with some materials in a way that causes error in determining the skeletal volume and consequently may lead to errors in the quantity of hydrogen absorbed by such a sample. These interactions may be in the form of helium adsorption or it is possible that the helium pressure may affect the density of the material. While not common for most materials, this issue will have the strongest effect on low density, physisorption materials and may be exacerbated by small sample sizes.

5.5.2 Gas Impurities

Gas impurity effects are generally much more severe in gravimetric methods than volumetric methods because samples are much smaller and the total amount of gas surrounding the samples is many orders of magnitude larger than in the volumetric case. This means that even at low impurity levels the relative exposure of the sample to impurities may be orders of magnitude higher. In addition, the weight increase due to contaminants can not be distinguished from increase due to hydrogen sorption and therefore gas impurities have the potential to greatly affect measurements; in the volumetric system, the partial pressure of contaminants is typically negligible compared to hydrogen and therefore doesn't affect measurements to the same degree. This makes it important to reach relatively high levels of vacuum in order to take accurate measurements.

In contrast to the volumetric method, the effects of gas impurities tend to lead to false positives, measurements that indicate a sample is a better hydrogen storage material than it really is. This is because weight increase due to sorption of impure species is mistaken for hydrogen sorption, although in reality the sorption of hydrogen is decreasing (poisoning). Once again, it is necessary to minimize gas impurity effects during testing in order to gain an understanding of a material's true hydrogen storage properties. When a gravimetric system is used in a flow-through mode, the sample is continuously exposure to fresh source gas, thus impurities in the source gas must be minimized. Use of high purity gas, non-permeable and non-contaminating tubing such as stainless steel, and, if necessary, passing the source gas through water and oxygen scrubbers will mitigate the effect of impurities.

The effects of impurities is increased at low temperatures where a (porous) sample can act as "getter" for molecular species condensing at temperature above the particular cryogenic temperature used. This can lead to large errors in gravimetric measurements. There has been considerable concern in the case of hydrogen storage on carbon nanostructures where important errors can be attributed to impurities in gases, vacuum quality and gas purity.

Because gravimetric measurements are much more sensitive to co-generation of other gases (evolved mass, not evolved moles) they often send up warning flags (like when the weight loss exceeds the total hydrogen content) even when the evolved gas is not being monitored.

5.5.3 Heat Transfer

Heat transfer effects are critically important to hydrogen storage measurements and are resolved from temperature data collected by thermocouples. Ideally, the thermocouple measuring the temperature of the sample material and the sample are in perfect thermal contact, allowing the thermocouple to best measure the temperature of the sample. In gravimetric systems, this is not the case. A thermocouple cannot be attached directly to the sample because it will affect the sample's measured weight and is therefore placed near but not touching the sample. This makes it difficult to measure the true temperature of the sample and resolve heat transfer effects. In cases where the thermal gradients in the vicinity of the sample holder are large enough that the temperature reported by the thermocouple does not represent the true temperature at the sample holder, calibration with known temperature standards is necessary. System design that minimizes thermal gradients near the sample is highly desirable.

5.5.4 Leaks

The effects of leaks on the gravimetric method vary widely depending on the type of experiment. One advantage of the gravimetric method is that leaks that occur during sorption testing have little effect on the measurement because the gas lost to the environment is not included in the indirect calculation of concentration like in the volumetric method. However, the flow of gas in the instrument caused by a leak can affect the forces measured by the cantilever. Leaks during gravimetric desorption testing can affect the sample material as well as the measurement. Sub-atmospheric pressures sometimes used for desorption promote gas contamination and can lead to poisoning, retardation and other issues associated with gas impurities. This is a serious consideration when evacuating the sample holder or degassing a sample at elevated temperatures under vacuum.

5.5.5 Sample Transfer

Some hydrogen storage materials are sensitive to atmospheric oxygen, carbon dioxide and/or water. Physisorbing materials readily adsorb atmospheric gases and vapors and must be baked out under vacuum for a sufficient time (3-12 hours) before hydrogen storage testing. Other materials, such as magnesium-nickel metal hydrides, oxidize rapidly and can not be exposed to oxygen. Both cases necessitate 'airless' sample transfer between storage containers and the hydrogen storage instrument. Airless sample transfer is difficult in gravimetric systems because the sample must be loaded onto a microbalance, a process that often exposes the sample to atmosphere. Some gravimetric and volumetric systems offer airless sample transfer devices but the process is typically awkward and while special designs make this manageable, typical systems

are prone to mistakes that can compromise a sensitive sample. One approach is to incorporate the entire instrument inside an inert gas glovebox. While this provides a much higher level of assurance against contamination, it can add considerable complexity and impracticality to the sorption testing of materials and general, use, maintenance and repair of the instruments.

5.5.6 Volume Dilatation

Volume dilatation during sorption affects weight measurements in gravimetric systems by changing the buoyancy forces acting on the microbalance. As the volume of the sample increases, the amount of hydrogen displaced by the sample also increases. This increases the buoyancy force acting on the volume that in turn affects the resultant force measure by the microbalance. This is a particularly challenging consideration because taring the microbalance with an inert material, a common technique used to minimize buoyancy effects, will not account for buoyancy effects due to volume dilatation. If necessary, these can be taken into account by post-data acquisition processing provided a measurement or reasonable estimate of the sample density in the sorbed state is available.

5.5.7 Thermal Gradients and Gas Flow Forces

Thermal gradients in the gas phase inside the chamber cause natural convection currents that can affect the microbalance, leading to noisy weight measurements. Once perturbed, the microbalance can take a long time to stabilize; therefore it is important to heat and cool the system slowly to minimize thermal gradients. Careful system design, including controlled flow channels and baffles to prevent establishing large convective cells, can help mitigate against thermal gas flow noise. In flow-through systems, gas flow drag forces on the sample holder and hang-down wires must be taken into account. These require either running a second, null experiment under identical conditions in the absence of the sample as a baseline for comparison of the sample run, or else calibration of the flow forces under various conditions of flow velocity (which generally changes with the kind of gas, temperature, and pressure).

5.6 Temperature-Programmed Desorption Method

Temperature-Programmed Desorption (TPD) refers to a wide range of experimental methods that rely on temperature variation and generally include mass spectroscopy to investigate and quantify desorption reactions. The technique can be used for both reversible and irreversible processes, with the latter referred to as Temperature-Programmed Reaction Spectroscopy (TPRS).

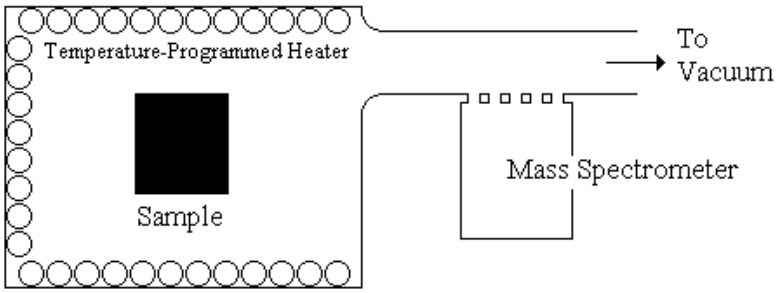

Figure 29. Schematic of typical Temperature-Programmed Desorption experimental set-up.

TPD measurements may be as simple as measuring pressure rise in a volumetric instrument or weight loss in a gravimetric instrument while ramping the sample temperature. However, TPD generally refers to spectroscopic desorption measurements. The basic set-up for TPD techniques is illustrated in Figure 29. The sample is loaded into the experimental apparatus (a temperature-programmed heater contained in a vacuum chamber) and charged with hydrogen until fully loaded. Note that hydrogen loading may also be performed in a separate apparatus prior to putting the sample in the TPD instrument. After the remaining gas has been drawn off, the computer-controlled heater slowly raises the temperature of the sample. This releases hydrogen that is evacuated to vacuum. A mass spectrometer connected to the evacuation line analyzes the relative composition of the desorbed gas and quantifies the amount of hydrogen desorbed by the sample. As with other methods (gravimetric and volumetric) that employ simultaneous mass spectrometry analysis, TPD systems have an advantage, in that it can distinguish between hydrogen and other constituents in the evacuated stream.

Concentration, temperature and time data is obtained through TPD measurements and can be used to determine capacity, kinetics and thermodynamic properties of a material. A common data representation for TPD experiments is shown in Figure 30.

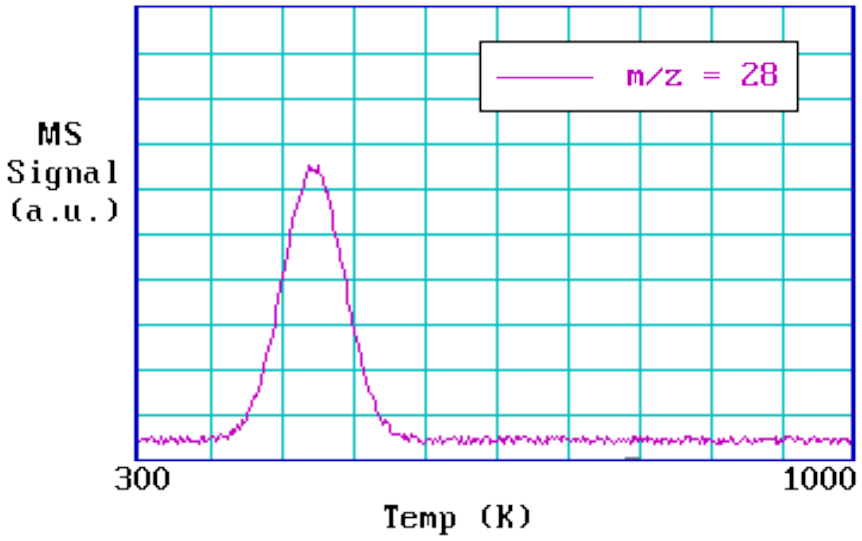

Figure 30. Typical data representation of single-component TPD experiment with CO.[78]

The area under the peak at ~475K in Figure 30 is proportional to the amount originally sorbed to the sample. In the case of full charging, it represents the capacity of the material. Kinetics information is obtained from the contour of the spectroscopic peak and knowledge of the relationship between temperature and time based on the computer program. Lastly, the temperature associated with the peak is related to the reaction enthalpy of hydrogen-substrate desorption. Unfortunately, TPD measurements can only be done at vacuum due to limitations in analytical equipment, effectively limiting the amount of thermodynamic information that can be collected. Quantitative analysis requires accurate calibration of the mass spectrometer against known flow rates. It is also important to understand that TPD or any dynamic type measurement of measurement gives results that are a convolution of both thermodynamic and kinetic properties of the hydrogen storage material. This may lead to miss-interpretation of the results. For example, does a decrease in desorption temperature of a material that is modified through the addition of a dopant mean that the thermodynamics of the host material has been altered? Or, is the dopant acting as a catalyst, or a thermal conductor, or modified the materials morphology such that kinetics are improved, increasing desorption rates at lower temperatures? For the development of new (reversible) materials it is important to have information on both the dynamic and equilibrium hydrogen sorption behavior of the storage material.

5.7 Differential Scanning Calorimetry Method [79]

Differential Scanning Calorimetry (DSC) is a thermal analysis technique used to investigate the thermodynamic properties of a material by measuring the energy necessary to maintain a sample material and an inert reference material at the same temperature over a range of temperatures. The relative heat flow to the sample material as a function of temperature can be used to determine thermodynamic properties such as specific heat and enthalpy.

Temperature variation in DSC is controlled by a computer and is typically linear in order to simplify calculation, although nonlinear temperature variation can be used as well. The specific heat at constant pressure C_p of a sample material (on a per mass unit basis) as a function of temperature is determined by the equation:

Equation 11

$$c_p(T) = \left(\frac{\partial h}{\partial T}\right)_p = \frac{q(T)}{\frac{dT}{dt}(T)}$$

where T is temperature, h is energy, q is heat flow and t is time. The heat flow can be taken from the data and the temporal temperature variation is based on the computer program controlling the experiment. In this way, the specific heat as a function temperature can be determined. Furthermore, the enthalpies of reactions can be determined from the measurement. For example, the enthalpy of crystallization is calculated by integrating the specific heat capacity determined from Equation 9 between the temperatures at which the heat flow varies ($T_{c,1}$ and $T_{c,2}$).

Equation 12

$$\Delta H_{crys} = \int_{T_{c,1}}^{T_{c,2}} c_p(T)dT$$

The two most commonly used methods for conducting DSC measurements are power-compensation DSC and heat-flux DSC. In the power-compensation method, the sample and reference material are placed in independent, identical furnaces. The furnaces are maintained at the same temperature over a variety of temperatures by varying the power input. The power input and temperature data are used to construct the DSC diagram. The indirect and direct variables in power-compensation DSC are flipped in heat-flux DSC. The sample and the reference material are placed in one furnace and exposed to the same heat flux. The variation in temperature between the sample and reference is used to determine the relationship between heat flux and temperature.

In the context of hydrogen storage, Differential Scanning Calorimetry is primarily used for desorption testing because DSC equipment is not typically designed to handle the

high pressures required for sorption with some exceptions. The advantage of DSC over other methods is that other thermal events such as melting or crystal structure changes may be observed. A significant limitation for testing hydrogen storage using DSC is that there is no way to determine the amount of hydrogen desorbed by a sample, only the total enthalpy of a given reaction. For instance, DSC alone would be unable to distinguish between materials that desorb 0.1 mol H_2 with an enthalpy of reaction of 30 kJ/mol H2 from one that desorbs 1 mol H_2 with an enthalpy of reaction of 3 kJ/mol H2. It is important to have an understanding of the enthalpy of reaction per mol hydrogen in order to compare thermodynamics across materials. This vital consideration for hydrogen storage should not be overlooked but can be remedied by coupling DSC with quantitative measurements of hydrogen uptake and release.

5.8 Differential Thermal Analysis Method

Differential thermal analysis (or DTA) is a thermoanalytical technique, similar to differential scanning calorimetry.[80] In DTA, the material under study and an inert reference are made to undergo identical thermal cycles, while recording any temperature difference between sample and reference. This differential temperature is then plotted against time, or against temperature (DTA curve or thermogram). Changes in the sample, either exothermic or endothermic, can be detected relative to the inert reference. Thus, a DTA curve provides data on the transformations that have occurred, such as glass transitions, crystallization, melting and sublimation. The area under a DTA peak is the enthalpy change and is not affected by the heat capacity of the sample.

A DTA consists of a sample holder comprising thermocouples, sample containers and a ceramic or metallic block; a furnace; a temperature controller; and a recording system. The key feature is the existence of two thermocouples. One thermocouple is placed in an inert material such as Al_2O_3, while the other is placed in a sample of the material under study. As the temperature is increased, there will be a difference in the temperatures (voltages) of the two thermocouples if the sample is undergoing a phase transition. This occurs because the input of heat will raise the temperature of the inert substance, but be incorporated as latent heat in the material changing phase.

Today most commercial instruments are no longer true DTA devices but rather have incorporated this technology into a Thermogravimetric analysis equipment (TGA), which provides both mass loss and thermal information. Even these instruments are being replaced by true TGA-DSC instruments that can provide the temperature and heat flow of the sample, simultaneously with mass loss.

5.9 TGA/Calorimetry Vital Measurement Practices:

- Crucibles should be clean and free of contaminants prior to performing experiments
- Thermally pre-treating crucibles over the experiment temperature range is good practice to eliminate unwanted signals during the experiments
- Be mindful of alloying or corrosive reactions with crucibles
- Be aware that the crucibles may act as a catalyst for unwanted side reactions
- Ensure that there is maximum contact between the sample-crucible and the crucible-sensor pan
- When using a crucible more than once in a series of experiments it must be replaced in exactly the same position (especially critical for heat capacity measurements using a reference). In general, it is good practice to place the crucibles in the exact position, regardless of whether or not the experiment is part of a series.
- Be aware that physically altering the sample (e.g., grinding, etc.) may introduce differing thermal events as compared to the unadulterated sample. In kinetic analyses, the crystal form, shape and size may be important. In contrast, there are cases where smaller particle sizes are advantageous.
- Be aware of the temperature and pressure limits, and chemical compatibility with crucibles. For example aluminum crucibles should never exceed its melting point of 600°C. To be on the safe side, the upper temperature limit probably should not exceed 500°C.
- Be fully aware of the possible reaction products (i.e., toxic, corrosive, flammable, etc.)
- Document and use the same crucible cleaning procedures every time. There may be different cleaning procedures for the different types of crucibles.
- Be mindful of the pressure limits of the sealed crucibles. A way to estimate the amount of evolved gases when the possible reactions are unknown is to perform TGA and measure the mass loss. The mass loss is then converted to the number of moles of gases per mass of the sample. The pressure can then be back calculated to ensure the pressure limits of the crucible are not exceeded.

- Examine the thermal analysis curves before undergoing a rigorous detailed analysis. Spurious thermal/mass events are often the result of crucible movement, bubbling, foaming, etc.
- Be aware of the effects of heating rate on the observed signal due to thermal lag. Thermal lag arises because of large heating rates (typically >30°C/min) coupled with large sample masses.
- Be aware of the significant effects of the composition and flow rates of the carrier gas on the mass and thermal signals. For example the mass signal is affected because of the buoyancy effects incurred resulting from the type and flow rate of the purge gas. The heat flow or temperature signals are also affected by the nature and flow rate of purge gas, in this case the thermal conductivity and heat capacity of the gas results in differing thermal analysis curves.
- It is imperative to perform a comprehensive calibration followed by periodic checks on all analytical instruments. If upon periodic checks the calibration is off, then a full comprehensive calibration is then required. Preliminary experiments should aim to answer the following the questions:
- How reproducible is the instrument signal when a sample crucible is removed and subsequently replaced in the apparatus?
- How reproducible is the instrument signal when the same crucible is removed and subsequently replaced in the apparatus with different operators?
- How sensitive is the instrument signal to crucible placement and crucible type?
- How sensitive is the instrument signal as a function of purge/gas type and flow rate?
- How sensitive is the instrument signal as a function of samples mass with respect to thermal lag?
- How sensitive is the instrument signal as a function of temperature?
- How reproducible is the instrument signal as a function of operator?
- Regularly perform calibration runs. In particular for TGA calibrations contain information on thermal and mass changes (e.g., buoyancy corrections) associated with the instrument and specific operating conditions.

5.10 Important Consideration: Gas Composition

All testing methods (with the possible exception of TPD spectroscopy) rely on the assumption that the change in the direct variable used for correlation during desorption is due to hydrogen gas alone. Unfortunately, this assumption is not always valid. During desorption, it is possible to evolve gases other than hydrogen by chemical reaction of the sample material itself. These evolved gases can affect pressure and weight measurements and can contaminate experimental data.

Unless the gas evolution properties of the material are well established, for many materials it may be highly incorrect to assume that the change in the [directly measured] correlation variable, such as weight or equilibrium pressure, is due entirely to hydrogen. In particular, this can produce seriously misleading results in making hydrogen storage measurements during desorption. In addition, impurities (water, oxygen…) in the hydrogen gas stream used to charge a sample may be gettered out of the hydrogen, causing a significant weight change that may be misinterpreted as hydrogen absorption. In terms of hydrogen absorption capacity measurement this contaminated gas problem is much more significant for gravimetric measurements than volumetric measurements because of the ratio of the quantity of gas to sample size and the fact that sample weight change is being equated to hydrogen content. In volumetric measurements the pressure change due to sorption of ppm level impurities would be minimal, if even measureable. Whenever possible we recommend using a secondary technique, such as mass spectrometry, to validate weight loss or gain measurements in gravimetric systems. Volumetric measurements should likewise be tested for evolution of gases other than H_2 which can lead to capacity loss or possibly decreased kinetics with cycling (e.g. nitrogen loss in amides) or detrimentally affect fuel cell catalysts (evolution of ammonia from amides).

One way to account for non-hydrogen gases is to use a mass spectrometer to determine the composition of the desorbed gas. The mass spectrometer is connected to the outlet line of the sample holder and tests a representative sample of the evolved gas, outputting the relative composition of the individual species via their partial pressures. One caveat when using mass spectrometers is the production of a virtual H_2O signal. Water and air are often present in the background spectrum, especially in the absence of a complete bake-out of the experimental equipment. However, depending on the state of the mass spectrometer being used, the filament itself can be partially oxidized and when testing H_2 for impurities, the H_2 can reduce the filament to create water. Although the mass spectrometer registers the water, it may not necessarily be coming from the material.

In some alanate-amide mixtures, the gas evolved from a sample during desorption is not all hydrogen. Trace amounts of ammonia can be found as well, as shown in Figure 28.

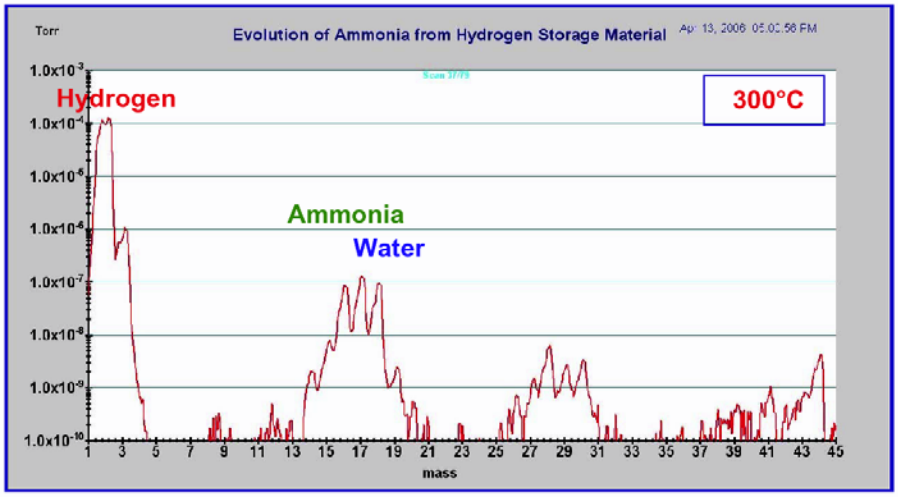

Figure 31. Residual gas analysis of alanate-amide sample discussed in the Kinetics section.[57]

Water is a common background contaminant, but is also found as a contaminant of hydrogen storage materials, generally due to adsorption from air due to improper sample handling prior to testing. The presence of ammonia is much more interesting in this case. Under elevated temperature, the alanate-amide mixture reacted to measureable amounts of ammonia as well as hydrogen, although the exact mechanism for the reaction is unclear. This type of unexpected gas evolution shows a critical need to apply other analysis to validate the gas composition assumption inherent in the testing methods. Simultaneous measurement of gas composition and (inferred) concentration is highly preferred until it can be assured that co-evolution of other species does not occur from the particular material. Gas phase infrared spectroscopy of polyatomic gases such as ammonia, water, carbon dioxide, carbon monoxide, etc, is a particularly powerful tool to complement mass spectrometry.

5.11 Important Calibration Consideration: Helium Adsorption

5.11.1 Background For The Issue Of Helium Adsorption

In both the volumetric and gravimetric capacity measurement techniques, it is usually necessary to calibrate the apparatus with the sample present and using a non-adsorbing gas to subsequently determine the Gibbsian excess hydrogen adsorption. In the volumetric case, the calibration determines the free space in the sample container; in the gravimetric, it is used to determine the skeletal volume of the sample so that buoyancy effects can be accounted for. Almost universally, helium is the gas of choice for these calibrations with its small size and ability to penetrate tiny pores and it is very

weakly interacting so that adsorption effects are minimized. It is especially suited in hydrogen sorption experiments because of hydrogen's correspondingly small size and they share a similar thermal conductivity which is important in measurements where the apparatus is non-isothermal. The critical assumption made during these calibration procedures is that helium is not adsorbed onto the sample. What are the consequences when this assumption fails and what procedures exist to compensate for this failure? This section discusses just this topic and it should be noted that Sircar has addressed this issue extensively for the case of an ideal gas[81,82,83] and that other authors have also investigated this issue.[84,85,86]

As a starting point in the discussion we ask: Under what circumstances will the non-adsorption assumption most likely fail? As we expect the helium atom to only interact with the surface atoms of the sample, samples with high specific surface areas will be the most problematic. This is further borne out by realizing that the intent for the volumetric and gravimetric calibrations is to effectively measure the skeletal density of the sample and that samples with a high surface-area-to-volume ratio will most likely be susceptible to errors introduced by helium adsorption. Additionally as the temperature of the sample and helium gas decreases, the relative influence of any helium-sample interaction will increase. Thus high-surface-area samples at low temperatures will have the largest helium adsorption effects. Still, this is a relative statement and it is found that there are significant effects for high-surface-area samples even at room temperature.

What influence does helium adsorption have on the instrument calibration? For the volumetric or "free space" calibration, the adsorption of helium reduces the pressure and results in the free-space volume being calculated larger than it actually is. When this calculated volume is then used to determine the hydrogen adsorption, the adsorption is underestimated. So ignoring the helium adsorption effects will underestimate the hydrogen adsorption but it will still yield a lower-bound estimate for the Gibbsian-excess hydrogen adsorption on the sample. Similarly, it can be shown for the gravimetric measurement that ignoring any helium adsorption during the calibration also results in underestimating the hydrogen adsorption and again produces a lower-bound estimate.[82]

Sircar[82,83] treated the case where the helium adsorption follows Henry's law:

Equation 13

$$n_{He} = m_s \quad K_{He}(T) \quad P_{He}$$

where n_{He} is the number of helium moles adsorbed, m_s is the mass of the sample, $K_{He}(T)$ is the temperature-dependent Henry's Law constant for helium on a particular sample type and P_{He} is the helium pressure. This is the "worst-case" scenario for not detecting helium adsorption and its interference with the calibration because for a given temperature and for an ideal gas, this helium adsorption exactly mimics an effective extra volume and shifts the apparent volumetric free-space calibration to a higher value. In other words, performing the calibration measurements as a function of pressure alone will not reveal the occurrence of helium adsorption.

If Henry's law is modified so that it is proportional to the helium density, ρ_{He}, instead of the pressure:

Equation 14

$$n_{He} = m_s \quad \overline{K}_{He}(T) \quad \rho_{He}$$

then the situation is identical except that the constraint of gas ideality is relaxed. In fact, the effective extra volume is the sample mass times the modified Henry's law constant, $m_s \overline{K}_{He}(T)$, as it has the proper units and has been shown as such.[82,83] The modified law is equivalent to the normal law when the gas is ideal, and in general, appears physically plausible as it linearly relates the adsorbed amount on the surface to the number of helium atoms near the surface of the material.

If the helium adsorption does not follow Henry's law (normal or modified), then in principle, one could detect that the helium adsorption was occurring by observing a pressure-dependent calibration result (assuming other causes of such behavior have been eliminated). However, this is not to say that the helium adsorption could be quantitatively determined since any linear (Henry's law) component would be masked as discussed above. Instead, it is anticipated that performing the calibration at various temperatures could reveal both its occurrence and its magnitude under the proper circumstances.[82,84,86] The reasoning behind this is the strong temperature dependence expected for any helium adsorption with it rapidly decreasing with increasing temperature. The most straightforward situation occurs when it is possible to measure the free-space volume (or equivalently the skeletal density) as a function of increasing temperature and observing the measurement reach an asymptotic value.[86] This value is the true value and carries the assumption that negligible helium is adsorbed at the higher temperatures. Additional assumptions needed are: 1) thermal expansion effects are either negligible or compensated for; 2) the sample can reversibly withstand excursions to the elevated temperatures; and 3) the necessary instrumentation, procedures, and calibrations exist to perform such measurements.

5.11.2 Best Practices For The Issue Of Helium Adsorption

These practices follow in no particular order. Any methodology used should be clearly reported with its respective data. It is also assumed that all other possible errors have been minimized through proper experimental protocols, well-calibrated instrumentation and verified data analysis procedures. It is useful to try several of the approaches listed below for comparison and to check for self-consistency.

5.11.2.1 Gibbsian Excess Lower Bound

As stated above, it is possible to assume that no helium adsorption is occurring in conjunction with performing a standard calibration using helium and the sample present (w/S). Then by processing the hydrogen adsorption data using that calibration result, one arrives at a lower-bound estimate for the Gibbsian excess adsorption. Although this is counter to the inclination to report the absolute best numbers possible, it provides a good solid number. This number will most likely be the highest adsorption number reported that simultaneously maintains a high degree of confidence. As many researchers may not be aware of the helium adsorption issue, the corresponding values reported in the literature may actually be this value *de facto*. This is a good reason why the methodology used to treat helium adsorption be explicitly described when reporting Gibbsian excess values.

5.11.2.2 Engineering Excess

It is possible to measure the free space or buoyancy with helium and with no sample (n/S) present to determine the empty volume (volumetric) or empty buoyancy (gravimetric) of the sample holder. If this empty value is then subsequently used for the calculations of hydrogen adsorption obtained with the sample present, a firm estimate of the engineering excess is obtained. This calculation is useful in answering the question on whether an empty pressure vessel is better at storing hydrogen than one filled with the material being tested. As the engineering excess values are lower than the Gibbsian excess lower bound, these numbers tend to be reported only when this particular question is being addressed. Still, it offers two advantages: 1) it is easy to measure the empty calibration with a high degree of confidence, and 2) in principle, this calibration measurement only needs to be performed once and can be used indefinitely as long as it can be proven that the sample vessel volume or buoyancy is constant over time and under repeated sample loadings and multiple instrument mountings.

5.11.2.3 Independent Skeletal Density

Direct knowledge of the sample's skeletal density coupled with the sample's mass and a n/S calibration will theoretically allow one to arrive at the true Gibbsian excess adsorption value. This is done by using the sample mass and skeletal density estimate to calculate the sample volume and then using that information to adjust the empty-sample-vessel calibration value. Unfortunately, the skeletal density is usually determined by helium pycnometry so the helium adsorption issue remains. However by using an independent measurement, such as apparent skeletal density versus temperature, it may be possible to obtain a good estimate of the true skeletal density. Furthermore, there may exist upper- and lower-bound estimates for the skeletal density and these could then be used to determine upper- and lower-bound estimates for the Gibbsian excess adsorption. These estimates should be compared to the one obtained from the Gibbsian excess lower bound discussed above.

5.11.2.4 Independent Helium Adsorption

Independent knowledge of the sample's helium adsorption properties allows corrections to be made to the w/S calibration. If the sample follows a modified Henry's law, the correction consists of subtracting the effective volume, $m_s \overline{K}_{He}(T)$, from the free space calibration volume for the volumetric case or by adding this volume to the sample volume for buoyancy correction. As the Henry's law constants are largely unknown for the wide range of new and novel materials being tested for hydrogen storage properties, having some predictor to estimate the Henry's law constant would be valuable. One possible predictor is to correlate the Henry's law constant with the surface area as measured by nitrogen BET.[85] In this way, a rough estimate of the Henry's law correction is made, as these materials are often tested for their surface area. It should be noted however that the BET-Henry's law correlation has a fair degree of scatter and should only be used as an estimate.

5.11.2.5 Recommendation for Low Temperature

The adsorption of helium onto the sample will drastically increase as the temperature is lowered. Rather than attempting to perform a w/S calibration at low temperatures and then correct for the helium adsorption, it is recommended to perform any w/S calibrations near or above ambient temperatures only. A low temperature calibration is still required to measure the volume at low temperature, but an empty sample holder can be used for that purpose. The sample volume measured at high temperatures can then be used to correct for the low-temperature volume to estimate the volume with the sample present. It is much easier to correct for the other weaker temperature effects in the sample (e.g., volume contraction) than to correct for the helium adsorption effects which has a much-stronger Arrhenius dependence with temperature.[56,87]

5.12 Reporting Measurement Results:

In order to collect high quality pertinent data from any experimental work, best practices require: 1) a good understanding of the principles of the measurement technique, 2) extreme care in performing the measurements with a focus on attention to details and a certain cautious skepticism of unusual results, 3) a solid knowledge of how to process and analyze the data, and 4) an appreciation of inherent limitations of the methods and data analysis.

Some guidance for reporting results of hydrogen storage materials have been suggested in recent publications.[4,88,89] The following are this document's recommended ***Best Practices for reporting experimental results***. The items listed below may not be the complete set of reporting requirements for all experimental work, but they are a good basis set. The purpose of these recommendations is to allow the scientific community to reproduce your results, exactly. **Data cannot be considered valid data if it cannot be reproduced independently.** Any variable or condition that can affect the results should be reported.

When in doubt, report it.

Sample Properties

- Identify all samples used in the experiment.
- Identify the source and purity of sample:
    - If vendor supplied, or
    - If prepared in-house.
- Document the synthesis method and sample purity (XRD, NMR, etc.).
- Document CAS number, Lot #, Batch #, etc.
- Document sample history, e.g.
- Indicate whether the sample was used as-received from vendor or was the sample treated (thermally, chemically, physically, etc.,) prior to running experiment. This includes activation of the sample under hydrogen, or degassing the sample. Include a full description of the conditions of these pre-treatment processes.
- Indicate the physical properties of the sample, e.g.:
    - Porosity, surface area, particle size, etc.

Experimental Conditions

- State the analytical equipment used (manufacturer, model #, etc.)
- Document the sample conditions: e.g. temperature program (thermal treatment) performed in the experiment (e.g., dwell times for isothermal steps, heating rates, initial and final temperatures).
- State precisely the sample atmosphere (environment) during the experiment (e.g., flow rates, purity, composition, pressure, etc.). Include the purity of hydrogen gas supply, any filtration, or purification.
- State precisely the type of sample holder or crucible used:
    - Dimensions and volume,
    - Composition (e.g., platinum, alumina, stainless steel, etc.,),
    - Type of sample holder or crucible (e.g., closed (sealed) or open),
    - Indicate pressure rating of closed/sealed crucible.
- Sample mass (indicate accuracy of balance).
- Indicate the long term stability of the balance for gravimetric measurements.
- For most measurements, but in particular gravimetric measurements it is valuable to report the total duration time of the measurement.
- Know the accuracy and precision of the measuring devices (thermocouples, pressure transducers, gravimetric balance, mass flow controller, volumes, spectrometer, etc.). Be sure to report the accuracy, baseline drift, precision, detection limits, etc., of the instruments used.
- Report the temperature stability of the instrument and sample.
- For volumetric measurement equipment, report the various dosing and sample holder volumes. Include the gas displacement volume of the sample and how it was derived.
- Reporting the leak rate of the instrument is important for volumetric measurements as the capacity is determined from measured changes in pressure. It is equally important to know and report leak rates for other experimental apparatus (gravimetric…) because positive pressure leaks may cause instability in the measurement and air leaks with the sample under vacuum may contaminate the sample.

- In the same regard, the type of vacuum pump and base pressure (on the sample) should also be reported when used.
- In addition, it is helpful to indicate the cleaning method, the loading method and the loading environment (e.g., argon filled glove box).

Data Acquisition

- Perform and report regular calibrations of equipment.
- Perform and report validation of experimental equipment by running standard or bench-mark samples. The best practice is to perform a validation experiment before every critical experiment. Validation samples should be appropriate for the instrument (see the manufacture's guidelines) and representative of the experimental conditions (Temperature, Pressure…) that will be used in the subsequent measurements.
- Describe in detail the calibration methods employed (indicate the composition, purity and temperature or mass range for all calibration standards employed).
- For volumetric measurements, the method used to determine the dead volume of the sample should be reported (instrument, inert gas type, temperature of the sample…).
- For gravimetric measurements, the buoyancy effect corrections applied to the data should be reported including any assumptions or measurements made in determining the sample's gas displacement volume.
- State the data sampling rate.
- State the time to reach equilibration, or the method used to determine the duration of a dose when doing equilibrium (e.g. PCT) measurements.
- State the method used to determine gas compressibility factors (important for both volumetric and gravimetric measurements and critical at high pressures or low temperatures).
- Describe the method used to compensate for variations in gas density with temperatures gradients. This effects both the bulk gas density corrections to capacity determination in volumetric measurements and the buoyancy corrections in gravimetric measurements.
- State exactly the type (and units) of capacity being reported. For physisorption experiments, state whether capacity being reported is "excess" or "absolute" capacity and, if "absolute" what assumptions were made in calculating the capacity.

- State the software used for data collection (LabView, Calisto, etc.).
- Indicate all signal conditioning/smoothing transforms.
- Report data regression/manipulation.
- Clearly state the equations used for calculation of sought after data (e.g., heat capacity, heats of reaction, etc.).
- State clearly the assumptions made during data regression (e.g., ideal gas behavior, $C_p(solid) \approx C_V(solid)$, etc.).
- Perform and indicate the statistical analyses on collected data and on the calibration standards (don't think your data is good, but rather know how good your data is!).

Results

- Quote errors and/or standard deviations.
- Do not report values to an unjustified number of decimal places (to how many figures is the value significant to?).
- Produce graphs that clearly present the results with an attempt to identify all thermal and/or mass change events.
- Make attempts to correlate chemical and/or physical transformations with observed thermal, pressure, and/or mass change events.
- Make sure results and the conclusions agree.

6 Summary

It is our intent that this overview of fundamental processes and measurement considerations will aid research and development of new and better hydrogen storage materials. In particular we hope to have clarified some of the recommended practices and caveats in performing high-quality experiments to measure the hydrogen storage properties of advanced materials.

Section 2: Kinetics Measurements

Measurement of hydrogen sorption and desorption kinetics is important for practical hydrogen storage system performance, advanced materials development and fundamental research on the mechanisms of hydrogen uptake and release.

In this chapter we will provide an overview of the purpose of kinetics measurements, introduce some modeling of mechanisms, discuss important considerations that affect kinetics measurements, and present some methods to improve kinetics.

The proper characterization of hydrogen storage properties is one of the most crucial and time-consuming steps on the road to the discovery and development of advanced and practical materials. Because of this, it is important that measurements, including kinetics measurements, are informative, reliable and consistent with accepted standards. The intent of this chapter is to describe some common practices accepted in the field of hydrogen storage and to highlight important considerations both positive and negative that can have a strong impact on kinetics measurements.

1 Introduction and Definitions

As an introduction, we will briefly review definitions in chemical kinetics in general and then discuss kinetics as it pertains to hydrogen storage materials.

1.1 Chemical Kinetics

The following description of kinetics involves excerpts from general textbooks on the topic. This is intended only as a general introduction to the field. For a more detailed discussion, please see the references at the end of this document.

> "Kinetics deals with the speed or rate at which reactions proceed and the rate of reaction are defined simply as the rate of change of concentration for reactants and products… The rate of a chemical reaction depends on several factors in addition to reactant concentration. In some cases the rate is influenced by the products, substances such as catalysts, or even chemically inert species. Of greater general importance is the fact that in almost all cases the rate varies with temperature, often very considerably.[16]

The following factors affect reaction rates:

1.1.1 Nature of the Reactants

"Depending upon what substances are reacting, the reaction rate varies. Acid reactions, the formation of salts, and ion exchange are fast reactions. When covalent bond formation takes place between the molecules and when large molecules are formed, the reactions tend to be very slow."[90]

1.1.2 Heterogeneous vs. Homogeneous Reactions

The physical state (i.e. solid, liquid, gas) of the reactants is also important. If the state of all of the reactants is the same, they will mix and the result will be a homogeneous reaction. If the reactants are of different phases or for some reason cannot mix, then the reaction is heterogeneous and limited only to the interface between the reactants. Heterogeneous reaction rates therefore scale with surface area. [15]

1.1.3 Concentration

"Concentration plays an important role in reactions. According to the collision theory of chemical reactions, this is because molecules must collide in order to react together. As the concentration of the reactants increases, the frequency of the molecules colliding increases, striking each other more often by being in closer contact at any given point in time. Imagine two reactants in a closed container. All the molecules contained within are colliding constantly. By increasing the amount of one or more of the reactants you cause these collisions to happen more often, increasing the reaction rate."[90] An equation that describes the relationship between the rate of reaction and the concentration of all species in the reactor is called a rate equation and is presented in detail in section 2.2.2 .

1.1.4 Temperature

"Temperature usually has a major effect on the speed of a reaction. Molecules at a higher temperature have more thermal energy. When reactants in a chemical reaction are heated, the more energetic atoms or molecules have a greater probability of colliding with one another. Thus, more collisions occur at a higher temperature, yielding more product in a chemical reaction. More importantly however, is the fact that at higher temperatures molecules have more vibrational energy; that is, atoms are vibrating much more violently, so raising the temperature not only increases the number of collisions but also collisions that can result in rearrangement of atoms within the reactant molecules." [90] Temperature has a profound effect on reaction rates, most often described by the Arrhenius equation. This is presented in detail in section 2.2.1 of this chapter.

1.1.5 Catalysts

A catalyst is a substance that increases the rate of a reaction without modifying the overall standard Gibbs energy change in the reaction… this definition is equivalent to the statement that the catalyst does not enter into the overall reaction; it is both a reactant and a product of the reaction.[26] A catalyst increases the rate reaction by providing a lower energy pathway from reactants to products (Figure 32).

"Ostwald defined a catalyst as 'a substance one adds to a chemical reaction to speed up the reaction without the catalyst undergoing a chemical change itself.' …this definition is not quite accurate. Catalysts do undergo chemical changes during the course of reaction. It is just that the changes are reversible, so that the catalyst is not consumed as the reaction proceeds. Example of catalysts include the acids in your stomach that you use to break down food, and the enzymes that people put in detergents to make the detergent work better. Most chemical processes use catalysts at some stage in the production process.

…One of the key features of catalysts is that they change the form of the rate equation. In the gas phase, rates of reactions are often proportional to the reactant concentrations to some simple powers. However, catalytic reactions follow much more complex rate equations. It is common for the rate of a catalytic reaction to be constant or even go down as the concentration of one of the reactants increases. This is quite different from gas-phase reactions, where rates generally increase with increasing reactant pressure.[15]

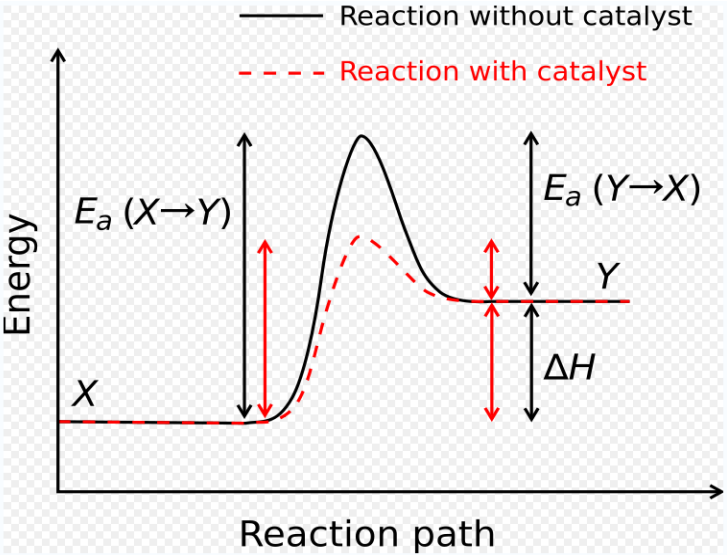

Figure 32. Generic potential energy diagram showing the effect of a catalyst in a hypothetical endothermic chemical reaction. The presence of the catalyst opens a lower energy reaction pathway (shown in red) with a lower activation energy. The final result is an increase in the rate of the reaction while the overall thermodynamics remain the same.[90]

1.1.6 Equilibrium

The concept of equilibrium is an important link between thermodynamics and chemical kinetics. Equilibrium does not determine the reaction rate of a system, but rather is defined by the statement "at equilibrium, the rate of any forward chemical reaction… must equal the rate of the reverse chemical reaction." This is most easily represented by the concept of the equilibrium constant.

For example, for the reaction ***A + B ↔ C + D,*** the equilibrium constant is defined as

Equation 15

$$K_{1,2} = \frac{k_1}{k_2} = \frac{[C][D]}{[A][B]}$$

Where k_1 is the rate of the forward reaction, k_2 is the rate of the reverse reaction, and brackets representation concentration. Therefore, if $k_1 = k_2$, the product of the concentration of the products will equal the product of the concentration of the reactants at equilibrium.[15]

"In chemical kinetics, reactions that simultaneously and independently proceed in two directions – the forward and reverse ones – but at different rates, are called opposing, two-way, or reversible. It is characteristic of reversible reactions that in a certain time after they begin the rates of the forward and the reverse reactions become equal and a state of chemical equilibrium sets in.

All chemical reactions are reversible, but in definite conditions some of them can proceed only in one direction up to the practically complete disappearance of the reactants. Such reactions are called irreversible. Usually reactions are irreversible in which at least one product is removed from the sphere of the reaction (when reactions proceed in solutions a product precipitates or evolves in the form of a gas), or which are attended by a great positive heat. When considering ionic reactions, a reaction is practically irreversible if its products include a very poorly soluble or poorly dissociated substance.[91]

While all chemical reactions are reversible, for the purposes of hydrogen storage they may not be because of practical considerations such as limits on achieving conditions of temperature, composition, and/or pressure to achieve reversibility. As described above, reactions may be rendered irreversible when one or more products are removed from the system. For example, precipitation of a solid or evolution of a gas from a homogeneous reaction solution effectively removes a product from the reaction system, causing the reaction to be irreversible. Another example of irreversibility occurs when the reverse reaction becomes thermodynamically highly unfavorable, such as is the case for many highly exothermic forward reactions. To drive such a reaction in reverse, the temperatures or pressures may be unachievable because of experimental or practical limitations, or because of high temperatures leading to decomposition of products and/or reactants.

1.1.7 Free Energy

The concept of Gibbs free energy change, ΔG is "the indicator of spontaneity of a reaction or physical change at constant T and P. If there is a net decrease of useful energy, ΔG is negative and the process is spontaneous." It is defined as:

Equation 16

$$\Delta G = \Delta H - T\Delta S$$

Where ΔH is the change in enthalpy, T is the temperature and ΔS is the change in entropy. The heat of formation, ΔH_f, and the entropy of formation, ΔS_f, are roughly independent of temperature, and therefore can be used to determine the spontaneity of the reaction at various temperatures by inserting them into Equation 16.[92] It is important to note that the Gibbs free energy only determines whether the reaction will occur, but says nothing about the speed of reaction. For that we must rely on kinetics."

1.2 Kinetics in Hydrogen Storage

For hydrogen storage, kinetics is generally taken to mean the rates of hydrogen sorption and desorption from a storage material occur. A primary distinction between capacity and kinetics in reversible systems is that capacity measurements are theoretically taken at thermodynamic equilibrium, independent of the time required to reach equilibrium, while kinetics investigates how the material approaches equilibrium and what influences this approach. The availability of hydrogen in a storage material is dependent on the kinetics of the material under the system operating conditions. While a material might demonstrate high hydrogen storage capacity, the amount of hydrogen practically available may be significantly less depending on the material's intrinsic kinetics versus what the application requires. A number of different intrinsic properties of a storage material may control kinetics including surface interactions, transport phenomena, hydrogen-substrate storage mechanisms and phase change.[93] External factors such as temperature and pressure (in the case or reversible systems) also have a profound effect on hydrogen sorption and desorption kinetics.

In its most simple form, a kinetics experiment provides a useful measure of the rate of hydrogen uptake or release from a storage material. Unfortunately, comparing kinetics data across materials and experimental setups can be complicated. For example, one way to compare kinetics is to consider average rates. A common practice is to define the average kinetic rate as the time to reach 95% of the full capacity. However, as is demonstrated in Figure 33, it is possible to derive the same average sorption rate for materials that, in fact, exhibit very different kinetic character. Thus, it is important not only to compare average rates but also to compare the shape of the kinetic curves. Factors that can influence the experimental rates are discussed in the section on experimental and analysis considerations (Section 3).

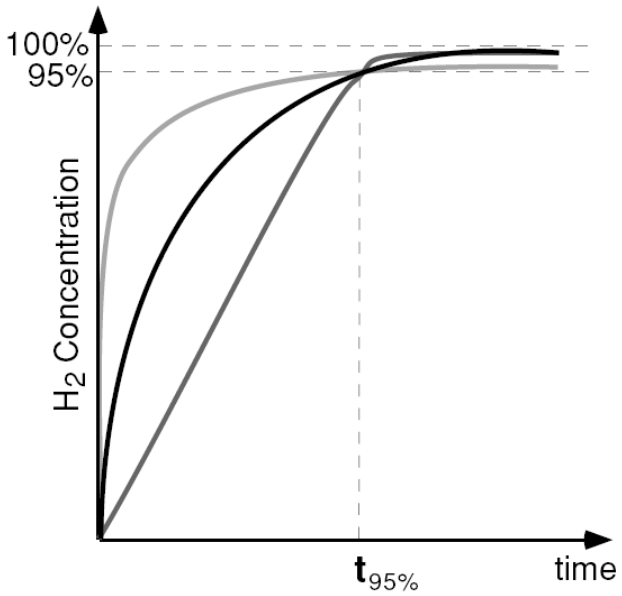

Figure 33. Hypothetical concentration versus time curves showing three different kinetic behaviors that have the same average rate at $t_{95\%}$.

1.3 Impact of Heat Transfer

Kinetics measurements are conducted to quantify the kinetics performance of hydrogen storage materials and identify the potential intrinsic mechanisms controlling hydrogen uptake and release. Identification of the kinetic mechanisms, most specifically the rate-controlling mechanism, is instrumental in developing materials with improved kinetics properties. It is not easy to perform measurements to accurately determine the potential intrinsic rate-controlling mechanism however. Early in hydrogen storage research, intrinsic material properties like surface effects, mass transport and storage mechanisms were generally assumed to be the rate-controlling mechanisms. In reality, heat transfer and other thermal effects dominate rates for nearly all reactions in hydrogen storage systems and measurements.[94]

In taking kinetics measurements, heat transfer (i.e. maintaining as much as possible a constant sample temperature) is the most important effect for which researchers must account. The temperature of sorption/desorption is the most influential variable in hydrogen storage kinetics for both chemisorbing and physisorbing materials. It is imperative that measurements are taken under isothermal conditions in order to minimize the effects of heat transfer and identify the potential intrinsic reaction mechanisms. Isothermal measurements are difficult in systems with poor heat transfer and fast intrinsic kinetics because the heat generated or taken up during hydrogen-substrate interactions can cause local temperature excursions that profoundly affect rates. All too often, rates reported in literature are in fact heat transfer rates because the sorption/desorption process is limited by an experiment's ability to supply or

dissipate energy. Heat transfer-limited kinetics measurements occur primarily because of improper equipment design and errors in experimental protocol. The effect of heat transfer on kinetics measurements is underscored by Dantzer in 1997: with regard to kinetic measurements on hydrogen sorption in $LaNi_5$, before 1983-1985, attempts to interpret data in terms of a microscopic [kinetics] model are questionable since no proof is provided on the isothermal conditions of the experiments.[58] The effects of heat transfer are addressed often to reinforce their importance to the field. Further discussion on steps that can be taken to minimize the effects of heat transfer can be found in the experimental and analysis considerations section 3 of this chapter.

2 Kinetic Theory

This section is designed to familiarize the reader with knowledge of the fundamental mechanisms of hydrogen uptake and release. It will also briefly review the process used to identify rate-limiting mechanisms through mathematical modeling.

Kinetic theory is a complicated and heavily researched field and a complete review of its content is beyond the scope of this work as an introductory document on hydrogen storage properties and testing. Accordingly, the kinetic theory section 2 is restricted to a brief overview. The authors will use references extensively in order to both summarize information and provide the reader with avenues for further inquiry into the subject of kinetic theory.

2.1 Fundamental Mechanisms of Reactions

In order to improve the kinetics properties and performance of potential hydrogen storage materials, it is important to gain a fundamental understanding of the underlying rate-controlling steps. The sorption and desorption of hydrogen by a material involves a number of important steps that occur in series and in parallel. For different sorption and desorption processes as well as for different hydrogen storage materials, the mechanisms controlling these steps differ. In general, there are three broad categories of kinetics mechanisms: surface interactions, mass (hydrogen, potentially the host elements) and energy transport (heat transfer), and bond breaking and bond forming mechanisms. Surface interactions, mass and energy transport and binding mechanisms are considered intrinsic processes. Mass and energy transport also depend on a number of extrinsic considerations including the particle size, packing density, the shape of the sample and sample holder, the thermal contact between the sample and sample holder, and the mobility and pressure of the gas. Any one mechanism of these parameters may be rate controlling, although heat transfer is often rate-controlling in practical application. Moreover, for reversible storage materials, the rate-controlling mechanisms may not necessarily be the same for sorption and desorption. Careful experimental control is required to develop mechanistic understanding of any chemical process.[59]

Sorption and desorption in physisorbing materials (at least) is a two-step process consisting of mass and energy transport and surface interactions/binding mechanisms. Hydrogen is only transported through the void volume of the material and physisorption occurs at the surface of the host material with minimal effect on the structure of the material. In this sense, surface interactions/binding mechanisms can be considered equivalent phenomena in physisorbing material and will be addressed in the physisorption binding mechanisms section below. In chemisorbing media, surface interactions and bulk diffusion present distinct steps in the process of hydrogen storage and one or both may play the key role in hydrogen storage kinetics. The following section on surface interactions will discuss the various surface interactions that affect hydrogen storage kinetics.

2.1.1 Binding Mechanisms

Hydrogen storage mechanisms differ for physisorption media and for storage media where the interaction between hydrogen and the storage material involve bond breaking and bond making between hydrogen and the host. The relative strength of the bonding situations between these two classes of storage greatly influences the kinetics and thermodynamics

2.1.1.1 Storage by Physisorption of H_2 on Surfaces

For physisorption, molecular hydrogen interacts with the surface via weak van der Waals forces and remains in molecular form, H_2. Storage through physisorption is primarily limited to porous and nano-structured materials, where high surface area-to-volume ratios contribute significantly to storage capacity. In these types of materials, the external surface structure dictates the accessibility of the internal pore structure and the internal surface area dictates the degree of physisorption. Hydrogen interactions with the surface can occur through dipole-induced dipole and induced dipole-induced dipole interactions (Figure 34), with heats of adsorption (physisorption) ranging from 4-10 kJ/mol depending on the nature of interaction.[12,95]

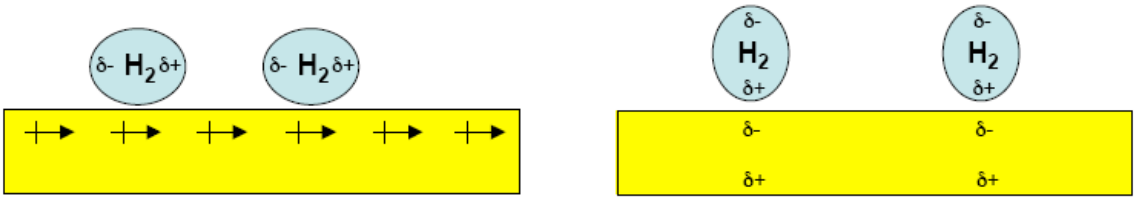

Figure 34. Left: Dipole-induced dipole van der Waals interactions. Right: Induced dipole-induced dipole van der Waals interactions.[95]

In Figure 33 below, the heat of adsorption is shown on the H_2 + M potential energy curve as E_P. Van der Waals forces dominate kinetic forces at low temperatures because molecules have relatively low kinetic energy under these conditions, allowing weak intermolecular forces to bond hydrogen to a substrate.

It should be mentioned that the energy of physisorption is enhanced in small pores owing to the overlap of attractive fields from opposite walls. Therefore, there is considerable interest in the development of porous materials with pore of nanometer dimensions. The extent of adsorption depends on the surface area and the micropore volume. The characterization of samples in terms of surface area is subject to controversy, especially for microporous materials. On these materials, the surface measured will depend on the size of the probe molecules, the model use (BET or Langmuir), the extent of micropores filling etc.

2.1.1.2 Storage of Hydrogen by Forming Hydrides

The dissociation of hydrogen and the subsequent bond formation to yield bulk hydrides or interstitial metal hydrides provides the basis for a substantial number of hydrogen storage materials. Depending on the type of hydride bond formed, hydrides may be classified as ionic, metallic(interstitial?) or covalent hydrides. A thorough review of the chemistry of hydrides can be found in the book “Hydrides” by Wiberg and Amberger and in particular on metal hydrides in the book “Metal Hydrides” edited by Muller, Blackledge, and Libowitz.[6] The important point is that the kinetics of hydrogen uptake and release may involve many complex steps including adsorption, dissociation, surface diffusion, bulk hydrogen diffusion, hydride formation, reactant diffusion, phase separation, catalysis, etc.

2.1.2 Mass Transport

The kinetics of hydrogen storage in reversible systems is strongly influenced by the mobility of hydrogen and potentially the storage material itself and the transport of energy through the storage media (material and gas). The mobility of hydrogen, reactants, and energy within the storage media involve a wide range of transport properties. For simplicity we have divided the discussion of transport mechanisms into physisorption and hydride storage media.

2.1.2.1 Physisorption

For porous materials, molecular hydrogen easily passes through macroscopic boundaries and is transported through the network of pores to the internal surfaces of the material. Transport through the internal networks is governed by porous media-specific transport laws. Darcy's Law is a well-known momentum transport constitutive equation in porous media that relates the velocity with respect to the porous media ν to the viscosity of the fluid (hydrogen in this case) μ, the diagonal permeability tensor K, and the piezometric pressure, P.[96]

Equation 17

$$\langle v \rangle = -\frac{1}{\mu}\left[\underline{K} \cdot \nabla \langle P \rangle\right]$$

Transport of fluids in porous media is the subject of extensive study and the reader is encouraged to review several books on the subject.[97], [98]

2.1.2.2 Hydrogen Diffusion in Metal Hydrides

For hydrogen mobility in metal hydrides, hydrogen transport in the bulk occurs via atomic diffusion through the interstitial sites of the host metal structure. The dynamics of interstitial motion cover a wide range of time scales, from 10^{14} Hz for vibrational motion to 10^{10} Hz for collective long-range diffusion. The mechanisms controlling local diffusion in metal hydride materials are highly temperature dependent. Values measured for long-range diffusion can vary over 12 orders of magnitude for different samples at different temperatures.[99] In the high-temperature region of practical interest to hydrogen storage research, a classic barrier-hopping model can be used to describe the diffusion of hydrogen through a metal hydride. The temperature dependence of the diffusion rate can be expressed by the relation

Equation 18

$$D = D_0 e^{\frac{-E_A}{k_B T}}$$

where D is the number of successful jumps per unit time, D_0 is the number of vibrations or attempts per unit time, k_B is the Boltzmann constant and E_A is the activation energy. At lower temperatures, quantum tunneling effects of hydrogen atoms become dominant.[100]

2.1.3 The Impact of Surface Interactions on Kinetics

As described above, hydrogen can be stored on the surface (adsorption) and in the bulk (absorption) of metal hydride materials. Hydrogen is weakly bound to the host's surface. For bulk metal hydride formation, only atomic hydrogen can pass through the surface layers and be transported into and out of the bulk. Therefore, the surfaces of metal hydride storage materials must dissociate molecular hydrogen into atomic hydrogen for storage. This is accomplished by the dissociation of H2 via the transfer of electrons to the sample material. Hydrogen dissociation on the surface of a metal hydride is shown in Figure 35. Generally, hydrogen exists as a diatomic molecule before interacting with the surface of the material (left side of the figure), dissociates at the surface into two atomic hydrogen atoms, and diffuses into the bulk of the material (small molecules in the lattice). Doping with metal catalysts is a common technique used to increase the efficiency of hydrogen dissociation at the surface of chemisorbing materials. A considerable number of investigations at the materials development and fundamental mechanism levels seek to maximize the ability of a material to dissociate hydrogen through doping and surface texturing.[101,102]

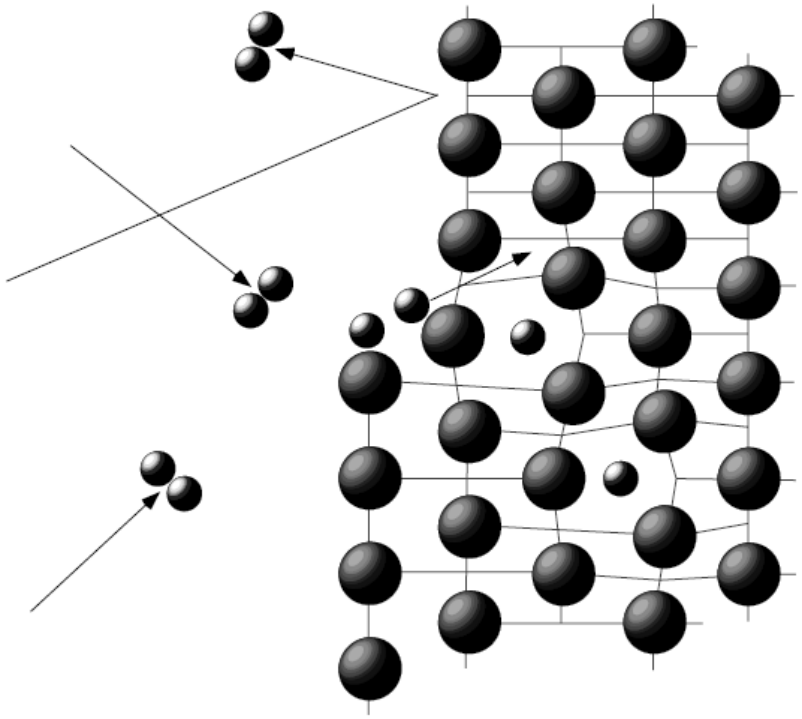

Figure 35. Schematic representation of the interaction of hydrogen with a clean crystalline surface.[60]

The interaction of hydrogen with the surface of a chemisorbing material is complicated by the fact that the surface or interfacial properties of the material may be substantially different than those of the bulk. The crystal structure, electronic, magnetic and dynamic properties, as well as the chemical composition of a material can be dramatically altered near the surface due to the discontinuity of the surface. By definition then, the surface layer consists of the atomic region that shows different properties from those of the bulk. For a clean single crystal, the surface layer is generally no thicker than the first few monolayers. Oxidized, contaminated, or multiphase materials may have a surface layer as thick as 10 nm. From the crystal structure point of view, atoms in the surface layer may relax or reconstruct. Surface relaxation may involve changes in the lattice dimensions and inter-atomic distances in the first few layers. Reconstruction consists of a rearrangement of atoms in the top atomic layers and often results in a loss or change of symmetry. Electronic states are also altered in the surface layer.

Details on the effects of surface contamination on kinetics is discussed in section 2.1.3.2 below.

2.1.3.1 Surface Energetics

Surface energetics governs the dissociative chemisorption of hydrogen in the surface layer. The potential energy of the interaction of gaseous hydrogen with a surface can be depicted using a simple two-dimensional set of potential energy curves (Figure 36). (Complex hydrides do not fit into this simple picture, since the absorption and desorption of hydrogen involve structural phase transitions.) Away from the surface the two curves are separated by the heat of dissociation, E_D = 218 kJ/mol H, which represents the amount of energy required to split H_2 into two hydrogen molecules. The interaction of gaseous hydrogen with the metal to form a stable solid solution or intermetallic is described by following the H_2 + M potential from its minimum (E_P) to its intersection with the 2H + M potential in the surface layer. If the potential energy curves intersect above the zero energy level, positive activation energy E_A is required for hydrogen dissociation; if the curves intersect below zero, dissociation is energetically favorable ($E_{NA} < 0$) and occurs spontaneously. After the curves intersect, dissociation occurs and the potential continues along the 2H + M curve as atomic hydrogen is transported into the bulk. The potential energy of hydrogen in the material reaches a deep minimum on the 2H + M potential (the heat of chemisorption, $E_C \approx$ 50kJ/molH) close to the surface/bulk interface, which dictates that only atomic hydrogen transports through the bulk of metal hydrides.

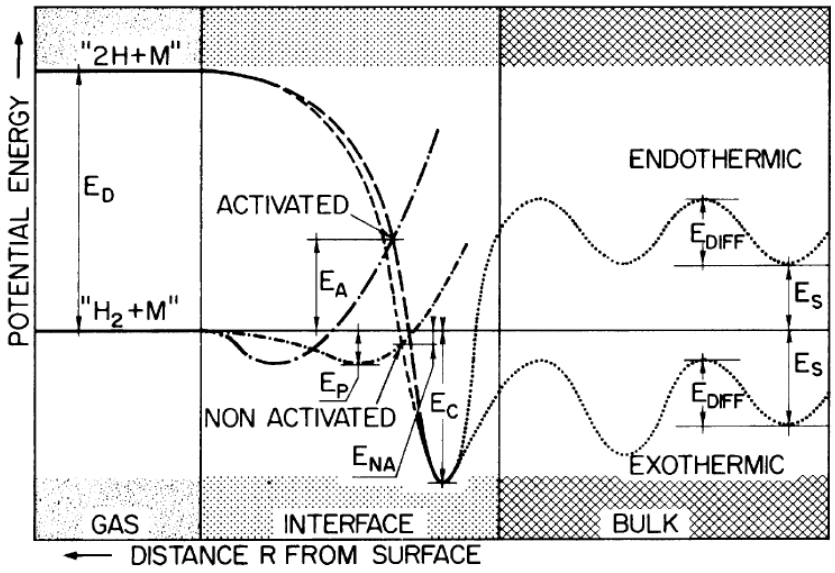

Figure 36. Potential energy curves for activated or non-activated dissociation and chemisorption of hydrogen on a metal surface, followed by the endothermic or exothermic solution of atomic hydrogen into the bulk.[103]

For chemisorption, some surface properties that can limit the overall hydrogen sorption rates (such as E_C and the sticking probability) become concentration dependent as the surface coverage of atomic hydrogen increases. The coverage, in turn, depends on the mobility of atomic hydrogen on the surface and into the bulk. Perhaps most importantly, diffusion from the very stable superficial chemisorption sites (E_C) into the bulk absorption sites (E_S) may be a rate-limiting step and is usually closely linked to surface structure. Thus, kinetics may be influenced by a feedback loop between concentration and surface interactions.

2.1.3.2 Surface Contamination

So far, the interaction of hydrogen with metals has been described by the ideal case of a clean elemental metal surface. Clearly, this model does not describe the real surface environment found on most samples. Elemental metals generally have surfaces that have been passivated by oxygen, thus preventing the dissociation reaction and the diffusion of atomic hydrogen into the bulk (Figure 37).

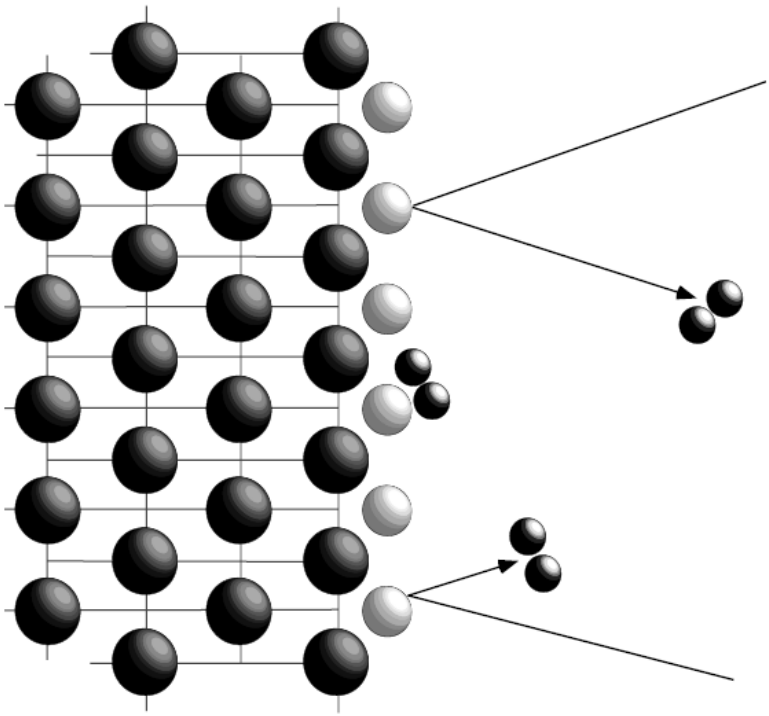

Figure 37. A schematic representation of surface passivation hindering the hydrogen dissociation reaction. Light-colored spheres represent oxygen occluding the surface of the material.[60]

Intermetallic compounds, on the other hand, often show highly reactive surfaces even after exposure to oxygen or other contaminants (H_2O, N_2, CO_2, etc.). This is due to reorganization in the chemical composition of the surface to minimize the surface energy. This form of surface segregation is an intrinsic property of alloys.

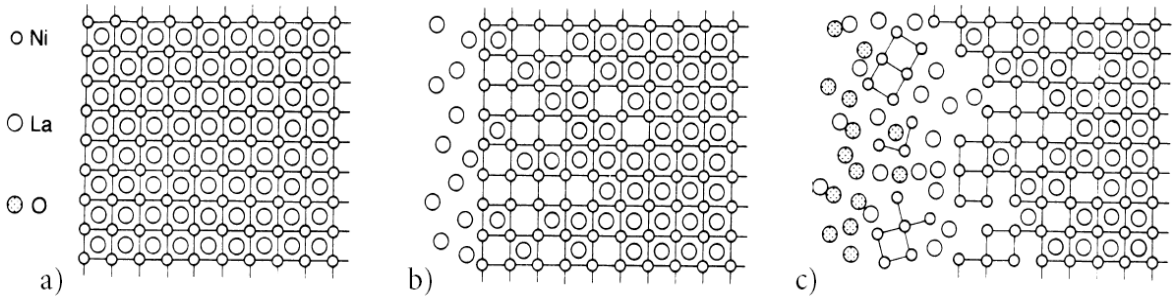

Figure 38. Surface segregation in the $LaNi_5$ system. a) fresh surface, b) surface enrichment of La lowering the surface energy, and c) selective oxidation of La and formation of Ni precipitates at the surface.[104]

Schlapbach et al. showed that surface segregation can be caused by selective oxidation of certain elements in the alloy.[105] In the case of $LaNi_5$, they found that the selective oxidation of La prevents the surface from becoming passivated. Using depth profiling by combining photoelectron spectroscopy and sputtering, they demonstrated that there was a surface enrichment of La, as well as the precipitation of metallic Ni in the subsurface. This suggests that the decomposed surface layer is permeable to molecular hydrogen that may dissociate in the subsurface on active Ni precipitates and on the un-oxidized host alloy (Figure 38). Surface segregation at room temperature has also been observed in many other hydride-forming intermetallic compounds such as ErFe, $ZrMn_2$, $TiMn_2$, $CeRu_2$, and Th_7Fe_3, and at elevated temperatures for the hydrogen storage compounds TiFe and Mg_2Ni.

An active surface does not necessarily guarantee rapid kinetics. TiFe provides a good example. This compound requires activation at high pressures and temperatures to absorb hydrogen. Yet, the detection of HD molecular species created through H_2–D_2 exchange interactions at the surface showed that this compound actually has an active surface even at room temperature. It is thought that the difficult activation is due to bulk diffusion properties.[106]

In practice, there are different ways to overcome the kinetic barriers of oxides and other contaminants on the surface (activating the material or sample). By heating under vacuum oxygen may diffuse from the surface into the bulk, essentially cleaning the surface. By heating under an inert gas flow unstable surface layers may be removed. By heating under hydrogen the oxides may be reduce and removed. Any one of these processes may cause surface segregation and the formation of a mixed surface layer consisting of nano-scale oxide and catalytic metal particles (such as La-oxides and Ni clusters on the surface of $LaNi_5$ as described above).[104]

2.1.3.3 Surface Hydriding

Hydride formation that occurs at the surface of the material can hinder the further transport of hydrogen into the bulk.[107,108] This phenomenon is depicted in Figure 39. When hydrogen dissociates at the superficial layer, it must be transported away from the surface through the first several monolayers of material. If the hydrogen transport properties of the material are poor, the hydrogen and substrate will react to form hydride at the surface. The hydride acts as a barrier to further hydrogen transport into the bulk and can significantly affect kinetic performance. The sorption rate eventually becomes limited by the diffusion of hydrogen through this hydride layer.

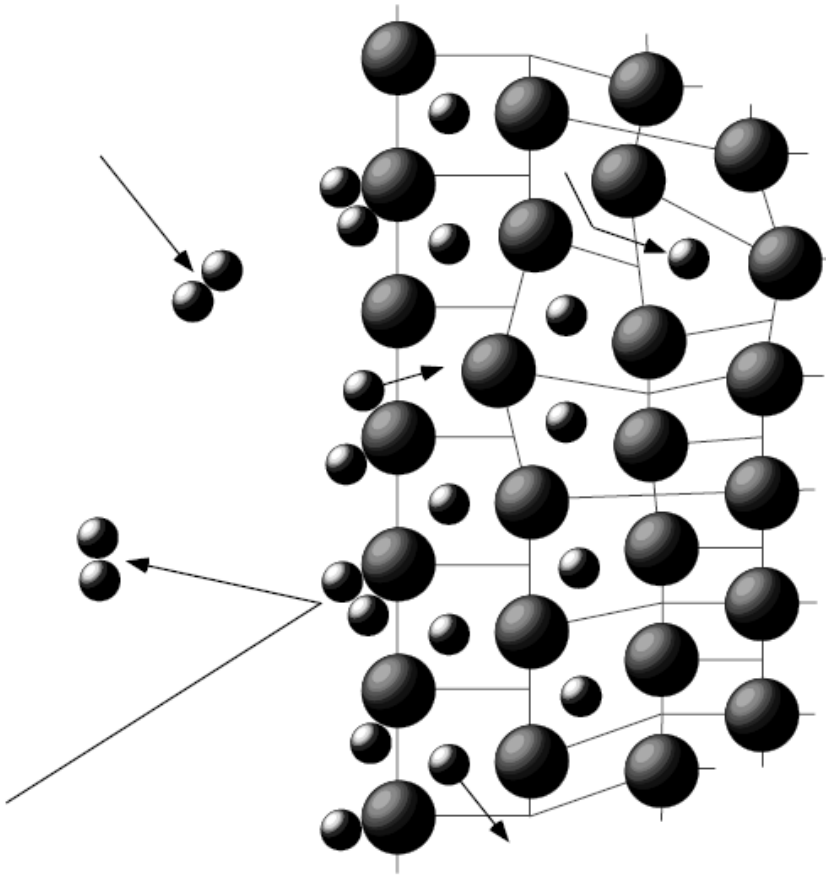

Figure 39. A schematic representation of the formation of a surface hydride which creates a diffusion barrier blocking the transport of atomic hydrogen into the bulk.[60]

2.1.4 Heat Transfer

Because of the exothermic nature of most hydrogen storage materials, heat transfer often plays the most critical role in the kinetics of hydrogen sorption and desorption. This topic was brought out early in this chapter because of the importance of heat transfer on the study of sorption kinetics. Consideration of heat transfer effects on experimental measurements are presented in detail in section 3.10 . At this point it is useful to discuss heat transfer within the context of the materials themselves.

Heat transfer in porous media occurs through the internal pore network and the material itself. Heat transfer performance is generally dictated by the pore size distribution relative to the mean free path of the hydrogen molecule at various temperatures and the structure (e.g. characteristic dimension, linkage) of the skeletal material.[109, 110]

At first glance, heat transfer in chemisorbing materials would seem to be governed by thermal conduction through the storage material itself. However, with few exceptions, hydrogen storage materials are often powders with limited particle-to-particle contact. Thus, heat transfer is generally governed by many of the same principles as porous media. For example, the large lattice expansion that occurs in hydriding metals and intermetallic compounds creates enough internal stress within the crystal lattice and grain boundaries that bulk samples will turn to powders on hydriding. With cycling these powders will break down into smaller and smaller particles. This is referred to as decrepitation. This process itself will change the thermal conductivity of the storage material. Thus, the repeated process of hydrogen sorption and release can have a strong influence on the kinetic behavior of the storage material system with cycling. Heat transfer in other hydrogen storage materials such as alanates and amides as well as nano-materials of any kind may also be affected by mass transport of the reactants and grain growth.

Over the years, a great amount of effort has been put into the design and development of materials and devices optimized for controlling material mobility and heat transfer in hydrogen storage systems.[111]

2.2 Kinetics Modeling

Mathematical models are used to provide insight into the rate controlling mechanisms of a material's hydrogen uptake and release. The model that best fits experimental observation is typically assumed to be the rate-limiting mechanism.

The kinetics modeling section will be structured around models for metal hydrides to illustrate the process of determining sorption mechanisms. Kinetics in metal hydrides can be mathematically modeled by the general relationship

Equation 19

$$\frac{dC}{dt} = K(T)F(C,P)$$

where K(T) is the temperature-dependent rate constant and F(C,P) is a function dependent on the hydrogen concentration in the material C and gas pressure P. A brief introduction will be given on the rate constant K(T) and how it is determined followed by a more in-depth discussion on modeling the hydrogen concentration function.

2.2.1 Temperature Dependence

When kinetics measurements are made at different temperatures, it is generally found that gas sorption and desorption rates are highly dependent on temperature. This is indicated in the temperature dependence of the rate constant K in Equation 20. In 1889, Arrhenius recognized that most chemical reactions occur at rates that increase exponentially with temperature. This empirical observation is valid in hydrides and can be conveniently written as

Equation 20

$$K(T) = Ae^{\frac{-E_A}{k_B T}}$$

where A is the frequency factor, E_A is the activation energy, k_B is the Boltzmann constant and T is the temperature. Note however, that the Arrhenius equation is actually only an approximation and, while it is a good approximation over the temperature range of interest for hydrogen storage, it works best in for temperature of about 50-100 K where the activation energy may be considered temperature independent.[15]

From Equation 20 we find that the activation energy E_A is given by

Equation 21

$$E_A = -k_B T \ln(K)$$

The activation energy of a reaction can be determined by measuring the rate constant K (T) at several different temperatures and then plotting ln(K) versus 1/T. This is known as an Arrhenius plot.

An example of such an Arrhenius plot is shown in Figure 40. This plot presents data for the same La_2Mg_{17} sample given in the example in the following section.[60] The rate constants were determined from a series of absorption measurements at different temperatures using the same pressure-dependent curve fitting approach as in Figure 42. A line was then fit to the Arrhenius data in Figure 40. The activation energy for the hydride formation reaction can be obtained from the slope of this ln(K) versus 1/T plot. The activation energy calculated from these measurements is 63.7 kJ/moleH_2.

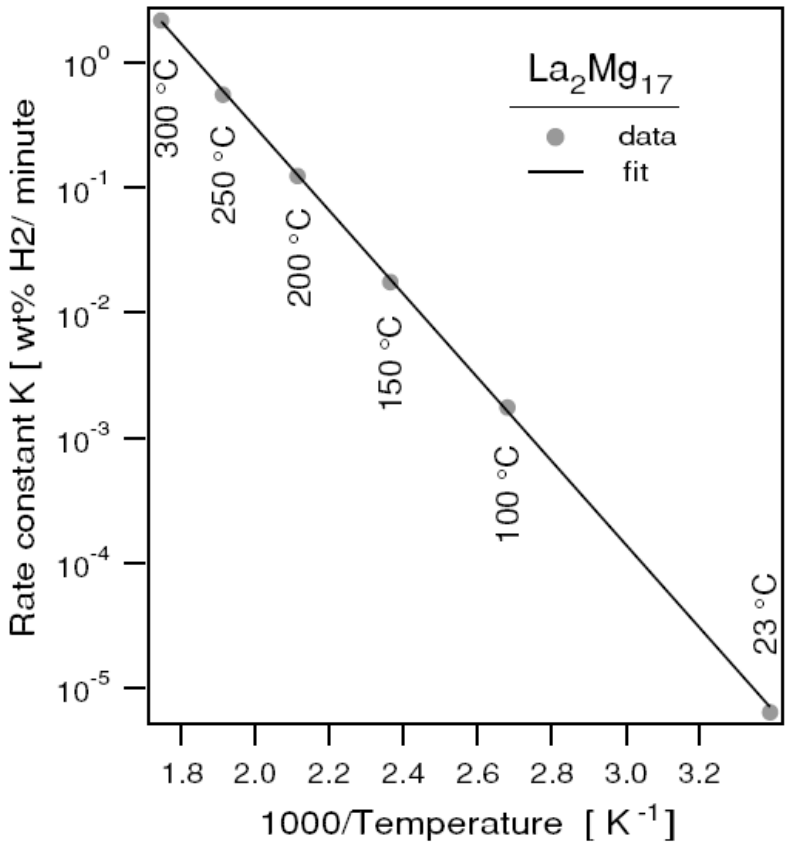

Figure 40. Arrhenius plot of rate coefficients K versus 1/T, for hydrogen absorption by La_2Mg_{17}.[60]

2.2.2 Concentration Dependence

The rate of adsorption and desorption is dependent on the availability of hydrogen in the sample. The hydrogen concentration function is used to model this availability and is often normalized to allow different kinetics measurements to be compared on the same plot. The functional dependence of concentration is modeled non-dimensionally as

Equation 22
$$F(\alpha) = \kappa(t / t_{1/2})$$

where the reacted fraction α is the concentration C normalized by the final concentration C_0, κ is an empirically-determined rate constant, and t is the time normalized by $t_{1/2}$, the time at half concentration ($C_0/2$).[112]

With great care, experimental data can be compared with theoretically derived models for different bulk-process rate limiting mechanisms (diffusion or reaction propagation). This type of mechanistic analysis was described early on by Sharp et al.[112] This is

presented below as a series of models that have been derived for different hydrogen transport mechanisms and geometries. The nine models presented, divided by mechanistic category, are compared to experimental data in Figure 41. In the absence of heat transfer and/or surface interaction effects, such an analysis can be used to determine the rate-limiting concentration driven mechanism of a material. The subscripts of the equations below denote the kinetics profile they describe in Figure 41.

Please note that it is extremely difficult to make measurements that are sufficiently isothermal and have little-to-no surface effect considerations. Such an analysis should be restricted to experimental configurations designed specifically for this type of analysis (see section 3.10) and well defined high-purity samples and gases.

2.2.2.1 Diffusion Models

Diffusion models can be used to describe one-, two-, and three-dimensional diffusion processes. A simple one-dimensional diffusion process with a constant diffusion coefficient can be described by

Equation 23
$$D_1(\alpha) = \alpha^2 = .2500(t/t_{1/2})$$

Two-dimensional diffusion into a cylindrical body gives

Equation 24
$$D_2(\alpha) = (1-\alpha)\ln(1-\alpha) + \alpha = .0426(t/t_{1/2})$$

Diffusion from the surface towards the center of a sphere is [113]

Equation 25
$$D_3(\alpha) = \left(1-(1-\alpha)^{\frac{1}{3}}\right)^2 = .0426(t/t_{1/2})$$

Another well-know model for a spherical body is [114]

Equation 26
$$D_4(\alpha) = \left(1-\frac{2\alpha}{3}\right) - (1-\alpha)^{\frac{2}{3}} = .0367(t/t_{1/2})$$

2.2.2.2 Reaction Models

Kinetics may be limited by the chemical reaction rate i.e. the rate of transition from solid solution to intermetallic. This mechanism can be modeled by

Equation 27
$$\frac{d\alpha}{dt} = \kappa(1-\alpha)^n$$

where n is the order of the reaction.[112] In some cases, solid-state reactions appear to follow first order kinetics

Equation 28 $$R_5(\alpha) = \ln(1-\alpha) = -.6931(t/t_{1/2})$$

If kinetics is controlled by a constant velocity propagation of the phase transition boundary, then useful relationships can be derived from Equation 27. The case of a cylinder, n = 1/2, gives

Equation 29 $$R_6(\alpha) = 1-(1-\alpha)^{\frac{1}{2}} = .2929(t/t_{1/2})$$

For a sphere of radius r in which the reaction proceeds from the surface towards the center with n = 2/3,

Equation 30 $$R_7(\alpha) = 1-(1-\alpha)^{\frac{1}{3}} = .2063(t/t_{1/2})$$

The above models of phase boundary propagation assume a virtually instantaneous and homogeneous nucleation of the product phase. In such a case the surface of a material is quickly covered by a hydride layer and the kinetics are described by the propagation of the phase boundary towards the center of the material. However, this is generally not how a hydride is formed. Typically the hydride phase nucleates at discrete locations in the bulk and grows outward. Hydride domains come into contact with each other as they grow and growth continues along the remaining reactant-product boundaries, eventually consuming the entire material. This process of nucleation and growth can be described by the following equations derived by Avrami and Erofe'ev [115] [116]

Equation 31 $$A_8(\alpha) = (-\ln(1-\alpha))^{\frac{1}{2}} = .8362(t/t_{1/2})$$

Equation 32 $$A_9(\alpha) = (-\ln(1-\alpha))^{\frac{1}{3}} = .8850(t/t_{1/2})$$

The following is an example presented to show how one could potentially determine the rate-controlling mechanism. The nine models described above are plotted along with the experimental hydrogen absorption data of a metal hydride sample in Figure 41. The models are shown in Figure 41 on a plot of α versus $t/t_{1/2}$. At low concentrations, it is clear that diffusion (Equation 23 through Equation 26, 1-4 in Figure 41) is the rate-controlling mechanism, although it is difficult to distinguish between the different diffusion models. However, this distinction becomes more obvious at higher hydrogen concentrations. The experimental data best fits curve 3, which describes diffusion from the surface to the center of a sphere. Therefore, absent heat transfer and/or surface interaction effects, this diffusion process is the mechanism that would best describe the rate limiting mechanism of hydrogen sorption in the metal hydride in question. Once again, it is important to remember that it is very difficult to accurately determine the intrinsic mechanisms of hydrogen sorption/desorption due to thermal effects. Heat transfer effects dominate kinetics for most measurements. Therefore, conclusions drawn from modeling must be kept in perspective when analyzing sorption/desorption mechanisms.

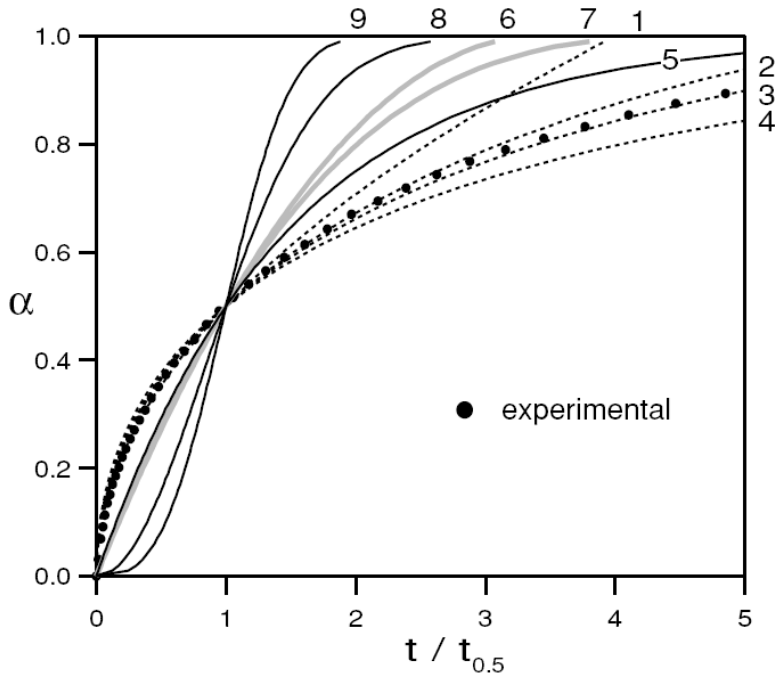

Figure 41. Various solid-state kinetics models.[112] 1) One-dimensional diffusion, 2) diffusion in a cylinder, 3+4) diffusion in a sphere, 5) 1st-order phase transformation, 6) constant velocity phase-boundary propagation in a cylinder, 7) constant velocity phase-boundary propagation in a sphere, 8+9) nucleation and growth.

2.2.3 Pressure Dependence

The volumetric method commonly used for measuring kinetics is not done at a constant pressure. Therefore, the pressure term in Equation 19 must be included to account for the effect that the changing potential energy of the surrounding gas will have on sorption kinetics. The following set of equations were proposed by Wang and Suda[117] for the sorption kinetics of the hydride phase transition:

Equation 33

$$\frac{dC}{dt} = K_h F_h(P, C)$$

Equation 34

$$K_h = Ae^{\frac{-E_h}{k_B T}}, F_h(P,C) = \left(\frac{P}{P_{eh}}\right)^a \left[1 - \left(\frac{P_f}{P}\right)^a \left(\frac{C}{C_f}\right)^b\right]$$

Equation 35

$$\frac{dC}{dt} = K_d F_d(P,C)$$

Equation 36

$$K_d = Ae^{\frac{-E_d}{k_B T}}, F_d(P,C) = \left(\frac{P}{P_{ed}}\right)^b \left[1 - \left(\frac{P}{P_f}\right)^a \left(\frac{C_f}{C}\right)^b\right]$$

K_h and K_d are the absorption and desorption rate constants, P_{eh} and P_{ed} are the equilibrium plateau pressures, Pf and Cf are the final pressure and concentration, and a and b are the orders of the relationships between the sorption rates and pressure and concentration, respectively. Corrections due to pressure change effects on rates can be overcome by simply adding pressure regulation or using relative volumes such that sorption results in measurable pressure changes but not significant with respect to reaction rates (quasi-isobaric).

As an example of relationships given in Equation 33 through Equation 36, experimental measurements of the hydrogen absorption kinetics of the intermetallic compound La_2Mg_{17} at 300°C are presented in Figure 42. The most linear behavior was found for reaction orders a = 2 and b = 1. This relationship proves to be valid for up to 95% of the absorbed capacity. The slow non-linear residual absorption at the bottom of the plot is most likely due to reestablishing thermal equilibrium after initial fluctuations in temperature caused by the exothermic hydriding reaction. The rate constant K_h from Equation 34 was determined from the slope of a linear fit of the upper part of the data.

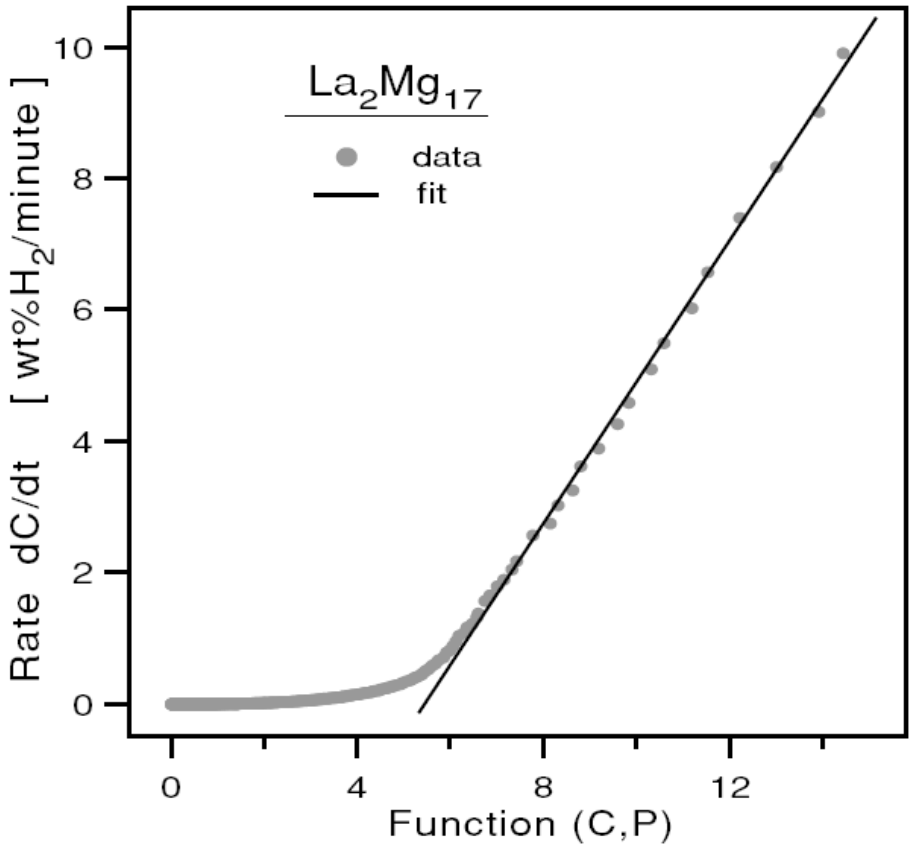

Figure 42. Linear fit to the rate dC/dt versus F(C,P) for hydrogen absorption of La_2Mg_{17} at 300°C. The rate coefficient K is found from the slope of the fit.[60]

3 Experimental and Analysis Considerations

Measured sorption and desorption rates are dependent on experimental and data analysis considerations as well as intrinsic material properties. As a consequence, experimental conditions and procedures that vary from system to system and from researcher to researcher can have a tremendous effect on measurements and the conclusions drawn from them. This makes comparisons between measurements with experimental equipment, different experimental conditions, different sample shapes, sizes, morphology and composition difficult if not impossible. Considerations that can have a significant effect on kinetics measurements will be discussed in this section along with suggestions to minimize their impact.

This section will rely heavily on examples from literature to support and illustrate the effects of various kinetics considerations. For more detailed information on specific considerations, refer to the reference of the cited example.

3.1 The Limitations of Kinetics Measurements

While a great deal can be learned from a good set of sorption and desorption kinetics measurements, from a materials discovery perspective, it is critical that the underlying hydrogen sorption process that is occurring is well understood. Unfortunately, kinetics measurements themselves often give very little direct information about these processes. In many ways kinetics plots look similar to each other. For that reason, basic sorption and desorption measurements should be complemented by a reliable set of supporting measurements. These may include characterization by PCT isotherm, TPD, X-ray and neutron diffraction, NMR, FTIR and Raman measurements among others.

To give an example, the measurement of hydrogen uptake or release (kinetics) may appear quite similar for extremely dissimilar chemical processes. Two examples are presented to show how desorption measurements from two different types of hydrogen storage materials can look quite similar (no distinguishing features other than being measured at different temperatures and showing differing overall rates) even though the mechanisms of hydrogen uptake and release are very different.

In the first example, the room temperature release of hydrogen from a classic AB_5 ($LaNi_5$-based) intermetallic hydride is shown in the kinetics measurement of Figure 43.

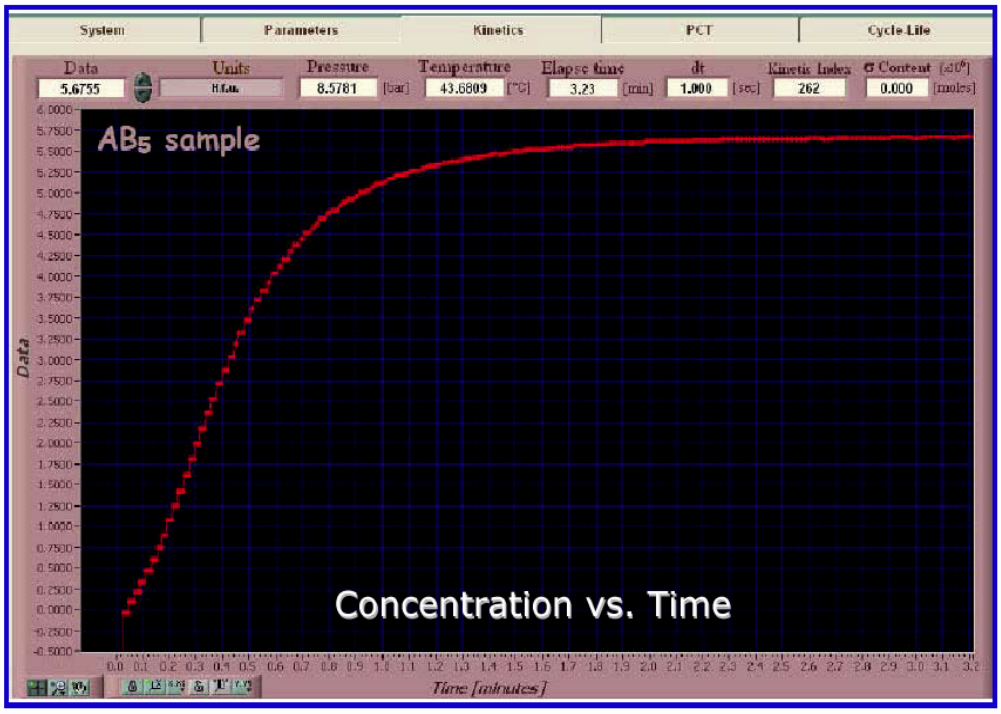

Figure 43. Kinetics measurement of $LaNi_5$ Intermetallic compound with a single phase transition. The experiment was conducted at room temperature. Units in H per formula unit released.[118]

Figure 43 was made by measuring the increase in pressure using a calibrated volumetric instrument as a sample of approximately 5 g desorbed hydrogen. For the most part, this material exhibits the classic kinetics profile of a single phase-transition from the intermetallic hydride compound to a metal alloy with some hydrogen in solid solution (commonly referred to as beta and alpha phases, respectively). An intermediate crystal structure transition is known to occur (gamma phase), but for current illustrative purposes the kinetics can be considered as a single chemical reaction. Atomic hydrogen is released from its interstitial binding site in the host metal's lattice, diffuses to the surface and combines with another hydrogen to form gaseous hydrogen, which gives rise to the measured increase in pressure.

The capacity change as a function of time represents the material's total hydrogen content change (in H per $LaNi_5$) during the desorption transition from $LaNi_5H_6$ to $LaNi_5$. This does not mean that the concentration of hydrogen in the hydride is changing but rather that the sample's total composition of the two phases is changing with time. The sample's total composition at any one time is:

Equation 37

$$\left(1-X\left(t\right)\right)LaNi_5H_6+X\left(t\right)LaNi_5$$

with boundary conditions X(t=0) = 0 and X(t=∞) = 1.

This transition from solid solution α-phase through the γ-hydride phase to the β-hydride phase in $LaNi_5$ is best observed by performing a series of equilibrium PCT measurements (Figure 44). Absorptions are shown for increasing temperatures in purple to red and desorptions at the same set of temperatures in blue. The flat portion (plateau region) of each measurement is present because of the equilibrium coexistence of the α-phase and β-phases (or γ-phase as the case may be). On moving from left to right along an absorption plateau the measured sample is being transformed, gas aliquot by gas aliquot, from the α-phase intermetallic alloy to the β-phase hydride. The reverse is true going from right to left across the desorption plateau.

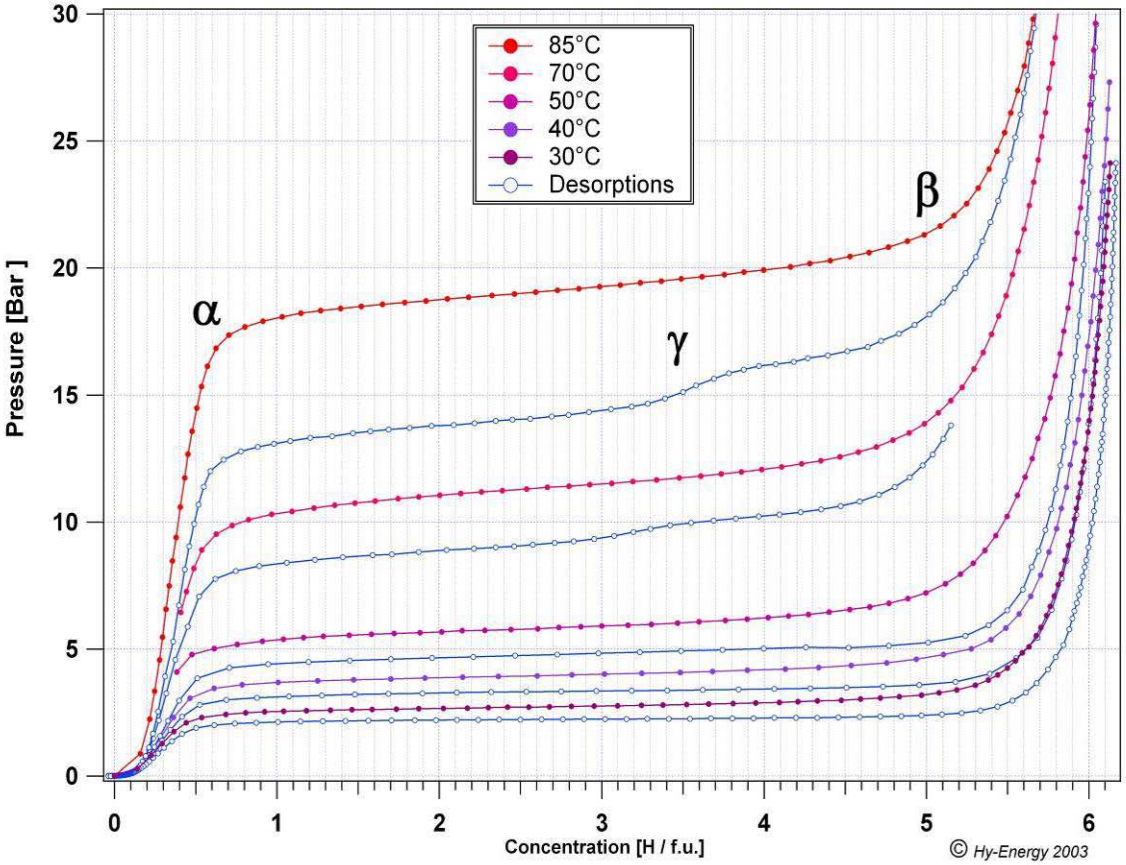

Figure 44. PCT measurements of $LaNi_5$, a classic metal hydride. The transition pressure at various temperatures illustrates the thermodynamic dependence of transition between the solid solution and intermetallic hydride phases.[118]

Hydrogen sorption through a single gas-solid phase transition such as the one above represents the ideal case for studying the mechanisms of hydrogen sorption kinetics. However, today's advanced hydrogen storage materials are becoming increasingly complex. They can consist of materials that undergo multiple hydriding reactions, complete structural decompositions and potentially the long-range transport of reactants other than hydrogen. And yet, these complex processes may present absorption and desorption kinetics that are quite similar at first glance to a classic hydride.

Our second example shows the measurement of the third cycle of gas desorption from titanium-doped alanate-amide mixture with a starting composition of

Equation 38

$$LiH + Al + 2LiNH_2 + Mg + TiF_3$$

It should be noted that, unlike the intermetallic hydride example above, this is not an isothermal measurement but rather a ramp and soak-style TPD measurement. However, within the isothermal portion of the measurement at t > 0.4 hours, the desorption resembles the classic kinetics curve of Figure 43 to a large extent.

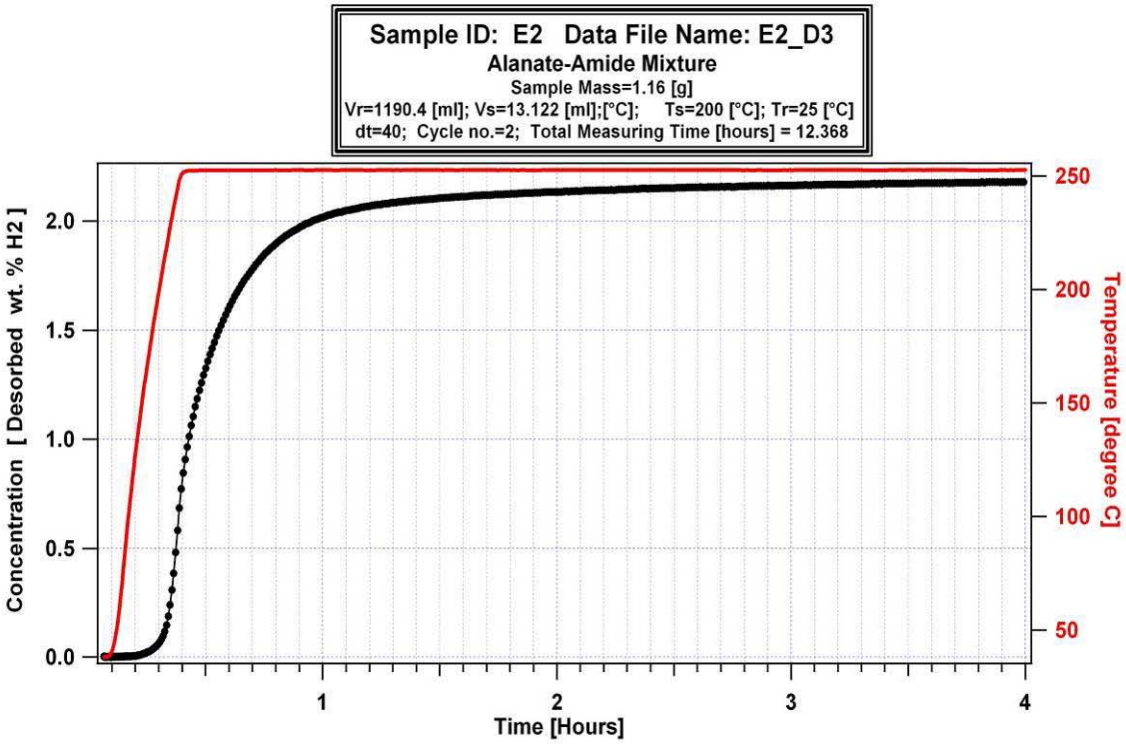

Figure 45. TPD measurement of the alanate-amide mixture described above.[57]

Without doing a more detailed PCT isotherm, it may be incorrectly assumed by looking only at the kinetics measurement that the desorption involves a single reaction. By performing an equilibrium desorption PCT measurement of the same sample (Figure 46) in the fourth cycle makes it clear that the continuous evolution of gas observed in the kinetics measurement of Figure 45 is the result of a complex series of chemical reactions instead of the single phase-transition as in classic hydrides.

Each of the three distinct plateaus corresponds to a different chemical transition within the material. This complex system has not been optimized or fully characterized by any means, but from what is known of its complex hydride and amide precursors, these reactions undoubtedly involve chemical decomposition and re-formation reactions. For hydride and amide products to form, this necessitates the long-range transport, not only of hydrogen, but also of other reactants including one or more species of Li, Al, and N. Later studies that coupled a high-pressure mass spectrometer to these same experiments showed the presence of ammonia in the evolved gas, adding additional complexity to the gas-solid system. [57]

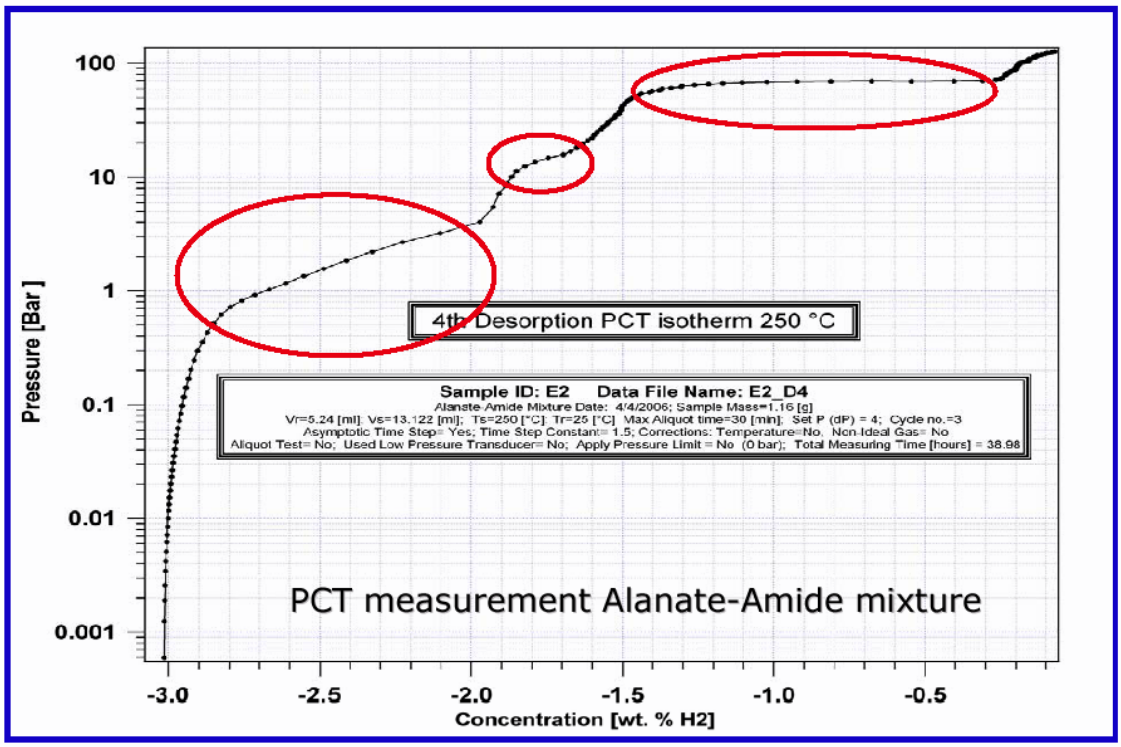

Figure 46. PCT diagram of the alanate-amide mixture described above.[57]

3.2 Discrete Kinetics Measurements

In the opening paragraph of Kinetics, it is noted that the difference between kinetics and capacity is that kinetics are inherently dynamic while capacity measurements are taken at thermal equilibrium. However, in principal, each data point on a PCT isotherm is the equilibrium concentration after the gas/material system has been perturbed from equilibrium. In fact, a volumetric PCT measurement consists of a series of small doses which, when measured with respect to time, individually represent measurements of kinetic properties. More precisely, with each dose (or aliquot of gas), a specified over-pressure (or under-pressure) is applied to the sample and the system is allowed to reach equilibrium through a dynamic process. The last data point of each kinetics measurement, which is assumed to represent equilibrium in composition, pressure and temperature, provides a single point on the PCT curve. This process is performed repeatedly until there are enough equilibrium data points collected to construct a full PCT diagram.

In a volumetric measurement where the quantity of gas is controlled (and thus the reactions are controlled), each dose is performed within a narrow band of concentration and pressure. In this sense the time-resolved data of a PCT measurement can be

thought of as a series of mini-kinetics measurements that can separate different portions of the overall sorption process. This is demonstrated using the same PCT isotherm measurement of the second example above.
Figure 47 presents the pressure time plot of the data that was used to create the PCT isotherm of Figure 46.

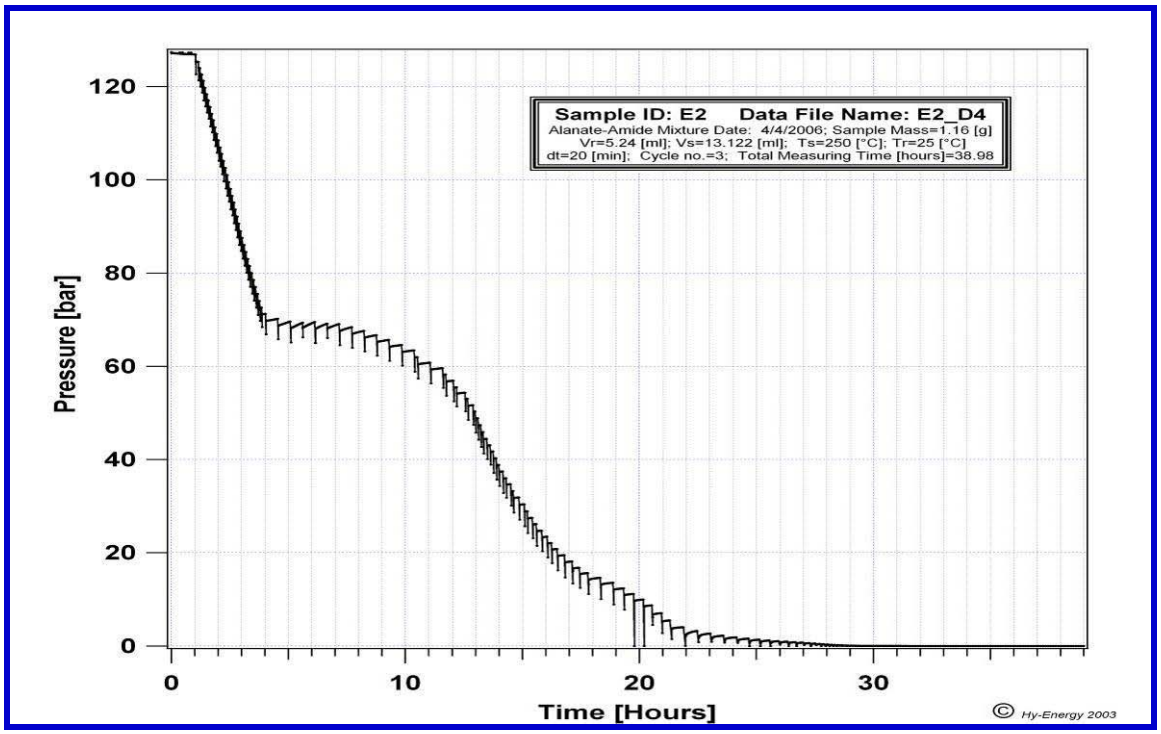

Figure 47. Pressure versus time plot of data used to create the PCT diagram of alanate-amide mixture in the preceding figure.[57]

By controlling the dosing pressure so that only one reaction occurs at a time, it is possible to determine relative reaction rates of each independent reaction. Indeed with the same applied pressure differential of 2 bar, the desorption rates for the three observed reactions from the highest to the lowest pressure plateaus are 0.29, 0.10 and 0.15 wt.%/hr. Note that such data is not only useful for determining the kinetics of individual reactions, but it also demonstrates that due to poor kinetics the final PCT isotherm was derived from relatively non-equilibrium conditions.

These examples serve not only to demonstrate the wide range of complexity encountered in the development of advanced storage materials, but also point to the importance of utilizing multiple methods of characterization in evaluating what may at first appear to be a simple sorption process. Given limited time and resources, the

ability to perform different measurements simultaneously in a single experiment becomes a real advantage in understanding complex systems.

3.3 Kinetics from TGA Measurements

Thermal gravimetric measurements (see Introduction section 5.5) are often used for kinetic analyses of chemical reactions. The progress of a solid state reaction is correlated to the fractional conversion (denoted as α) which is normally directly related to the mass change at time, t, relative to the total mass change observed for the reaction. Note that this holds only for material systems in which only one gas is released (H_2); that is, it does not distinguish multiple products such as both hydrogen and ammonia release from amides and AB samples. The fractional reaction is defined as

Equation 39

$$\alpha(m) \equiv \frac{m_i - m}{m_i - m_f}$$

Where m_i is the initial mass of the solid, m_f is the final mass of the solid, and m is the sample mass as a function of temperature/time. There are number of methods for determining the solid-state kinetics. The most often used methods are presented below without derivation.

3.3.1 Single Run Methods for Kinetics Analyses

Single run methods are the simplest and fastest approach to evaluating kinetics parameters. Using these methods the kinetic parameters can be obtained from a single TG run. The kinetic plots are examined by assuming various possible $f(\alpha)$ or $g(\alpha)$. After choosing the most appropriate form of $f(\alpha)$ or $g(\alpha)$ by comparing the linearity of the plots, E_a and A are calculated from the slope and intercept of the "most linear" plot. The single run method in differential form is applicable for kinetic rate data obtained under all temperatures conditions. However, this integral form of this method can only be used when a constant heating rate (β) is employed because an approximation function $p(x)$ for the exponential temperature integral has been used for deriving the kinetic equation:

Equation 40

$$g(\alpha) = \frac{A}{\beta}\int_{T_o}^{T}\left(e^{\frac{-E_a}{RT}}\right)dT \approx \left(\frac{AE_a}{\beta R}\right)p(x)$$

Various form of $p(x)$ have been proposed for the integration of the kinetic equation under non-isothermal conditions with linear heating rates. The Coats and Redfern integral method is a method derived by using an asymptotic expansion of the $p(x)$ function:

Equation 41

$$p(x) \cong \frac{e^{-x}}{x^2}\left(1-\frac{2}{x}\right)$$

3.3.2 Isoconversional Methods for Kinetic Analyses

This method uses data points at constant α_i (i.e., isoconversional points) extracted from the different series of kinetic rate data obtained from multiple TG runs. The value of E_a can be obtained at a constant value of α from the slope of the isoconversion kinetic plots. The isoconversion method has advantages in that the value of E_a can be determined without assuming a kinetic model, and the efficacy of:

Equation 42

$$\frac{d\alpha}{dt} = g(T)\cdot f(\alpha) = \left(Ae^{\frac{-E_a}{RT}}\right) f(\alpha)$$

Can be confirmed checked by confirming that E_a is constant through the course of the reaction. The isoconversional method in differential for is known as the Freidman Method, and is applicable to all kinetic data collected under any temperature conditions.

The isoconversional integral method analysis has been proposed by Ozawa with the following approximation of the $p(x)$ function:

Equation 43

$$\log p(x) \cong 2.315 - 0.4567x$$

Ozawa's method is applied to the non-isothermal kinetic data sets recorded at various heating rates (i.e., β_i). With a known value of E_a, the generalized time (denoted as θ) proposed by Ozawa is introduced for determining the "most" appropriate model function and the value of A:

Equation 44

$$\theta = \int_0^t e^{\left(\frac{-E_a}{RT}\right)} \mathrm{d}t$$

The generalized time (θ) is defined at the reaction time required to attain a specified α at infinite temperature. Using the generalized time (q) the kinetic equations at infinite temperature can be written as:

Equation 45

$$\frac{\mathrm{d}\alpha}{\mathrm{d}\theta} = Af(\alpha) \qquad and \qquad g(\alpha) = A\int_0^{\theta} \mathrm{d}\theta = A\theta$$

The values of $\mathrm{d}\alpha/\mathrm{d}\theta$ and θ can be calculated at a specified α from the kinetic rate data via:

Equation 46

$$\frac{\mathrm{d}\alpha}{\mathrm{d}\theta} = \frac{\mathrm{d}\alpha}{\mathrm{d}t} e^{\left(\frac{-E_a}{RT}\right)} \qquad and \qquad \theta = \frac{E_a}{\beta R} p(x)$$

The "most" appropriate kinetic model can be chosen from the linearity of $\mathrm{d}\alpha/\mathrm{d}\theta$ versus $f(\alpha)$ or from $\mathrm{g}(\alpha)$ versus θ, where the intercepts of the most linear plots is correlated to the value of A.

3.3.3 Peak Methods for Kinetic Analyses

The peak method is known as the Kissenger Method and has been widely used for the determination of E_a from the change in the peak top temperature (denoted as T_p) as a function of the differential kinetic rate data at various heating rates (β_i). Although the Kissenger method is derived assuming a first order rate process, in many cases the logarithmic term on the right-hand side of:

Equation 47

$$\ln\frac{\beta}{T_p^2} = \ln\left[\frac{\mathrm{d}f(\alpha_p)}{\mathrm{d}\alpha}\left(\frac{AR}{E_a}\right)\right] - \frac{E_a}{RT_p}$$

is approximately constant. Consequently, the value of E_a can be calculated from the slope of the plot of:

Equation 48

$$\ln\left(\frac{\beta}{T_p^2}\right) \text{ vs. } \frac{1}{T_p}$$

There are a number of software packages capable of performing many kinetic rate regressions. In addition, there are also many reference works that cover the applications and derivations of the various methods presented in much greater depth.

3.4 Matching Experimental Setup with Purpose

Perhaps more than any other type of measurement, the manner in which kinetics measurements are performed will greatly depend on the purpose of the measurement. The purpose of measurements is the deciding factor in determining the measurement method to be used, the design of the experiment or a series of experiments, and ultimately the size of the sample and the design of the containment. This section will provide some guidelines to help the reader understand the purpose of kinetics measurements at the different levels of research and highlight considerations associated with measurements at each level.

3.4.1 Experiments for System Performance

The kinetic rates of a hydrogen storage system are determined by a number of factors in addition to the intrinsic kinetic properties of the storage material. Some of the factors that affect kinetic rates at the system level include heat transfer between the storage material, material housing and environment, the operating over- or under-pressure relative to thermodynamic equilibrium and the packing density of the storage material. Heat transfer plays an important role in the kinetic performance of storage systems because some materials require the delivery and dissipation of significant amounts of energy during charging and discharging. Dedrick presented an example of the extreme energy releases characteristic of some metal hydrides upon charging: hydriding 5 kg of sodium alanate storage material in 2.5 min releases an average of 668 kW.[119] The ability to handle sorption/desorption energy loads such as those for sodium alanate necessitates the use of sophisticated thermal management systems such as internal plates, fins and tubing in system performance measurements.[59] System-level considerations like thermal management devices must be included in the design and evaluation of the kinetic performance of a storage system.

For a system level understanding, this may mean, for example, designing experiments to be able to examine material from different sections of a test bed after performing kinetics measurements under a different set of charging or discharge conditions. In such a case, being able to access the material multiple times would be important. Or perhaps it is the heat produced and heat transfer that is the focus of interest. Then one may want to instrument a test bed with multiple temperature sensors at different position in

the material and then to run a series of kinetics measurements under different test conditions.

To gain useful system performance information, enough material should be tested to provide results representative of the material's behavior in a full-sized operating storage system. In general, this means between 10 grams and 1 kilogram of storage material. 100 grams is probably a good tradeoff between the practical issues of synthesis and handling of the materials and a characteristic, uninterrupted volume of material that would be found in a large-scale system. For kinetics measurements it will be important to be able to measure hydrogen flow rates into or out of the test bed. If the material performance is already fairly well characterized, it may be possible to use flow meters to study sorption/desorption rates at a system level. However, with the exception of Coriolis-based flow measurement devices that maintain accuracy over two decades, conventional flow meters generally have fairly narrow dynamic measurement ranges (often less than one decade). This is a severe limitation when sorption/desorption rates may vary over several orders of magnitude depending on state of charge, temperature and pressure.

Mass change measurements on a system scale are also possible, but complicated by the connections between the system on a balance and the need for hydrogen transfer and potential heating or cooling. System scale kinetics measurements are most easily performed volumetrically using a normal regulator for sorption and a backflow regulator for desorption to maintain a constant or simulated pressure profile on the storage system. In its most simple form the amount of material is limited by the largest practical calibrated volume for a single desorption dose.

One example of scale up measurements are the experiments performed by Gary Sandrock on Ti-doped alanates.[120] Hydrogen absorption/desorption studies were performed on a simple high-pressure cylindrical vessel shown in Figure 233 designed to simulate the heat transfer and gas impedance conditions of a larger bed. This 316 SS reactor has a 4.6cm OD, 0.38cm wall thickness, about 11.4cm internal length, and was pressure rated to 3000 psia (204 atm) at 360°C. It was loaded with about 100 g of bicatalyzed $NaAlH_4$ (78 g of $NaAlH_4$ and 22 g of $Ti(OBu^n)_4$ + $Zr(OPr)_4$). The reactor had internal thermocouples but no internal heat exchange structure. The reactor was heated within an air furnace. Absorption kinetics and capacity were measured volumetrically and desorption measured with flow meters backed up by a wet test meter (a device to measure gas flow by counting the revolutions of a shaft upon which water-sealed, gas-carrying cups of fixed capacity are mounted).

Figure 48. Scale up (100 g) reactor with end cap removed in Ar-glovebox to show catalyzed alanate.[121]

The higher than expected initial charging kinetics, combined with limited heat transfer, results in exothermic temperature excursions, as is common with hydrides. An example is shown in Figure 234 for the 4th hydrogen absorption. The fully dehydrided bed was heated to 155˚C and then charged with hydrogen at 172 atm. Within one minute, the exothermic hydriding reaction resulted in an internal temperature of 234 ˚C.

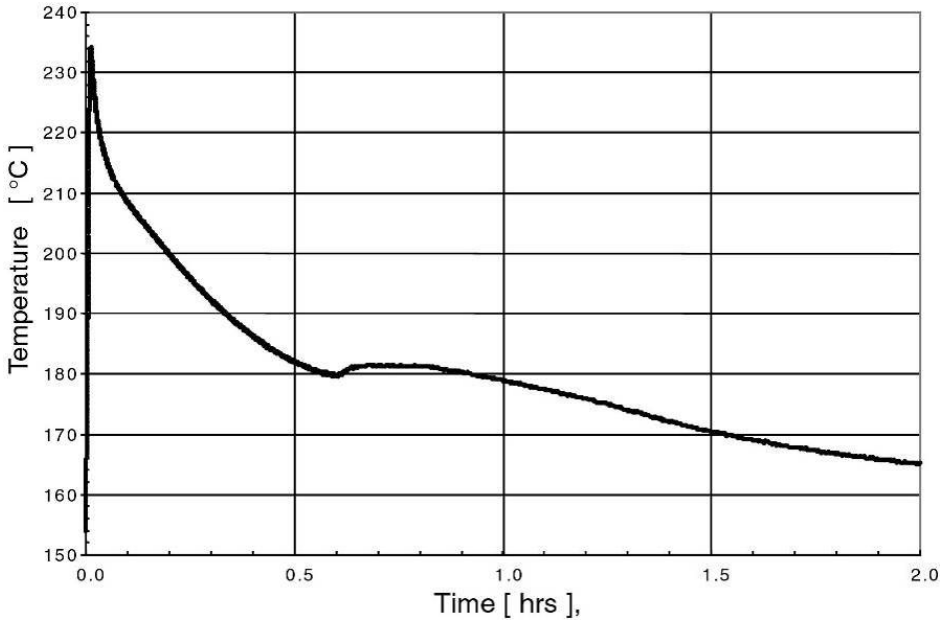

Figure 49. Exothermic temperature excursion during scale up bed charge half-cycle (P_i=172 atm, T_i=155˚C).[121]

This is essentially the van't Hoff temperature for $NaAlH_4$ at this applied pressure. However, the melting point of $NaAlH_4$ is only 182˚C; thus, any $NaAlH_4$ formed during the first 0.5 hr of Figure 234 would do so directly into the liquid phase. As one can see in the figure, a thermal arrest occurs at 182˚C due to solidification during cooling (about t = 0.6-0.8 hr). This is precisely as expected and shows that liquid $NaAlH_4$ was formed during the exothermic temperature excursion associated with the rapid initial charge.

It is natural to ask if such melting could be detrimental to the subsequent performance of the alanate bed. From subsequent absorption and desorption measurements, the answer seems to be "no" or at least "not much". In fact that series of scale up experiments pointed to a possible benefit of partial melting. When the reactor was opened between cycles 4 and 5 (photograph shown in Figure 16) the material in the bed was found to be sintered into a porous, solid mass. Such a structure may have distinct advantages for actual applications. In particular, such a sintered structure should reduce particulate migration, increase packing densities, allow expansion, and provide a constant internal gas impedance and enhanced safety.

Later, a more advanced test bed (Figure 47) was developed which had thermocouples placed at regular radial spacings and at different depths within the bed to examine heat transfer properties of the material during charge and discharge measurements.[122]

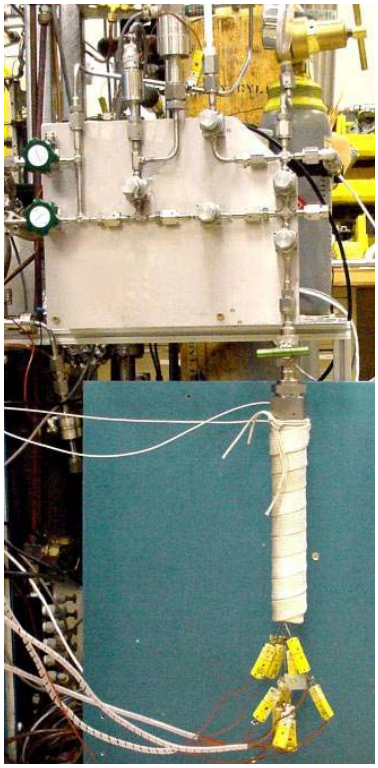

Figure 50. Image of scaled up Alanate test bed with series of internal and external thermocouples.[122]

3.4.2 Experiments for Materials Development

Kinetics measurements for materials development must focus on the intrinsic kinetics of the storage material in order to effectively compare materials. This can be difficult for materials with highly exothermic or endothermic reactions and good intrinsic kinetics because heat transfer often masks the intrinsic kinetic character of the materials. Intrinsic kinetics testing emphasizes testing at isothermal conditions and conducting measurements under identical conditions (pressure, temperature, sample size etc.) using identical measuring equipment in order to minimize the effects of heat transfer. The importance of testing kinetics under identical conditions using identical measuring equipment and setup is illustrated in the many dozens of papers before 1982 reporting absolute absorption and desorption rates for $LaNi_5$. Reported kinetics rates at half capacity varied between < .01 min^{-1} to 35 min^{-1} at 5 atm and 298 K.[123] The measurements in the review were performed with different quantities of material on completely different equipment without special considerations for heat transfer. Therefore conclusions drawn from these measurements concerning intrinsic kinetics are questionable at best. There are a few special instances when non-isothermal kinetics measurements are informative, particularly when applied to developing functional hydrogen storage applications.

For research focused on materials development, a good approach is to run a series of comparative measurements on different samples while ensuring that all other material properties (sample size, packing density, purity…) and measuring conditions remain as consistent as possible. The experimental setup, sample size and measurement technique should be centered on simplicity and the ability to make comparative measurements as efficiently as possible.

Heat transfer and measurement of the true sample temperature at low gas pressures, in addition to buoyancy corrections at high gas pressures, make kinetics measurements by gravimetric methods difficult if not impractical. These complications are due to the limitation that the sample in a gravimetric analysis system cannot make physical contact with a thermal mass for heat exchange. This can be accommodated by reducing sample size or, in the case of desorption, by using a carrier gas in flow through mode to maintain the sample temperature. Volumetric kinetics measurements on samples ranging in size from a few milligrams to a couple of grams are quite straightforward. A major consideration is that, in particular for materials with elevated enthalpies of formation (> 10 KJ/mol H_2) and good intrinsic kinetics, sorption/desorption rates may be limited more by heat transfer in the measuring equipment than by physical or chemical sorption mechanisms. The flexibility in sample holder design and sample compositions (addition of thermal ballasts) can overcome this problem. With this in mind, it is still very relevant to measure sorption rates under imperfect (non-isothermal) conditions in order to obtain relative hydrogen uptake and release rates and to develop modified materials with improved kinetic performance. However, it is exceptionally important

that materials are measured under essentially the same conditions (pressure, temperature, sample size, perhaps sample packing density) using identical measuring equipment and setup to be able to make quantitative and even qualitative comparisons between materials. Comparison of the intrinsic kinetic properties under the aforementioned instrumental limitations can be further qualified by considering or measuring, for example, differences in the isobaric heat capacity and thermal conductivity among the materials under investigation.

A classic example of such a successful comparative analysis with the goal of developing optimized hydrogen storage materials was the systematic study of increasing levels of $TiCl_3$ additives in $NaAlH_4$.[126] By performing these measurements under identical conditions a clear trend in kinetic performance was observed ultimately leading to key findings in understanding the effect of Ti additives on alanates. Another example of comparative measurements for improved performance of storage materials was through the investigations of many different types of alanate additives by Anton et al.[102]

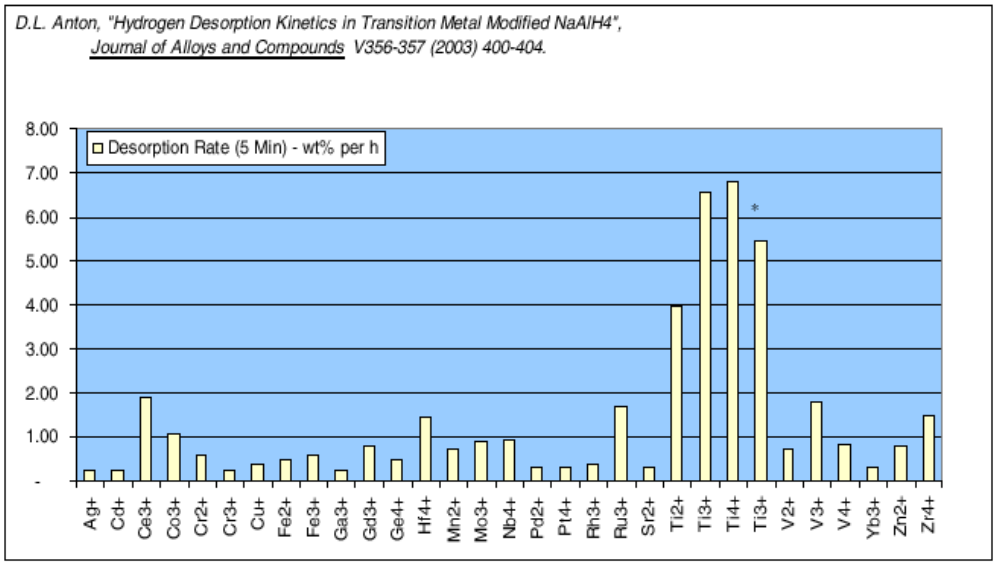

Figure 51. Investigation of different additives for improvement of kinetics of $NaAlH_4$. Dopants are transition metals and rare earth ions.

3.4.3 Experiments for Fundamental Studies

Fundamental mechanism studies look to identify and understand intrinsic kinetic phenomena. Like those for materials development, fundamental investigations require isothermal conditions in order to eliminate the effects of heat transfer. Investigation of hydrogen diffusion mechanisms, the effects of catalysts on hydrogen dissociation, and

the nature of hydrogen/sample material interaction are examples of research at the fundamental level. If the purpose of a kinetics measurement is to study intrinsic mechanisms, it is absolutely necessary to design the experimental measurement equipment to achieve essentially isothermal conditions.

For these basic science experiments, simplicity (reducing the number of free experimental parameters) is key. While it may not be possible to determine rate-limiting mechanisms without specially designed sample cells, sorption and desorption kinetics measurements on standard equipment and laboratory scale samples (e.g. 1 gram) can provide not only relative measurements for materials optimization but also some fundamental insight into sorption processes. Gary Sandrock's work on Ti doping in sodium alanates provides a good example of how detailed kinetics measurements and the determination of activation energies have been employed for improved understanding and development of better hydrogen storage materials.[124] Hydrogen desorption rates were measured at several temperatures for the decomposition of $NaAlH_4$. For convenience, these rates were determined using a linear fit to the initial portion of each desorption kinetics measurement. The desorption rates for both undoped and 4 mol.% $TiCl_3$-doped $NaAlH_4$ are plotted on a log scale versus 1/T in Figure 52. This is essentially an Arrhenius plot. The effect that Ti doping has on the desorption behavior of $NaAlH_4$ is apparent from these measurements.

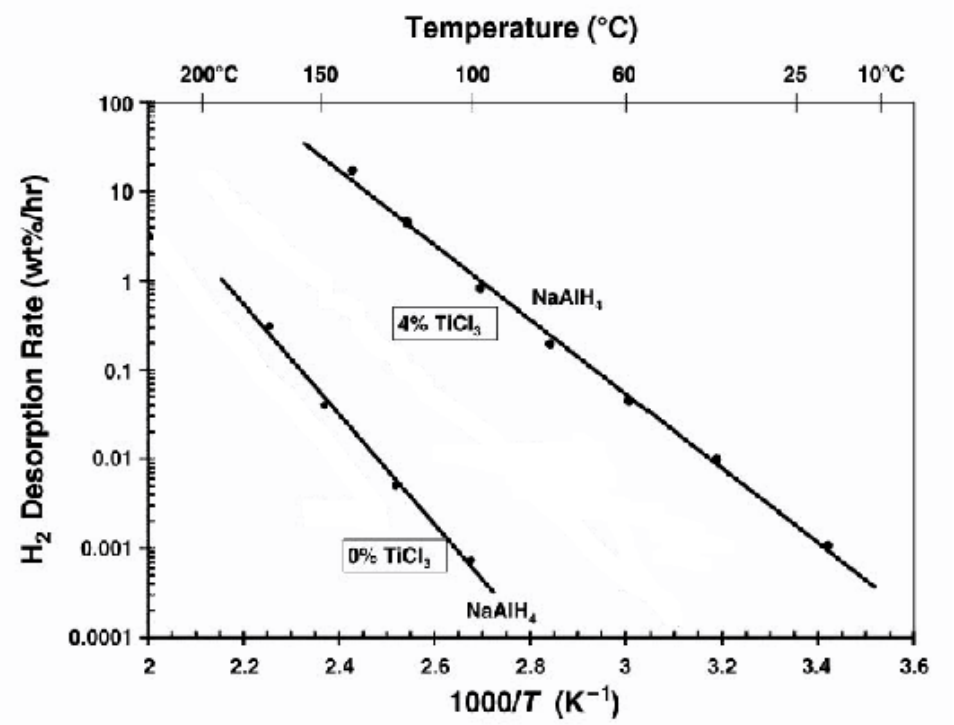

Figure 52. Log desorption rates versus inverse temperature plotted for $NaAlH_4$ with no $TiCl_3$ and 4 mol% added $TiCl_3$ [Original plot modified for simplicity, Na_3AlH_6 removed from figure].[124]

The activation energies calculated from this plot as well as other Ti doping levels are presented in Figure 53. This series of kinetics measurements demonstrate that adding only small amounts of $TiCl_3$ to the alanates significantly reduces the activation energy for hydrogen desorption. It is interesting to note from Figure 53 that increasing the level of $TiCl_3$ in $NaAlH_4$ shows little change in the activation energy. Thus, the chemistry of the Ti-enhanced kinetics is unchanged with Ti concentration. Further improvement in the desorption rates by increased $TiCl_3$ doping is observed through an increase in the pre-exponential factor *A* of Equation 20. This indicates that performance is improved by the increased distribution and access to titanium in the material.

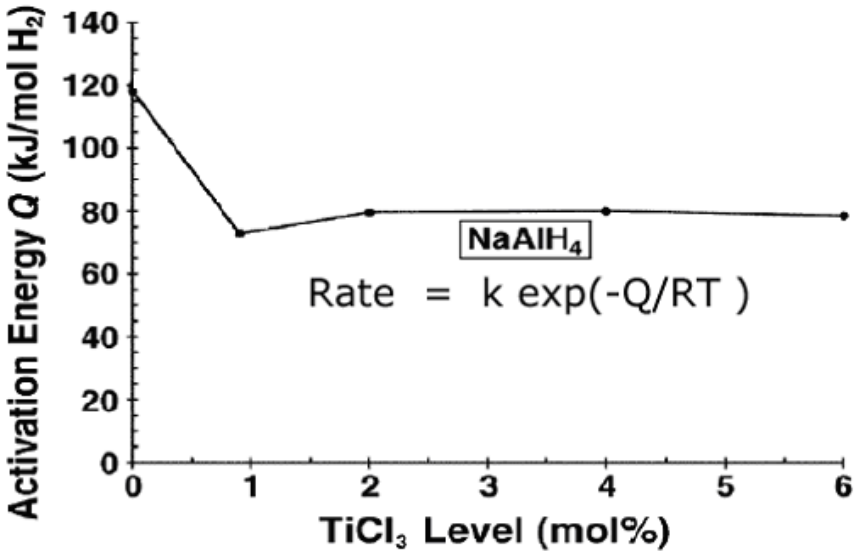

Figure 53. Activation energies Q (= E_A) for $NaAlH_4$ decompositions as a function of added $TiCl_3$ [modified for simplicity, Na_3AlH_6 removed from figure].[124]

If the purpose of the kinetics measurements are indeed to study fundamental mechanisms then it is absolutely necessary to design the experimental measurement equipment to achieve essentially isothermal conditions and at an even higher level of precision, isobaric measurements. This was in fact done with painstaking detail by Goodell et al. for hydrogen absorption and desorption in $LaNi_5$. Their thermal ballast technique is described in detail in the Thermal Effects section 3.10.1 of experimental considerations.

3.5 Efficient Testing

Evolution of hydrogen storage material discovery, development and characterization is directly dependent on the ability to conduct measurements with speed and efficiency. Kinetic activity is often the limiting factor in hydrogen testing. For example, the time required to reach equilibrium in performing PCT measurements is directly dependent on the kinetics of the sample material. Any technique that reduces sample characterization time will help in improving the pace of material discovery and development.

An excellent example of efficient testing used by Gary Sandrock drastically reduces the time required to determine the activation energy of a sample with slow kinetics.[125] To develop an Arrhenius diagram necessary to determine the activation energy of a chemical reaction, several experiments must be performed at different temperatures to determine the relationship between the rate constant K and temperature. Instead of performing a series of isothermal experiments, Sandrock's method changes the temperature of the sample in steps, as shown in Figure 54.

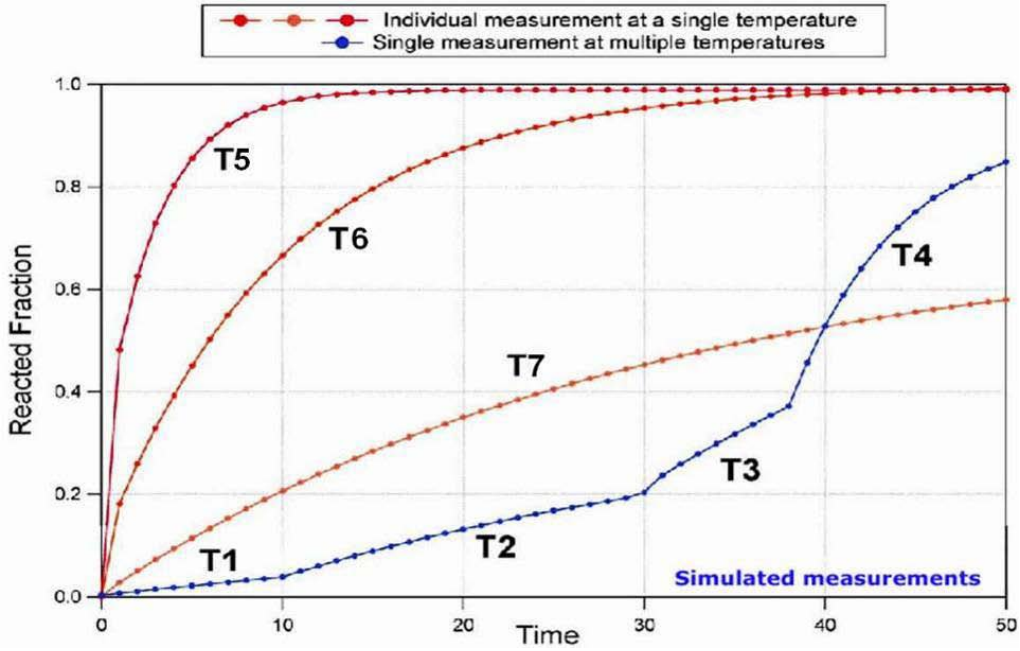

Figure 54. Example of efficient testing in determining the activation energy of a sample with slow intrinsic kinetics. The figure itself is a kinetics measurement used to relate the rate constant to temperature.[57]

Several rate measurements can be performed using this method in the same amount of time as a single isothermal measurement. It is important to remember that the temperature is stepped instead of ramped because isothermal conditions are still

required to perform kinetics tests. For such type of measurements to be valid the sample holder and heater design should allow temperatures to be changed and establish a steady on a time scale that is short compared to the kinetic rates. This technique can only be used with samples that have slow enough intrinsic kinetics that the sample temperature can be increased in several steps before the sample completely desorbs. In addition, rates should be measured when the sample is below about 60% conversion to avoid the impact of changes in reactant concentration on the rate measurements.

3.5.1 Kinetics and Capacity

With respect to kinetics measurements it is important to review how capacity is reported. In particular, it may be more useful to examine relative sorption rates of materials based on what we term here as "active capacity" in contrast to "material capacity".

Today, hydrogen storage capacities are typically presented in units of weight percent (wt.%), where wt% is defined as:

Equation 49

$$wt.\% = \frac{mass_{H_2}}{mass_{sample} + mass_{H_2}} * 100\%$$

This makes sense from a practical perspective, because it is a measure of how much hydrogen can actually be delivered from a storage material. And, in this vein, it is important to recognize that ultimately the practical hydrogen storage capacity must be on a systems level that includes the material, containment vessel, heat transfer system, controls and balance of plant.

3.5.2 Active Capacity

From the perspective of a materials development level, it is equally important to be able to quantify capacity in terms of the active material only. In particular, where this becomes important is in the evaluation of improvements of kinetic performance. Since rates are typically being measured in units of wt.% per time, to make a comparative analysis of the effect on kinetics of different catalysts or additives, rates should be compared on an active wt.% capacity basis and not on material wt.% capacity. Thus, for this purpose, we may define:

Equation 50

$$Material\ wt.\% = \frac{mass_{H_2}}{mass_{sample} + mass_{H_2}} * 100\%$$

Equation 51

$$Active\ wt.\% = \frac{mass_{H_2}}{mass_{active\ sample} + mass_{H_2}} * 100\%$$

The mass of the active sample only includes the mass of material that participates in hydrogen storage and the mass of the sample is the total weight of the sample including both the active and inactive material in the sample. Another possible way to perform such a comparative analysis is to use rates based on reacted fraction per time rather than absolute capacity values. As will be seen in the next section, for comparative kinetics it can be very important to present capacity in terms of reacted fraction or active wt.% rather than true wt.%.

A specific example is presented here to demonstrate the difference between "material capacity" and "active capacity" and to aid in understanding the impact of this differentiation in evaluating relative kinetics of a series of different samples.

In this example, $NaAlH_4$ doped with $TiCl_3$ reacts during the milling preparation process to form NaCl according to:[122]

Equation 52

$$NaAlH_4 + xTiCl_3 \rightarrow xTi + 3xNaCl + 3xAl + (1-3x)NaAlH_4 + 3xAl + 6xH_2$$

This means that only

Equation 53

$$\frac{54(1-3x)}{54+154.5x}$$

of the sample, representing the fraction of active sodium alanate to the total sample, is active for hydrogen uptake and release. Without taking this into account, improvements in alanates by doping with 6 mol% vs. 2 mol% $TiCl_3$ would be underestimated by up to 30% (Figure 55). In this case, this has little impact on the conclusions with respect to the level of dopant since the correction actually improves the rates with increasing levels of doping. However, another example may serve to demonstrate how this effect could impact such an evaluation.

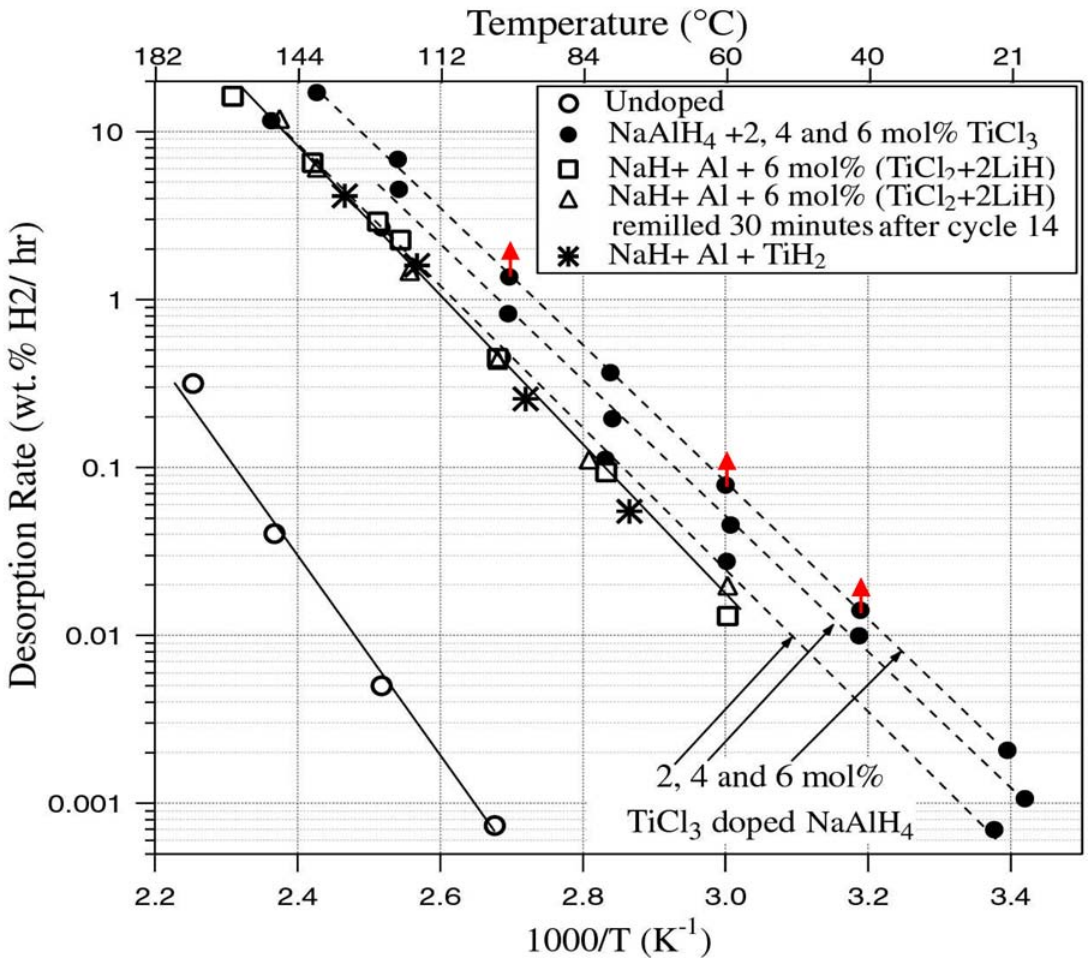

Figure 55. Arrhenius plot comparing desorption rates of $NaAlH_4$ Generation II, III-D, and III-E alanates (rates: II on a material weight basis, III-D and III-E on a NaH + Al weight basis). Red arrows indicate change in data points on converting from a material to an active weight basis.[126]

To investigate the effects of active capacity versus material capacity on kinetics measurements, a sample was tested using only TiH_2 instead of $TiCl_3$.[126] In this case, a mixture of NaH, Al, and TiH_2 in a 1:1:1 composition was mechanically milled and tested for hydrogen absorption and desorption. From an applications perspective, TiH_2 as a precursor should overcome the problem of capacity loss associated with the formation to Na-halides when using Ti-halide precursors. This composition did absorb hydrogen (130˚C and 82 bar H_2) to form $NaAlH_4$. In this case, the inactive component (TiH_2) makes up almost half of the samples mass. Thus rates would be off by a factor of 2 if capacity were measured on wt.% basis using the sample's total weight. However, by plotting rates on an active material mass basis (NaH + Al), the desorption rates are nearly identical to those of the indirectly doped material and the 2 mol% $TiCl_3$ doped alanates

(Figure 55). Had the total weight of the sample been used, an incorrect conclusion may have been drawn about Ti-hydride vs. Ti-halide additives. With optimization, kinetics may be achieved without a severe degradation in hydrogen storage capacity. This example of kinetic analysis based on active versus material weight capacity serves to demonstrate that even small details in how the analysis is performed can have a big impact on the conclusions and ultimately on decisions concerning the direction of materials research and development.

Note that it may be better to report results for this type of analysis in terms of reacted fraction. Capacities reported as wt% of the active material can be misleading if not fully and carefully explained, because the capacity reduction that accompanies additives and catalysts is suppressed.

3.6 Activation Effects

Activation effects are important in kinetics measurements because the kinetic character of a reversible storage material can change drastically during the first five to ten cycles. The change in kinetic character is most significant early in cycling and gradually approaches the intrinsic kinetic character of the material. In application, a hydrogen storage material will typically cycle hundreds, if not thousands, of times so it is important to characterize the intrinsic kinetics in order to evaluate a material's suitability for end-use. It is also important to run samples of new materials through several absorption/desorption cycles to determine their true intrinsic kinetic character. While the activation process is time-consuming, it is better than missing a viable storage material because its kinetic properties appear uninteresting after the first few cycles.

Pre-reacted sodium alanate is an excellent example of kinetic activation effects. Figure 56 is kinetic data taken from a cycling experiment on sodium alanate and clearly shows the drastic impact activation effects can have on kinetic character.

Each desorption measurement is taken in a fixed time interval so the increasing hydrogen desorption indicates that the kinetics of the sample are improving. The rate of hydrogen evolution increases markedly the first five cycles and gradually approaches the intrinsic kinetic rate from cycle 5-13. The class of pre-reacted sodium alanates would have been completely disregarded if judgment were passed based only on the kinetic character and capacity of the first few cycles.

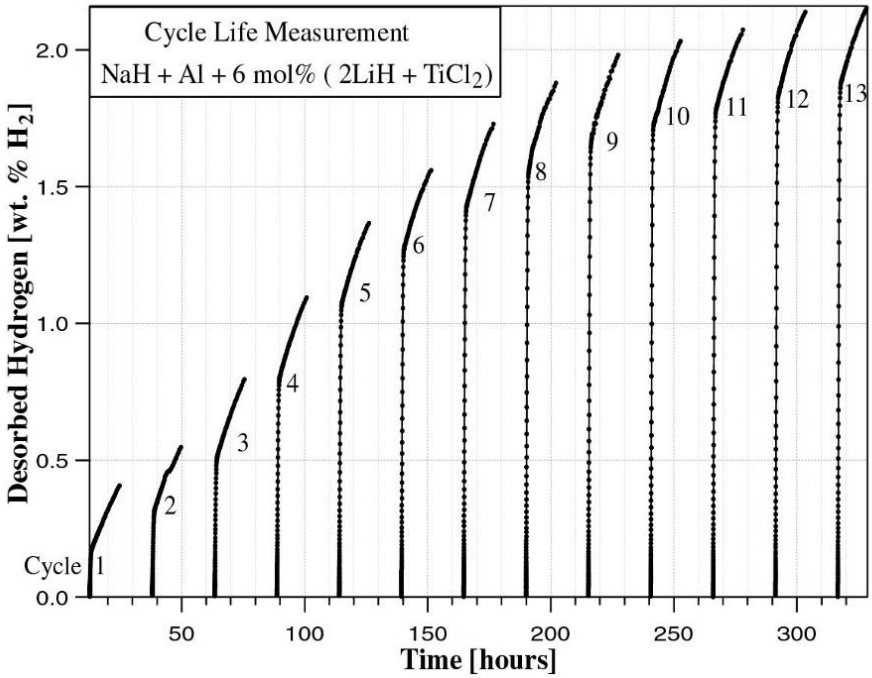

Figure 56. The kinetic activation effects of pre-reacted sodium alanate. The marked increase in desorbed hydrogen indicates increasing kinetic rates.[126]

Digging a little deeper into the kinetic character of sodium alanate, it is interesting to note that there are two distinct rates in each desorption cycle in Figure 56. Each represents a separate step in the two-step equilibrium desorption reaction.

Equation 54

$$NaAlH_4 \rightarrow \frac{1}{3}Na_3AlH_6 + \frac{2}{3}Al + H_2 \rightarrow NaH + Al + \frac{3}{2}H_2$$

The difference in the kinetic rates of the two reactions is probably due to the difference in the thermodynamic stability of $NaAlH_4$ and Na_3AlH_6. $NaAlH_4$ is less stable than Na_3AlH_6 and forms at a higher equilibrium pressure (Figure 57). In these desorption measurements, the under-pressure is below both equilibrium plateau pressures, allowing the decomposition of both alanate phases. However, the pressure difference driving the desorption reaction from $NaAlH_4$ to Na_3AlH_6 (DP_d (1)) is greater than for Na_3AlH_6 than for NaH (DP_d (2)), leading to higher kinetic rates for $NaAlH_4$ than Na_3AlH_6. It is important to note that the situation is exactly the opposite during absorption measurements. The lower plateau pressure of the NaH to Na_3AlH_6 transition would provide a greater driving pressure differential (DP_a (2)) compared to the Na_3AlH_6 to $NaAlH_4$ transition (DP_a (1)). Thus, in absorption, higher kinetic rates would be observed for the reverse NaH + Al to Na_3AlH_6 step in the reaction of Equation 54.

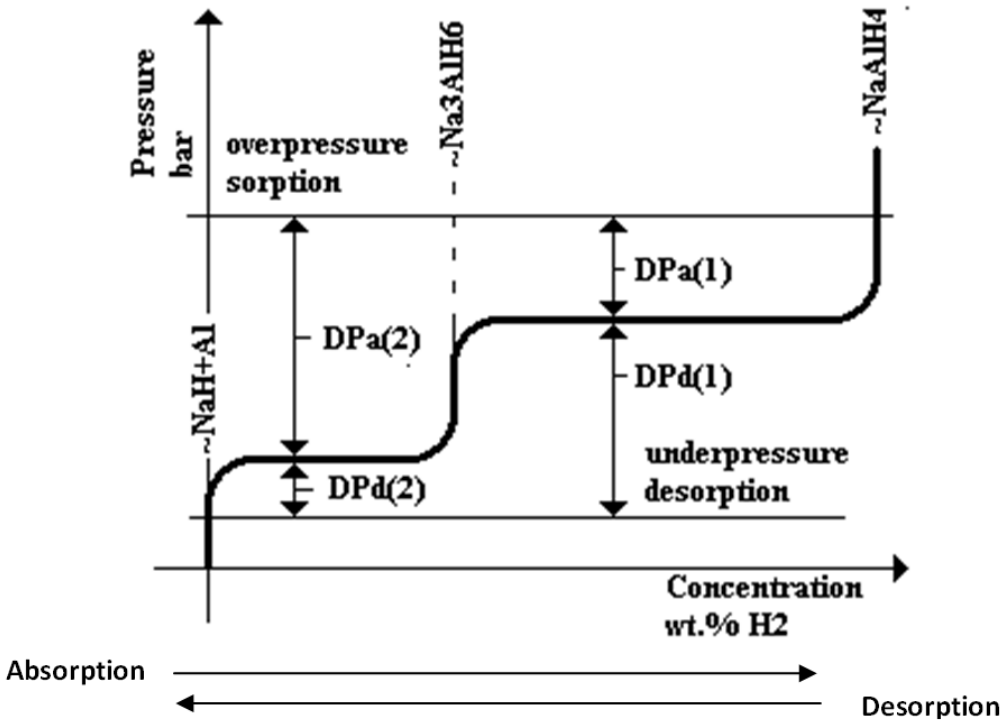

Figure 57. The reaction follows the equilibrium pressure (darkest line) from bottom left to top right for absorption and top right to bottom left for desorption. The horizontal section of the equilibrium pressure line represent phase transitions (reactions), the vertical lines represent the alanate compounds as indicated.

At first glance it appears that only the first reaction in Equation 54 is affected by activation because nearly all of the increased desorption capacity occurs during the first section of each desorption profile. As the material is cycled, the $NaAlH_4$ to Na_3AlH_6 reaction becomes more active while the Na_3AlH_6 to NaH reaction remains constant. This is easily rationalized with the aid of Figure 57. Before the first hydriding of the material, the sample is in its as prepared NaH + Al state. After the first charging which is incomplete (a1), the sample is dehydrided (d1) but can not completely desorb all of the hydrogen taken up in the first absorption due to the poor desorption kinetics of the second Na_3AlH_6 to NaH step and the fixed absorption/desorption times used for each cycle. This creates a permanent offset in total hydrogen concentration. During subsequent cycles (a2-d2 and a3-d3), only the $NaAlH_4$ to Na_3AlH_6 reaction improves (activates) because the NaH to Na_3AlH_6 to has *already* been taken to completion in the first cycle. It is important to remember that Figure 56 presents desorption rates only and not both sorption and desorption rates.

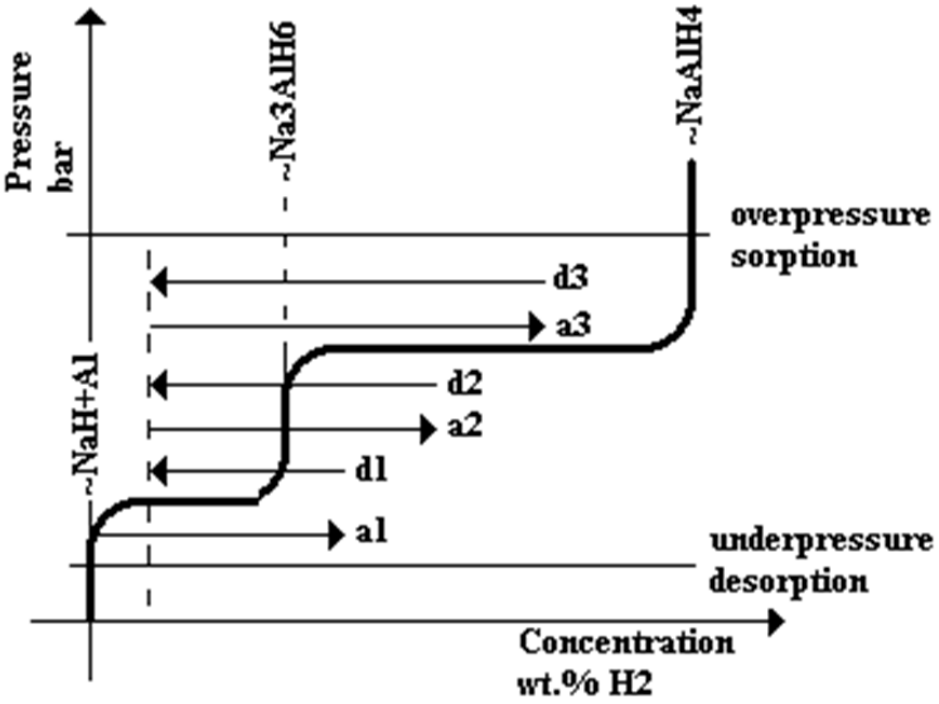

Figure 58. Concentration offset caused by incomplete desorption. Due to thermodynamic limitations, the sample cannot be fully desorbed during the experiment, which causes the concentration to offset.

3.7 Gas Impurities

3.7.1 Retardation

Retardation in kinetics occurs when impurities such as CO_2, H_2O and NH_3 in the H_2 gas stream react with storage material surfaces, leading to decreased kinetic activity. The gas stream impurities occlude catalytic sites and diffusion pathways and can be difficult to desorb from the storage material because of their high thermodynamic activity. These effects influence the mechanisms discussed in the theory section 2.1 . The primary retardation considerations for physisorbing materials like porous media are decreased surface area due to physisorbed impurities and the occlusion of internal pore networks; blocked catalytic sites and diffusion pathways affect chemisorbing materials like metal hydrides. Unlike poisoning, retardation does not significantly affect ultimate hydrogen storage capacity: the sorption curve of a material experiencing retardation asymptotically approaches the original hydrogen storage capacity of the material, albeit at a slower rate.

Sandrock et al. presents an excellent example of the retardation effects of NH_3 on $LaNi_5$ during cycling.[127] Although Figure 59 only shows the beginning of the sorption curve, each arc eventually approaches the ultimate hydrogen sorption capacity dictated by cycle 0. The effects of retardation are often reversed by flushing and subsequent use of high-purity H_2.

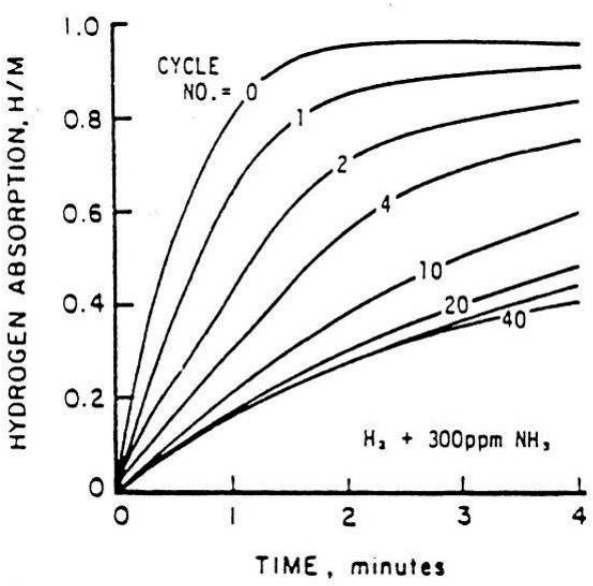

Figure 59. Effects of retardation of NH_3 on isobaric sorption curve of $LaNi_5$ during repeated cycling.[127]

3.7.2 Gas Impurity Effects on Kinetic Performance

An important consideration is whether fresh or recycled gas is used during cycling kinetics measurements. For recycled gas measurements, the temperature of the sample is increased and decreased with each cycle with the sample exposed to the same gas in a fixed gas volume. Thus, the total amount of impurities in the hydrogen gas/system remains the same. When fresh gas is used for every cycle, gas impurities may have a much larger impact on the retardation of the material's kinetics. This is because the gas impurities are strongly bound to the surface of the material and are not released upon desorption. With cycling, the concentration of impurities on the sample increases, degrading the material's storage performance. In this sense the storage material is simply acting as an impurity getter. The advantage with gettering storage materials is that the hydrogen delivered to the application (e.g. fuel cell) will be much higher purity than that provided by the gas supplier. The disadvantage, of course, is that the performance of the storage system may be significantly affected.

As a side note, kinetics measurements performed on gravimetric systems in flowing gas mode, impurities in the gas stream that react with the sample will be observed as a slow linear increase in weight rather that the curved behavior expected for a true kinetics curve (much like leaks in a volumetric system discussed below). Such behavior should be taken as an indicator that impurities are present in the hydrogen gas stream.

3.8 Leaks

Leaks cause kinetic sorption/desorption profiles to appear linear in time, as opposed to true sorption profiles that exhibit curvature. An example of a leak is demonstrated in Figure 60, where the expected capacity of the sample is 1.39 wt.%. Sorption steadily increased with a linear behavior until a fitting was tightened about two hours in to the experiment. With respect to new materials, one should weigh on the side of skepticism and review the setup and measurements if the results appear too good to be true.

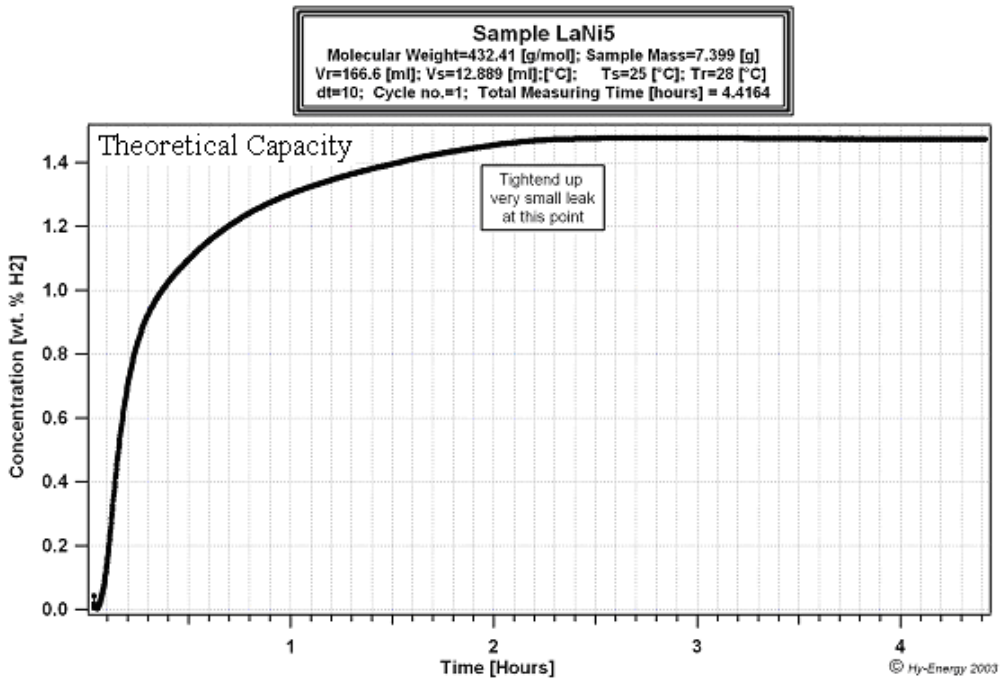

Figure 60. Example of a leak on kinetics measurement. A little after an hour in to the experiment, the leak was eliminated.[118]

3.9 Pressure Effects

Observed kinetic rates are highly dependent on the pressure differential between the gas reservoir and the sample reactor that drives the sorption/desorption reaction. The theoretical description of the effect of pressure on kinetics was presented in section 2.2.3 . and the experimental results can be measured as shown in the example of Figure 62 in section 3.9.1 below.

From an experimental perspective, In order to investigate the intrinsic kinetic properties of a material, it is important to reduce the degree of variation in pressure differential during testing. If the system pressure changes significantly during a sorption/desorption reaction, the changing pressure differential will affect the observed kinetic rates and mask the intrinsic kinetic properties of a material. It is, however, important to balance loss in sensitivity in the measurement due to the smaller total pressure change with the ultimate impact that a changing pressure may have on the kinetic behavior. In the volumetric method, this is done by appropriate selection of the volume reservoir so that the system pressure change is relatively sufficient for accurate measurements but not large compared to the driving pressure differential during reaction.

3.9.1 Reservoir Selection

In volumetric measurements, it is important that the dosing volume, sample holder volume and dosing pressures are selected to match not only the size of the sample but also the type of measurement. One simple way to estimate an appropriate selection is to calculate an assumed amount of gas that the sample will absorb and divide this by the number of doses that are needed to collect a reasonable set of data. For an absorption kinetics measurement the dosing volume should be large enough to be able to dose enough gas to completely charge the sample with the final pressure being greater than any plateau pressure and still result in enough of a pressure drop to make an accurate measurement. A typical value would be 110% of the capacity of the sample at the resulting pressure. For a desorption kinetics measurement the same is true with the sample being able to nearly completely desorb all of its gas to the reservoir volume. A typical value would be 95% of the capacity of the sample at the resulting pressure. For PCT isotherm measurements the volume of the reservoir and dosing pressures essentially determine how many data points will be collected on an isotherm. A good rule of thumb is that the size of the reservoir and pressure step should be selected to completely charge or discharge the sample in about 30 doses. This of course is dependent on the size of the sample, its capacity and charging pressures.

As a particular example, the effect of pressure on kinetics is illustrated in Figure 61 for a 1 g sample of $LaNi_5$. When using a volume reservoir that is too small (10 ml, dashed line), there is not enough hydrogen to hydride the entire sample to $LaNi_5H_6$. Therefore

the pressure in the system must be the plateau pressure of $LaNi_5$. The amount of hydrogen in the reservoir is:

Equation 55

$$n = \frac{PV}{RT} = \frac{5bar * .01L}{.083\frac{bar * L}{mol * K} * 298K} = .002molH_2$$

A small portion of the hydrogen remains as a gas in the system to satisfy the thermodynamic plateau pressure.

Equation 56

$$n = \frac{PV}{RT} = \frac{1bar * .01L}{.083\frac{bar * L}{mol * K} * 298K} = .0004molH_2$$

The remaining hydrogen, .0016 mol H_2, enters the $LaNi_5$ sample to create .234 g of $LaNi_5H_6$. Because there is not enough hydrogen in the 10 ml reservoir, the system pressure drop is from 5 bar to 1 bar and is equal to the driving pressure differential; such a situation would greatly affect the observed kinetics.

In contrast, a 400 ml reservoir (solid line) under the same conditions has enough hydrogen to hydride the entire sample. The amount of hydrogen in the 400 ml reservoir is:

Equation 57

$$n = \frac{PV}{RT} = \frac{5bar * .4L}{.083\frac{bar * L}{mol * K} * 298K} = .08molH_2$$

After complete hydriding, there is .073 mol H_2 that remains in gas phase. The pressure associated with .073 mol H_2 is:

Equation 58

$$P = \frac{nRT}{V} = \frac{.073mol * .083\frac{bar * L}{mol * K} * 298K}{.4L} = 4.5bar$$

In contrast, a large reservoir under the same conditions has enough hydrogen to hydride the entire sample. After complete hydriding, there is enough H_2 remaining in the gas phase to maintain a pressure of 4.5 bar. The change in system pressure during hydriding is about 0.5 bar (solid line), much less than the 4 bar pressure differential driving the sorption reaction. Data from the large reservoir experiment would have measured sorption to full capacity. The larger reservoir also provides the quasi-isobaric sorption kinetics of the $LaNi_5$ sample as the rates are not impacted by a significant change in the driving which is logarithmic with pressure differential.

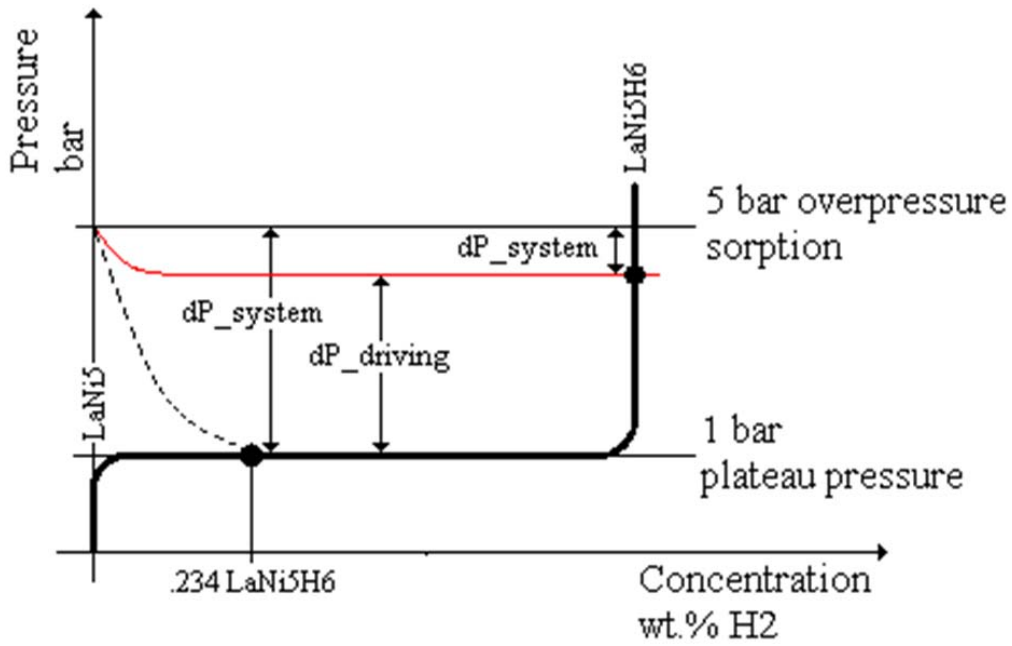

Figure 61. Diagram of the pressure in sorption/desorption system during hydriding reaction. The dashed line represents a test using a reservoir that is too small and the solid red line represents a test using a sufficiently large reservoir.

Another example is presented below to show the important effect of the driving pressure on kinetics. A series of absorption and desorption measurements were performed on $NaAlH_4$ by Weifang Luo who then fit the data with an empirical rate model.[128] In this model, the absorption and desorption rates were dependent not only on temperature but also on the driving pressure (ΔP is the difference between the equilibrium pressure at a given temperature and the applied pressure). The model was validated by comparing predicted desorption curves with measured curves for changing pressures and temperatures. Once validated, the model was then used to predict absorption and desorption rates over a wide range of pressure and temperatures. Absorption rates for the formation of $NaAlH_4$ from Na_3AlH_6, Al and H_2 are presented in Figure 62. These results have important consequences for how such materials would be used in a hydrogen storage application and a first look may be counter intuitive. That is because the plateau pressures increase with temperature for a given applied pressure and the driving pressure differential decreases. Therefore, it is possible that even though mobility increases with temperature, there are practical conditions where it is better to operate at a lower temperature to have faster hydrogen charging of the storage material. This can be seen if one compares the absorption rate at 120°C versus 140°C at a charging pressure of 50 bar in Figure 62.

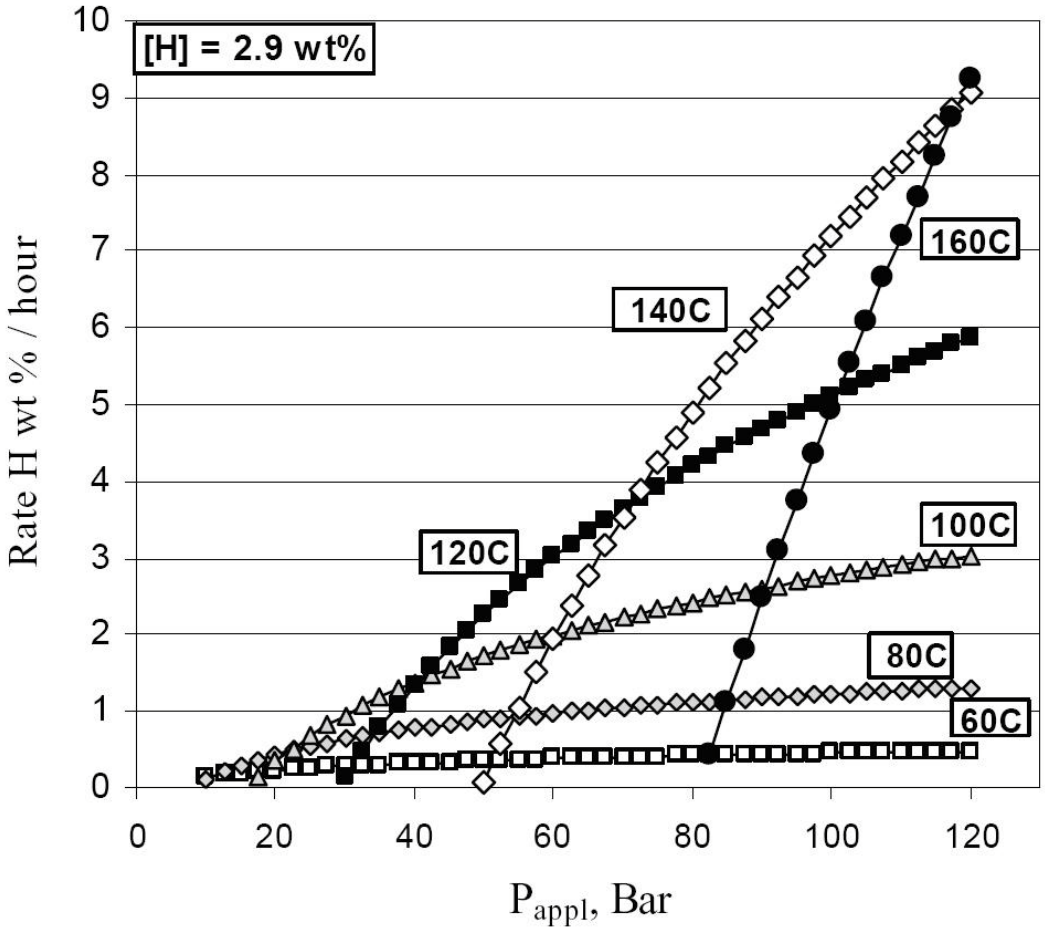

Figure 62. Calculated formation rates of $NaAlH_4$ at several temperatures and applied pressures.[128]

3.10 Thermal Effects

Arguably the most significant factor in accurate kinetics measurements is the interplay of thermal effects in the hydrogen storage material, material holder and measurement system. The importance of thermal effects has been discussed on several occasions in this recommended practices manuscript and will be reiterated. Isothermal or controlled scanning temperature conditions are required to take meaningful fundamental kinetics measurements, in particular when attempting to identify rate-limiting mechanisms. Unfortunately, large temperature variations can occur locally due to the exo- and endothermic reactions and inadequate material thermal conductivity.

3.10.1 Thermal Ballast

Several techniques have been developed to ensure isothermal conditions and minimize thermal effects. Goodell and Rudman were two of the first to obtain approximately isothermal conditions in the kinetics testing of hydrogen storage materials.[123] Their method is simple: 'thermal ballast' is added to the hydride to increase the heat capacity of the sample and dampen the thermal gradients in the system. Ballast material is carefully paired with the hydride being tested to ensure porosity, non-reactivity and minimal contamination. The effect of ballast on the temperature excursions upon hydriding is defined by

Equation 59

$$\Delta T = \left(-\frac{\Delta H}{6.2R} \right) \ln\{1 + (1-b)x_P\}$$

with ΔH the heat of reaction, b the atomic fraction of ballast and x_P the fractional hydride composition of the sample. Equation 59 is presented graphically in Figure 63.[94] To give an example of the significant thermal effects at work in kinetics studies, 98% of a $LaNi_5$–ballast sample must be thermal ballast in order to limit the temperature change during reaction to within 10K of ambient temperature.

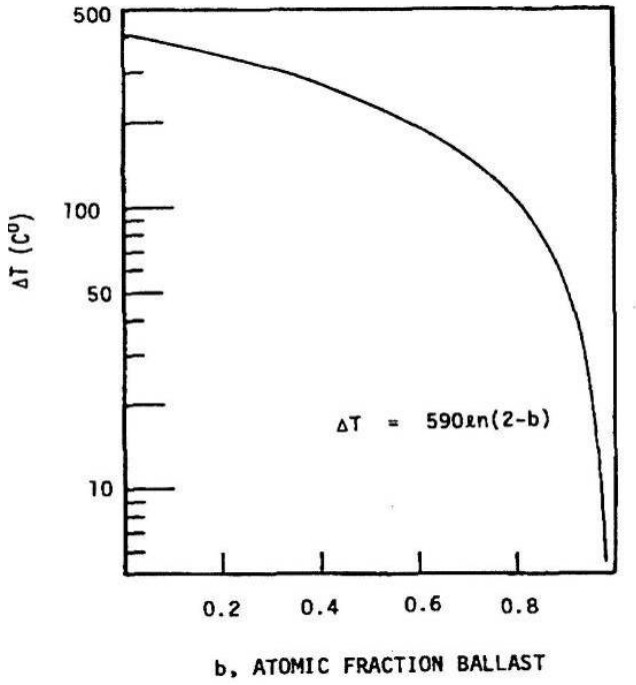

Figure 63. Dependence of the change in the adiabatic temperature during hydriding on the fraction of thermal ballast for the $LaNi_5$-H system.[94]

3.10.2 Heat Transfer-Maximizing Cell

The second method used to eliminate heat transfer effects is to employ a specially designed testing cell to maximize heat transfer to the sample. Maximum heat transfer is accomplished by using a reaction bed that is as thin as possible along with a thermocouple in the bed itself. Supper et al. designed a specialty cell to eliminate heat transfer effects and study the influence of other parameters on kinetics.[129] In the Supper cell, a thin disk of sample material is sandwiched between a porous metal disk that allows for gas transfer and an integrated water-copper heat pipe that acts as an isothermal heat source or sink. The heat pipe is regulated using an external water loop.

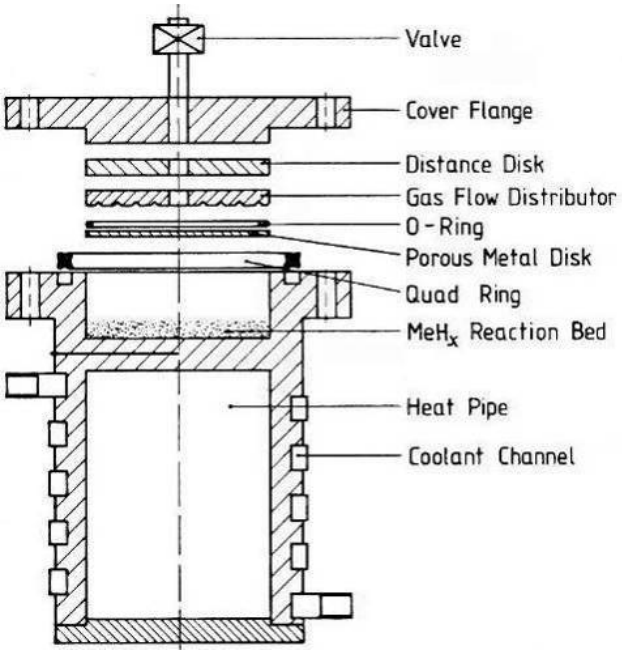

Figure 64. Schematic diagram of the Supper heat-pipe-cooled fast reactor specially designed cell to eliminate heat transfer effects during kinetics testing.[129]

The Supper cell in Figure 64 was used to investigate the effects of temperature and sample thickness on kinetics in $LaNi_{4.7}Al_{.3}$. For the sample with 1 mm bed thickness, increasing the temperature of the sample enhanced the kinetics of the material in agreement with Arrhenius' law.

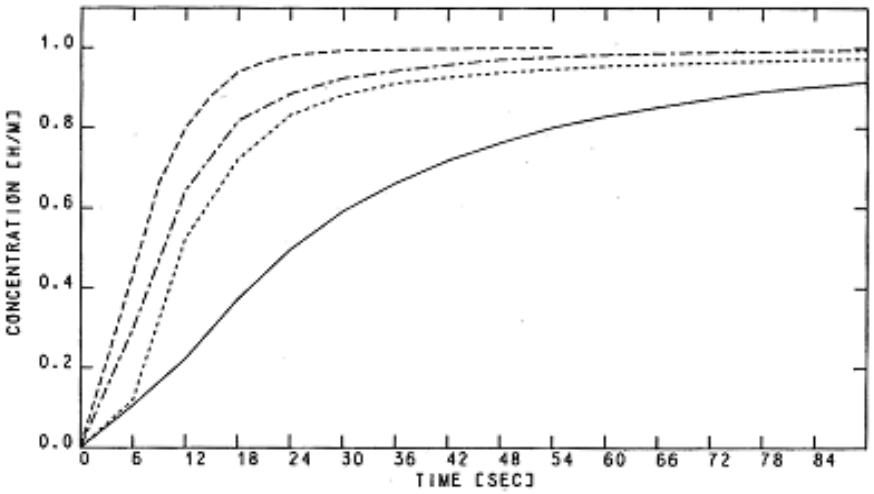

Fig. 3. Absorption reaction rates for $LaNi_{4.7}Al_{0.3}$ (bed thickness, 1 mm; distance from equilibrium, 2 bar): ——, 293 K; · · · ·, 303 K; — · —, 313 K; — — —, 323 K.

Figure 65. Measurements taken with the Supper Cell on $LaNi_{4.7}Al_{0.3}$ to investigate the effects of temperature and sample thickness on kinetics. Sample bed thickness of 1 mm.[129]

3.10.3 Effect of Sample Thickness

The effect of increasing sample thickness on the kinetics at various temperatures in the example above is worth noting. As the thickness of the sample bed is increased, the relation between temperature and kinetics is inversed; reaction rate decreases with elevating temperature, as seen in Figure 66. Supper et al. provide an excellent explanation: the increased thickness of the bed increases the temperature in the bed as the reaction proceeds because the heat of reaction cannot be removed effectively. The van't Hoff thermodynamic relation dictates that the increase in temperature of the sample requires a commensurate increase in the equilibrium pressure in the system. The increased equilibrium pressure reduces the driving pressure differential at higher temperatures because the experiments were all performed at the same distance from equilibrium at the initial sample temperature. This decrease in the true pressure differential because of non-isothermal conditions in turn decreased the rate of reaction. This example of the effect of sample thickness on kinetics shows the complexity of heat transfer effects in drawing conclusions from experimental observation.

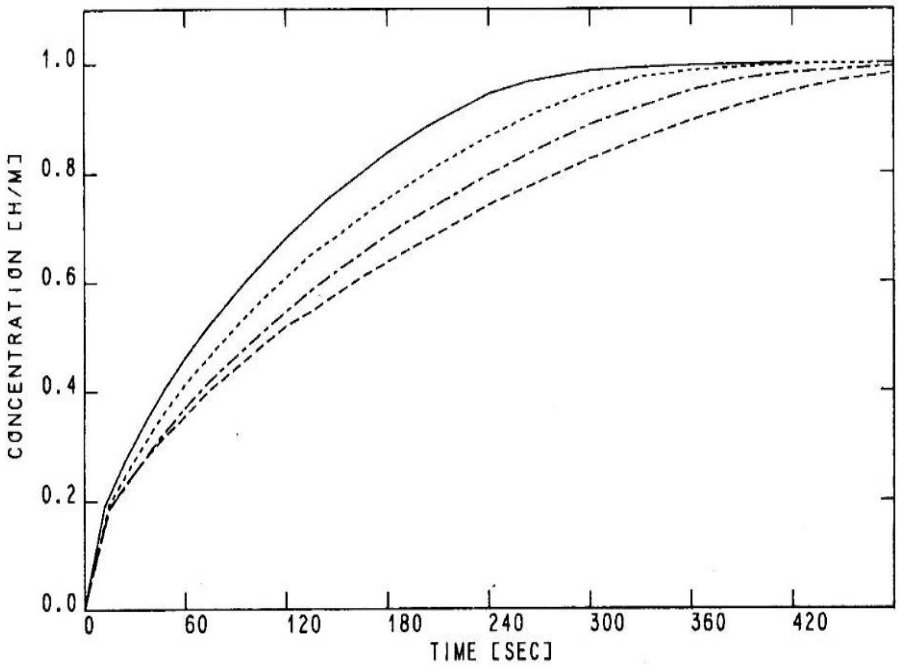

Fig. 6. Absorption reaction rates for $LaNi_{4.7}Al_{0.3}$ (bed thickness, 6 mm; distance from equilibrium, 2 bar): ——, 293 K; - - -, 303 K; — · —, 313 K; — — —, 323 K.

Figure 66. Measurements taken with the Supper Cell on $LaNi_{4.7}Al_{0.3}$ to investigate the effects of temperature and sample thickness on kinetics. Sample bed thickness of 6 mm.[129]

4 Approaches to Improve Kinetics

The kinetic behavior of a material is controlled by mechanisms that are determined by specific material properties. Consequently, it should be possible to improve kinetics by altering these material properties.

4.1 Alloying

By alloying hydrogen storage materials with catalysts and/or other foreign substances, it is possible to improve kinetics in a variety of ways. In chemisorbing materials, catalysts aid in the dissociation of hydrogen at the gas/material interface and allow for more rapid diffusion of atomic hydrogen into the bulk. A stylized view of how this may affect the rate-controlling mechanisms is presented in Figure 67. Although oxygen (white) may passivate one metal (dark gray), the introduction of a second element (light gray) may provide active sites for dissociation, and may also create diffusion paths into the bulk. Metal hydrides can also be blended together to manipulate the thermodynamic and kinetic properties of the base material.

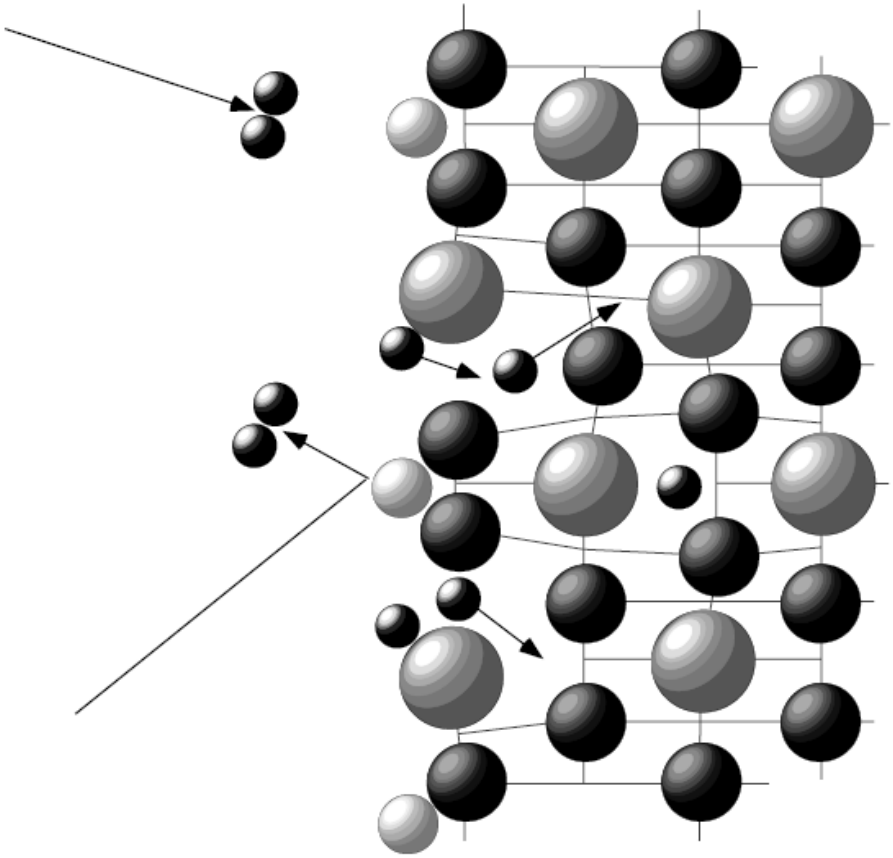

Figure 67. The presence of a second element, either in solution or as a compound, can improve kinetics by providing active sites for dissociation and creating a diffusion path through the lattice.[60]

4.2 Grain Boundaries

Intimate contact between two different phases may improve kinetics by enhanced diffusion through inter-phase grain boundaries (Figure 68). Intimate contact between separated phases can be produced by mechanically milling a mixture of phases together, by vapor deposition of one phase onto the others, or by the solid-state disproportionation reaction of a compound upon hydriding.

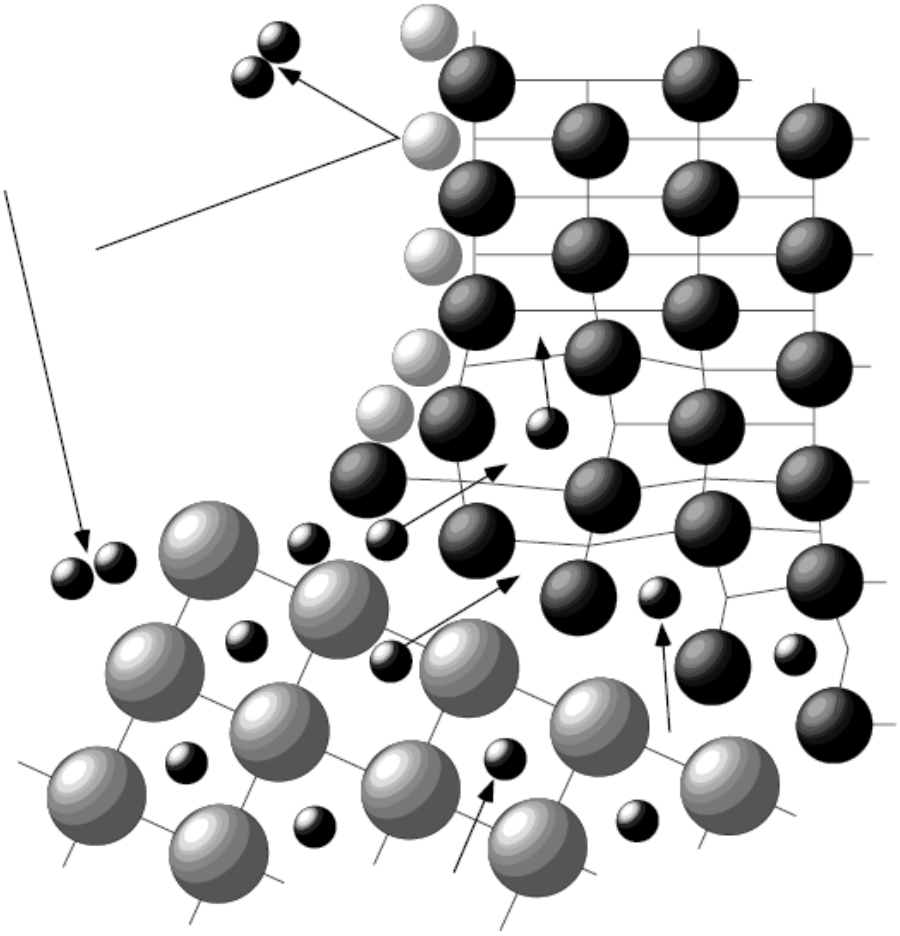

Figure 68. Intimate contact between two different phases may allow atomic hydrogen to diffuse through an active phase and cross the phase boundary into the passivated phase.

4.3 Decrepitation

Kinetics may be enhanced by crack formation due to lattice expansion during hydrogen sorption. In metal hydrides, these cracks bring clean metal surfaces into contact with hydrogen. The oxygen-free surface may promote the hydrogen dissociation reaction and diffusion into the bulk. This process may also be enhanced in multi-phase systems by cracks that form along inter-phase boundaries because of the different amount of lattice expansion in separate hydride-forming as well as non-hydride phases. Such a situation is pictured in Figure 69.

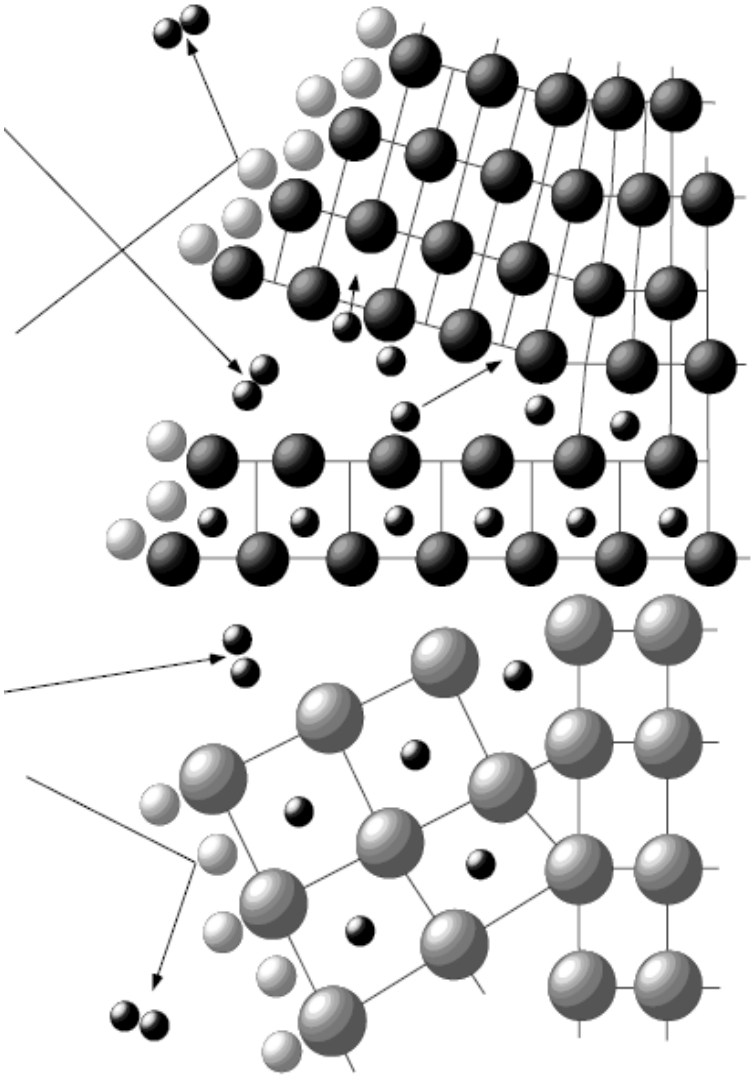

Figure 69. Lattice expansion and crack formation along phase boundaries create clean metal surfaces for dissociation and diffusion.

4.4 Nano-Structuring

Kinetics may be inhibited by diffusion through the lattice of chemisorbing media or through the internal pore network of high-surface area physisorbing materials. In both cases, nano-structuring can increase the diffusivity of hydrogen. In chemisorbing media, nano-structuring increases the surface area-to-volume ratio, which allows for greater access to the bulk and shorter diffusion paths (Figure 70). Diffusion pathways through the internal pore network of physisorbing media are often tortuous and can become occluded. Nano-structuring can offer more direct diffusion pathways and greater access to internal surfaces.

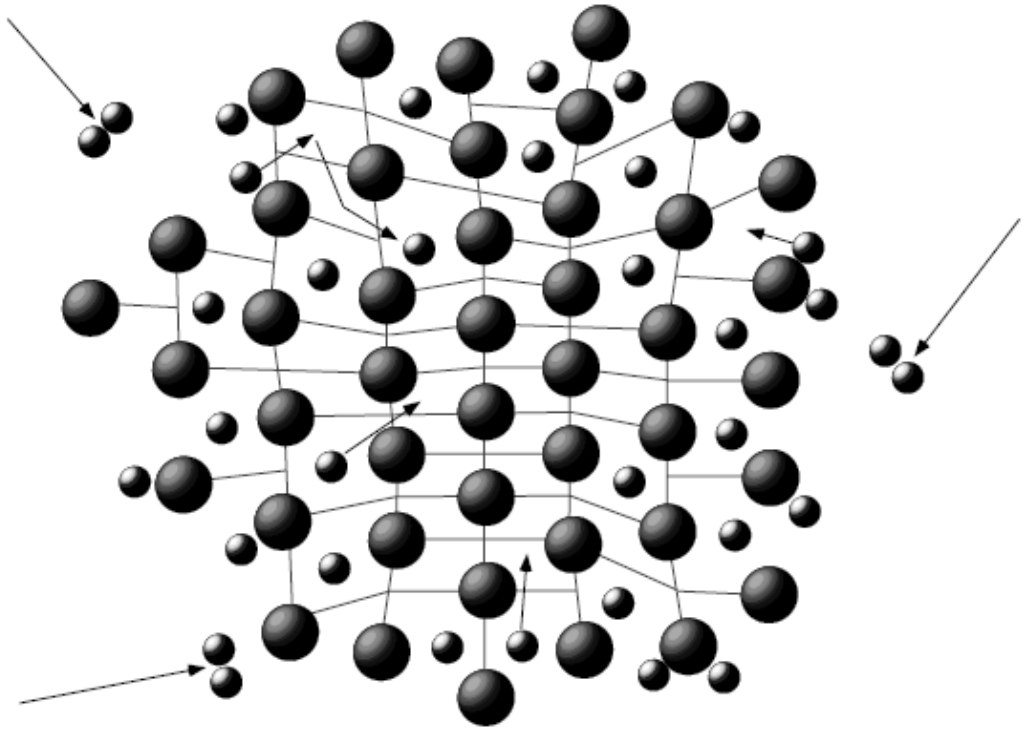

Figure 70. Poor kinetics due to a surface hydride diffusion barrier can be overcome by increasing the material's surface area to bulk ratio (i.e. decreasing the particle size).[60]

4.5 Example of Improvements

An example of enhanced sorption kinetics by altering material properties is the observed rapid absorption and desorption kinetics of Mg-hydride formation in multi-phase composite materials based on Mg, Mg_2Ni and La. A combination of the above concepts was ascribed to improved kinetics measured in these composite materials.[60] The composites were produced by mechanically milling La_2Mg_{17} together with $LaNi_5$. In the process, fine particles of $LaNi_5$ were encompassed by the softer La_2Mg_{17} to create an intimate contact between the two phases (Figure 71). In a second step the composites

underwent a phase and morphology transformation during the rapid absorption and desorption of hydrogen at 300°C. This resulted in the disproportionation of the La_2Mg_{17} and $LaNi_5$ phases. Morphological changes occurred as the La coalesced into fine particles and the Ni combined with Mg in a solid-state reaction to form larger grains of Mg_2Ni. During desorption cycles the remaining Mg likely diffused and sublimated to form a matrix around the other phases. The final product was a composite of fine particles (<1 micron) composed of Mg_2Ni covered with small grains of La-hydride all held together and coated with Mg (Figure 72).

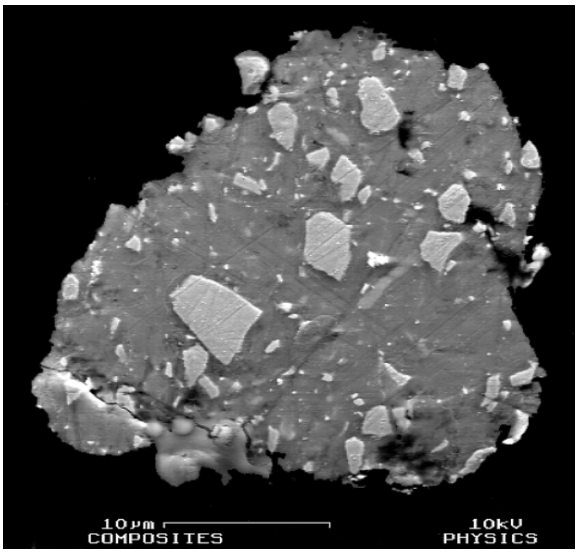

Figure 71. SEM-BSE image of the cross-section of a composite particle formed by mechanically milling La_2Mg_{17} together with $LaNi_5$. The lighter phase is the $LaNi_5$.[60]

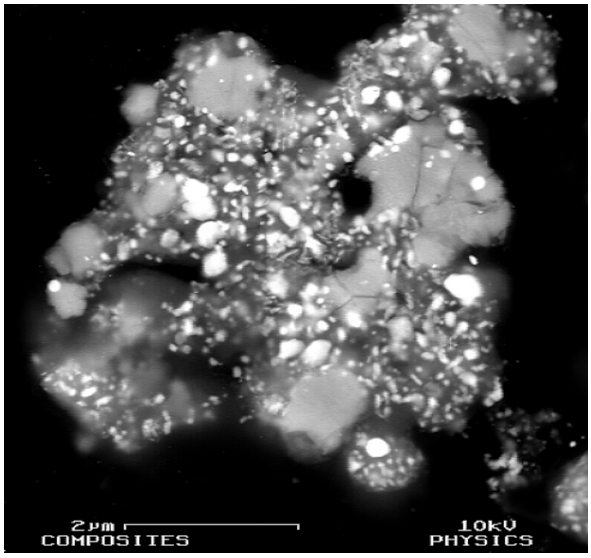

Figure 72. SEM-BSE image of the cross-section of a composite particle after cycling under hydrogen at 300°C. The lightest phase is La, the medium-grey phase is Mg_2Ni, and the dark matrix is the Mg phase.[60]

The kinetics of these composite materials proved to be far superior to those of the individual Mg and Mg_2Ni phases. A study of the relative kinetics of each phase in the composite revealed that the probable mechanisms for the enhanced kinetics were enhanced catalytic dissociation of hydrogen on the Mg_2Ni and La phases, rapid diffusion along inter-phase boundaries and a reduction of the MgH_2 diffusion barrier due to the extremely large surface area of the Mg phase.

5 Kinetic versus Thermodynamic Issues

In pursuit of the ultimate hydrogen storage material it is important to separate kinetic effects from the thermodynamic properties of a material. This is because a material may be kinetically hindered, requiring high temperatures and pressures to achieve reasonable hydrogen sorption/desorption rates, and these high operating conditions are regularly mistaken as inherent thermodynamic properties of the sample. All too often, a material is hastily excluded from hydrogen storage consideration on the basis of its initially observed inability to sorb/desorb hydrogen at moderate temperatures and pressures. In reality the equilibrium thermodynamics may be perfectly adequate for a useful hydrogen storage system but poor kinetics require testing outside a practical range of temperatures and pressures. Figure 73 shows what is considered the range of standard operating conditions for a Proton Exchange Membrane (PEM) fuel cell (shown in grey). As an extreme example, consider a hypothetical material that can thermodynamically operate at room temperature, but which is kinetically hindered such that much higher temperatures would be required to overcome the kinetic barriers. Because the equilibrium pressure increases with increasing temperature Figure 73, it is possible that the kinetic barrier could suppress hydrogenation over the entire range of experimentally accessible pressures, i.e., by the time a temperature is reached where the kinetics allow reaction, the required pressure is too high to be achieved.

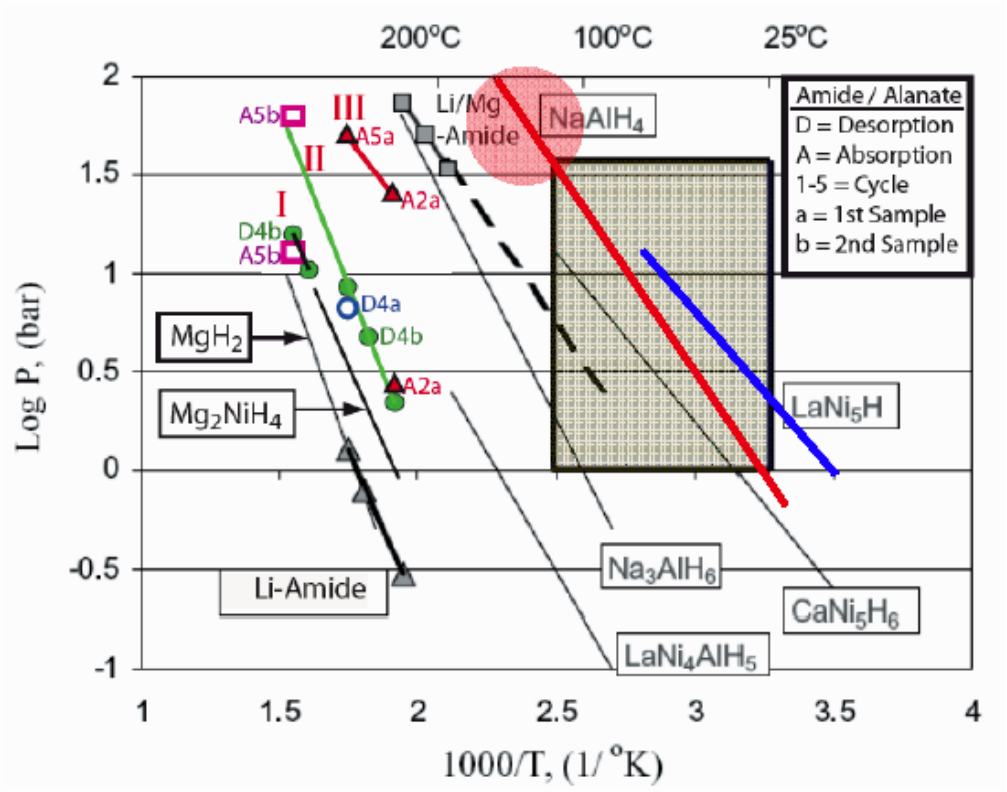

Figure 73. Equilibrium thermodynamics of some commonly researched hydrogen storage materials. The boxed area represents the range of practical operating conditions for a PEM Fuel Cell.[126]

A classic example of the relationship between kinetics and thermodynamics is investigated in the work by Bogdanovic and Schwickardi on the effect of Ti-additives on the hydrogen sorption properties of alanates.[130] Prior to their work, alanates were not seriously considered as hydrogen storage materials because of the extreme pressures and temperatures required for hydrogen absorption. Bogdanovic et al. systematically doped sodium alanate with varying levels of titanium compounds and found that this significantly improved kinetics and by consequence reversibility. This opened the doorway to what followed as an intensive worldwide study of the alanate family as practical hydrogen storage materials. Until the Bogdanovic work, little was done to determine the thermodynamics of the sodium-alanate system because it was nearly impossible to reach thermodynamic equilibrium due to slow intrinsic kinetics of the pure alanate system. Only after the discovery of greatly enhanced kinetics in samples doped with titanium precursors was it was even feasible to make equilibrium PCT measurements, and even these achieve only partial equilibrium conditions at lower pressures and temperatures due to kinetic limitations.

Section 3: Capacity Measurements

1 Introduction and Definitions

Hydrogen capacity is the material property that has had the greatest focus of attention in the race to discover and improve the ultimate hydrogen storage material. While the other critical materials properties (kinetics, thermodynamics, stability, safety, cost and flavor) may have been pushed into the shadows by comparison, it is true that without a reasonably high capacity, a material can not be considered viable for on-board hydrogen storage. And yet, despite all of its appeal and the perceived simplicity of the concept, the hydrogen storage capacity of a material has not been, in fact, either well defined, or (in many cases) very easy to measure, particularly when the measurement of and accounting for gas-phase species other than hydrogen is brought into play. Unfortunately, focus on the glitter of what is not always gold has, on occasion, lead to the expenditure of great efforts, minds, and money on unproductive paths. From this perspective, it is the aim of this chapter to help to clarify the different definitions, practical relevance, and best practices in the measurement of hydrogen storage capacity.

1.1 Hydrogen Storage Materials Classifications

The mechanisms of hydrogen uptake in a material can be separated into "Physisorption", or "Covalent" and "Interstitial", with a cross-over mechanism referred to as "Spillover". These mechanisms are defined in the introduction section 3 .

A material's hydrogen storage capacity is strongly dependent on the hydrogen-material binding mechanisms responsible for hydrogen uptake. Hydrogen storage mechanisms differ among molecularly bound hydrogen that is physisorbed, and hydrogen that is dissociated and covalently bound or occurs in the interstices of metal atoms in alloys. The strength of the hydrogen interactions among these various modes of hydrogen binding affects the overall manner in which a hydrogen storage material will be used in a real application. Because of the different energetics among the classes of hydrogen storage materials, different measurement approaches and definitions of storage capacity are needed to fully describe the hydrogen storage characteristics of these separate classes of materials. For this reason, we will review the hydrogen storage capacity definitions with respect to the different categories of storage materials differentiated by the type and strength of hydrogen binding mechanisms.

To begin with, we separate hydrogen storage materials into three different classes described in the Introduction section 5 :

1) **Physisorbed hydrogen storage materials** that store hydrogen by molecular physisorption or weak atomic chemisorption. These typically have high hydrogen storage capacities at cryogenic (77K) storage temperatures but some ambient temperature applications are being explored as well.

2) **On-board reversible hydrogen storage materials** that store dissociated hydrogen either covalently or as interstitially bound hydrogen. These are able to take up and release hydrogen at moderate temperatures and pressures allowing the materials to be directly recharged with hydrogen *in-situ* on a vehicle

3) **Off-board regenerable hydrogen storage materials** that store dissociated hydrogen as covalently bound hydrogen materials, but that require more complex off board chemical processes for regeneration.

These classes of materials tend to parallel the focus of the US DOE's three different hydrogen storage materials development Centers of Excellence:

1) Sorption,
2) Metal Hydride, and
3) Chemical Hydrogen Storage.

In reality the boundaries are not distinct and there is much overlap between the materials and research centers.

1.1.1 Physisorbed Hydrogen Storage Materials

Hydrogen storage by physisorption or weak chemisorption of H_2 on high-surface-area materials, such as activated carbon, nanostructured materials, and metal organic frameworks (MOFs) has the advantage of inherent reversibility, cyclability, generally rapid release and recharging kinetics and high capacities at moderate pressures (ca. 30 bar). Physisorption generally involves weak interactions of molecular hydrogen with the surface. However, surface adsorption of hydrogen can also include spillover of atomic H and Kubas type binding of molecular H_2. Because these interactions are rather weak, materials that store H_2 by physisorption have the drawback of low storage capacities at near ambient temperatures. Gravimetric storage densities only reach acceptable levels at cryogenic temperatures (77K). Up to now, most physisorption studies have focused on the storage capacity of the materials and have not included thermal performance of the storage system. The net storage capacity of an adsorption based system over a wide range of pressures and temperatures as well as system thermal requirements are important for real world applications. Recent analysis on a systems basis suggest that a 5 kg hydrogen tank of 150 liters capacity of high-surface-area activated carbon (77K and up to 350 bar) will offer an advantage over cryogenic-compressed hydrogen storage if the residual mass of physisorbed hydrogen in the tank is retrieved by heating. The results of this study are summarized in a recent paper by M.A. Richard et al.[131]

In physisorption, intermolecular forces between hydrogen molecules and surface atoms create a region near the surface of the material where the local hydrogen density is greater than in the bulk gas. This region is called the adsorbed phase, or more colloquially the boundary layer (BL), and may extend several hydrogen molecule diameters from the solid surface (shown in Figure 74a).[81] As in other transport fields, it is difficult to quantify the extent of the hydrogen BL because the density, used to define the boundary layer, asymptotically approaches that of the free gas phase. In order to avoid ambiguity, the physical chemist J.W. Gibbs proposed the concept of Gibbsian surface excess (GSE), a measure of the additional hydrogen stored in the boundary layer. GSE allows for the unambiguous and practical determination of the extent and advantage of the adsorption of molecular hydrogen to the surface of a material with respect to the hydrogen storage materials themselves and also with respect to the complete storage systems. The reader is referred to Sircar for a more detailed analysis of GSE theory and application.[81]

A material's excess hydrogen capacity is a measure of the Gibbsian surface excess (shown in Figure 74b). It is this "excess hydrogen storage capacity" which is the preferred capacity representation for physisorption materials like nano-structured carbon, aerogels and MOFs. The complete set of definitions of physisorption capacities and their relation to GSE are presented in more detail below in section 1.4 .

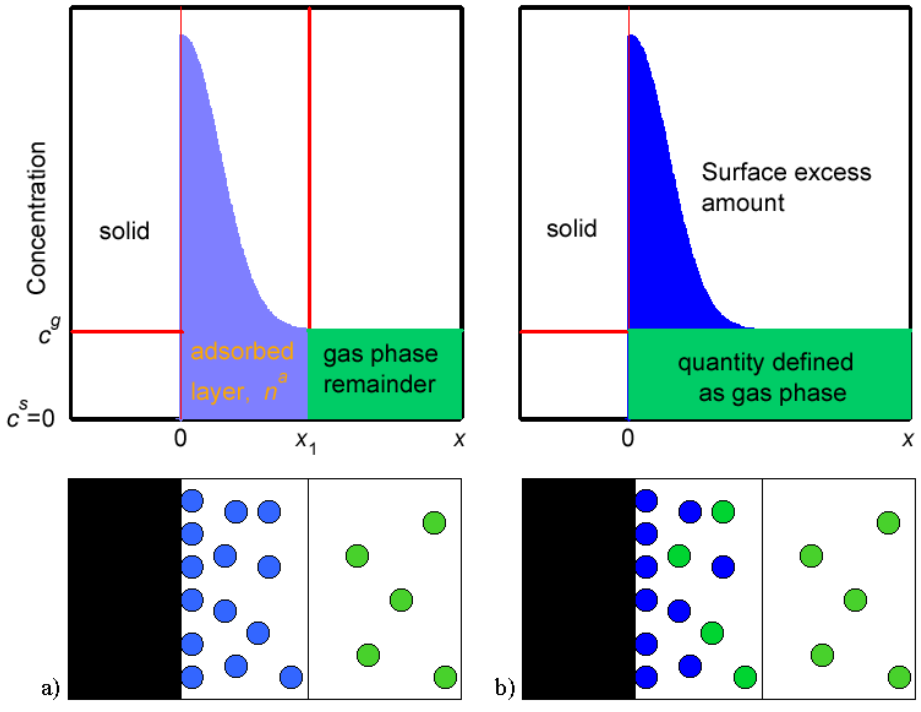

Figure 74. Schematic illustration of (a) physisorbed hydrogen and (b) the distinction between excess and bulk gas phase hydrogen.

1.1.2 On-Board Reversible Hydrogen Storage Materials

On-board reversible hydrogen storage materials consists of a wide range of materials, with the sole requirement that the thermodynamics allow the discharged materials to be recharged on-board a vehicle under reasonable pressures and temperatures Many if not all of the members of this class of storage material release hydrogen endothermically. If the release of hydrogen is very endothermic, heat might have to be supplied to the material to achieve reasonable rates. However, recharging endothermic release materials with hydrogen of course releases heat, and managing the rate of this heat release is often a challenge for on-board regeneration. Within this class of materials, the thermodynamics of release on the order of 30 kJ/mol H_2 provides the ideal stability for the reversible uptake and release of hydrogen at room temperature and 1 atmosphere. Solid on-board hydrogen storage materials include among other things, interstitial metal hydrides, covalently bound metal hydrides including multi-component hydride systems and metal amides, borohydrides, etc. With respect to these "reversible" materials the interstitial metal hydrides and covalent complex metal hydrides have received the most research focus over the last few decades. A brief look at these two classes of materials is presented here in view of capacity measurements.

There are three general types of metal hydrides: interstitial metal hydrides, covalent metal hydrides, and covalent complex metal hydrides. Interstitial metal hydrides are materials such as $LaNi_5H_x$, where hydrogen atoms are found in interstitial sites within the metal atom substructure. The hydrogen bonding is often complex but relatively weak, involving multicenter bonding between hydrogen and the metal. Examples of complex saline hydrides include lithium aluminum hydride, $LiAlH_4$, and sodium borohydride, $NaBH_4$. Covalent metal hydrides are discrete compounds such as MgH_2, AlH_3, among others, where the bonding between hydrogen and metal is very covalent and localized and strong. Complex covalent hydrides are compounds such as metal borohydrides, metal amides, and mixtures thereof, and the bonding between hydrogen and either B or N, etc is highly covalent and strong.

Most metal hydride formation reactions are exothermic and relatively stable below their dissociation temperatures. This means that under suitable activation conditions, the formation reaction will be spontaneous, and the hydrogen will remain stored within the material until a certain desorption temperature is reached.

Hydrogen absorption in reversible interstitial metal hydrides may involve a number of complex, multiple-step mechanisms, such as: Adsorption – Disassociation – Dissolution – Nucleation and Growth and may lead to bulk discrete metal hydride compound formation. Figure 75 illustrates the sequential dissociation of molecular H_2 at the surface, diffusion of atomic hydrogen through the crystal metal lattice to form a hydrogen-metal solid solution that in some circumstances may reach a critical concentration where the nucleation and growth of bulk metal hydride phase occurs.. Hydrogen desorption, follows the reverse path.

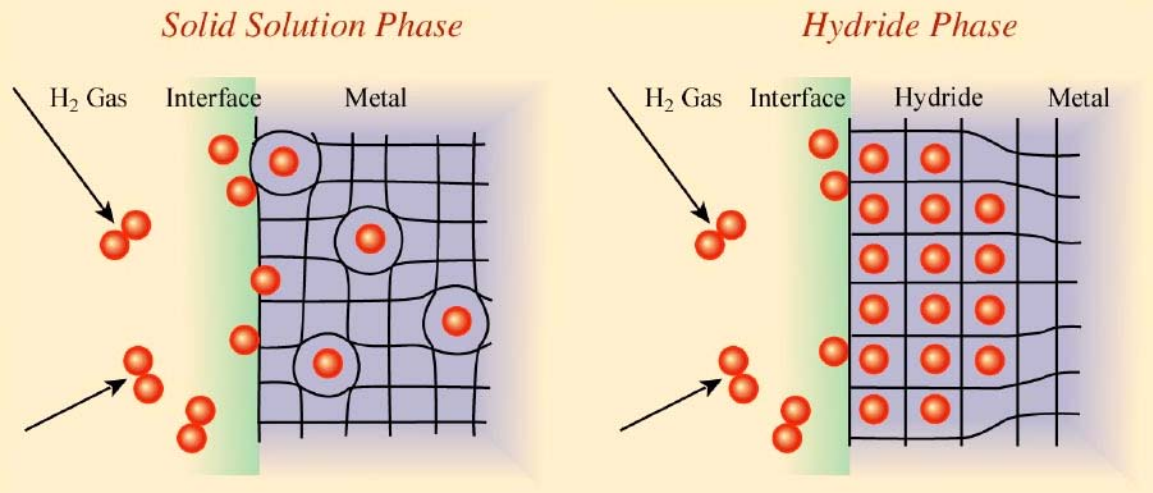

Figure 75. Potential energy curves for the activated or non-activated dissociation and chemisorption of hydrogen on a clean metal surface, followed by the endothermic or exothermic solution of atomic hydrogen into the bulk.

Thus, the equilibrium hydrogen capacity of an interstitial hydride will be dependent on the temperature and pressure conditions of the sample. The idealized PCT diagram of Figure 76 show how hydrogen concentration varies with pressure for different temperatures (T_1, T_2 and T_3). Assuming a flat plateau (which may or may not be the case for a metal hydride) the capacity of a sample at a given temperature will be the concentration of hydrogen in solution in the metal (alpha-phase) below the plateau pressure or the concentration of hydrogen in solution in the hydride (beta-phase) above the plateau pressure. The hydrogen capacity for any pressure at a temperature T_2 is indicated by the red portions of the T_2 isotherm. The capacity becomes continuous at the critical pressure and temperature Tc. For a metal hydrogen system with a sloping plateau, the capacity is simply the equilibrium hydrogen concentration at a given temperature and pressure (the extreme case being amorphous metal hydrides)

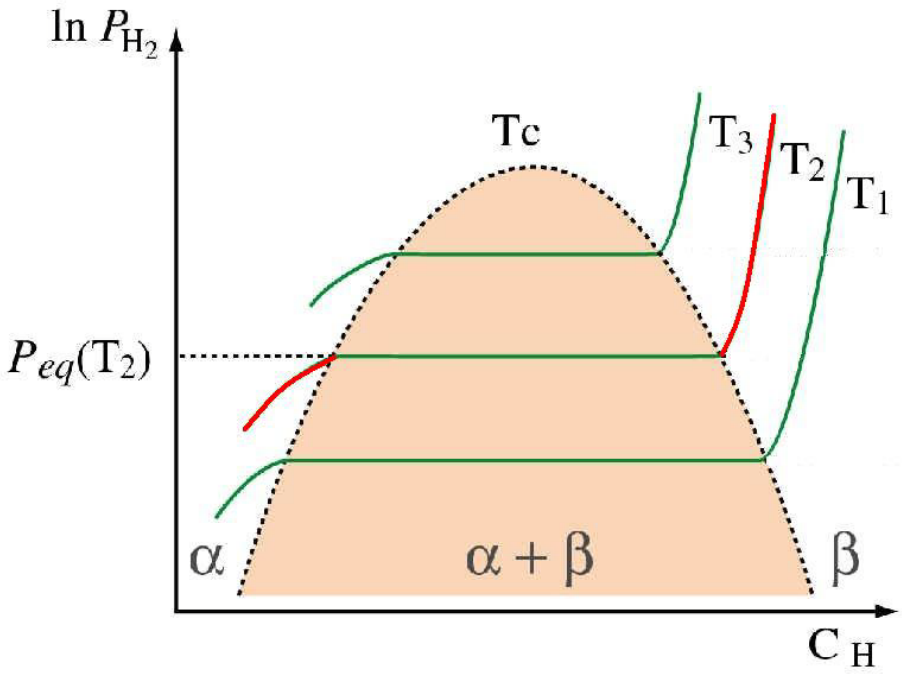

Figure 76. Illustration of a PCT Pressure Composition Temperature phase diagram for hydrogen-metal solid solution α-phase and metal hydride formation β-phase. Temperature isotherms are shown for increasing temperatures T1, T2 and T3.

Complex hydrides generally release and absorb hydrogen through bond-breaking decomposition and recombination reactions sometimes through discreet intermediate phases. Many complex hydride systems, such as $NaAlH_4$, involve multi-step chemical reactions that have multiple dissociation temperatures corresponding to different stable intermediate states. Using the example of sodium alanate again,[30] the practical decomposition of $NaAlH_4$ occurs in two steps. The first step shown in Equation 60 will occur at room temperature with added Ti-dopants, albeit at extremely slow rates, and at 220 ^{o}C without additives. This step accounts for 3.64 wt% of hydrogen, or half of the total theoretical storage capacity of 7.28 wt%.

Equation 60 $\mathbf{3NaAlH_4 \rightarrow Na_3AlH_6 + 2Al + 3H_2}$

The reaction in Equation 61 occurs at ~250 °C, releasing another 1.82 wt% of hydrogen.

Equation 61 $\mathbf{Na_3AlH_6 \rightarrow 3NaH + Al + 3/2H_2}$

The remaining 1.82 wt% hydrogen remains as stable NaH which is not released under practical conditions. Thus, the total theoretical capacity of the sodium alanate system is 5.46 wt.%. The actual measured capacities will generally be much lower that the theoretical capacity due to 1) addition of additives to the total sample weight, 2) the reaction of additives or impurities with the alanate to form inactive phases and 3) incomplete reactions due to poor kinetics or segregation of reactants.

The PCT measurements of the Ti-doped Na-Al-H system in Figure 77 show the reactions of Equation 60 and Equation 61. Because these complex hydrides absorb and desorb hydrogen through chemical decomposition / recombination reactions and the measurements allowed enough time for the system to reach equilibrium, the plateaus are essentially flat. Thus, while the hydrogen concentration during the measurements varied with dosing and time between 0 and 2.5 H/Al, the hydrogen capacity of this material is either 1.0 H/Al or 2.5 H/Al depending on the applied pressures and temperatures.

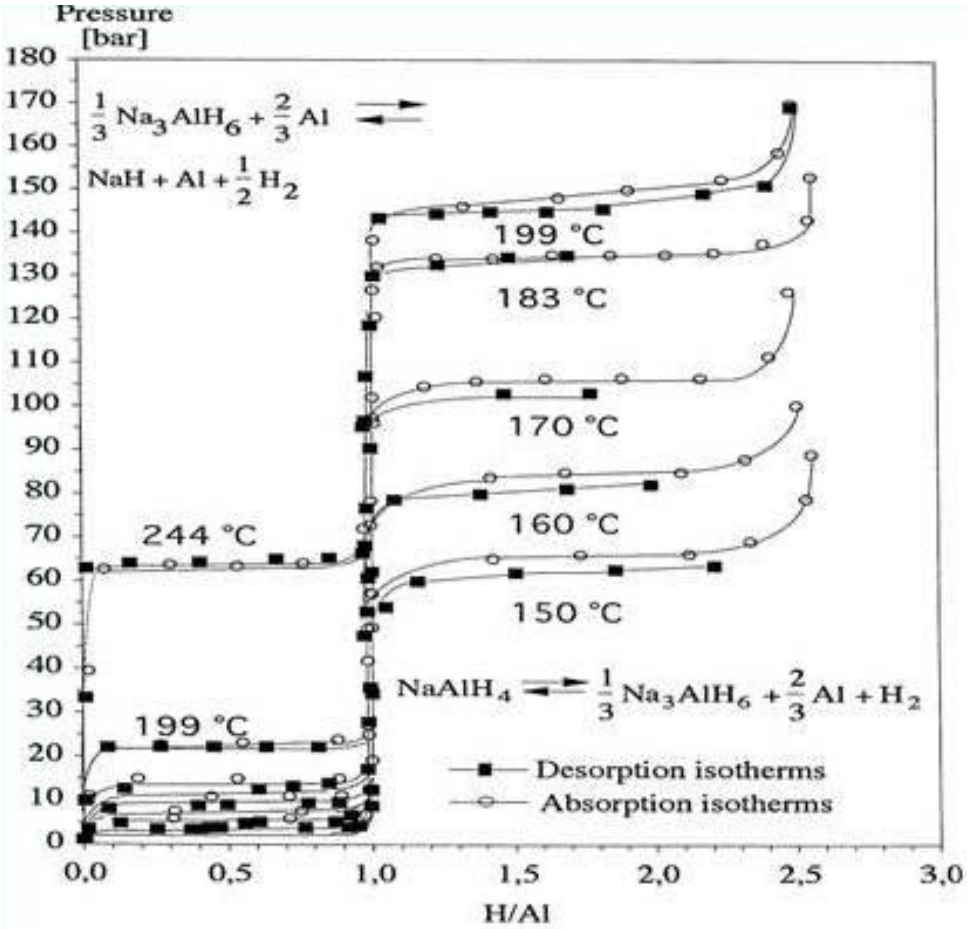

Figure 77. PCT measurements at different temperatures for the decomposition and rehydriding of $NaAlH_4$ and Na_3AlH_6.[132]

1.1.3 Off-board Regenerable Hydrogen Storage Materials

There are numerous approaches to hydrogen storage that result in "spent fuel" that is not feasible to regenerate on-board, and these storage materials are considered here. The key feature of these materials is that they typically release hydrogen in an overall exothermic set of reaction sequences, and the dehydrogenated products are too thermodynamically stable to rehydrogenate in a practical sense. These materials may require chemical regeneration in an off-board process. Perhaps the most explored example of an off-board regenerable storage material is ammonia borane (AB), NH_3-BH_3, a molecular solid that releases hydrogen stepwise to liberate hydrogen, heat, and "BNH_x", where x is determined by the severity of the dehydrogenation conditions. Losing one mole or 6.5 wt. % of H_2/mole of AB results in the known compound cyclotriborazane. Losing two moles or 13 wt. % of hydrogen generates the molecular compound borazylene. Loss of additional hydrogen (up to 16 wt. % may be readily delivered) presumably results in the formation of cross-linked borazylene units, forming so-called polyborazylene, and other BNHx oligomers or polymers.

Regeneration of polyborazylene with H_2 pressure is too endothermic and not feasible in a practical sense, and so spent AB must be regenerated using a chemical process. Another subclass of potentially off-board regenerable covalent hydrogen storage materials are certain organic hydrocarbon compounds, where hydrogen is stored as C-H bonds, and released endothermically. Researchers at Air Products have led the way in exploring a variety of endothermic hydrogen release compounds.[133] Another example of an off-board regenerable storage material that received some attention is the simple molecular solid sodium borohydride. Controlled hydrolysis of concentrated aqueous solutions of sodium borohydride release hydrogen and generate sodium borate. Rehydrogenation of sodium borate is too endothermic, and so regeneration of the borohydride from the borate in an energetically efficient pathway is a significant technical challenge. In all of these cases, the bonds that are being broken are quite strong and covalent B-H or N-H bonds, with bond strengths on the order of 300-400 kJ/mol.

In addition to the importance of the on-board storage capacity and the hydrogen release rates, the energy efficiency of the off-board regeneration of spent fuel is a key contributor to the overall energy efficiency of the fuel cycle. Chemical hydrogen storage provides a diversity of options and could also be used for hydrogen delivery where it offers the opportunity for a liquid or solid fuel infrastructure with the potential for no direct hydrogen handling by the consumer.

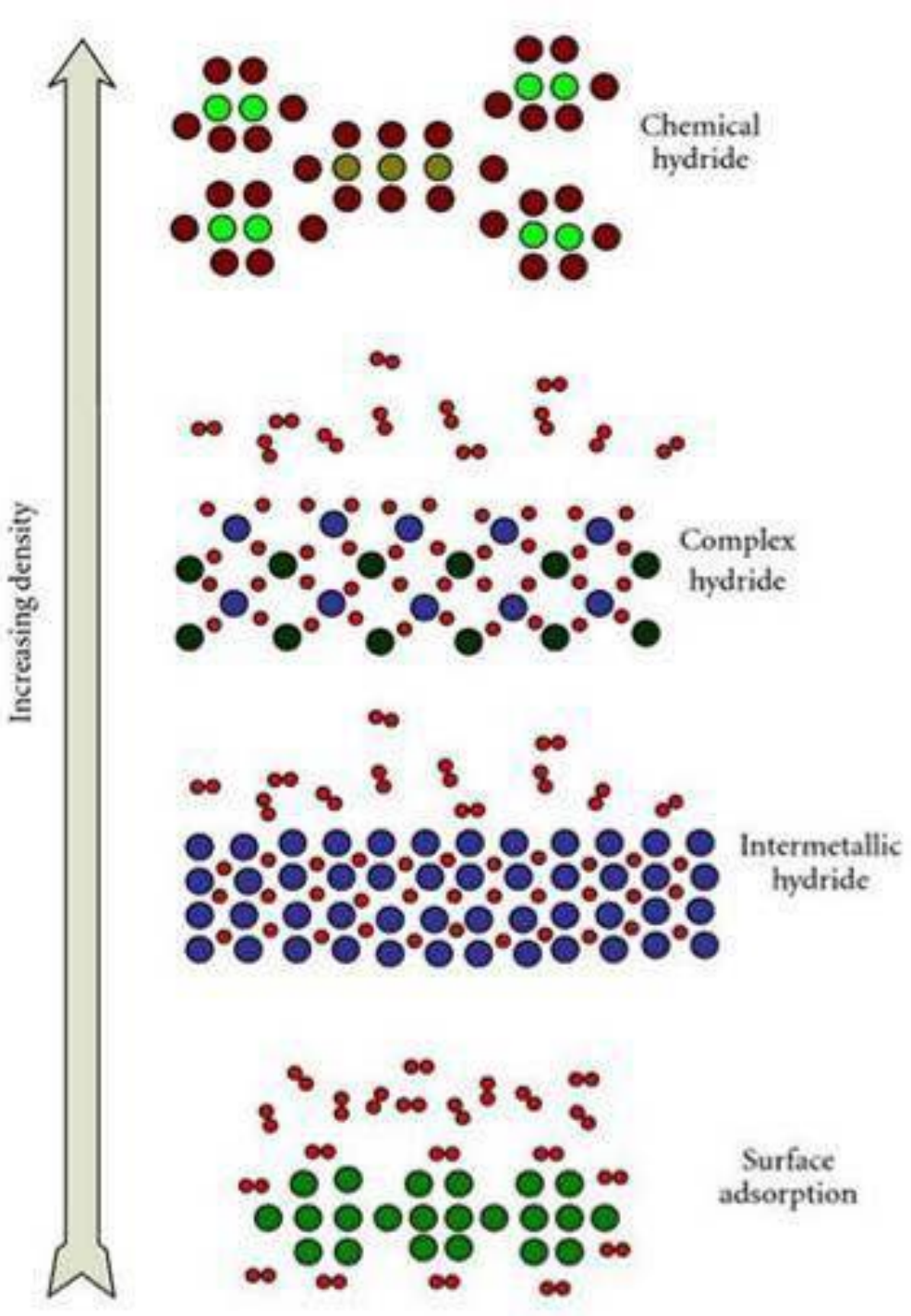

Figure 78. Schematic representation of nature of differences in binding and density of hydrogen ranging from surface adsorption to chemical hydrides. Chemical hydrides can show significantly higher density of deliverable hydrogen as compared to other hydrogen storage materials.

1.2 Definitions of Capacity With Respect to Hydrogen Storage

The general concept of hydrogen storage capacity is straightforward. Unfortunately, behind the conceptual simplicity is the difficult task of making the translation from laboratory measurements of gas sorption to reliable values for the practical amount of hydrogen that can be stored for use on-board a hydrogen fuel cell vehicle. At an initial level, "storage capacity" values depend on a wide range of precise and often confusing definitions being used in the field of hydrogen storage research. For example, the term "Total Capacity" is used in different ways. It can refer to the total amount of hydrogen stored by a storage *system* as well as the amount stored within a storage *material*. It is important to be able to distinguish between the various capacities reported in literature and understand which capacities are most informative at different levels of hydrogen storage research. The definitions that are used for capacity can be very different depending on whether the context is; understanding fundamental sorption processes, developing improve materials, or hydrogen delivery at system level. For this reason, we begin this section with, what we hope to be a concise and definitive summary of the different capacity definitions as they relate to different material types and research focus.

Definitions of capacity can be divided into two overlapping categories, those based on the where the hydrogen located (gas, near surface or in the bulk of a material) and those based on the physical considerations that limit the quantity of deliverable hydrogen (pressure, temperature and time).

The two most instructive capacities at the materials development and system performance levels are the total material and system capacities. The total material capacity is the maximum amount of stored hydrogen that is associated with the storage material itself; this includes hydrogen stored by compound formation or absorbed in the material, hydrogen physisorbed to the surface of the material and any gaseous hydrogen within the pores of the material. For chemical hydrides and traditional metal hydrides, the total material capacity is typically equivalent to the atomic hydrogen stored within the bulk of the material because of metal hydrides' minimal porosity and negligible storage contribution made by adsorption. For porous materials, the hydrogen stored as a gas within the pores and physisorbed to the surface can be significant as the porosity or total surface area increases. The total system capacity is determined by adding the total material capacity and the hydrogen stored as a gas in the free (unoccupied) volume of the total storage system. Being able to determine the total system capacity is critical for practical applications because this represent the total amount of hydrogen available to a fuel cell, combustion engine, or other real world devices.

Another important consideration is that, for the purpose of the research being conducted for which this document has been created, hydrogen is stored to be used as

an energy carrier. Because this covers hydrogen storage in a wide range of forms, compressed, liquid, physisorbed, onboard reversible or off-board rechargeable hydrogen it is sometimes difficult to make useful comparisons of storage methods based only on the quantity of hydrogen stored. Ultimately it is the energy storage capacity (or efficiency) that is important. It seems reasonable then, that eventually materials and systems will need to be evaluated on a complete wells-to-wheel energy balance basis. Such an analysis would need to account for all energy inputs in producing the hydrogen to be stored, the transportation and dispensing and perhaps cooling (physisorption) of the hydrogen to the storage system (for on-board regenerable materials), the energy required to release or initiate release of the hydrogen, and for off-board systems, the energy input required to regenerate the fuel from spent fuel, and the transportation and dispensing of fuel and spent fuel to and from the reprocessing plant.

Currently, such a complicated wells-to-wheels analysis is premature, even though certain aspects are being worked on, but will not be covered here. However, hydrogen storage capacity at a materials level and best approximations at a systems level are key parameters in evaluating the potential for materials to meet the goals of a practical hydrogen energy economy. With respect to hydrogen storage capacity, it is critical that the terminology, measurement methods, and relationship to stored energy are well understood and employed.

An important consideration with respect to these measurements is that, while hydrogen capacity is of significant technologically of interest, in many of the materials systems being explored, the potential for generation of volatile gas-phase impurities exists, and the various impacts of these impurities must be assessed as well as the total hydrogen storage capacity. How gas-phase impurities influence the capacity measurement, or how the presence of gas-phase impurities might impact the reversibility of the material, or the loss of material from the system, and the impact of gas-phase impurities on the downstream uses of the hydrogen stream must be considered when developing methodology to accurately and precisely determine the true hydrogen capacity of a system and the quality of the hydrogen stream released.

1.2.1 Synopsis of Capacity Terminology

Material Hydrogen Content: the total quantity of hydrogen that is present in a material.

Reversible capacity: the quantity of stored hydrogen for on-board reversible materials that can actually be taken up and subsequently released by a material under reasonable (Laboratory) pressures and temperatures (-196 to 500^{o}C and 100 mtorr to 300 bar).

Usable capacity: the total quantity of stored hydrogen that can be released by a material within the operating range (high and low) of temperatures and pressures found in a mobile storage application (USDOE operating targets: Temperature of -196 °C [LN2] to 85^{o}C [PEM fuel cell] and a delivery pressure range of 3 to 40 bar).

Onboard Irreversible capacity: the quantity of stored hydrogen that can be released but not reabsorbed by a material under temperature and pressure conditions reasonably achievable in a mobile storage application.

GSE (Gibbs Surface Excess): Gibbs proposed a model to represent the gas-solid adsorption system as a two dimensional interface which is arbitrarily located within the bulk gas phase that creates a new adsorbed phase, called the Gibbsian adsorbed phase.[134] In Gibbs' view, the gas-phase properties extend unchanged up to the solid surface. Differences between the actual and the unchanged properties are attributed to a hypothetical surface layer. The surface excess adsorption is the difference between the actual amount of gas adsorbed and the amount of gas that would be present in this adsorbed layer if the density of the adsorbed phase was the same as the equilibrium (bulk gas) phase.

Excess adsorption amount (sometimes refer to as excess capacity): Extra hydrogen present due to adsorption of the gas to the surface of a material. Excess capacity is the measured surface excess adsorption capacity of a material. It represents excess hydrogen per unit sample over what would be present if the bulk gas density prevailed all the way to the surface, it can be positive, negative or zero. It is the material hydrogen storage capacity that is determined directly using volumetric and gravimetric methods.

Maximum excess adsorption amount: The peak excess hydrogen adsorption capacity at a specific temperature for a range of pressures.

Absolute adsorption capacity: the total amount of hydrogen present in the space where the attractive potential from the surface is effective (adsorbed phase). This is all of the gas in the adsorption boundary layer including the bulk phase gas and the surface excess gas. Because the boundary layer is a hypothetical construct, the absolute adsorption capacity can not be measured experimentally. It can be a useful conceptual quantity but relies on uncertain assumptions regarding the arbitrary placement of the dividing line and surface shape between adsorbed and bulk gas.

Total material capacity: all hydrogen actually absorbed in the bulk, as well as, all gas adsorbed to the surface of a material and present as a gas within the pores and cracks of individual particles of a material. Thus, total adsorption often includes compressed gas, which is not present in the adsorption boundary layer.

Active material capacity: is a measure of how much hydrogen can actually be delivered from the portion of the material that actively stores the hydrogen. It excludes the mass of material such as catalysts or thermal conductivity additives that do not store the hydrogen. This is a useful quantity when making materials performance comparison for kinetics studies.

Theoretical material capacity: all hydrogen that could theoretically be absorbed in the bulk and adsorbed to the surface of a material and as a gas within the pores and cracks of individual particles of a material.

Total system capacity: all hydrogen actually absorbed in the bulk and adsorbed to the surface of a material and as a gas within the pores and cracks in a material and in the free volume of the storage container.

System excess capacity (also referred to as "engineering" excess capacity): Is the capacity of a storage tank filled with a hydrogen storage material and hydrogen over and above the amount of hydrogen stored in the same tank at the same hydrogen temperature and pressure if the tank were empty (no hydrogen storage material). It answers the question: At what point is it better to have an empty tank?

Gravimetric material capacity: the total quantity of stored hydrogen with respect to the mass of the storage material (may be energy/mass material, mass H_2/mass material, wt.% [wt-H/(wt-material + wt-H)], wt-ratio [wt-H/wt-material], etc.).

Gravimetric system capacity: the total quantity of stored hydrogen with respect to the mass of the storage system including the vessel and ancillary equipment to operate the storage system (may be energy/mass material, mass H_2/mass material, wt.% with respect to the material mass, etc.).

Volumetric material capacity: the total quantity of stored hydrogen with respect to the apparent volume of the storage material (may be energy/volume material, mass H_2/volume material, wt.% with respect to the material volume, etc.).

Volumetric system capacity: the total quantity of stored hydrogen with respect to the total volume of storage system including the vessel and ancillary equipment to operate the storage system (may be energy/volume material, mass H_2/volume material, wt.% with respect to the material volume, etc.).

1.2.2 Capacity vs. Concentration

Before concentration and capacity can be discussed in depth, it is important to differentiate between capacity, a material property, and the concentration variable in hydrogen storage measurements.

Concentration and capacity provide information about the hydrogen content of a sample. Concentration is the temporal measure of hydrogen content in a sample and is the most fundamental variable in hydrogen storage; it is also the one important variable that cannot easily be measured directly in the material. In all cases, calculated relationships are used to determine hydrogen concentration from measurable (independent) variables. Concentration is the fundamental quantity needed for determining capacity and many other storage properties, including kinetics, thermodynamics and cycle life. Factors that affect concentration measurements will invariably affect the determination of other vital properties of a hydrogen storage material.

A simple example illustrates the difference between concentration and capacity. Figure 79 shows an idealized PCT isotherm of $LaNi_5$, a well-known hydrogen absorbing material, at two different stages of hydriding. At a specific temperature with a corresponding plateau pressure of 1 bar, the theoretical material capacity of $LaNi_5$ is 1.38 wt.% H_2 corresponding to $LaNi_5H_6$. Neglecting hydrogen in solution in the alloy or the hydride, this is the maximum steady-state hydrogen concentration achievable at a given temperature. Thus, the capacity of a storage material is equal to the maximum concentration when fully hydrided (or 1.38 wt.% for $LaNi_5H_6$ as shown in Figure 79). The sample's hydrogen concentration is a measure of hydrogen content which depends on pressure, temperature, time (kinetics and thermodynamics), and the quantity of hydrogen to which the sample is exposed. For example, a sample that has only been exposed to enough hydrogen in one dose to convert half of the sample to the $LaNi_5H_6$ hydride will have a hydrogen that increases in time from 0 to 0.69 wt.% H_2. When equilibrium is achieved, the sample's final concentration will be 0.69 wt.% H_2. Regardless, the sample's capacity under these conditions is still 1.38 wt.% H_2.

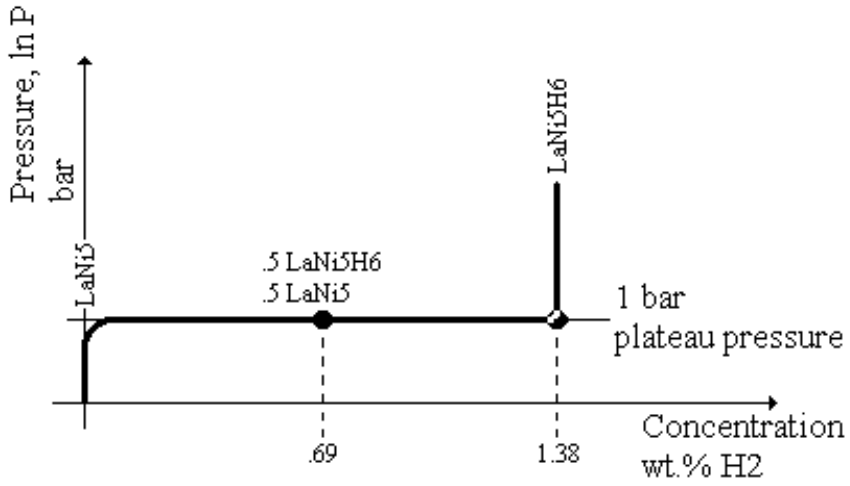

Figure 79. Illustration of the relationship between concentration and capacity for a flat plateau hydride.

In this regard, concentration is treated as a variable and not a property of a material. Thus, concentration is used to describe the *state* of the material in the same way temperature is used. A material's capacity, on the other hand, is a specific material property that is dependent temperature and pressure.

From the broadest definition, "capacity" represents the maximum steady-state hydrogen content in a material and capacity measurements are central to developing materials and systems that meet the criteria established by the US Department of Energy (DOE) for on-board hydrogen storage. However, hydrogen capacity can be

defined in a number of different ways which depend not only on how hydrogen is stored in a material (binding mechanisms) but also on the issues being addressed with respect to capacity (fundamental vs. application questions). Hydrogen binding mechanisms and important definitions of "capacity" are presented in the next two sections.

1.2.3 Reversible vs. Usable Hydrogen Capacity

An important consideration when referring to the hydrogen storage capacity of chemical compounds is to identify the actual amount of stored hydrogen that can be practically used. We refer to this as the "Reversible Capacity" regardless of whether the recharging process will be on-board or off-board a vehicle. This is the amount of hydrogen that can be released and recharged to a material under reasonable conditions. Here we define these conditions as the pressures and temperatures achievable in a typical laboratory environment (-196 to 500^{o}C and 100 millitorr to 300 bar). In many cases, there is some hydrogen that remains chemically bound to its host that will not be used under any condition and thus will not count towards the usable capacity of the material or system.

It is important to stress the difference between "Usable Capacity" and "Reversible Capacity". The definition of both are somewhat ambiguous, since laboratory conditions and the conditions required for absorption and desorption of hydrogen in a real world application vary significantly. For example, the DOE has target for a fuel cell vehicle system is an operating temperature range of -40 to 85^{o}C and an operating pressure range of 3 to 40 atm for hydrogen supply during vehicle operation, but determines the filling time based on a temperature of 20^{o}C. We have modified the definition to include physisorption materials at -196^{o}C. The upper temperature limit could also be modified depending on whether some form of storage system heating is used and if the hydrogen energy conversion device is another type of fuel cell than the low temperature PEM or an internal combustion engine. Here we define the conditions for "Usable Capacity" as the pressures and temperatures needed for the operation of PEM fuel cell transportation system without hydrogen storage system heating (-196 to 85^{o}C and 3 to 40 bar). Such a system is referred to as "passive" in contrast with "active" systems in which the residual hydrogen associated with the operating pressure of the system can be extracted by heating or pumping.[135]

1.2.4 Hydrogen Content vs. Reversible Capacity

Usable capacity was discussed in section 1.4.7 , 1.5 and 1.6 above with respect to the minimum required pressure limitations of physisorption material, on-board storage materials and off-board hydrogen storage materials. For physisorption, the 3 bar pressure required by the fuel cell may severely limit the accessible amount of hydrogen

stored in the adsorption materials if cryogenic temperatures of the storage system are to be maintained. For the other hydrogen storage materials, the same pressure limit holds, except that generally much less of the hydrogen storage capacity is locked up in the 0 to 3 bar pressure range. Typically, most of the stored hydrogen will be in an optimized chemical system that releases most of the hydrogen at a pressure above the required pressure of the application (fuel cell).

It is important to make the distinction between the hydrogen "content" of a material system and the reversible (or usable) capacity. In materials other than physisorption materials, a large amount of hydrogen may be inaccessibly tied up in a very stable hydride phase that can not be released given the practical pressure and temperature conditions of the application. There are many hydrogen systems that have hydrogen contents that are much higher than the actual practical reversible hydrogen storage capacity. Some examples of hydrogen content are given in Figure 80.

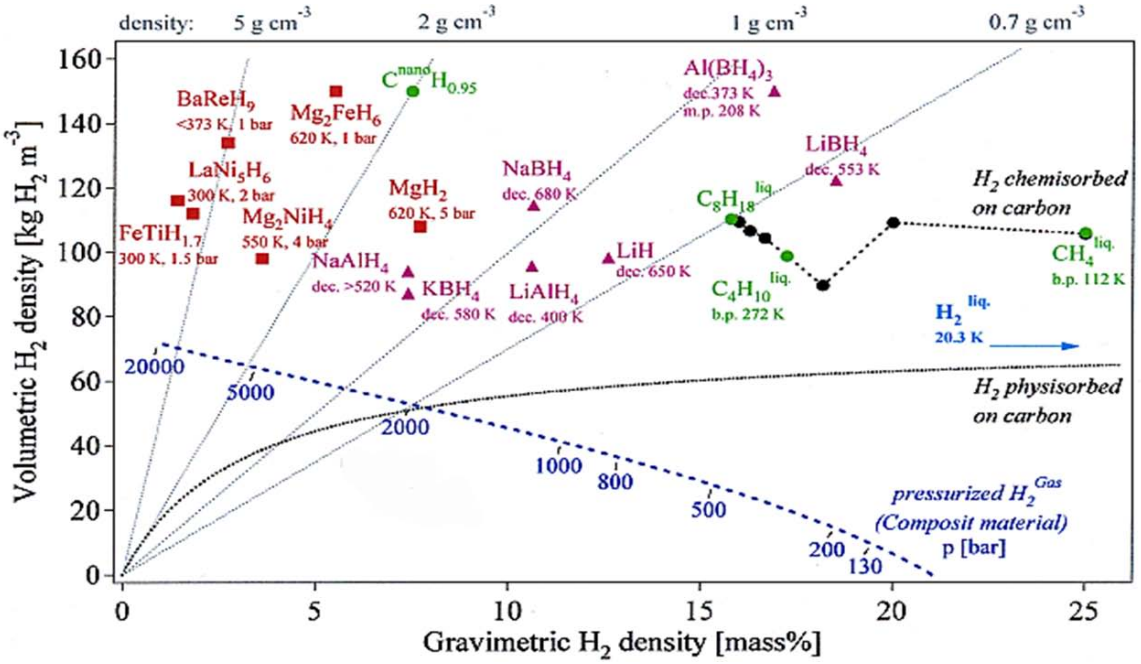

Figure 80. Hydrogen content of different hydrogen storage materials.[3]

Taking the well studied alanate $NaAlH_4$ as an example, the pure compound has a hydrogen content of 4H per $NaAlH_4$ or 7.4 wt.%. However, for all practical purposes, the reversible hydrogen storage capacity is less than 4 wt.%. This is because a large portion of the hydrogen in this system is tied up as irreversible NaH in the sequential reactions:

Equation 62 $\mathbf{NaAlH_4 \rightarrow 1/3\ Na_3AlH_6 + 2/3Al + H_2 \rightarrow NaH + Al + 3/2H_2}$

The first reaction releases a theoretical 3.7 wt.% and the second an additional 1.9 wt.%. The true reversible capacity is further reduced by weight and secondary reactions of the addition of kinetic enhancing additives (typically Ti-compounds) as well as the kinetic limitations of the reactions.

As nature is inclined to make hydrogen storage a challenge it seems that we find our selves surrounded by very high hydrogen content compounds (water at 12.5 wt.% being one of them) that can not be considered practical hydrogen storage materials. The grand challenge then is to discover ways to modify some of these high hydrogen content materials to reversibly take up and release hydrogen under practical conditions.

1.2.5 Active Capacity (All Materials)

Another material capacity definition that can apply to all types of materials whether hydrogen is physisorbed or chemisorbed is what we refer to as "Active Capacity". This is the capacity of hydrogen stored in a material measured with respect to the mass of the active component of the material. That is the portion of the material that actively participates in desorption or sorption processes. All other components of the total hydrogen storage material are excluded, such as: catalyst reaction byproducts (e.g. NaCl…), heat transfer material and media (e.g. carbon, aluminum powder or structures…), macrostructure support material (e.g. mesoporous carbon or silicon confinement or template material, thin film substrates…).

This definition of capacity is most useful for fundamental or materials development studies, in which one is comparing, desorption or sorption properties of different modifications of the same material. From a materials perspective, "Active Capacity" is a measure of how much hydrogen can actually be delivered from the portion of the material that actually stores the hydrogen. This is particularly important for kinetics studies and is addressed in detail in 3.5.1 and 3.5.2 of the kinetics chapter. Since rates are typically being measured in units of wt.% per time, to make a comparative analysis of the effect on kinetics of different catalysts or additives, rates should be compared on an active wt.% capacity basis and not on total capacity. Thus, for this purpose, we have defined the "Entire Material Capacity" including active and inactive material components as:

Equation 63

$$Entire\ \ wt.\% = \frac{mass_{H_2}}{mass_{sample} + mass_{H_2}} * 100\%$$

and the "Active Material Capacity" as:

Equation 64
$$Active\ wt.\% = \frac{mass_{H_2}}{mass_{active\ sample} + mass_{H_2}} * 100\%$$

It is also of value when comparing improvements in the capacity of the active component by the modification of catalysts or other additives that will themselves affect the weight of the storage material. If the total capacity is used for comparison rather than the active capacity, it is possible that a heavier additive that improves the storage capacity of the main component of the material will appear less effective than a lighter additive than has a less beneficial effect and this could lead to the incorrect conclusion about which additive is potentially more effective in improving capacity.

1.3 Units of Measured Hydrogen Capacity

It is useful to start with a discussion of the most commonly used units of hydrogen storage capacity.

Hydrogen per formula unit [H/f.u.] has been a common unit in the study of hydrides in that the discovery of hydrides and research on the properties of hydrides generally focused on single phase hydride compounds. However, the current research on materials for hydrogen storage often involves multi-component materials. For this reason, hydrogen capacity today is most commonly presented in units quantifying hydrogen on a per-mass or per-volume basis. Typical units are:

Mass hydrogen per mass sample (wt. ratio) [g/g]: $\frac{M_{Hydrogen}}{M_{solid}}$

Weight Percent hydrogen (wt.%) [g/g]: $\frac{M_{Hydrogen}}{M_{solid} + M_{Hydrogen}} \times 100$

Moles hydrogen per mass sample (moles H) [Moles H/g]: $\frac{moles_{Hydrogen}}{M_{solid}}$

Volume hydrogen per mass sample (STP Vol. H_2) [liters/g]: $\frac{Liters_{H2}}{M_{solid}}$

Note that the first definition (wt. ratio) may be most useful in some cases as it is naturally related to other *specific* quantities of interest. It is thus readily compatible for comparison and correlations with quantities such as specific surface area (m^2/g), specific volume (ml/g), and other concentrations (mol/g). On–the-other-hand, second definition (wt.%) is somehow more representative of the performance of the material.

1.4 Physisorption Materials

The hydrogen storage capacity of physisorption materials involves some complex details that are important to understand including the differentiation between "excess capacity", "absolute capacity" and "total capacity" as well as the potential for significant impurity effects due to the large surface area of this class of materials. These details can be overlooked and cause confusion on how to report hydrogen storage capacities and have occasionally lead to mistaken representation of capacity results in the field of hydrogen storage research.

It is vitally important for physisorption measurements of any kind, that capacity data is properly labeled as either "excess", "absolute", or "total" capacity. And equally important that any assumptions made in determining the capacity values are clearly reported.

The basic result that is generated from both volumetric and gravimetric measurements is "excess" hydrogen capacity. From a best practice point of view and consistency in the field, the measured hydrogen "excess" capacity is what should be reported. Everything else, absolute and total capacity, is an estimate based on this physical measurement and will only be as valid as the assumptions made in making these estimate. It is important from a system storage perspective to have a good idea of "absolute" and "total" capacities, but it is equally important to report how these values were determined and what assumptions were made when presenting such values.

Detailed concepts and definitions of material and system capacities for physisorption materials are presented in this section. However, a simple illustration is given below in Figure 81 to clarify the three most common capacity terms (*"excess", "absolute", or "total" capacity)* for physisorption materials.

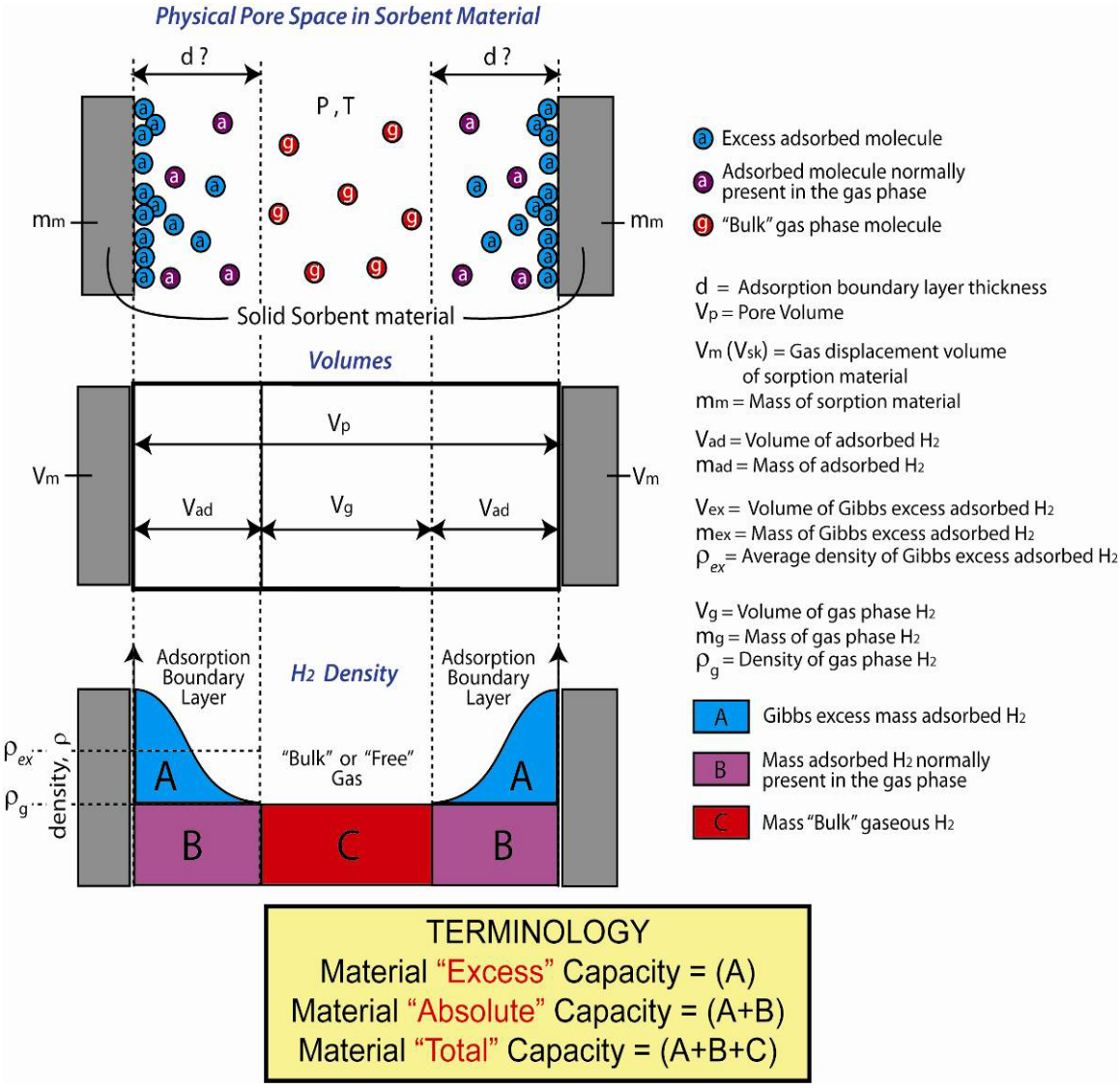

Figure 81. Illustration of physisorption hydrogen storage material capacity terminology.[29]

Physisorption hydrogen storage materials rely on the interaction of molecular hydrogen and the solid surface of storage materials with extremely high surface areas. Physisorption is restricted to adsorption and occurs when the forces involved are weak intermolecular forces, also known as van der Waals forces. It is useful to make a distinction between molecular physisorption, in which the H-H bond in the gas phase is preserved in the sorbed state, and chemisorption, in which the H-H bond is broken during the sorption process. Physisorption is usually accompanied by multilayer molecular adsorption at the surface of the material depending upon temperature.

The important quantities pertaining to physisorption hydrogen storage by a solid adsorbent (s), the adsorbate (a) and the adsorptive gas (g) are illustrated for a simple Gibb's excess schematic diagram in Figure 82.

The adsorptive gas phase is described by a real gas equation of state $\rho_g(H_2, P, T)$, as a function of pressure (P) and temperature (T)where ρ_g is the real gas density of the sorptive gas in the storage container in the absence of any sorbent interactions. The volume of the adsorbent material (V_m) is the volume of the sorbent which is impenetrable to the adsorptive gas. For a porous material V_m is referred to as the skeletal volume (V_{sk}). Typically, the skeletal volume is assumed to be equal to the helium volume (V_{He}). That is the gas displacement volume of the sample using helium gas as a probe.

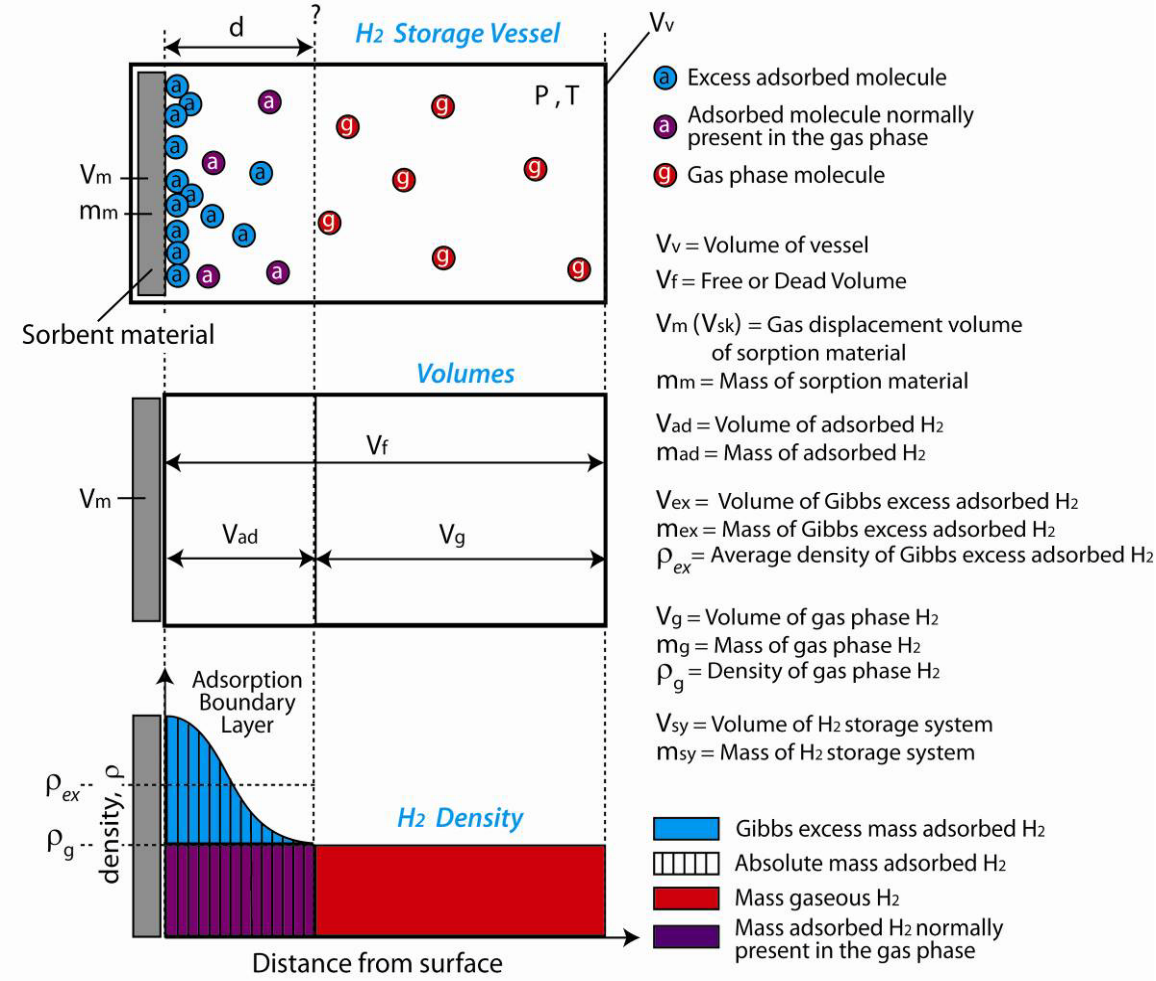

Figure 82. Illustration of the Gibbs surface excess mass for a physisorption material in a storage vessel or measurement volume Vv.[29]

The free gas volume (V_f) (sometimes called the "dead volume") is the difference between the instrument vessel volume V_v (or at a storage system level, the total storage tank $V_{empty\ vessel}$ volume, see section 1.4.11) and the material volume, and is expressed as $V_f = V_v - V_m$. The free gas volume V_f is often measured directly using helium gas and the volumetric technique. For this approach to be valid it is important that the that helium does not physisorb to the sample surface in significant quantities. This is probably a valid assumption for most materials at room temperature and pressures lower than 10 bar. However, at high helium pressures (100 bar) or low temperatures (77K) this assumption may no longer be valid. The adsorbed phase volume (V_{ad}) designates the volume where adsorptive molecules are "influenced predominantly" by the adsorbent interaction potential. Near saturation, the characteristic decrease of the excess isotherms has been related to the mass of gaseous hydrogen displaced by this volume.[31]

It should be noted however, that is not the only possible reason for an observed maximum in the excess capacity isotherm. It may also be caused by an error in the use of helium to determine V_f if helium adsorption onto the sample is not taken into account. This is illustrated in Figure 83 for low temperature measurements of hydrogen adsorption on high-surface-area activated carbon fiber materials. In this example a 10% increase in the apparent (temperature corrected) free volume V_f causes a significant reduction and the appearance of a maximum in the excess capacity. While this effect has been exaggerated in this example for illustrative purposes, errors in helium volume calibrations at low temperatures due to helium adsorption are a real concern.

One simple way to test for such effects is to perform the same helium volume measurement at low temperature on the sample to be tested and on a low surface area material (example: glass or steel beads) having the same gas displacement volume (as determined by known bulk density of the materials). A significant difference in measured volumes would indicate significant helium adsorption by the high-surface-area sample material.

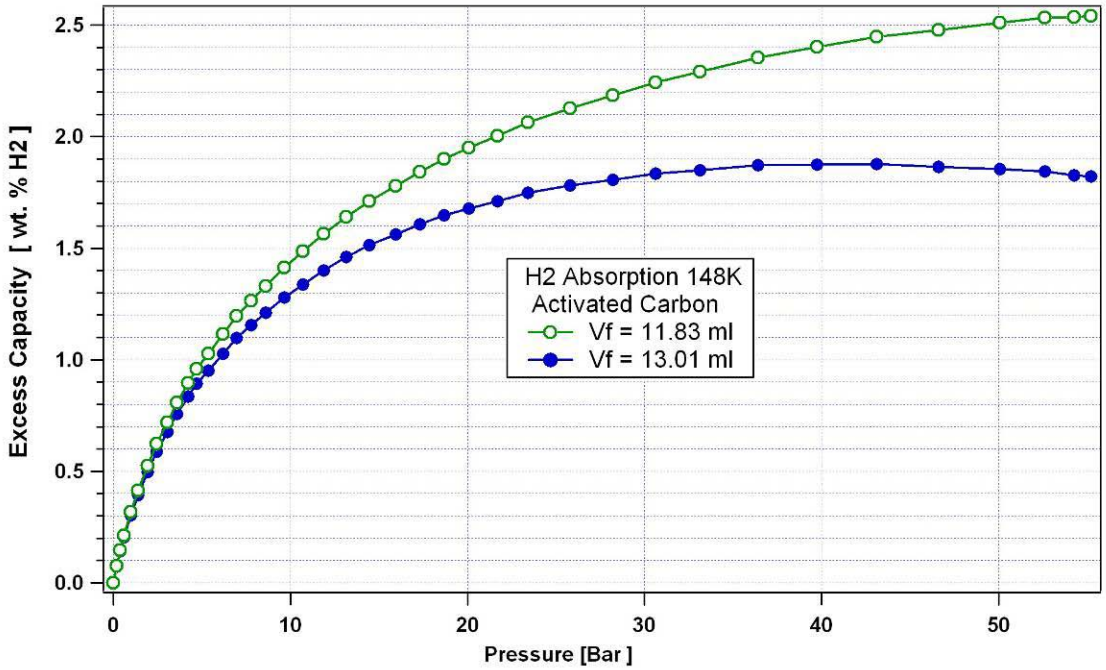

Figure 83. Illustration of the effect of error in the free volume determination on surface excess hydrogen adsorption capacity measurements.

In a microporous material, the adsorbed phase volume (V_{ad}) could be related to the total pore volume if the pores are small enough that all gas in the pores experience van der Waals attraction to the material at the same time (i.e. due to overlap of the potential from opposite walls). The adsorbed phase density in Figure 81 is plotted in the lower diagram as a function of distance from the sorbent surface. On the sorbent surface the density is higher than that of the gas phase, and cannot be directly measured. The quantities which are typically known before an experiment are the total vessel volume (V_v) (or system vessel volume ($V_{empty\ vessel}$) in the case of an actual storage tank), and the mass of the sorbent, m_m. The quantities which are measured during a typical capacity measurement experiment are the free gas volume V_f (to provide sample skeletal volume $V_{sk} = V_V - V_f$) the pressure (P) and temperature (T) of the bulk adsorptive gas, and in the case of gravimetric measurements, the total mass of the adsorptive system (m_T), which is the mass of the sample plus adsorbed gas $m_T = m_m + m_{ad}$ corrected for buoyancy.

1.4.1 Density of Porous Solids

A key aspect of being able to measure "excess adsorption capacity" through either gravimetric or volumetric measurements is to be able to determine the skeletal density of the physisorption material.[136] This is typically done by helium pycnometetry. That is helium at a measured pressure and temperature in a calibrated volume is released into a sample vessel of a known empty volume and the pressure re-measured. The volume of the sample vessel with the sample inside is determined from the resulting pressure. The difference between the empty sample vessel volume and the measured volume gives the skeletal volume of the sample and together with the samples mass, the skeletal density of the porous material.

These measurements involve a few important assumptions: 1) that helium is accessible to all the pores of the adsorbent, 2) that there is no significant helium adsorption under the measuring conditions, 3) the equation of state and temperature distribution is adequately accounted for in the gas mass balance determination and, 4) that there are no impurities in the helium gas before or after exposure to the sample.

With respect to these assumptions it is generally held that pores which have a diameter of less than 2.25 Å (the Lennard-Jones kinetic diameter) are not accessible to helium will also not be accessible to hydrogen. It is also generally assumed in the literature that helium at ambient conditions (near or below 1 bar and room temperature) will not be adsorbed to the materials surface in any significant quantity.[81]

As shown later in Figure 87 the adsorption capacity is generally proportional to the pore volume or more exactly the specific surface area of the material. Thus, measuring the specific surface area of a sample material can provide much insight into the physical chemical interpretation of hydrogen physisorption. Such measurements are also made through gas adsorption studies.[137]

It is useful when discussing the surface properties of solids having large specific surfaces, to distinguish between the ***external*** and the ***internal*** surfaces. The external surface includes all the protrusions and all cracks that are wider than they are deep. The internal surface consists of the walls of all cracks, pores and cavities which are deeper than they are wide. Despite being somewhat arbitrary, the distinction between an external and an internal surface is useful in practice. A wide range of porous solids have an internal surface greater by several orders of magnitude than the external surface. The total surface of a solid thus being predominantly internal and for a given mass of solid, the surface area is inversely proportional to the size of the constituent particles.[138,139]

It is useful to have a good knowledge of the range of pore sizes in a porous solid. The pore sizes in a porous solid must be of a suitable size to admit, hold, and discharge individual gas molecules. If the pores are too small, the gas molecules can not enter. If

they are too large, most of the molecules of gas in the pore behave as a gas under pressure with rapid movement and molecular collisions. They are not packed as tightly and bound to the surface in the adsorbent structure.[140]

The individual pores may vary greatly both in size and in shape within a given solid and between materials. The conventional classification for pore size has been defined by the International Union of Pure and Applied Chemistry (IUPAC) and is summarized below. The classification is arbitrary and was developed on the basis of the adsorption of nitrogen at 77K on a wide range of porous solids.[141] The basis of the classification is that each of the size ranges corresponds to characteristic adsorption effects.

CLASSIFICATION OF PORES ACCORDING TO THEIR WIDTH [139]

PORE TYPE	**WIDTH**
Micropores	Less than ~ 20Å
Mesopores	Between ~ 20 and ~ 500 Å
Macropores	More than ~ 500 Å

Porous materials may contain pores made up of highly regular structures or cracks, crevices, and tortuous passageways. For all of these materials three distinctly different types of density measurements are possible, one that includes and one that excludes these pores. And a third definition that defines sample volume in terms of the volume of a container into which a known quantity of material (powder or pieces) can be filled or packed. This last density includes not only the pore spaces within the material but also the spaces among the particles or pieces. The following is a summary of these three different density definitions:

1. Skeletal density: also termed the absolute or true density, excludes both the intraparticle spaces that may be in the particles and the interparticle spaces.
2. Apparent density: also termed as the envelop density, includes the intraparticle but excludes interparticle spaces.
3. Packing density: also referred to as bulk density includes both intra- and interparticle spaces.

Note that the term “bulk density” causes some confusion because it is variously used for both apparent density and packing density. For example, the density obtained from filling a container with the sample material and vibrating it to obtain near optimum packing is also called “bulk density”.[86] This would be what is referred to here as the packing density. Similarly, X-ray density may be equivalent to skeletal density for porous solid materials and apparent density for crystalline open framework materials.

For reporting hydrogen storage capacity measurements, it is important to make clear the distinction between the *apparent density* and *skeletal density*, which are different for highly microporous materials. The apparent density includes both the volume occupied by skeletal framework of the adsorbent and the pore volume:

Equation 65

$$\rho_A = \frac{m}{V_{sk} + V_{pore}},$$

where *m* is the mass of the adsorbent. The apparent density can be determined from the slope of the helium buoyancy correction. For a crystalline sample, the apparent density is the same as the crystallographic density. On the other hand, the skeletal density does not include the pore volume:

Equation 66

$$\rho_{sk} = \frac{m}{V_{sk}}.$$

These three different definitions of density use quite different equipment to be measured. Helium can fill all open spaces including that of the pores of sizes as small as 0.3 nm. Therefore, the resulting density from using helium is the skeletal or absolute density which is being ever more frequently referred to simply as the "helium density".

Note however, that the assumptions listed above, ***in particular that helium does not adsorb to the material during helium density measurements***, are not always valid for many high-surface-area materials.[142] Because knowledge of the skeletal density of the material is crucial to the accuracy of both gravimetric and volumetric measurements, great care should be taken in the determination of the skeletal density of samples being measured. This is discussed in more detail in sections 2.3.1.7 below.

The relationship between materials and system volumes can be expressed as follows:

Equation 67

$$\textbf{Free Volume: } V_f \approx V_{He}$$

Equation 68

$$V_f = V_{pore} + V_{void} + V_{empty\ vessel} - V_{pk}$$

Equation 69

$$V_f = V_{empty\ vessel} - V_{skeletal}$$

These different volumes as we have defined them here and the related densities are represented schematically in Figure 84.

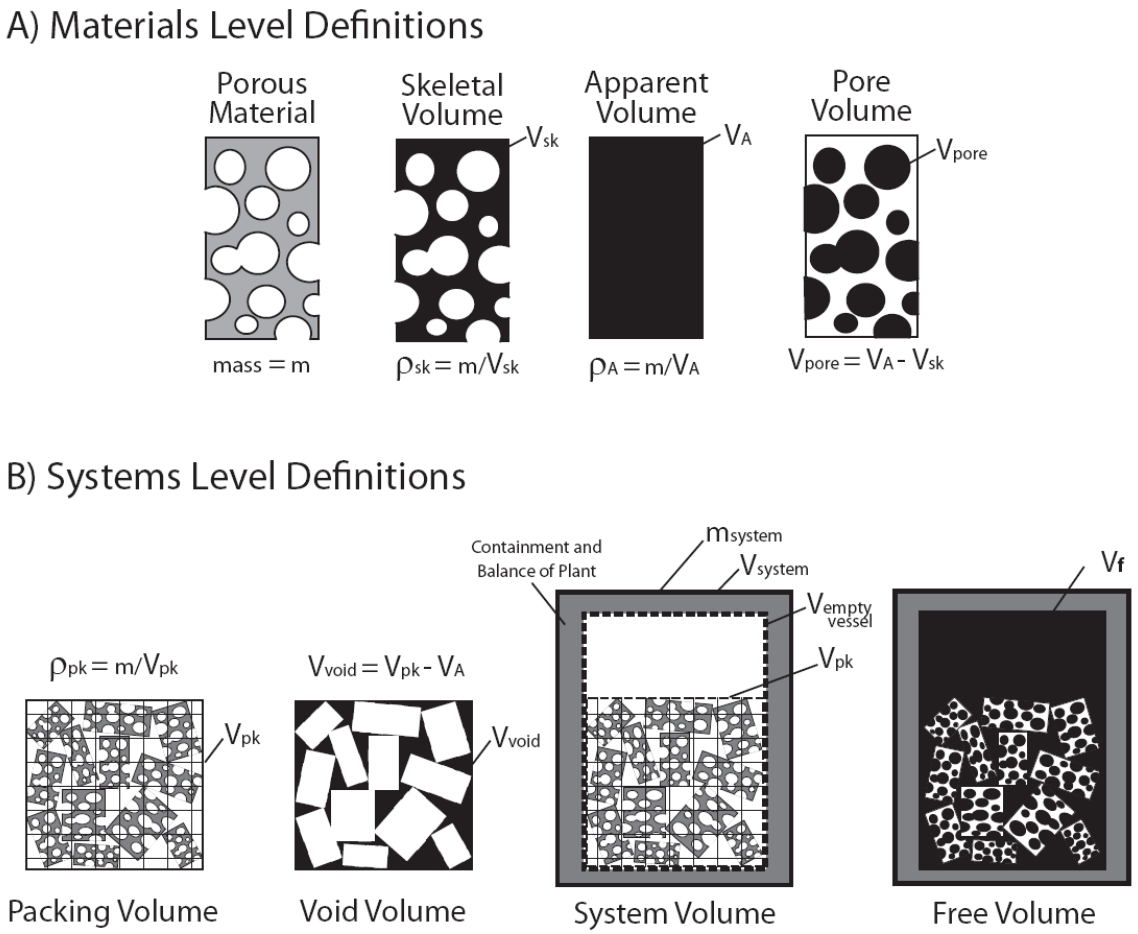

Figure 84. Volume and Density Definitions: Illustration of volume and density definitions relevant to hydrogen storage capacities at a materials and systems level.

1.4.2 Material Gibbs Surface Excess Adsorption Capacity

The "Gibbs surface excess capacity" is the term for adsorption amount, since it is the quantity which is directly measured during a volumetric adsorption experiment. This is the additional amount of adsorbate which is present on the adsorbent surface over and above the density of the free gas phase. Note that although "excess" capacity is a term

that is often used, it is not standard. Strictly speaking, the wording "capacity" does not apply well to excess amounts adsorbed (as excess is, by definition, a fraction of a capacity).

The excess amount is given by the cross-hatched area in Figure 81. The expression for the Gibbs surface excess amount is,

Equation 70 $$m_{ex} = m^* - \rho_g(V_f) = m^* - \rho_g(V_V - V_m)$$

Where m* is the total mass of hydrogen gas in the experimental vessel or system. The Gibbs surface excess hydrogen m_{ex} is the quantity which is measured in a standard volumetric measurement. To illustrate this, consider a single gas expansion step. An initial dose of H_2 in a reference vessel has a known mass, m^* as determined by the temperature, pressure of the gas and volume of the reference vessel. It is then expanded into the sample vessel by opening a valve.

The total free volume (or "dead volume") is given by $V_f = V_V - V_m$, where V_m is the sample volume determined initially from helium expansion measurements and V_V again is the total calibrated volume of the instrument. After the gas is dosed into the sample vessel, one waits for the system to reach an equilibrium state, and then measure the temperature and pressure of the free gas. The bulk gas density ρ_g (H_2, p, T) is determined using a real gas equation of state, and the excess adsorption amount is calculated from Equation 70. The implicit assumption made here is that the bulk gas phase extends to the surface of the adsorbent.

The "Gibbs surface excess capacity" is the *standard* expression for adsorption for hydrogen capacity of physisorption storage materials

1.4.3 Material Maximum Excess Adsorption Capacity

The *maximum capacity* is a materials property that specifies the maximum amount of H_2 that can be adsorbed by a material. The standard method of specifying H_2 adsorption capacity in the literature seems to be maximum adsorption amount at 77K. Nevertheless hydrogen adsorption may continue to increase considerably below 77K as shown in recent reports.[143,32]

For supercritical H_2, the maximum adsorption amount should correspond to H_2 monolayer completion on the adsorbate surface. In theory, the same maximum should be reached at all temperatures in the limit of high pressure. However, this is not the case for micropores filling. Assumptions on physisorption are often misleading because they are based on the Langmuir model, oversimplified, especially for microporous systems. Micropores filling appears as a dominant mechanism for adsorption in many porous materials. The Dubinin formalism makes provisions for adsorbed phase expansion with temperature and energetic heterogeneity. Thus, the maximum amount adsorbed in microporous materials corresponds to the entire filling of the adsorption space. Temperature dependence of the adsorption capacity may occur as a result of volumetric expansion of the adsorbed phase.[143,144] In fact, the maximum H_2 excess adsorption amount decreases with temperature for most adsorbents (see Figure 85). Zhou *et al.* observed an exponential decrease in the maximum adsorption amount with temperature for activated carbons.[161]

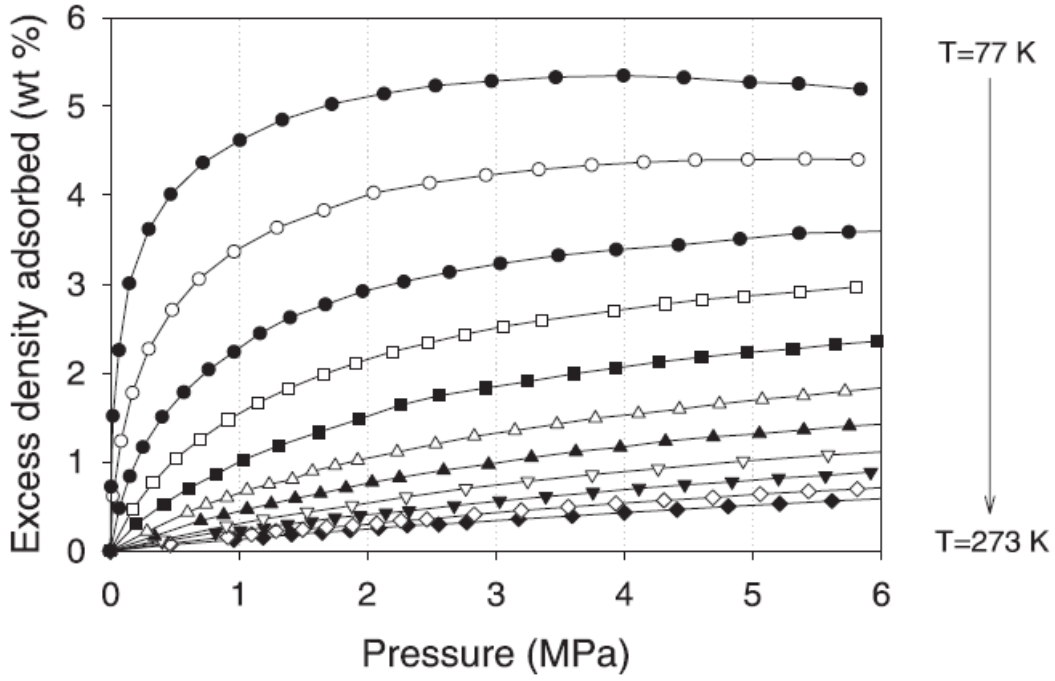

Figure 85. High pressure H_2 adsorption isotherms on the superactivated carbon AX-21TM.[145]

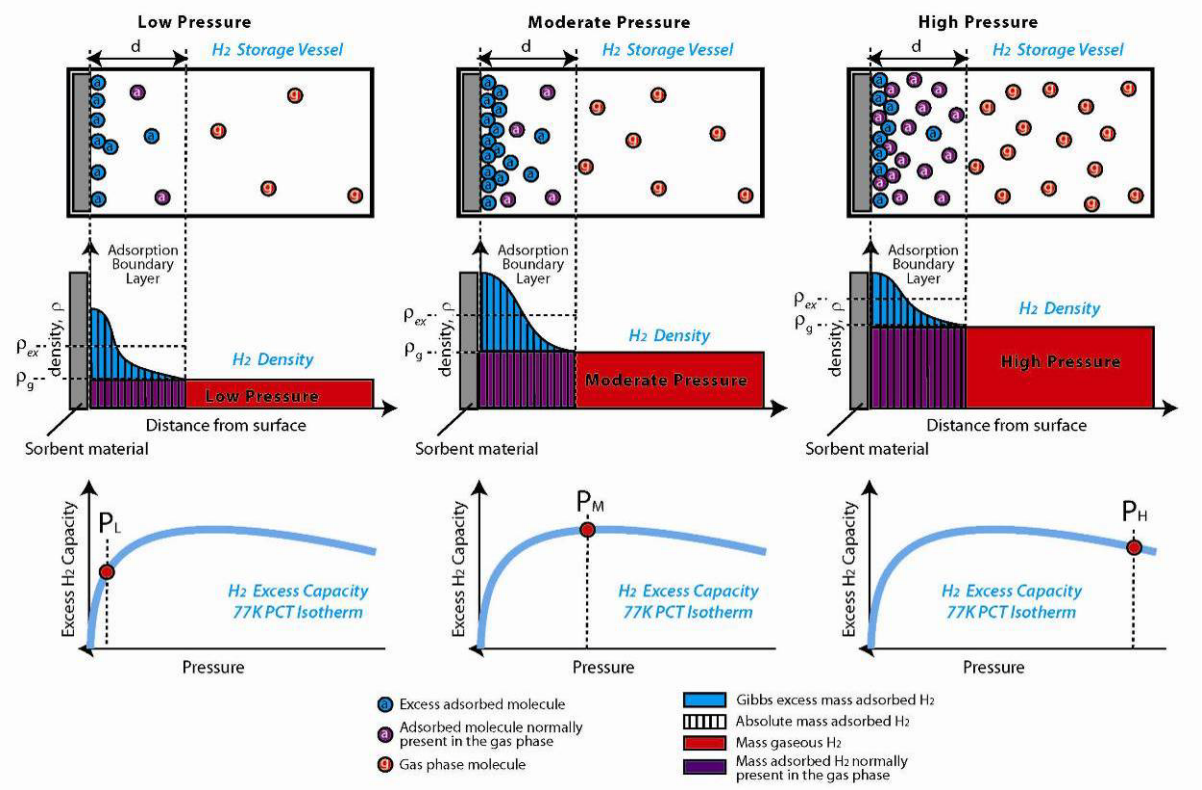

Figure 86. Illustration of the shape of excess capacity curve and the point of maximum excess capacity for physisorption material at 77K.

In supercritical H_2 isotherms, there is often a point where the density of the free gas phase begins to increase faster than the adsorbate density. In these conditions, high density gas is being displaced by the nearly saturated adsorbed phase. This translates into a maximum in the plot of surface excess amount versus pressure. This phenomenon is represented schematically in Figure 86. The top row of the figure shows H_2 molecules in the gas phase (red) and in the adsorbed phase (blue and purple) close to the adsorbate surface. Blue H_2 molecules represent the excess hydrogen present due to adsorption over-and-above that which would be present in the gas phase regardless of physisorption (purple). The second row is a representation of the hydrogen density close to the material surface. Again the hydrogen density is divided between "excess" hydrogen (blue region), adsorbed hydrogen (vertical hatched region), adsorbed hydrogen adsorption over-and-above that which would be present in the gas phase regardless of physisorption (purple), and gas phase hydrogen (red). The bottom row shows the "excess" hydrogen amount as a function of pressure. As the pressure is increased (three columns from left to right) the excess hydrogen amount increases up to a maximum until a point where the adsorbed hydrogen that would be present in the gas phase regardless of adsorption overtakes the amount of excess hydrogen due to physisorption.

This effect is observed in the 77K measurement shown in Figure 85 where a maximum is reached at about 35 bar. The schematic drawings of Figure 86 have been prepared to illustrate this phenomenon. As the measured pressure (red data point in PCT isotherm at bottom of each figure) increases (left to right, P_L, P_M and P_H), the excess H_2 capacity is over-taken by the concentration of H_2 in the gas phase. Thus, the Excess H_2 capacity reaches a maximum, typically at 30-40 bar at 77K, followed by a decreasing excess capacity with increasing pressure.

1.4.4 Excess Hydrogen Adsorption Capacity and Surface Area

Another benchmark for the physisorption capacity of a material is the N_2 BET surface area. The maximum H_2 adsorption at 77 K has been found to scale approximately linearly with the N_2 BET area in most adsorbents. However, the difference in the molecular cross-section can yield to differences between the H_2 and N_2 capacity.

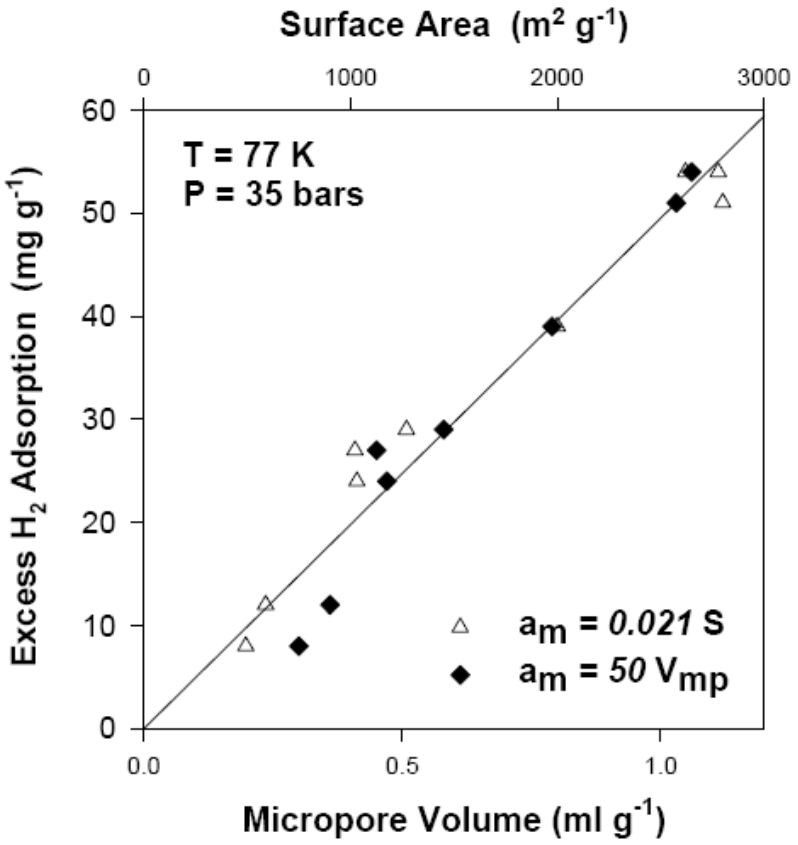

Figure 87. Data demonstrating the "Chahine Rule"; the excess H_2 adsorption capacity is linearly proportional to micropore volume.[146]

This relationship has been validated in the testing of a variety of microporous adsorbents where it has been found that the excess hydrogen storage capacity scales with the total micropore volume (and thus surface area) of the materials.[146] This observation, shown in Figure 87, is known as the "Chahine Rule". It implies that the hydrogen storage capacity of physisorption materials is clearly optimized by increasing a given materials surface area or pore volume.

1.4.5 Material Absolute Hydrogen Adsorption Capacity

In the field of hydrogen storage as well as gas sorption in general, there is a lot of variation in terminology. In particular, between the terms "absolute adsorption quantity" and "total adsorption quantity". While these terms are often used synonymously, we prefer to use the IUPAC term of "absolute adsorption" for the surface adsorbed hydrogen and to reserve the term "total" for "total material hydrogen capacity" and "total system hydrogen capacity" which both relate to hydrogen storage capacities at an applications level.

The concept of "absolute adsorption quantity" is a conceptual construct based on the hypothetical concept of a two dimensional surface layer of thickness d, in which adsorbed gas resides. It is not a measurable quantity. By definition, the "absolute adsorption quantity" is the total number of adsorptive molecules present within this adsorbed phase volume V_{ad}. Therefore; it includes all the molecules present in the space in which the attractive field from the surface is effective. As the space V_{ad} reaches saturation, the absolute amount exhibits the characteristic plateau associated with most adsorption models. In fact, the usual adsorption models, including the traditional Dubinin-Astakhov and Langmuir models refer to the absolute amount. Consequently, the relationship between absolute models and (excess) measurements is crucial for scientific understanding and analysis of adsorption data, especially near saturation. The absolute amount can reach considerably higher values than the excess amount. In that connection, it can provide (alongside with total adsorption) a better assessment of the performance of a microporous materials, especially if comparisons are to be made on similar basis with other types of hydrogen storage materials. The schematic diagram of Figure 81 is shown again below to help illustrate these three different hydrogen storage capacity terms.

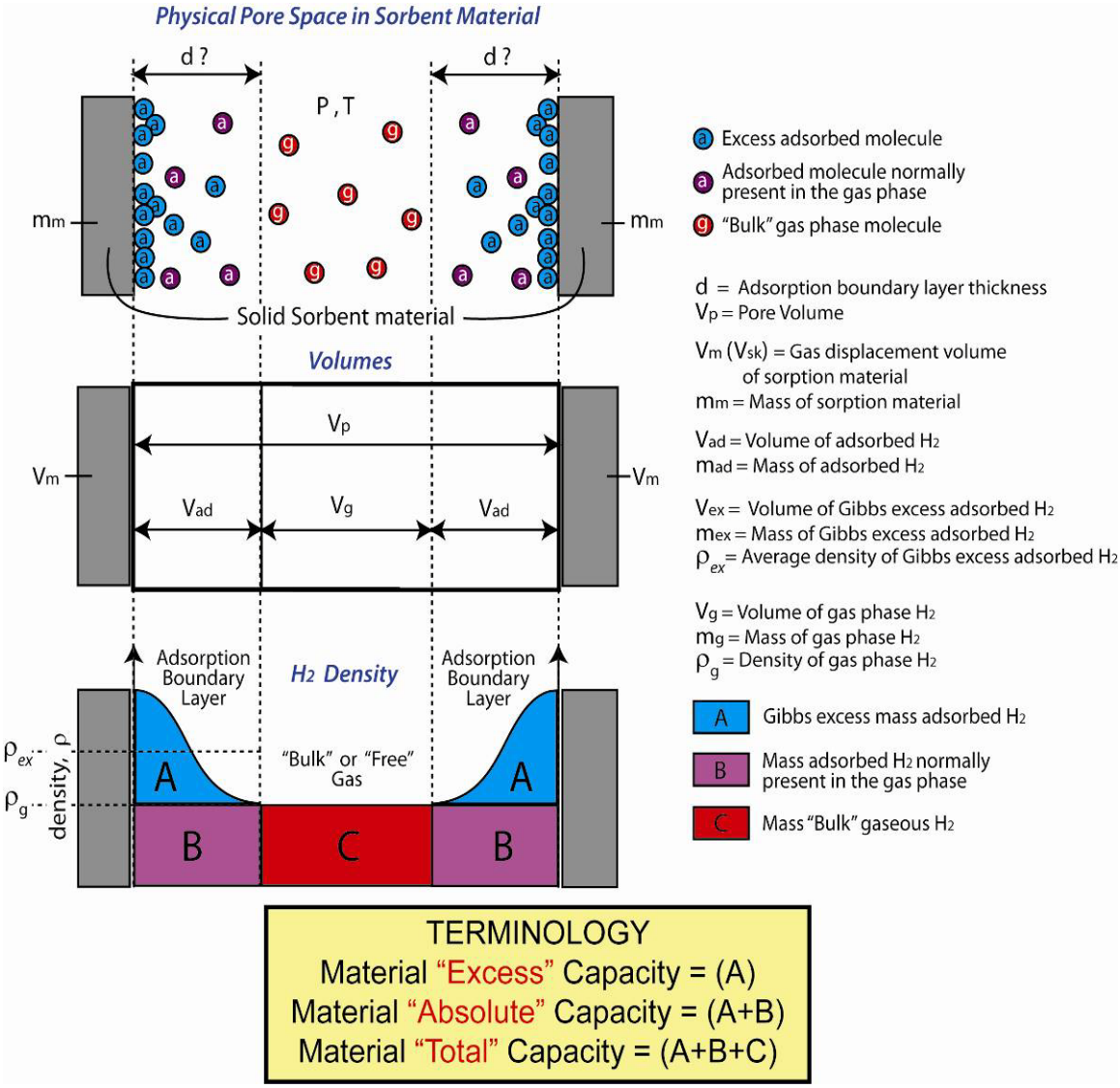

Figure 88. Illustration of physisorption hydrogen storage material capacity terminology.[29]

In studies of H_2 adsorption by highly porous materials,[147,148] the absolute adsorption amount can be related to excess measurements such as:

Equation 71

$$m_{ad} = m_{ex} + \rho_g V_{ad}$$

where m_{ex} is the surface excess amount, ρ_g is the bulk gas density, and V_a is the volume of the adsorbed phase, as approximated from the saturation amount of the N_2 isotherm for example. Note that for a microporous material, the assumption can be made that $V_{ad} \sim V_{pore}$ i.e. the microporous volume corresponds essentially to the space where the attractive potential from the surface is effective.[31] The assumption in this case is that the pore volume is small enough that all gas within the pores experience adsorption to the material surface within the pores. This assumption may break down when the pore radius falls in the mesopore range (r>2 nm).

Equation 71 must be considered when excess adsorption measurements are to be modeled at high pressures and low temperatures.

The adsorbed phase volume can be measured near saturation and used to calculate absolute isotherms. So, despite being difficult to measure as very low temperatures are required, the absolute sorption isotherm can be a valid and important for evaluating physisorption materials.

However, as mentioned above, the critical assumption for estimating the absolute uptake is the thickness of the adsorption boundary layer. This thickness is dependent on the assumed density of the physisorbed layer. Typically one defines an equivalent "adsorbed hydrogen density" for a fixed thickness, rather than an "equivalent adsorption" volume or "equivalent boundary layer thickness" at the ambient hydrogen density. These terms are represented schematically in Figure 89. This convention is commonly used because it is often assumed that the pore size in a micro-porous material is equivalent to the adsorption volume. Or, stated another way, that all of the hydrogen gas in the pores are physisorbed to the material surface. This is convenient because the pore size distribution can be measure to some degree of accuracy using mercury intrusion porosimetry or gas sorption analysis. Unfortunately, assuming that the pore size is equivalent to the adsorption volume is a rather arbitrary and often inaccurate assumption.

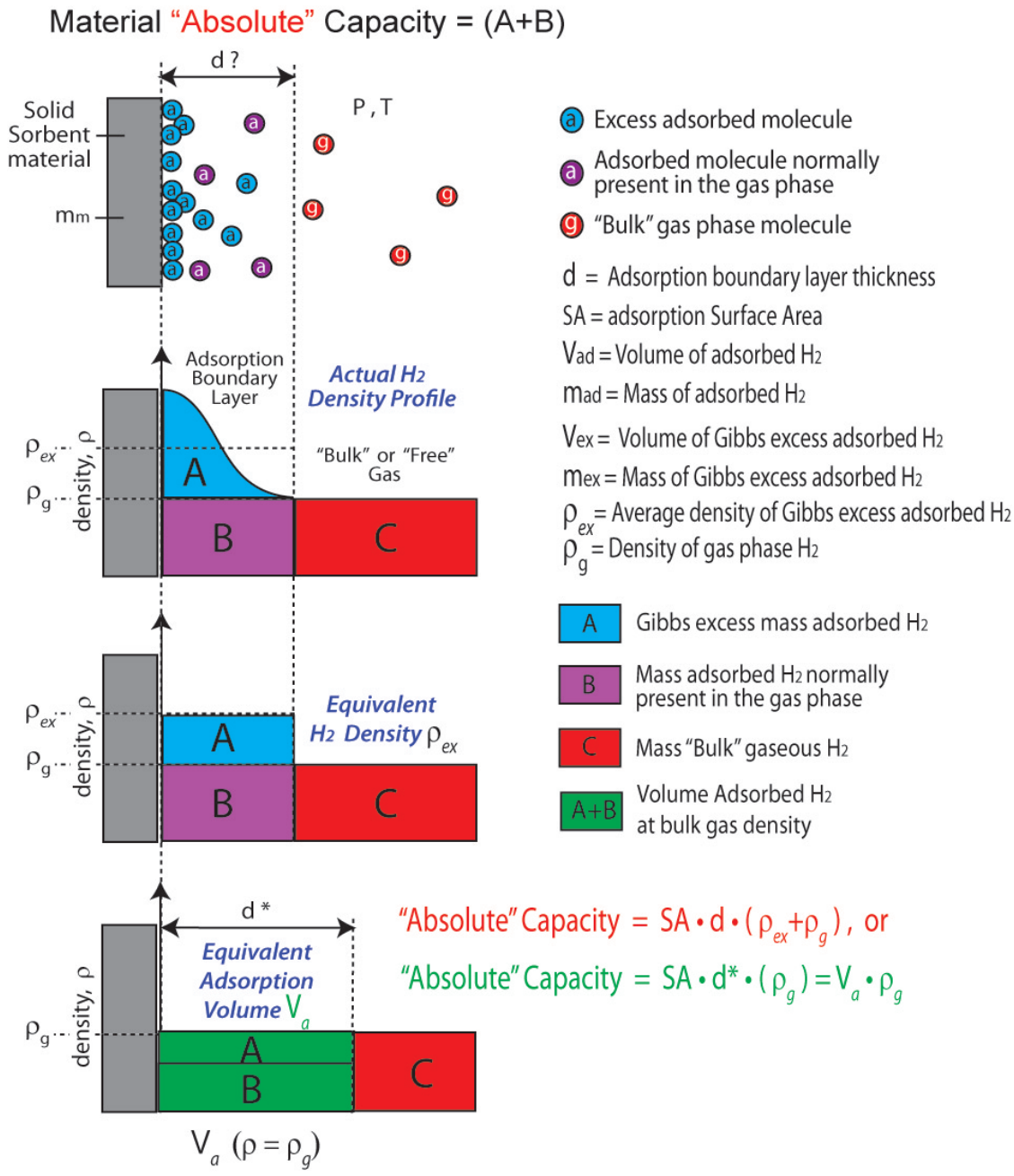

Figure 89. Illustration of the conversion of adsorbed gas density to an equivalent "Adsorption Volume" or equivalent boundary layer thickness.

Conversely, using the method of choosing an assumed adsorbed hydrogen density to determine the adsorption volume is also not without the possibility of producing significant errors. For example, assuming an adsorption density equal to that of liquid H_2, produces a small adsorption boundary layer thickness value (d) and in most cases will underestimate the absolute hydrogen uptake. As you reduce the assumed density of the adsorbed hydrogen the boundary layer will increase. Obviously one can get to a point where too low an assumed hydrogen density will give you a boundary layer that is

much greater than it should be and will overestimate the absolute hydrogen uptake. This concept is shown schematically in

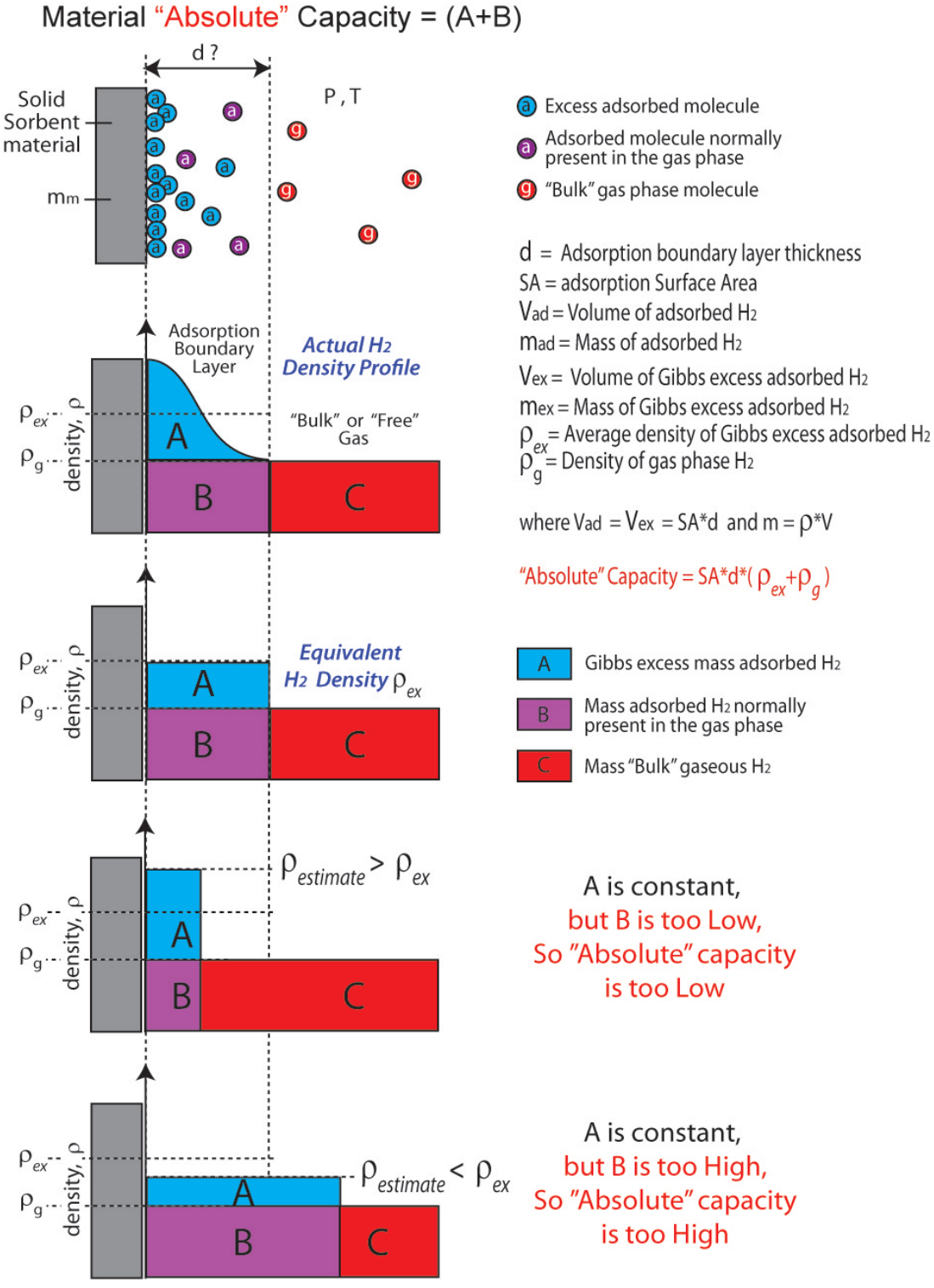

Figure 90 below.

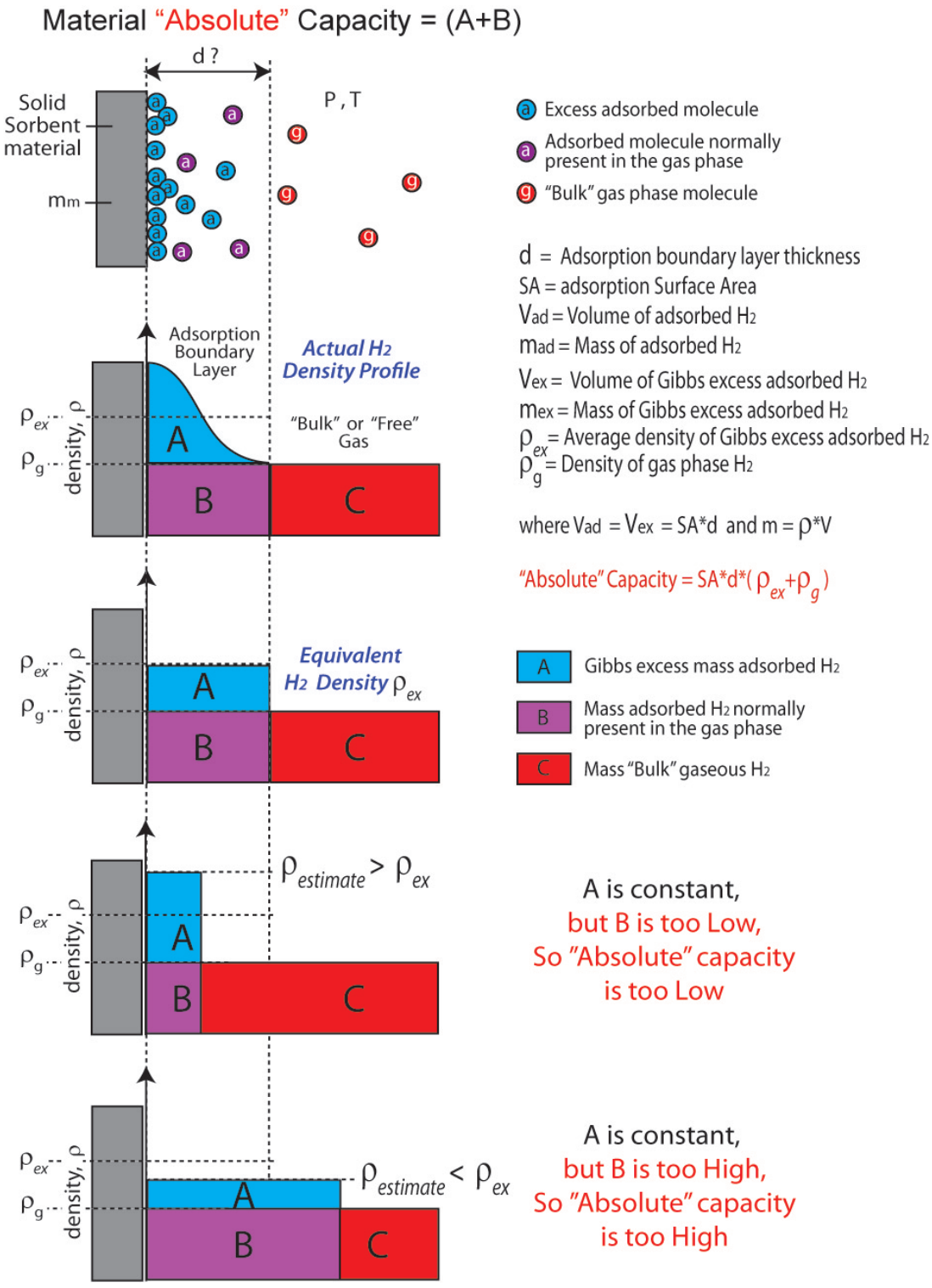

Figure 90. Illustration of the dependence of physisorbed hydrogen.

1.4.6 Material Total Hydrogen Adsorption Capacity

The total material storage capacity, however, is the sum of the capacity due to adsorption on the surface and the capacity due to compression within the space of the pores of the adsorbent. The total material capacity is useful in comparing physisorption materials with the other classes of materials in that it compares the total amount of hydrogen actually stored within the apparent volume of the materials. Thus, this measure of capacity is equivalent regardless of whether the hydrogen is absorbed in the bulk, adsorbed to the surface or present as a gas within the pores of a material.

The various "Materials" capacity definitions for porous materials are depicted schematically in Figure 91 below.

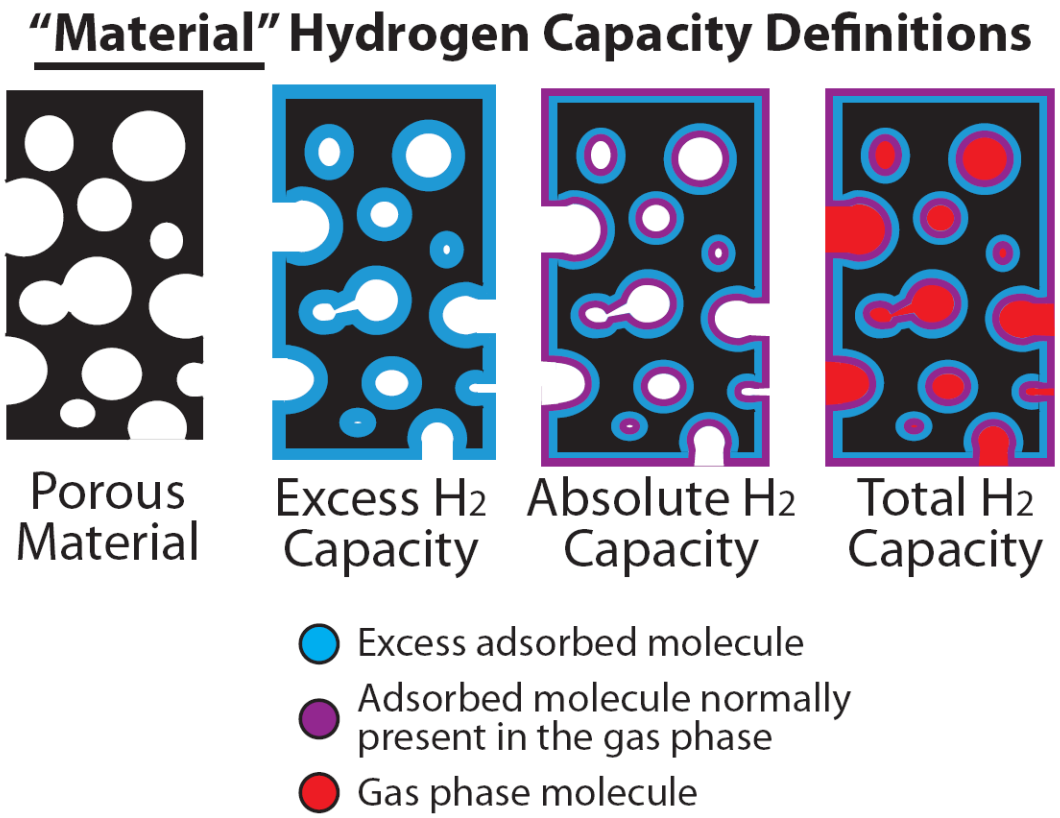

Figure 91. Porous Materials Capacity Definitions: Illustration of the "Excess H_2 Storage Capacity", "Absolute H_2 Storage Capacity" and "Total H_2 Storage Capacity" at a materials level.

An example of an evaluation of excess and total hydrogen capacity is given in the following excerpt on hydrogen uptake measurements in porous media (MOFs) by Dinca et al.[148] Here the term "bulk density" is synonymous with what we refer to as "apparent density".

> "The volume of the sample holder and the connecting gas manifold was previously determined using H2 and He at 298 K and at 77 K. Hydrogen was used to determine the free-space volume correction for a nonporous sample of known volume; this correction accounted for the change in effective sample volume observed when cooling the sample holder from room temperature to 77 K. The adsorbent was then introduced into the sample holder, and He gas was used to determine the volume of the sample at room temperature. Since He gas penetrates the pores of the sample without being adsorbed onto the surface, the volume measured with He corresponds to the volume of the framework walls, also referred to as the framework skeleton. Consequently, the skeletal density of the material, d_{sk}, can be obtained from the following expression:
>
> $$d_{sk}\ m/V_{sk}$$
>
> Here, m is the sample mass expressed in g, and Vsk is the sample volume in cm^3, as determined using He expansion at room temperature. In order to obtain an accurate assessment of the value of the skeletal density, the volume of the sample, V_{sk}, was measured 20 times, and the average of these was used as the final value. Excess adsorption is defined as the amount of gas taken up by the surface of a porous adsorbent above and beyond the quantity of gas that would have occupied the adsorbent pore volume under the same temperature and pressure conditions in the absence of an adsorbent. The total storage capacity, however, is the sum of the capacity due to adsorption on the surface and the capacity due to compression within the space of the pores of the adsorbent. The total adsorption capacity can therefore be expressed as follows:
>
> $$C_{\text{tot}} = C_{\text{exc}} + \frac{100 \times d_g V_{\text{pore}}}{1 + d_g V_{\text{pore}}}$$
>
> Here, C_{tot} is the total adsorption capacity expressed in weight percent (wt.%), C_{exc} is the excess adsorption in wt.% and is the quantity being measured, d_g is the

density of the compressed gas (here H_2) at a given temperature and pressure in g/cm^3, and V_{pore} is the specific pore volume in cm^3/g. In the equation above, the second term of the sum on the right-hand side represents the contribution of the compressed H_2 inside the pores to the total adsorption. Note that the denominator must contain the term $d_g V_{pore}$ for the capacity to be expressed in units of wt.%. Omitting this term would correspond to units of grams of H_2 adsorbed per 100 g of adsorbent, and not to wt % of H_2 adsorbed. The compressed gas density, d_g, is the density of H_2 gas as a function of pressure at a given temperature. In the current experiments, the software package GasPak (v. 3.41) was used to plot the density of H_2 at 77 K as a function of pressure. If the bulk density of the sample, d_{bulk}, is known, the specific pore volume can then be calculated as follows:

$$V_{pore} = \frac{d_{sk} - d_{bulk}}{d_{sk} d_{bulk}}$$

The volumetric density of H_2 adsorbed inside the sample can be obtained simply by multiplying the adsorbed quantity with the bulk density of the sample, $d_{bulk.}$

$$C_{vol} = Q_{ads} d_{bulk}$$

Here, C_{vol} is the volumetric H2 capacity expressed in g/L, and Q_{ads} is the total quantity of H_2 taken up in mmol/g. The excess quantity of H_2 adsorbed may instead be used in this equation if "excess" volumetric capacity is the desired quantity.[148]

The results of this evaluation are shown in Figure 92 for the measurements of hydrogen uptake by two different metal-organic-framework materials. Where:

1′: $[Mn\text{-}(DMF)_6]_3[(Mn_4Cl)_3(BTT)_8(DMF)_{12}]_2$ is the partially desolvated form of:

1: $[Mn(DMF)_6]_3[(Mn_4Cl)_3(BTT)_8(H_2O)_{12}]_2 \bullet 42DMF \bullet 11H_2O \bullet 20CH_3OH$.

1m′: $Mn_3[(Mn_4Cl)_3(BTT)_8(CH_3OH)_{10}]_2$ the desolvated form of

1m: $[Mn(CH_3OH)_6]_3[(Mn_4Cl)_3(BTT)_8(CH_3OH)_{12}]_2 \bullet 42CH_3OH$.

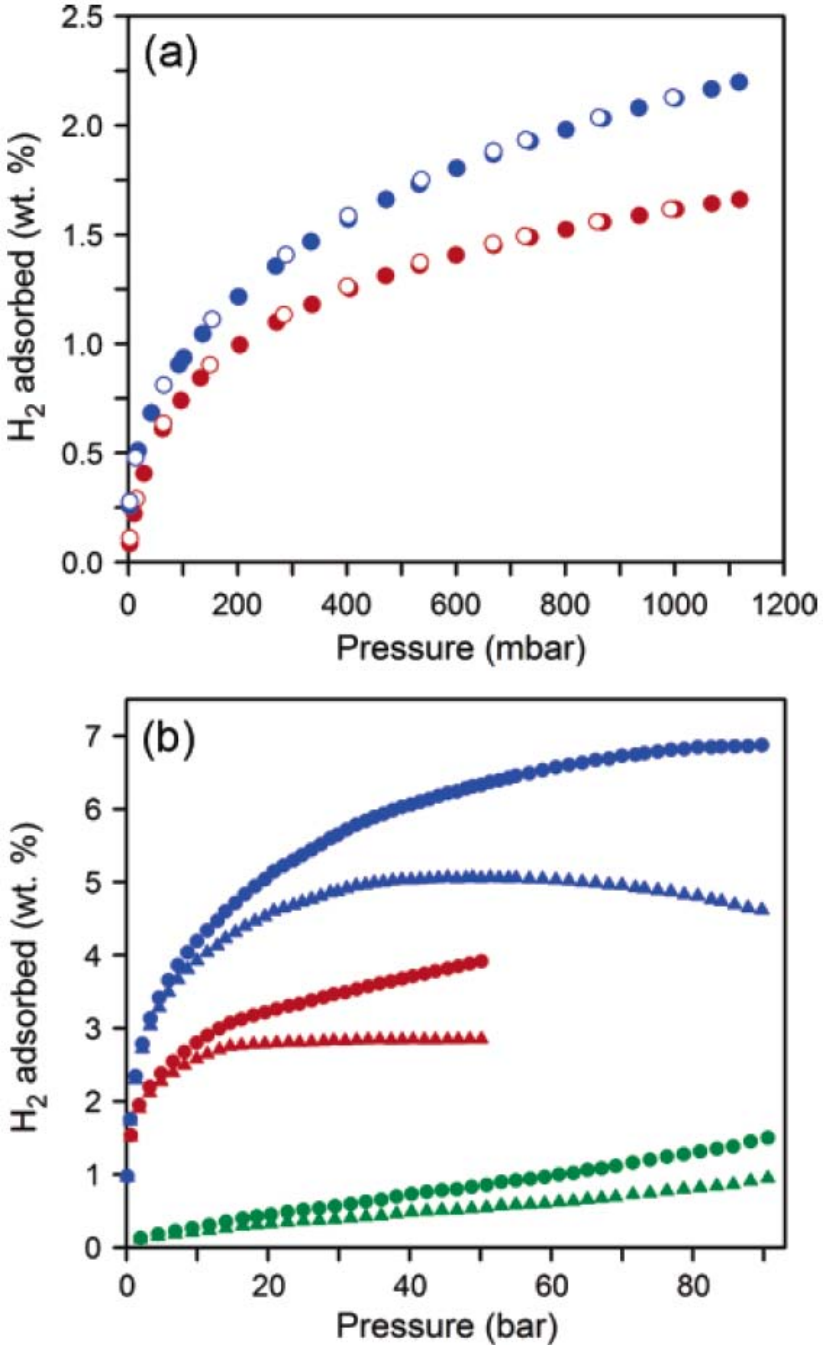

Figure 92. H2 adsorption isotherms (a) below 1.2 bar and (b) up to 90 bar within the MOFs 1' (red) and 1m' (blue) at 77 K, and within 1m' at 298 K (green). Triangles and circles represent excess and total material H2 adsorption, respectively, while filled and open symbols represent adsorption and desorption data, respectively.[148]

1.4.7 Physisorption Materials: Usable Hydrogen Capacity

The DOE has set the target minimum supply pressure for a storage system at 3 atm. It is useful to introduce the concept of *usable capacity* (see Figure 93). This refers to amount of H_2 that can be desorbed at pressures between 3 and 100 atm. Therefore, the usable capacity is given by the difference between the maximum excess adsorption amount and the equilibrium excess adsorption amount at 3 atm. Once again, the usable capacity will depend on temperature although in this case there is precedent for using 77 K as the standard temperature. This measure also depends on the shape of the isotherm.

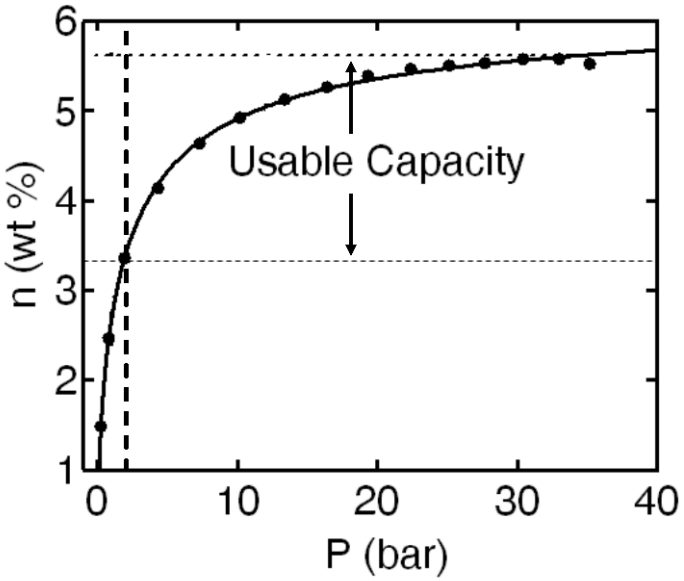

Figure 93. Illustration of the "usable capacity" above 3 atm pressure.

1.4.8 Material Gravimetric and Volumetric Hydrogen Densities

For applications it is not only the material gravimetric hydrogen densities that is important but also the volumetric hydrogen density. Calculating the maximum gravimetric density is straightforward, as it is simply the mass percent of the maximum H_2 excess adsorption amount at the storage temperature T (typically 77K) relative to the mass of the adsorbent,

Equation 72
$$\text{Max Gravimetric density} = \frac{m_{ex}^{\max}(\mathrm{T}, \mathrm{H}_2)}{m^s + m_{ex}^{\max}(T, \mathrm{H}_2)} \times 100.$$

To determine the material volumetric density, the density of the adsorbent must be known. The skeletal density and apparent density were described earlier in the section 1.4.1 on helium density measurements.

To calculate the material volumetric capacity, it is conventional to use the apparent density to convert from a mass-mass ratio mg g^{-1} to a mass-volume ratio g L^{-1},

Equation 73

$$\text{Max Volumetric density} = \frac{m_{ex}^{\max}(\mathrm{T}, \mathrm{H}_2)}{m^s / \rho_A}$$

1.4.9 Reversible Physisorption

Physisorption, by definition, is always reversible. The interaction energies responsible for H_2 physisorption are typically on the same order as the thermal kinetic energies of the H_2 molecules, so only a negligible fraction of adsorption sites are occupied at ambient conditions. The physisorbed H_2 molecules do not dissociate or form chemical bonds. Therefore, all of the adsorbed molecules can be recovered by decreasing the pressure or raising the temperature. If a minimum operating pressure or maximum operating temperature is present, however, then only a fraction of the adsorbed phase will be desorbed. This leads to the concept of usable capacity defined earlier.

1.4.10 Kinetically Limited Physisorption

Hydrogen adsorption occurs rapidly for most sorbent systems. However, the adsorbed hydrogen diffuses within the pore network of the adsorbent, and therefore reaching a true equilibrium state can require an indefinite amount of time. “Technical equilibrium” can therefore be defined as a state where the change in adsorbate mass, as a fraction of the total adsorbate mass, is less than a specific value ε (for example, $\varepsilon = 1e^{-5}$).

1.4.11 System-Level Hydrogen Storage Capacity

At a hydrogen storage systems level, one would like to measure the total quantity of hydrogen contained in the storage vessel. This amount includes both the hydrogen that fills the free volume of the vessel and the hydrogen that is bound on the adsorbent. This number is influenced by both the entire system volume (including all ancillary devices needed to operate the storage system) and the sorption properties of the adsorbent. Thus, it is highly dependent on storage system design which in-turn is highly dependent on the particular storage material it incorporates. For the purpose of this total system capacity section we represent such a system simply as an external volume with an internal volume that contains a storage (in this case physisorption) material. This is shown schematically in Figure 94.

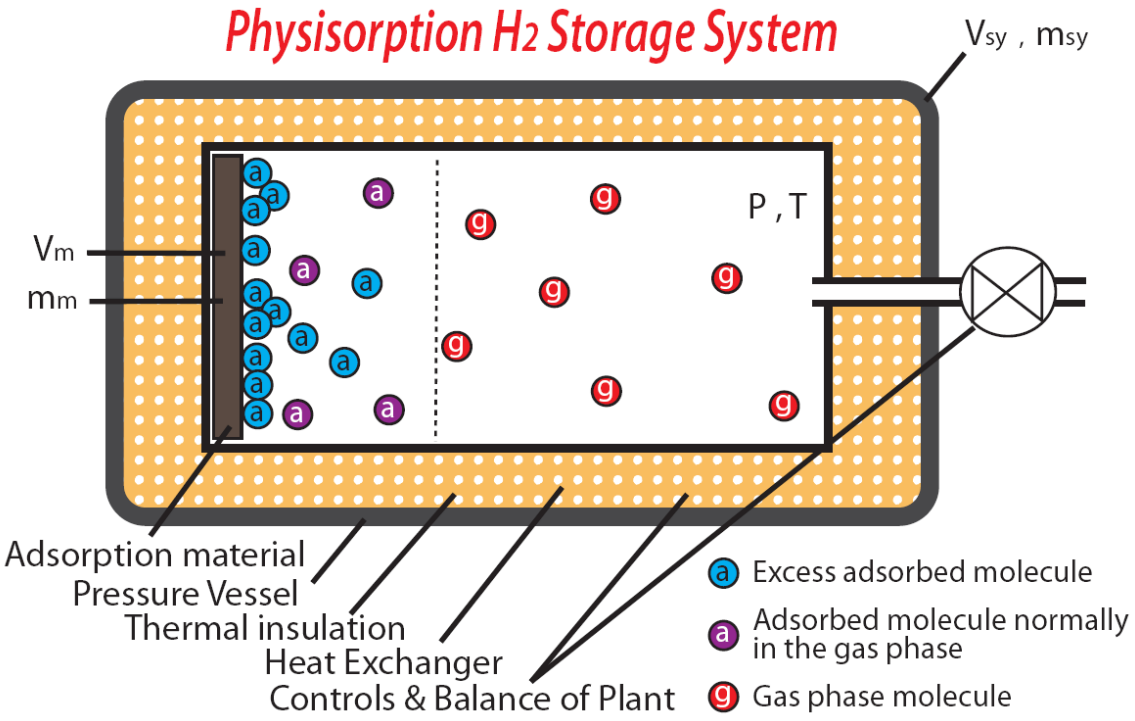

Figure 94. Simplified representation a physisorption material hydrogen storage system.

The amount of total hydrogen stored in the system depends, therefore, on the temperature, pressure and available free gas volume of the system as well as the extent of the sorbent's adsorption boundary layer. Hydrogen in a system can be found inside and outside the macroscopic boundaries of the storage material, especially in porous media. The pore volume of porous materials (representing the collective pore network) can contain both free hydrogen gas and hydrogen adsorbed to the internal microscopic surface area of the pores.

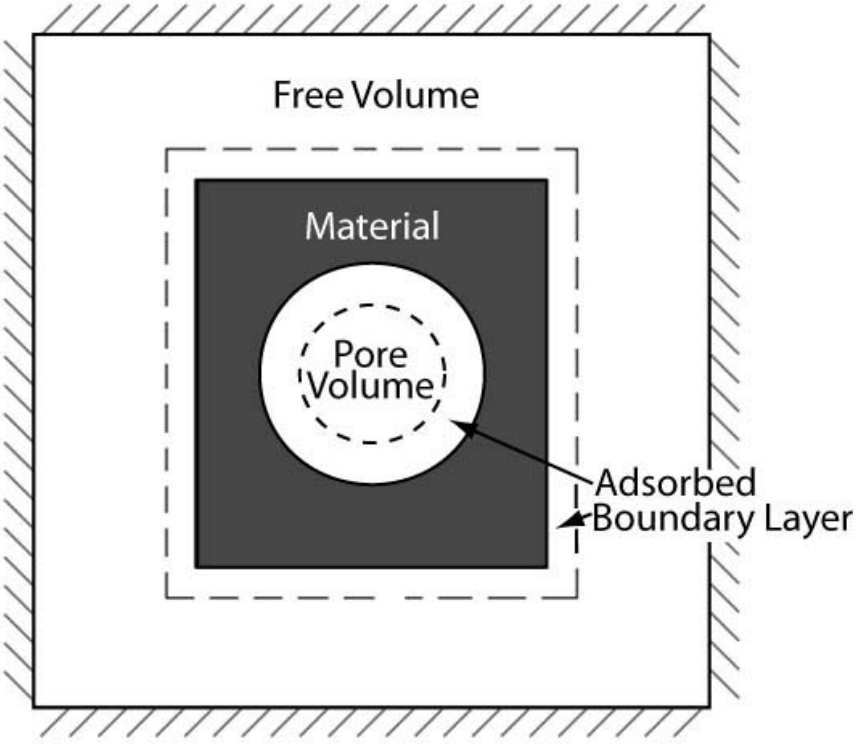

Figure 95. Simplified diagram of a porous material. The outermost boundary represents the free gas volume of the hydrogen storage system; the central pore volume represents the collective accessible pore network.

Figure 95 illustrates the various components and regions of a hydrogen storage system. Hydrogen is stored as a free gas in the void volume inside the material and in the unoccupied volume of the storage system. It is also stored as adsorbed hydrogen (absolute material capacity) in the physisorption boundary layers of the pores and surface of the sorbent material. For porous materials, the amount of hydrogen stored in the adsorbed boundary layer inside the pore volume and on the exterior material surface combined with the non-physisorbed gas in the pore volume is termed the total material hydrogen storage capacity. The total system capacity includes the total material capacity as well as gaseous hydrogen in the unoccupied free volume of the storage system.

Thus, hydrogen storage capacity at a systems level can be broken down into the separate components of how and where hydrogen is stored in a physisorption system. Each component of the total hydrogen stored depends directly on the measurement and reporting of capacity. This is shown schematically in Figure 96.

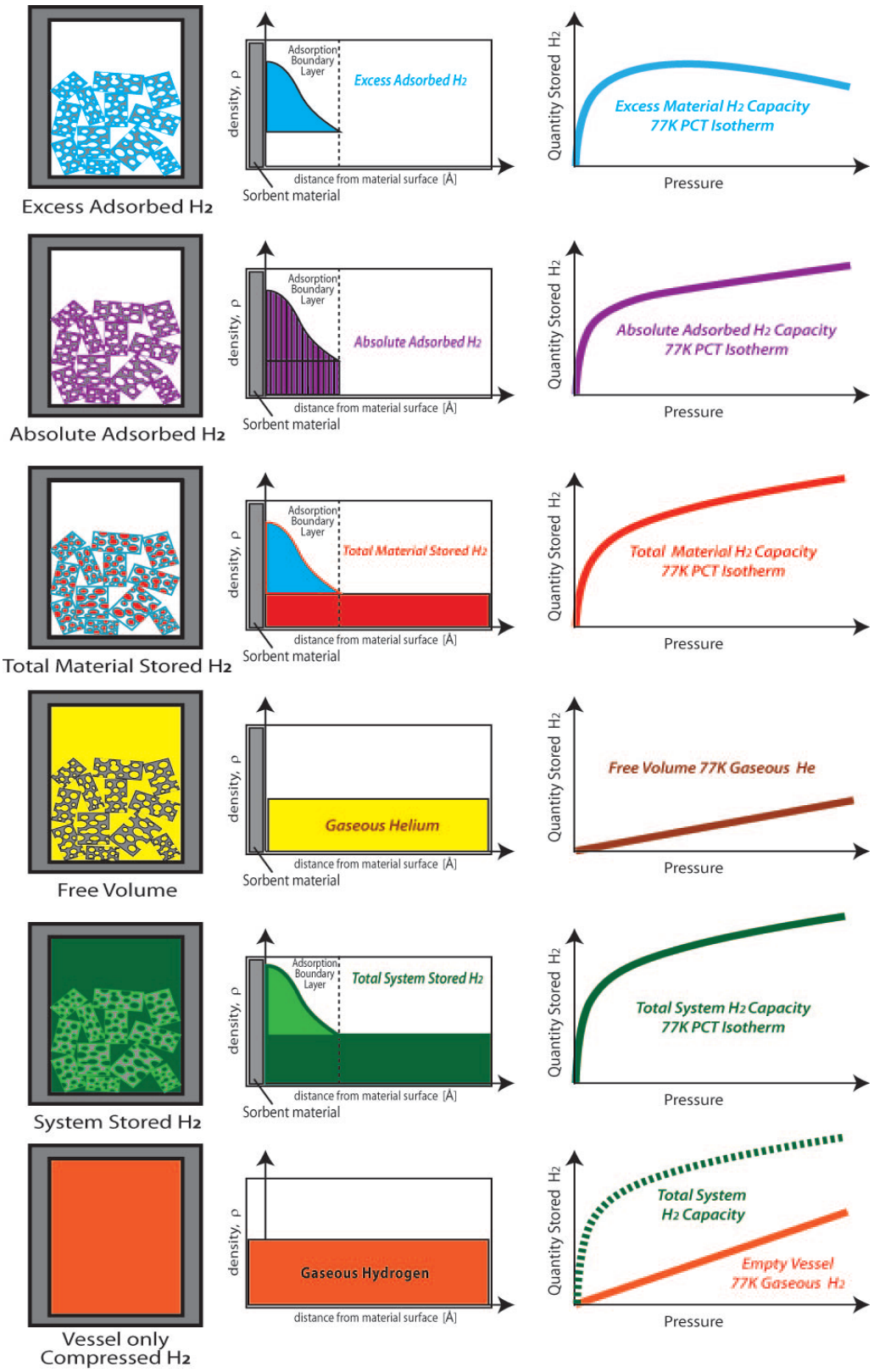

Figure 96. A breakdown of the separate components of the hydrogen storage system capacity for physisorption materials.

In the first column is a pictorial representation of the hydrogen storage system composed of a tank (including heat transfer and control systems), the physisorption materials, and free gas space within the tank and in the porous materials. The second column indicates which component of the total stored hydrogen is being accounted for and the relationship of the hydrogen to the surface of the adsorbent material. The third column depicts the portion of the total hydrogen capacity curve versus gas pressure attributable to each particular stored hydrogen component.

The first three rows show the components of stored hydrogen on a materials basis: Excess Capacity, Absolute Capacity, and Total Material Capacity. Again, Excess Capacity (on a mass basis) and Total Material Capacity (on a volume basis) are the most useful for determining the amount of hydrogen that can be practically stored by the material itself. This is followed by the free gas space of within the storage system (gas volume within the materials and in the empty space within the storage vessel. This is usually measured by filling the system with helium from a calibrated volume and noting the change in pressure. The forth row is the total quantity of stored hydrogen within the physisorption storage system at any given pressure and one temperature (isothermal). The fifth, and final, row depicts the amount of hydrogen that could be stored in the vessel under the same pressure and temperature conditions in the absence of any sorbent material. Obviously, the physisorption material storage system is only viable if the total system stored hydrogen (row 4) is significantly greater than the vessel only stored hydrogen (row 5).

A simple example used by Bhatia and Myers provides a good explanation of the relationship between system excess hydrogen capacity N_{ex}, system absolute adsorb hydrogen capacity N_{ad}, and the hydrogen gas stored in the free volume of the storage system N_f (illustrated in Figure 97).[149] The amount of gas adsorbed at the surface of a material N_{ad} increases and then saturates as given by a Langmuir adsorption isotherm:

Equation 74 $$N_{ad} = N_{max}KP/(1+KP)$$

Where N_a is the moles of adsorbed gas, N_{max} is the maximum moles of adsorbed gas at saturation, K is the equilibrium gas constant and P is pressure. The amount of gas N_f in the free volume (V_f) of the adsorbent system increases linearly with pressure P given by the ideal gas equation:

Equation 75 $$N_f = PV_f/RT$$

Where V_f is the gas volume, R is the gas constant and T is temperature. The excess is given as the difference between these two quantities.

The adsorption equilibrium constant K depends exponentially on temperature according to:

Equation 76 $$K = \exp(S_{ad}/R - H_{ad}/RT)$$

Where S is the entropy and H the enthalpy of adsorption. The result is that the amount of adsorbed gas versus pressure saturates at very low pressure as the temperature is decreased. On-the-other-hand, the volume contribution changes linearly with temperature. This results in saturation of adsorption at low P at low T causing a maximum in the excess capacity at a moderately low pressure, while at higher T the maximum is shifted to higher pressure.

Thus, it is key to identify the temperature where the maximum excess hydrogen can be stored for a given upper pressure limit of a storage system.

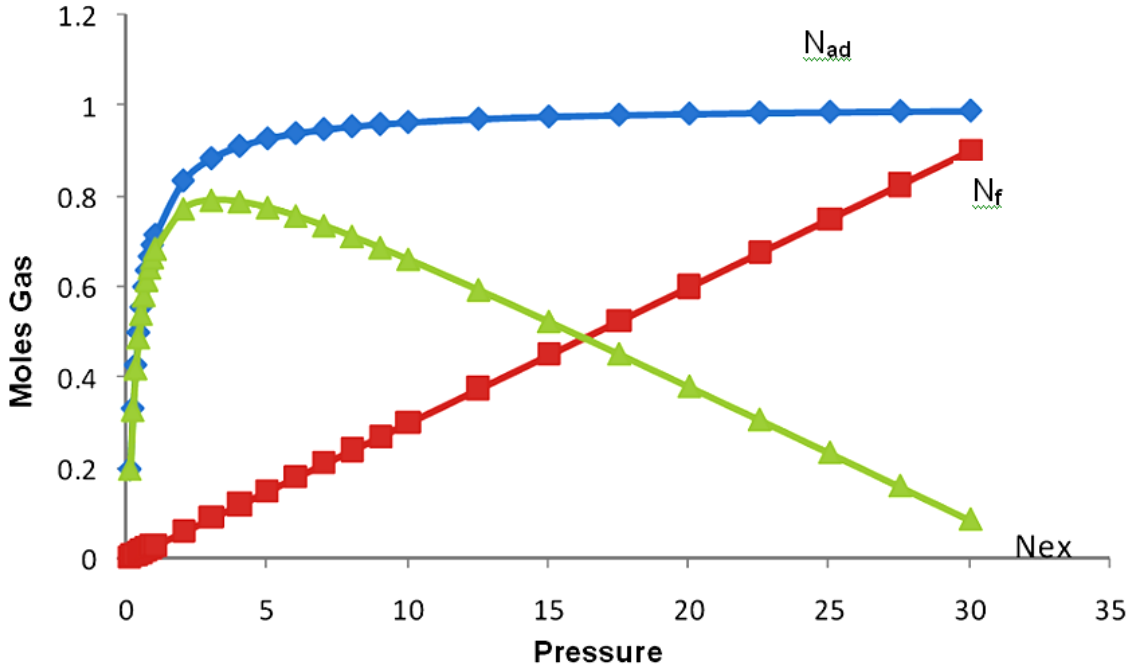

Figure 97. Schematic plot of different components of adsorbed gas as a function of pressure (N=moles gas, Blue N_{ad} = absolute adsorbed gas (e.g. Langmuir model), Red N_f = gas in the free volume of the material storage system, Green N_{ex} = excess adsorbed gas).[150]

With this in mind, there will always be a point of diminishing returns for physisorption hydrogen storage systems as the pressure is increased to very high pressures, in which more hydrogen would be stored in a given vessel ($V_f = V_v$) by removing the adsorption material. That is more hydrogen could be stored as a gas at a certain high pressure in the volume (Vsk) occupied by the adsorption material itself than is stored as excess adsorbed hydrogen by physisorption to the adsorption material. An example of this is presented in the section 1.4.11 below on modeling of a hydrogen storage system using high-surface-area activated carbon.

A very nice example of the advanced modeling of the system storage capacity as a function of pressure and temperature was recently submitted publication by M.-A. Richard et. al. The model for the material sorption capacity they used was the modified Dubinin-Astakhov micropore filling model given by; [151]

Equation 77

$$n_a = n_{\max} \exp\left[-\left[\frac{RT}{\alpha + \beta T}\right]^2 \ln^2\left(\frac{P_0}{P}\right)\right]$$

where, T and P are the temperature and the pressure, R is the universal gas constant, the parameter n_{max} is the limiting adsorption in mol kg^{-1} and the parameter P_0 is the pressure corresponding to the limiting adsorption (no longer the saturation pressure since it is applied in the supercritical region).

They validated their model by comparing calculated results with experimental capacity measurements performed on samples of high-surface area activated carbon samples of Maxsorb MSC-30™ (~ 3000 m^2g^{-1}) obtained from Kansai Coke and Chemical Co. Ltd.

Using this model, they determine the net hydrogen storage densities in a 150 L tank containing 40.5 kg of Maxsorb MSC-30™ for different temperatures (60 to 298 K), and pressure up to 35 MPa. The amount of hydrogen in the tank was calculated using:

Equation 78

$$m_{H_2} = V_{\text{tank}} \rho_{c,bulk} M\left(n_a + \rho_g V_g\right)$$

where V_{tank} is the volume of the tank (0.15 m^3), $\rho_{c,bulk}$ is the apparent or bulk density of the activated carbon (270 kg m^{-3}), M is the molar mass of hydrogen and n_a, the absolute amount of hydrogen adsorbed in Maxsorb MSC-30™ obtained from Equation 78 and expressed in mol kg^{-1}. The molar density of hydrogen, [mol m^{-3}], at a specified temperature and pressure was obtained using the modified Benedict-Webb-Rubin

(MBWR) equation of state implemented within the *NIST 12 Standard database* tables.[76] At a minimum discharge pressure of 0.25 MPa, a non-negligible quantity of residual hydrogen remains in tank at low temperature. For instance, at 77 K the residual mass of hydrogen was about 1.36 kg. The net hydrogen storage capacity of the system at a particular temperature, also called delivery, was calculated by deducting this residual hydrogen. The net isothermal storage capacity in the 150 L activated carbon tank, *i.e.* the storage capacity calculated while assuming that the temperature remains constant during discharge, is presented in Figure 98. The equivalent gravimetric hydrogen storage density of the material is shown along the right hand *y*-axis. The thick black line represents the break even curve where a cryogenic compressed gas 150 L tank at the specified pressure and temperature results in the same storage capacity. It shows that, with a target of 5 kg of hydrogen stored, the capacity advantage of adsorption-based storage over cryogenic compressed gas is small and even disappears below 93 K.

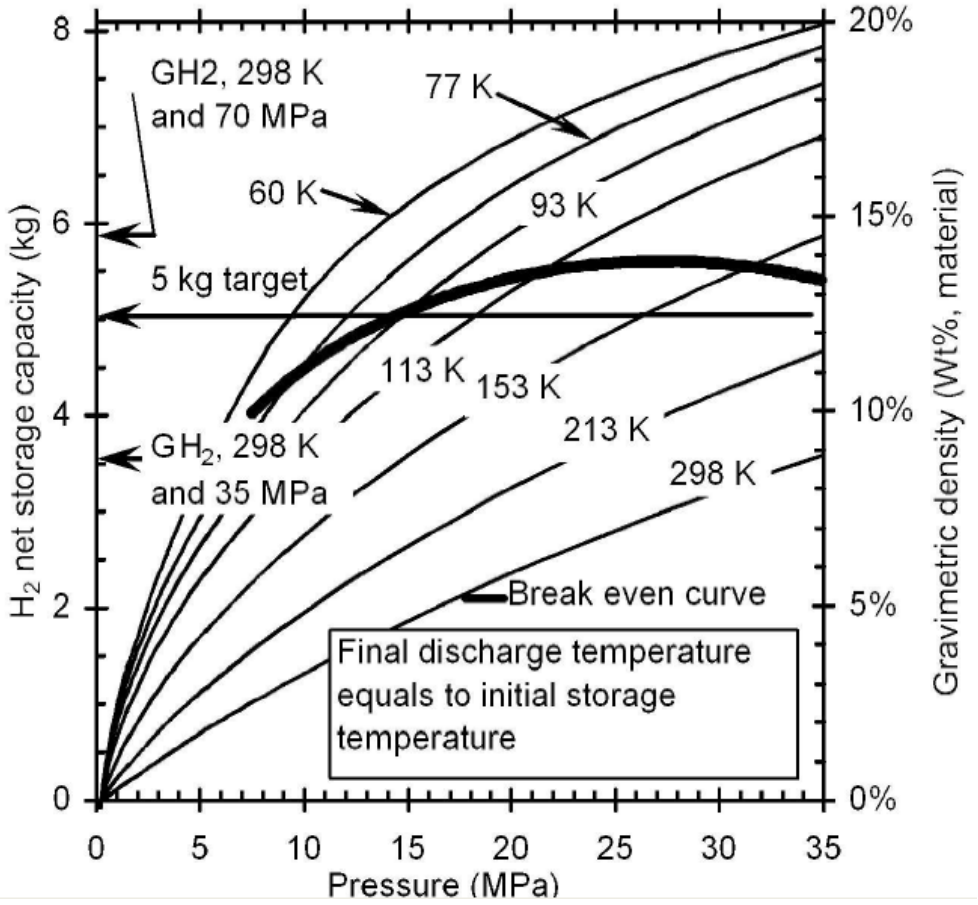

Figure 98. Isothermal net H_2 storage capacity of a 150 L tank filled with Maxsorb MSC-30TM activated carbon (heating up to initial temperature for discharge, outlet pressure 0.25 MPa). The "break even curve" (where a cryogenic compressed gas at the specified pressure and temperature would

result in the same storage capacity) and the amount of gas stored by compression at 35 and 70 MPa at room temperature is also presented.[131]

In their paper, M. A. Richard et. al. pointed out that, although the storage capacity is often calculated assuming isothermal discharge, it is important to note that the tank temperature is likely to vary during discharge. Since desorption is endothermic, the temperature will decrease if the tank is adiabatically discharged. Heating, supplied by either heat leaks or a heating system, is necessary to keep the temperature constant. From a net storage capacity point of view, it would be much more interesting to further heat the tank to reduce the residual hydrogen at 0.25 MPa. In the 150 L tank, the residual mass at this pressure drops from 1.36 kg at 77 K to, respectively, 0.75, 0.23, 0.09 and 0.03 kg at 100, 150, 200, and 298 K. A temperature of about 200 K is sufficient to discharge most of the hydrogen. The storage capacity of a system with a final discharge temperature of 298 K is shown in Figure 99.

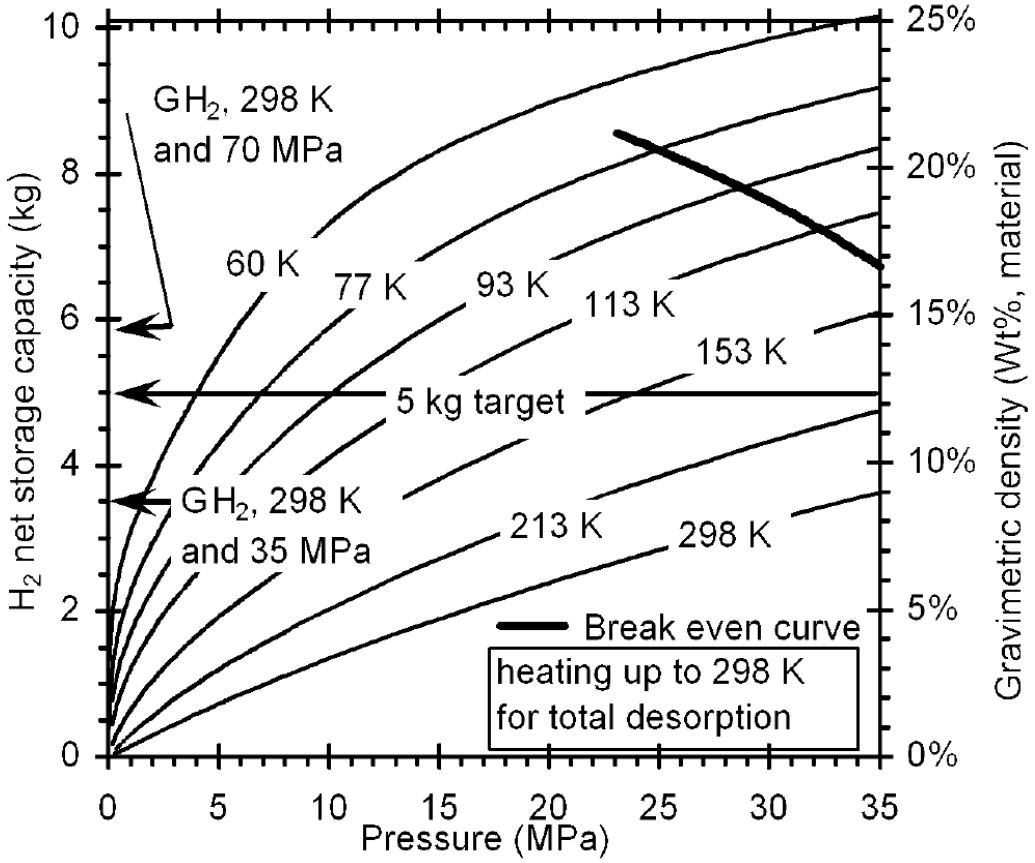

Figure 99. Calculated Net H_2 storage capacity of same 150 L tank as in Figure 98 heating to 298 K for discharge, with an outlet pressure 0.25 MPa. The heating advantage with respect to the "break even curve" can be seen. Room temperature compressed gas at 35 and 70 MPa also noted.[131]

The target of 5 kg of stored hydrogen can be reach at a much lower filling pressure. It can be seen that below 15 MPa, the net 5 kg target is reached below 113 K. The lower the temperature, higher is the hydrogen storage. Through this analysis, M. A. Richard et. al. found that, with heating, adsorption-based storage provides a larger capacity than cryogenic compressed gas.

The materials ability to greatly improve the storage capacity depends (among other things) on both the material's excess storage capacity and the extent to which the material efficiently fills the space within the storage vessel. These two, sometimes competing, effects are depicted in the drawings of Figure 100. The figure shows the typical case of a moderately dense, high-surface-area material with a corresponding moderate amount of stored hydrogen. The second case portrays a physisorption material with a low surface area to bulk ratio. The third case depicts the other worst case scenario of a high-surface-area material a low apparent density or packing density. The final figure shows the optimal material which will have a high-surface-area material with a reasonably high packing density.

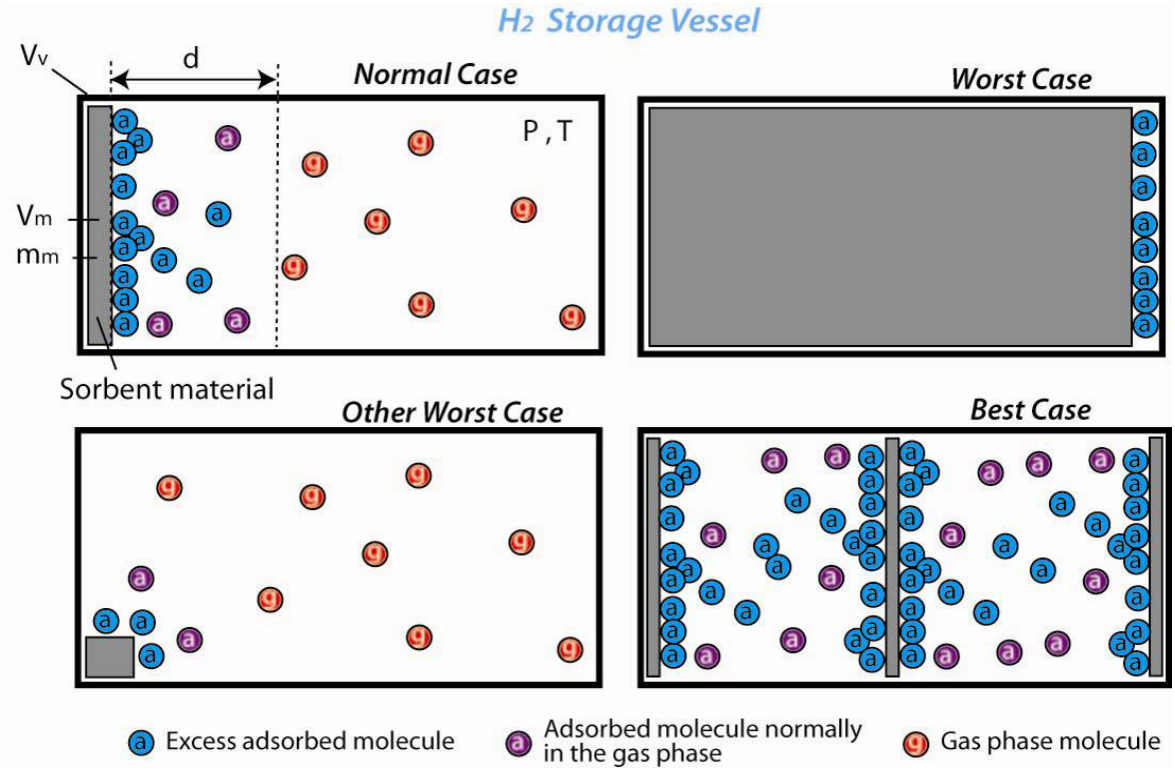

Figure 100. Representation of different physisorption system hydrogen storage capacity scenarios.

1.5 On-board Reversible Hydride Materials

Capacity measurements are most often presented in the form of Pressure-Composition Isotherm (PCT) plots. The plateau pressure at which hydriding occurs material is material-specific and is based on intrinsic thermodynamic equilibrium properties. Unfortunately PCT data must be treated with care because it is difficult to make true equilibrium measurements as reactions near equilibrium proceed extremely slowly.

In this sense there is some difference between metal-hydride and complex-hydride (or chemical-hydride) systems. Complex-hydride systems often involve chemical decomposition-recombination reactions involving hydrogen and one or more of the material's constituent elements or compounds. In this case, all of the hydrogen is bound or released in a reaction that occurs (thermodynamically) at a given combination of pressure and temperature. No extra hydrogen is stored between reactions. In PCT measurements, this is observed as a discrete jump in pressure between plateau pressures.

At the other extreme are the disordered alloy hydrides, amorphous hydrides, and quasicrystal hydrides. In these materials, hydrogen binding sites have an unlimited range of nearest and next-nearest neighbor combinations such that interstitial sites exist of hydrogen over a wide and homogeneously distributed range of binding energies. The end result is that these materials do not have flat pressure plateaus, but rather exhibit monotonically increasing hydrogen capacity with increasing pressure.

In between the two extremes, stochiometric metal-hydrides exhibit flat plateau pressures, but also some small amount of hydrogen is stored as a solid solution below the hydride plateau. This hydrogen would be released if the pressure dropped below the plateau or minimum fuel cell operating pressure. However, typically less than 10% of the stored hydrogen is found in this solid solution phase.

1.5.1 Reversible and Usable Hydrogen Capacity

Figure 101 shows two extreme examples of PCT measurements and the resulting reversible and usable capacities. Figure 93a represents the ideal case with a flat plateau, as is often seen in AB_5 materials such as $LaNi_5$. If the plateau region falls within the useful pressure range for the system, then the usable capacity will be close to the reversible capacity. Figure 93b shows the opposite extreme of a material with a severely sloping plateau. This behavior is often seen in AB_2 materials and can result in a usable capacity that is significantly lower than the reversible capacity.

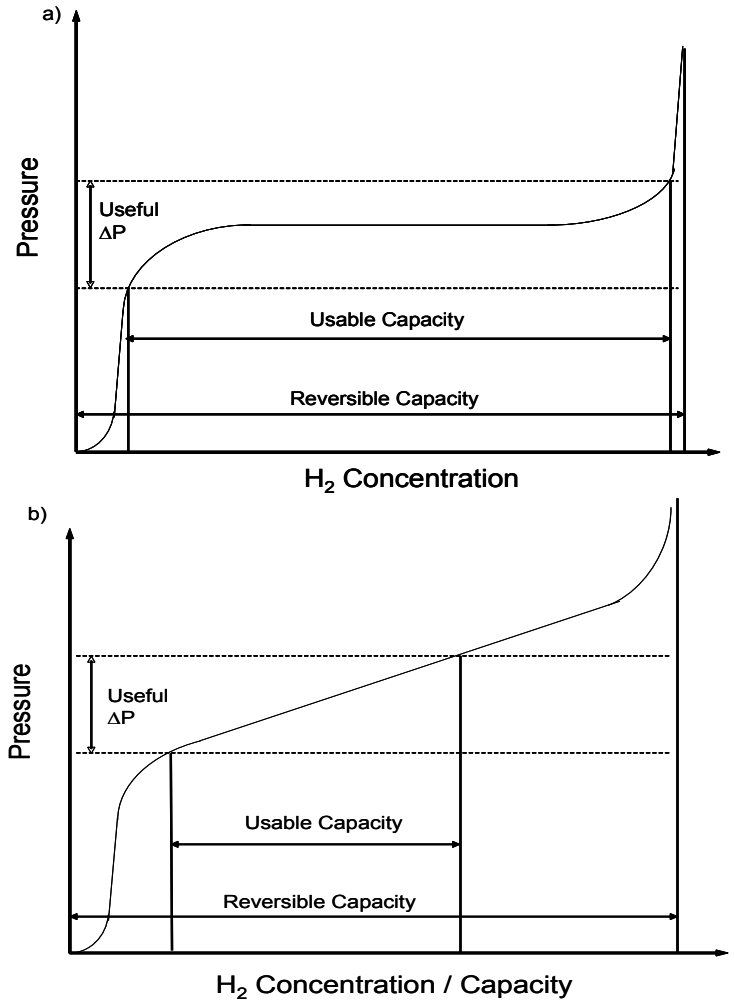

Figure 101. Pressure versus concentration isotherms (PCT plots) for a) an idealized material with a flat plateau, commonly seen in AB_5 materials and b) a real material with a largely sloping plateau, as is often seen in AB2 materials. The reversible and usable capacity is shown on each plot to demonstrate the potential effects of a sloping plateau.

Some materials have multiple dissociation steps, and therefore have multiple plateaus in a PCT plot. One of the most studied examples of this is sodium alanate, $NaAlH_4$, which decomposes in 2 steps to NaH, Al and H_2 gas via the following reactions:

Equation 79 $$3NaAlH_4 \rightarrow Na_3AlH_6 + 2Al + 3H_2$$

Equation 80 $$Na_3AlH_6 \rightarrow 3NaH + Al + \frac{3}{2}H_2$$

A third dissociation reaction is possible for NaH, but it is generally considered impractical as it normally occurs only at much higher temperature.

It is also possible to have multiple plateaus due to a mixture of materials. Ivanov et al. conducted PCT measurements on samples of Mg and Co that had been ball-milled in a 2:1 atomic ratio and then hydrided. The desorption isotherms were measured and are shown in Figure 102. Each plateau corresponds to a different alloy formed during the ball milling and hydriding. Based on enthalpy of formation calculations, the top plateau is likely the result of unalloyed MgH_2, while the bottom and middle plateaus are assigned to Mg_2CoH_5 and Mg_3CoH_5 respectively.[152] It is clear from Figure 102 that not all of the pressure plateaus for a given material or mixture will fall within the desired pressure range at a given temperature. This is another example of a case where the usable capacity could be significantly less than the reversible capacity.

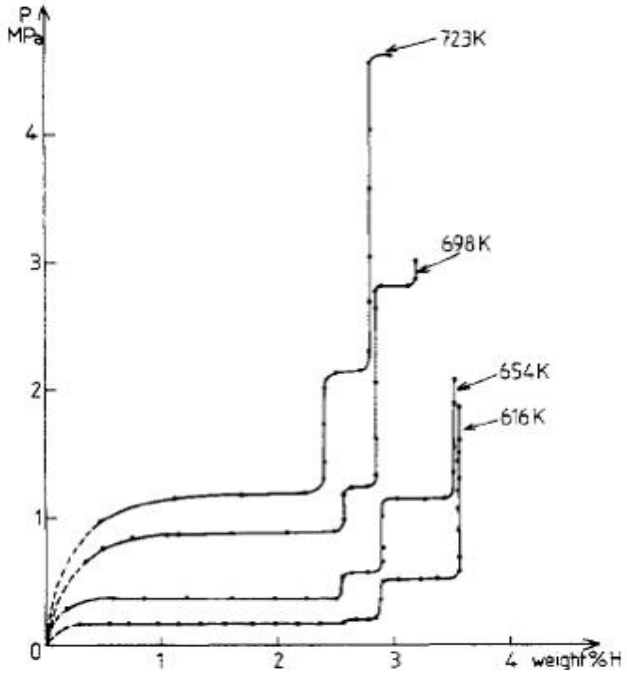

Figure 102. Desorption isotherms of the Mg-Co-H system demonstrating multiple plateaus, each representing a different dissociation reaction.

Since PCT measurements assume equilibrium, no information on kinetics is available and it is impossible to determine if the required fuel supply rates can be achieved at these temperatures and pressures. This information would be necessary to determine the actual amount of hydrogen available to a fuel cell in a real application. The dynamic availability of capacity is dependent on kinetics and is considered a separate measurement and optimization problem from equilibrium capacity.

PCT capacity measurements are one of the primary tools in evaluating a material's potential for utilization in the hydrogen storage space. Capacity is typically the first property measured during evaluation of possible storage materials because it is often the least mutable; most research begins with materials that exhibit high storage

capacity and subsequently tries to improve their kinetic and thermodynamic properties via catalysis etc. The excessive focus on capacity is sometimes misguided however. Most hydrogen storage research is conducted with hope of reaching the US DOE on-board hydrogen storage system performance targets; these targets mimic the performance of gasoline-powered internal combustion engines and are quite demanding.[153] If no material is found that meets all of the US DOE targets, what property targets can be compromised? Some end-users might prefer a car that has a 140-mile range and 'fills up' in 5 minutes instead of one with a 300-mile range but takes 45 minutes to charge.

1.5.2 System-Level Hydrogen Capacity

It is necessary to include system level considerations in the final design for hydride materials. The concerns are similar to those presented in section 1.4.10 on physisorption materials, such as the need to include the support structure and ancillary device volumes and weight in addition to that of the sample. A schematic of a representative hydride storage system is shown in Figure 103**.**

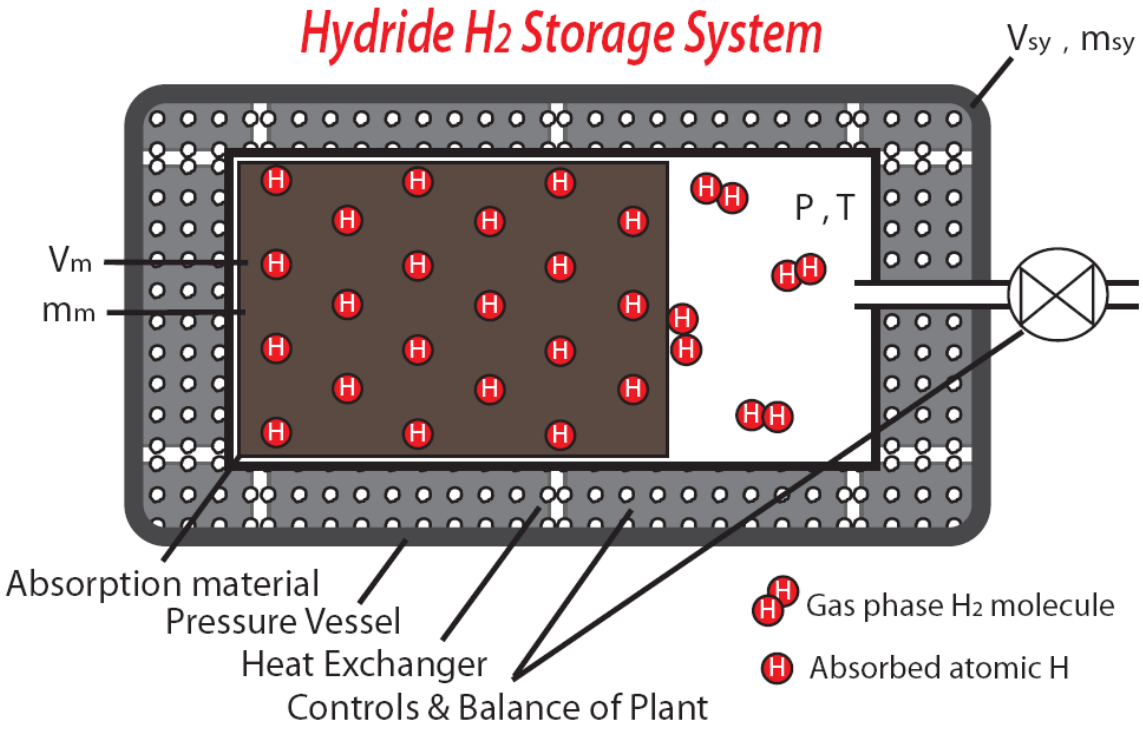

Figure 103. Simplified representation of a Hydride Hydrogen Storage System

One additional consideration of interest for hydride systems is the lattice expansion of the material upon hydrogen absorption. This expansion is often on the order of 30% and must be accommodated by an equivalent amount of free volume in the system design. The ideal material would have a large storage capacity with minimal lattice expansion. However, the sample volume increase is often correlated with increasing hydrogen content in the sample.

Figure 104 represents some possible scenarios. The first image shows a reasonable storage capacity and a normal lattice expansion of roughly 30%. The second image is of a worst case scenario where a material with a reasonable storage capacity has such a large lattice expansion upon hydrogenation that most of the system must be free (dead) space. The third image shows another worst case scenario of a material with minimal lattice expansion, but with a low storage capacity. The last image shows the ideal case of a material with a high storage capacity and a small lattice expansion.

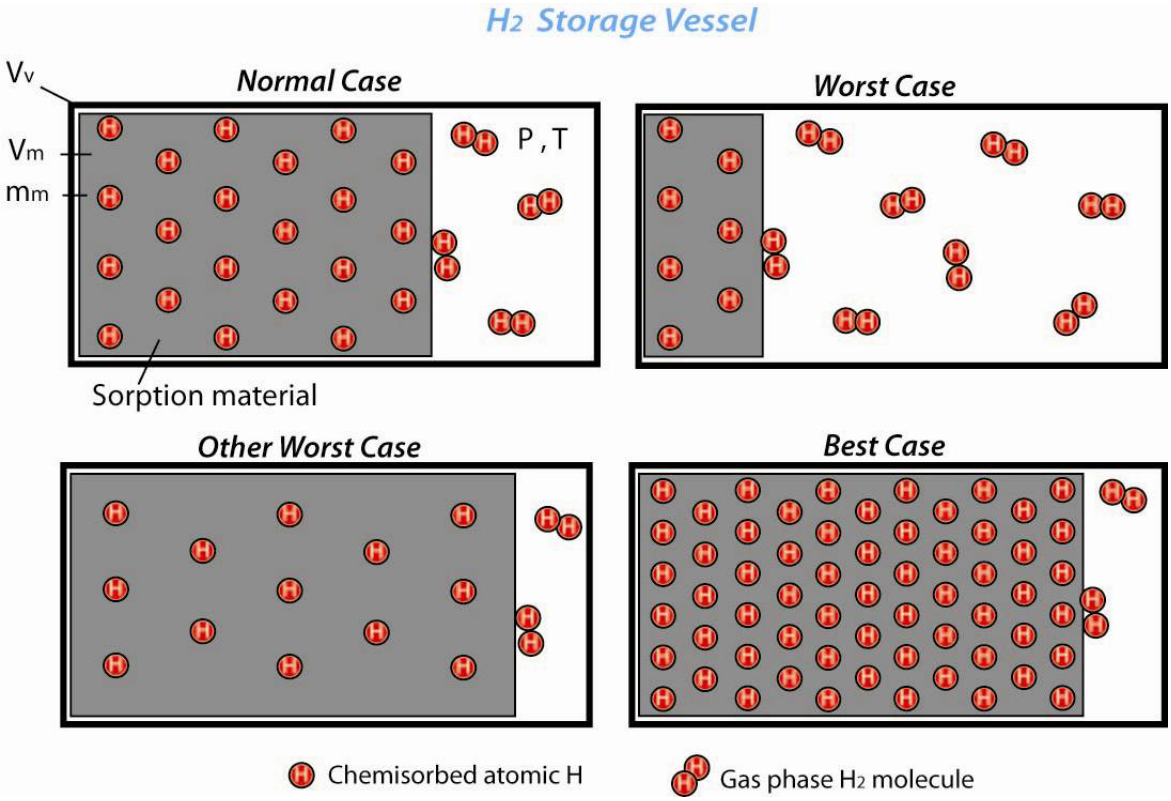

Figure 104. Representation of different hydride systems hydrogen storage capacity scenarios

1.6 Off-board Regenerable Hydride Materials

Chemical hydrides such as ammonia borane and N-ethyl carbazole contain large amounts of hydrogen bonded to lighter elements such as B, C or N. In general, hydrogen release from these materials proceeds in a stepwise manner, as discreet chemical intermediates are formed at each stage of dehydrogenation. For example, ammonia borane contains about 19 wt% hydrogen. It loses this hydrogen in a three step process during thermolysis (Equation 81 - Equation 84). The first step which proceeds at temperatures ranging from 70-120°C results in a 6.5 wt.% loss of hydrogen. The second step corresponds to 6.5-9 wt.% hydrogen which is released at temperature in the range of 120-160°C. Further heating at 160°C or even up to temperatures of 500°C or higher results in almost no hydrogen release. This hydrogen is about 3 wt.% of the parent compound and bonded strongly to a polymeric BNH_x material.

Equation 81 $nNH_3BH_3 \rightarrow (NH_2BH_2)n + (n-1)H_2$ **(<120°C) (intermolecular)**

Equation 82 $(NH_2BH_2)n \rightarrow (NHBH)n + H_2$ **(120 - 160°C) (intramolecular)**

Equation 83 $2(NHBH)n \rightarrow (NHB\text{-}NBH)n + H_2$ **(>160°C) (cross linking)**

Equation 84 $(NHBH)n \rightarrow BN + H_2$ **(160 - 500°C) (boron nitride)**

The first three steps correspond to usable hydrogen capacity of ammonia borane while the hydrogen released during step 4 requires relatively high and unpractical temperatures. Thus, the fourth step is not typically used for predicting the usable hydrogen capacity. However, this hydrogen still contributes to the total hydrogen content of the system and points to the difference between the “Usable Capacity” and “Hydrogen Content” for chemical hydrides. Several variants for release of hydrogen from ammonia borane have been actively explored, including the catalytic release, and additive-induced release of hydrogen from these materials. The added mass of a catalyst or additive must be accounted for in the useable hydrogen weight.

As another example, N-ethyl carbazole contains more than 10 wt.% hydrogen however only 6.2 wt.% of hydrogen (based on the pure compound) is accessible for release under practical conditions; release above this amount leads to irreversibility. N-ethyl carbazole and other derivatives release hydrogen endothermically, and depend extensively on aromatic stabilization energies and catalysis to drive the reaction forward. Again, the mass of the catalyst must also be accounted for in the useable hydrogen capacity.

Hydrolysis or solvolysis reactions in compounds such as $NaBH_4$ or NH_3BH_3 have been explored. However, severe limitations exist due to the amount of solvent (water or alcohols) that is needed for the reactions, which must be included and ultimately reduces the overall usable hydrogen capacity.

1.7 US DOE Hydrogen Storage Capacity Targets

The US Department of Energy Hydrogen Storage Program set technical targets for the properties that an onboard hydrogen storage system will have to have to be considered viable for use with a Hydrogen Fuel Cell Vehicle. The targets are based on the requirement of an on-board hydrogen storage in the range of approximately 5–13 kg to enable a driving range of greater than 300 miles for the full platform of light-duty automotive vehicles using fuel cell power plants. From an applications perspective, these targets define some of the critical properties that researchers must be able to accurately measure for a material to be evaluated with respect its ability to meet the program goals. It is important to note that the targets are defined on a "System" basis and not on a materials only basis. The storage system includes interfaces with the refueling infrastructure, safety features, the storage vessel itself, all storage medium including catalysts or additives, any required insulation or shielding, all necessary temperature/humidity management equipment, any regulators, electronic controllers, and sensors, all on-board conditioning equipment necessary to store the hydrogen (compressors, pumps, filters, etc.), as well as mounting hardware and delivery piping.

The original system capacity targets set by the US DOE to be achieved by 2010 and 2015, respectively, are summarized in Table 9.

Capacity Type	2010 Targets	2015 Targets
Gravimetric, *system* (kg H_2 / kg system)	6.0	9.0
Gravimetric, *material* (kg H_2 / kg system)	12.0	18.0
Volumetric, *system* (kg H_2 / L system)	0.045	0.080
Volumetric, *material* (kg H_2 / L system)	0.090	0.160

Table 9. Summary of the original US Department of Energy capacity targets. The material capacities are assumed to be 2 times larger than the system capacities.[154]

These were modified in February 2009 and the new US DOE are shown below in Table 10.

Capacity Type	2010 Targets	2015 Targets
Gravimetric, *system* (kg H_2 / kg system)	4.5	5.5
Gravimetric, *material* (kg H_2 / kg system)	9.0	11.0
Volumetric, *system* (kg H_2 / L system)	0.028	0.040
Volumetric, *material* (kg H_2 / L system)	0.056	0.080

Table 10. Summary of revised US Department of Energy capacity targets.[154,155]

We have added material capacities based on a rough assumption that the material capacities will be required to be 2.0 times larger than the equivalent system gravimetric capacities, in order to compensate for the weight penalties introduced by the storage container. This of course, will vary significantly depending on the material and system design. The system volumetric capacity includes a 20% penalty for storage systems that are not conformable to geometry of conventional gasoline tanks.[154] Again, we have used a rough 2 times factor to arrive at a materials basis volumetric capacity.

Please refer to the following document for more detail on the US DOE Targets for on-board hydrogen storage systems

http://www1.eere.energy.gov/hydrogenandfuelcells/pdfs/freedomcar_targets_explanations.pdf

The hydrogen storage material capacities of current state of the art materials as of mid-2008 are presented in Figure 105 and Figure 106 below. Note that no material meets the DOE gravimetric or volumetric system capacity targets.

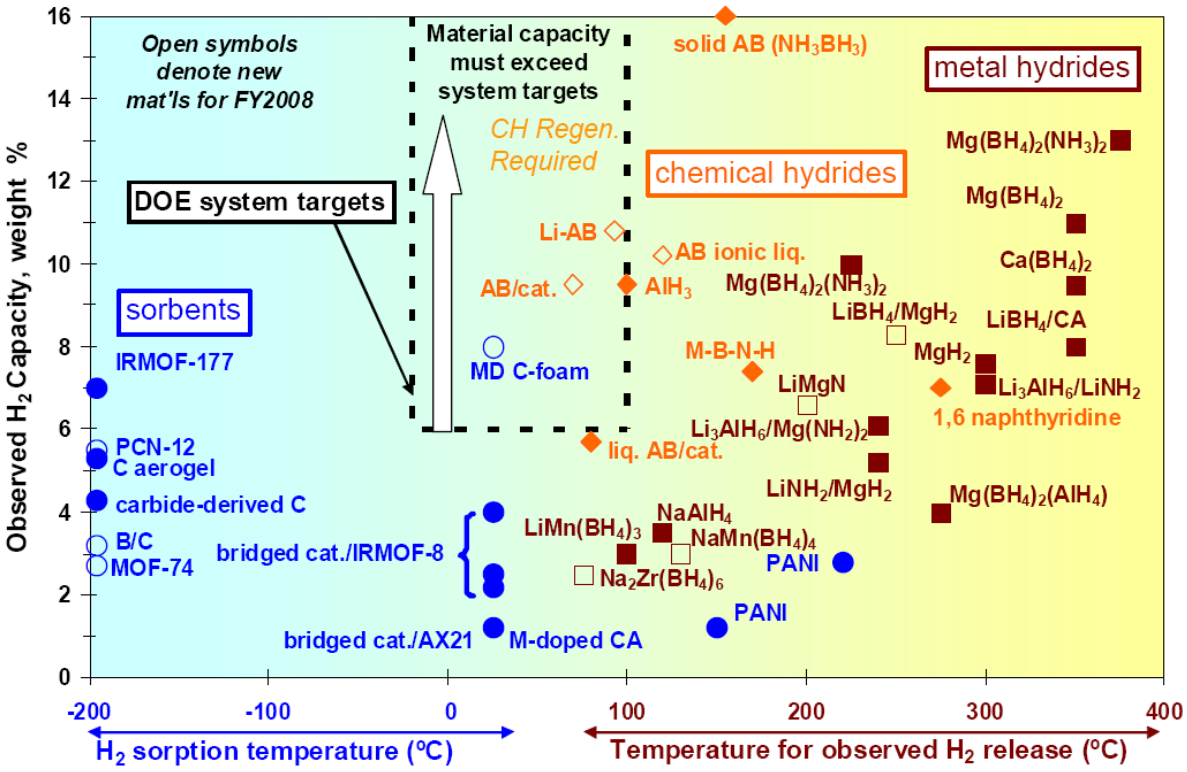

Figure 105. Current state of the art, material hydrogen capacity vs. temperature.[156]

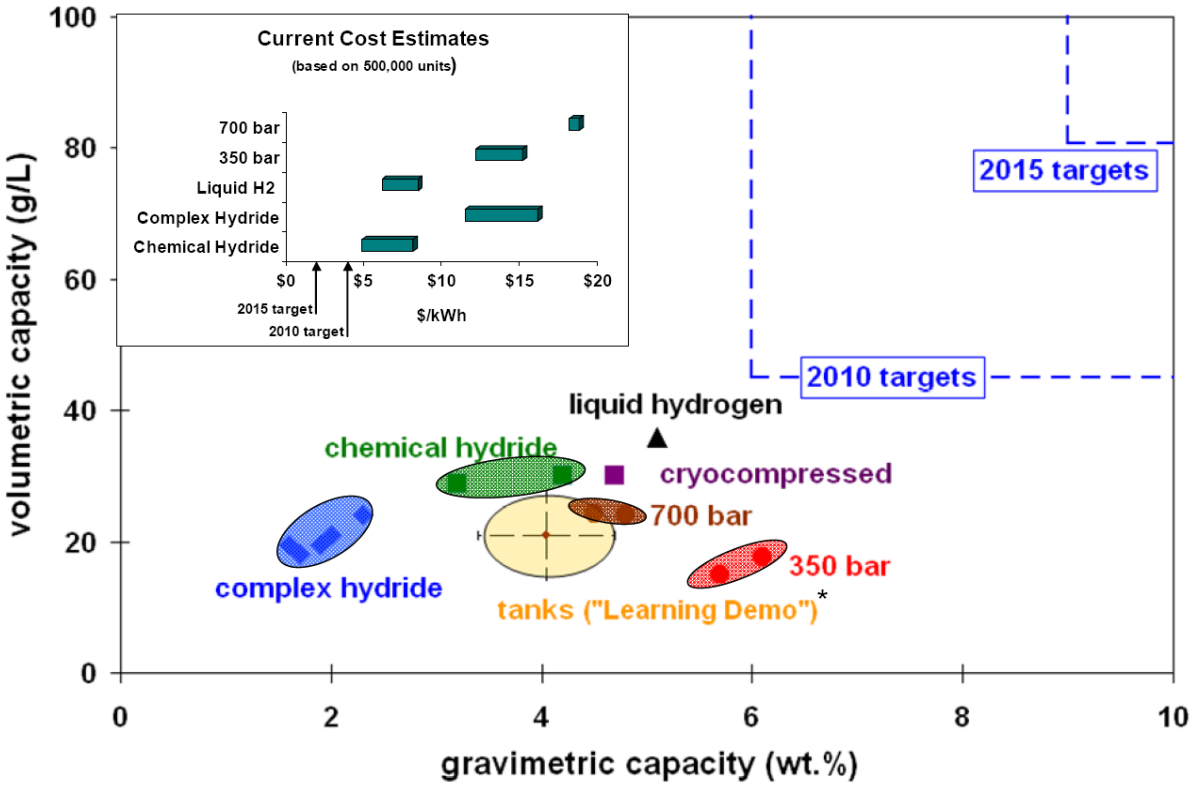

Figure 106. Current state of the art, system gravimetric vs. system volumetric capacities and target.[156]

2 Experimental and Analysis Considerations

While the measurement of the hydrogen storage capacity of a material would seem to be a straight forward endeavor, there are many issues associated with both the experimental methods and evaluation of data which can have a very large effect on the final result. In the following sections the most important of these considerations will be presented with examples to help avoid the common pitfalls in measurements of capacity.

2.1 Matching an Experiment to the Purpose of a Measurement

As with kinetics measurements, the methods and equipment used to measure hydrogen capacity depend to a great extent on the purpose of the measurement. That is, are the measurements being performed to determine capacity at a system performance, materials development, or fundamental science level? Experimental setup and analysis are discussed below in the context of these three broad classes of the purpose of a measurement.

2.1.1 Experiments for System Performance

To gain useful system performance information, enough material should be tested to provide results representative of the material's behavior in a full-sized operating storage system. In general, this means between 10 grams and 1 kilogram of storage material. 100 grams is a good tradeoff between the practical issues of synthesis and handling of the materials and a characteristic, uninterrupted volume of material that would be found in a large-scale system.

If the hydrogen storage capacity of a system is high enough it may be possible to weigh the system before and after charging or discharging on an accurate balance to be able to determine the system hydrogen storage capacity.

If the material performance is already fairly well characterized such that the range of hydrogen desorption and/or absorption rates of the material are known and the identity and quantity of impurities has been identified, it may be possible to use flow meters covering these ranges. By measuring the flow rates with respect to time, the cumulative hydrogen released or absorbed can be calculated at a given time, and the total capacity can be determined. However, with the exception of Coriolis-based flow measurement devices which maintain accuracy over two decades of response, conventional flow meters generally have fairly narrow dynamic measurement ranges (often less than one decade). This is a severe limitation when sorption/desorption rates may vary over several orders of magnitude depending on state of charge, temperature and pressure; and especially on the material itself.

For capacity only measurements, a flow controller can be used to determine the total system capacity. One will not necessarily be able to extract rate information, but as long as the material can absorb or desorb at rates greater than the flow controllers maximum setting, the rate should be steady and provide a good measure of the total absorbed or desorbed capacity. A consideration, however, is that the operation of the flow controller may be affected by or limited by the pressure differential, and any potential impurities. The pressure in the hydrogen storage bed will be a function of the thermodynamics of

the material, the temperature and the rate of gas flow into or out of the bed. A miss-match between the flow controller's rate setting and the materials rate of absorption or desorption will cause a change of pressure that will in turn effect material rates. This may lead to pressures that are too high for the system or instrumentation or a flow situation that is difficult to control. Using a flow meter and pressure regulator, the system will generally find an equilibrium between flow rate and bed pressure that is hopefully within the flow meter's measurable range.

If it is the capacity and not necessarily rates that one wishes to determine then the volumetric approach (PCT measurement) using a large calibrated dosing volume, and multiple doses, will work fine and be quite accurate. Given a scaled-up system containing a relatively small sample (50-100 grams) and a large enough calibrated volume, it is feasible to make single dose measurements that provide rate information as well as total capacity.

One example of scale up measurements are the experiments performed by Gary Sandrock on Ti-doped alanates.[122] A scaled-up test bed was constructed, to evaluate the engineering properties of the alanate material on a scale that would represent the material behavior in real-world applications. The bed was loaded with 72 g of 4 mol% $TiCl_3$ catalyzed $NaAlH_4$ and consisted of a 24.5 cm long stainless steel tube 3.17 cm diameter by 0.21 cm wall thickness (Figure 107). These dimensions are perhaps typical of one element one might find in practical vehicular-sized storage system. The intent was to study rate behavior and to model same from combined kinetics and heat transfer points of view. For that reason, two axial thermocouple wells were included (one centerline and one at the half-radius). Thermocouples were placed at top, middle and bottom in each well, and also at equivalent places on the outside diameter (total of nine measuring thermocouples). The instrumented reactor, wrapped with electrical heating tape, was evaluated a large reservoir volumetric apparatus. It was designed for isobaric charging, followed by non-isobaric discharging into a large calibrated volume.

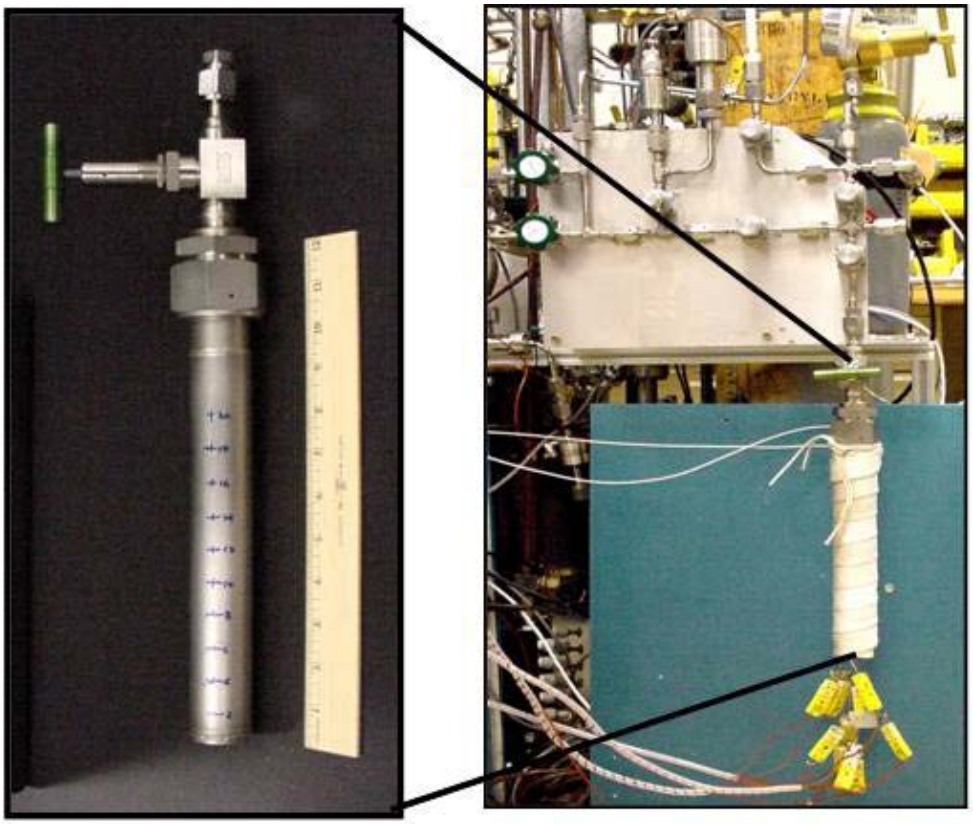

Figure 107. Image of scaled up Alanate test bed with a series of internal and external thermocouples.[122]

Charging runs on the test bed were done at 125˚C with 60, 75 and 90 atm applied hydrogen pressure. Discharging runs were performed at 80, 100, 125 and 150˚C. The 100˚C discharge curve is shown in Figure 108. The capacity appears to level off at 2.2 wt.% after 3 hours. However, this represents only the decomposition of the $NaAlH_4$ phase (first step). The decomposition of Na_3AlH_6 (second step) is present but is a much slower process at 100˚C. The temperature was then increased to 150˚C to complete the Na_3AlH_6 decomposition.

Note that addition applications relevant information was taken from the marks placed on the reactor (Figure 107). These were used as reference points to determine if any expansion deformation of the test bed took place during the cycling. No measurable deformation was found.

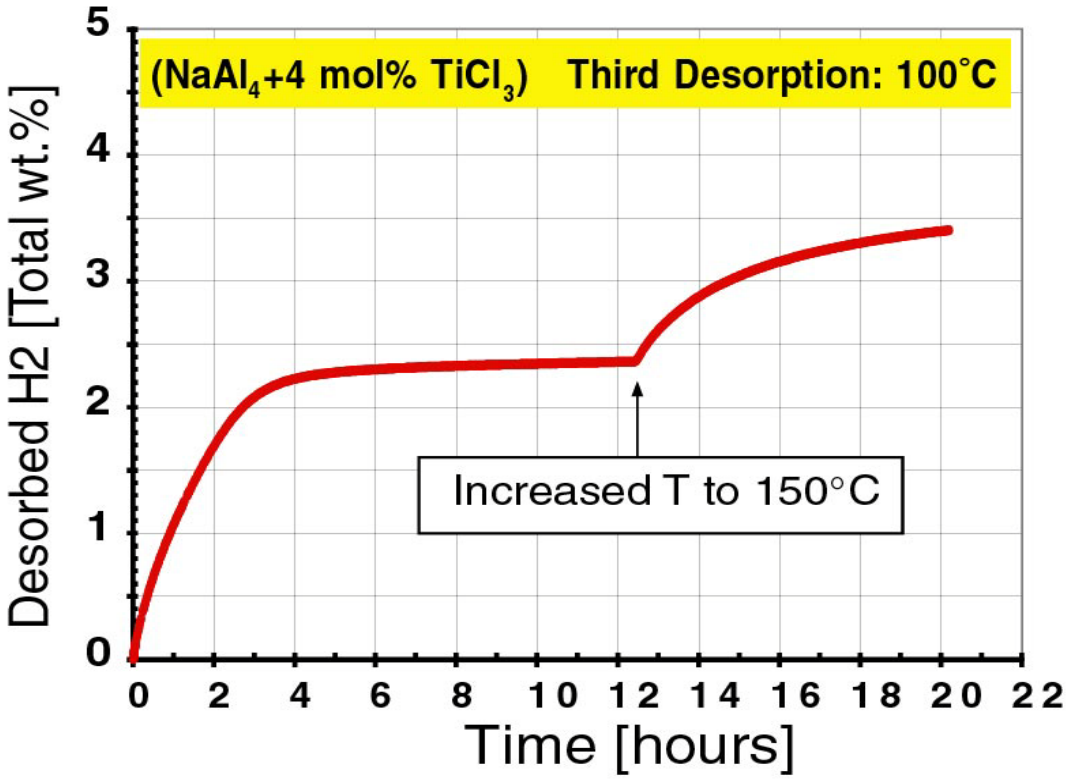

Figure 108. Third hydrogen desorption from scaled-up test bed (capacity on a materials only basis).[122]

These experiments not only provide a good example of a typical experimental setup for examining material properties on a scaled-up system performance level, but also demonstrate how capacity measurements are effected by rates of absorption and desorption which are in turn dependent on temperature and pressure. Had one only measured only at 100˚C the usable capacity would be about 2.4 wt.%. Whereas, at 150˚C the usable capacity approaches 3.5 wt%.

The scale and structure of the sample is integral to the determination of the reversible or usable capacity. This is largely due to the impact of kinetics on capacity measurements. For the determination of reversible or usable capacity, it is important to define more than just the temperature and pressure parameters, but also a required flow rate for dehydrogenation or reaction time for the hydrogenation reaction.

On-board reversible hydride storage materials are characterized by their short hydrogenation times. The usable capacity is capped by the amount of hydrogen that can be loaded in an amount of time similar to that of loading a gas tank. Therefore the kinetics of the reaction is integrally related to the reversible or usable capacity for

onboard storage materials, and similar considerations as to sample size and surface area must be considered for capacity measurements (see kinetics section).

Physisorption-based gas storage systems will contain a large sorbent bed. Operation will consist of cyclical processes, with an alternating adsorption and desorption sequences. Filling the sorbent bed with superactivated carbon can increase both gravimetric and volumetric densities relative to compressed H_2 in the same empty bed at the same temperature and pressure. This "gain" parameter appears to be maximized at low temperatures and pressures for any given activated carbon.[157] An example of the cryo-adsorption method is given in Figure 109, in which the volumetric density is expressed relative to the total volume of the sample cell instead of the apparent volume of the adsorbent. In order to qualify as a true measure of systems performance, however, the mass of the storage cell needs to be included in the gravimetric density. The volumetric densities also need to be validated for real engineering-scale storage tanks (as opposed to small laboratory sample cells). Particularly interesting is the effect of granular carbon adsorbent versus powder carbon adsorbent on the volumetric density, as apparent in Figure 109. Adsorption in an exothermic process, so the same sort of heat dissipation problems brought up in §3.3.1 needs to be addressed for a physisorption-based storage system.

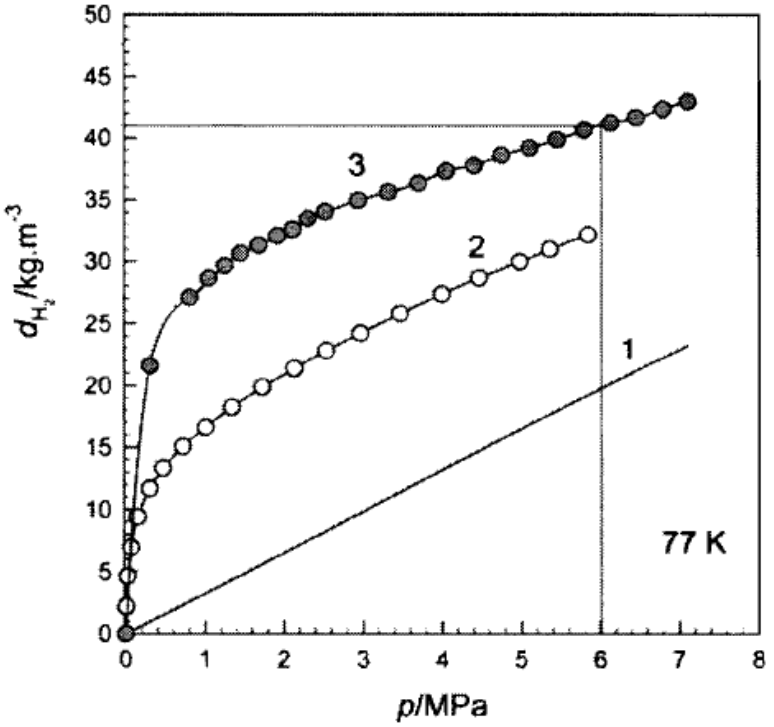

Figure 109. Volumetric density of H_2 in (1) an empty sample cell, (2) a sample cell filled with superactivated carbon powder, and (3) a sample cell filled with superactivated carbon granules.[30]

As and example of an off-board regenerable hydride hydrogen storage system we refer to the work of Kojima et al. who demonstrated the use of $NaBH_4$ hydrolysis to power a 10kW scale hydrogen generator.[158] The schematic of the reactor is shown in Figure 110. They report the gravimetric and the volumetric H_2 densities of the system were 2 wt.% and 1.5 kg H_2/100 liter, respectively. The volumetric density was similar to that of the compressed H_2 at 25 MPa. The hydrogen generator successfully provided a maximum H_2 generation rate of 120 normal liters/min. Assuming a standard PEM (polymer electrolyte membrane) fuel cell operated at 0.7 Volts, generating 120 normal liters/min was equivalent to12 kW. However additional considerations for the energy storage of a mobile system include the extensive heat management required, in addition to a fuel tank and by product tank. In particular, the requirement of a byproduct tank adds complexity and volume that is not ideal for volumetric capacity efficiency.

These studies are still relatively new and cover only a small portion of the parameter space of practical systems. Extensive testing and modeling is required for maximizing the volumetric and gravimetric efficiency for scale up and to be able to make reasonable predictions of system hydrogen storage capacity from material capacity measurements.

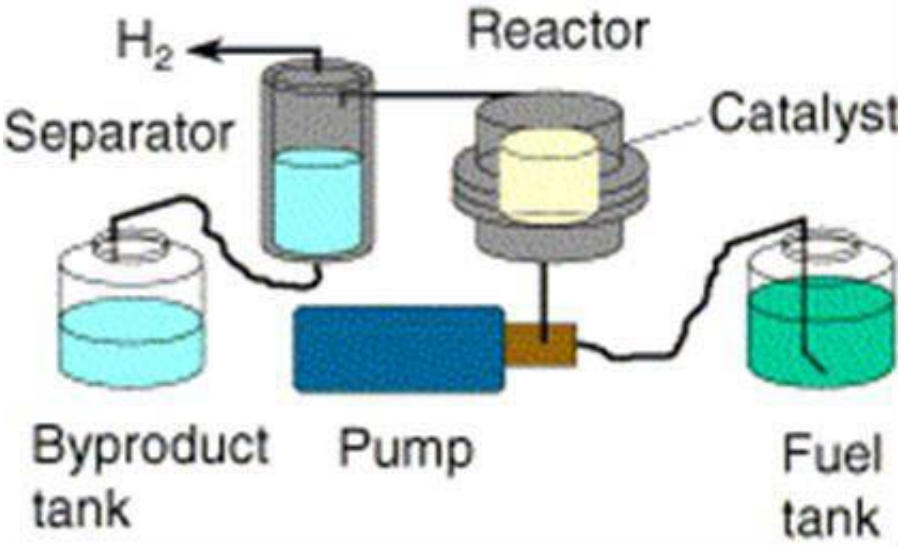

Figure 110. 10kW scale hydrogen generator using $NaBH_4$ hydrolysis.

2.1.2 Experiments for Materials Development

In experiments for materials development, it can be necessary to test many different samples, and therefore smaller sample size can be useful, ranging from a few milligrams to a few grams. Depending on the type of capacity measurement, this may be of only minor importance, or it could lead to almost meaningless results. In determining the theoretical or total capacity of a material, measurements are taken until some sort of equilibrium or steady-state is reached, in which case sample size is much less important. However, if the reversible or usable capacity is being measured, then a small sample could lead to an overestimation of the capacity of a bulk sample that would be used in a real system. It is common that the rate of hydrogen uptake and release is one of the most limiting factors in on-board reversible storage materials, and this effect will not likely be accurately represented by testing on a thin film or other small sample.

Identical experimental conditions are critical to useful results when measuring reversible or usable capacity. Direct effects from temperature and pressure conditions clearly can change results, but other indirect effects may come from heat transfer impacting kinetics or sample size effects on hydrogen diffusion. Even the structure of the material can be important. For example, grain size generally has a strong effect on the kinetics of hydriding, as well as the degree of complete hydriding and therefore a sample of the same weight, size, shape and material composition, but with different grain structures could lead to different results for the measured capacity.

Materials development for physisorption-based systems can be organized into two categories:

1. Increasing the “effective” specific surface area (SSA). The modifier “effective” is used because surface area in microporous materials is not necessarily well-defined.
2. Increasing the adsorption enthalpy.

Different approaches of developing high surface area adsorbents have been adopted for different classes of materials. For activated carbons, the H_2 storage capacity is known to increase linearly with the N_2 BET surface area.[159] The final SSA depends on the quality of the starting carbon precursor, and on the specific purification and activations processes used. An example of a self-contained experiment is a study of the adsorption capacity of a steam-activated coconut char as a function of activation time (shown in Figure 111).[160] Here, a direct correlation between activation time and material capacity (albeit for methane) was determined. In general, the highest surface areas have been reported for KOH treated superactivated carbons.

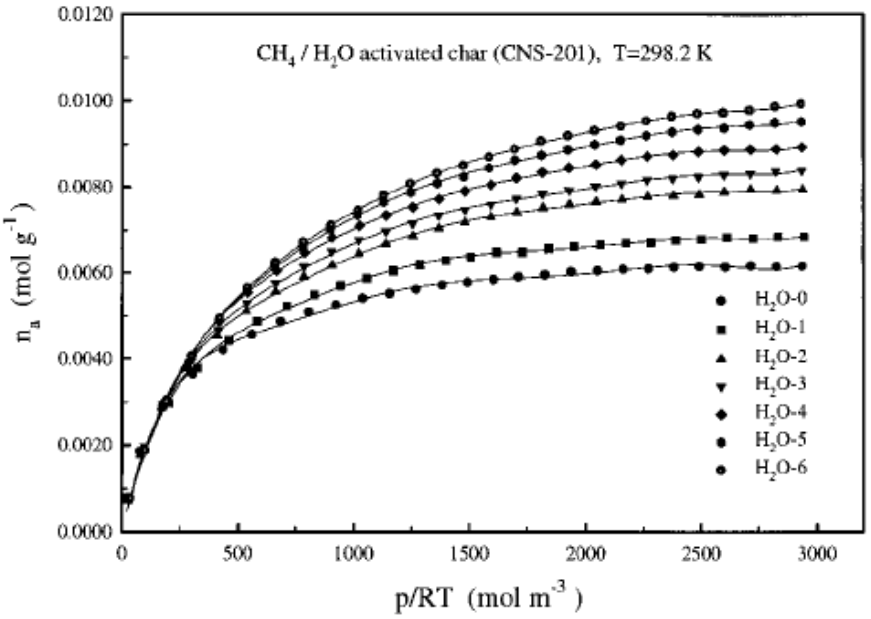

Figure 111. High pressure methane adsorption isotherms of steam-activated coconut char, with varied activation times. The traces H_2O-O through H_2O-6 correspond to activation times between 0 and 140 hours.[160]

In general, the number of variables (activation time, activation type, starting material) is large, making a single comprehensive study of activated carbons (under identical conditions) difficult. For metal-organic frameworks, materials development is limited by the inherent difficulty in designing and synthesizing new structures. The same difficulty applies to carbon nanostructures (e.g. nanofibers), compounded by the weak reproducibility between different synthesis and purification techniques.[159]

Development of materials with enhanced adsorption enthalpies is necessary to achieve reasonable storage capacities at ambient temperatures. Examples of comprehensive studies on the effect of surface functional groups on the adsorption enthalpy of activated carbons are available in the literature (see Figure 112).[161] Once again, however, the energy heterogeneity and complex surface morphology of activated carbons makes direct comparisons difficult. Materials development of metal-organic frameworks, with respect to optimizing adsorption enthalpy, has focused on maximizing the density of exposed unsaturated metal atoms. Due to the complexity of MOF design and synthesis, however, there does not yet exist a truly systematic experimental approach. The same difficulties apply to other designer sorbents as well.

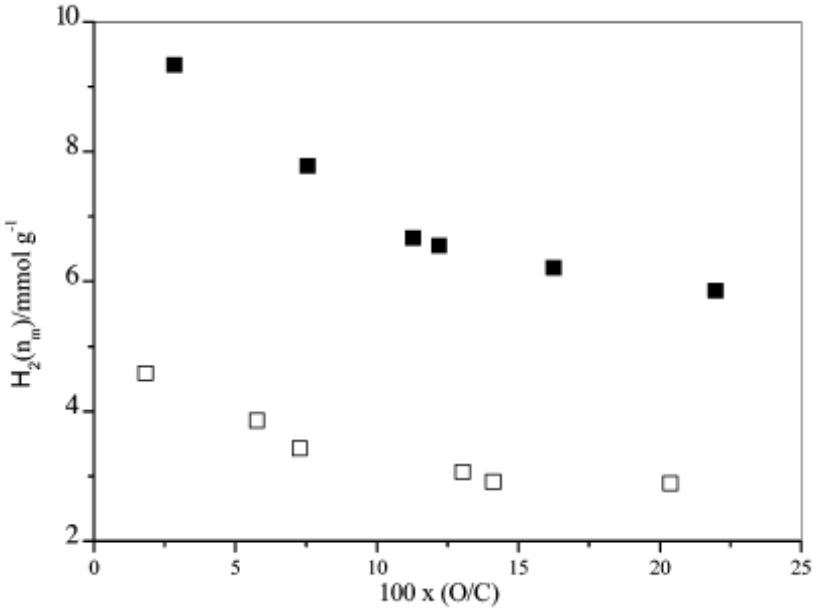

Figure 112. Variation of the maximum H_2 adsorption amount versus the oxygen/carbon ratio: (□) steam-activated coconut shell carbons (■) polyacrylonitrile-derived activated carbons.[161]

Work on developing improved chemical hydrides follows similar requirements to on-board reversible hydrides for systematic measurements to be able to make reliable comparisons between materials. In one example, in an effort to lower the decomposition temperature of ammonia borane, Xiong et al have adopted an approach that has been applied in the manipulation of the thermodynamic property of compounds through chemical alteration to modify ammonia borane.[162] The method consists of substituting one H in the NH_3 group in BH_3NH_3 with a more electron-donating element. The idea is to alter the polarity and dihydrogen interactions of ammonia borane to produce a substantially improved dehydrogenation profile.

Chemical modification of ammonia borane to lithium amidoborane ($LiNH_2BH_3$) and sodium amidoborane ($NaNH_2BH_3$) show substantially different and improved dehydrogenation characteristics with respect to ammonia borane itself. These alkali-metal amidoborane materials are formed through the interactions of alkali-metal hydrides (LiH and NaH) with ammonia borane, which lead to the replacement of a single ammonia borane hydrogen atom by a lithium or sodium atom. It has been observed that more than 10 wt.% and 7 wt.% of hydrogen desorbs from $LiNH_2BH_3$ and $NaNH_2BH_3$, respectively, at around 90°C. In addition to the improved dehydrogenation properties, volatile gas impurities such as borazine that are formed during dehydrogenation of ammonia borane are eliminated. However some impurities such as ammonia appear to be enhanced.

With respect to these comparative measurements of hydrogen release capacity, measurements based on constant pressure systems are more reliable where the actual volume of hydrogen released is measured. It is extremely important that off-gas analysis of these materials is performed, as gases and volatiles other than hydrogen may be released from chemical hydrogen storage, amides, borohydrides, and other complex hydride materials, in particular. It is critical to identify the species or volatiles that formed to determine for the safe use of such materials and the impact they may have on the hydrogen energy conversion device (e.g. the fuel cell components). Also, the potential loss of materials from the system may be problematic for either reversible on board complex hydrides, or for off board regenerable systems.

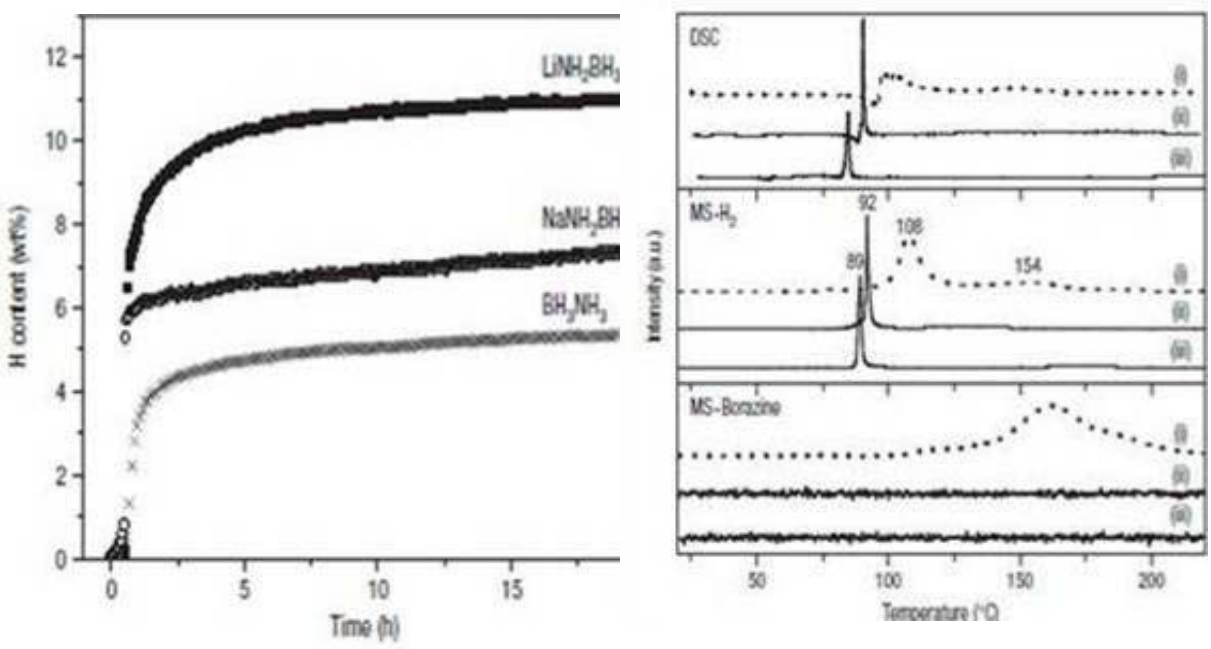

Figure 113. Kinetics of hydrogen desorption from alkali amidoboranes and post-milled BH_3NH_3 samples at about 91°C (left); the right panel indicates the DSC trace, as well as the mass spectrometer traces of hydrogen and borazine from these three materials. The metal amidoboranes release significantly less borazine than the parent ammonia borane.

2.1.3 Experiments for Fundamental Studies

Experiments on the fundamentals of reversible or off-board regenerable hydride materials may study things like the appropriate amount and distribution of a catalyst in a sample to optimize kinetics tradeoffs with weight capacity (in general, catalysts don't contribute to hydrogen capacity). If the catalyst is introduced to improve the kinetics, sample size is still crucial to predicting realistic results for the final application of materials, but may be less important in fundamental studies.

Special care should be taken when extrapolating from fundamental studies to estimates for system level performance. Many factors involved in testing smaller samples will lead to unreasonably high predictions of metrics like loading time and usable capacity. This is because fundamental studies are often done on small samples, sometimes just a few milligrams or even micrograms, where the mass and heat transport may substantially differ from a full-scale test. With respect to off-board regenerable materials, exothermic reactions may lead to runaway reactions on large scale systems which are not observed in measurements on small samples. Hydrogen release from aminoborane is exothermic but not much is known about thermal effects on capacity or effect of runaway reactions on capacity.

With respect to physisorption materials, theories for supercritical H_2 isotherms are still not as well developed as the theory for subcritical isotherms. Understanding of H_2 adsorption enthalpies and packing densities within pores of various sizes and geometries have been usually limited by the lack of hydrogen adsorption isotherms measured over a wide range of temperatures and pressures. However, recent results obtained on metal-organic frameworks down to 50 K and 30 bar have revealed that the packing density of hydrogen in pores of nanoscale dimensions can reach that of the liquid state.[163] In the same report, the adsorbed phase was also found to behave like an incompressible fluid, suggesting an upper limit to the packing of hydrogen interacting with such small pores (Figure 107). The above-cited characteristics could be modeled using a Dubinin-Astakhov equation involving pseudo-saturation pressures. Therefore, such extended measurements have proven to be useful on fundamental perspective as well as for exploring the physical limits of physisorption material for practical applications. Volumetric measurements on small masses of materials and at low temperatures and high pressures involve stringent requirements in terms of pressure and temperature stability. Blank tests are imperative to make a basic assessment of the performance of the system. Moreover, as mentioned earlier, the volume of the system must be small enough (i.e. to get sufficient sensitivity on small sample masses).

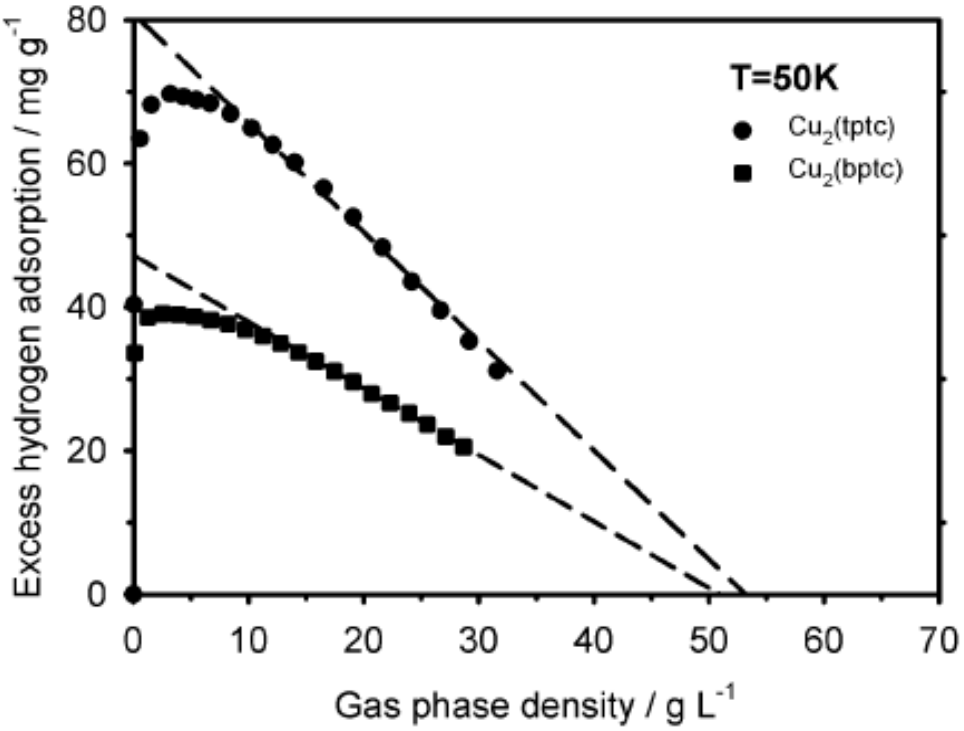

Figure 114. Excess hydrogen adsorption isotherms performed on copper-based MOFs near saturation. Notably the extrapolated excess curves down to Nex=0 are shown. At this point the adsorbed phase density equals that of the gas phase (about 50g/L); revealing the ultimate hydrogen packing density under such conditions.[163]

2.2 Material Properties that Affect Capacity Measurements

2.2.1 Materials Preparation and Handling

Materials preparation and handling can have a dramatic effect on performance results but is often an overlooked step in understanding and performing hydrogen sorption measurements. Thus, the determination of a sample's purity or at least its chemical composition is clearly important. For reversible materials, it is critical to measure hydrogen uptake and release over several cycles as the formation of unintended by-products (NaCl, H2O, NH3, LiH, other stable hydrides…..) versus true hydrogen storage will typically present a decrease in the apparent hydrogen storage capacity of the material. Mass-spectrometry of the evolved gases is highly recommended. In addition, because the manner in which impurities can produce misinterpreted results is generally differently in volumetric versus gravimetric measurements, it is highly recommended that unexpected or too-good-to-be-true results from one technique be carefully evaluated using at a minimum the other measurement technique.

The most obvious consideration in the synthesis or preparation of a sample for use in quantifying the hydrogen storage capacity of a material are impurities or wholly inactive side products in the sample. Impurities, in addition to potentially detracting from overall capacity, may have an effect on the actual hydrogen uptake or release capacity and/or kinetics.

The presence of unaccounted for-secondary hydrogen absorption phases may skew the interpretation of the capacity of a material if all of the hydrogen uptake or release is attributed to only one component of a multi-component sample. For example, the presence of a catalytic metal that itself forms a reversible hydride. Or the presence of unstable oxides that may react with hydrogen to form water. These issues are often most consequential for high-surface-area materials because the level of impurities generally scale with the amount of active surface area. Impurity issues are also most difficult to identify in high-surface-area materials because while impurities may be present in significant quantities, they may be dispersed in only a few monolayers, present as nano-particles, or amorphous in nature and, therefore, not readily observable using common analytical methods such as standard X-ray diffraction.

The secondary component may not be a hydride former at all, but may cause hydrogen release through a side reaction. For example, a sample of unreacted $NaAlH_4 + xTiCl_3$ may produce more hydrogen on its first desorption than expected from the decomposition of $NaAlH_4 \rightarrow NaH + Al + 3/2H_2$. This is because in the process of decomposition NaH may react with $xTiCl_3$ to form xNaCl releasing $x/2H_2$.[164] In this case, the impurity or additive, could contribute to an overestimation of hydrogen storage capacity of the actual active storage material based on measurement of the initial quantity of released hydrogen. Such side reactions are clearly an important consideration in the determination of the hydrogen storage capacity of off-board rechargeable chemical hydrides.

The presence of unaccounted for “inactive” impurities can lead to an underestimation of the capacity of the active component of a storage material. This may be the most common and often the most difficult problem to address. If secondary components are present difficult to detect impurities (e.g. nanocrystalline, poorly crystallized or glassy phases), they will be difficult to quantify or even identify in using standard techniques such as X-ray diffraction If the impurities are of the same composition as the storage phase, but only structurally different than the hydrogen sorption component, it becomes extremely difficult to assess the true hydrogen capacity of a material based on a sample of an unknown mixture of phases. For example, in the case of nanostructured carbon materials (specifically single wall carbon nanotubes, SWCNTs) it has been very challenging to determine how much of a sample actually consists of SWCNTs versus amorphous carbon, graphite, multiwall carbon nanotubes, how catalysts used in the synthesis and other components introduced in processing and purification are associated with the various phases and their roles, etc. Different techniques such as

TEM and pulsed neutron diffraction have been used to try to quantitatively determine the actual SWCNT content of samples.[165] With impurity concentrations on the order of 30-40% even in highly purified samples, a thorough analysis of a sample's elemental and structural composition is needed before measured quantities of ab/adsorbed hydrogen can be ascribed to any single material as its true hydrogen storage capacity.

The properties of most hydrogen storage materials are very sensitive to impurities, both as solid contaminants and gas phase impurities. It is well known, for example, that the addition of small amounts of additives (alloying or impurities metals) to hydride-forming alloys used in nickel-metal hydride batteries will cause large changes in electrical capacity, kinetics and cyclability. A great amount of work has been carried out in perfecting the composition (now ~ 10 elements) of AB5 battery alloys. One such example is shown in Figure 115 where the Ni portion of the AB5 alloy $LaNi_5$ has been substituted with small quantities of other elements to improve the long-term cycling capacity.[166] With the commercialization of gaseous hydrogen storage materials and systems, it is very likely that similar compositional "fine tuning" will be employed to improve storage material performance.

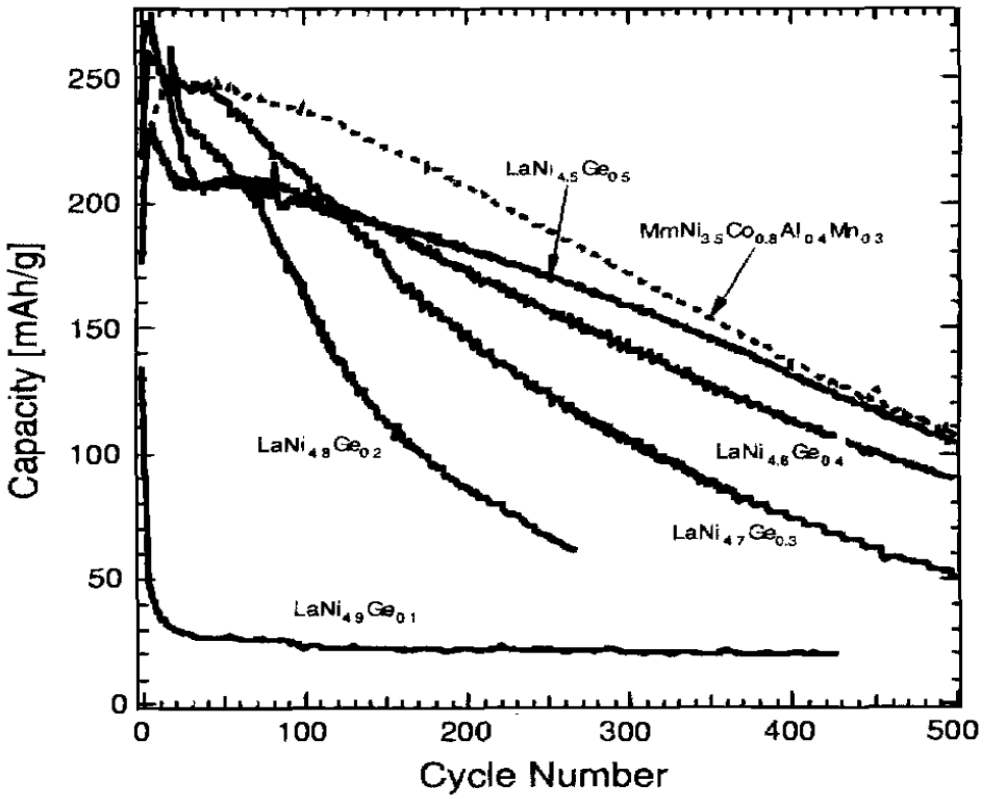

Figure 115. Cycle life behavior of $LaNi_{5-X}Ge_X$. alloys with comparison to a good commercial mischmetal-based, multi-component alloy also evaluated at JPL.

An important consideration is that solids contaminates can have similar beneficial or negative effects on a material's performance. For example, it is very common to use ball-milling preparation to introduce catalysts, create defects, or produce nano-structured materials. The milling pot and balls themselves may introduce metals into the samples (Fe, Cr, W, C….). Enhancement of the kinetics may not necessarily be coming solely from intentionally added catalysts, but rather the components of the ball mill may be participating as well. This has been observed by comparing the diameter milling balls when they are new with those that have been used for many hours of milling. The amount of material loss due to mechanical attrition was significant.

An additional consideration with respect to the mechanical milling preparation of materials is the possibility of the introduction of gas-phase impurities that may be deleterious to the materials synthesis. One generally performs milling of the sample in an inert gas environment. There are two ways to do this. One is to introduce the entire mechanical mill into an inert gas glove box, and even then, ppm level of oxygen and water may affect the outcome of the anticipated products. There is also the added complications of needing to setup the milling machine in the glovebox, potential perform maintenance or repairs in the glovebox as well as all of the vibration problems the mill imposes on the glovebox and delicate instruments and items in the glovebox.

The other method is to simply seal the milling vial in an inert gas glove box and subsequently perform the milling outside of the glove box. This second method may leave open question of how well the milling vial is sealed against introduction of oxygen and moisture from the surrounding air that could leak into the vessel if the vessel is poorly sealed. The seals on milling vials are typically made of an elastomer and are not particularly suited to seal against a pressure differential. So, for example, as the vial heats up on milling, so too will the inert gas in the vial heat and expand building up pressure in the vial. The excess pressure may be released across the elastomer seal to equalize the pressure. After milling if the milling vial will cool and the pressure will drop inside of the vial. If it is still in an air environment there is a chance that the lower pressure in the vial will draw air into the vial contaminating or reacting with the sample materials. Introduction of ambient air into the vessel during milling could obviously alter the desired composition and in turn affect the hydrogen storage properties of the materials or even cause unanticipated chemical reactions within the vial that could lead to potential safety concerns.

A well-controlled series of sorption tests of the materials after exposure to known quantities (ppm levels) of contaminants should provide insight into the sensitivity of the materials to impurities during preparation and/or testing. However, it is difficult at best to perform hydrogen sorption testing on materials in an ultra-high purity environment, and it is unlikely that in the real world application for which the materials are being developed that any hydrogen storage system will ever operate under UHP conditions.

2.2.2 Impurity Effects and Capacity Testing Protocols

The same contamination issues that occur in materials preparation hold for the actual gas-sorption testing of materials. This again may include both solid-phase and gas-phase contamination. Above all, it is recommended that only UHP (Ultra High Purity 99.999% or better) test gases be used for both the inert gas (helium) free (dead) volume calibrations and hydrogen in the sorption tests. The gas manifold system should be of an appropriate design to enable highly effective purging of any gas transfer lines. It is very important to follow all gas-line and instrument purge instructions when connecting a new cylinder of gas to the test equipment. If there is any residual air or moisture in the line or any section of the instrument connected to the gas cylinder when the cylinder valve is opened then the expensive UHP gas of your cylinder has just been contaminated and no longer meets testing requirements. It is recommended that gas-lines and instrument components be pumped down to at least 10^{-2} millitorr or better followed by a flushing with the test gas (quick open and close in a safe manner of the gas cylinder valve). This process should be repeated at least three times before the test gas is finally opened up to the instrument.

The same procedure should be followed every time a new sample is loaded into the instrument or a sample cell is attached to the instrument. There will certainly be air in the connections between the cell and the instrument. The unusual procedure is to pump the connecting lines or cell down to rough vacuum.

A variety of vacuum pumps may be used for degassing of samples or in the gas-line purging and gas sorption measurement processes. Important considerations are that the pump is compatible with the working gases and potential out-gassed products, and that the vacuum pump itself does not contaminate the measurement instrument or sample. Oil-free vacuum systems are generally preferred because of the potential that oil vapor can back-stream into the system causing contamination. Although oil vapor filters can reduce this, they are unlikely to eliminate it entirely. A study by Bojon et al showed that a turbomolecular pumping station, backed by a rotary oil pump, did not significantly contaminate a UHV system during operation, but water and hydrocarbon contamination was introduced upon stoppage of the pump.[167] Volumetric systems designed for hydrides can operate without UHV-capable pumps; in this case, it is very important that the vacuum pump does not introduce contamination and therefore an oil-free device, such as a scroll pump, should be used.[4] The greatest potential problem in this case is the potential failure or powering down of an oil-based vacuum pump with the chance that the oil is then aspirated into the testing equipment.

The authors feel that there is not strong evidence to suggest that evacuation of gas lines or the sample itself using a UHV (Ultra High Vacuum) pumping system such as a turbomolecular pump versus a rough vacuum (1-100 millitorr) pump system has a

significant impact on the performance of the materials. Realistically, the vacuum level at the sample itself is limited by the conductance of the gas lines and filters between the vacuum pumps and sample.

The pumping speed of a pump is only one of the many factors involved in the lowest achievable vacuum of a given system. The size and shape of the tubes or chamber being evacuated can be of even greater importance. The out-gassing rate of the tube or chamber walls, known as the gas load, also limits the working vacuum achieved from a pumping system.

When low enough pressures are reached, the density of gas in the tubes is so low that intermolecular effects, or viscous forces, become less important, while the interaction with the walls becomes more important. This latter regime is termed molecular flow, and the flow properties can be described mainly by the geometry of the tubes. This is described by the conductance, which in the molecular flow regime can be approximated as:

Equation 85

$$C = 78\frac{D^3}{L}$$

Where D is the diameter of the tube and L is the length, both in inches. C is in units of liters/s. The effective pumping speed is then defined as:

Equation 86

$$\frac{1}{S_{eff}} = \frac{1}{S_{Pump}} + \frac{1}{C}$$

The minimum achievable pressure is then given by:

Equation 87

$$P = \frac{Q}{S_{eff}}$$

Where Q is the gas load due to out-gassing from the walls and any leaks present.[168] Figure 116 presents the results for the maximum achievable vacuum for a 10 in. long tubing system for a typical gas load of $5x10^{-9}$ Torr-L/s[169] and pumping speeds for a standard roughing pump and turbomolecular pump.

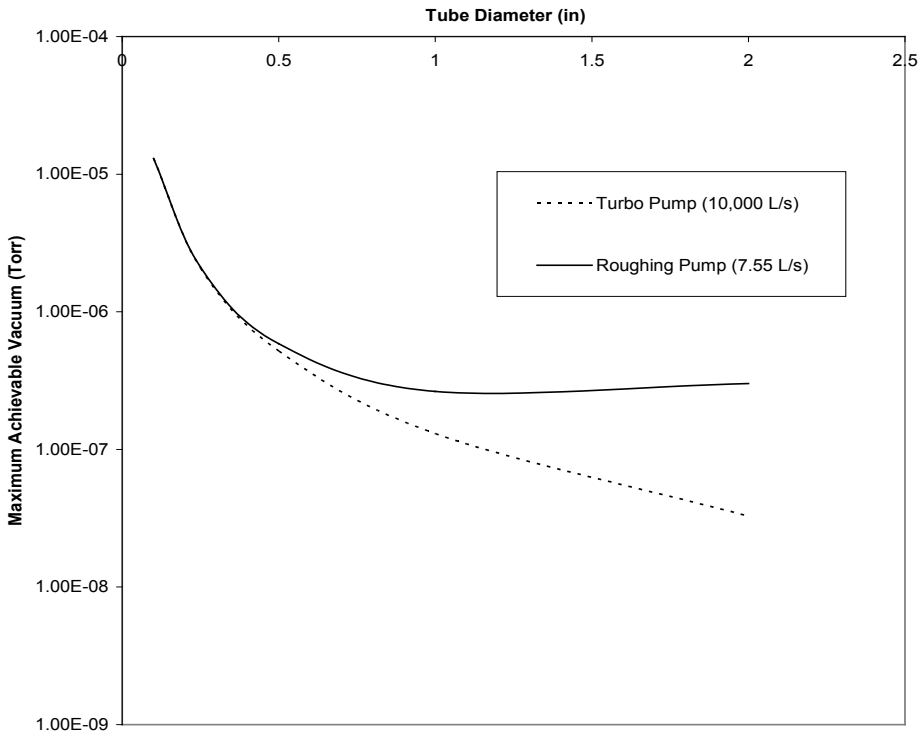

Figure 116. Achievable vacuum for a roughing pump and turbo pump for various tube diameters.

From the figure, it is clear that for tube diameters less than approximately 0.5 in. there is no significant advantage to using a turbomolecular pump over a roughing pump. Thus the ultimate vacuum level at the sample for most measurement instruments is generally not significantly better whether a UHV or rough vacuum pumping system is used.

The heating of the sample under vacuum has much more impact on reducing impurity levels (or degassing) than achieving UHV conditions. That being said, if UHV levels are deemed necessary, they will be most effective when the pumping station is connected via large diameter (0.5 inch or greater) directly to the sample cell.

For physisorption materials such as activated carbon, it is almost always necessary to bake out the sample at an appropriate temperature to remove physisorbed impurities such as water, carbon dioxide, solvents from preparation, etc. before performing gas sorption measurements.. To accurately observe the characteristic gas (hydrogen) sorption properties of the sample one must ensure that all active adsorption sites in the material and the diffusion path to these sites are free of any interfering contaminants.

Physisorption materials, because of their high surface area are particularly susceptible to the adsorption of moisture. To give an appreciation of this, prior to the testing of a

high-surface area activated carbon sample (ca. 1 gram), it was exposed to air in a relatively low humidity environment. The sample was then heated in a closed evacuated sample vessel for approximately 30 minutes. Upon cooling the sample vessel, water droplets were observed to have condensed in the unheated gas lines connected to the sample vessel.

These physisorbed "contaminants" can be present in significant quantities adding very large amounts to the weight of the sample. Thus, for volumetric gas sorption measurements the sample should be weighed after the bake-out and sorption measurements to get the true sample mass for determining the sample's hydrogen storage capacity. Ideally, the sample should be transferred airlessly to an inert gas glove-box where the sample can be weighed minimizing the risk of air exposure (resulting in adsorption of contaminant mass). The same is true for gravimetric measurements where the sample should be fully degassed and transferred to the balance for weighing before gas sorption testing is done. In general, with volumetric equipment, the degassing can be done *in-situ* on the gas sorption testing instrument. This is also normally the case with gravimetric instruments, and the mass of the sample can be measured *in-situ* before the start of sorption measurements.

In one study, bake out of activated carbon materials at elevated temperatures reduced the sample mass significantly.[170] In the referenced paper, activated carbon was ball milled for up to 1000 hours. For samples ball-milled up to about 100 hours, the mass loss was about 2-5%, with most of this occurring below 200 °C. Further heating to 1000 °C led to slightly more mass loss (up to 7% for the 100 hour milled sample). The sample ball-milled for 1000 hours had a 20% mass loss during heating to 1000 °C. Another study found that MOF-5 looses about 12.5% of its mass due to heating up to 523 K (due to water and solvent elimination) but is stable up to 723 K.[171]

Regardless of what type of analytical gas sorption measurement instrument is used, an important consideration is that in the bake-out process the sample may release gases, vapors or even liquids (volatile organic solvents, borane, ammonia, low vapor pressure metals, molten alanates…) that can contaminate the instrument. This may cause serious irreparable damage to the instrument or impact the reliability of subsequent measurements. An example is that of sodium aluminum hydride ($NaAlH_4$) which melts at 182°C. If a sample of alanate is rapidly heated and suddenly exposed to vacuum, the liquid can coat and decompose on the inside of the sample cell or may even be aspirated into the instrument leaving behind solid decomposition products (aluminum and NaH). With these considerations in mind it may make sense depending on the material to perform the bake-out on a separate evacuation manifold and then transfer the sample to the measurement instrument after the bake-out. This is one of the advantages of the volumetric method in that sample cells are generally designed for simple airless sample transfer from the sample preparation system (glove box), to a bake-out degassing station if required, and then to the measurement instrument.

Bake-out conditions

The following are typical bake-out or degassing conditions for different physisorption materials.

Material	Temperature (K)	Vacuum (Pa)	Time (h)	Reference
Activated Carbon	673	10^{-4}	48	[172]
Carbon Nanotubes	420		24	[173]
Carbon Nanotubes	673	10^{-3}	>1	[174]
MOF-5	400	10^{-2}	14	[175]
IRMOF-8	400	10^{-2}	14	175
Cu-MOF	400	10^{-2}	14	175

Table 11. Typical degassing conditions for different sorption materials.

An important caveat to these generic bake-out conditions is that some materials (MOFs in particular) are only moderately stable. They may decompose or become structurally alter at elevated temperatures, causing a significant change in their ability to store hydrogen. It is advisable to do some materials analysis such as X-ray diffraction measurements before and after a test bake-out to ensure that the bake-out itself does not alter the material. DSC measurements on a sample up to the desired bake-out may also indicate any thermally induced instabilities in the materials that necessitate performing bake-out at lower temperatures.

Under certain circumstances, hydrogen evolution capacity can be strongly affected by measurement conditions and interactions between reaction components. For example, during the hydrolysis of $NaBH_4$ with steam to produce hydrogen, higher yields of hydrogen were obtained at the lower temperature of 110 °C and raising the temperature to 140 °C decreased the reaction rate and yield.[176] The lower rates and yields at higher temperature are counterintuitive, but this was tentatively attributed to mass transfer limitations in the particles. Examination of the reactor contents after the experiments at both temperatures revealed that the solid particles were agglomerated. The agglomerated material was soft and wet after the 110 °C experiment and hard and dry after the 140 °C experiment. Presumably, the $NaBH_4$ on the surface of the particle absorbs water, reacts, and forms a layer of sodium metaborate ($NaBO_2 \cdot xH_2O$). This material will retard steam diffusion through the $NaBH_4$ particle, decreasing the production of hydrogen. The lower reaction rates at higher temperatures may be explained if the less hydrated form of $NaBO_2 \cdot xH_2O$ is less permeable to water vapor.

Another explanation for the temperature effect could be that the reaction initiates only after the $NaBH_4$ absorbs water. In that case the water absorbed by the hydride could be affected by the temperature such that condensation and absorption of the water is

suppressed at the higher temperatures. This may explain the physical difference between the wet product from the 110 °C reaction and the dry product from the 140 °C experiment.

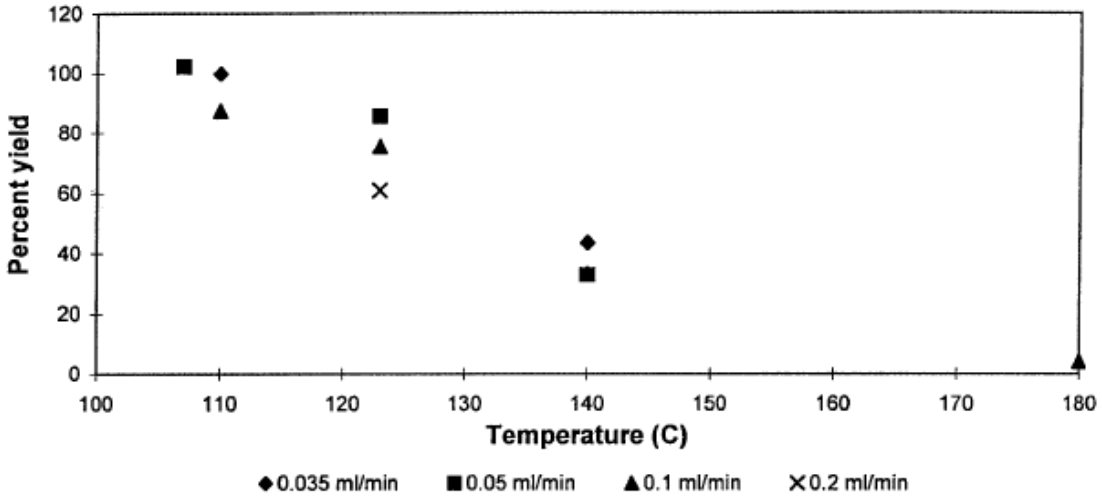

Figure 117. Hydrogen yield as a function of temperature in the steam hydrolysis of $NaBH_4$ At higher temperatures the surface composition changes to borate hence preventing interaction of steam with the hydride ultimately decreasing the hydrogen delivery capacity.[176]

2.2.3 Surface Conditions

Imperfect materials preparation and handling often has the greatest impact on the surface of the material. The next sections give a detailed description of some of the different ways that surface contamination can affect the hydrogen storage properties of materials including both capacity, kinetics and cyclability.

2.2.3.1 Surface Passivation

Surface passivation is a common problem in the study of metal hydrides as many of the materials of interest, such as Mg and Li, are readily oxidized by water or oxygen. Even a thin surface oxide layer and block hydrogen diffusion into the bulk of the sample, leading to drastic reductions in the measured capacity value. Depending upon the nature of the surface coating, the effects of surface passivation can be mitigated by annealing or cycling the sample.

For fundamental studies, this problem is often mitigated by using a capping layer to protect the surface. However, extreme care is still necessary to limit surface oxidation

since even trace amounts of oxygen or water can contaminate the sample surface. For example, thin films are deposited in high vacuum conditions, but even at a pressure of 10^{-6} Torr, the primary constituent of the residual gas in the chamber is water vapor evaporating from the chamber walls. In a worst-case scenario where all of the molecules are water vapor and all impinging molecules stick to the surface, the monolayer formation time is about 3 seconds.[33] Therefore it is possible that in imperfect vacuum conditions there may be some surface passivation even before the capping layer can be deposited. Similar logic also applies in the case of using glove boxes to limit exposure to an oxidizing atmosphere.

Since it is impossible to limit any exposure to oxidizing elements, samples should be subjected to exactly the same conditions as much as possible. This includes establishing a standard cleaning procedure for targets before deposition (e.g. sputtering for 15 seconds before opening the shutter to begin deposition), setting a standard vacuum level for deposition and exposing a sample to ambient or glove box conditions for the same amount of time.

Surface oxidation or passivation can have as strong an impact on bulk or powder samples as it does with thin film samples. Oxidation of the surface may prevent the dissociation of molecular hydrogen gas to atomic hydrogen at the surface or prevent the diffusion of hydrogen from the surface into the bulk. This is true of many of the intermetallic hydrides. Figure 118 shows the activation of a coarse granular sample of $LaNi_5$ that was exposed to 30 hydrogen absorption/desorption cycles.

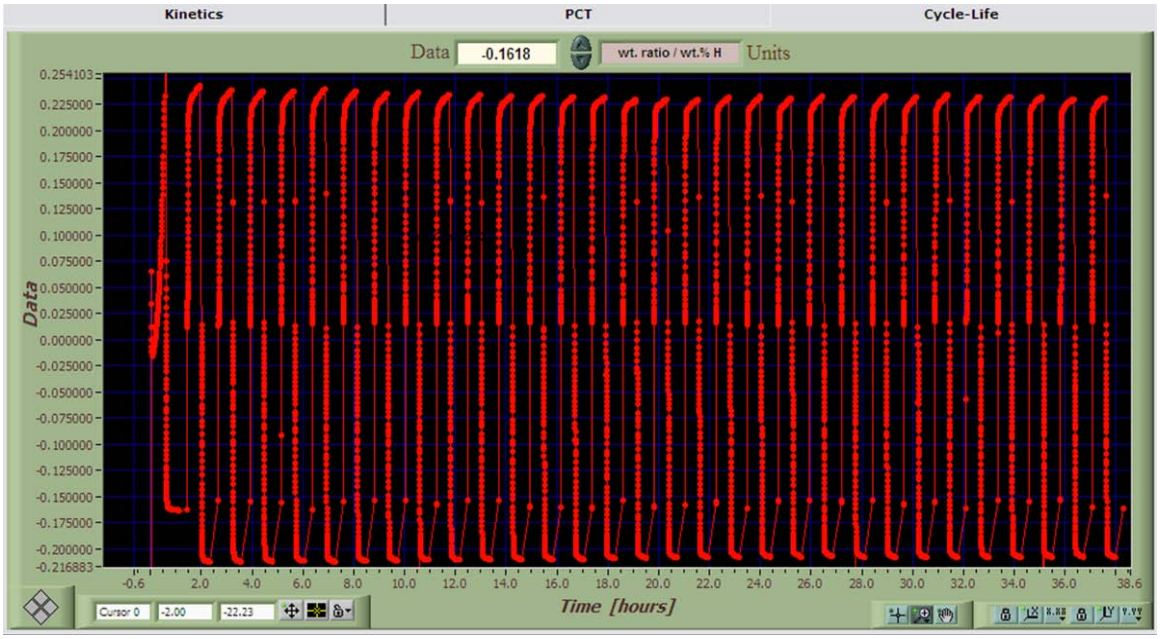

Figure 118. Cycling measurements on $LaNi_5$.[177]

The sample partially activated in the first two absorption cycles, and was unchanged in the cycles that followed. However, the total hydrogen capacity was just slightly less than 0.25 wt.% which is significantly lower than the expected $LaNi_5H_6$ capacity of 1.39 wt.%. Thus only about $1/6^{th}$ of the sample was actually hydrided ***($LaNi_5 \rightarrow 5/6LaNi_5 + 1/6LaNi_5H_6$)*.** This was verified by the visually observation that the only a small fraction of the coarse $LaNi_5$ alloy had decrepitated into the fine grey powder of the hydride (Figure 119).

Figure 119. Photo of incompletely hydrided LaNi5.[177]

It is likely that oxygen contamination formed an oxide barrier fully passivating the surface of most of the alloy particles. To fully hydride the sample, the oxide surface of the remaining particles would have to be breached (activated) by repeated cycles of charging the sample with hydrogen at high pressure (up to 100 bar) at elevated temperatures (up to 100°C) followed by evacuation of the sample. For those who perform such an activation process on $LaNi_5$, it should be noted that the activation process itself induces the formation of a metastable phase of the hydride that is often observed as a second plateau at much higher pressures than normal in the initial PCT measurements. This plateau usually disappears with the first desorption. An example of this is shown in Figure 246 where the room temperature absorption exhibits a second higher pressure plateau that is not observed in the subsequent desorption.

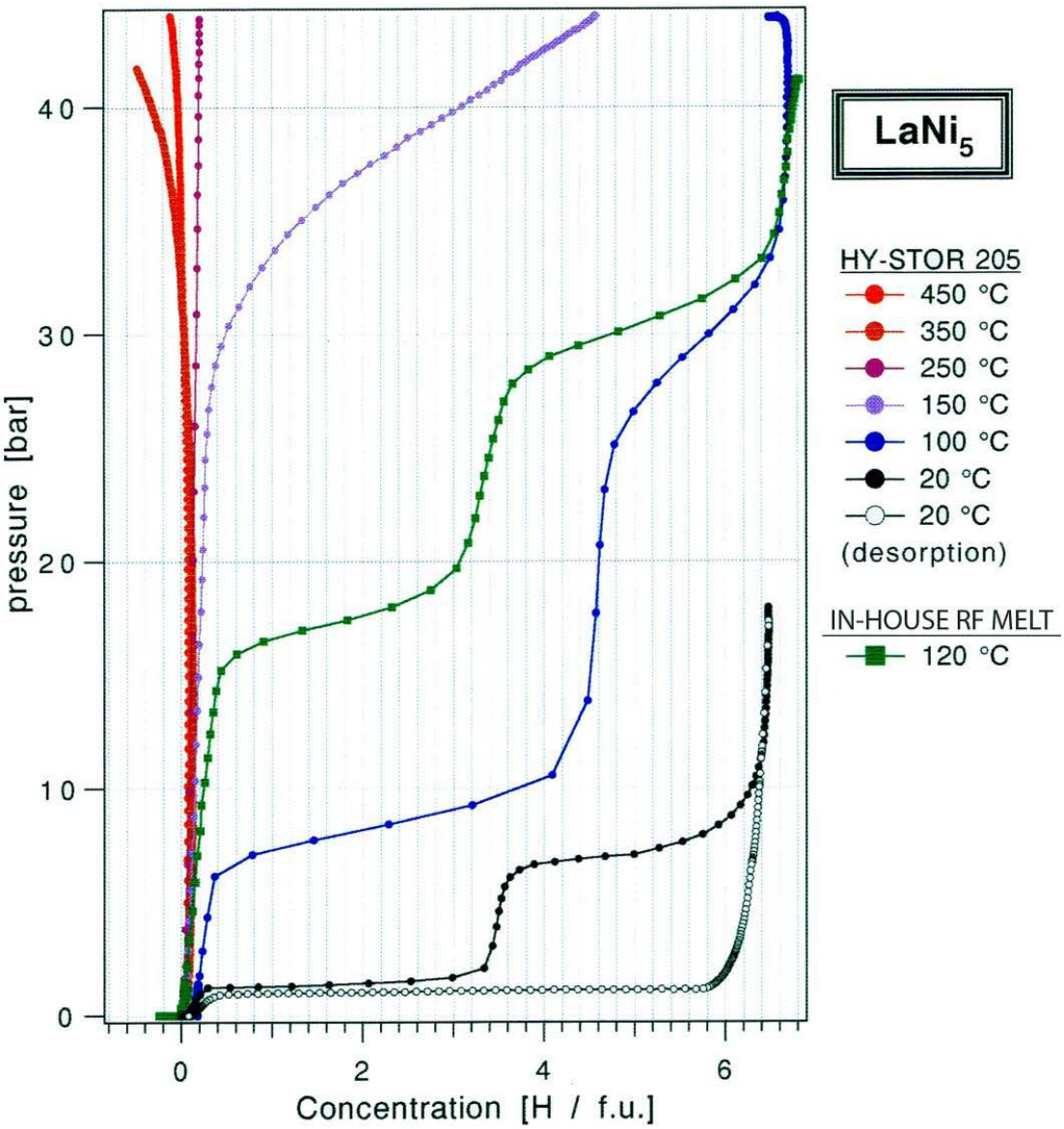

Figure 120. PCT measurements of $LaNi_5$ after heating under hydrogen.

2.2.3.2 Poisoning

Sandrock and Goodell define four basic types of negative effects from impurities in the hydrogen stream used for hydrogenation: poisoning, retardation, retardation and recovery, and reaction. Figure 121 shows examples of each process. Poisoning and retardation are similar in that they involve the blocking of surface sites required for the dissociation of H_2 involved in hydrogen absorption. Poisoning involves a stronger interaction between the impurity and sample surface, and therefore leads to a reduction in capacity as well as kinetics, while retardation simply slows the reaction kinetics. The negative effects of both can generally be restored by heating in a pure hydrogen atmosphere. In some cases, termed retardation and recovery, restoration of

reaction kinetics will occur simply with cycling. Reaction is a more severe interaction between the impurity and sample surface, leading to corrosion and permanent loss of capacity. An example of impurities effects on $LaNi_5$ and Ti(Fe,Mn) is shown in Figure 121.

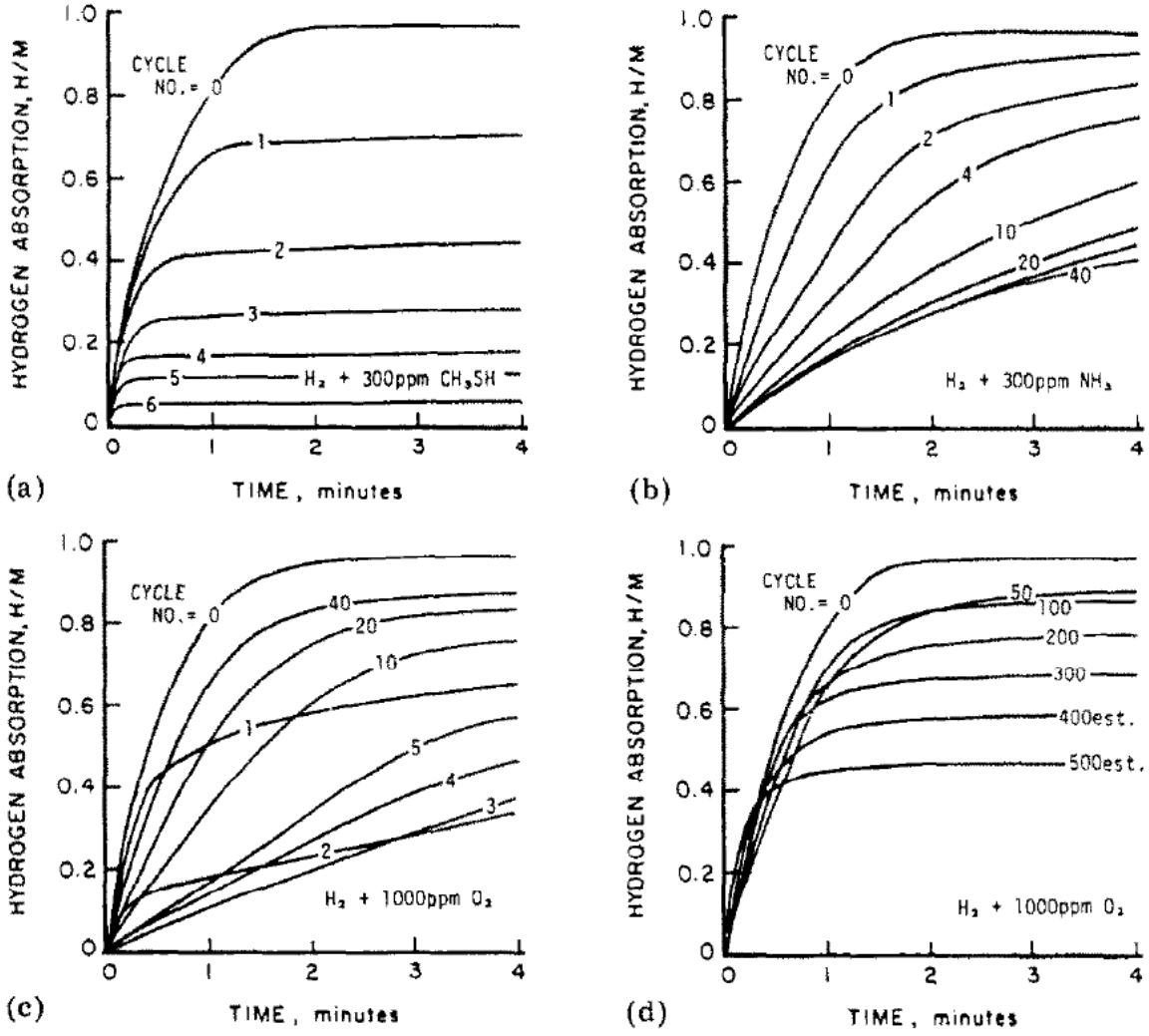

Figure 121. Illustration of the effects of different types of alloy-impurity interactions on absorption-time profiles during repeated cycling: (a) poisoning; (b) retardation; (c) retardation-recovery; (d) reaction. The curves are for LaNi5 tested at 25°C and 345 kPa; only the first 4 min of 15 min absorption is shown.[127]

See section 3.7.1 in the Kinetics section for a description of how impurities such as Co_2 and H_2O in the H_2 gas stream can lead to retardation. This can have a critical impact on the evaluation of reversible capacity measurements where kinetics are critical. However, depending on the reaction conditions, the impurity, and the storage material, poisoning can also have an impact on the total capacity.

The physical and chemical activation of carbons can remove impurities, but can also introduce complex surface morphologies and create surface functional groups ($C_xO_yH_z$), which either enhance or depress adsorption capacities. Many adsorbents are water or air sensitive and should be handled in a high purity glovebox. For example, many metal-organic frameworks react with water and their crystallinity is observed to degrade over relatively short periods of time. Alkali metal doped carbons are particularly reactive. As a good practice, the same strict handling procedures should be followed for physisorption samples as for air-sensitive metal hydride materials.

Surface poisoning is not a very critical issue for chemical hydrides like ammonia borane. However it is very crucial for metal amidoborane ($LiNH_2BH_3$). Surface poisoning, though not critical for ammonia borane reactions, still has an impact on capacity measurements and an enhanced effect on the kinetics. Ammonia borane is water stable but slowly reacts with water to form borate coatings on the surface which can diminish the hydrogen capacity over time. This process is slow to cause an appreciable decrease in capacity during a period ranging from a month to a year. For $LiNH_2BH_3$ the capacity is significantly impaired if the material is exposed to air or moisture, since it rapidly reacts with air or moisture to undergo side reactions. The purity of ammonia borane can have an impact on Figure 122 of ammonia borane from different sources.[178]

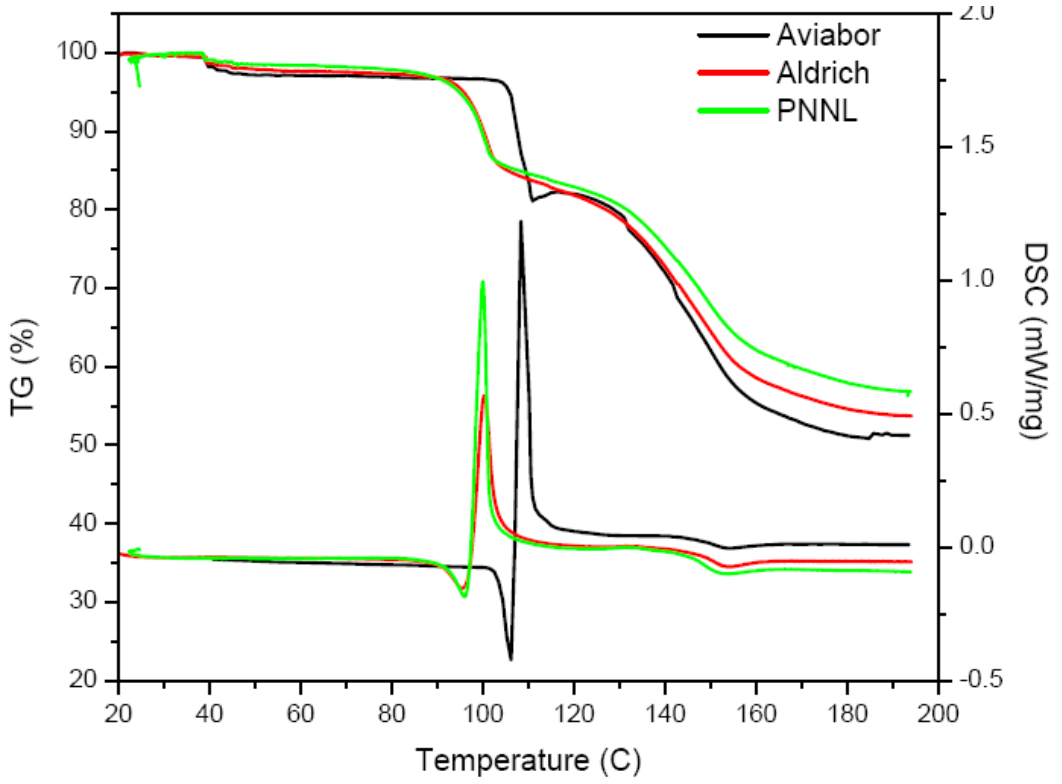

Figure 122. Effect of the purity of ammonia borane on the onset of H_2 release.

2.2.4 Capacity and Kinetics

Capacity measurements of reversible materials should be taken at thermodynamic equilibrium, regardless of the time required to reach equilibrium. However, the amount of hydrogen uptake or released from a reversible storage material is dependent on the kinetics of the sorption process which is strongly dependent on the type of material and the pressure and temperature conditions. While a material might demonstrate high hydrogen storage capacity, the actual amount of hydrogen practically available may be significantly less depending on the material's intrinsic kinetics as well as the system's ability to deliver hydrogen due to heat transfer, gas flow through the material and other considerations.

Therefore, while we consider Capacity to be the amount of hydrogen released after an infinite amount of time (equilibrium) at a given temperature and pressure. In reality, the kinetics of many materials are so slow that one must take a hydrogen capacity measurement after some reasonable period of time. An example would be to take the final measurement when the material capacity has reached 95% of its asymptotically projected capacity.

The wide range of hydrogen storage materials leads to a somewhat unfair comparison of the capacity of different materials that may actually deliver the reported quantity of stored hydrogen at sorption rates that may be different by six or more orders of magnitude. For this reason we strongly recommend that the time to reach the reported capacity is reported along with capacity information.

Another important consideration is that the output of a measurement device tends to change or drift with time (pressure transducers, mass balance devices, temperature, hydrogen leak rates….). Thus, the measurement of capacity over long periods of time is more prone to errors that relatively short measurements.

Understanding of kinetics of hydrogen release is as crucial to irreversible off-board regenerable hydrides as it is for reversible metal hydrides and other systems. Kinetics studies of hydrogen release from ammonia borane have been undertaken by several institutes. This is a very complicated analysis due to the induction period that is observed during the initial times at lower temperatures and which can lead to measurement errors. The study of kinetics requires a detailed understanding of the mechanism with which the reaction proceeds. Gutowska et al, studied the effect of nanophase scaffolding on the kinetics of hydrogen evolution from ammonia borane in mesoporous SBA-15.[179] enabling release of hydrogen at higher rates at lower temperature. Neat ammonia borane takes significantly longer relative to that when the scaffold is present (conversion is incomplete after 37.5 hours at 70 °C). However, at higher temperatures, almost all the ammonia borane is converted to products and the reaction is significantly faster providing a more accurate estimate of the extent of

reaction and ultimately the stored hydrogen capacity of the materials. Other additives, and catalysts have been used to not only remove the induction period, but to enhance the rate of hydrogen evolution from AB. These experiments have led to a reasonable level of understanding of the molecular mechanism of hydrogen release from ammonia borane.

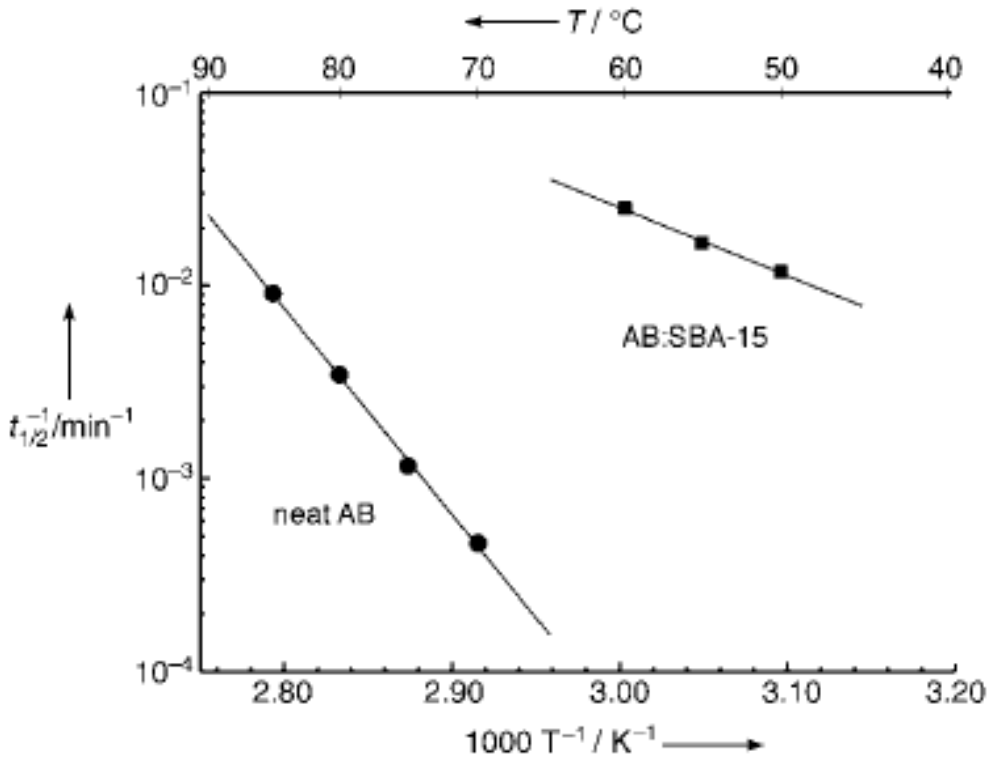

Figure 123. Arrhenius plots of the temperature-dependent rate data yields a straight line. The slope is proportional to the apparent activation energy for hydrogen loss from neat ammonia borane (neat AB; Ea = -184 kJ/mol H2) and ammonia borane in the scaffold (AB:SBA-15; Ea = -67 kJ/mol H2).

2.2.5 Capacity and Thermodynamics

A reversible hydrogen storage material's equilibrium hydrogen storage capacity is dependent on the material's temperature and the surrounding gas pressure. In other words, the capacity at a given pressure and temperature at infinite time depends on the equilibrium thermodynamics of the gas-solid reactions.

In the first example, the room temperature release of hydrogen from a classic AB_5 ($LaNi_5$-based) intermetallic hydride is shown in the kinetics measurement of Figure 43.

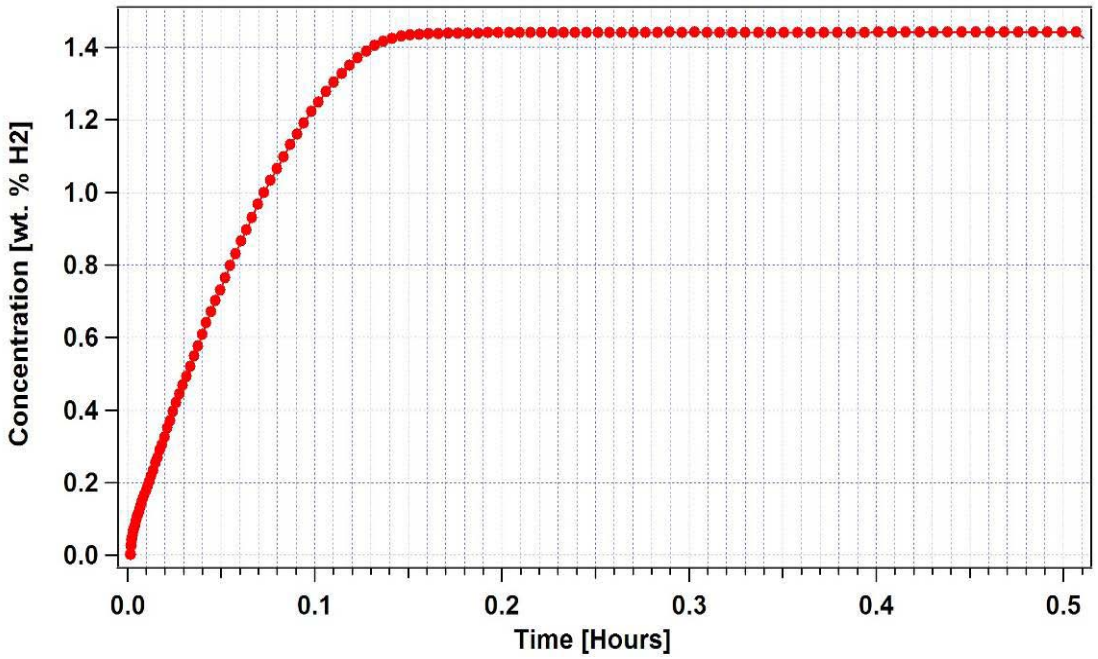

Figure 124. Kinetics measurement of $LaNi_5$ Intermetallic compound with a single phase transition. The experiment was conducted under isothermal conditions at room temperature. Units in H per formula unit released.[180]

Figure 124 was made by measuring the increase in pressure using a calibrated volumetric instrument as a sample of approximately 4.5 g desorbed hydrogen. The capacity change in wt.% is plotted as a function of time. This represents the sample's total hydrogen content change during the desorption transition from $LaNi_5H_6$ to $LaNi_5$. This does not mean that the concentration of hydrogen in the hydride is changing but rather that the sample's total composition of the two phases is changing with time. The sample's total composition at any one time is:

Equation 88
$$(1 - X(t))LaNi_5H_6 + X(t)LaNi_5$$

with boundary conditions X(t=0) = 0 and X(t=∞) = 1.

While this single dose desorption of hydrogen indicates that the sample was in the fully hydrided state (1.4 wt.% = $LaNi_5H_6$) in fact the sample's hydrogen storage capacity depends greatly on the pressure and temperature conditions at in the charged state.

This is best observed by performing a series of equilibrium PCT measurements of the transition from solid solution α-phase through to the β-hydride phase in $LaNi_5$ (Figure 125). Absorptions are shown for two different temperatures (30°C purple) and (85°C red). The flat portion (plateau region) of each measurement is present because of the equilibrium coexistence of the α-phase and β-phases. On moving from left to right along an absorption plateau the measured sample is being transformed, gas dose by gas dose, from the α-phase intermetallic alloy to the β-phase hydride.

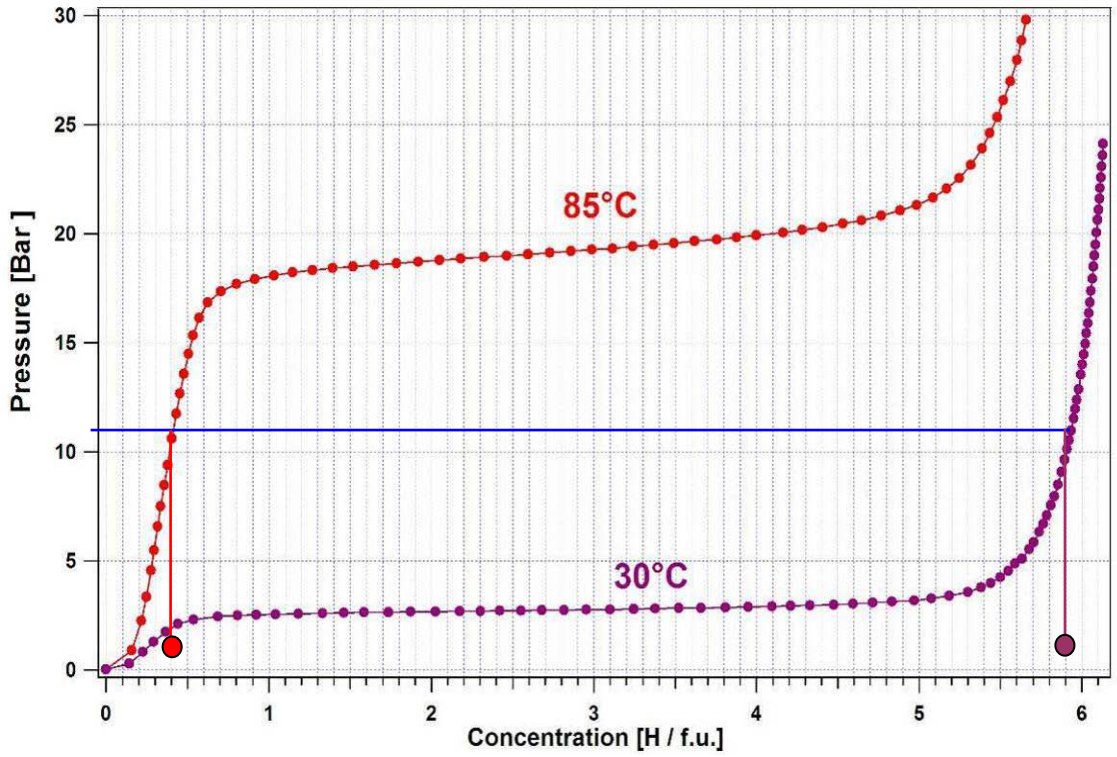

Figure 125. Equilibrium PCT measurements of $LaNi_5$, a classic metal hydride at two different sample temperatures.[118]

If we pick a specific pressure (10 bar for example) the fully charged state or hydrogen storage capacity of the material will be very different (0.3 or 5.9 H/f.u.) depending on whether the sample is at 30°C or 85°C.

Our second example presents the same concept for a different type of material. In this case the sample is a multiphase complex hydride and amide mixture with a starting composition of:

Equation 89 $$LiH + Al + 2LiNH_2 + Mg + TiF_3 .$$

The measurement of the third cycle of gas desorption from titanium-doped alanate-amide mixture is shown in Figure 126. It should be noted that, unlike the intermetallic hydride example above, this is not an isothermal measurement but rather a ramp and soak-style TPD measurement. However, ultimately a final hydrogen capacity of 2.2 wt.% release at a final temperature of 200°C and 200 mbar.

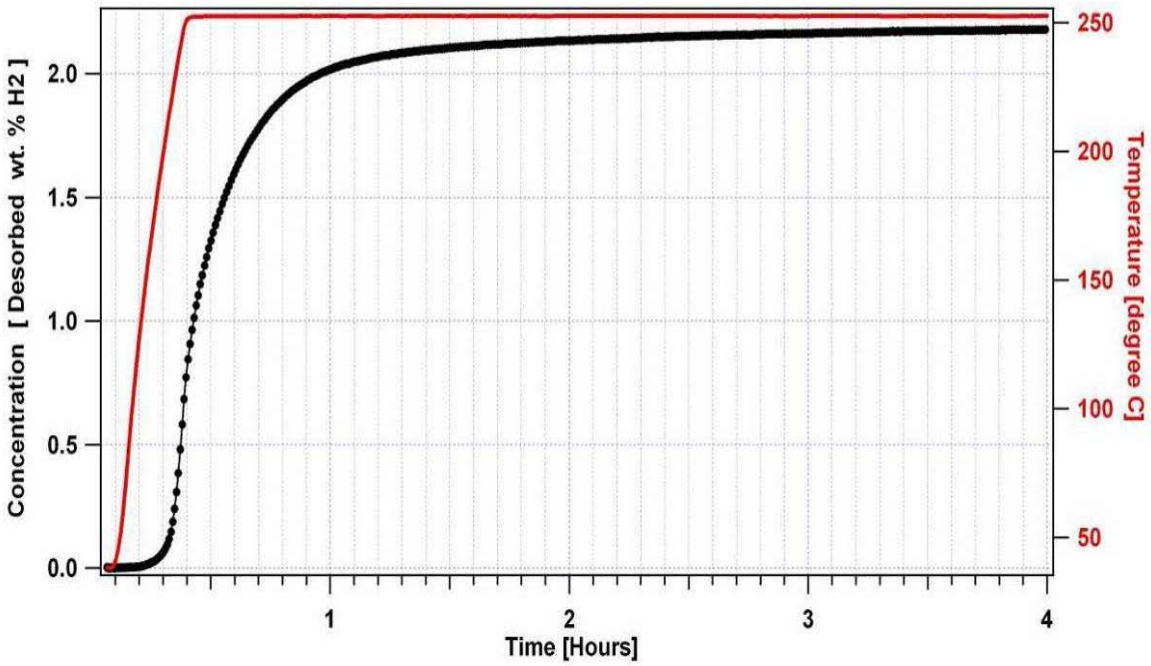

Figure 126. TPD measurement of the alanate-amide mixture.[57]

Without doing a more detailed PCT isotherm, it may be incorrectly assumed by looking only at this single dose desorption measurement that the desorption involves only one reaction. By performing an equilibrium desorption PCT measurement of the same sample (Figure 127) in the fourth cycle it becomes clear that the continuous evolution of gas observed in the kinetics measurement of Figure 45 is the result of a complex series of three separate chemical reactions instead of the single phase-transition as in classic hydrides.

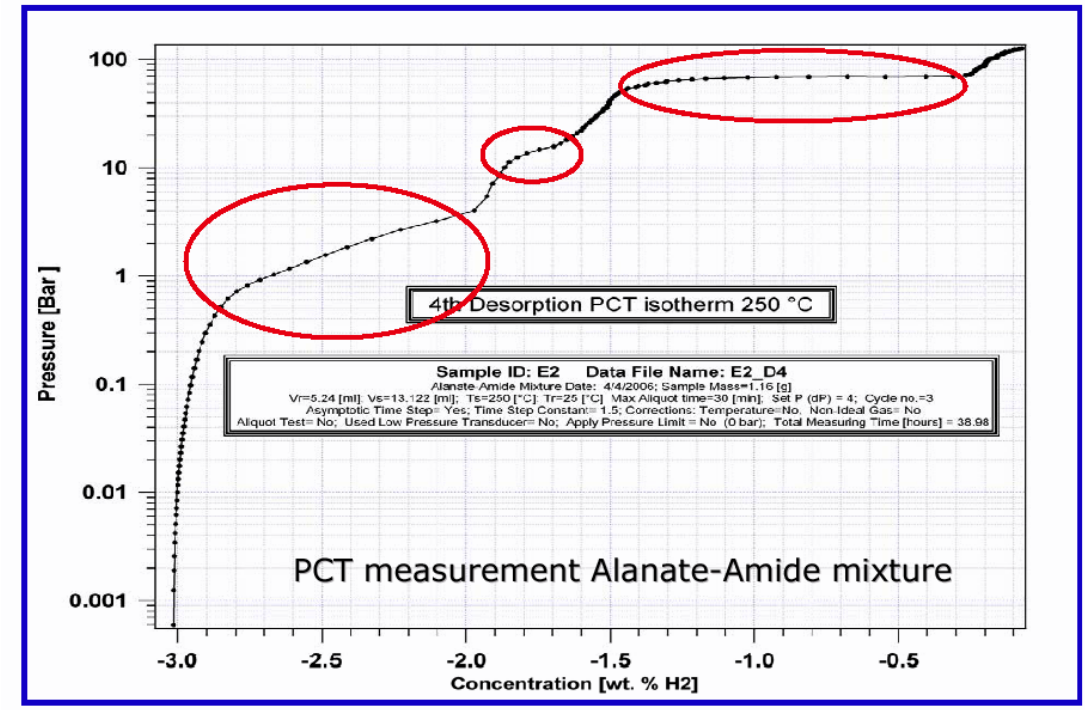

Figure 127. PCT diagram of the alanate-amide mixture.[57]

Each of the three distinct plateaus corresponds to a different chemical transition within the material. In this case the materials hydrogen storage capacity will depend on whether the thermodynamic conditions (pressure and temperature) have been met to cause one, two or all three hydrogen uptake reactions.

For hydrogen physisorption materials, the enthalpy of molecular hydrogen binding is relatively weak (on the order of 4-6 kJ/mol H_2). Thus, significant hydrogen uptake is found only at low temperatures. The standard measurement of physisorption capacity is usually taken at liquid nitrogen (77K) and room temperature (298K). However, measurements at a series of temperatures between 77K and 298K are often performed to make an accurate determination of the isosteric heat of adsorption. Measurements at 77K and 298K are shown in Figure 128 for MOF-177, currently one of the highest capacity physisorption materials. The 77K isotherm shows a maximum excess capacity of about 7.5 wt.% at 60 bar hydrogen pressure. At room temperature the excess physisorption capacity at 60 bar is only about 0.4 wt.%. This behavior is typical for all physisorption materials with the possible exception of spill over materials which appear to have high capacity, albeit slow kinetics at room temperature.[181]

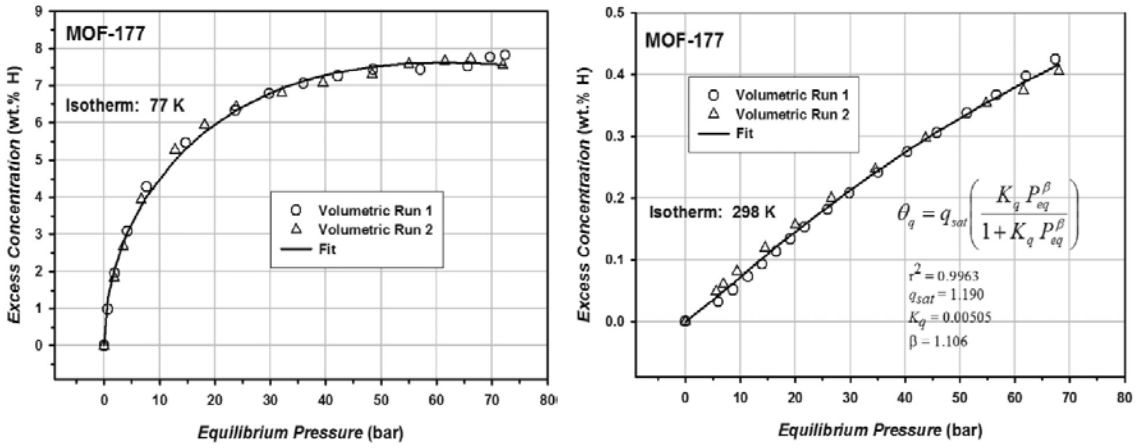

Figure 128. Example of capacity as a function of temperature and pressure for MOF-177 physisorption materials (Left: 77K , Right: 298K).[182]

Off-board rechargeable chemical hydrides are, by definition, not thermodynamically reversible within the temperatures and pressure range of the hydrogen delivery. Thus, with the exception of Usable Capacity vs. hydrogen content discussed above, it is kinetics and not thermodynamics that will impact the measurement of a chemical hydrides hydrogen storage capacity. Also, as these materials are irreversible, the rate and extent of hydrogen release are invariant with applied hydrogen pressure.

2.2.6 Impact of Hysteresis on Capacity

Reaction kinetics are probably the most fundamental factor in determining the technologically usable or reversible capacity of on-board reversible materials. This is because the time of reaction is important in both the absorption and desorption reactions to provide reasonable filling times at the pump and usable flow rates of hydrogen to the fuel cell.

Nearly all capacity measurements on reversible materials (with the exception of usable capacity) represent storage capacity at thermodynamic equilibrium. One of the many benefits of measuring capacity at equilibrium is that it minimizes the number of free variables, improving reliability and reproducibility. The accuracy of an equilibrium capacity measurement is directly related to the kinetic properties of tested material; the better the kinetic properties, the faster the material approaches thermodynamic equilibrium. Most testing equipment has safeguards against data collection at non-

equilibrium (sorption-rate feedback etc.) but a fundamental understanding of the relationship between capacity and kinetics is still central to conducting good research and drawing accurate conclusions from capacity data.

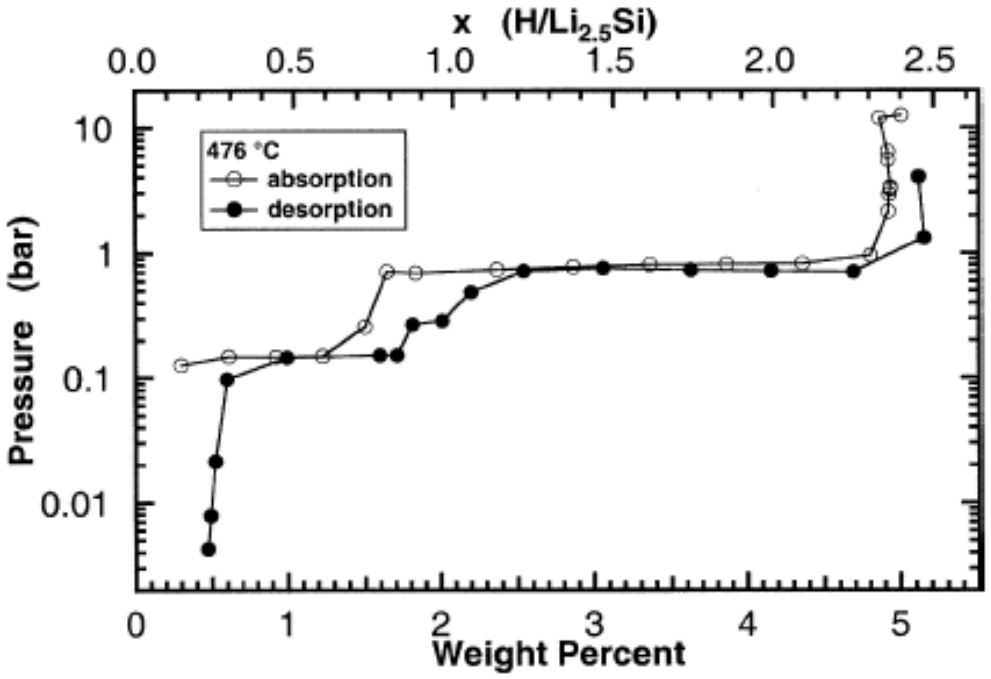

Figure 129. PCT measurement of lithium hydride destabilized by silicon. The first plateau (0.5 wt.% - 1.5 wt.%) corresponds to the transition from $Li_{2.35}Si$ to $Li_{1.71}Si$ + 0.64LiH. The second plateau corresponds to the transition from $Li_{1.71}Si$ to Si + 1.71LiH.[31]

One of the many phenomena affected by equilibrium (or non-equilibrium) measurements of reversible hydrogen storage materials is hysteresis. The effect of hysteresis is often seen in PCT measurements of metal-hydrides. The plateau pressure can be different depending on whether the measurement is made during absorption or desorption, and the even the location of phase transitions can differ. For example, a study by Vajo et. al on lithium hydride destabilized by silicon shows a different total capacity and a different hydrogen concentration value for the transition between the two stochiometric phases of lithium silicides (Figure 129)[31]. However, the plateau pressures are consistent during absorption and desorption.

In contrast, L. Guoxian et. al performed a PCT test on Mg mechanically milled with $FeTi_{1.2}$.[32] This plot (Figure 130) shows three sets of absorption and desorption curves at three different temperatures. At each temperature, the absorption curve shows a slightly higher-pressure plateau than the desorption curve, which is typical.

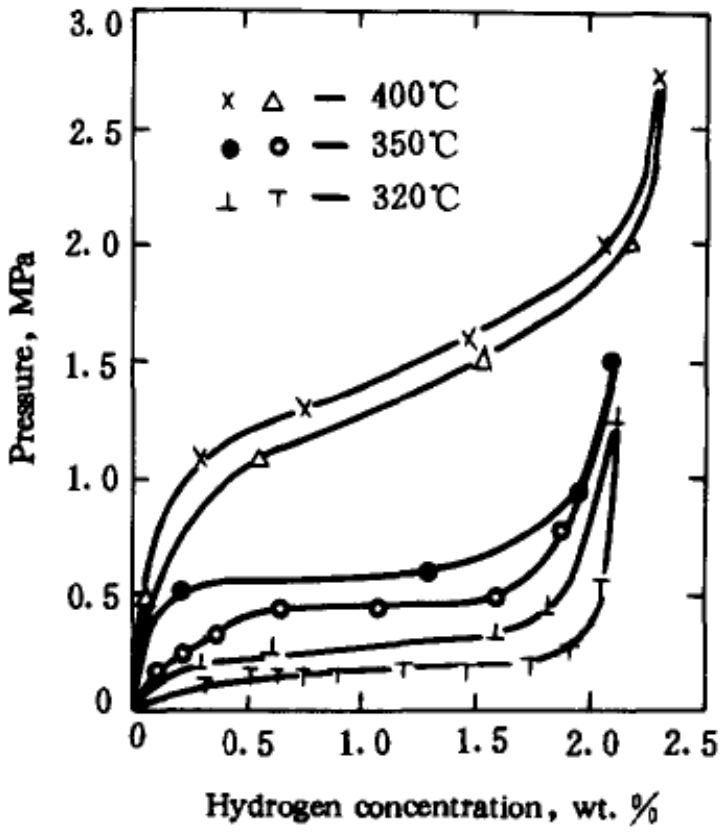

Figure 130. Hysteresis effects on the plateau pressure of PCT curves of Mg mechanically milled with $FeTi_{1.2}$.[32]

In general, the difference in pressure measured between absorption and desorption may be in part due to a hysteresis effects related to the thermodynamics of the process hydriding and dehydriding. This intrinsic hysteresis is observed for nearly all metal hydrides. Hysteresis is of considerable interest for practical applications of metal hydrides as it represents a loss of efficiency in energy storage. Intrinsic hysteresis has been the focus of much study since the investigation of the phenomena in the Pd-H system by Ubbelohde in 1937.[183] A number of models and theories have been proposed concerning the origin of hysteresis.[184,185,186,187,188] The subject of the cause and implications of intrinsic hysteresis will be presented in more detail in the next chapter on thermodynamics.

Because of hysteresis effects in metal-hydrides, the capacity at a given pressure will be dependent on whether one references the absorption or the desorption data. Likewise, hysteresis may have a profound effect on the actual hydrogen storage capacity of a material system for many applications. This is demonstrated in Figure 131 for a hypothetical material with a realistic amount of intrinsic hysteresis.

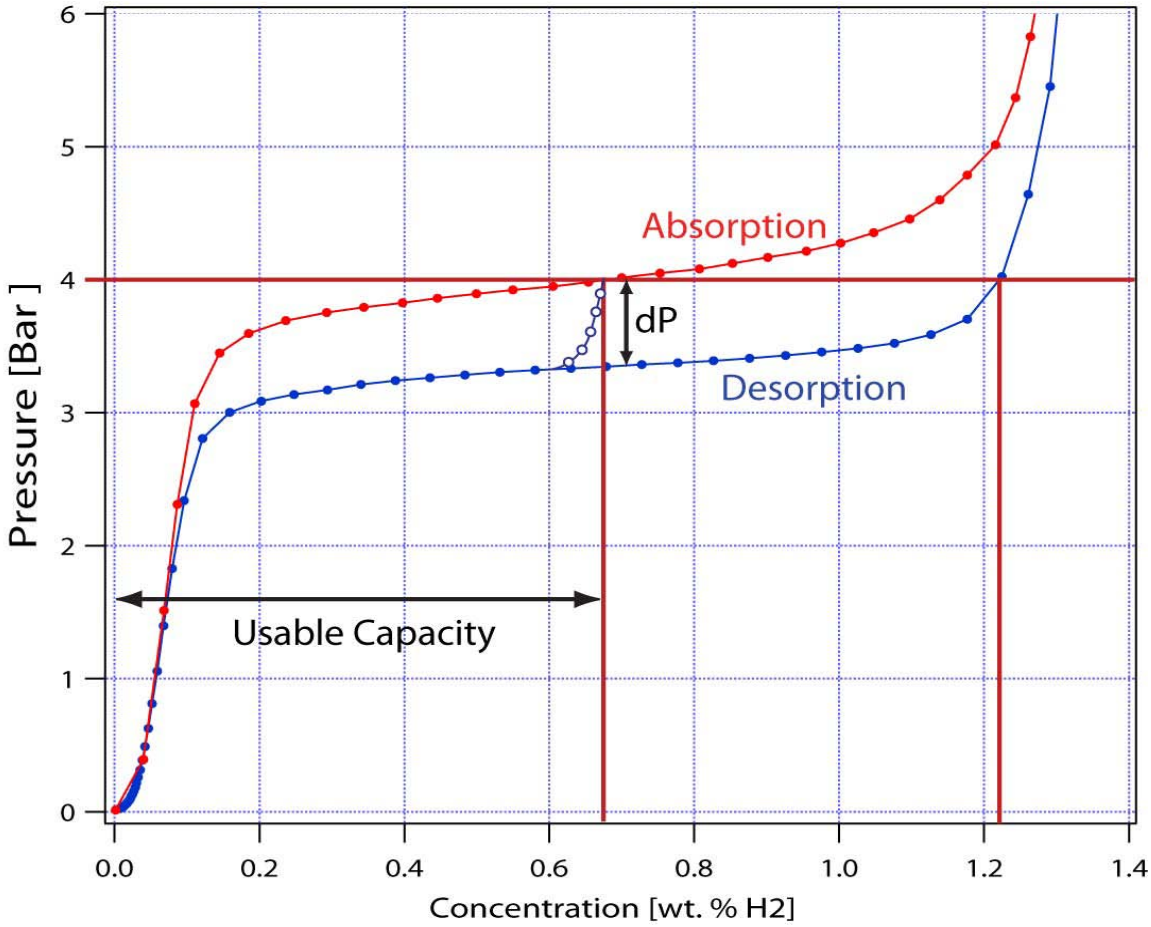

Figure 131. Depiction of absorption (red) and desorption (blue) pressure concentration profiles for a material at one temperature. Open (blue) circles represent the effective desorption curve were the material only charged with hydrogen at a maximum pressure of 4 bar.

At a given constant operating temperature, the intrinsic material hysteresis presents itself as a difference in pressure dP between absorption and desorption PCT isotherms. This means that if the upper pressure limit of a storage system was 4 bar, the full theoretical capacity (1.2 wt.%) that could be discharged from the material could not be achieved in practice. This is because the maximum amount of hydrogen that could be absorbed before reaching equilibrium at 4 bar is only about half this capacity (~0.66.wt%). The effective desorption curve is shown as open circles. Thus, the usable capacity of such a material under these operating conditions is effectively half of its total hydrogen capacity.

From the practical perspective of the result obtained from PCT measurements it is important to understand that the difference between measured absorption and desorption pressures may be simply due to kinetic effects and the inability to reach true equilibrium at each step within a reasonable period of time. It is difficult to distinguish the two effects without looking at the time dependency of the approach to an equilibrium pressure at each data point in a PCT measurement. Ideally, one would want to have a test at each data point to ensure that equilibrium has been reached before moving on to the next data point. This is often accomplished with automated equipment by setting a lower limit on the rate of concentration change that must be achieved before automatically moving to the next data point.

One simple approach to distinguish between hysteresis due to kinetics (non-equilibrium measurement) and intrinsic hysteresis (material property) is to run a series of PCT absorption and desorption isotherms for different durations of time (different dosing rates for volumetric measurements, different increasing pressure rates for gravimetric measurements). An illustration of this is shown in Figure 132. The figure shows that as the time to allow the absorption and desorption process is increased the plateau pressures will drop for absorption and increase for desorption. Given enough time the measurements should reach a steady state equilibrium conditions such that making longer duration measurements will no longer change the results.

In theory, it should be possible to extrapolate the time resolved pressure changes in volumetric measurements to obtain final equilibrium pressures.[189] Recent results on the hydrogenograghy of Mg-Ni-H thin films have employed such an analysis for evaluating equilibrium pressures using optical transmission measurements under controlled pressure.[190] A caveat to this is that there is some evidence that final equilibrium pressures may not be identical depending on whether hydrogen is introduced to the sample in doses or continuously.[72]

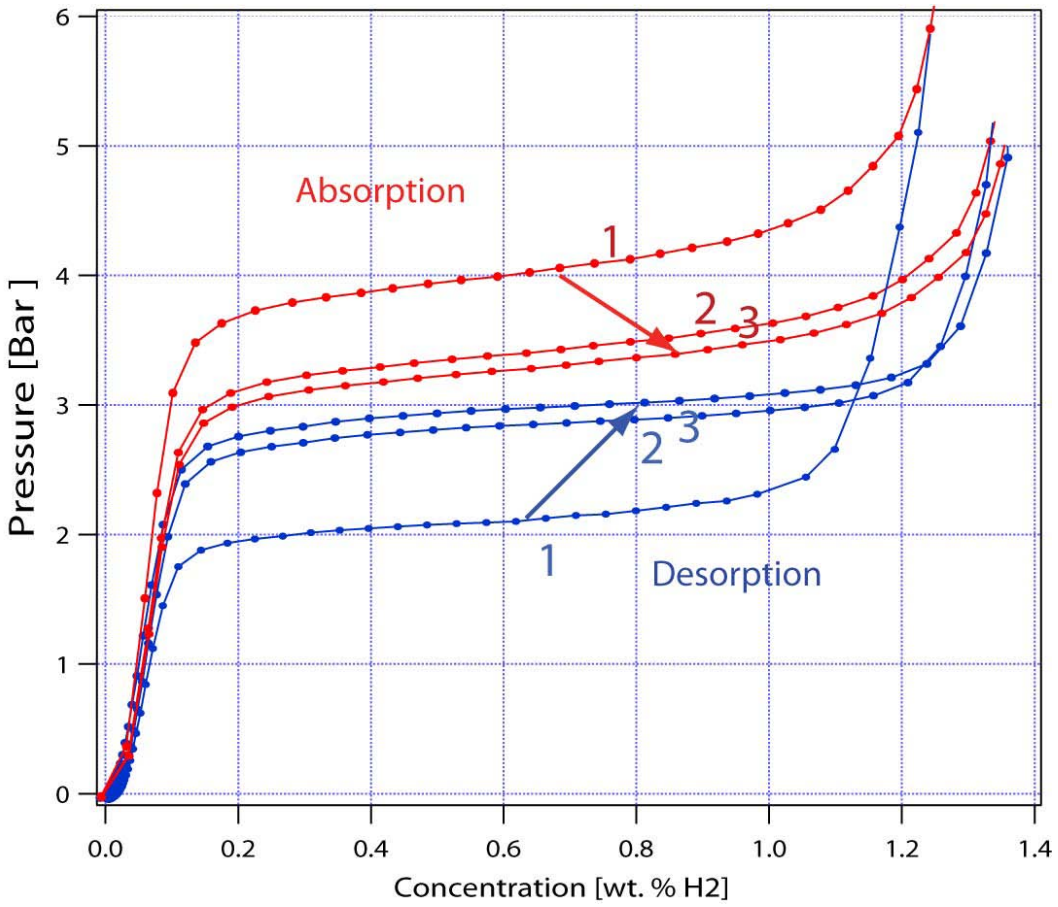

Figure 132. Depiction of absorption (red) and desorption (blue) PCT measurements made over increasingly long (1,2,3) periods of time.

Ultimately, it simply very important to verify that the hydrogen/material system has reached a close approximation to thermodynamic equilibrium when making PCT measurements. This is best achieved by observing the hydrogen concentration change vs. time during the measurement and proceeding with the measurement at a pace that is slower than required to reach 95% of the reaction at each data point if possible. In all fairness, many of today's materials have such poor kinetics that this is not achievable in a reasonable amount of time (< time to finish a thesis). In such cases, it is important to indicate that results represent non-equilibrium conditions and may have some impact both on the capacity of the material presented and any evaluation of thermodynamics. When it is possible to measure the relevant rates of absorption or desorption, it is highly valuable to present these values as well. Methods to overcome the measurement time issue with respect to thermodynamic measurements will be presented in the next chapter.

With regard to adsorption storage materials, physisorption of H_2 on surfaces and within pores is typically a fast process. There are some instances where adsorption actually prompts a structural change in the host adsorbent, resulting in indefinitely long equilibration times. Hysteresis. However, is not usually observed for Langmuir-like supercritical adsorption of hydrogen. Typically, caused by uptake measurements that are kinetically limited, i.e. have not reached equilibrium.

2.2.7 Activation Effects

For most reversible materials, hydrogen storage capacity is not maximized immediately. In both chemisorbing and physisorbing media, notably metal hydrides and high-surface area materials, reaction with hydrogen is initially obstructed by impurities caused by exposure to contaminants such as ambient air during preparation.

In metal hydrides this leads to a natural oxide film barrier on the sample surface that inhibits hydride formation. Removing the oxide film activates the hydride and maximizes its hydrogen storage potential. Activation occurs in a two-step process: small amounts of atomic hydrogen penetrate the oxide layer to form the first hydride nuclei, after which the bulk hydride fragments into smaller particles through a process called decrepitation. Oxide layer penetration and nuclei formation can take anywhere between seconds to days at room temperature and occurs via a variety of different mechanisms depending on the sample. Decrepitation is a phenomenon caused by the stresses placed on the usually brittle metal phase by the expanding hydride phase and yields a substantial increase of uncontaminated, oxide-free surface area. Most decrepitation occurs during the first few hydride/dehydride cycles and tails off during subsequent cycles. FeTi is an example of a metal hydride that is difficult to activate due to more passive and dissociatively inactive natural oxide films on the surface of air-exposed particles and partly the result of higher toughness than other intermetallic alloys. Figure 133 illustrates the degree to which FeTi requires multiple cycles to be fully activated.

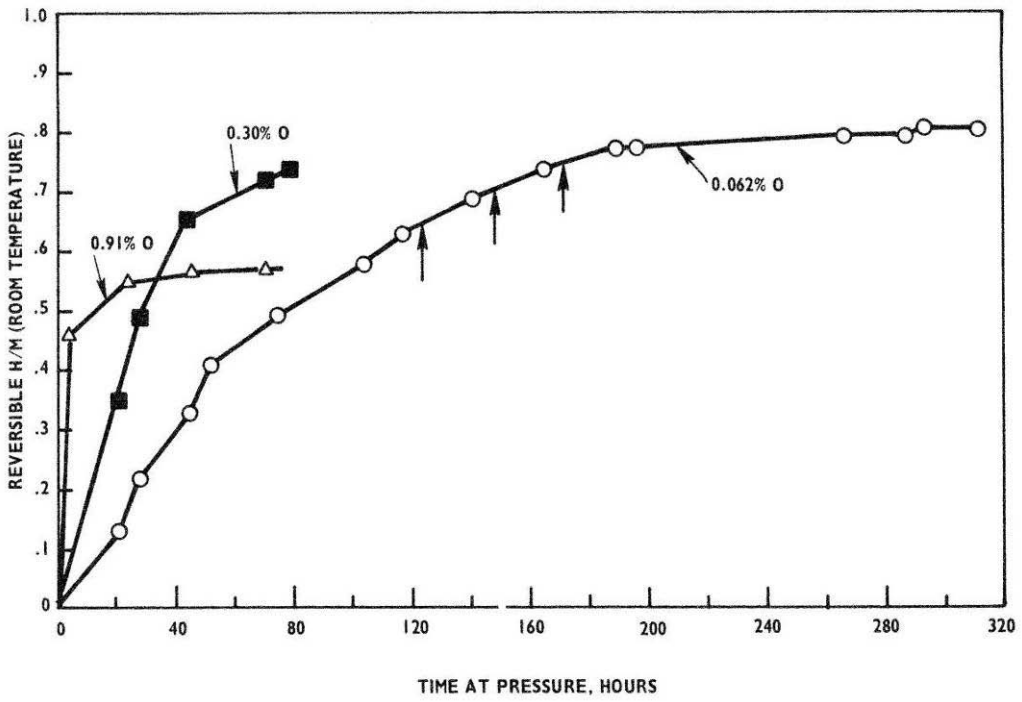

Figure 133. Effect of FeTi Oxygen-content on second stage activation. Initial particle size -30 mesh +50 mesh. Rome temperature P ~ 67 atm. Each data point represents a dehydriding cycle. Arrows indicate sample cycled but no data taken.[191]

Porous media and other physisorption materials also experience activation effects, although of a different nature than chemisorbing materials. Physisorption is dominated by van der Waals forces, which do not differentiate between potential sorbents. Physisorption samples exposed to the environment form a barrier of physisorbed air constituents, which take up surface area on the sample and must be removed before maximum hydrogen storage can be achieved. Because the physisorption mechanism weakens with increasing temperature, it is usually only necessary to flush the sample with hydrogen at an elevated temperature to eliminate the constituent barrier.

Zeolites, activated carbons, and other microporous materials will typically contain residual water and other contaminants. Activation consists of degassing the material at high temperatures (150 – 400 °C depending upon the material and its thermal stability) under dynamic vacuum. It is best to perform the activation process *in-situ*, immediately prior to experiments so that there is no chance for contamination between the activation and the actual experiment. A "perfectly clean" surface requires ultra-high vacuum and very high temperatures (>1000 K), however the goal of activation should be to remove "most" of the residual species without modifying or destroying the adsorbent itself.[56] For some samples that might decompose at high temperatures (e.g. some metal-organic frameworks), a different activation procedure might be used. Generally, a

rough vacuum of 10 to 100 mtorr is sufficient for the degassing of most physisorption materials. In any case, the conductance through standard tubing limits the effective vacuum that can be achieve at the sample position in most experimental setups regardless of the vacuum that the pumping system may achieve.

In reversible chemical hydrides the hydrogen uptake and release can be strongly effected by such factors as, distribution of catalytic additives, distribution of reactants, completion of initial unstable reaction processes to final reversible reactions, particle size, morphology of the material on a macroscopic and microscopic level, surface contaminants, etc. Thus, the hydrogen storage capacity of a material can change dramatically during the first five to ten cycles. It is important to run samples of new materials through several absorption-desorption cycles to determine the actual steady state capacity of the material. The first few absorptions/desorption cycles may be very misleading with respect to the materials true storage capacity.

A good example that was shown in the section on kinetics applies also to capacity. This was the pre-reacted Ti-additive sodium alanate system. Figure 134 is desorption data taken from a cycling experiment this material. It clearly shows the impact activation effects can have on capacity of the material with cycling.

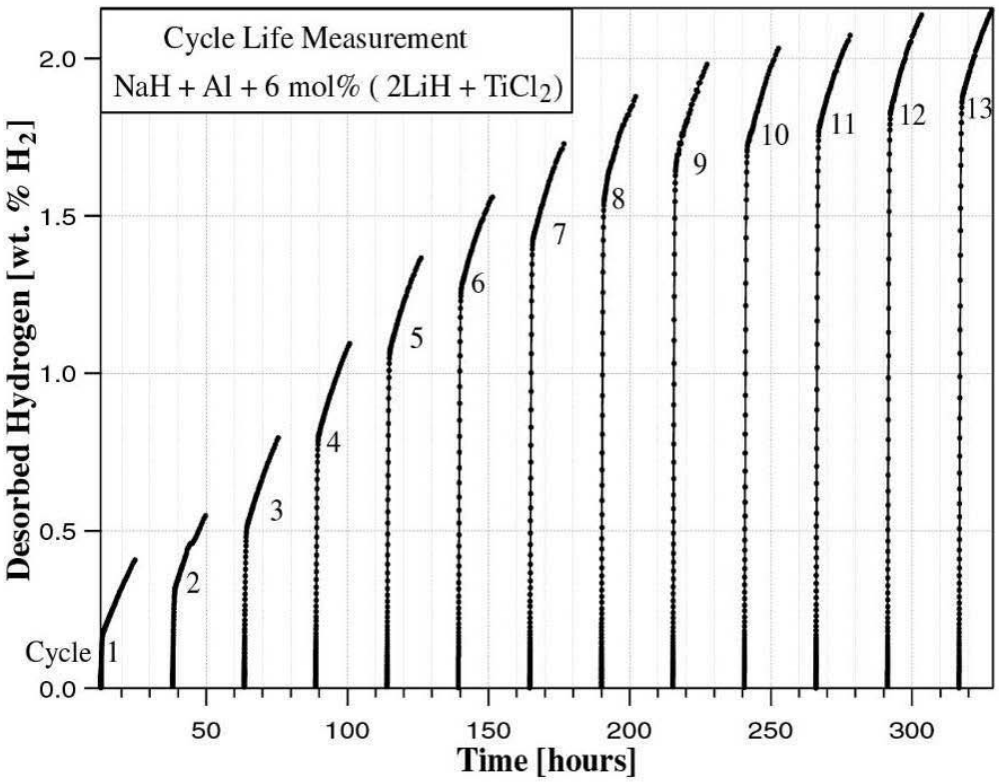

Figure 134. The activation effects of pre-reacted sodium alanate.[126]

Because each desorption measurement is taken over a fixed time interval the amount of hydrogen desorbed is limited by the kinetics of each desorption and subsequent absorption. Thus, the capacity increases with each cycle, in particular with respect to the first part of the desorption which is due to the first decomposition in the two step reaction given below.

Equation 90

$$NaAlH_4 \rightarrow \frac{1}{3}Na_3AlH_6 + \frac{2}{3}Al + H_2 \rightarrow NaH + Al + \frac{3}{2}H_2$$

The increasing capacity with each step can be explained by the reactions proceeding further to the left in the reverse of the reaction above to form more $NaAlH_4$ with each subsequent absorption. This is likely due to an increasing distribution of the Ti-additive throughout the mixture with each cycle.

Had this been a new material that was tested only over one or two cycles, it might have been abandoned as an uninteresting hydrogen storage candidate with only a maximum of 0.5 wt.% storage capacity. Regardless of the sorption mechanism, it is important to account for activation effects when performing capacity measurements on hydrogen storage materials.[59]

2.3 Special Method Dependent Considerations

2.3.1 Volumetric

The volumetric method was presented in section 5.3 of the introduction (recommended reading). Due to the importance of issues that impact the accuracy of these measurements for determining capacity the method is presented here in more detail.

2.3.1.1 Volumetric Physisorption Measurements

The determination of the excess adsorption in the volumetric process can be represented in four steps as shown in Figure 135. 1): from left to right: A) The volume containing the sample to be tested is first evacuated. Then gas is introduced into a calibrated volume where the gas pressure is measured after coming to thermal equilibrium with its surroundings. B) The valve between the two known volumes is opened and gas expands to fill the region containing the sample. C) Gas molecules adsorb onto the sample (blue) until an equilibrium pressure is reached and measured. Some molecules within the physisorption layer would be present in the gas phase at the same pressure in the absence of physisorption (red). D) The excess capacity consists of the blue molecules only.

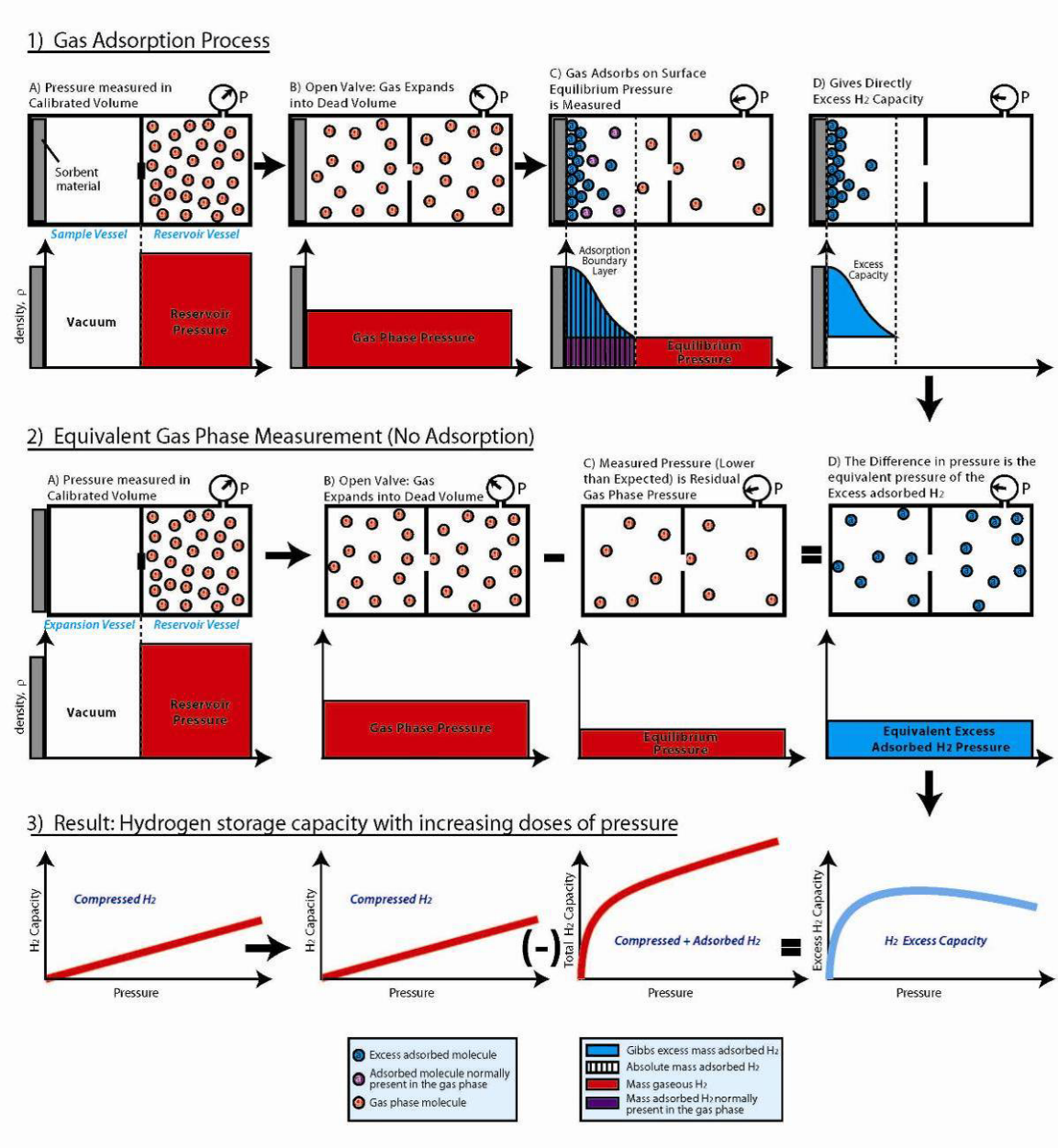

Figure 135. Depiction of the excess adsorption as determined by the volumetric method. 1) A step by step description of the volumetric measurement process as it actually occurs. 2) Depicts the equivalent gas expansion process, which is how the excess adsorbed gas is measured. 3) A graphic representation showing how as the excess capacity is measured as a function of final measured pressure (C) by subtracting the expected (no sorption) quantity of hydrogen stored in the total volume from the measured amount of hydrogen in the total volume.

Figure 135.2) depicts a practical method for determining the excess capacity. From left to right: steps A) and B) are the same as before. In practice, the adsorbed gas is not measured directly. Rather, the adsorption of the gas results in a pressure lower than the expected pressure purely based on the volume expansion, as shown in C). The excess capacity shown in D) is then the difference between the expected pressure and the measured pressure.

Figure 135.3) shows the resulting excess hydrogen storage capacity of the material as a function of pressure. The excess material capacity is the measured capacity of the total system volume less the capacity of the system due only to compressed hydrogen in the same volume in the absence of physisorption.

2.3.1.2 Volumetric Measurements of On-board Reversible Hydrides

The determination of the hydrogen storage capacity in the volumetric process can be represented in four steps as shown in Figure 136. 1), from left to right: A) The volume containing the sample to be tested is first evacuated. Then gas is introduced into a calibrated volume where the gas pressure is measured after coming to thermal equilibrium with its surroundings. B) The valve between the two known volumes is opened and gas expands to fill the region containing the sample. C) Gas molecules dissociate on the sample surface and are chemisorbed on the surface of the sample and then diffuse into the bulk of the material (green) until an equilibrium pressure is reached and measured. At equilibrium, some hydrogen remains in the gas phase at the equilibrium pressure (red). D) The hydrogen capacity consists of the green atoms only.

It should be noted that even reversible hydride materials have some surface area that will physisorb a finite amount of (excess) hydrogen that should be accounted for in the total capacity. This physisorbed hydrogen is already included in the storage capacity in as an intrinsic in the volumetric measurements method. That is, the volumetric method, accesses the mass balance of hydrogen in the gas phase and all unaccounted for hydrogen is what is stored by the material through both absorption and physisorption. For most reversible hydride materials the specific surface area is small and physisorbed hydrogen capacity is insignificant. However, nano-particle materials may have high enough specific surface areas that the portion of total stored hydrogen due to physisorption is relevant.

Figure 136.2) depicts a practical method for determining the hydrogen absorption (and physisorption) capacity. Steps A) and B) are the same as before. In practice, the sorbed gas is not measured directly. Rather, the absorption of hydrogen results in a pressure lower than the expected pressure purely based on the volume expansion, as shown in C). The capacity shown in D) is then the difference between the expected pressure and the measured pressure.

Figure 136.3) shows the resulting hydrogen storage capacity of the material as a function of pressure. The material capacity is the measured capacity of the total system volume less the capacity of the system due only to compressed hydrogen in the same volume in the absence of physisorption.

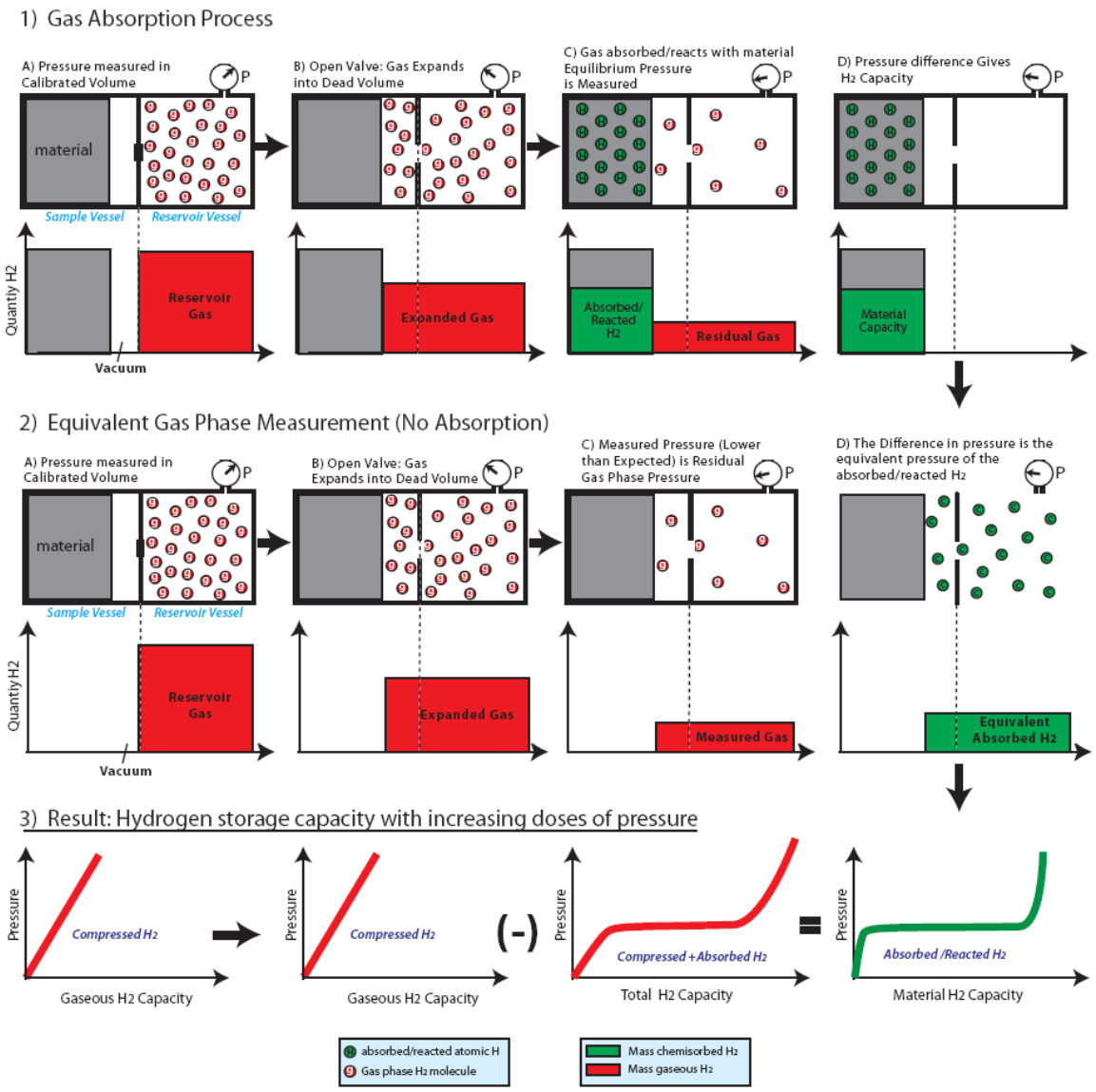

Figure 136. Depiction of hydrogen capacity measurements as determined by the volumetric method. 1) A step by step description of the volumetric measurement process as it actually occurs. 2) Depicts the equivalent gas expansion process, which is how the total sorption of hydrogen is measured. 3) A graphic representation showing how as the capacity is measured as a function of final measured pressure (C) by subtracting the expected (no absorption) quantity of hydrogen stored in the total volume from the measured amount of hydrogen in the total volume.

These simplified descriptions of the volumetric capacity measurement assume a perfect knowledge of the gas vessel volumes, gas temperatures, gas pressures, gas density and the mass and skeletal volume of the sample. An error in determining any one of these quantities will result in an error in the determination of a material's hydrogen storage capacity. Some common errors and issues associated with volumetric measurements are presented below.

2.3.1.3 Volumetric Sorption Dose

Equation 33-Equation 36 in the kinetics section demonstrates how a small single dose measurement can lead to imperfect kinetics measurements for a 1 g sample of $LaNi_5H_6$. The same example can be used to demonstrate the impact of a poorly planned single dose on capacity measurements.

As stated before, when using a volume reservoir that is too small (10 ml, dashed line), there is not enough hydrogen to hydride the entire sample to $LaNi_5H_6$, so it is impossible to reach the theoretical capacity due to a flaw in the experimental design. The amount of hydrogen in the reservoir is

Equation 91

$$n = \frac{PV}{RT} = \frac{5bar * .01L}{.083\frac{bar * L}{mol * K} * 298K} = .002molH_2$$

The entire dose is not absorbed by the sample, since enough gas must remain in the system to satisfy the equilibrium pressure. The amount of hydrogen required to maintain the equilibrium pressure in this example is

Equation 92

$$n = \frac{PV}{RT} = \frac{1bar * .01L}{.083\frac{bar * L}{mol * K} * 298K} = .0004molH_2$$

The remaining hydrogen, .0016 mol H_2, enters the $LaNi_5$ sample to create .234 g of $LaNi_5H_6$. If the experiment were stopped here, the measured capacity would be roughly 3.2%.

In contrast, a 400 ml reservoir under the same conditions has enough hydrogen to hydride the entire sample. The amount of hydrogen in the 400 ml reservoir is

Equation 93

$$n = \frac{PV}{RT} = \frac{5bar * .4L}{.083\frac{bar * L}{mol * K} * 298K} = .08molH_2$$

After complete hydriding, there would be .073 mol H_2 remaining in the gas phase. This would yield the full theoretical capacity of 13.8%. Therefore any measured capacity value short of the theoretical capacity is due to the properties of the sample rather than the amount of hydrogen available.

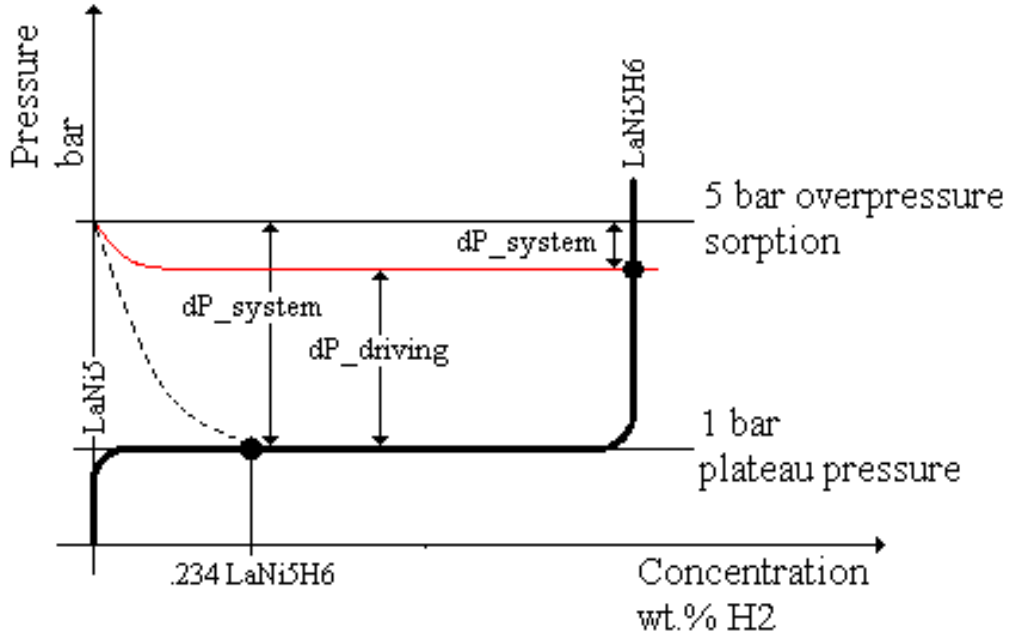

Figure 137. Diagram of the pressure in sorption/desorption system during hydriding reaction. The dashed line represents a test using a reservoir that is too small and the solid red line represents a test using a sufficiently large reservoir.

2.3.1.4 Gas Density Gradients

In typical volumetric adsorption experiments, the sample vessel is kept at a low temperature while the reference volume remains at room temperature. The density profile of the free H_2 gas in not constant throughout the free volume therefore. A common approximation is to divide the system into two isothermal regions connected a small region with a linear temperature gradient. It is important to minimize density fluctuation throughout the free volume, for example by maintaining a constant liquid N_2 fill line. The linear correction factor in the temperature gradient zone can be calibrated by empty reactor measurements.[147]

2.3.1.5 Temperature Control

Immersing the sample in a liquid N_2 bath (77 K) or a liquid Ar bath (87 K) is the simplest means of temperature control. To achieve greater temperature range, inexpensive LN_2-based cryostats can be developed to provide a stable sample temperature in the range T > 77 K. The design of the cryostat should minimize the temperature gradient region. One way of doing this is incorporate a separate heating element at the sample-reference interface, as shown in Figure 138.

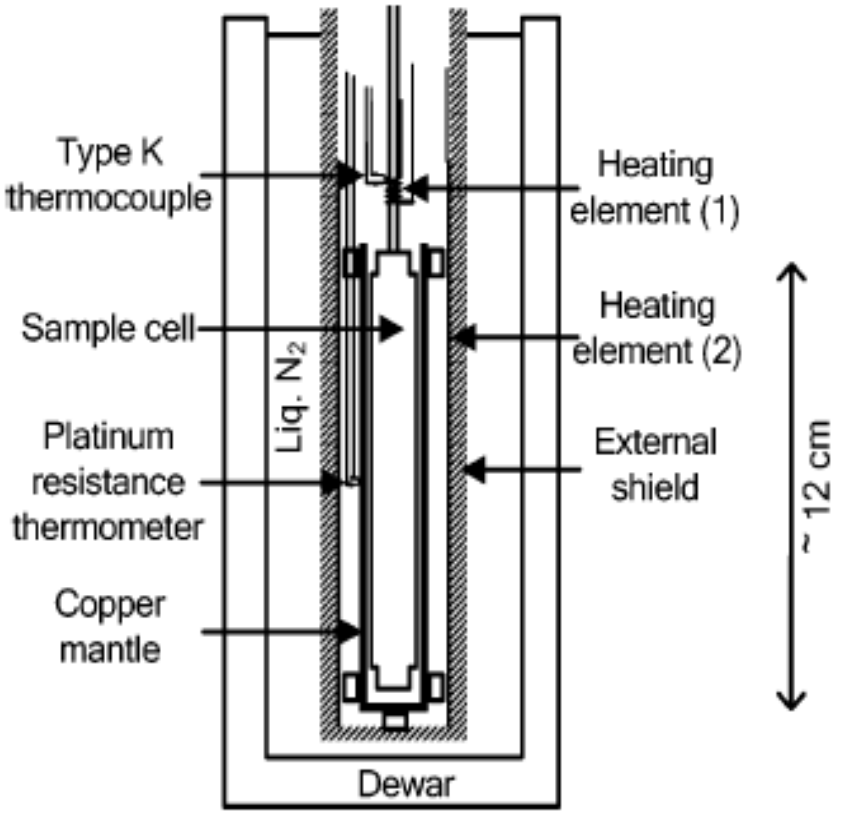

Figure 138. Schematic view of a cryostat designed for H_2 physisorption measurements.

Figure 139 shows the volumetric measurement of the evolution of hydrogen during the decomposition reaction of the chemical hydride ammonia borane at various temperatures. At 95 °C, the decomposition rate for the as-received sample is very slow and after 4500 s about 3% hydrogen was desorbed. By increasing the temperature the

same amount of hydrogen is desorbed in shorter times and the final desorbed amount slightly increased. The maximum hydrogen amount desorbed at 140 °C after 4500 s was 5.2%. The amount of hydrogen released observed by Benedetto et al is lower than the previously reported one by Wolf et al.[192,211] This result cannot be explained taking in consideration only the material purity (90%). They observed that part of the material is pushed up from the thermalized zone as a consequence of the thermal decomposition, remaining non-reacted. They further discuss the effect of ball milling and addition of platinum based catalysts on dehydrogenation from ammonia borane.

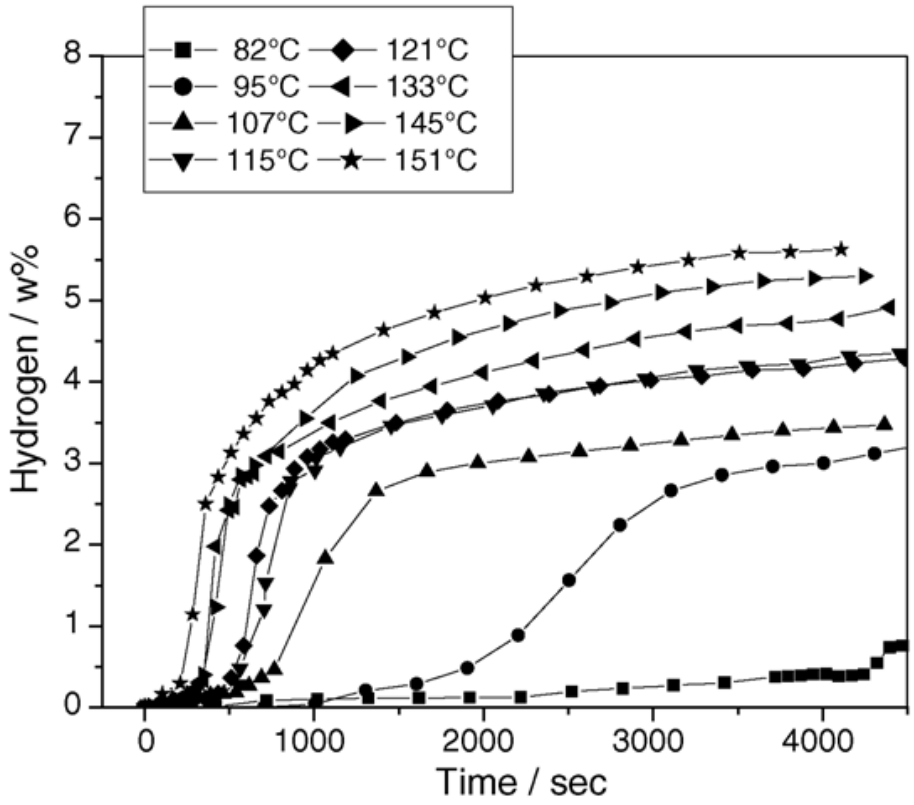

Figure 139. Volumetric hydrogen evolution during the decomposition reaction of ammonia borane.[192]

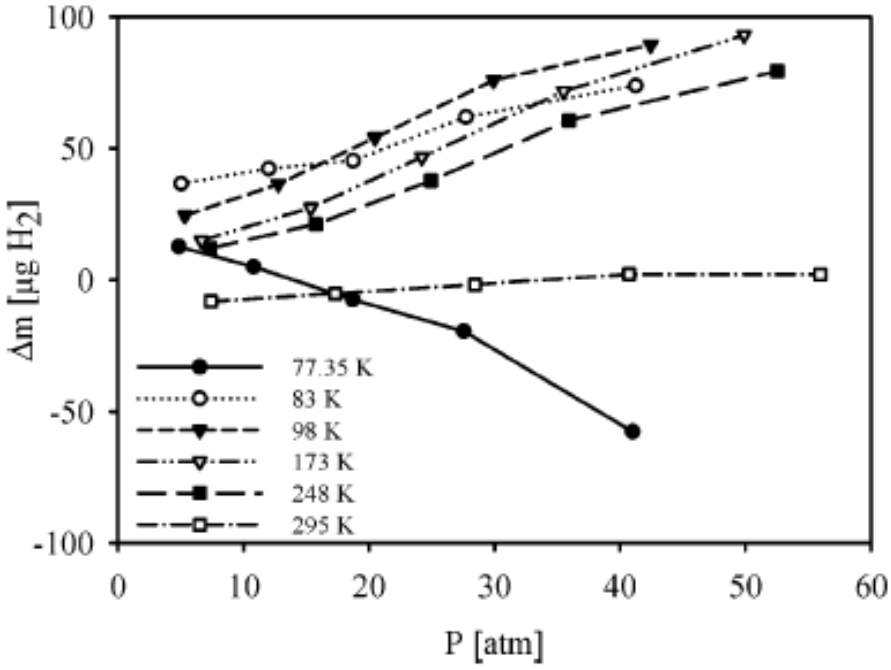

Figure 140. Blank tests performed at several temperatures in the 0–50 atm range.[145]

If the adsorption isotherms are acquired in a stepwise fashion using sequential doses of H_2, then the errors in each step will accumulate. This results in the increase of blank adsorption with pressure.

2.3.1.6 Real gas behavior

At low temperatures and high pressures, the real gas equation of state for H_2 starts to deviate from the ideal gas equation (Figure 141). If the sample vessel is at 77 K while the reference volume is at room temperature, then applying the ideal gas equation for a known amount of gas will result in an "effective volume," as explained in Chapter 2. While the pressure is constant throughout the instrument volume, the density is larger in the 77 K region. To calculate the H_2 density in the 77 K region, standard thermodynamic tables or H_2 equations of state can be used to determine the compressibility factor.

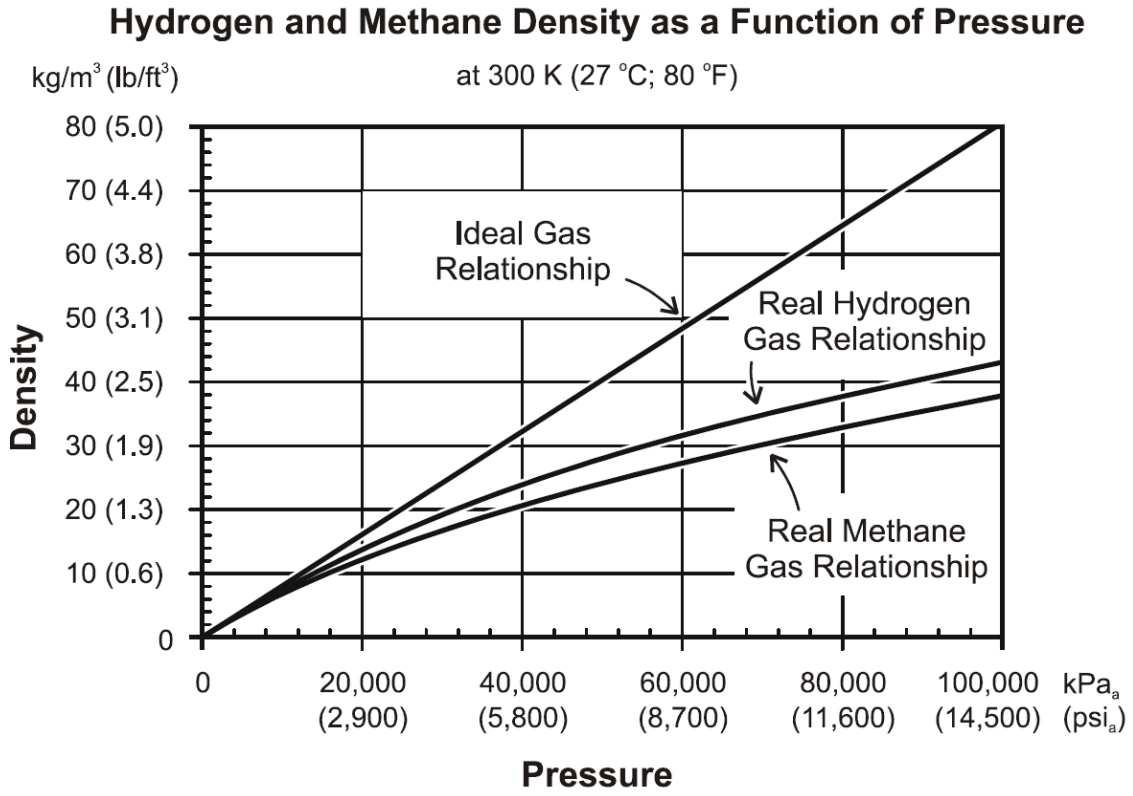

Figure 141. Hydrogen density as a function of pressure at room temperature.[193]

2.3.1.7 Blank Sample Measurements

There are a number of reasons to make measurements on blank samples (non-absorbing samples of low surface area, or empty sample cell). One of the main reasons is to validate the accuracy of experimental measurements at the temperatures and pressures that will be used for measurements on actual storage materials. A blank measurement under these conditions should give a quantity of sorbed gas that is very close to zero. The amount by which the measurement is non-zero is an indication of the accuracy of the measurement system and data analysis. The effective H_2 uptake or release in these blank tests should be small relative to the uptake expected from the sample. If the expected sample uptake is very small at the measurement conditions (e.g. hydrogen spillover adsorption at room temperature and low pressures), then it is especially critical that the "blank" H_2 uptake should be small. If the instrument volumes and pressure gauges are well calibrated, the void volume is well characterized, and the temperature gradients are properly accounted for, then H_2 uptake in blank tests can be on the order of 100 μg (see Figure 140).

Another reason for doing blank sample measurements is to empirically characterize the response of the instrument to a set of measurement conditions. For example, it is possible to determine the equivalent room temperature gas volume of a sample cell that is being held at a temperature far from room temperature using a blank sample rather than the actual sample to be measured. While it is more typical to use inert gas (generally Helium) measurement on the real sample to determine an "apparent volume" there may be some concern that the sample itself will adsorb significant amounts of the inert gas causing large errors in the "apparent" void volume of the sample cell. This becomes an important concern for high-surface area materials being measured at low (cryogenic) temperatures where inert gas uptake may be large.

In such cases, the void volume of the sample cell, with the sample in it, is usually determined from helium expansion measurements at room temperature and low pressures (under 5 bar). Under these conditions the effect of helium adsorption is generally considered to be small enough to have little impact on the volume calibration. By using a blank sample measured with hydrogen under the same conditions as the sample will be measured a "Temperature Correction Factor" can be determined (see introduction section 5.3.3 for more on temperature gradient corrections). These tests are run under identical conditions, but instead use inert, non-porous materials (e.g. stainless steel rods, silicon granules, glass beads) which have as close as possible the same gas displacement volume as the actual sample to be measured. The correction factor determined from these tests is the ratio of the apparent (at temperature) void volume of the cell containing the blank sample to the physical void volume of the cell containing the sample at room (or instrument) temperature. This ratio will be pressure and temperature dependent. Once this "Temperature Correction Factor" is determined using the blank sample, it can then be applied to correct the room (or instrument) temperature void volume value of the actual sample at equivalent experimental temperatures and pressures. This correction then compensates for the temperature induced density change in the gas in different isothermal and gradient sections of the instrument to aid in calculating the actual amount of hydrogen ad/absorbed by the sample at low temperatures.

2.3.2 Gravimetric Methods

The gravimetric method was presented in section 5.4 of the introduction (recommended reading). Due to the importance of issues that impact the accuracy of these measurements for determining capacity the method is presented here in more detail.

The gravimetric method is conceptually simple, but can be challenging in practice. In its most simple form, a sample is exposed to hydrogen at increasing pressures and the change in the weight of the sample is measured. The weight change of the sample is caused by two opposing forces, the ad/absorption of gas by the sample whose mass causes an additional gravitational pull on the sample and the buoyancy force of the difference in the density of the sample (and adsorbed gas) and the surrounding fluid (gas). These opposing forces must be accounted for regardless of whether the majority of hydrogen is absorbed in the bulk of the material or adsorbed to the surface. Because the buoyancy portion of the measurement is dependent on knowledge (or counter-balancing) of the pressure and temperature of the gas, measurements at elevated pressures or extreme temperatures become very sensitive to the behavior of hydrogen in the surrounding gas phase.

2.3.2.1 Gravimetric Physisorption Measurements

Physisorption measurements are most often performed at liquid nitrogen temperatures and this presents one end of the temperature extreme challenges for gravimetric measurements. In this light, we start with a description of the measurement with respect to physisorption. Figure 142 shows the adsorption process (a) and the equivalent depiction of the forces that contribute to the weight change of the sample on adsorbing gaseous hydrogen (b). All adsorbed hydrogen, whether excess hydrogen molecules or hydrogen molecules that would be present in the gas phase anyway, add to the mass of the sample. The density of the free (or bulk) gas that does not experience adsorption creates and opposing buoyancy force on the sample and adsorbed gas that decreases the measured weight of the sample. To determine the absolute adsorbed hydrogen requires some knowledge of the gas displacement volume of the sample together with the volume and ***density*** of the adsorbed gas. Because the thickness of the adsorption layer is generally not known exactly, based on pore size or monolayer coverage are often used to provide a rough estimate of the adsorbed gas volume. This also requires some assumption of the density of the gas in this layer. The density of the adsorbed hydrogen will likely be somewhere between that of liquid hydrogen and gaseous hydrogen (at the temperature and pressure of the gas surrounding the sample). Making estimates of this adsorbed hydrogen density that is either too low or too high can strongly affect the estimated “absolute” hydrogen storage capacity and may lead to unrealistically high values for hydrogen storage. Therefore, the absolute adsorption hydrogen storage capacity of physisorption materials is not often used or easily determined.

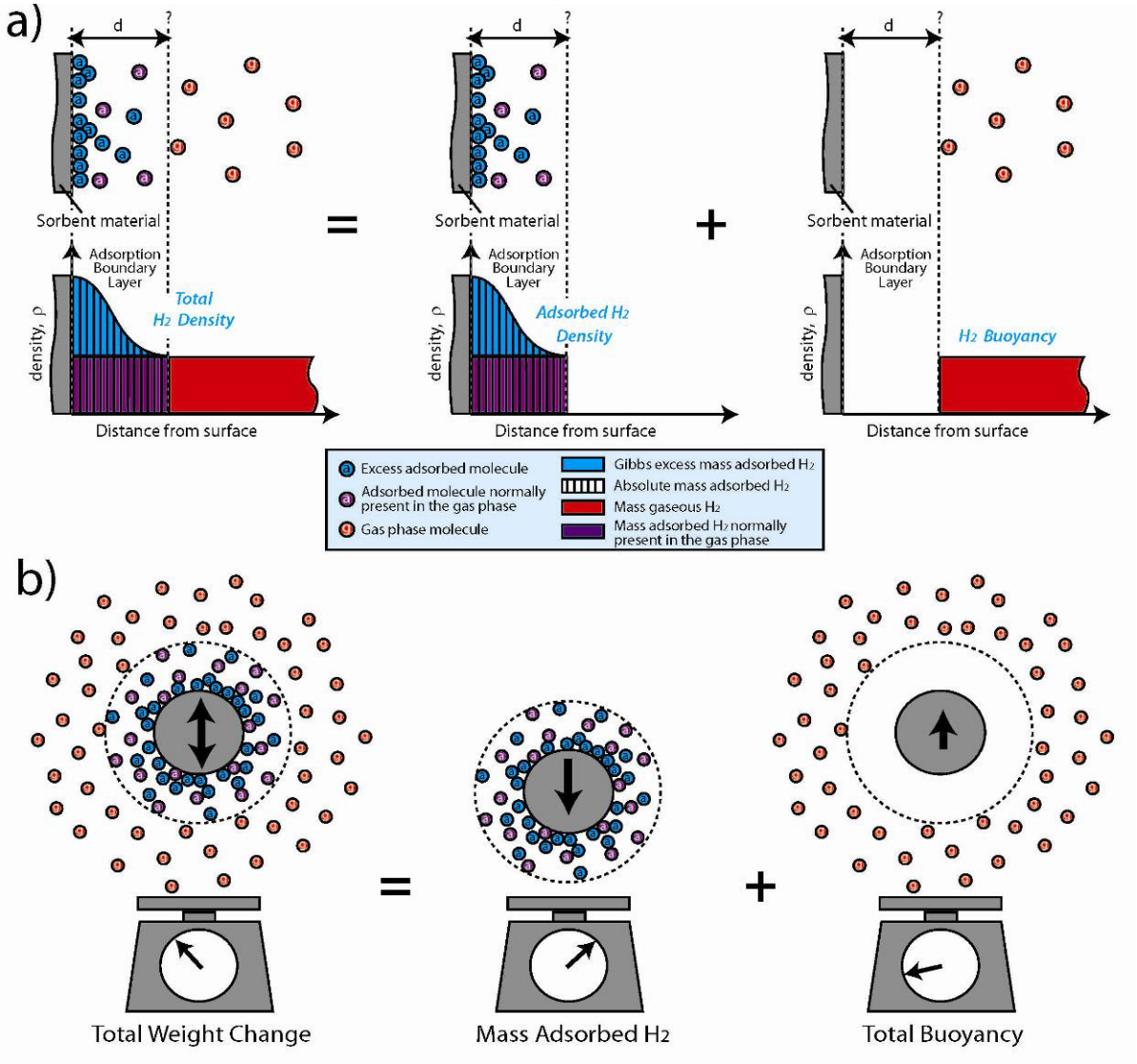

Figure 142. Depiction of the measured weight change of a sample caused by physisorption and buoyancy of the surrounding gas using the gravimetric method. a) The physical process of adsorption. b) Adsorbed molecules contribute to the weight of the sample (blue + purple), while the hydrogen molecules (red) displaced by the sample (and physisorbed gas) contribute to a buoyancy force opposing gravity.

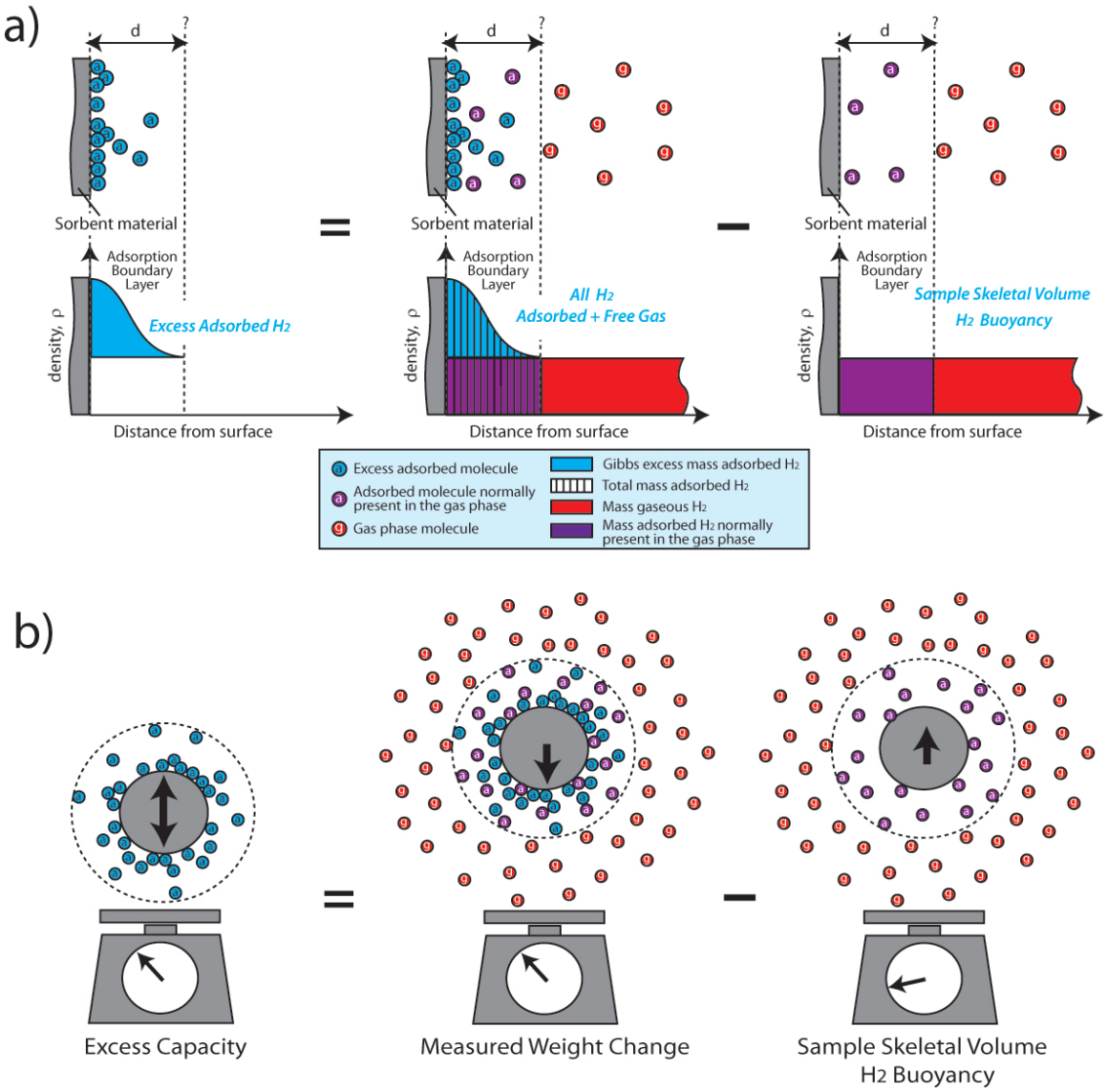

Figure 143. Depiction of the excess capacity as measured by the gravimetric method. a) The physical process of adsorption. b) The buoyancy force caused by hydrogen molecules (red + purple) displaced by the sample only (skeletal volume) is subtracted from the total measured weight change to give the "Excess" hydrogen storage capacity of the material.

The excess capacity is more readily determined than absolute capacity in that only the buoyancy force of the sample itself (and not the buoyancy on the adsorbed layer) is needed to correct the measured weight change of the sample. Figure 143 shows the adsorption process and the forces involved in determining the excess capacity.

As before, all hydrogen atoms in the adsorbed layer contribute to the mass of the sample. The volume of the sample plus this adsorbed layer displace a volume of hydrogen, leading to a buoyancy force counteracting gravity equal to the density of hydrogen at the local pressure and temperature surrounding the sample times the displaced volume. However, the adsorbed gas that would normally be present in the adsorption layer (purple) first add to the mass of gas adsorbed to the sample (purple and blue), but are subtracted out of the excess mass by being included again in the counteractive buoyancy force on the sample only. Simply put, the "excess" hydrogen capacity is determined by including the adsorbed hydrogen that would normally be present in the adsorption layer (purple) in the buoyancy term by using only the gas displacement volume of the sample for determining the buoyancy force. Thus, no assumptions for the thickness or density of the adsorption layer are required in determining "excess" capacity.

It is vitally important for physisorption measurements of any kind, that capacity data is properly labeled as either "excess", "absolute", or "total" capacity. And equally important that any assumptions made in determining the capacity values are clearly reported.

The base result that is determined from both volumetric and gravimetric measurements is "excess" hydrogen capacity. From a best practice point of view and consistency in the field the hydrogen excess uptake is what you should report. Everything else, absolute and total capacity, is an estimate based on this physical measurement and will only be as valid as the assumptions made in making that estimate.

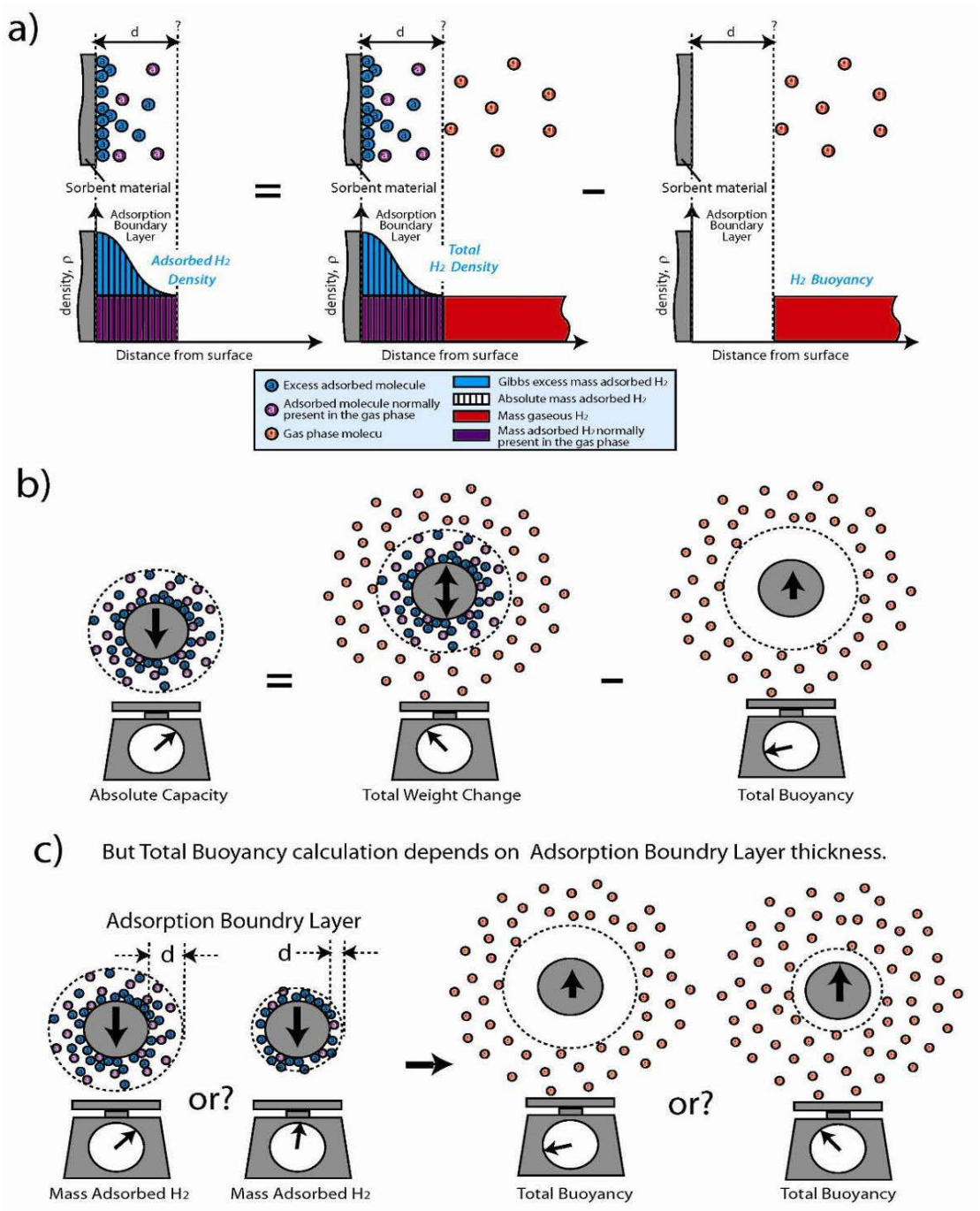

Figure 144. Depiction of the absolute storage capacity of a sample as measured by the gravimetric method. a) The physical process of adsorption. b) The buoyancy force of hydrogen molecules (red) displaced by the sample and the adsorbed hydrogen is subtracted from the total measured weight change to give the "Absolute" hydrogen storage capacity of the material. c) In a porous sample, it can be difficult to determine the thickness and volume of the adsorption boundary layer, which leads to difficulty in evaluating the "Absolute" hydrogen storage capacity.

The gravimetric method poses a similar problem in determining the absolute capacity directly from the measured mass of the sample. Figure 144 shows the adsorption process and the assumptions that are made in determining the absolute capacity. All hydrogen atoms in the adsorbed layer contribute to the mass of the sample. The volume of the sample plus this adsorbed layer displace a volume of hydrogen, leading to a buoyancy force counteracting gravity equal to the density of hydrogen at the ambient pressure times the displaced volume.

It is difficult to determine the volume of the adsorbed phase under usual experimental conditions, making it difficult to calculate the total buoyancy force. In practice, the buoyancy force is calculated as if the volume of the sample remains unchanged. In this case, the reported value is the Gibbs excess capacity. It is much more difficult to determine an accurate value for the absolute capacity. This concept can be most easily related using the following definitions:

M = measured mass of the sample = mass of the sample (Ms) + mass of total adsorbed gas (Ma) – total buoyancy (Mbt)

Mbs = buoyancy force due to the sample volume

Mba = buoyancy force due to the volume of the adsorbed phase

With these definitions and the apparent mass due to buoyancy is the density of the ambient hydrogen (ρ_{H2}) times the displaced volume, we can write:

Equation 94 $$M = Ms + Ma - Mbs – Mba = Ms + Ma – \rho_{H2}Vs - \rho_{H2}Va$$

Thus,

Equation 95 $$M = Ms + Ma – \rho_{H2}(Vs+Va)$$

Making use of

Equation 71, which relates the excess and the absolute amounts adsorbed, we obtain:

Equation 96 $$Mex = Ma – \rho_{H2}Va = M – Ms + \rho_{H2}Vs$$

Therefore the excess capacity is determined by a relatively straightforward calculation. Estimating the absolute amount adsorbed would require conditions in which the term $\rho_{H2}Va$ becomes large and measurable (e.g. at very low temperature and high pressure).

Note that the volume Vs can be determined from a helium displacement curve considering the relationship for buoyancy correction

Equation 97
$$F_b = g\rho\Delta V = g\rho\left(\frac{m_s}{\rho_s} - \frac{m_t}{\rho_t}\right)$$

Where F_b is the buoyancy force, g is the gravitational constant, ΔV is the differential gas displacement volume of the sample and the tare, ρ is the density of the gas, ρ_s is the density of the sample, m_s is the mass of the sample, ρ_t is the density of the tare, and m_t is the mass of the tare.

For an asymmetrical apparatus in absence of tare weight, the buoyancy force exerted on the sample will simply be:

Equation 98
$$F_b = g\rho\Delta V = g\rho\frac{m_s}{\rho_s} = g\rho V_s$$

Therefore, the corresponding correction on an actual hydrogen adsorption measurement can be performed as a function of (P,T) considering a factor (~1/2) between the bulk He and H_2 gas densities under similar (P,T) conditions. This approach is similar in essence to the free (dead) space measurement using helium in the volumetric approach.

Gravimetric instruments including Thermal Gravimetric Analysis instruments were discussed in the introduction section 5.4 and 5.5 above. There are several considerations with respect to the accuracy of hydrogen capacity measurements using gravimetric instruments.

2.3.2.2 Issues Involving Impurities

Of primary importance in the accuracy of mass-change measurements of hydrogen capacity is the certitude that mass change is due exclusively to hydrogen uptake or release. Therefore, two key factors are the purity of the gas (supply and environment) and the behavior of the sample itself.

Because gravimetric measurements generally involve small highly active samples exposed to relatively large quantities of gas any impurities in the gas are likely to be chemisorbed or physisorbed to the sample causing a non-hydrogen weight change that may mistakenly be attributed to hydrogen uptake. Impurities in the gas can come from the gas supply itself. Therefore, UHP hydrogen and calibration gasses (99.999% purity) is absolutely recommended. However, impurities in the gas can also come from, inadequate purging of gas lines when connecting gas cylinders to the instrument. For this we recommend at a minimum, 3 cycles of evacuating lines to at least 100 millitorr and purging with fresh gas. Impurities can also come from any leak in the instrument or lines connected to the instrument. When the sample cell is held under vacuum, air and moisture will be drawn into the sample cell through poor seals, back flow through vacuum pumps (especially if not operating properly) or other leaks. Impurities may also come from residual vapor left behind in the instrument or as a result of components or residue from prior experiments degassing when the instrument is heated. Clearly the introduction of the sample into the mass balance without exposure to air is problematic. Sometimes, bake out of the sample after air exposure is sufficient. In this case it is important to ensure that any moisture or other contaminants have not condensed somewhere else within the instrument only to contaminate the sample upon the introduction of gas. Some samples simply can not be exposed to air or moisture at all and will require that the measurement instrument is installed inside of a glove box or has a sophisticated sample transfer system that is 100% air-free.

Another source of error in high-surface-area physisorption materials is the presence of oxides on the surface of the material that may react with hydrogen in the presence of catalysts to form water. Hydrogen uptake in the material as water would increase the sample weight giving the appearance of stored hydrogen. A check for this is that the water should be released as vapor in a subsequent desorption and the sample would loose weight with each desorption cycle.

A good cross-check would be to measure the same materials using the volumetric method. During desorption the evolved water will not produce a significant increase in pressure during desorption (at low temperatures) as hydrogen desorption would. An apparent desorption by the gravimetric measurement and none given by a volumetric measurement would indicate the formation of water or some other non-hydrogen species. The formation of hydrocarbons (methane…) at active or catalyzed sites on high-surface-area carbon materials may present a similar (false positive) behavior.

The sample itself may change mass through melting (spattering or flowing off the sample holder), evaporating, or evolving gaseous components (such as NH_3 from amides) during heating. This weight loss concurrent with hydrogen release might be misinterpreted as purely the desorbed hydrogen capacity. Continued mass loss with each desorption cycle is a sign of such a situation. Again comparison with measurements made using the volumetric method would also help to resolve such issues.

Sometimes mass spectroscopy infrared spectroscopy, or gas chromatography of the evolved gasses can identify impurities or decomposition of the sample. This, however, depends on the set up of the analytical system and operating temperatures of the sample and gas lines. Many volatiles released by the sample (NH_3, BH_3, H_2O, CH_4….) may condense out in the system before reaching the analytical detector and escape detection.

2.3.2.3 Instrumental Stability

Besides the purity of the gas and the sample properties there are instrumental sources of error to be evaluated. One consideration is the stability of the measurements over time. Some sources of noise or drift to consider are: mechanical vibrations, temperature variations within the lab, temperature stability of the measurement instrument itself, stability of the gas pressure, or (in the case of flowing gas systems) stability of the gas flow rates, any transfer of heat from the sample chamber to the mass balance measurement system. A good test of stability is to systematically run blank samples under the same conditions as the test sample will be measured.

2.3.2.4 Instrumental Effects on Buoyancy Corrections

The weight reported from a gravimetric measurement system is not necessarily the total weight of the sample, but rather can be significantly affected by buoyancy forces on the sample and system components. While it is possible to correct for these effects, loose assumptions can create a large degree of uncertainty in gravimetric measurements. Thus, gravimetric measurements are seriously affected by buoyancy.[194] Since density values of dispersed or porous materials are often not well known, the complete compensation of buoyancy by means of a counterweight on the basis of a given density value generally fails.[142] It is therefore typical to measure the remaining buoyancy effect by using helium at 77K or at ambient temperature.

These buoyancy effects can have a big impact on Gravimetric and Thermal Gravimetric Analysis, especially when using small samples relative to the size of the sample holder. For example, if a 1 mg magnesium sample is measured in a sample holder made of quartz that weighs 1 g, the volume of the sample will be only 5.754×10^{-4} cm^3 compared to 0.375 cm^3 for the sample holder. If the magnesium is heated from room temperature to 300 °C, the buoyancy force on the sample and its holder, given by ρgV, where ρ is the density of the hydrogen gas and V is the volume of the sample and holder, will decrease dramatically. In this example, the weight of the sample is only 9.8×10^{-6} N, while the buoyancy force decreases by 1.723×10^{-7} N due to the decrease in the density of hydrogen gas at higher temperature. This would lead to an apparent storage capacity of 1.76% without any hydrogen absorbed at all. This problem can be partially overcome by

using a system with a tare or running a test measurement under the exact same temperature and pressure conditions but with nothing in the sample holder and subtracting the apparent weight change from the real data.

An example of the activation and tare process for a 1 gram sample of activated carbon is shown in Figure 145. In this example, a) the sample was degassed in vacuum at 573K, then b) cooled to 77K in vacuum. The initial temperature difference generated a thermal gas flow, resulting in a sudden decrease in the indicated mass of the sample. An initial zero point reading was taken at c after considerable equilibration time. On the introduction of helium (d and f), an instantaneous degrease in the indicated mass of the sample is observed as a result of buoyancy in helium. Following this immediate buoyancy effect, a slow increase in the mass occurs, which is ascribed to the adsorption of helium. Evacuation (e and g) causes a fast increase in the indicated mass as a result of the lack of buoyancy, followed by a slow mass decrease ascribed to the desorption of helium. A final zero point shift at the end of g is attributed to the sorption of contaminating vapor. This degassing and zeroing process is followed by a nitrogen adsorption measurement at point h.

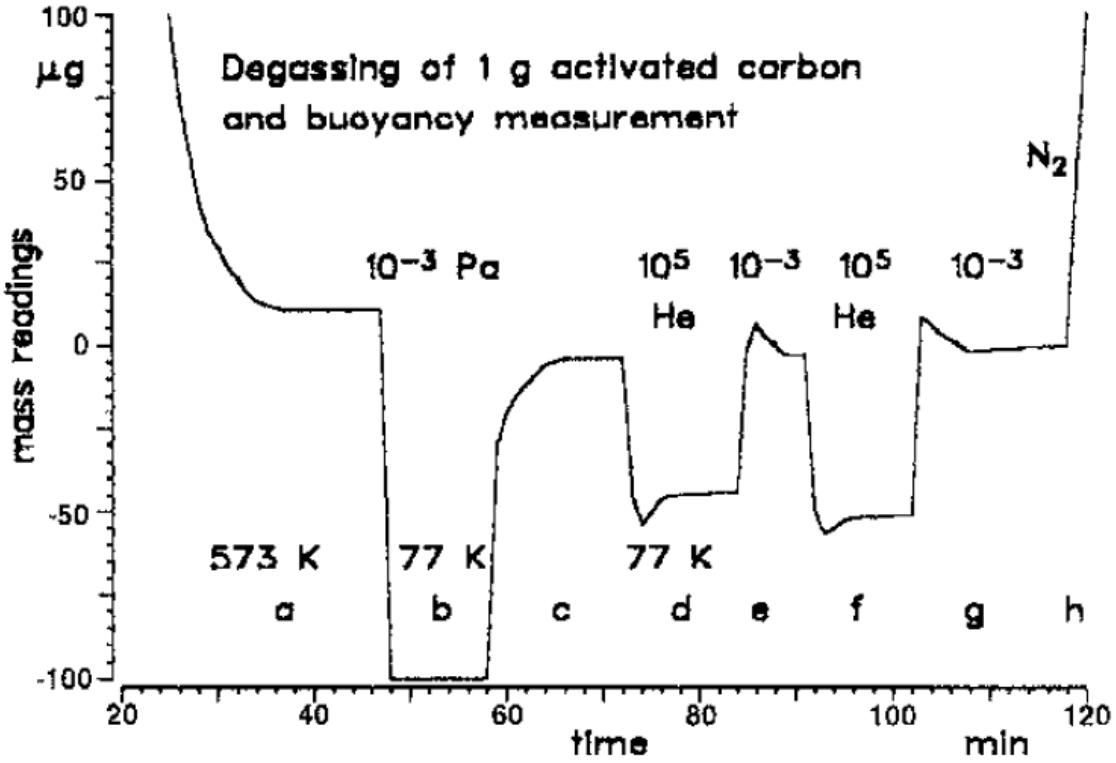

Figure 145. Gravimetric record of the activation and zeroing process of a sorbent sample of 1 g activated carbon, counterbalanced by quartz glass, in vacuum and in a helium atmosphere.

For asymmetric balances (spring or magnetic suspension balances), the influence of buoyancy must be corrected computationally, taking into account the fact that the buoyancy of the balance parts occur at different temperatures than that of the sample, and that this temperature distribution may also vary with pressure.

In a symmetrical microbalance, the balance consists of a sample in a sample holder on one side, with an inert tare of similar mass and density to the sample on the other to reduce the buoyancy effect. The variation in mass due to buoyancy is then given by:[74]

Equation 99
$$\Delta m_B = \rho_{gas}(\Delta V) = \rho_{gas}\left(\frac{m_s}{\rho_s} + \frac{m_{sh}}{\rho_{sh}} - \frac{m_t}{\rho_t}\right)$$

Where Δm is the change in measured mass due to buoyancy, ρ_{gas} is the density of the gas, m_s, m_{sh} and m_t are the mass of the sample, the sample holder (assuming there sample holder in addition to the normal balance components) and the tare respectively. Similarly, ρ_s, ρ_{sh} and ρ_t are the densities of the sample, the sample holder, and the tare, respectively. Since the buoyancy force opposes gravity, this term must be added to the measured mass to determine the true weight of the sample.

For asymmetric balances (spring balances or magnetic suspension balances), the influence of buoyancy on the sample and instrument components must be corrected computationally, taking into account that the buoyancy of the balance parts occurs at temperatures different from that of the sample. The variation in mass due to buoyancy is then given by:

Equation 100
$$\Delta m_B = \rho \Delta V = \rho(P_s, T_s)\left(\frac{m_s}{\rho_s} + \frac{m_{sh}}{\rho_{sh}}\right) + \rho(P, T_x)\left(\frac{m_B}{\rho_B}\right)$$

where $\rho(P_s,T_s)$ is the density of the hydrogen gas at the sample, $\rho(P,T_x)$ is the density of the hydrogen gas at various points along the components of the balance (P is constant, but T_x will vary), m_s and ρ_s are the mass and density of the sample, m_{sh} and ρ_{sh} are the mass and density of the sample holder (assuming there sample holder in addition to the normal balance components) and m_B and ρ_B are the mass and density of the balance components (bucket, pan, beam, and the hang-down wires).

It should be noted that once the buoyancy correction is added, the calculated quantity is the excess hydrogen adsorbed. Alternatively, if an accurate model for the volume occupied by the adsorbed gas is available, the absolute adsorption can be calculated.[195] However, there are still many subtleties involved that can still lead to inaccurate results.

For example, in some cases variations in the temperature throughout the measurement system need to be accounted for computationally. [142]

2.3.2.5 Thermal Errors in Buoyancy Corrections

In a typical gravimetric instrument, the heating furnace, water bath, or cryostat surrounds the sample cell containing the balance pan(s) on the bottom and sides. Heat will be transported into the cell from above causing a temperature gradient in the cell's components and any gas that is present. For 77K measurements at low pressures (<100 Torr) a temperature difference of up to 15K has been observed between the sample and cryostat even in the most well designed systems.[196] Any remnant thermomolecular flow at low pressures will shift the zero point of the mass measurement of the sample. Thermomolecular flow has the greatest effect at pressures at which the mean free path of the gas molecules (λ) is comparable to the characteristic length L (L= the diameter of the balance cell).[197] The Knudsen number *Kn* is given by:

Equation 101 $$Kn = \lambda/L$$

For pressures below *Kn* = 1, the thermomolecular flow creates a pressure difference where the maximum pressure difference is given by Knudsen's law:

Equation 102 $$P_1/P_2 = (T_1/T_2)^{1/2}$$

For the typical microbalance cell tube of 2 cm in diameter the maximum thermomolecular flow is observed in the pressure range of 0.1 to 1 Pa. These pressure differences should be accounted for in any computation of buoyancy corrections of components of the balance and sample (hang-down wires, pan,…) under such conditions.

At higher pressures thermally induced convection of the gas will occur also affecting the mass measurement. These are difficult to correct for computationally and therefore require optimal design of the balance and cell. In one example, the use of deflecting metal shields mounted above the sample, and long (1m) and very thin (30μm) hang-down wires, reduced convective disturbances to about 10 μg (1g activated carbon sample at 77K).[142] The effect of thermal convection issues increase with increasing pressure, increasing temperature differential and decreasing sample size.

2.3.2.6 Sample Density Errors in Buoyancy Corrections

Another source of error comes from determining the true skeletal density of the sample. This is of particular importance in porous solids where the porosity is often not well known. The skeletal density is usually determined from helium pycnometry as outlined in the Capacity section 1.4.1 Density of Porous Solids. However, the assumptions involved, such as neglecting the adsorption of helium, can lead to significant errors. In some materials large amounts of helium can be adsorbed.[198] One study has shown the estimated volume to off by 20% when the helium calibration was used on a nonporous Al wire of known density and mass. [199]

Given that the buoyancy correction to the mass change of a sample is:

Equation 103 $$\Delta m = \Delta F/g = \rho_{H2}(m_s/\rho_s)$$

Where m_s, ρ_s are the mass and density of the sample and ρ_{H2}. is the density of hydrogen at the sample pressure and temperature, then the buoyancy correction on a weight % basis given by:

Equation 104 $$\Delta wt.\% = 100\cdot(\rho_{H2}/\rho_s)/(1+(\rho_{H2}/\rho_s))$$

The weight percent buoyancy correction can therefore be calculated as a function of the skeletal density of a sample for a given pressure and temperature of hydrogen gas surrounding the sample. Some examples of these corrections are shown in Figure 146 for measurements at 77K and 298K of hypothetical samples with skeletal densities of 0.5, 1.0 and 4.0 g/ml.

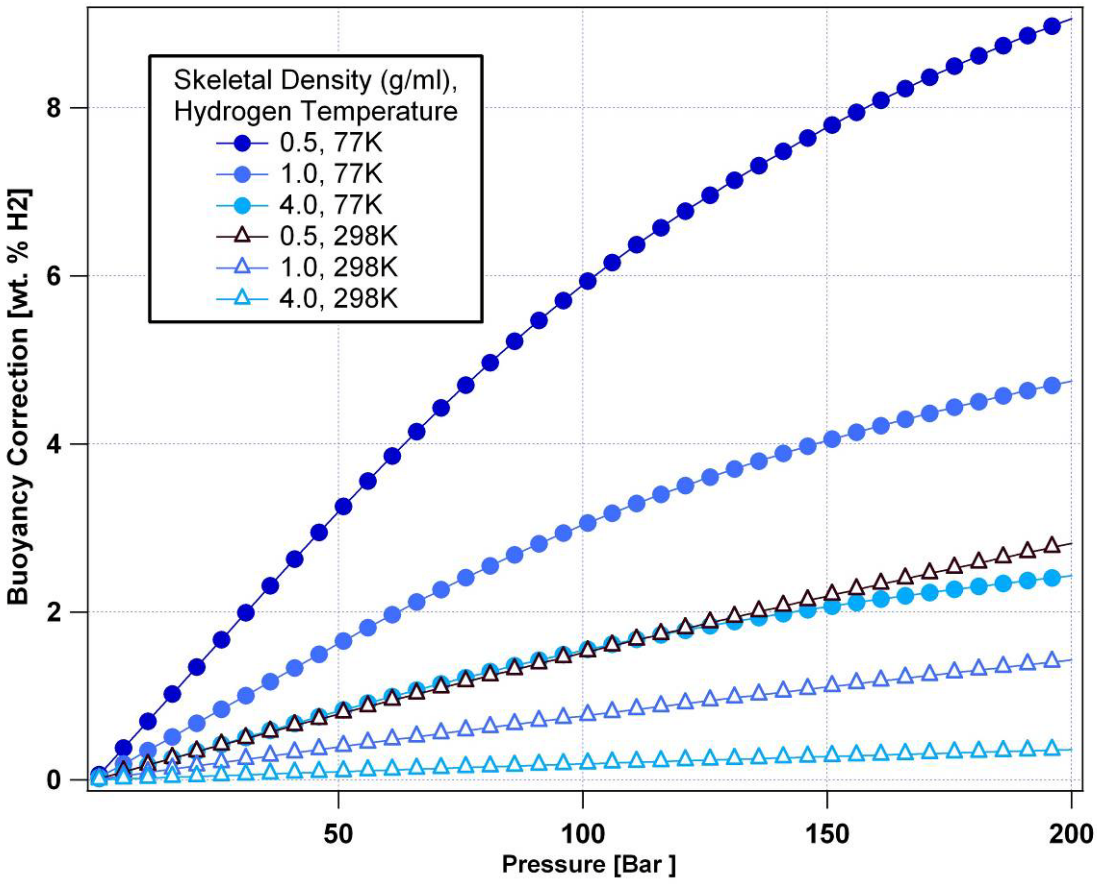

Figure 146. Buoyancy corrections for different sample skeletal densities at 77K and 298K.

The skeletal density of a sample can be determined gravimetrically using the buoyancy effect. Assuming arms of a symmetrical balance of equal mass, density and length, the mass difference $\Delta F/g$ from buoyancy between a sample and counterweight is given by:

Equation 105

$$\Delta F/g = \rho_{He}(m_s/\rho_s - m_c/\rho_c)$$

Where m_s,ρ_s and m_c,ρ_c are the mass and density of the sample and counterweight respectively. In one example, the density of 1 g of activated carbon was determined by such a helium measurement at 77K to be 1.9×10^3 kg/m^3. This was about 10% higher than the same measurement performed using nitrogen at room temperature.[142] One explanation for such differences is that microporous materials with pore diameters less than 0.26 nm[200], which are accessible for the small helium atoms, are not for larger molecules such as nitrogen.[201,202]

One significant source of error comes from neglecting the volume expansion of the sample upon hydrogen loading. This has a similar effect to errors in the volume measured by helium pycnometry. For example, the volume of Mg can expand by as much as 33% on hydriding. Similarly, the gas adsorbed on the surface of a porous medium can have a significant contribution to the volume.[131] The error associated with neglecting the volume change upon hydrogen loading is presented in Table 12. These are high estimates for the error, since the ideal gas law was used to calculate the density of hydrogen at high pressure and low temperature. More accurate values for hydrogen density can be calculated using the Bender Equation of State, the Modified Benedict-Webb-Rubin Equation of State or an equation developed by NIST. [203]

Material	P (atm)	T (K)	Error
Mg	1	273	0.02%
Mg	200	273	4.40%
Mg	200	77	15.60%
Activated Carbon	1	273	0.01%
Activated Carbon	200	273	2.20%
Activated Carbon	200	77	7.90%

Table 12. Maximum error due to volume expansion during hydrogen loading at various temperatures and pressures.

2.3.3 Sources of Errors in Volumetric and Gravimetric Measurements

One of the greatest challenges to accurate measurements of the interaction of hydrogen with storage materials it the fact that hydrogen is the smallest and lightest of all gas molecules. Measurement techniques that are considered standard in the investigation of other gases are significantly more challenging for hydrogen. Both volumetric and gravimetric measurements are common for gas uptake measurements such as BET where gases such as nitrogen and argon are measured at pressure generally below 1 bar.

With gravimetric measurements an important consideration is that nitrogen gas is 14 times heavier and Argon gas 20 times heavier than gaseous hydrogen. In other words, 14 to 20 times as much hydrogen must be adsorbed to a material to give the same weight change as the same molar adsorption of nitrogen or argon respectively. Or conversely, at least an order of magnitude higher sensitivity is required to accurately measure hydrogen uptake as most other gases. This is not the case for volumetric

measurements where pressure change is directly proportional to moles of gas uptake independent of what the gas is.

Volumetric measurements are subject to errors caused by gas leaks or essentially a loss in the total accounting of all hydrogen present (mass balance). Hydrogen being the small molecule that it is exacerbates the absolute requirement for measurements to be made with as low a leak rate as possible. Clearly all seals between gas handling components should be leak free (generally metal-to-metal seals). But in addition, hydrogen will diffuse through all materials at some rate which is dependent on temperature and pressure. Teflon is an example of a materials that is particularly permeable to hydrogen, even some steels are not ideal for hydrogen applications (316L steel is most commonly used in instruments for hydrogen sorption measurements) and all steels have limitations with respect to high pressures and temperatures of hydrogen.
Impurities in either the hydrogen gas supply or the sample materials present some of the greatest issues for hydrogen capacity measurements. This is because most materials that are highly reactive or interactive with hydrogen will be the same with impurities (oxygen, water, nitrogen….). This is particularly true of high-surface-area materials. An important consideration is that the errors caused by impurities present themselves in very different ways depending on the measurement technique. Impurities in the gas that react with the sample generally show a large increase in mass in gravimetric measurements that is indistinguishable from hydrogen uptake and may indicate high hydrogen weight percent capacity. The opposite is true for volumetric measurements where impurities in the gas may deactivate the sample, reducing the apparent hydrogen uptake.

Impurities in the sample that cause un-intended hydrogen uptake (hydride-forming additives, water-forming oxides,…) would be expected to give invalid results in both gravimetric and volumetric techniques if not properly accounted for. Regardless, the formation of extraneous hydrogen compounds are often not reversible, therefore, a significant loss in reversible capacity (of reversible materials) with cycling would indicate the possibility if impurities in the sample.

Uncertainty in the skeletal density (gas displacement volume) of new materials creates errors in both gravimetric and volumetric measurements. In gravimetric measurements the error is directly proportional to the required buoyancy correction. In volumetric measurements error in the density of the sample is proportional to the total calibrated free gas volume.[73] An example of these impact of uncertainty in a sample's skeletal density is shown in Figure 147 for 77K hydrogen absorption measurement on a 23 mg sample of activated carbon using a volumetric instrument with a total free gas volume of 1.78 ml. Given an underestimation of the sample skeletal density of 0.85 g/ml vs. actual 1.7 m/ml the resulting error in the measurements due to error in the free gas volume of the instrument (volumetric) or in the buoyancy correction for the sample are shown in the figure.

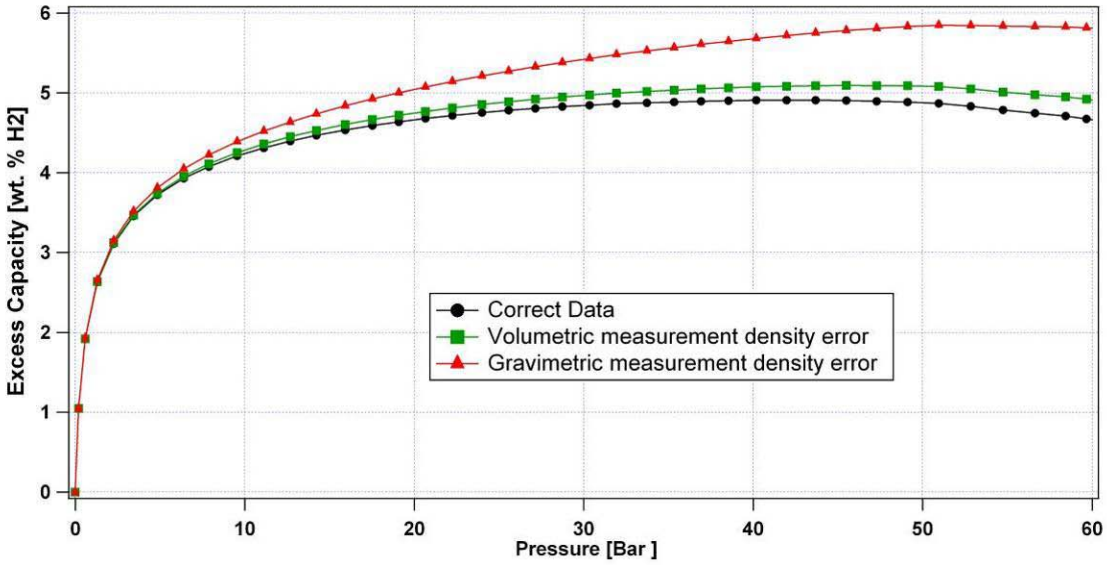

Figure 147. Error in capacity by gravimetric and volumetric measurements due to a 50% error in estimating the skeletal density of a sample (50% lower than actual). Sample 23 mg activated carbon at 77K.

These corrections are only for errors in sample volume and do not include temperature gradient effects on both buoyancy corrections (gravimetric) or apparent volume temperature corrections (volumetric).

It should also be noted that, in contrast to gravimetric measurements, the zero point calibrations of isotherm measurements is not effected by thermomolecular flow issues (buoyancy corrections) at low pressures. [197,204,205]

2.3.4 Thermal Gravimetric Analysis

TGA (Thermal Gravimetric Analysis) generally refers to a combination of gravimetric and mass-spectrometry analysis. As such, it can be used to detect the presence of chemisorbed gases. This is typically negligible on most carbon adsorbents due to van der Waals repulsion, but it can occur in unique geometries like single-walled carbon nanotubes.[159] TGA can be used effectively in tandem with isotope substitution to characterize and validate hydrogen spillover. An example for a spillover sample dosed first with H_2 followed by D_2, is shown in Figure 148.[206] This has been interpreted as successive H_2 and D_2 dissociation on the spillover sites, recombination at the interface between the two isotope layers, and desorption at the same spillover sites.

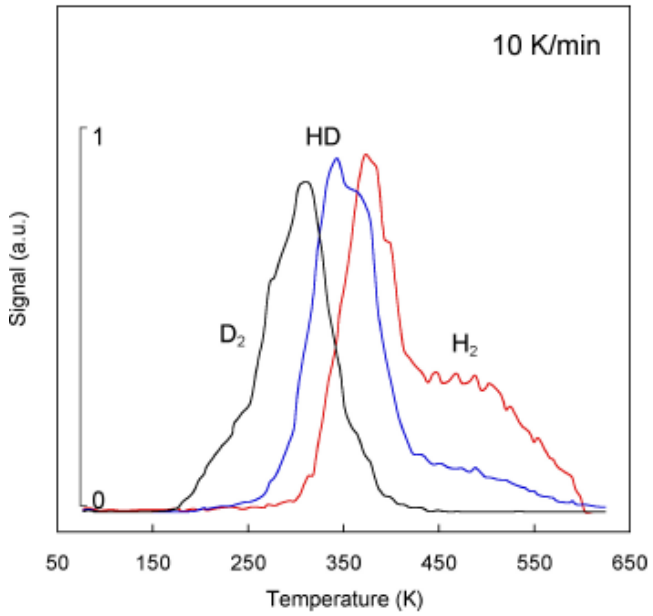

Figure 148. TGA desorption trace for a spillover sample that was dosed first with H_2 followed by D_2.[206]

The decomposition of the off-board rechargeable chemical hydride polyamino borane (Second dehydrogenation step of Ammonia borane) is given by:

Equation 106 $(NH_2BH_2)n \rightarrow (NHBH)n + H_2$

Typical TGA-curves for this decomposition at different heating rates (1, 5 and 10 °C min−1) are shown in Figure 149 a). A single mass loss step was observed at all heating rates. It is clearly evident that a mass loss is detectable in the same temperature range in which hydrogen release and heat evolution were determined. The final value of the mass loss depends significantly on the heating rate used. With rising heating rate the final mass loss increases from 7.1 wt.% at β = 0.1 °C/min to 20.3 wt.% at β = 10 °C/min. The formation of boron nitride at a temperature of 250°C is not probable, as follows from the volumetrically detected release of only 1.1 mol hydrogen per mol H_2BNH_2.

In Figure 149 b) results of thermogravimetric and volumetric investigations are compared. Volumetric results were converted into mass loss data. The release of 1.1 mol H2, which was detected by volumetric investigations, corresponds to a mass loss of only 7.6 wt.%. The results for the mass loss from thermogravimetric and volumetric investigations are nearly in agreement at a heating rate of 1 °C/min. The amount of

gaseous products evolved in addition to hydrogen should be very small at 1 °C/min. The thermal decomposition of polymeric aminoborane $(H_2BNH_2)x$ is accompanied by the evolution of different gaseous products as follows by volumetric and thermogravimetric investigations.

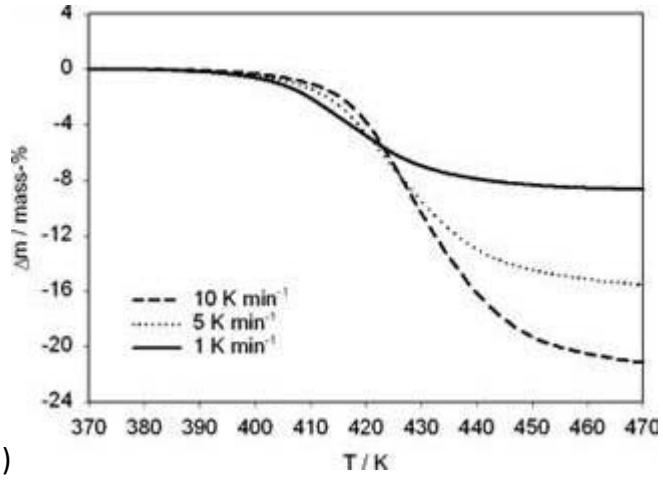

a)

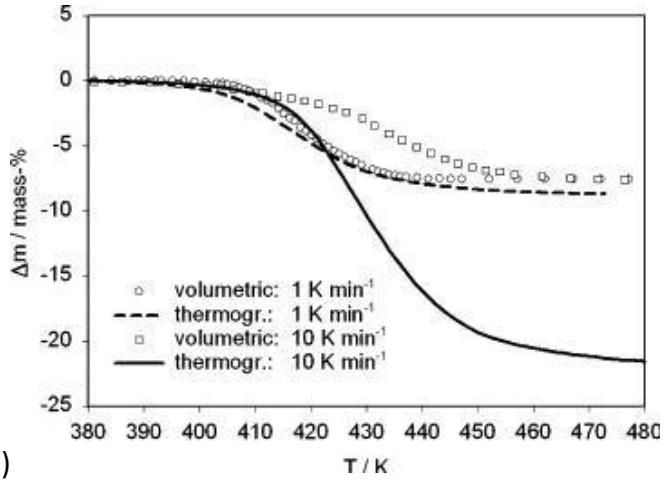

b)

Figure 149. a) Mass loss on the thermal decomposition of polymeric aminoborane (H2BNH2)X versus temperature b) Experimental data for the mass loss (TG, line) in comparison with the mass loss data calculated from the released amount of hydrogen (volumetric measurements, points), (heating rates 1 and 10 °C/min).[207]

Gravimetric measurements are often used for measuring capacity for many hydrogen storage materials. However, in ammonia borane it is very difficult to obtain accurate information about the capacity using simple TGA measurements. The key issues that could skew measurements are:

- Foaming: Ammonia borane foams extensively in the range of 90-110 °C during hydrogen release. This often creates mechanical errors in the instrument balance thus reporting an erroneous weight loss.
- Sublimation: Sublimation of the storage material is more common on samples which are heated under TG conditions. Undetected loss of some of the sample via sublimation may result in a significant error in estimating hydrogen capacity.
- Non-hydrogen volatiles: Other volatile intermediates or byproducts such as ammonia and borazine also contribute to an overestimation of hydrogen capacity if not properly accounted for.

These errors though significant under certain conditions can be minimized by use of smaller sample sizes in larger sample cups equipped with a lid (with a small orifice) that can minimize sublimation and foaming issues. Volatile byproducts or intermediates can be quantified by other techniques mentioned in section dealing with gas composition analysis and corrected for those measurements.[208]

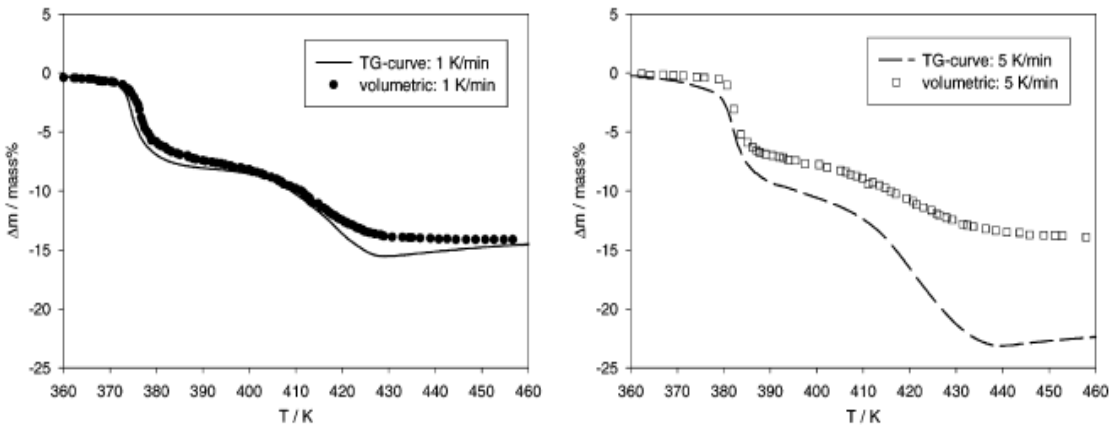

Figure 150. Comparison between mass loss data detected thermogravimetrically (line) and calculated from volumetric results (points) (heating rate 1 K/min (a), 5 K/min (b))

TGA is less accurate than either the volumetric and gravimetric methods and is not typically used for measuring capacity.

2.3.5 Temperature Programmed Desorption

TPD (Temperature Programmed Desorption) often refers to the quantification of desorbed gas most commonly using a mass-spectrometer to measure gases evolved from a sample while ramping the temperature of the sample at a constant rate. Alternatively, infrared spectroscopy may be used when MS is problematic, i.e. if there are complex mixtures of gases to be studied. The method is generally referred to as TDS (Thermal Desorption Spectroscopy). The experimental difficulty in this method is the proper calibration of the mass-spectrometer to provide quantitative measurements of evolved gas.

The quantities of gases evolved may be derived experimentally from the measured area under the MS response vs. time curve by comparison to a calibrated volumetric dose of the gases delivered to the system under the identical conditions used for the TDS experiment. Alternatively, calibration of hydrogen may be achieved by decomposing a metal hydride sample with a very well known hydrogen content or by carefully weighing a hydride sample before and after desorption. In addition to the calibration, good response times are needed in coupled DSC–MS systems. That means that the time lag between the signal detected by the DSC and that detected by the MS should be small. It is also desirable that the shape of the MS signal accurately reflects decomposition reaction of the sample. Both characteristics, time lag, and shape of the MS signal, are taken into account by the response time function of the system which is mainly affected by the flow and type of carrier gas and the geometry of the experimental system. An example of such a system was reported by Fernández, C.R. Sánchez.[209]

A simple TPD alternative to study the gas–solid interaction of hydrides can be studied using the using a thermo-volumetric analyzer (TVA), based on a modified Sievert's type apparatus. A TVA system uses a calibrated high pressure reactor vessel and calibrated reservoir vessel. The temperature of the reactor vessel is usually controlled a PID temperature controller that can ramp the temperature of the sample at a constant rate. As the sample desorbs the hydrogen pressures inside the vessels are recorded using high precision pressure transducers. These values are then converted into capacity via the volumetric method. As with all volumetric and gravimetric devices, it is not possible to be sure that the evolved gas pressure or mass loss is purely due to hydrogen without performing some form of gas analysis. It is also important to note that TPD methods are by design dynamic not equilibrium measurements. Thus, great care should be taken in evaluating stabilities and capacities to individual hydride phases.

An example of TPD measurements can be seen in the thermal decomposition of Zr and Ti doped sodium aluminum hydride system by Zidan et al. One such measurement is shown in Figure 151.[210]

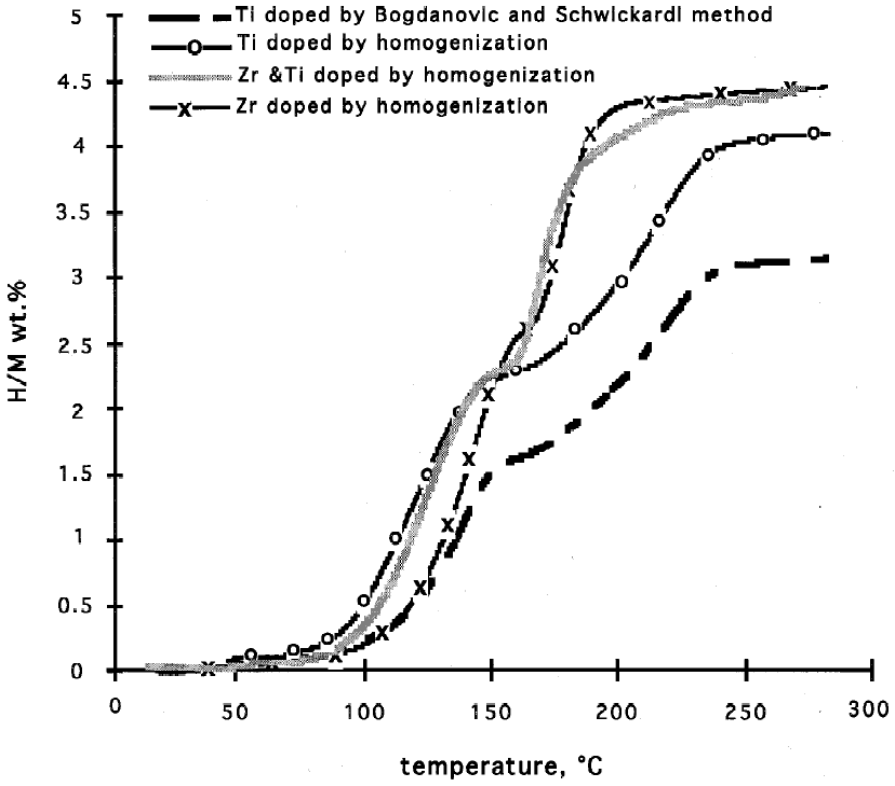

Figure 151. Thermal-programmed desorption (28°C/min) of hydrogen from various doped samples of $NaAlH_4$ after three cycles of dehydriding / rehydriding.[210]

2.3.6 Differential Scanning Calorimetry

Differential scanning calorimetry, DSC, is a direct method of determining the adsorption or desorption enthalpy of a material, but it rarely used for reversible sorption due to experimental complexity. The isosteric method for calculating adsorption enthalpy, is far more widespread and provides results directly on a per mole H_2 basis without requiring separate measurements of hydrogen capacity. Various methods of adsorption calorimetry have been developed to measure adsorption amounts. For more information, refer to the book "Adsorption by Powders and Porous Solids" by Rouquerol et al.[56]

For irreversible off-board regenerable materials DSC may be the only way to measure heats of decomposition. Isothermal DSC measurements are a reliable method to determine the heat of the reaction provided that the products formed at known and are identical at all temperatures.

For the results to be valid it is important that the extent of the decomposition is measured. This can be done ex-situ by analyzing the sample through a secondary technique (XRD) before and after a DSC measurement or *in-situ* by measuring the quantity of hydrogen released. The second method is preferred as it directly provides the heat of decomposition on a mole H_2 basis which is critical for hydrogen storage. An important caveat is that the evolved gas should be analyzed to ensure that the main constituent is hydrogen for a correct determination of the enthalpy.

As and example, the first decomposition step of ammonia borane to evolve one mole of hydrogen was studied in great detail by Wolf et al using DSC operating in the isothermal mode at temperatures between 343 and 363 K.[211] Isothermal measurements are suitable for the investigation of the slow decomposition reaction of borazane in the solid state below the melting temperature. Figure 152 shows typical calorimetric curves obtained at different temperatures. A single exothermic peak was detected in all cases. The rate of decomposition strongly depends on the temperature. The amount of hydrogen released during the process is also significantly affected by the temperature. As the temperature of the dehydrogenation is decreased the amount of time it takes to release the hydrogen is significantly increased. At 343 K (70 °C) it takes about 40 hours to release the predicted 6.5 wt% hydrogen and at 363 (90 °C) that time is decreased to 6h. Longer decomposition runs do not result in a further increase of the detected hydrogen amount. Additionally they inferred that the mean enthalpy of decomposition reaction is nearly independent of the temperature and is equal to $\Delta H = -(21.7 \pm 1.2)$ kJ/mol BH_3NH_3. Gutowska et al. observed that the inclusion of Ammonia borane in mesoporous scaffolds such as SBA-15 significantly decreases the exothermicity of reaction.[179] The rate of release of hydrogen from ammonia borane is greatly enhanced in this case. So, to get reliable data, it is critical to measure heat of reaction for dehydrogenation on the composites at much lower temperature (50 °C).

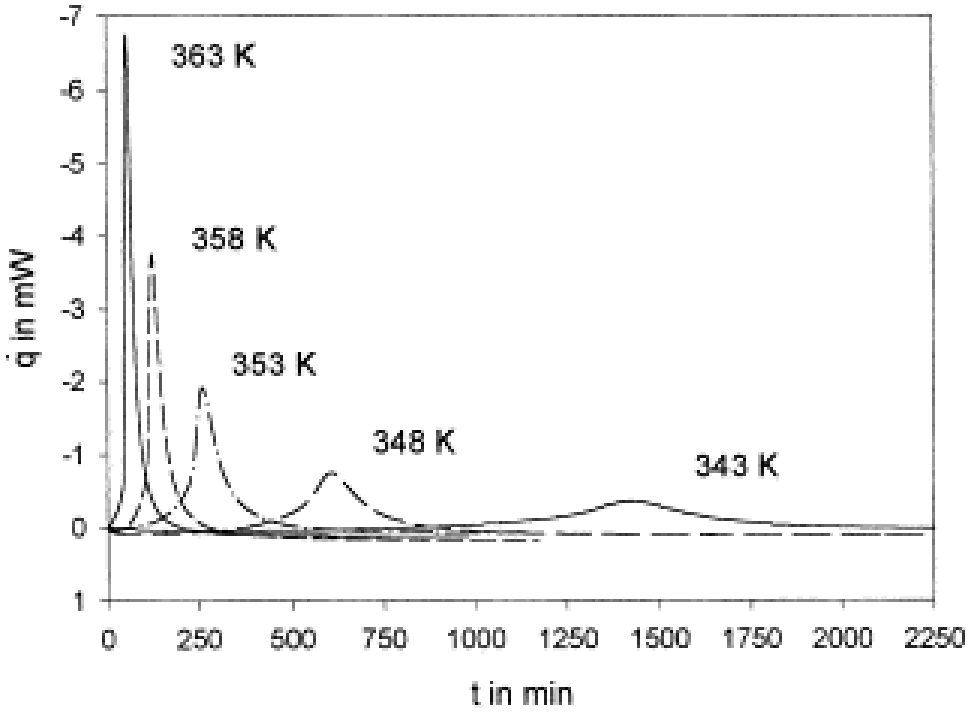

Figure 152. DSC curves of isothermal decomposition of BH_3NH_3 at temperatures between 343 and 363 K.

DSC measurements are vital in understanding the extent of dehydrogenation from ammonia borane. The DSC technique has similar sources of errors as found in TGA measurements. It is critical to understand that at lower temperatures the extent of dehydrogenation is significantly slower and hence it is very important and sometimes difficult to determine the start and end point of the thermal event. At 70 °C the thermal event in Figure 152 requires approximately 2250 minutes (37.5 hrs). The amplitude of the signal is very low during these measurements as compared to the ones performed at higher temperatures e.g. at 90 °C. These errors can be minimized by choosing a larger sample size, which as mentioned previously for TGA measurements can cause other errors.[211]

2.4 Experimental Considerations

2.4.1 Desorption vs. Sorption Testing

There are two methods available to test storage capacity: charging an uncharged sample and discharging a charged sample. The more accurate, and less intuitive, approach is to begin with a fully charged sample and measure the maximum amount of hydrogen it can desorb. The desorption approach is preferred because of the lower pressures and larger reservoir volumes associated with desorption, in contrast to the higher pressures and smaller volumes required to drive the sorption reaction. Lower pressures and larger reservoir volumes significantly reduce the errors associated with measurements and capacity calculations.

To illustrate the advantage of desorption-based capacity testing, consider a 1 g sample of storage material with an excess material capacity of 10 wt.% hydrogen (.05 mol H_2) that is tested with both methods at room temperature. During sorption, the amount of gas in the reservoir must be much greater than that in the sample and the equilibrium pressure in the system must be much greater than the pressure of maximum sorption. A gas reservoir of 200 ml and 20 bar contains .16 mol H_2. If the pressure transducer used is rated to 200 bar and is accurate to +/- 1%, then the corresponding error is .016 mol H_2, over 30 % of the excess material capacity of the sample (10 wt.% +/- 3 wt.%)! In comparison, if a larger reservoir (1 L) and vacuum are used for desorption and the low-pressure transducer is rated to 10 bar with the same +/- 1% accuracy, the corresponding error measurement is .004 mol H_2. This represents an error of only 8 % of the sample (10 wt.% +/- .8 wt.%). With this simple calculation it is apparent that desorption testing, with its associated lower pressures and higher volumes, delivers more accurate results than the sorption-based alternative.

Since H_2 is only physisorbed at low temperatures, it is necessary to perform adsorption before a desorption experiment can be attempted. Desorption testing in isolation does not makes sense in this context. However, if desorption is the only process the experimenter is interested in, then the sample can be fully charged in a single adsorption step, followed by a multi-step desorption. Since hysteresis is not typically observed in supercritical H_2 adsorption, the desorption trace usually is equivalent to the adsorption trace. (Hysteresis is typically associated with capillary condensation of subcritical gases in mesopores). Desorption is endothermic, while adsorption is exothermic. Therefore, kinetics may be different for the two processes. Appropriate equilibration times should be used each process to ensure “technical equilibrium” is achieved.

2.4.2 Gas Composition

Both gravimetric and volumetric methods rely on the assumption that weight change and equilibrium pressure change during sorption is due to hydrogen gas alone. Unfortunately, this assumption is not always valid. During dehydriding, it is possible to evolve gases other than hydrogen by chemical reaction of the sample material itself. These evolved gases can contribute to weight change and equilibrium pressure change measured with gravimetric and volumetric methods, respectively, and can contaminate experimental data. One way to account for non-hydrogen gases is to use a residual gas analyzer (RGA) to determine the composition of the desorbed gas. The RGA is connected to the outlet line of the sample holder and tests a representative sample of the evolved gas, outputting the relative composition via the partial pressures of the individual species. A residual gas analyzer commonly used to determine the composition of evolved gas during hydrogen storage experiments is shown in Figure 154.

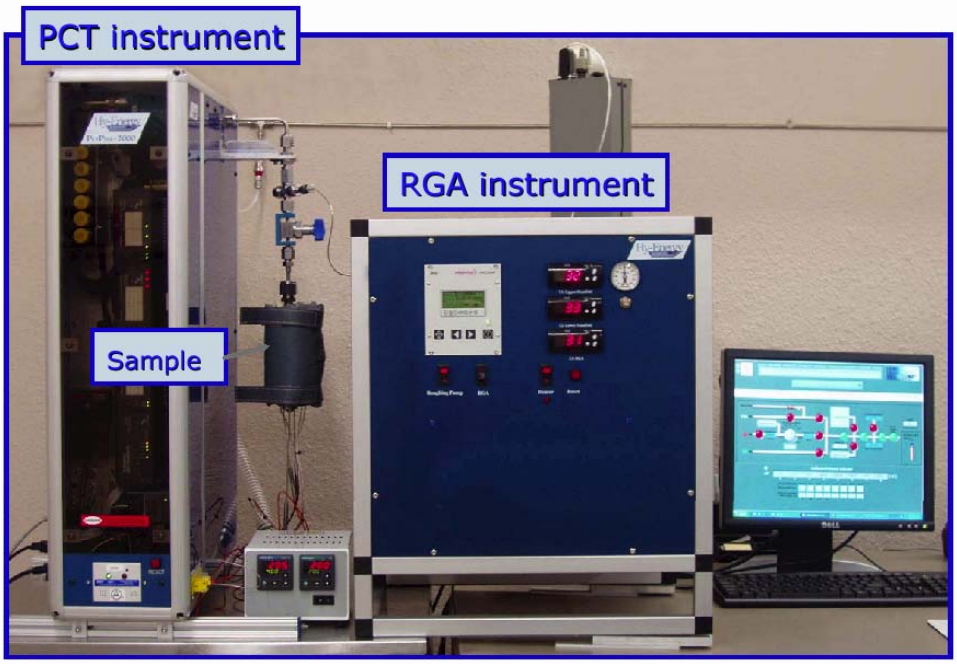

Figure 153. Residual Gas Analyzer set-up.

In a titanium-doped alanate-amide mixture (LiH + Al + $2LiNH_2$ + Mg + TiF_3), the gas evolved from the sample during desorption was not entirely hydrogen. Trace amounts of water and ammonia were found as well, as evidenced in Figure 155.

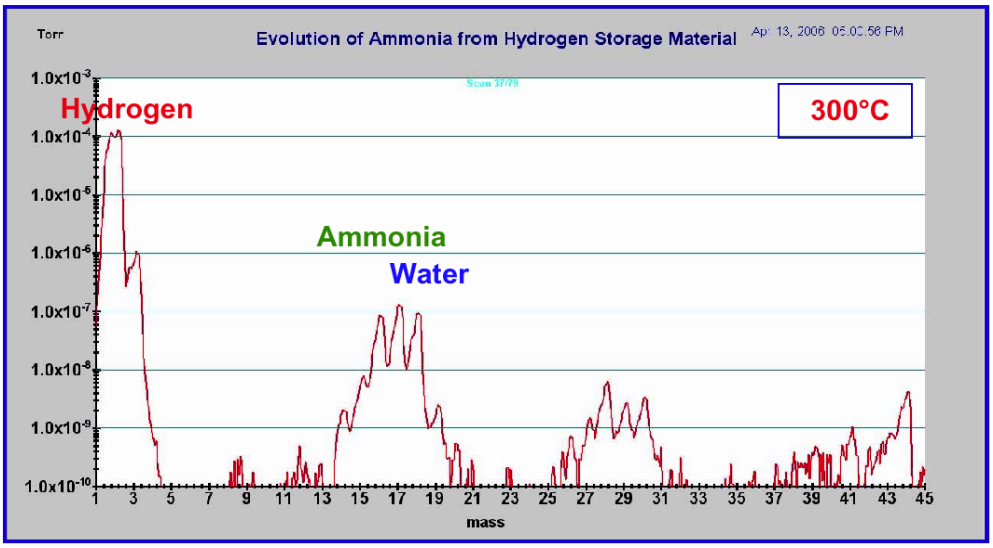

Figure 154. Residual gas analysis of alanate-amide sample discussed in the Kinetics section.[212]

Water is a common contaminant of hydrogen storage materials, generally due to adsorption from air due to improper sample handling prior to testing. The presence of ammonia is much more interesting in this case. Under elevated temperature, the alanate-amide mixture reacted to form ammonia although it is unclear the exact mechanism for the reaction. This type of unforeseen gas evolution reaction warrants accounting for desorbed gas composition variation and the use of a residual gas analyzer to validate the assumptions inherent in the gravimetric and volumetric methods.

Unexpected gas evolution is less common in metal hydrides since the metals involved tend to be stable in metallic form after releasing hydrogen.

Purity of the hydrogen gas that is released is a key criterion for long-term performance of a fuel cell. The 2010 and 2015 targets specify the need for H_2 gas to be 99.9 % pure. Chemical hydrides such as ammonia borane, lithium borohydride, and magnesium borohydride are likely to produce volatile byproducts during the reaction which could possibly poison the fuel cell if not mitigated. The analysis of the hydrogen generated is critical for determining the species generated during hydrogen release these materials. A TGA or volumetric instrument coupled with a mass spectrometer is a powerful tool for this study. The use of gas phase FTIR to quantitatively analyze the gas collected may also provide a reliable analysis of gas phase composition. Additionally a gas chromatograph (GC) equipped with a thermal conductivity detector (TCD), a flame ionization detector (FID) and/or a MS detector can provide for the identification and quantification of gaseous products.

Ammonia borane dehydrogenation releases hydrogen in a three step process as shown previously (Equation 81 - Equation 84). During dehydrogenation ammonia borane undergoes a stepwise cyclic trimerization process resulting in the formation of borazine which is an inorganic analogue of benzene cyclic $(BHNH)_3$. Coupled TG-MS analysis clearly shows a peak of mass 80 (one of several due to the presence of B-10 and B-11 in the trimer leading to a manifold of peaks around m/e = 80) in the dehydrogenation of ammonia borane at higher temperatures, consistent with the loss of volatile borazine.

However, one must be careful using these techniques or a combination of any techniques listed above. It is critical to understand the mechanistic decomposition chemistry of a particular compound, as well as the limitations of mass spectrometry. It is difficult with low resolution quadrupolar mass spectrometers that are typically used in these studies to distinguish between species having masses within 1 unit of one another. For example N_2 and B_2H_6 both give rise to major peaks at mass 28. A detailed analysis of the mass spectrum is required to differentiate between the two species to confirm the presence or absence of diborane during the decomposition of borohydrides.

In the example given earlier, borazine that arises from certain ammonia borane dehydrogenation processes, is difficult to quantify, as accurate preparation of standards of known concentration is experimentally challenging because of chemical stability problems. Because of this fact, there are no commercially available standards for borazine. Therefore, standards must be prepared in the lab as needed from freshly synthesized borazine The most routinely used techniques for borazine quantification include gas chromatography, mass spectroscopy, and nuclear magnetic resonance spectroscopy.. While this discussion has focused on borazine, similar caution should be applied to developing analytical methods for the identification and quantification of any byproduct or gas-phase impurity.

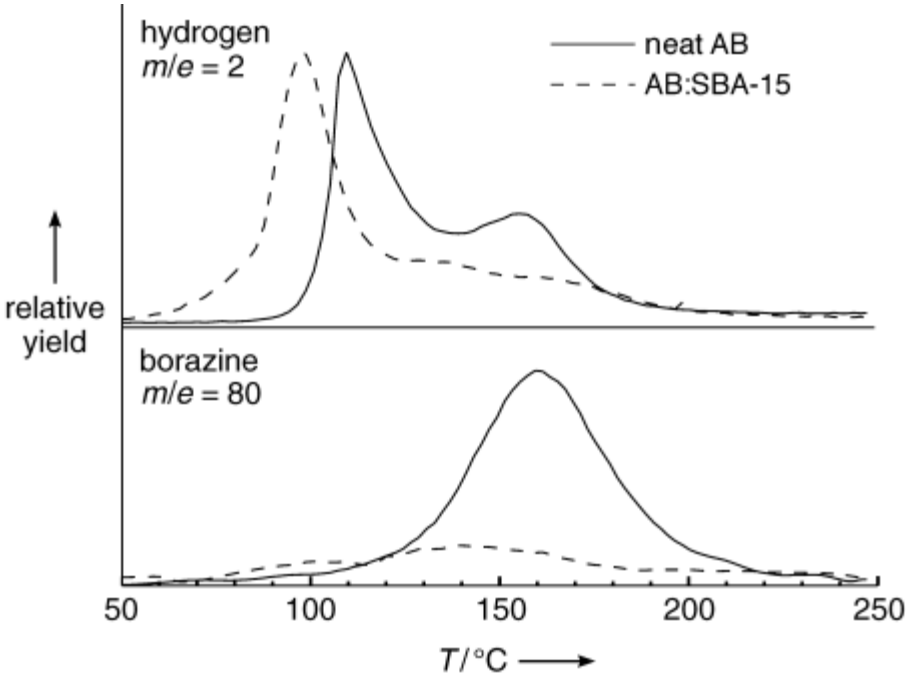

Figure 155. TPD/MS (1 °C/min) of volatile products generated by heating neat ammonia borane (solid line) and AB:SBA-15 (dashed line); m/e=2 (H_2) and m/e=80 (borazine, c-(NHBH)3).

2.4.3 Leaks

Leaks in the connections of volumetric hydrogen storage testing equipment can cause errors in the data. Leaks usually cause unexpectedly high capacities; in a kinetics measurement, they cause absorption or desorption profiles to appear linear in time, as opposed to true sorption profiles that have a curved profile. During sorption testing at above ambient pressures, gas leaked to the environment is mistakenly thought to be sorbed to the sample. Leaks during sub-ambient desorption also affect the capacity by increasing the reading of the amount of gas desorbed with time. For emphasis, for both sorption and desorption, measurements taken with leaking equipment report that the amount of hydrogen gas sorbed or desorbed by a material is greater than it would be otherwise. An example of this is demonstrated in Figure 60, where the expected capacity of the sample is 1.39 wt.%. Absorption steadily increased with a linear behavior until a fitting was tightened about 2 hours in to the experiment. With respect to new materials, weigh on the side of skepticism and repeat the setup and measurements if the results appear too good to be true. Plateau pressures at exactly 1 atm are possible and desirable but highly unlikely.

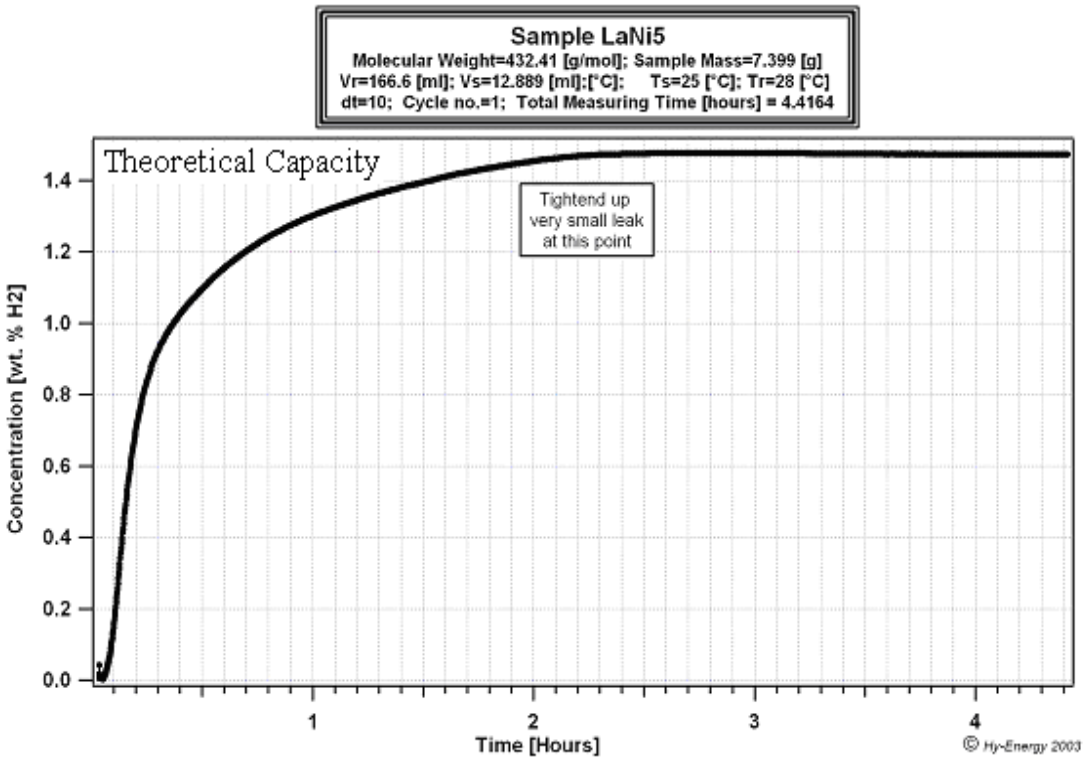

Figure 156. Example of a leak on kinetics measurement. A little after two hours in to the experiment, the leak was eliminated.[118]

Sorption testing of On-board reversible materials is often done at higher pressure where a leak might be more obvious, especially in a static measurement. However, for practical applications pressures near atmospheric are desirable for supply to a fuel cell and for safer fueling.

2.4.4 Discrete Compositions

A volumetric PCT measurement consists of a series of small gas doses that control the concentration of gas given to or evolved from the sample (Figure 157). The last data point of each kinetics measurement, which is assumed to represent equilibrium in composition, pressure and temperature, provides a single point on the PCT curve (Figure 158). This process is performed repeatedly until there are enough equilibrium data points collected to construct a full PCT diagram. Details of these measurements are presented in the introduction section; Volumetric Method 5.3 .

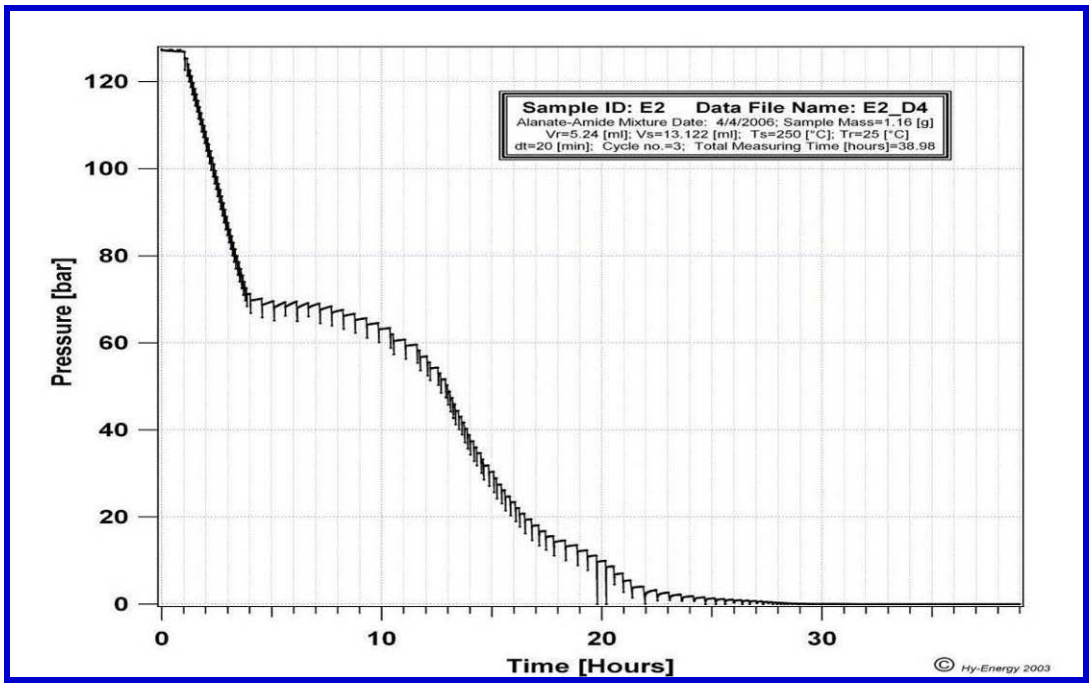

Figure 157. Pressure-time plot of data used to create the PCT diagram of the alanate-amide mixture in the figure below.[57]

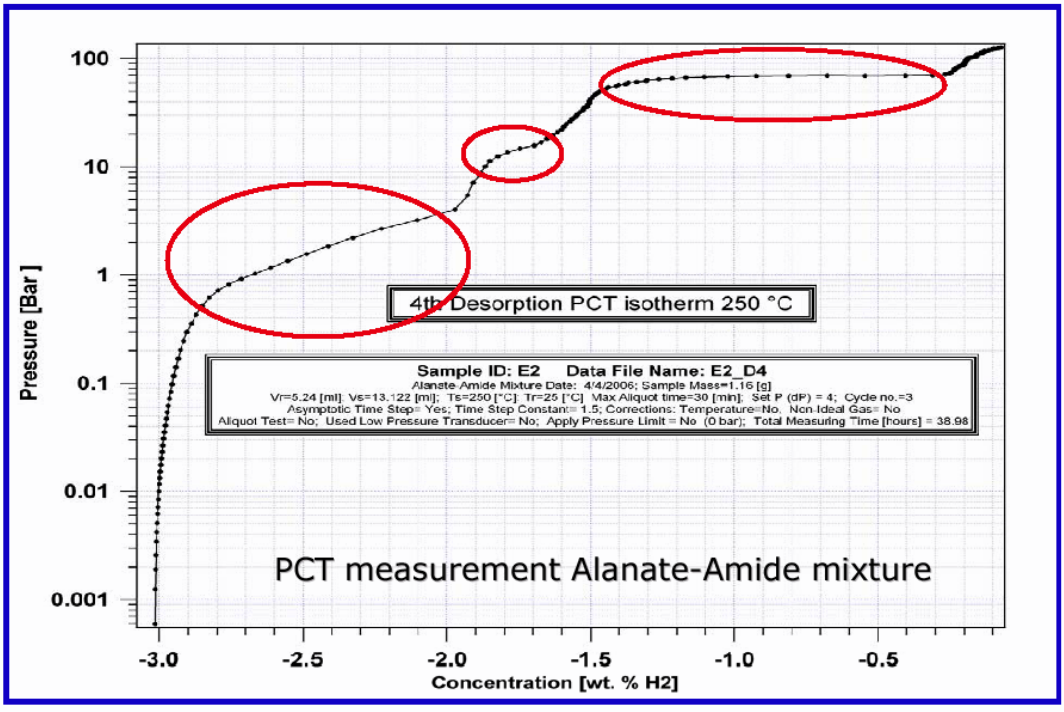

Figure 158. PCT diagram of the alanate-amide mixture.[57]

An advantage of the volumetric method is that this dosing in concentration steps rather than pressure steps enables one to go a specific concentration and stop the measurement to "Prepare or Synthesize" a sample. This method has been used, for example to prepare new compounds by deuteriding to specific compositions to prepare samples for Neutron diffraction measurements and crystallographic analysis.

In addition, a full equilibrium PCT measurement will enable the determination of the range of pressures and temperatures at which different hydrides exist. While plateau pressure vary slightly, this information can then be used to prepare deuterided samples, *in-situ* during NPD (Neutron Powder Diffraction) studies to determine the crystal structure and deuterium site occupations of each individual deuteride phase. An example of this is can be seen in the PCT measurements by Chotard et al. for hydrogen absorption in $LaMgNi_4H_X$ (Figure 159). These measurements were used to determine the hydrogen content and thermal stability of the various hydride phases, and compared to the *in-situ* deuteriding NPD measurements and crystal structure refinements.[213]

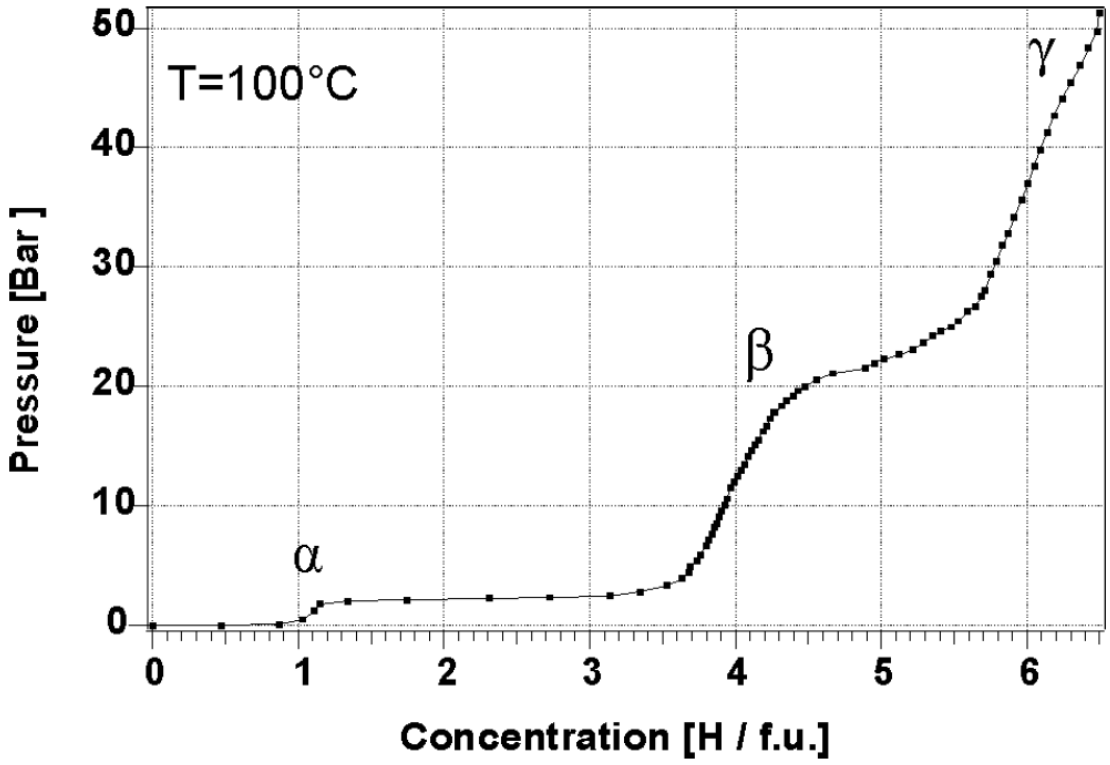

Figure 159. Pressure-composition-isotherm of LaMgNi4 - H system during absorption at 100°C and approximate upper phase limits (α, β, γ).[213]

2.4.5 Effect of Sample Size

The size of a sample determines the quantity of gas that is adsorbed. In both volumetric and gravimetric measurements, the ability to make accurate capacity measurements improves when making measurements on larger samples. In order to make sensitive volumetric measurements, the amount of hydrogen sorbed/desorbed by the sample should cause a pressure change in the calibrated volume of the system which is at least 10x the resolution limit of the measuring pressure transducer. A specialized volumetric instrument consisting of a small 7.5 ml sample cell and 7.6 ml reference cell was reported in Ref. 145, which was capable of making precise measurements of small adsorption volumes. Similarly, in gravimetric measurements the sample's weight change on sorption/desorption should be at least 10x the resolution limit of the balance.

In order to investigate the effect of sample size on adsorption amount, the experimenter can measure a series of isotherms using different masses of adsorbent. If the isotherms appear relatively independent of the adsorbent mass, then it can be concluded that sample size is not a significant factor. On the other hand, if the isotherms do depend on the mass of adsorbent, this is an indication of either experimental error or of a sample size which is too small.

The ability to make good capacity measurements has been an issue that is particularly problematic for physisorption materials because of the very small quantities of sample that are sometimes available (CNTs) and also because of the low packing density of high-surface area material which effects both buoyancy corrections for gravimetric measurements and the amount of sample vs. the free gas volume in the sample holder of volumetric measurements. While it has generally been assumed that small sample quantities limit measurements to gravimetric techniques, in fact, quite accurate measurements can be made on well designed volumetric equipment. Such measurements are shown in Figure160 for hydrogen sorption on 2 milligram samples of single-wall and multi-wall carbon nanotubes at room temperature. [214]

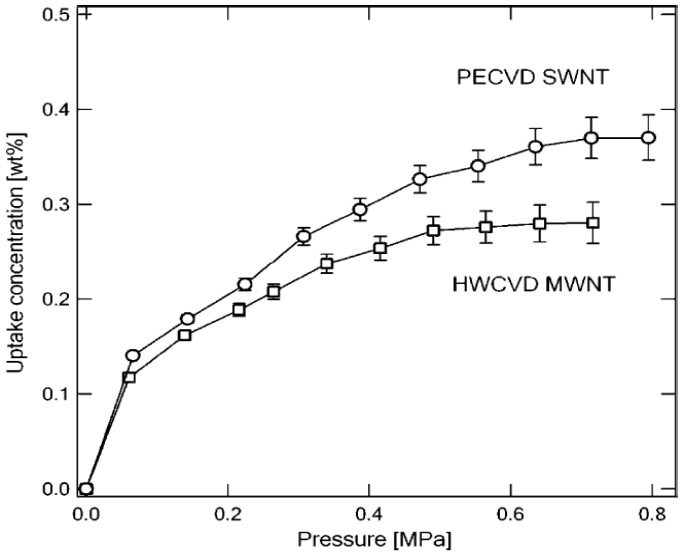

Figure160. Example of volumetric measurements on very small quantities of physisorption materials. Room temperature PCT isotherms from 2 mg PE CVD SWNT and HW CVD MWNT.[214]

To validate the measurements, similar runs were made a small blank sample (stainless steel) and on an activated carbon sample (39 mg) at room temperature (Figure161**a**). These showed no absorption for the blank sample and characteristic absorption for the carbon sample.

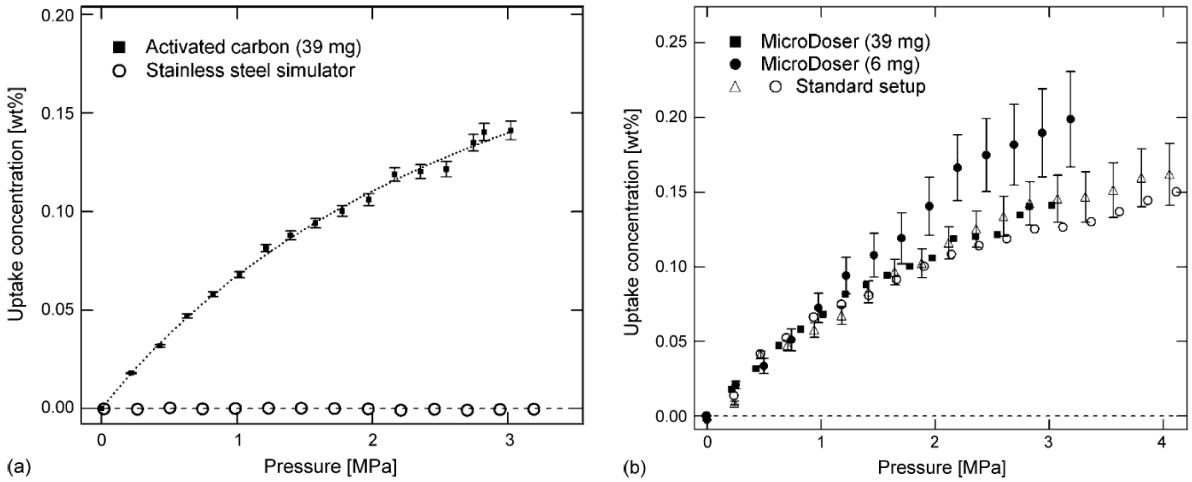

Figure161. Example of effect of sample size on the accuracy of measurements for physisorption materials. (a) Hydrogen uptake PCT isotherm of 39 mg of activated carbon sample and a stainless steel blank with the same gas displacement volume, and (b) comparison of measurements using the MicroDoser (39 and 6 mg) with those obtained using the standard sample holder setup with a 251 mg activated carbon sample (open triangles and circles).[214]

This was followed by measurements using a standard volumetric instrument on 251 mg of the same activated carbon sample and a 6 mg sample using a MicroDoser volumetric device (Figure161b). Some deviation was observed in the smallest sample and the results were similar for the 39 and 251 mg samples measured using different devices.[214] Overall, the results were quite reproducible and indicate that SWNT and MWNT hydrogen sorption behavior at room temperature are similar to activated carbon.

Most studies related to chemical hydrides are performed on a small scale as mentioned previously. Significant work needs to be performed to better understand these issues. A measurement on a large sample is inevitable when generating data for sample size effect on capacity. The main issue for measurements will be the exothermicity of the reaction. At larger scales, heat transfer from the samples to the external environment may be inefficient, and hence the temperature of the sample may rise, increasing the rate of hydrogen evolution yet further convoluting the measurement. Ensuring efficient heat transfer is a key to the accuracy of these measurements. Techniques such as providing for a large but thin layer of material in good thermal contact with a relatively massive thermostated heat source may mitigate these types of problems.

As mentioned in the sections DSC and TGA measurements, there are complications due to the contradictory requirements for sample size. It would be optimum for TGA to start with smaller amounts of sample to minimize mechanical errors associated with foaming. However, at lower temperatures the hydrogen release is significantly slower hence producing a very low amplitude signal that can create errors in the DSC measurement.

Thin films are popular in fundamental studies due to the increasing complexity of new materials. Thin film deposition techniques such as sputtering and pulsed laser deposition (PLD) can be readily tuned to make films of varying composition to study many material compositions in one sample. Another advantage in using thin films in fundamental studies is that the effects of kinetics can be dramatically reduced in the limit of extremely thin films. However, it is important to maintain a focus on the goals of the experiment at hand when deciding whether to use a thin film or a bulk sample where heat and mass transfer are decidedly different. For example, it does not make much sense to spend a lot of time measuring the reversible capacity of a thin film, since kinetics play such an important role in determining the reversible capacity of a practical system.

Capping layers are often used in fundamental studies of metal hydrides due to their highly oxidizing nature. Often the capping layer is also a catalytic material such as palladium, which allows the experiment to be run under more reasonable temperature and pressure conditions. However, it is important to keep in mind that a catalytic capping layer may lead to dramatic improvements in a thin film with short diffusion lengths, but may be much less effective in a bulk sample where the catalytic effect would be concentrated in a surface layer only.

2.4.6 Efficient Testing

Progress in the discovery, development and fundamental characterization of hydrogen storage materials is dependent on the ability to perform measurements with speed and efficiency. The hydrogen storage capacity of a material is usually the first characteristic that is measured and used as a "select-or-dismiss" gauge in the rapid scanning / discovery phase of research. For this reason, it is critical that the measurement of storage capacity is not only efficient but accurate. Improved accuracy, in its own way, increases efficiency. Any technique that reduces sample characterization time or improves accuracy will help in improving the pace of material discovery and development.

In bench scale studies for off-board chemical hydride material screening, gas burette systems have been routinely used to determine hydrogen gas release kinetics of sodium borohydride and ammonia borane systems. For low pressure measurements, simple gas burettes with manual measurements at intervals are easy to set up but are not adequate to study fast kinetics (e.g. reaction half times of less than minutes) or to carry out high throughput testing. Automated gas burettes of various designs have been reported in the literature. Piston-cylinder-type burette systems can measure gas volume changes at constant pressure if they are equipped with a linear actuator that is driven by a pressure controller. Zheng et al reported on details of a gas burette system using only pressure and temperature sensors, which is capable of continuously recording the gas evolved as a function of time to a computer.[215] In this system, the moles of gas generated are calculated from the volume, pressure, and temperature change of the gas phase assuming ideal gas P-V-T behavior as a function of time. Integrating the quantity of gas evolved over time yields a measurement of capacity. While the burette pressure and all process temperatures are measured directly, the volume of the gas in the burette is calculated by relating the burette pressure to the liquid level difference between the burette and a reservoir containing the working fluid. The pressure in the reactor can also be calculated similarly. Thus, at any moment the amount of gas released was simply the difference between the number of the moles of gas in the system and the moles of gas before the reaction.

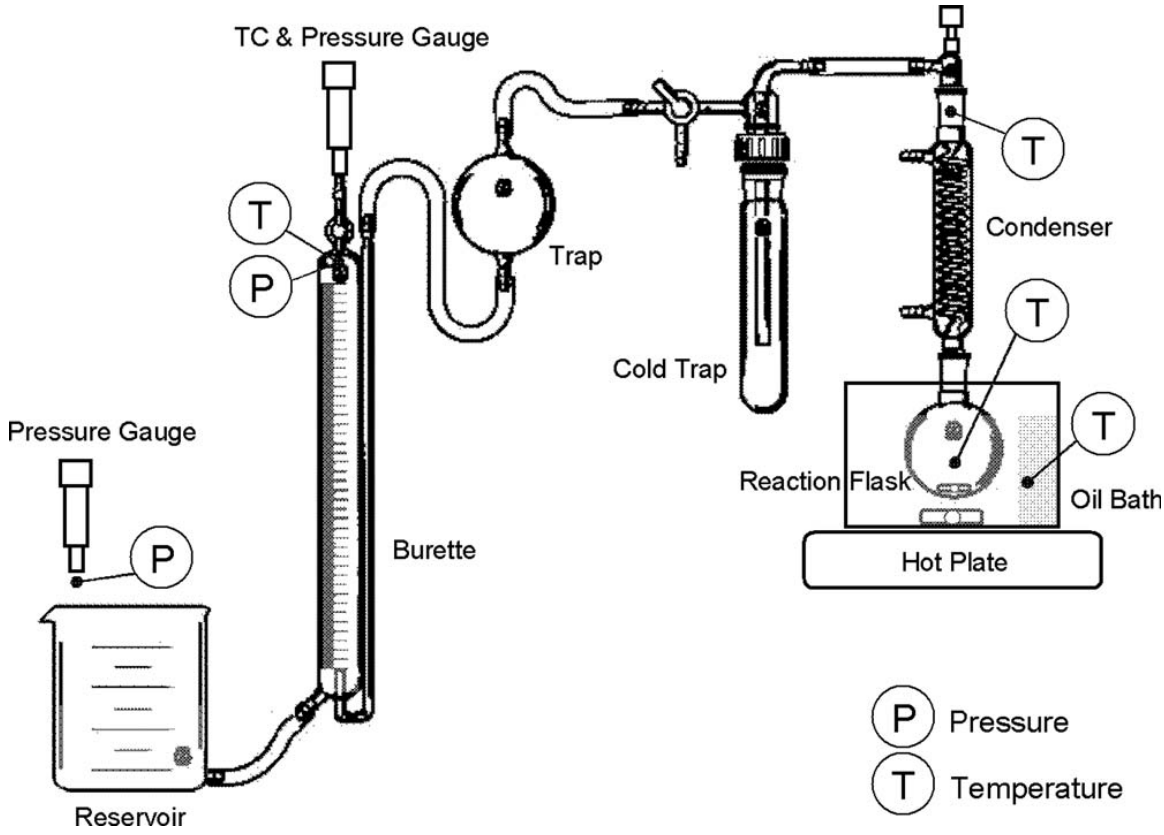

Figure 162. Schematic of a automated burette system used for Capacity and Kinetics measurements.

2.4.7 Thermal Effects

Large temperature variations can occur locally due to the exo- and endothermic reactions and inadequate material thermal conductivity. The need to achieve equilibrium in reversible systems has been well documented in the introduction and kinetics sections. Thermal equilibrium is also extremely important in capacity measurements, particularly reversible metal hydrides which are typically largely exothermic during hydrogen loading. Total capacity measurements should always be made under conditions as close to equilibrium as possible, but this may be difficult and time consuming.

Reversible and usable capacity measurements may be more focused on practical applications rather than maintaining equilibrium during testing. However, it is still important to consider the heat transfer effects. For example, an insulated sample may yield unrealistically high reversible capacity numbers because of the heating effect during absorption, whereas a practical application may result in more heat transferred away from the sample and therefore reduced performance.

2.5 Potential Materials Improvements

2.5.1 Doping

In most fundamental studies, small sample sizes are used. This can simplify a study significantly, but can also be misleading. For example, for a small sample, it is easy simply to deposit a catalyst on the surface, since diffusion lengths are typically small and the catalytic effect should work on most of the sample. However, this principle does not apply very well to a bulk sample, where the surface area to volume ratio is much less advantageous. It is often necessary to distribute a catalyst throughout a bulk sample to achieve full effectiveness.

Doping has been shown to be an effective way to distribute a catalyst throughout a material to make reversible hydrogen storage feasible. Bogdanovic and Schwickardi demonstrated that doping sodium alanate with transition metals, particularly Ti, improves reaction kinetics and reduces the temperature associated with and equilibrium hydrogen pressure of 1 atm. For example, by doping $NaAlH_4$ with 2% $Ti(OBu)_4$ they were able to evolve about 4.5 wt% hydrogen in 1 hr versus 22-24 hrs for the undoped sample.[34]

2.5.2 Grain/particle Size Effects

Decreasing grain/particle size in a potential hydrogen storage material can lead to a significant increase in sorption/desorption rates due to the increase in grain boundaries and therefore an enhancement of hydrogen diffusion throughout the sample. Since this is purely a kinetics effect, it will only enhance the reversible or usable capacity, not the total capacity. Therefore this technique is of particular interest for on-board reversible materials where the fueling time is a more significant parameter.

2.5.3 Alloying

Many potential materials for on-board reversible storage, such as MgH_2 and LiH, have favorable total capacities, but are too thermodynamically stable for practical applications. It is impossible to overcome thermodynamic barriers by addressing the kinetics alone, so much research has been focused on reducing the thermodynamic stability of materials with a high total capacity. One technique is to alloy the stable metal with a metal that forms a less stable hydride such as Ni or Al. For example,

Mg_2NiH_4 has been showing to have an enthalpy of formation of -65 kJ/mol H_2, compared to -75 kJ/mol H_2 for MgH_2. However, the addition of nickel leads to a significant reduction in total capacity (down to 3.6% from 7.7%), while still falling short of the ideal enthalpy of formation of -39.2 kJ/mol H_2. The ideal enthalpy of formation in this case is determined as the value that would lead to an equilibrium hydrogen pressure of 1 atm at 100 °C as determined by the Van't Hoff equation.

2.5.4 Capping Layers

Capping layers can be very useful in preventing oxidation and as a simple catalyzing layer for fundamental studies. This can speed up the search for potential materials, but does not necessarily translate into good system level performance. Many of the commonly used materials, such as Pd, are heavy and expensive, and therefore not practical for real applications. In addition, a capping layer will be much more effective on a thin film than a bulk sample.

2.5.5 Chemical Hydrides Materials Improvements

A combination of theory and experiments is being used to design molecules with improved capacity of off-board regenerable materials. Certainly most of the off-board regenerable chemical hydrides have very high capacity to begin with. Additions of catalysts or additives to influence the kinetics of release clearly impacts the gravimetric capacity of the material. If far more efficient additives and catalysts can be developed, reduced amounts of catalysts can be added which will mitigate some of the effects of the additives on the capacity. Theoretical studies can predict certain stable species which may not have been synthesized as yet but have the potential to contain useful amounts of hydrogen with potentially improved thermodynamics of release.

Another approach to high capacity materials is to focus on compounds that can potentially couple exothermic and endothermic release processes within the same molecule, with the goal to provide near-thermoneutrality. Two examples of such an approach are outlined below. One involves the tuning of the electronic properties of aromatic hydrocarbons to potentially couple an exothermic oxidation reaction with endothermic dehydrogenation in an attempt to 'assist' dehydrogenation toward lower heat input requirements. A second example relies on an attempt to couple the exothermic dehydrogenation of a B-N fragment of a molecule that also contains C-C fragments that are dehydrogenated endothermically, again with the goal of coupling of the thermodynamics of two potentially cooperating reactions to drive towards lower intensity de/rehydrogenation cycles.

The first example comes from the group at Air Products led by Alan Cooper and Guido Pez. This team has focused on the development of liquid hydrogen carriers derived from the reversible hydrogenation of aromatic organic molecules. This team has a series of patents in this area.[216,217] This general topic has been recently reviewed by Crabtree.[218] Liquid carriers are likely to be more readily integrated into existing fueling infrastructures, and are a highly desired format for a hydrogen carrier.

Releasing hydrogen from saturated cyclic hydrocarbon carriers by catalytic dehydrogenation is in general quite endothermic, but may be performed with reasonable rates and high yields to produce cyclic aromatic hydrocarbons. The prototypical example of this is the reversible catalytic cycle of hydrogen plus napthalene to produce decalin, as indicated in Equation 107.

Equation 107

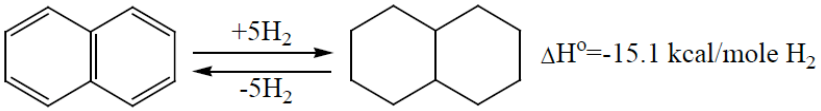

The hydrogenated hydrocarbons are readily dehydrogenated catalytically with very high yields, making these liquid carriers recyclable. The Air Products team demonstrated that by the judicious choice of appropriate nitrogen or oxygen substituted hydrocarbons, that the dehydrogenation temperatures could be reduced but not to temperatures accessible using the waste heat of an operating fuel cell. To attempt to circumvent this barrier, they demonstrated the very clever idea of coupling an exothermic oxidation reaction with the endothermic dehydrogenation, all within the same storage molecule. As indicated in the figure below, heat from the exothermic oxidation of one portion of the molecule (step 3) nearly balances the heat required to drive the endothermic dehydrogenation reactions (step 2), thus in principle mitigating the need to add heat to the system by burning some of the produced hydrogen, which would reduce the effective storage capacity. One potential drawback to this approach is that one mole of hydrogen is consumed in making water during the recycling of the oxidized spent fuel (step 1). Nonetheless, this autothermal approach was demonstrated in the laboratory to operate efficiently at temperatures in the vicinity of 200 °C with high yields (>99%) in each of the three steps required to complete the cycle, and was demonstrated to be recycled multiple times.

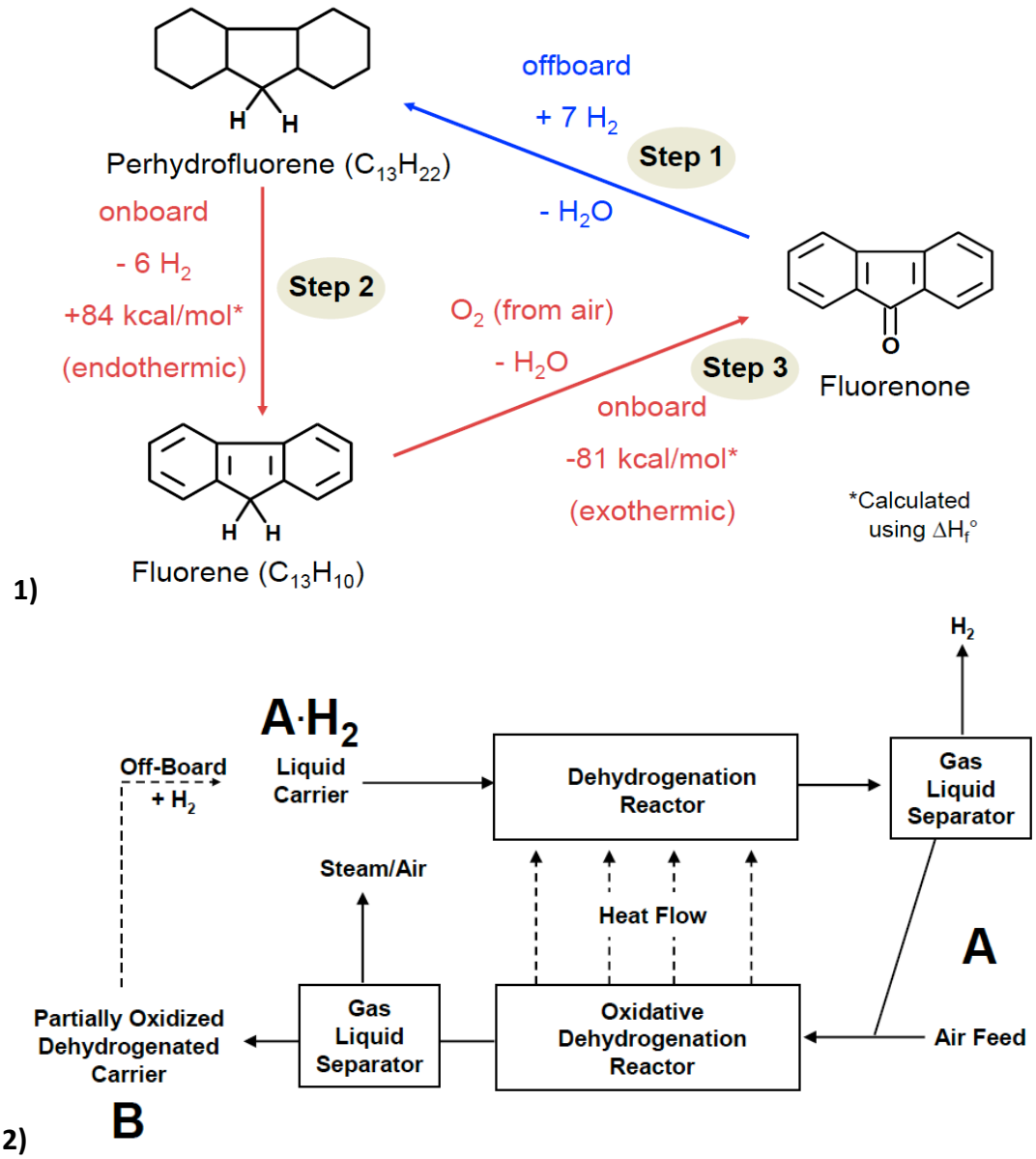

Figure 163. 1) The three step autothermal cycle demonstrated by Cooper et al (preceding page). 2) The block diagram indicating of a potential reactor scheme to transfer the heat of the onboard oxidation reaction (step 3) to the endothermic onboard dehydrogenation reaction (step 2). The spent fuel 'B' is then rehydrogenated in an off board catalytic regeneration process.

A second example comes from the group at the University of Oregon led by Shih-Yuan Liu. Liu's group has developed new synthetic routes to hybrid organic/inorganic benzene like systems.[219,220] These materials are based upon the substitution of boron and nitrogen in a benzene ring. While materials such as borazine have been known for close to 100 years hybrid materials such as the 1,2-dihydro-1,2-azaborine (Figure 164) were only prepared in 2008.[221]

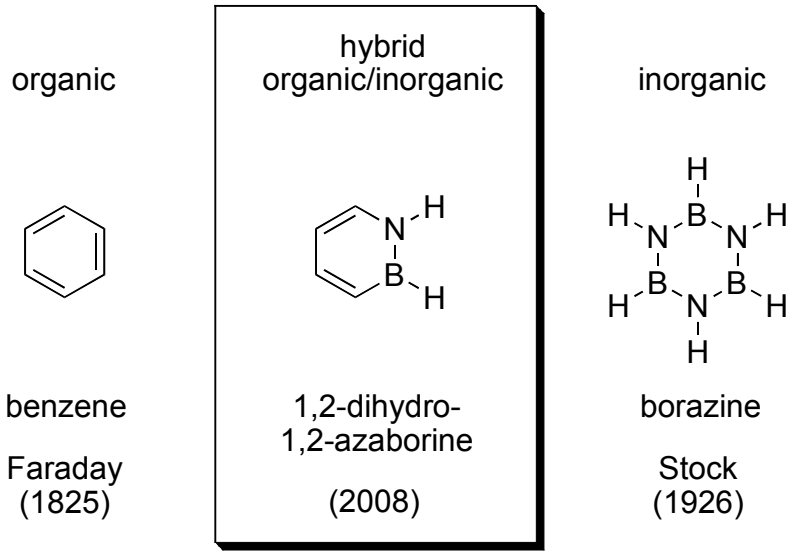

Figure 164. Benzene, borazine and hybrid materials 1,2-dihydro-1,2-azaborine.

With a synthetic route to these elusive compounds it is now possible to assess the possible of coupling the exothermic H_2 desorption from the *B-N* bond with the endothermic H_2 desorption from *C-C* bond in a cyclic system. The key goal here, like in the Air Products approach, is to tune the thermodynamics for the overall H_2 absorption/desorption process and approach a more thermoneutral system. Calculations in collaboration with David Dixon at the University of Alabama indicate that the coupled release of hydrogen from these organic-inorganic hybrids is much more favorable than in either benzene or borazine alone.

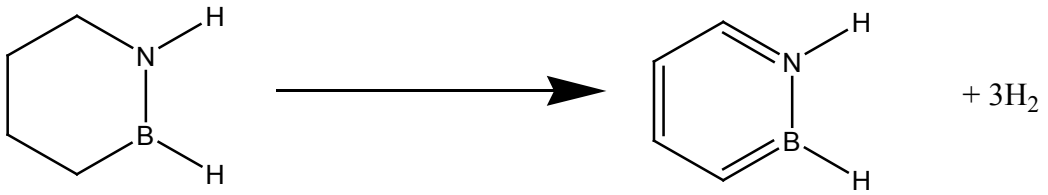

$\Delta H = 23$ kcal/mol, $\Delta G = -2$ kcal/mol

While the development of this hydrogen storage system is only in its infancy Lui's synthetic methodology is extremely versatile and the systematic tuning of these molecules may lead to a system that provides the correct balance of thermodynamics and kinetics for a liquid based onboard storage media. In particular the development of the fused ring systems will enable an approach which effectively unites the Air-Products systems with the ammonia borane chemistry,[222] see Figure 165.

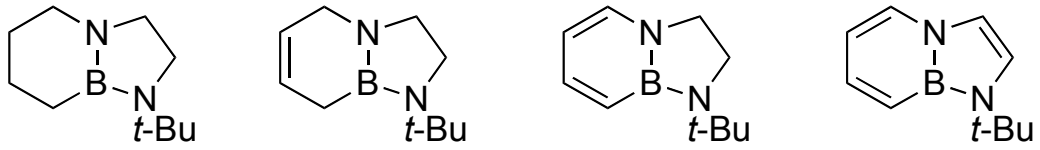

Figure 165. Fused ring systems.

While the development of new materials from Liu's group has been impressive over the last year, significant challenges still remain. In particular, the development of catalysts that enable the coupled hydrogen release from both the C-C and B-N bonds are required.

2.5.6 Physisorption Materials Improvements

The extent of physisorption is generally proportional to the surface area and porous volume of the adsorbents. As a result, optimization of these materials for high hydrogen storage capacities on a gravimetric basis usually involves the maximization of these two structural properties. The class of materials known as Metal-Organic-Frameworks (MOFs) is particularly interesting in this regard, as both the surface area and pore volume of these materials can be tuned during the synthesis. In particular, this can be done by judicious choices of organic linkers and secondary building units SBU.[223]

It has been found, for example, that the pore size, as well as the amount of hydrogen adsorbed, is related to the length of the linker unit of the particular MOFs (see Figure 166).[224] Moreover, the same changes in the length of the linker unit were shown to lead to differences in the magnitude of the adsorption enthalpies.[163] The preparation method can also be improved to get higher storage capacities on certain MOFs, as shown for the IRMOF-1.[225] Post-synthesis optimization approaches are also investigated. These approaches include, among others, doping with metals and acidic treatments aiming at creating high affinity sites, especially on carbon structures. In the latter case, the resulting effects appear be a higher affinity for the hydrogen, and higher adsorption at relatively low pressures.[226]

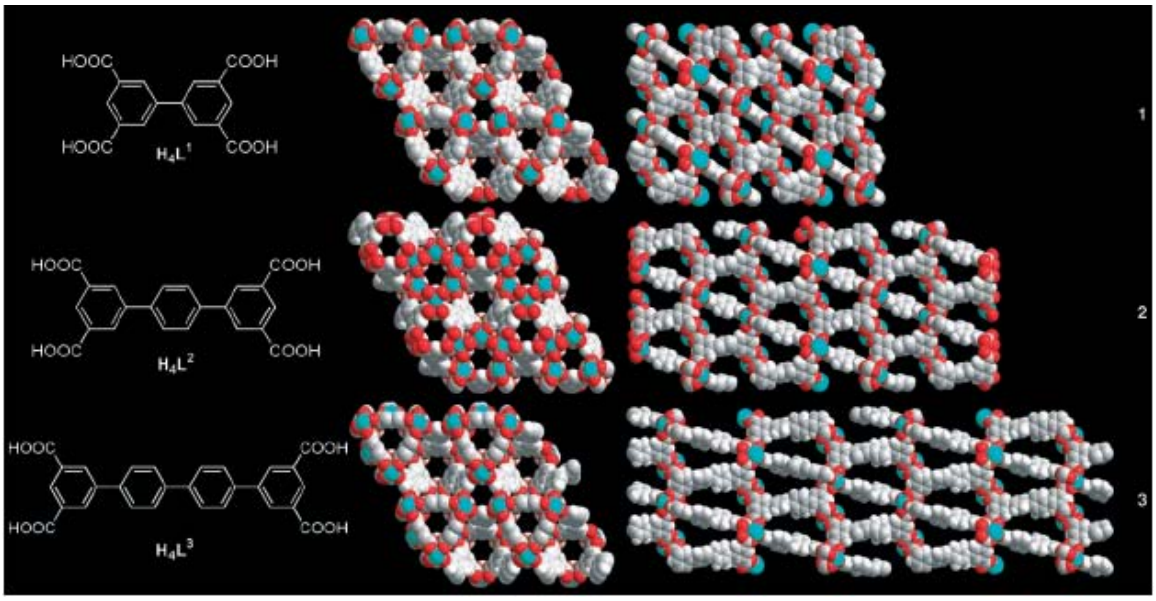

Figure 166. The pore size of microporous Metal-Organic Frameworks materials can be tuned during the synthesis to optimize the adsorption properties of the material. In this case, different linker sizes were used to vary the pore width.[224]

Section 4: Thermodynamic Measurements

The study of thermodynamics determines fundamental properties of hydrogen storage materials that can only be changed by altering the physical structure or composition of the material. Knowledge of these properties can help determine whether the desired performance is possible, but does not present the complete picture. Knowledge of the kinetics and other factors will ultimately determine whether the theoretical performance is achievable.

This section will give a brief introduction to the basic concepts of thermodynamics and then focus on the difficulties that can arise in making accurate measurements and interpreting the data.

1 Introduction and Definitions

The following is a brief introduction to the general concepts of thermodynamics and some of the basic applications to hydrogen storage materials.

1.1 Basics of Thermodynamics

Thermodynamics is the study of equilibrium states and the transitions between them. For the measurement of any thermodynamic variable such as temperature or pressure to make sense, the system must be in equilibrium. However, this is rarely the case in real applications, particularly for temperature, which often varies throughout a system. A common assumption used to get around this difficulty is that a system is in local thermodynamic equilibrium when measurements are made in systems with thermal gradients. Reaction kinetics in many hydrogen storage material systems may be very slow and reaching true thermodynamic equilibrium may be difficult or impossible in a reasonable time scale. This is particularly true of hydride materials (alanates, borohydrides and destabilized hydride mixtures) that require the mobility of not only hydrogen, but also other constituent elements to form or decompose the hydride. For thermodynamic measurements to be valid one must be cognizant of these kinetic

limitations and ensure that appropriate equilibrium conditions have been achieved or accounted for.

1.1.1 Laws of Thermodynamics

The laws of thermodynamics cannot be directly proven, but rather are based on practical observations that have been shown to be consistent over centuries of experience. They describe the specifics of how energy heat and work can be transported in thermodynamic processes. The laws are stated and summarized below:

0th law – If two thermodynamic systems are in thermal equilibrium with a third system, then they are in thermal equilibrium with each other. This law validates the comparison of temperature measurements between separate systems.

1st Law – Energy can neither be created nor destroyed. It can only change forms. This law is simply a statement of the conservation of energy.

2nd Law – It is impossible for any system to operate in such a way that the sole result would be an energy transfer by heat from a cooler to a hotter body. This statement is the Clausius statement. Other phrasings are available which bring out other subtleties of the 2nd law. The basic concept is that the net change in entropy of a system and its surroundings cannot be negative. In practice, the net change in entropy will always be positive.

3rd Law – As temperature approaches absolute zero, the entropy of a system approaches a constant minimum. This law serves to define the concept of absolute zero temperature, as well as making calculations of absolute entropy possible.

1.1.2 First Law of Thermodynamics

The first law of thermodynamics, conservation of energy, merits further discussion, as it is useful in many different forms. The most basic formulation is presented in Equation 108, which simply states that the total energy in the universe is the combination of the energy in the system under study and the energy in its surroundings.

Equation 108

$$E_{Universe} = E_{System} + E_{Surroundings}$$

In general, energy can be exchanged between the system and its surroundings in the form of work or heat. Work energy comes in many different forms. For example, mechanical work is the force times the displacement of an object, while electrical work is the potential difference between two points on an objects path times its electric charge.

More information can be determined from the first law when the surroundings are considered to be a reservoir for thermal and mechanical energy to make it easier to evaluate gains and losses in energy. This is shown in Equation 109.

Equation 109

$$E_{Universe} = E_{System} + E_{Thermal-res} + E_{Mechanical-res}$$

A more familiar form of the first law arises from considering changes in heat, $q = -\Delta E_{thermal-res}$, and work, $w = -\Delta E_{mechanical-res}$, or on an infinitesimal scale $\delta q = -dE_{thermal-res}$ and $\delta w = -dE_{mechanical-res}$. A negative sign is included because we are considering changes in heat and work of the system. The first law can now be expressed in differential form as shown in Equation 110. The subscript system is dropped because the change in energy of the universe is always zero. It is also important to note that δw is included as a positive term in Equation 110, implying that work done on the system is considered positive. Another commonly used sign convention includes δw as a negative term, meaning that work done by the system should be considered to be positive.

Equation 110

$$dE = \delta q + \delta w$$

In Equation 110, the symbol for the increment of energy and the increments of heat and work are different. The symbol δ emphasizes that the infinitesimal increments of *q* and w are not perfect differentials, meaning that in a transformation their changes depend on the path followed by the system moving from an initial state to a final state. Consider a property *E* of a system, identified and well defined, that takes a value E_i when the system is in state *i* (initial) and a value E_f when the system is found in state f (final). The change in the property *E* will then be $dE = E_f - E_i$, whatever the path linking the two states. This statement introduces a state function whose differential *dE* is exact. The energy of a system satisfies this relation and may be identified as being one of its properties, but this does not apply to heat or work. Stated differently, work and heat cannot be assigned to one given state of the system but they belong to the process of transformation of the system.

1.1.3 Classical Thermodynamics

The basis of classical thermodynamics is a macroscopic view of the materials of interest. Properties are averaged across an entire system and it is assumed that the individual behavior of molecules can be ignored. While classical thermodynamics will be sufficient to study most aspects of hydrogen storage systems, some approaches to improve performance may require knowledge of interactions on the molecular scale. This often requires quantum mechanical calculations which fall under the realm of statistical thermodynamics.

1.1.4 Statistical Thermodynamics

Statistical thermodynamics, also known as statistical mechanics, considers matter from the microscopic viewpoint. Both classical and quantum statistics are used to determine the behavior of individual molecules in a system. The macroscopic values of properties are determined by averaging over a large number of molecules. Statistical Thermodynamics is particularly important when there are small length scales in a problem or in systems with rarefied gases so that the assumption of a continuum becomes invalid.

1.1.5 State Variables

The state of a system is defined by a set of independent variables, such as pressure, temperature, internal energy and volume. The specific variables required to define the state vary with the type of system, as discussed in the next section. Typically, once three state variables are determined, all other state variables can be calculated from known relationships.

One important aspect of state variables is that they can be defined at any point with no knowledge of the process required to get there, as noted in section 1.1.2 . Other important variables, such as heat and work, are path dependent, and therefore cannot be used to define the state of a thermodynamic system. An example of this is presented in Figure 167, showing two hypothetical processes to change the system from state 1 to state 2. The pressure and volume at states 1 and 2 can be measured and do not depend on whether path A or B was followed. However, the amount of PV work performed, represented by the area under the curves if the processes are reversible, clearly depends on the path, and therefore cannot be used to uniquely define the state.

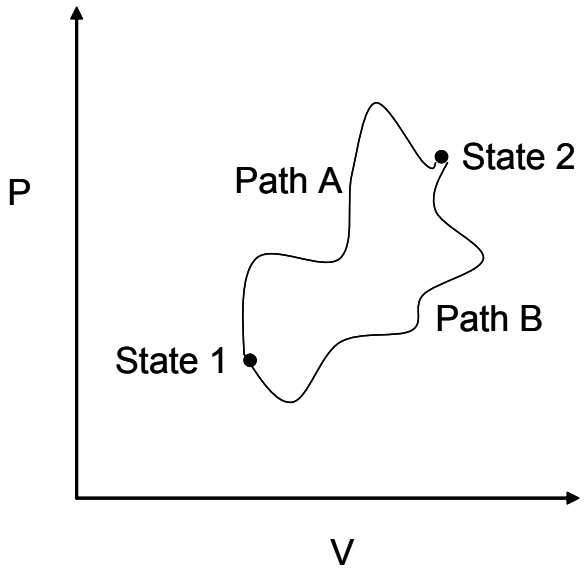

Figure 167. Image depicting the distinction between path dependent and independent variables.

It is also useful to consider the concept presented in Figure 167 mathematically. First, consider points 1 and 2 in the P-V space connected by two hypothetical piecewise smooth curves designated Path A and Path B. Let *F(x,y,z) = F(r)* be a continuous vector function whose partial derivatives exist. Then the line integral of the function F over Path A or B between the initial point 1 and final point 2 will in general depend not only on F and on the end points of the path but also on the path along which the integral is carried out. If F is a force then the line integral is the work done by the applied force in the displacement on a body of mass m. The result shows that the work done equals the kinetic energy, and that the amount of work done will differ if a different trajectory is selected.

Equation 111

$$Y = \int_{1}^{2} F(r) \cdot dr$$

A path independent variable is one which produces the same value in integrating from 1 to 2 along any path.

For a closed curve, the independence of path of the line integral is obtained if and only if its value around the closed path is zero. If we have independence of path, integration from 1 to 2 along Path A and B gives the same value. A and B taken together form a closed curve. Now, when integration is done from 1 to 2 along A and then in the opposite direction along B (the integral is multiplied by -1) the sum of the two contributions is zero.

We know from mechanics that Equation 4 represents the work done by a force F in a displacement of a body of mass m. Then we learn that work may be independent of the path if and only if it is zero for displacement around any closed curve. Moreover, the first part of the discussion tells us that this happens if and only if *F* is a gradient of a function (potential). *F* and the vector field defined by *F* are called conservative, because in this case mechanical energy is conserved. That situation occurs only for an adiabatic transformation observed in a closed system where. In other words, δq = 0. Here, we stipulate that we are dealing with a closed curve. For example the kinetic energy of a body represents the ability of a body to do work by virtue of its motion. If the body moves in a conservative force field, like gravity, then after the completion of a loop the body returns to its initial position with the same kinetic energy it had at the starting point.

1.1.6 Thermodynamic Systems

The definition of the system under consideration is fundamental to the study of thermodynamics. A thermodynamic system is separated from its surroundings, often called the environment, by an arbitrarily defined boundary. The properties of the boundary, such as whether it is fixed or flexible, or allows the exchange of quantities such as mass or energy, determine the type of system. The state of each type of system can be completely determined by the measurement of a set of independent variables. In most cases, only three state variables are required, but by taking advantage of constant properties defined in a given system, this requirement can usually be reduced to only two, as outlined below.

1.1.6.1 Isolated System

The most basic system, and therefore also the most idealized, is the isolated system. This is a system that has no exchange of mass or energy with its surroundings. Therefore, the internal energy is a constant, and only two other variables, such as the pressure and temperature, are required to completely define the state of an isolated system.

1.1.6.2 Closed System

A closed system is defined by flexible theoretical boundaries surrounding a fixed mass. Energy is allowed to transfer across the boundaries of the system, but no mass. For a gas system undergoing no reactions, the number of moles is constant, and out of the

easily measured variables pressure, volume and temperature, only two need to be determined to define the state of the system. Of course, most systems involving hydrogen storage materials will involve reactions, so this assumption is not usually valid.

1.1.6.3 Open System

An open system, otherwise known as a control volume, is a system of fixed volume. The boundaries are rigid, and both mass and energy are allowed to transfer across the boundaries. The boundaries are arbitrary, but a well chosen system can greatly simplify the analysis. The constant volume means that only two other state variables are required to define all other state variables.

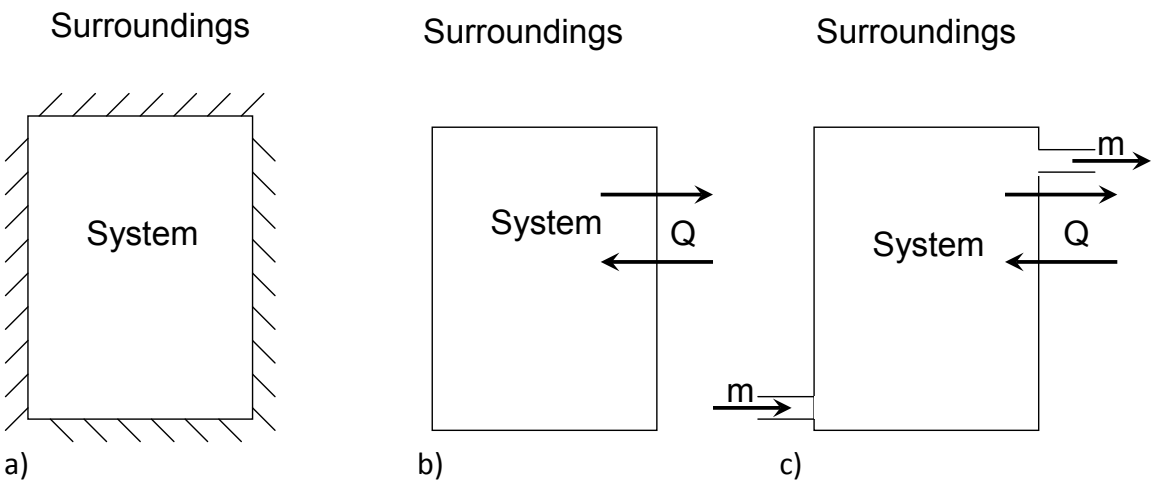

Figure 168. Diagrams of a) isolated system, no exchange with surroundings, b) closed system, only exchanges heat with surroundings, and c) open system exchanging both heat and mass with surroundings.

1.1.7 Equilibrium

In Section1.1.6 of the Kinetics section of this best practices document, chemical equilibrium was defined as a condition where the forward rate of a reaction was equal to the rate of the reverse reaction, so that there was no change in the overall chemical nature of the system. The definition of thermodynamic equilibrium is broader, encompassing thermal, mechanical, phase and chemical equilibrium, to name a few. The

simplest method to determine if a system is in equilibrium is to isolate it from its surroundings. When there are no longer any changes in its observable or measurable properties, then the system is in equilibrium.

Equilibrium can also be described as a minimum in a thermodynamic potential. The Helmholtz free energy is used to describe systems with constant temperature and volume and is defined by Equation 112, where *U* is the internal energy, *T* is the temperature and *S* is the entropy of the system.

Equation 112

$$A = U - TS$$

The Gibbs free energy describes systems at constant temperature and pressure and is defined by Equation 113, where H is the enthalpy of the system.

Equation 113

$$G = H - TS$$

It is clear from this definition that there can be no temperature gradients in a system in equilibrium. Since the assumption of equilibrium is essential to thermodynamics calculations, the concept of local thermal equilibrium (LTE) is used instead. LTE can be applied to systems where the variation in properties across space and time is small enough that the molecules surrounding a given point can be assumed to be in equilibrium. This assumption breaks down in systems with large variations in properties or low densities, so that molecules are unlikely to have enough collisions to establish equilibrium even locally.

1.1.8 Reversibility

A process is thermodynamically reversible if the system and its surroundings can be returned to its original state. An equivalent statement is that a process is reversible if each step in the process can be achieved through infinitesimal changes to properties of the system without loss or dissipation of energy so that the system is in equilibrium throughout the entire process. In practice, this is impossible, since all real processes lead to a net increase in entropy of a system and its surroundings. Additionally, it would take infinitely long for a system to adjust to infinitesimal changes. However, it is possible for a process to be approximately reversible if the system responds rapidly to small changes. Another approximation in an internally reversible process is that all irreversibilities are assumed to occur in the surroundings so that the system could return to its original state.

1.1.9 Practical Use and Limitations of the First Law

The first law of thermodynamics is discussed briefly above, but before we can use it to make calculations of changes in enthalpy, *H*, or internal energy, *U*, we must recognize that both of these properties are state functions. This means that they are path independent functions with well defined properties at all points and their differential form is exact. *U* and *H* can be defined as a function of any two of the three state variables *p*, *V* and *T*, but the choice is important as it can lead to significant simplifications. For example, considering *U* as a function of *T* and *V* allows us to define the heat capacity of a system as the change in internal energy at constant volume. Another reasonable choice is to consider *H* a function of *T* and *p*. In this section, we will focus mostly on calculations of enthalpy, since that is the more commonly used property for hydrogen storage measurements, but a similar derivation is also possible for the internal energy.

Since the derivative of enthalpy is exact, we can write a differential change in enthalpy as a function of *T* and *p* as:

Equation 114

$$dH = \left(\frac{\partial H}{\partial T}\right)_p dT + \left(\frac{\partial H}{\partial p}\right)_T dp$$

The $\left(\frac{\partial H}{\partial T}\right)_p$ term in Equation 114 is commonly referred to as the heat capacity at constant pressure, C_p, which is a measurable quantity. The second term must be manipulated further to arrange it in measurable form, which can be done by considering how the change in enthalpy depends on temperature when the volume of a system is held constant rather than the pressure. This is obtained by dividing both sides of Equation 114 by *dT* and imposing the volume constraint on *H*, as shown in Equation 115.

Equation 115

$$\left(\frac{\partial H}{\partial T}\right)_V = C_p + \left(\frac{\partial H}{\partial p}\right)_T \left(\frac{\partial p}{\partial T}\right)_V$$

The $\left(\frac{\partial p}{\partial T}\right)_V$ term can be modified using the rule for cross partial differentiation, as shown in Equation 116.

Equation 116

$$\left(\frac{\partial p}{\partial T}\right)_V = -\left(\frac{\partial V}{\partial T}\right)_p \Big/ \left(\frac{\partial V}{\partial p}\right)_T$$

It is useful to introduce the two measurable quantities, the isobaric coefficient of thermal expansion, α (Equation 117), and the isothermal compressibility, κ (Equation 118).

Equation 117

$$\alpha = \frac{1}{V}\left(\frac{\partial V}{\partial T}\right)_p$$

Equation 118

$$\kappa = -\frac{1}{V}\left(\frac{\partial V}{\partial p}\right)_T$$

A similar modification can be performed on the $\left(\frac{\partial H}{\partial p}\right)_T$ term of Equation 115, again using the rule for cross partial differentiation and recognizing the definition of C_p, as shown in Equation 119.

Equation 119

$$\left(\frac{\partial H}{\partial p}\right)_T = -\left(\frac{\partial T}{\partial p}\right)_H \left(\frac{\partial H}{\partial T}\right)_p = -\left(\frac{\partial T}{\partial p}\right)_H C_p$$

The coefficient to the C_p term is defined as the Joule-Thomson coefficient, μ_{JT}, creating the final form of Equation 115 shown in Equation 120:

Equation 120

$$\left(\frac{\partial H}{\partial T}\right)_V = \left(1 - \mu_{JT}\frac{\alpha}{\kappa}\right)C_p$$

1.1.10 Heat Capacity

When energy is transferred to a system as heat the temperature of the system generally increases. The relation between the amount of heat transferred and the temperature is of practical importance. For an infinitesimal transfer, the change in temperature is proportional to the heat transferred. This coefficient is commonly designated by *C* and called the heat capacity or the specific heat. It depends on the size, composition and mass of the system and is defined by Equation 121.

Equation 121

$$C = \frac{\delta q}{dT}$$

Since δq is not exact, *C* will depend on the path of transformation. Most transformations take place at either constant pressure or constant volume. When this distinction is important, a subscript *p* or *v* is added to indicate whether the heat capacity of a constant pressure or constant volume process is used, respectively. The heat required to bring a change of temperature *dT* is therefore $C_p dT$ or $C_v dT$ according to the constraints imposed on the system.

Note that it is usually easier to do and control experiments at constant pressure than at constant volume. This explains why experimental values of C_p are more accessible than C_v in spite of the fact that it is easier to predict theoretical values of C_v rather than those of C_p. This distinction can commonly be ignored for simple analyses of solid hydrogen storage materials.

The constant volume heat capacity C_V is given by the change in internal energy (U) with respect to changes in temperature:

Equation 122

$$C_V(T,V) \equiv \left(\frac{\partial U}{\partial T}\right)_V$$

For a constant pressure process, heat capacity C_P is given by the change in enthalpy (H) as a function of changes in temperature:

Equation 123

$$C_P(T,P) \equiv \left(\frac{\partial H}{\partial T}\right)_P$$

Consider a non-reactive system where the change in internal energy as a function of temperature at constant volume. The change in internal energy (with rearrangement) is

Equation 124

$$\Delta U = \int_{T_1}^{T_2} C_V(T)dT$$

Now, consider a change in temperature and volume of the substance. The process can be broken into two separate processes, one with constant temperature the other at constant volume. This can be written as $A(T_1,V_1) \xrightarrow{\Delta U_1} A(T_1,V_2) \xrightarrow{\Delta U_2} A(T_2,V_2)$, where the total change in internal energy from state 1 to state 2 is the sum of the individual steps: $\Delta U_{total} = \Delta U_1 + \Delta U_2$. We can calculate ΔU_2, by using the formula

Equation 125

$$\Delta U_2 = \int_{T_1}^{T_2} C_V(T)dT$$

How do we calculate the ΔU_1 where there is a change in volume? For ideal gases and (to a good approximation) liquids and solids, U depends only on temperature. Therefore, for step 1 (which is isothermal) $\Delta U_1 \approx 0$. This holds true for all substances except non-ideal gases. In summary

Equation 126

$$\Delta U = \int_{T_1}^{T_2} C_V(T)dT$$

To summarize Equation 126 is valid with the following caveats:
Ideal gas: exact
Solids or Liquids: good approximation
Real gas: valid only if the volume (V) is constant

Now consider heating a substance at constant pressure and consider the resulting change in enthalpy. Analogous to the internal energy, enthalpy depends strongly on temperature. If ΔH is the change in enthalpy resulting from only a temperature change at constant pressure then the heat capacity is defined as:

Equation 127

$$\Delta H = \int_{T_1}^{T_2} C_P(T)dT$$

Following the same procedure as before, the change in enthalpy for a two-step process can be broken into $A(T_1, P_1) \xrightarrow{\Delta H_1} A(T_1, P_2) \xrightarrow{\Delta H_2} A(T_2, P_2)$. The first step ($\Delta H_1$) is an isothermal pressure change. The internal energy has been shown to be nearly independent of pressure (i.e., $\Delta U \approx 0$). Therefore, the enthalpy, $\Delta H = \Delta U + V\Delta P$, reduces to $\Delta H = V\Delta P$. Both U and H are independent of pressure for ideal gases. Consequently, unless gases are at or above their critical pressures, it is normally safe to assume both $\Delta U \approx 0$ and $\Delta H \approx 0$ for gases undergoing isothermal pressure changes. If ΔH is a function of pressure such that the ideal gas law assumption is invalid, then tabulated values of $\Delta H(T, P)$ are needed or a thermodynamic relation is required. The second step (ΔH_2) is the isobaric temperature change, which by definition is

Equation 128

$$\Delta H = \int_{T_1}^{T_2} C_P(T)dT$$

Because enthalpy is a state function (just as internal energy is) the total enthalpy change for the two-step process is $\Delta H_{total} = \Delta H_1 + \Delta H_2$. In summary the total enthalpy change can be calculated as follows:

Equation 129

$$\Delta H_{total} = \int_{T_1}^{T_2} C_P(T)dT$$

To summarize Equation 129 is valid with the following caveats:
Ideal gas: exact
Real gas: exact only if the pressure (P) is constant
Solids and liquids: exact

Equation 130

$$\Delta H_{total} \approx V\Delta P + \int_{T_1}^{T_2} C_P(T)dT$$

Heat capacities are physical properties of materials, and are often tabulated in a variety of reference works including Perry's Chemical Engineering Handbook or can be found on the web at NIST Chemistry Webbook. The units of heat capacity are energy per unit amount per temperature. Specific heat capacity is the heat capacity on a per mass bases, molar heat capacity is on a per mole basis, and volumetric heat capacity is on a per volume basis (very rarely used). The temperature dependence on heat capacity is often given in polynomial form. The form given in the NIST Chemistry Webbook is the Shomate equation. There are simple relationships between C_p and C_V, two such cases are $C_p \approx C_V$ (solids and liquids) and $C_p = C_V + \mathrm{R}$ (ideal gases). Heat capacities can be used to calculate entropies, enthalpies of reaction at temperatures other than 298K, and consequently the Gibb's free energy of reaction for temperatures other than 298K.

1.1.11 Joule-Thomson Effect

In thermodynamics, the Joule–Thomson effect (or Joule–Kelvin effect) is the temperature change that a gas or liquid undergoes when it is forced through a small opening without an exchange of heat with the environment.[19,20] This procedure is called a throttling process or Joule–Thomson process.[21] The effect is named for James Prescott Joule and William Thomson, 1st Baron Kelvin who discovered it in 1852 following earlier work by Joule on Joule expansion, in which a gas undergoes free expansion in a vacuum. At room temperature, all gases except hydrogen, helium and neon cool upon expansion by the Joule–Thomson process.[227,228]

The adiabatic expansion of a gas may be carried out in a number of ways. The change in temperature experienced by the gas during expansion depends not only on the initial and final pressure, but also on the manner in which the expansion is carried out.

If the expansion process is reversible, meaning that the gas is in thermodynamic equilibrium at all times, it is called an isentropic expansion. In this scenario, the gas does positive work during the expansion, and its temperature decreases. It is important: to understand that the cooling of a gas by pure isentropic expansion is not Joule-Thomson cooling, although it is sometimes erroneously called this.

In a free expansion, on the other hand, the gas does no work and absorbs no heat, so the internal energy is conserved. Expanded in this manner, the temperature of an ideal gas would remain constant, but the temperature of a real gas may either increase or decrease, depending on the initial temperature and pressure.

In the Joule-Thomson process a gas at high pressure expands into a region of lower pressure via a valve or porous plug under steady state conditions and without change in kinetic energy. Thus, enthalpy remains unchanged. The temperature can either increase or decrease during this process. Each real gas has a Joule–Thomson (Kelvin) inversion temperature above which expansion at constant enthalpy causes the temperature to rise, and below which such expansion causes cooling. This inversion temperature depends on pressure; for most gases at atmospheric pressure, the inversion temperature is above room temperature, so most gases can be cooled from room temperature by isenthalpic expansion.

The cooling or heating of the gas in Joule-Thomson expansion is caused by the combination of the following two opposing physical mechanisms. The first is that, as a gas expands, the average distance between molecules grows. Because of intermolecular attractive forces (see van der Waals force), expansion causes an increase in the potential energy of the gas. If no external work is extracted in the process and no heat is transferred, the total energy of the gas remains the same because of the conservation of energy. The increase in potential energy thus implies a decrease in kinetic energy and therefore in temperature.

The second mechanism has the opposite effect. During gas molecule collisions, kinetic energy is temporarily converted into potential energy. As the average intermolecular distance increases, there is a drop in the number of collisions per time unit, which causes a decrease in average potential energy. Again, total energy is conserved, so this leads to an increase in kinetic energy (temperature).

Below the Joule–Thomson inversion temperature, the former effect (work done internally against intermolecular attractive forces) dominates, and free expansion

causes a decrease in temperature. Above the inversion temperature, gas molecules move faster and so collide more often, and the latter effect (reduced collisions causing a decrease in the average potential energy) dominates causing a temperature increase.

The rate of change of temperature *T* with respect to pressure *P* in a Joule–Thomson process (that is, at constant enthalpy *H*) is the Joule–Thomson (Kelvin) coefficient μ_{JT}. From Equation 131 μ_{JT} can be expressed in terms of the gas volume V, its heat capacity at constant pressure C_p, and its coefficient of thermal expansion α as:

Equation 131

$$\mu_{\mathrm{JT}} \equiv \left(\frac{\partial T}{\partial P}\right)_H = \frac{V}{C_{\mathrm{p}}}(\alpha T - 1)$$

For an ideal gas, μ_{JT} is always equal to zero: ideal gases neither warm nor cool upon being expanded at constant enthalpy.

All real gases have an inversion point at which the value of μ_{JT} changes sign. The temperature of this point, the Joule–Thomson inversion temperature, depends on the pressure of the gas before expansion.

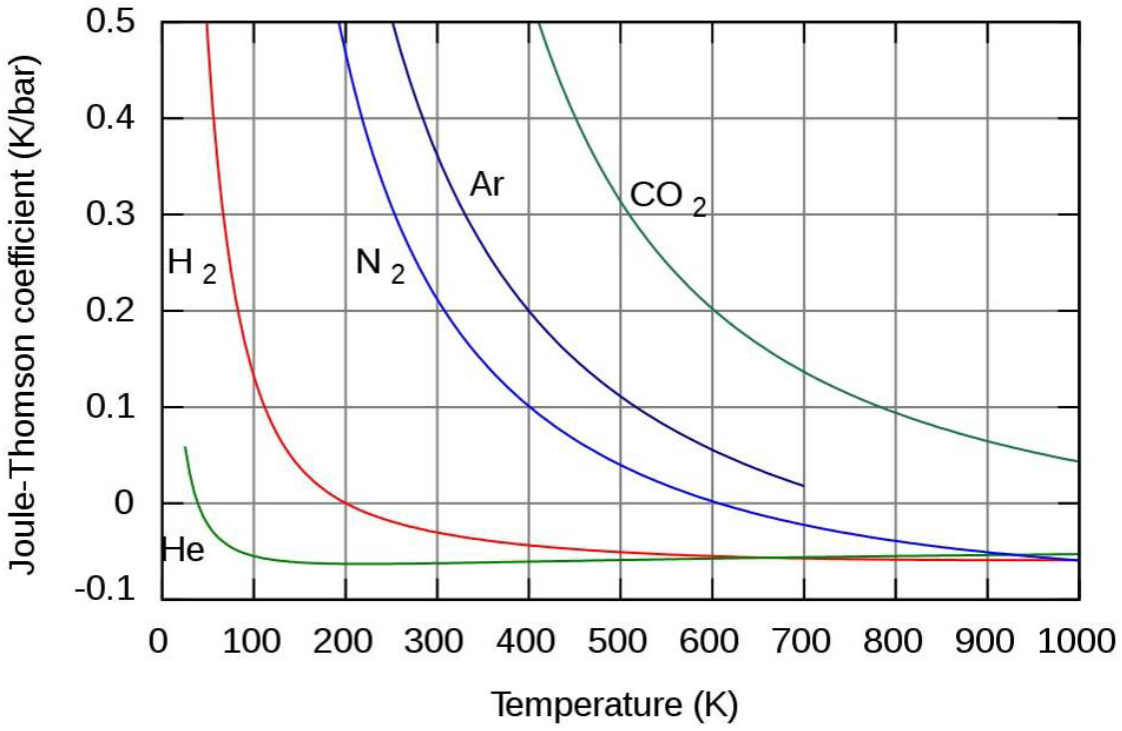

Figure 169. Joule-Thomson coefficients for various gases at atmospheric pressure.[229]

Helium and hydrogen are two gases whose Joule–Thomson inversion temperatures at a pressure of one atmosphere are very low. Thus, helium and hydrogen warm up when expanded at constant enthalpy at typical room temperatures.

In practice, the Joule–Thomson effect is achieved by allowing the gas to expand through a throttling device (usually a valve) which must be very well insulated to prevent any heat transfer to or from the gas. No external work is extracted from the gas during the expansion. A typical application for the effect is the "Linde" technique, where the cooling effect is used to liquefy gases (e.g. for the cryogenic production of liquid oxygen, nitrogen, and argon). Only when the Joule–Thomson coefficient for the given gas at the given temperature is greater than zero can the gas be liquefied at that temperature by the Linde cycle. For this reason, simple Linde cycle liquefiers cannot normally be used to liquefy helium, hydrogen, or neon.

The Joule-Thomson process (and consequently the coefficient, μ_{JT} of Equation 131) is of particular interest for hydrogen storage measurement applications, since it is an indication of how the temperature of a gas will change during an adiabatic expansion. Because hydrogen is one of the only gases which has a negative μ_{JT} at room temperature, if hydrogen expands at constant enthalpy, which will occur any time hydrogen flows through a valve from a region of higher pressure to a region of lower pressure, the temperature of the hydrogen gas will increase.

This is clearly a common process in many hydrogen storage measurements involving dosing of gas. However, this heating effect is typically small compared to the transient thermal (quasi-adiabatic) effects of a rapid expansion of hydrogen from one volume to another. In the case of volumetric measurements, gas in the sample cell will experience a brief increase in temperature in ad/absorption measurements due to compression and a transient temperature drop with each desorption dose (expansion) of gas out of the sample cell. To demonstrate that transient temperature (and thus pressure) excursion are mainly due to quasi-adiabatic expansion rather than Joule Thompson heating, measurements were performed in a Sievert's instrument using 4 different gases (H_2, He, Ar, CO_2). A thin (1/32") Type-K thermocouple was inserted into the center gas space of an empty sample cell. The temperature of the gas in the cell was monitored in time as gas at a high pressure was dosed to the sample cell from one of the instrument's reservoirs followed by a release of pressure from the sample cell into the reservoir at a lower pressure. The temperatures of the reservoir and sample cell were both at room temperature during the measurements.

Figure 170 shows the change in gas temperature in the sample cell upon dosing and releasing gas into the cell. The gas temperature in the sample cell increased on dosing and decreased on releasing pressure from the sample cell independent of the gas. The

Joule Thomson coefficients for H_2 and He are negative and Ar, CO_2 are positive under the test conditions, therefore it is reasonable to conclude that Joule Thomson heating of hydrogen does not play a significant role in the observed temperature variations. What is important is that the temperature excursions were significant (2°C) and of relatively long duration (up to 2 minutes) before thermal equilibrium was re-established.

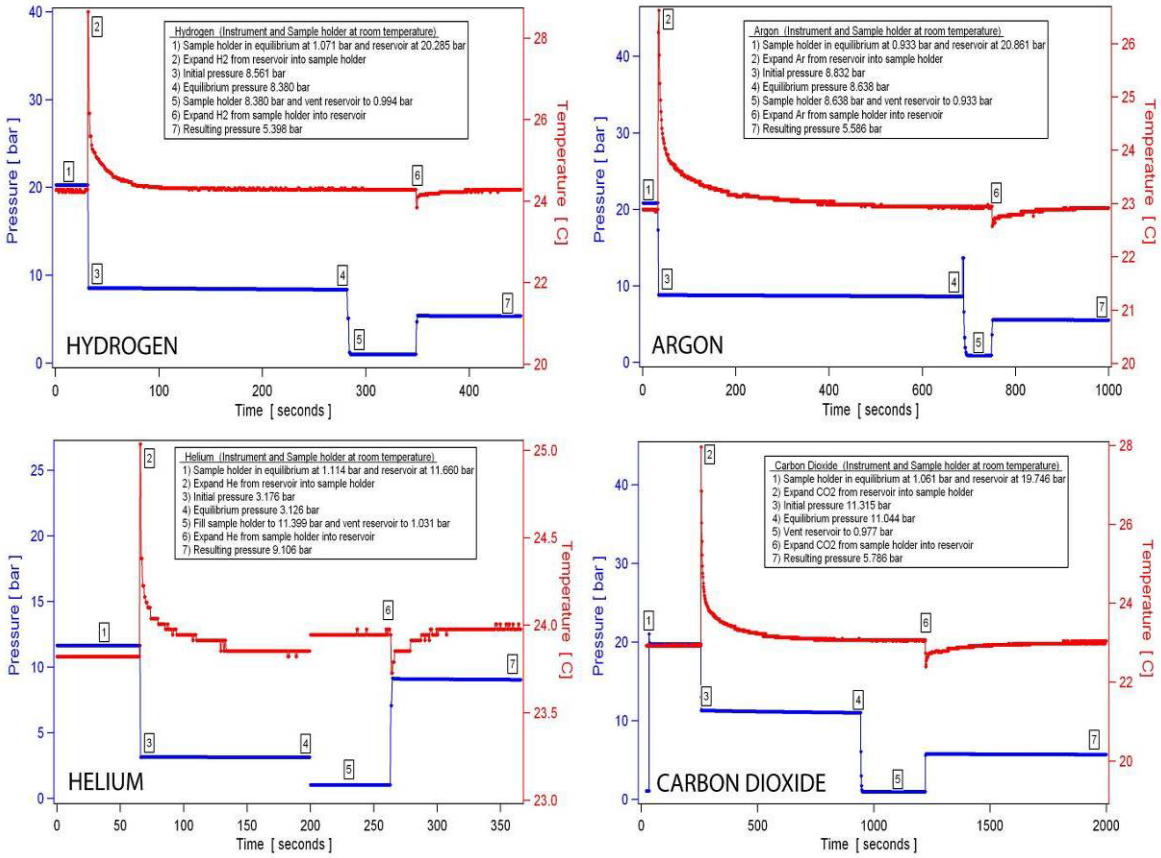

Figure 170. Thermal effect of gas expansion to and from a Sievert's instrument's sample holder for various gases at room temperature.

It is important to recognize that these transient gas-expansion temperature effects have an impact on the initial sample temperature as well as the pressure readings in the seconds (to minutes) following a gas dose. This, in turn, will have important consequences on interpretation of data in hydrogen sorption PCT or kinetics measurement. Specifically, the extrapolation of time resolve sorption capacity data back to time=0.0 (the moment of the dose) or the evaluation or modeling of initial sorption kinetics in such measurements can be subject to large errors. It is very difficult in this time domain to de-couple actual gas sorption phenomena from transient gas expansion effects.

1.1.12 Enthalpy of Formation

Enthalpy *H* is defined as the sum of internal energy *U* and the product of pressure *P* and volume *V*:

Equation 132

$$H = U + pV$$

Since internal energy is an arbitrary quantity which only has meaning relative to a reference state, the same is true of enthalpy. For simplicity, the enthalpy of elements in their most basic stable form is set to 0 at 298.15 K and 1 bar. For example, the stable form of hydrogen is the molecule H_2, not monatomic H. The standard enthalpy of formation of a material, denoted ΔH_f^o, is the difference in enthalpy between the constituent elements in their most stable form and the enthalpy of the final product at the standard temperature and pressure. ΔH_f^o for H_2 is therefore 0 kJ/mol. Note that this determination of 0 enthalpy is arbitrary, so some materials will be more stable and have a negative enthalpy of formation. Materials with a negative ΔH_f^o release heat during their formation, known as an exothermic process, while materials with a positive ΔH_f^o absorb heat during their formation, known as an endothermic process.

The enthalpy of a reaction is a more general term defined as the change in enthalpy during a given reaction. The terms endothermic and exothermic are still applied to reactions with a positive and a negative change in enthalpy as above.

It can be helpful to explicitly write out the reaction from which the enthalpy of formation is calculated, as shown in Equation 133 for magnesium hydride. Note that the chemical state of the elements is often included. For elements that have more than one common form, the exact state is often specified. For example, the standard state of carbon is graphite, not diamond.

Equation 133

$$Mg(s) + H_2(g) \leftrightarrow MgH_2(s)$$

The standard enthalpy of formation can not always be directly measured, since many compounds cannot be formed simply by combining their constituent elements. In such cases, the overall enthalpy of formation can be determined when it is divided into chemical reaction steps that are individually easier to measure. This method is based on Hess's law.

Hess's law states that the energy change for any chemical or physical process is independent of the pathway or number of steps required to complete the process

provided that the final and initial reaction conditions are the same. In other words, energy change is path independent, only the initial and final states being of importance. This follows from the principle of conservation of energy and is expressed in the first law of thermodynamics.

Thus, Hess's law allows the enthalpy change (*ΔH*) for a reaction to be calculated even when it cannot be measured directly. This is accomplished by performing basic algebraic operations based on the chemical equation of reactions using previously determined values for the enthalpies of formation.

Hess's Law states that enthalpy changes are additive. Thus the ΔH for a single reaction can be calculated from the difference between the heat of formation of the products and the heat of formation of the reactants:

Equation 134
$$\sum \Delta H^{\circ}_{\text{reaction}} = \sum \Delta H^{\circ}_{\text{f(products)}} - \sum \Delta H^{\circ}_{\text{f(reactants)}}$$

where the o superscript indicates standard state values.

If the net enthalpy change is negative (*ΔHnet* < 0), the reaction is exothermic and is more likely to be spontaneous; positive *ΔH* values correspond to endothermic reactions. Entropy also plays an important role in determining spontaneity, as some reactions with a negative enthalpy change are nevertheless spontaneous.

As an example, the standard enthalpy of formation for complex hydride materials such as sodium borohydride $NaBH_4$ can not be determined by direct reaction of its elemental components (Equation 135). However, $NaBH_4$ is often formed from sodium borate $NaBO_2$. Thus, the heat of formation can be determined from the is determined from the heat of hydrolysis (Equation 136 and Equation 137), where the enthalpy of formation of $NaBO_2$ is given by the elemental reactions presented in Equation 137.

Equation 135
$$Na(s) + B(s) + 2H_2(g) \leftrightarrow NaBH_4(s)$$

Equation 136
$$NaBH_4(s) + 2H_2O(l) \leftrightarrow 4H_2 + NaBO_2(aq)$$

Equation 137
$$\Delta H_f(NaBH_4) = \Delta H_f(NaBO_2) - \Delta H(hydrolysis)$$

Equation 138 $NaBO_2 \leftrightarrow Na + B + O_2$, $O_2 \leftrightarrow 2O$, and $2H_2 + 2O \leftrightarrow 2H_2O$

The enthalpy of formation is often presented in terms of energy per mole of product. However, in reversible hydrogen storage studies, it is the enthalpy of de/hydrogenation that is of interest, and this is more commonly presented as energy per mole of H_2. Note that the enthalpy of formation and the enthalpy of de/hydrogenation is not always the same if the reaction involves other products than just a hydride.

1.1.13 Entropy of Formation

Another important thermodynamic property is the entropy of formation, ΔS_f^o. Unlike standard enthalpies of formation, the value of standard entropy $S°$ is an absolute. In other words, an element in its standard state has a nonzero value of $S°$ at room temperature. According to the third law of thermodynamics, the entropy of a pure crystalline structure can be 0 (J/molK) only at 0 K. However, this could only be true for a 'perfect crystal' without any frozen in entropy (defects, dislocations), which is never completely possible because crystals always grow at a finite temperature.

Changes in entropy are associated with phase transitions and chemical reactions. Chemical equations make use of the standard molar entropy of reactants and products to find the standard entropy of reaction:

Equation 139 $$\Delta S°_f = S°products - S°reactants$$

The standard entropy of reaction helps determine whether the reaction will take place spontaneously. According to the second law of thermodynamics, a spontaneous reaction always results in an increase in total entropy of the system and its surroundings:

Equation 140 $$\Delta S_{total} = \Delta S_{system} + \Delta S_{surroundings} > 0$$

1.1.14 Free Energy

From the 1st law of thermodynamics:

Equation 141 $$dU = dq + dw$$

Where, U is the internal energy, q is the heat transferred to the system from the surroundings, and w is the work done on a system by the surroundings. A system that is at constant temperature and pressure, does only pV work. Since p is constant the only work that is done is expansion work:

Equation 142 $$dw=-pdV$$

At equilibrium, and with fixed a composition (i.e. no addition of material) the change in heat flow to the system q is proportional to the temperature T and the change in entropy S:

Equation 143 $$dq = TdS$$

From Equation 141 the internal energy is a function of entropy and volume:

Equation 144 $$dU = TdS - pdV$$

From Equation 132 the change in Enthalpy (*H*) is given by:

Equation 145 $$dH = dU + pdV$$

The Gibbs Free energy (G) is that portion of the total system energy that is available for useful work (non-PV work). When T and P are constant, we can use Gibbs expression for free energy.

Equation 146 $$dG = dU + pdV - TdS$$

or

Equation 147 $$dG = dH - TdS$$

The driving force of a reaction is *dG* and is comprised of two parts, change in enthalpy (*dH*) and change in entropy (*dS*). The magnitude and direction of the driving force depends on the magnitude and direction of *dH* and *dS*. Neither by themselves controls a reaction.

For a reaction proceeding in incremental amounts toward equilibrium, the change in the total Gibbs free energy is proportional to ΔG, where

Equation 148 $$\Delta G = (\Sigma x_i G_i)_{products} - (\Sigma x_i G_i)_{reactants}$$

Where x_i is the stoichiometric coefficient and G_i is the free energy per mole of each chemical component. The sign of the Gibbs free energy tells us if a reaction will happen, and in what direction.

$\Delta G < 0$, and G_{Total} decreases as the reaction proceeds. Thus, the reaction is spontaneous.
$\Delta G = 0$, the reaction is at equilibrium (has stopped) and G_{Total} is at a minimum.
$\Delta G > 0$, the reaction is not spontaneous, but proceeds in the opposite direction.

1.2 Thermodynamics of On-board Reversible Hydride Materials

On-board reversible hydrides for hydrogen storage cover a wide range of materials including: various intermetallic metal hydrides, complex metal hydrides, amides, and destabilize hydride mixtures consisting of two or more reactants (one or more of which is a hydride), etc. What is important is that these materials chemically react with hydrogen to store atomic hydrogen and are able to release hydrogen in a reversible, mildly endothermic desorption or decomposition. Baring kinetic limitations, on-board reversible hydrides should be able to be exothermically rehydrogenated under reasonable temperature (< 300°C) and pressure (< 200 bar) conditions.

A considerable amount of research has been done on interstitial intermetallic compounds (IMCs). These represent a specific class of hydrides that can be obtained by the direct reaction between single phase solid metals, alloys, or metallic compounds and hydrogen gas. This class of hydrides provides good examples of the most pertinent aspects of the complex thermodynamics of hydrogen storage using on-board reversible hydrides.

1.2.1 Metal Hydride Phase Diagrams

It is instructive to begin examining the thermodynamics of on-board reversible hydrides with a discussion of metal-hydride phase diagrams. A phase diagram is a 2-D or 3-D plot comparing thermodynamic variables, usually including lines representing equilibrium states and/or phase boundaries. Usually, phase diagrams consist of a 2-D projection of this 3-D parameter space. Metal hydride phase diagrams typically represent 2-D projections of isotherms of temperature, onto a plot of gaseous hydrogen pressure in equilibrium with the metal and/or hydride versus hydrogen concentration in the metal. The phase diagram now represents the phases containing hydrogen in the metal lattice.

PCT measurements, discussed in previous sections of this document, are therefore a useful tool for constructing phase diagrams. Figure 171 is an example of PCT measurements used to construct a phase diagram for the Pd-H system. Here the PCT measurements are represented by symbols on a solid line. The phase boundaries are plotted as a single curved dashed line which separates hydrogen dissolved in Pd metal on the exterior left portion of the curve (blue), hydrogen dissolved Pd hydride on the exterior right portion (red) of the curve and the two-phase hydrogen-metal solid solution and hydride in the center region (purple).

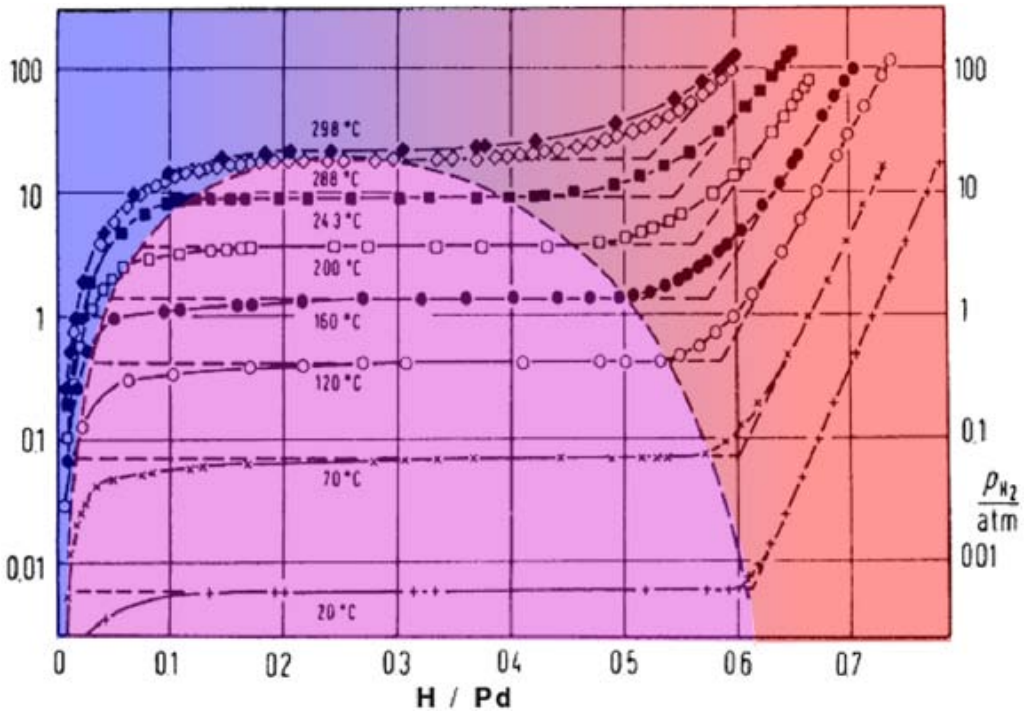

Figure 171. Example of a phase diagram for the Pd-H system determined from PCT measurements.[230]

At low pressure and concentration, hydrogen is typically present in solid solution, termed the α-phase. This can be seen on the left hand side of Figure 171 as the region of increasing pressure in the PCT plots (blue area). Hydrogen continues to be absorbed into the metal as pressure is increased, until eventually H-H interactions become important, At this point a hydride, denoted the β-phase or the β hydride phase, is formed locally by the occupation of particular interstitial lattice sites. The nucleation and growth of the β-phase may occur at free surfaces, at inter-grain boundaries, or throughout the bulk of the metal, depending on nucleation and diffusion mechanisms.

Under idealized equilibrium conditions, the hydrogen gas pressure reaches a constant pressure at which the hydrogen gas, α-phase and β-phase are all in equilibrium. This is observed as a plateau in the PCT diagram. Thus, the existence of an equilibrium plateau signals the co-existence of the two phases, similar to the plateau of the familiar water phase diagram. This two phase (α-phase and β-phase) region is the purple area in the Pd-H phase diagram above. As the β-phase grows the sample's total hydrogen content increases. Eventually all of the α-phase is transformed into the β-phase, represented by the intersection of the PCT curve with the rightmost side of the dashed line (red area in Figure 171). The pressure again rises and the overall hydrogen concentration continues to increase as hydrogen is dissolved as a solid solution in the β hydride phase. Above the critical temperature (shown here as 298°C for Pd-H) there is a smooth transition from the α-phase to the β-phase.

The slope and length of the equilibrium plateau is of particular importance for hydrogen storage applications. A flat plateau enables the reversible uptake and release (commonly referred to as absorption and desorption) of hydrogen from a metal simply by raising or lowering the surrounding hydrogen pressure above or below the plateau pressure. In raising the pressure or by heating and cooling the material. Hydrogen is absorbed in forming the β-hydride phase. Hydrogen is released by lowering the pressure or heating the material transforming the hydride back into the α-phase. This change in pressure (or temperature) can be minor (1 to 2 bar for the classic alloy $LaNi_5$ at 22°C) compared to the pressures needed to store a significant amount of hydrogen by pressurization (200 bar). The length of the plateau determines how much hydrogen can be reversibly stored in a metal hydride. The ease with which this amount of hydrogen is reversibly absorbed or desorbed is a different matter entirely, and it involves not only the thermodynamic stability of the hydride but also the kinetic mechanisms that control the rates of hydrogen uptake and release. The thermodynamic stability is determined by the enthalpy of formation, which will be discussed in the next sections.

1.2.2 Free Energy of Formation

The potential energy of a hydride is closely related to its domain of stability which can be obtained from the knowledge of the free energy of formation of the hydride. For a metal or any IMC, the hydrogenated form is an ordered phase, as opposed to the solid solution where H atoms are randomly distributed on the available interstitial sites.

Thus, the free energy of formation of the hydride compound may be defined as the free energy of reaction for the reaction between one mole of hydrogen gas with the pure metal (or IMC). Consequently the corresponding hypothetical reaction of formation is written as:

Equation 149 $$2xM(solid) + H_2(gas) \rightarrow 2M_xH(solid)$$

For the standard conditions, pure M (metal, alloy, or intermetallic compound) and H_2 gas at 1 bar pressure, one obtains:

Equation 150 $$\Delta G_f^O(2M_xH) = \Delta G_r(n)$$

Here, ΔG_f^O represents the standard free energy of formation which is equal to the free energy of reaction ΔG_r for the M_xH compound at the temperature T.

Equation 149 is for an idealized reaction between hydrogen and a metal. For many metal (and intermetallic) hydrides, the hydride phase begins to form at the limit of a saturated solid solution. Often heats of formation are reported from plateau pressure data that does not take the heat of solution into account (see next sub-section). In addition the enthalpy of uptake and release of hydrogen are generally not identical (hysteresis). On-the-other-hand, while equating measured enthalpies to the free energy of formation is not necessarily correct; it nevertheless may be used as a first approximation to compare stability differences between hydrogenated compounds.

Unfortunately, this approximation with these fundamental discrepancies has become common practice for many reported values of the free energy of formation of hydride compounds. It is the recommendation of this document that such measured (van 't Hoff) values be reported as enthalpies of reaction (from solid solution or another hydride) and state whether they are made from equilibrium absorption or desorption measurements.

1.2.3 Reversible Phase Transformations

In the following we assume that the hydrogenation reaction obeys the **Gibbs thermodynamic**, which states that the thermodynamic equilibrium must be reached under reversible conditions. A diagram of the hydrogen-metal-hydride phase diagram is depicted in Figure 172.

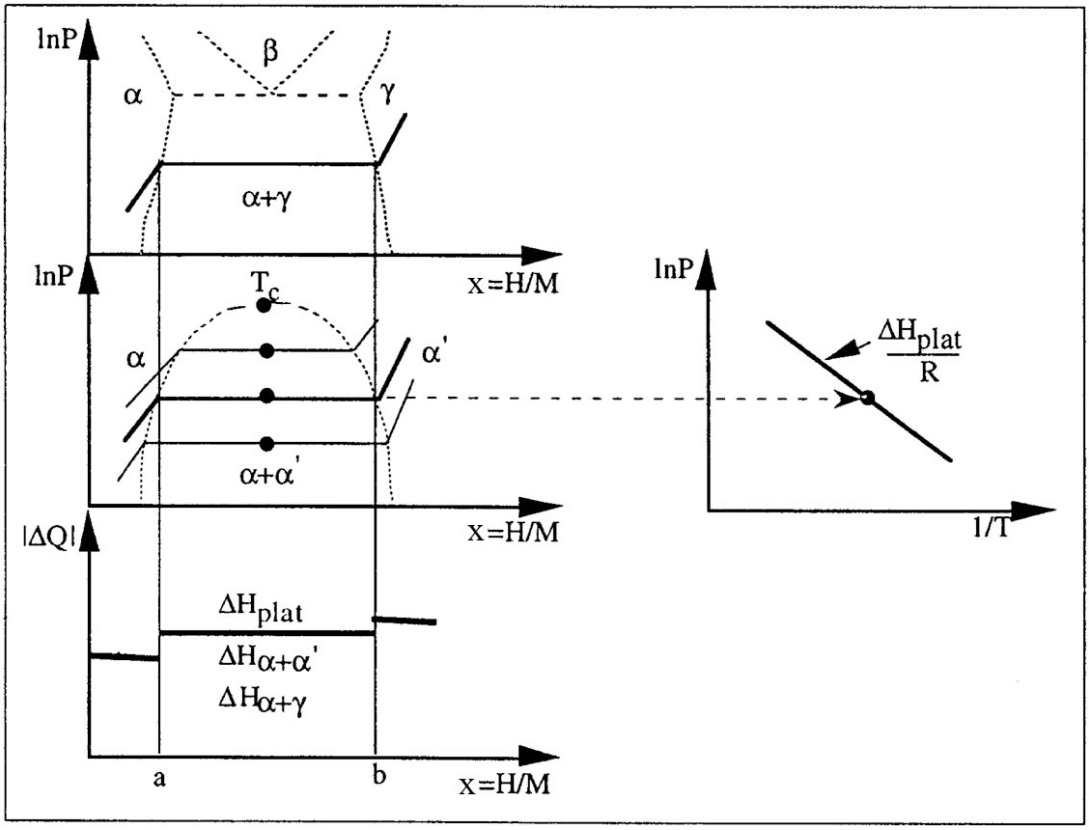

Figure 172. Ideal case, reversible conditions. Top-Left) isotherm in which hydrogen induces a structural change, Middle-Left) isotherms in which the structure is maintained. Right: van 't Hoff plot. The line must stop at Tc. Bottom-left) Heat evolved during the abs/des processes.[231]

On the right side of the figure the diagrams describes the solid solution formation with increasing hydrogen concentration (x=H/M) whose domain depends on the temperature and also on the endo- or exothermic character of the reaction. At the phase boundary 'a' the solid solution is saturated and further hydrogen absorption causes the hydride phase to precipitate. At the composition 'b' all the solid solution has been transformed, the single phase hydride MH_b remains. At 'b', all the 'accessible' interstitial sites of the MH_b phase are filled but further hydrogen absorption may be obtained depending on the applied pressure and temperature conditions. Then a non-stoichiometric compound will be formed. This could be described equally as well, as a new solution of hydrogen in the non-stoichiometric compound.

For isothermal conditions and assuming the formation of only one hydride, hydrogenation of the compound is described by the following reactions, where a and b (atomic ratio) are the phase boundary compositions. These equations are for equilibrium conditions where gaseous hydrogen $H_2(g)$ is in equilibrium ($p=p_{eq}$) with the

solid phases: solid metal (or alloy, or intermetallic) phase *M(s),* the hydrogen in metal solid solution phases $MH_{\alpha}(s)$, the solid hydride phase $MH_{\beta}(s)$, and hydrogen in solution in the solid hydride phase $MH_{\delta}(s)$. Note that the labeling of the α-phase and β-phase here refers to the solid solution and hydride phases, but in fact, can be any hydride phases that coexist.

The equilibrium state between gaseous hydrogen, the metal and the hydrogen-metal solid solution at composition X_{α} is given by:

Equation 151
$$M(s) + \frac{x_{\alpha}}{2} H_2\left(g, p_{eq} < p_{plat}\right) \leftrightarrow MH_{x_{\alpha}}(s)$$

Where the equilibrium pressure (P_{eq}) is below the hydride formation pressure (P_{plat}) (i.e. $P_{eq} < P_{plat}$).

At the limit of saturation of hydrogen in the metal solid solution phases X_{α} = a and Equation 151 becomes:

Equation 152
$$M(s) + \frac{a}{2} H_2\left(g, p_{eq} = p_{plat}\right) \leftrightarrow MH_a(s)$$

At this point ($P_{eq} = P_{plat}$) and the hydrogen gas phase is in equilibrium with α-phase solid metal-hydrogen solution and the solid β-phase metal-hydride. The coexistence of the two solid phases is called “the two phase region” and equilibrium is described by:

Equation 153
$$MH_{x_{\alpha}}(s) + \frac{x_{\alpha} - x_{\beta}}{2} H_2\left(g, p_{eq} = p_{plat}\right) \leftrightarrow MH_{x_{\beta}}(s)$$

At the limit of complete conversion of the α-phase to the β-phase metal-hydride X_{β} = b and Equation 153 becomes:

Equation 154
$$MH_a(s) + \frac{b-a}{2} H_2\left(g, p_{eq} = p_{plat}\right) \leftrightarrow MH_b(s)$$

As hydrogen from the gas phase continues at higher pressures ($P_{eq} > P_{plat}$) to form a hydride-hydrogen solid solution phase $X_\beta = b$:

Equation 155
$$MH_b(s) + \frac{x_\delta}{2} H_2\left(g, p_{eq} > p_{plat}\right) \leftrightarrow MH_{x_{b+\delta}}(s)$$

The thermodynamic behavior related to the three reactions (Equation 151, Equation 153, and Equation 155) follows the Gibbs phase rule. Thus, for Equation 151 where two elements are present (hydrogen and one homogeneous compound) and two phases (solid and gas phases), the variance of the system is equal to two. Therefore, the hydrogen concentration in the solid phase increases as the hydrogen pressure is increased. The formation of a new phase (hydride in Equation 153) reduces the variance and, thus, the system looses a degree of freedom. This means that under equilibrium conditions the hydrogen pressure remains constant during the transformation while the overall hydride composition of the system increases. The equilibrium hydride formation pressure is generally referred to as the plateau pressure (P_{plat}).

For most applications, it is preferable that the hydrogen content of the solid solution should remain small and the plateau pressure of hydride formation should be flat to optimize and simplify the management of the hydrogen gas uptake and release.

At the phase boundaries (a and b), it is assumed that the system is in equilibrium. In the case of chemical equilibrium, the equality between the chemical potentials (μ) leads to the following relationships between the saturated solid solution (μ_M^α), the hydride phase (μ_M^β), and the gaseous hydrogen phase (μ_{H_2}).

Equation 156
$$\mu_M^\alpha(p,T,a) = \mu_M^\beta(p,T,b)$$

Equation 157
$$\mu_H^\alpha(p,T,a) = \mu_H^\beta(p,T,b) = \frac{1}{2}\mu_{H_2}(p,T)$$

and for the two phase region assuming hydrogen is an ideal gas,

Equation 158
$$\mu_H^\alpha = \mu_H^\beta = \frac{1}{2}\mu_{H_2} = \frac{1}{2}\left[\mu_{H_2}^o + RTlnp_{plat}\right]$$

or after rearranging and introducing the relative chemical potential $\Delta\mu_{plat}$ for the reversible transformation α ↔ β one obtains:

Equation 159

$$\Delta\mu_{plat} = \mu_H^{\alpha} - \frac{1}{2}\mu_{H_2}^{o} = \mu_H^{\beta} - \frac{1}{2}\mu_{H_2}^{o} = \frac{1}{2}RTlnp_{plat}$$

The relative chemical potential, $\Delta\mu_{plat}$, corresponds to the Gibbs standard free energy for Equation 153 with hydrogen gas at 1 atm pressure and MH_a and MH_b in the standard state.

Equation 160

$$\Delta G = \Delta\mu_{plat}$$

A chemical reaction will proceed in the direction of lower Gibbs free energy (ΔG <0). Thus, ΔG determines whether the reaction will be spontaneous or not. From Equation 159 the products and reactants are in equilibrium when there Gibbs free energy of each are equal. From this, the well known relationships for the enthalpy (ΔH_{plat}) of the phase transformation α ↔ β are realized:

Equation 161

$$\Delta H_{plat} = \frac{d\left(\frac{\Delta G}{T}\right)}{d\left(\frac{1}{T}\right)}$$

and from Equation 159.

Equation 162

$$\frac{\Delta H_{plat}}{R} = \frac{1}{2}\frac{dlnp_{plat}}{d\left(\frac{1}{T}\right)}$$

Equation 162 is one form of the equation that is referred to as the van 't Hoff equation and relates the amount of heat evolved during the formation of a hydride to the plateau pressure. This relationship is illustrated in the right hand diagram of Figure 172.

Another more commonly used form of the van 't Hoff equation is found by expressing the change in Gibbs free energy ΔG in terms of the change in enthalpy ΔH and entropy ΔS (from Equation 147) such that:

Equation 163

$$\Delta G = \Delta H - T\Delta S = \Delta\mu_{plat} = \frac{1}{2}RTlnp_{plat}$$

Or equivalently:

Equation 164

$$\frac{1}{2}\ln\left(p_{plat}\right)=\frac{\Delta H_f}{RT}-\frac{\Delta S_f}{R}$$

With knowledge ΔS_f and ΔH_f, it is possible to determine the relationship between temperature and equilibrium pressure of hydride formation. By assuming that the change in entropy was mainly due to the change from H_2 gas to H in solid solution in the metal (i.e. a ΔS of ~130 kJ mol^{-1}), Gremaud et. al determined the ideal value of ΔH_f for Mg_2Ni system as -39.2 kJ/mol H_2 for a dissociation pressure of 1 atm at 300 K.[232,233] A better standard might be the DOE targets, which require a dissociation pressure of 3 bar at 85°C. This yields a slightly easier target of ΔH_f = -43.3 kJ/molH_2.

This target will be valid for any procedure to reduce ΔH_f that does not significantly change ΔS_f. Note however, that this is not always the case. The contribution of the entropies of solid reactants and products to the overall entropy change is generally overlooked in most conventional metal hydride systems, where gaseous H_2 is the main source of the entropy change.[234] However, in complex hydrides containing light elements (Li, B, N, etc.), the entropies of solid reactants and products can contribute significantly to the overall entropy change. As an example, the decomposition of $Mg(BH_4)_2$ to MgH_2, B and H_2 involves an entropy change of 91.3 J/K mol-H_2 rather than 130.7 J/K mol-H_2 (the entropy of H_2); ~ 29.4 J/K mol-H_2 is from the entropies of solid reactants and products.[235] In fact, a 10% variation in entropy change will result in a difference in temperature of a few tens of degrees Kelvin. Thus, the thermodynamics of decomposition / recombination hydrogen storage material systems that involve light element hydrides as one of the discharged state products, may be strongly effected by the entropy of formation of these products. A notable example is LiH which has an entropy of formation of ΔS^o = 20.04 (J /K mol-H_2).[236] Because of the low ΔS the corresponding ΔH_f for systems involving LiH or other light elemental hydrides may be higher than the -43.3 kJ/molH_2 to produce an equivalent equilibrium pressure of 3 bar at 85°C. This may be an important consideration in not only in the development of new storage materials, but also in the heat transfer requirements of storage systems using such materials.

1.2.4 Van 't Hoff Plots

Van 't Hoff plots are a commonly used method for determining the thermodynamics properties of hydrogen storage materials. The one caveat is that they can be used only when reversible hydrogen uptake and release occur at pressure and sample temperatures within the range of the measurement equipment. Hydriding measurements have been performed at very high pressures. An example of which is the attempts to hydrogenate Al to form AlH_3. Baranowski and Tkacz claimed to form AlH_3

from Al metal using high-pressure hydrogen (28 kbar) at 300 °C [237]. However this pressure is much too low in view of the free energy of formation for AlH_3 via the direct reaction of Al metal with hydrogen gas.[238] While this method is the most direct the hydrogen pressures required are much too large to be practical for any application (28 kbar is approximately thirty times the pressure at the bottom of the Mariana Trench, 11 km below sea level). In most laboratory environments, typical van 't Hoff pressure measurements are made in a range of pressures between a millibar and up to 200 or perhaps even 300 bar.

Van 't Hoff plots are generally generated from a series of PCT measurements at various temperatures. The "equilibrium" desorption plateau pressure from each isotherm is plotted on a log scale vs. the inverse of temperature, as shown in Figure 173. The slopes of all of the hydride materials presented in Figure 173 are negative, as expected, indicating endothermic dehydrogenation reactions. Also note that the x-axis is presented in terms of 1000/T, as is commonly done for simplicity. The van 't Hoff equation, (Equation 164) can be used to relate the slope to the enthalpy of reaction and the y-intercept to the entropy of reaction.

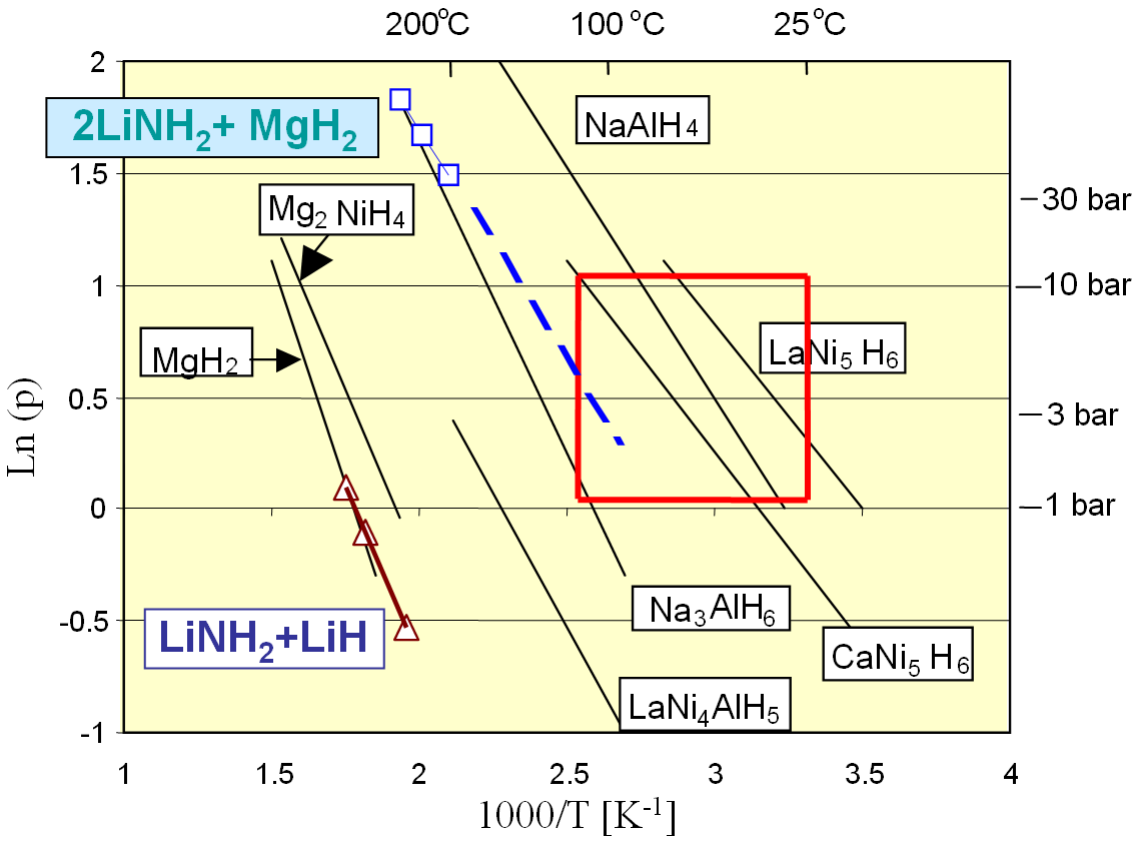

Figure 173. Example Van 't Hoff Plot

Van 't Hoff plots are also useful for comparing the operating temperature and pressure of various materials. The boxed area in Figure 173 shows the materials which fall in the desired operating range for PEM fuel Cell applications. It is important to keep in mind that while a material may look favorable on a van 't Hoff plot, no information is given for the storage capacity of the materials. For example, $LaNi_5H_6$ has favorable thermodynamic properties, but a theoretical storage capacity of only 1.38 wt.%.

A van 't Hoff plot contains a lot of valuable information, but only if constructed properly. Figure 174 demonstrates the standard process for generating a van 't Hoff plot from a series of PCT measurements.[3] There are a few interesting aspects highlighted in this figure which merit further discussion. First, note that all of the points used in the van 't Hoff plot are taken from a point on the pressure plateau corresponding to the same hydrogen concentration. A common choice is the center of the pressure plateau. This consistency is particularly important for materials which exhibit sloping plateaus.

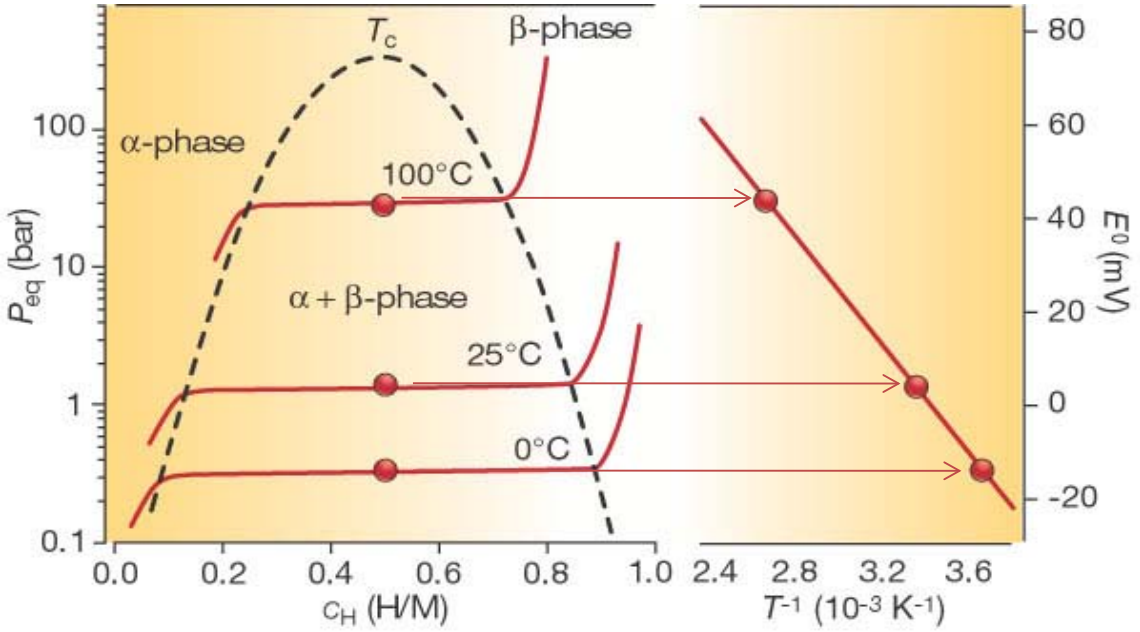

Figure 174. Example of the construction of a van 't Hoff plot from a series of PCT measurements.

While reversible decomposition-recombination chemical hydrides, as well as many metal hydrides show a flat pressure plateaus, many other metal hydrides show a large slope even under equilibrium conditions. The slope of the plateau is due to lattice defects or atomic disorder. In general, a higher degree of disorder will lead to more of a slope in the equilibrium pressure. An extreme example is shown in Figure 175 comparing PCT measurements of crystalline and amorphous $Zr_{50}Ni_{50}$. The crystalline sample shows only a minor slope, while the amorphous material has such an extreme slope that essentially no plateau is observable.

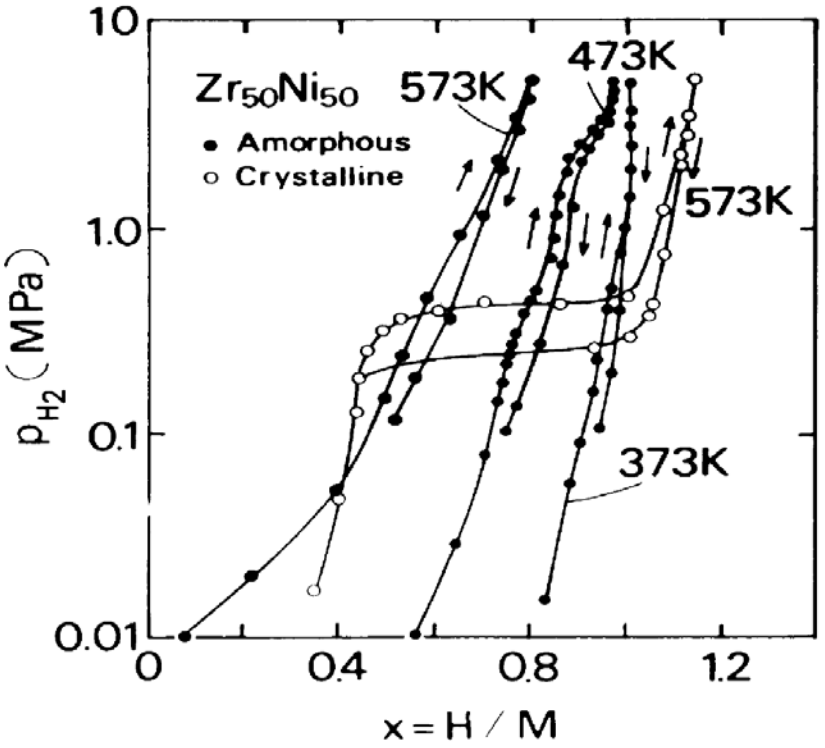

Figure 175. PCT plots for amorphous and crystalline $Zr_{50}Ni_{50}$. The amorphous measurements do not show a pressure plateau.[99]

For such materials it may be difficult to produce a van 't Hoff plot in the traditional sense of taking pressures from mid-plateau PCT measurements. Many properties of hydrogen in amorphous metals, such as the 'plateau-less' appearance of the PCT measurements, can be understood in terms of a density distribution of these interstitial site energies n(μ).[239,240,241] In other words, the number of sites within an energy interval of μ to μ+dμ which are occupied by hydrogen. This distribution was referred to as the density of states (DoS) function in Kirchheim's original work on the subject.[242] The DoS can be determined directly from PCT measurements by taking the derivative of the hydrogen concentration (C) with as a function of the pressure (lnP):

$$DoS(\mu) = \left.\frac{\partial C(p,T)}{\partial \ln(p_{eq})}\right|_T$$

Equation 165

It may then be possible to use the maximum in the DoS to define a pressure that represents the average equilibrium van 't Hoff pressure. Thus, plotting and comparing average enthalpies of formation for various amorphous hydrides.

A very important consideration is that the slope of the van 't Hoff plot, as implied by Equation 164, is linear and negative when the pressure is plotted on a log scale versus the inverse of temperature. However, the van 't Hoff equation is an approximation, so not all measured profiles will fit a linear profile. One of the most important assumptions is that the enthalpy of formation is independent of temperature. If nonlinear effects appear to be important, the nonlinear integrated form of the van 't Hoff equation shown in
Equation 166 can be used.[243]

Equation 166 $$RT\ln\left(\frac{P_{eq}}{P_0}\right) = \Delta H^o_{T_0} - T\Delta S^o_{T_0} + \Delta C^o_P\left(T - T_0\right) - T\Delta C^o_P \ln\left(\frac{T}{T_0}\right)$$

In
Equation 166, T_0 is an arbitrary reference temperature. Another important aspect of constructing van 't Hoff plots from PCT curves that is not shown in Figure 174 is whether the pressure plateau points are taken from absorption or desorption measurements. These values will typically differ due to hysteresis, even if perfect equilibrium is achieved. Lower plateau pressures are obtained from desorption measurements than absorption measurements. The specific application will determine whether absorption or desorption points are preferred, but desorption points are more commonly reported. This is because the desorption temperature is one of the most important variables affected by the thermodynamics. With limited fuel cell or ICE waste heat available on board a vehicle, materials development often aims at attempting to reduce the enthalpy of reaction in order to lower the required desorption temperature.

Some important considerations in the construction of a van 't Hoff plot from PCT measurements:

Because PCT plateaus are often sloping it is critical to take the equilibrium pressures of each isotherm at the same hydrogen concentration.

With respect to these plateau pressures, it is important to ensure that the hydrogen concentration at which the equilibrium plateau is measured is still within the two-phase region of the hydride of interest. For example, at an equivalent hydrogen concentration of 3 H/f.u. (hydrogen per formula unit) for $LaNi_5H_6$ appears to be mid-plateau between the α- and β-phase, but this is right at the concentration at which the γ-hydride phase $LaNi_5H_3$ is formed. Thus, P-equilibrium measured at this concentration may belong to the γ-hydride or the β-hydride or in between. In other cases, at higher temperatures as the two-phase region narrows (typically asymmetrically) a fixed hydrogen concentration may fall into the single-phase α solid solution or β hydride phase and the equilibrium

pressure measurement will not represent a valid phase transition point on the van 't Hoff plot.

It is very important in making PCT or other measurements to ensure that equilibrium has actually been achieved. A plateau pressure measurment is meaningless for the construction of a van 't Hoff plot if the sample is still (albiet slowly) absorbing or desorbing hydrogen. The best way to confirm equilibrium at a steady temperature is to observe the change of pressure with time. The measured pressure will assymptotically approach equilibrium. A good rule of thumb is to assume that equilibrium has been essentially reached when the pressure has approached 98% of the assymptotic value. For many hydrogen sorption materials, the kinetics of absorption or desorption or both may be so slow that it is not reasonable to wait the amount of time that it would take to reach 98%. In this case, it is not uncommon to take enough data to be able to extrapolate (with and exponential or double exponential fit of the data) to a final assypmtotic value and use this value for the van 't Hoff plot. This is somewhat controversial in that it is not actually a measured data point, but may be one option for materials with extremely slow kinetics. Certainly, it is clearly necessary to report such an extrapolation in detail in any publication of thermodynamics data so obtained.
Interstitial metal hydrides that form from hydrogen and a single phase metal, intermetallic compound, or metal alloy (Mg, Pd, LaNi5, MmNi5…) will have different equilibrium plateau pressures for absorption and desorption (hysteresis). This is explained in detail in the next section. The difference in plateau pressures and consequently the enthalpy and entropy of formation can be significantly different for absorption and desorption. For this reasion is it extremely important in reporting these values and van 't Hoff data to specify whether the data was derived from absorption or desorption measurements.

It is equally important to note that such hysteresis is not present in hydrides formed from multiple constituents ($NaH+Al+H_2 \rightarrow Na_3AlH_6$….) and the tranformation from reactants to products in these chemical formation/decomposition hydrides takes place at discrete hydrogen concentrations corresponding to the stoichiometric hydride. That is, there is little to no solubility of hydrogen in such hydrides. Never-the-less, reported results should indicate whether data was collected during absorption or desorption measurements.

1.2.5 Irreversibility Associated with Phase Transformations

In the idealized reversible hydride reaction, the plateau pressure is correlated to a reversible heat evolved (absorbed) during the process of formation (decomposition) of the hydride. However, one of the main causes of errors in measuring or ascribing

measured values to the thermodynamic stability of hydrides comes from the irreversibility associated with the hydride transformation.

The thermodynamic behavior of real systems is far more complex than the idealized one. This is due in part to hysteresis which is present in most first order phase transitions, and also with difficulties in operating under isothermal conditions. The intrinsic property of hysteresis introduces meta-stabilities in the system, and significant experimental constraints have to be applied, to avoid artifacts in the thermodynamic studies of hydrogenated powdered materials.

To better understand the impact of intrinsic hysteresis, it is important to first review the ideal, i.e. reversible and at equilibrium, scenario with no hysteresis for a standard intermetallic hydride. The Gibbs phase rule gives a variance of one for two components and three phases, H as a gas and two solid phases of an intermetallic hydride before and after reaction with hydrogen. This was presented in Equation 153 in the previous section describing the reaction occurring along the plateau of an isotherm, where a is the hydrogen content at the left boundary, i.e. that of the α-phase, and b is the hydrogen content at the right boundary, i.e. that of the β-phase. This description produces a single reversible isotherm for a given temperature, such as that shown in Figure 174.

However, in real systems hysteresis is present, and the plateau pressure for the absorption and desorption reaction will differ, and a different version of Equation 153 must be written for each case. Furthermore, the end points a and b will no longer match, and a different phase diagram must be drawn for the absorption and desorption reaction, clearly leading to a different enthalpy of reaction for each case. The plateau regions in this case can only be described as metastable since the equilibrium states are unknown due to hysteresis and sloping plateau effects. Stationary metastable states and reproducibility is possible in theory by finding a set of parameters that generate a constant minimum entropy production per cycle, but this has proved difficult in practice.

Hysteresis in the $\alpha \rightarrow \beta$ transformation can be described in more detail with the help of Figure 176 where x is considered an independent variable. At the point A, increasing x will cause the system to follow the 'AB' path. Below x_1, the system is stable, between x_1 and x_2, the system is metastable. The transformation occurs at x_2 according to the 'BC' path. When the direction is reversed from x_2 to x_1, the y variable follows a different route because the system is not reversible. The system moves through the metastable β states from C to D. The $\beta \rightarrow \alpha$ transformation will start at D. For metal-H system, x represents pressure and y the composition, ABCD represents a complete hysteresis cycle (loop).

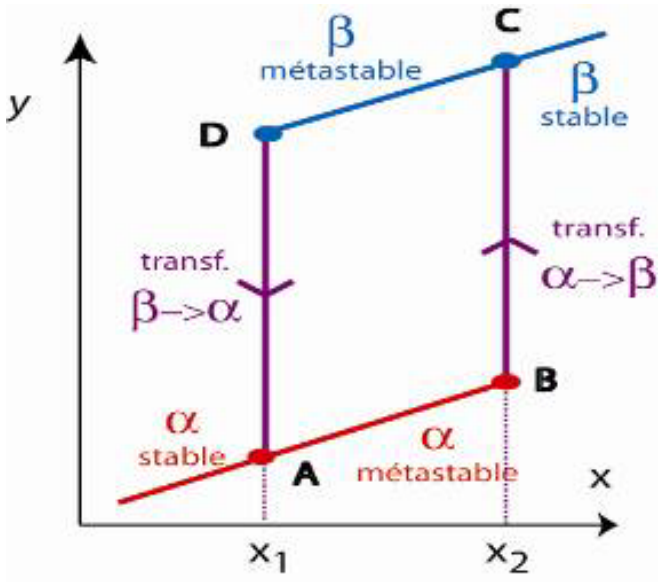

Figure 176. Hysteresis cycle (where x is an independent variable).

It should be noted that the definition of the cycle must obey two main criteria:
i the cycle must be described through quasi-static steps
ii) the path followed during the production of n cycles must be reproducible, because hysteresis is an intrinsic property of the system.

This unambiguous definition of the cycle is neglected in many thermodynamic studies. Note that severe experimental constraints on the control parameters of the reaction must be respected to achieve reproducibility of these hysteresis loops. It is clear that non re-reproducibility may cause dramatic differences in the determination of the heat of transformation and consequently on the estimation of the heat of formation.

Most of the time, thermodynamic characterizations of MH systems are carried out using Sievert's type equipment, sometimes using a coupled volumetric device with a calorimeter. If the discussion of such measurements is restricted to the pressure hysteresis (excluding sloping plateaus) then an ideal case of flat plateaus is presented schematically in Figure 177, for an isothermal case.

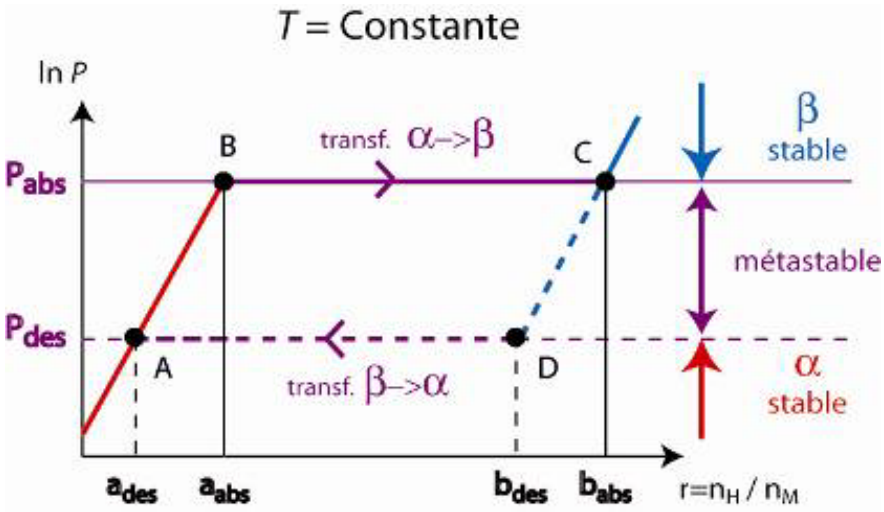

Figure 177. Ideal hysteresis in an isothermal plot of lnP = f(composition).

For a closed cycle (A,B,C,D,A in Figure 177), the different thermodynamic paths followed during the absorption and desorption processes produce:

Equation 167 $$P_{ab} > P_{des} \qquad a_{ab} > a_{des} \qquad b_{ab} > b_{des}$$

The consequence of this is that the single reaction of Equation 153 does not hold anymore and must be replaced by the two following reactions:

B→C) for the hydride formation from the saturated solid solution,

Equation 168 $$\frac{1}{b_a - a_a} MH_a(ab) + \frac{1}{2} H_2(P_{ab}, gas) \rightarrow \frac{1}{b_a - a_a} MH_b(ab)$$

D→A) for the hydride decomposition,

Equation 169 $$\frac{1}{b_d - a_d} MH_b(des) \rightarrow \frac{1}{b_d - a_d} MH_a(des) + \frac{1}{2} H_2(P_{des}, gas)$$

As a result, separate free energies of transformation are obtained for absorption and desorption:

Equation 170 $$\Delta G^{\alpha \rightarrow \beta} = \frac{1}{2} RTlnP_{ab} \qquad \Delta G^{\beta \rightarrow \alpha} = \frac{1}{2} RTlnP_{des}$$

The difference in the pressure plateau for absorption and desorption measurements will clearly have an effect on the van 't Hoff plots generated from PCT measurements producing different van 't Hoff plots for absorption and desorption as illustrated in Figure 178.

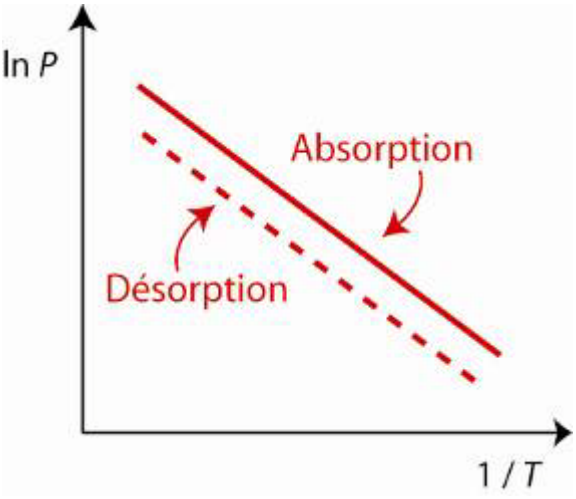

Figure 178. Absorption and Desorption van 't Hoff plots.

This leads to separate enthalpies of transformation for absorption and desorption:

Equation 171

$$\frac{\Delta H^{\alpha\to\beta}}{R} = \frac{1}{2}\frac{dlnP_{ab}}{d\left(\frac{1}{T}\right)} \quad \textbf{and} \quad \frac{\Delta H^{\beta\to\alpha}}{R} = \frac{1}{2}\frac{dlnP_{des}}{d\left(\frac{1}{T}\right)}$$

This may be quite important with respect to actual applications. In some cases (mobile applications) the pressure and temperature (and heat requirements) of desorption may be the critical determining factor of a materials performance. Whereas, in other cases (heat pumps….) the enthalpy of one or both absorption and desorption will have an important impact on the operation of a system.

There is no reason why the enthalpies calculated from the derivation of the free energy should be equal. This will be the case only for a restricted ideal hysteresis loop (as described above, with flat plateaus). At this point, it is crucial to understand that enthalpies for a reversible hydride material derived from PCT measurements are meaningful only if it has been experimentally demonstrated that the criteria for cycle reproducibility have been respected. From the intrinsic material properties perspective, this means that the material has been through sufficient activation cycles that sequential PCT isotherms are essentially identical. From the experimental measurement

perspective, it means that measurement errors or artifacts are insignificant with respect to the desired accuracy of the determined enthalpies. If not, then it is not surprising that the thermodynamic data will differ. Moreover, equilibrium states are never truly reached. Proceeding with the quasi-static steps to describe a cycle, simply means that it is possible to access the most stable meta-stable state, and not more than that.

The corresponding transformation enthalpies measured directly with a calorimeter do not include the extra energy 'cost' contained in the free energy term. This explains why the enthalpies should be equal (within the experimental error of the equipment) for absorption and desorption. The free energy loss along the cycle is lost to the external world in the form of heat. It can be demonstrated that it is part of the total entropy production of the cycle, and surprisingly it is lost in the two reversible branches AB and CD of the cycle (Figure 177).

One of the merits of physisorption materials lies in the full reversibility of hydrogen adsorption generally without significant hysteresis, which can be attributed to their low heats of adsorption typically less than 15 kJ/mol. However, hysteresis in H_2 adsorption / desorption have been observed in some MOFs. This has been explained by expansion and contraction due to flexibility in the framework structure.[244]

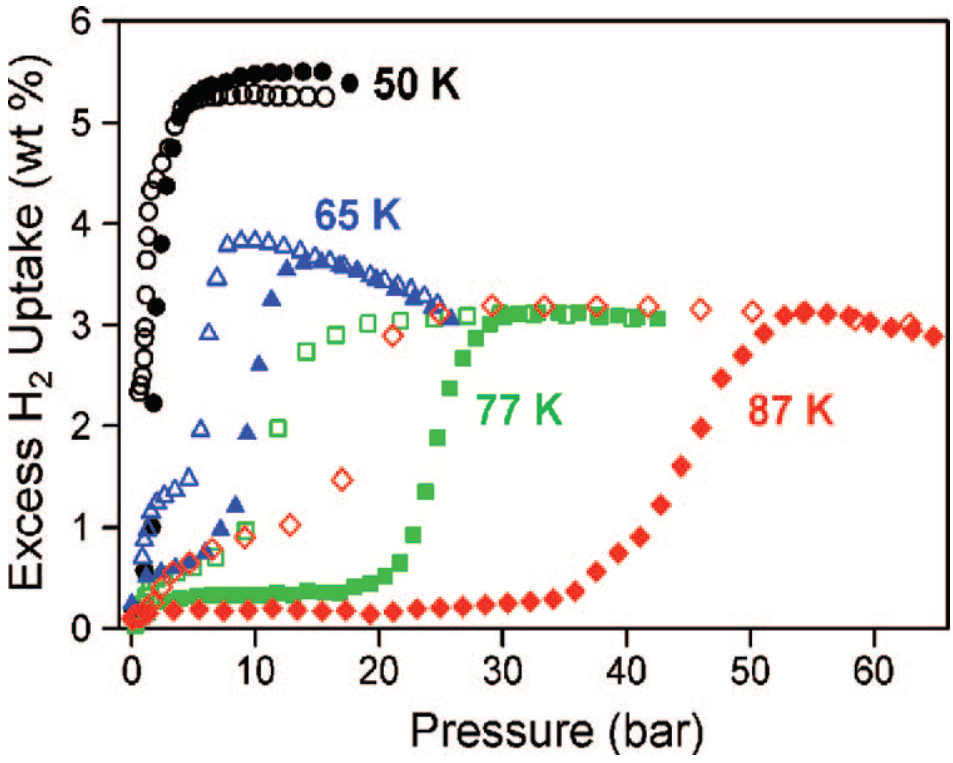

Figure 179. Hydrogen adsorption hysteresis observed in the flexible MOF materials Co(1,4-benzenedipyrazolate).[244]

1.2.6 Entropy Analysis

Hysteresis introduces an additional degree of freedom since $P_{abs} > P_{des}$ and, unfortunately, it also adds an extra energy cost with each cycle. This energy cost is proportional to the log of the difference in absorption and desorption plateau pressures. Thus, for real applications, slightly more energy is consumed through material entropy generation on cycling that is may be apparent through idealized thermal analysis of a material.

The total Gibbs free energy loss on completing and absorption (α-phase $\rightarrow$ β-phase) followed by a desorption(β-phase $\rightarrow$ α-phase) returning to the original point in temperature, pressure and composition is given by:

Equation 172

$$\Delta G_{loss} = \Delta G^{\alpha\rightarrow\beta} - \Delta G^{\beta\rightarrow\alpha} = \frac{1}{2} RT \ln \frac{P_{ab}}{P_{des}}$$

The entropy generated can be calculated without the need to understand the physics of its origin. According to Prigogine and Defay, during the course of a reaction, the entropy variation for a closed system is made of two contributions:

Equation 173

$$dS = \delta S_e + \delta S_i$$

where δS_e represents the entropy flows due to the heat transfers with the external surroundings, while δS_i represents the contribution from internal transformations within the system. Thus, δS_i corresponds to the entropy production per cycle, with: $\delta S_i = 0$ for a reversible process and $\delta S_i > 0$ for an irreversible process.

The effect of the irreversible contribution can be evaluated. If the system describes a complete loop, coming back to its initial state (that is that the generation of internal entropy δS_i is transferred by entropy flow through heat transfer with the external surroundings δS_e).The total entropy variation of the system then, is zero such that:

Equation 174

$$\oint dS = 0 = \oint \delta S_e + \oint \delta S_i$$

and

Equation 175

$$\oint \delta S_e = -\oint \delta S_i$$

where the symbol $\oint$ indicates integration over a closed loop.

The total entropy produced can be determined since it is possible to calculate the entropy flow exchanged with the external environment, thus:

Equation 176

$$\oint \delta S_e = \frac{\oint \delta q}{T}$$

where $\oint \delta q$ is the total heat exchanged along the different steps of the cycle. The free energy loss observed along the cycle can be directly correlated through this equation. From Equation 172, Equation 175 and Equation 176 one finally obtains:

Equation 177

$$\oint \delta S_i = \frac{\oint \Delta G_{loss}}{T}$$

Equation 177 indicates that when the basic criterion of reproducibility of the cycle is satisfied, Equation 177 takes the form:

Equation 178

$$\oint \delta S_i = Constant$$

When Equation 178 is not satisfied, then modifications of the thermodynamic parameters correlated to the phase transformation will be observed, resulting in different values for heats of transformation when measured, specifically by PCT van 't Hoff analysis.

Under ideal conditions, the best way to evaluate the enthalpy of formation of reversible hydrides remains a direct measurement with a calorimeter combined with a high precision gas dosing instrument. The ability to be able to measure quantitatively the hydrogen content of the material simultaneously is critical as will be shown in a later section (Thermodynamics section 2.2.3). Calorimetry alone is not sufficient. Using calorimetry, the heat detected should not be particularly sensitive to the entropy production term, which is generally not the case for the enthalpy derived from the van 't Hoff plot, see Equation 171 and Equation 177.

1.2.7 Intrinsic Hysteresis - Potential Causes

Hysteresis is a significant component of almost all cyclical scientific measurements. Across all reversible experiments, the two most common causes of hysteresis are equipment error and insufficient time to reach equilibrium at each measurement point. These are referred to as extrinsic effects. However, hysteresis can also be an indication of a different physical response when a variable, such as temperature or pressure, is ramped up or down. This is referred to as intrinsic hysteresis. Section 2.2.6 of the Capacity chapter discussed how various types of hysteresis affect PCT measurements. Here we will discuss the ways in which thermodynamics can influence both intrinsic and extrinsic hysteresis.

Intrinsic hysteresis is observed for nearly all metal hydrides. It is of considerable interest as it represents a loss of efficiency in energy storage and has been the focus of study since the investigation of the phenomena in the Pd-H system by Ubbelohde in 1937.[183] A number of models and theories have been proposed concerning the origin of hysteresis.[184] The most promising models focus on the variation in plastic deformation and dislocations during hydride formation and decomposition[245,246,247,248] which is supported by experimental evidence of dislocations during both formation and decomposition reactions.[249,250]

It is clear that the effects of intrinsic hysteresis on metal hydride measurements are significant, but the causes are less clear. The next few sections discuss some of the most likely contributions, but no complete theory has yet been identified.

1.2.8 Mechanical Strain energy

Absorption of hydrogen typically leads to expansion of the material's lattice, often causing deformations. If the deformation simply involves the stretching of atomic bonds without any breaking (Figure 180), it is called elastic deformation and excess energy is stored in the stretched bonds. This excess energy is referred to as mechanical strain energy.

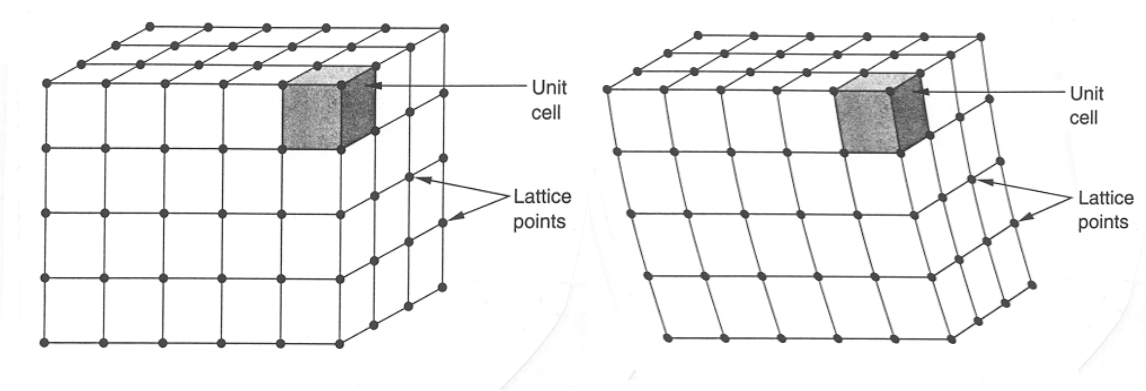

Figure 180. Representative image of an unstrained (left) and a strained (right) lattice. Excess energy is stored in the stretched bonds in the right-hand image.

1.2.9 Dislocations

Plastic deformation occurs when the strain is so great that bonds break and dislocations are formed which can move through the lattice. A typical type of dislocation, an edge dislocation, is shown in Figure 181. This formation of dislocations has been observed in many metal hydrides during both absorption[249] and desorption.[250]

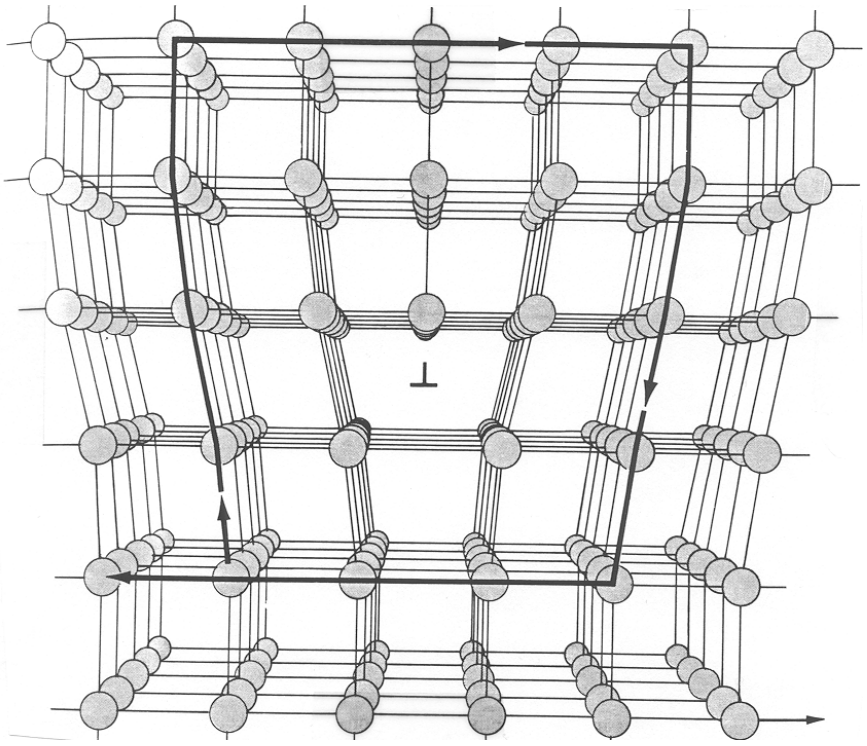

Figure 181. Representative image of an edge dislocation in a lattice.[251] Excess energy is stored in the bonds stretched by the dislocation.

Flanagan and Clewley have presented a theory to explain hysteresis based on a mechanism where dislocation arrays of comparable densities are produced during both hydride formation and hydride decomposition in a hysteresis cycle.[184] The hysteresis energy loss is observed to be the same, to within experimental error, for each cycle and therefore it was concluded that dislocations which are produced during each phase change are subsequently annihilated, leaving the dislocation density at a large saturation value. According to this theory, after the first cycle of $\alpha \rightarrow \beta$ and $\beta \rightarrow \alpha$ phase changes, a further cycle returns the sample to its initial highly dislocated state. The energy expended to create the new dislocations subsequently appears as heat which is transferred to the surroundings. The work done by the surroundings on the system is equal to the heat subsequently gained by the surroundings. The entropy of the surroundings thus increases as expected for an irreversible process. It is clear that either formation or decomposition of the hydride phase is an irreversible process since a small reversal of either leads to the traverse along a hysteresis scan and not to a reversal along a plateau. The authors described the extra free energy required for plastic deformation (on hydride formation and decomposition) as a new term, ΔH_{dis}. This energy is lost as heat during the hydride formation and decomposition processes, leading to a state ΔH_{dis} above equilibrium at the end of both the hydrogen absorption and desorption process, as shown in Figure 182.

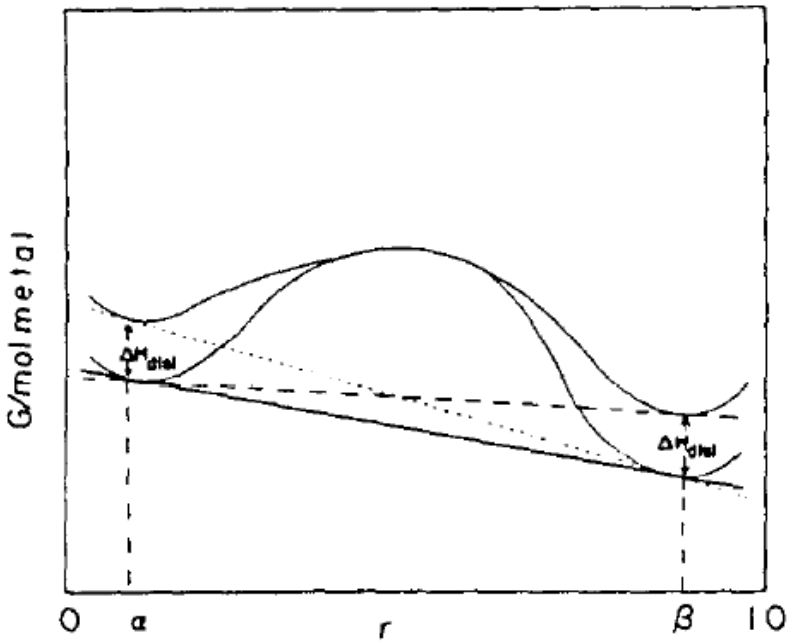

Figure 182. Schematic representation of the effect of plastic deformation, which accompanies hydride formation and hydride decomposition, on the integral free energy (per mole of metal). The tangent slopes $(dG/dr)_{T,p}$ give the chemical potential of hydrogen. Solid line: hypothetical equilibrium tangent slope; Dashed line: - - -, slope obtaining during hydride formation; Dotted line: · · · · · · slope obtaining during hydride decomposition.[184]

1.2.10 Interfacial Energy/Particle Size Effects

Many hydrogen storage materials have a granular structure. At the interface between two grains, there is a region of stretched bonds to accommodate the different orientations of the lattice. A similar effect can be observed near the boundaries of small particles. As discussed in section 1.2.8 these stretched bonds represent excess energy stored in the lattice. An example of such an interface is shown in Figure 183. Smaller grain or particle sizes will lead to more interfacial or boundary areas, which can change the thermodynamics of the reaction. However, whether the enthalpy of reaction is shifted upwards or downwards depends on the material and the interface. Theoretical and experimental work is needed to understand the exact effects on a case by case basis. For example, if the surface energy of the hydride phase is lower than that of the unhydrided phase, as is the case for Mg and MgH_2, then the enthalpy of formation is expected to decrease with decreasing particle or grain size.[252]

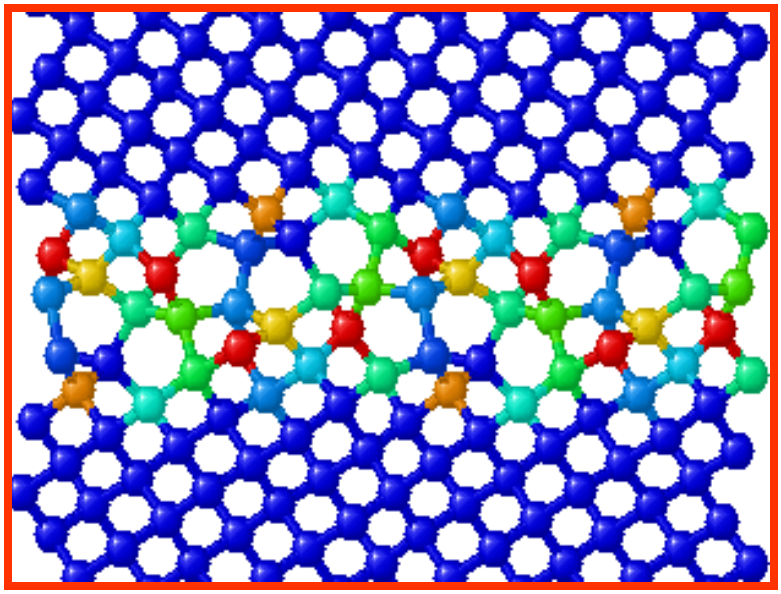

Figure 183. Representative image of strain in a lattice at the interface between two grains or particles.

1.3 Thermodynamics of On-board Rechargeable Physisorption Materials

1.3.1 Isosteric Heat of Adsorption

Physisorption of hydrogen in porous materials such as carbon nanotubes, activated carbon, zeolites, and coordination polymers or metal-organic frameworks (MOFs), is an exothermic process, and the isosteric (constant coverage, or constant excess hydrogen capacity) heat of adsorption (Q_{st}) or adsorption enthalpy (ΔH) is a direct indicator of the strength and heterogeneity of the interaction between the adsorbate and the adsorbent.

The isosteric enthalpies of adsorption of hydrogen on a wide range of porous materials have been listed in Table 2 of the article "Adsorption and desorption of hydrogen on metal–organic framework materials for storage applications: comparison with other nanoporous materials." by K. M. Thomas.[253] The enthalpies for hydrogen adsorption on porous materials have the following ranges: (i) activated carbon materials: 1.4-12.5 kJ mol^{-1}, (ii) zeolites: 5.9-18.2 kJ mol^{-1}, (iii) silica adsorbents: 5.4-10.4 kJ mol^{-1}, and (iv) MOFs: 5.1-13.5 kJ mol^{-1}. All the Q_{st} values are significantly higher than the enthalpy of vaporization of 0.9 kJ mol^{-1} for H_2 at 20.28 K implying significant hydrogen adsorption energies for all of these high surface area materials.[253]

While the above adsorption enthalpy values for porous materials are too low for any significant hydrogen uptake at ambient temperatures, the higher values of reversible ambient hydrides require proportionately more heat transfer for most applications. Thus, an intermediate weak non-dissociative chemisorption with facile adsorption and desorption characteristics would be preferred for storage applications.

1.3.2 Determination of Isosteric Heats of Adsorption from Isotherm Measurements

The determination of isosteric heat of adsorption for hydrogen is a very important aspect of characterizing the potential for various porous materials to be used for on-board hydrogen storage applications.

The isosteric heat of adsorption, Q_{st} of an adsorbate-adsorbent system is the change in enthalpy of the system upon the reversible transition of unit mass of any component from one phase (gas-phase for adsorption) to another (adsorbed phase). Like the heats of conventional phase-transitions, isosteric heat of adsorption can be described by Clausius-Clapeyron thermodynamic correlation.[254]

Equation 179 $$Q_{st} = -R\,[\partial \ln(P)/\partial(1/T)]_{\theta}$$

The adsorbed phase in this definition implies the absolute amount of adsorbate present in the solid adsorbent. **Experimentally measured adsorption on the other hand is the surface excess adsorption (n_{ex})** which is related to absolute adsorption (n_a) by

Equation 180 $$n_a = n_{ex} + (\rho_g \times V_a)$$

In the case of vapor-phase adsorption, the gas-phase density (ρ_g) is negligible compared to adsorbed-phase density (ρ_a); so surface excess can be assumed to be equal to the absolute amount. However, for high pressure gas supercritical gas adsorption, absolute adsorption significantly differs from surface excess due to non-negligible gas density. Therefore, if the isosteric heats of adsorption are determined at a constant excess instead constant absolute, it can become unphysical. **Thus, for supercritical gas adsorption, it is important to estimate isosteric heats based on the absolute adsorption.[255] Note, however, that this requires assumptions about the adsorption volume that have a significant effect on the resulting "absolute capacity" and the "absolute isosteric heat of adsorption" derived from these assumptions (see section 1.3.3).**

In addition, isosteric heat of adsorption is a coverage dependent property and single values of isosteric heats of adsorption apply only to initially adsorbed molecules, i.e., in the Henry's law region dictated by low coverage where the adsorbate molecules act independently.

To determine the isosteric heat of adsorption, the most frequently used method is the application of the Clausius–Clapeyron equation (Equation 179) to results obtained from measured hydrogen adsorption isotherms. Adsorption Isosteres are a function relating the equilibrium pressure to the temperature at a constant value of the amount, or excess amount, of substance adsorbed by a given amount of solid (IUPAC). Plotting lnP vs. 1/T of H_2 for a given adsorption isostere enables the determination of the isosteric heat of adsorption from the slope of the isostere Q_{st} = -slope × R (Figure 184).

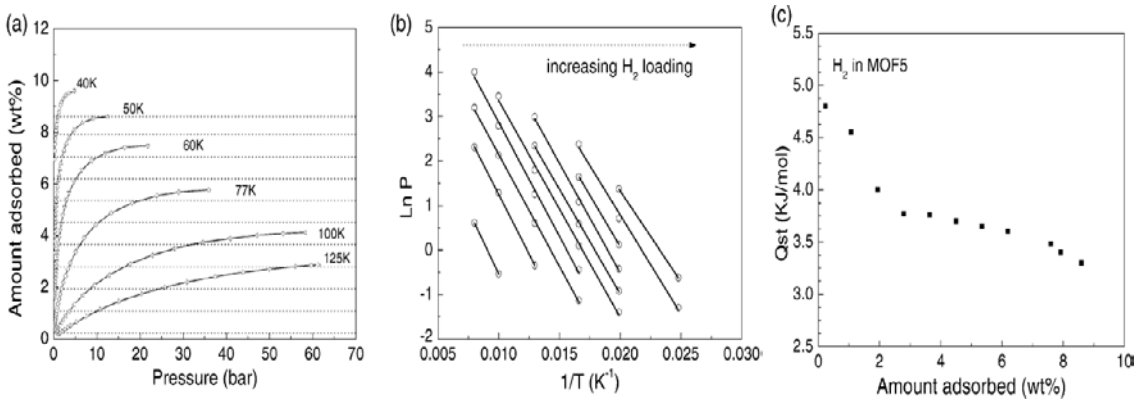

Figure 184. (a) Excess adsorption isotherm data of H_2 in MOF-5, used in the heat of adsorption calculation. Dotted lines indicate P-T data at fixed hydrogen concentrations. (b) The ln P vs. 1/T plot of H_2 in MOF-5 at various wt.%. According to the Clausius-Clapeyron equation, the isosteric heat of adsorption Q_{st} = -slope × R. (c) Q_{st} plot for H_2 adsorption in MOF-5, as derived from (b).[143]

Typically, the isosteric heat of adsorption is calculated from the adsorption isotherms measured at 77 K and 87 K since these temperatures can be realized easily by liquid nitrogen and liquid argon, respectively.[256] However, this small temperature range usually leads to a very high uncertainty in the heat of adsorption. To ensure the isosteric heat of adsorption determined with higher accuracy, it requires at a minimum three closely spaced (in temperature) adsorption isotherms (Figure 185).

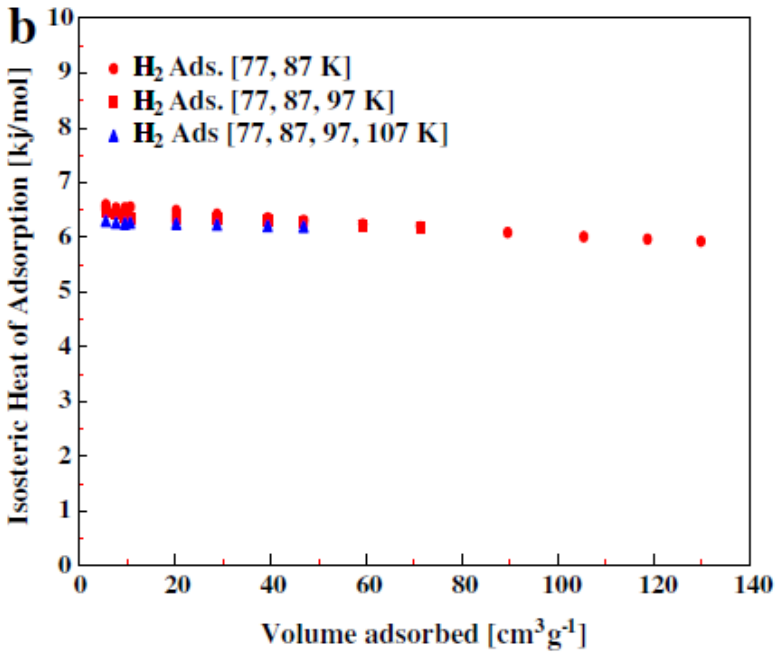

Figure 185. The isosteric heat values calculated from different number of adsorption isotherms.[18]

The critical step in determining isosteric heats of adsorption from isotherm measurements (Figure 184a) is to be able to accurately create plots of equilibrium pressures (ln*P*) vs. temperatures (*1/T*) at constant (in this case "excess") concentrations (Figure 184b). To do this, one must be able to interpolate between equilibrium pressures data points at a specific concentration from the isotherm measurements. This interpolation is usually done using a model to fit the isotherm data. Once the *lnP* vs. *1/T* (Figure 184b, essentially van 't Hoff plots) are created one then determines the isosteric heat of adsorption from the slope at each concentration (via the Clausius-Clapeyron equation). In this manner the isosteric heat of hydrogen adsorption can be then plotted as a function of concentration (Figure 184c). However, these hydrogen adsorption enthalpy calculations are very sensitive to errors with the accuracy of models for interpolating between isotherm points. These effects being critical in the low pressure region.[10]

In the low pressure region the relationship between the concentration of adsorbed hydrogen (n) and pressure (P) at constant temperature are often assumed to be linear. This is essentially Henry's law and modeling the low pressure isotherms consists of determining the Henry's law constant k_H.

Henry's law (formulated by William Henry in 1803) states that, at a constant temperature, the amount of a given gas that dissolves in a given type and volume of liquid is directly proportional to the partial pressure of that gas in equilibrium with that liquid. In the case of a gas adsorbed to a solid surface:

Equation 181

$$n = k_H P$$

where *P* is the pressure of the adsorbate, n is the specific surface excess amount of the adsorbate and k_H is a constant with the dimensions of moles of gas divided by pressure. When the temperature of a system changes, the Henry constant will also change. This is why some people prefer to name it Henry coefficient. There are multiple equations assessing the effect of temperature on the constant. The van 't Hoff form of the constant is:

Equation 182

$$k_H = k_H(T^o) \exp\left[-C(1/T - 1/T^o)\right]$$

Where k_H for a given temperature is the Henry's Law constant, *T* is the temperature, T^o refers to the standard temperature (298 K) and *C* is a constant for a given gas which is proportional to the enthalpy of adsorption.

For hydrogen adsorption the Henry's law (linear) range of pressure vs. concentration is dictated by low coverage (assumes adsorbate molecules act independently). Thus Henry's law applies for differential enthalpy of adsorption at zero coverage.

The differential enthalpy of adsorption at zero coverage is then given by:

Equation 183

$$\left(\frac{\partial H}{\partial n}\right) = RT^2 \frac{\partial(\ln k_H)}{\partial T}$$

1.3.3 Determination of Isosteric Heats by Modeling of Adsorption Isotherms

At higher pressures more complex relationships between adsorbed hydrogen concentration and equilibrium gas pressure are required. As mentioned above**, for supercritical gas adsorption, it is important to estimate isosteric heats based on the absolute adsorption.[255] Thus, for hydrogen storage applications it is beneficial to consider isosteric heats of adsorption determined from "absolute" adsorption isotherms, as well as from the directly measured "excess" adsorption isotherms. To do this requires assumptions about the adsorption volume that have a significant effect on the resulting "absolute capacity" and the "absolute isosteric heat of adsorption" derived from these assumptions. This section describes some of the methods for the evaluation of Isosteric Heats of Adsorption from a series of adsorption or desorption isotherms. Recommendations for the Best Practices in presenting isosteric heats of adsorption are given in section 1.3.6 .**

While extremely important for the evaluation of physisorption hydrogen storage systems, analysis at this level of detail has not been common practice up to this point and very few result are present in the literature. One such example is given below for the difference in isosteric heats of adsorptions calculated using the measured "excess" adsorption isotherms vs. "absolute" adsorption isotherms determined using an assumed boundary layer thickness *t* and bulk gas density ρ_g, to derive the n_a "absolute" quantity of adsorbed hydrogen from measured n_{ex} "excess" adsorption isotherms using Equation 180.[257]

Measured "excess" adsorption isotherms are shown on the left of Figure 186 for the physisorption activated carbon material MSC-30.

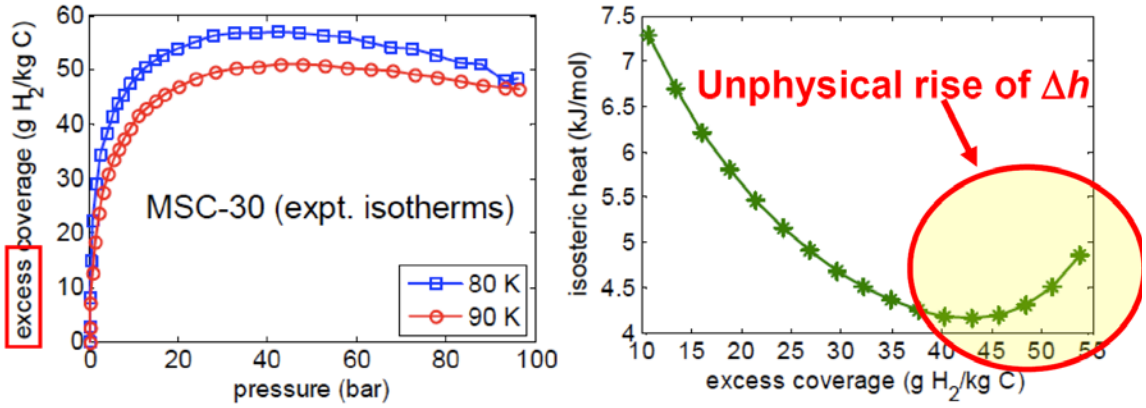

Figure 186. (Left) Measured "excess" adsorption isotherms. (Right) Calculated isosteric heat of adsorption from "excess" adsorption isotherms.[257]

The isosteric heats of formation are shown on the right side of the same figure calculated using the two isotherm version of the Clausius-Clapeyron relation:

Equation 184

$$\Delta H = \frac{RT_1T_2}{T_2 - T_1}\ln\left(\frac{P_2}{P_1}\right)$$

The increasing heat of adsorption at higher hydrogen coverage was assessed to be unphysical.[257] For this reason the "excess" adsorption isotherms were converted to "absolute" adsorption isotherms by adding the amount of adsorbed hydrogen in the adsorption boundary layer of thickness *t*, that would be present as bulk (in the absence of physisorption) hydrogen at pressure *P* to the "excess" adsorption isotherms. This is shown diagrammatically in Figure 187.

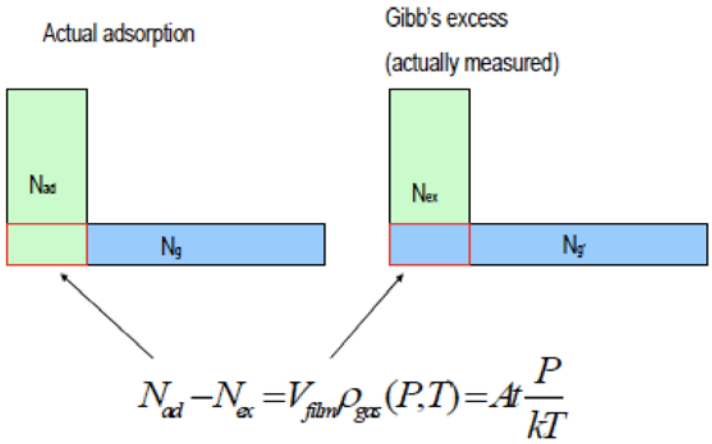

Figure 187. (Left) Actual ("absolute") adsorbed hydrogen vs. (Right) measured "excess" adsorbed hydrogen, the difference (red rectangle) being equal to *AtP/kT*.[257]

The calculated "absolute" adsorption isotherms are shown on the left of Figure 188 for the physisorption material MSC-30. The isosteric heats of formation calculated using the two isotherm version of the Clausius-Clapeyron relation are shown on the right side of the same figure. One can see not only a significant difference in the shape of the isosteric heat of adsorption plot (continuously decreasing with hydrogen coverage) but also a general lowering of the calculated values of the isosteric heats of adsorption.

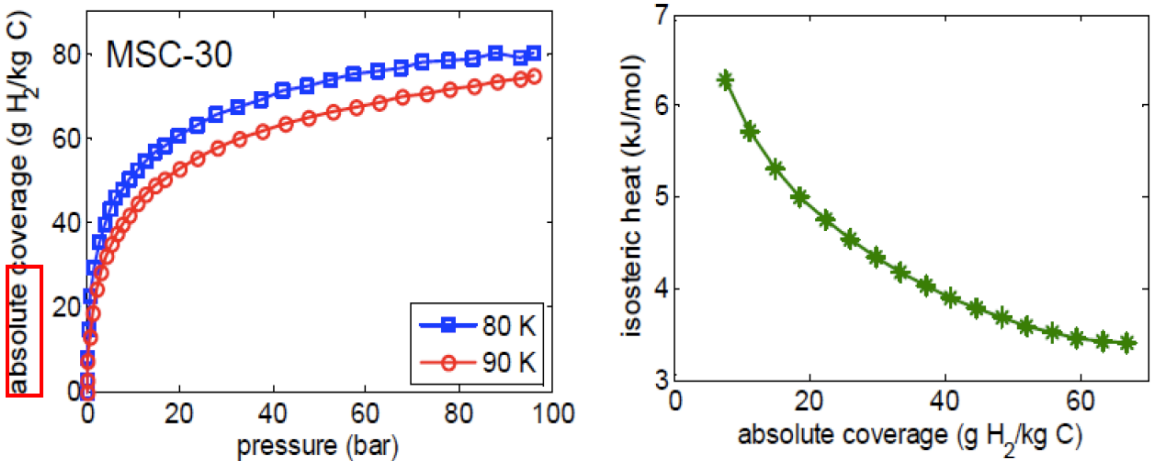

Figure 188. (Left) Calculated "absolute" adsorption isotherms. (Right) Calculated isosteric heat of adsorption from "absolute" adsorption isotherms.[257]

The author's conclusions were:[257]

- Except for at very low coverage, compute isosteric heat from *absolute adsorption* instead of *excess*.
- Computer simulations provide required microscopic information on film volume and/or thickness.
- Product: isosteric heats valid at *all* pressures and coverages.

This example demonstrates that the difference between isosteric heats of formation determined from measured "excess" adsorption isotherms and calculated "absolute" adsorption isotherms can be quite significant.

It should be noted however, that the calculated "absolute" adsorption isotherms required some assumptions (or simulations) of the adsorption volume as well as the determination of bulk gas density based on either an ideal gas but preferably (at low temperatures and elevated pressures) accurate real gas density.

The calculation of absolute adsorption from the experimental excess adsorption data requires knowledge of the adsorption volume (V_a in Equation 180). Unfortunately, this cannot be presently determined using any experimental technique. Therefore, a number of analytical and empirical models have been developed to describe "absolute" hydrogen adsorption properties (isotherms).

For the most part, three models (Viral Method 1, Viral Method 2, and the Langmuir-Freundlich equation) have been mainly used for interpolating isotherm pressure values for specific amounts adsorbed from isotherm data, and for calculating the isosteric enthalpies of adsorption.[258] The following describes these three models, the Dubinin-Astakhov (DA) model, and a more recently developed parametric model based on an advanced modification of the DA model for hydrogen adsorption.[151]

It should be noted that, in using these models to correctly determine isosteric heats of adsorption the adsorbed amount *n* is the "absolute" capacity as a function of pressure.

1.3.3.1 The Virial Method 1

This method uses the following virial equation:

Equation 185

$$\ln(n/p) = A_0 + A_1 n + A_2 n^2 \ldots\ldots$$

where *n* is the amount adsorbed, *p* is the pressure and A_0, A_1 and A_2 are constants. The van 't Hoff isochore is then used to determine the isosteric enthalpy of adsorption at specific surface coverages. The isosteric enthalpies of adsorption at zero surface coverage are obtained from the A_0 values.

1.3.3.2 The Virial Method 2

The method is based on the following virial equation:

Equation 186

$$\ln(p) = \ln(n) + (1/T)\sum_{i=0}^{m} a_i n^i + \sum_{j=0}^{n} b_j n^j$$

where p is pressure, n is "absolute" amount adsorbed, T is temperature, and a_i and b_j are temperature independent empirical parameters. This method provide the equilibrium pressure p and concentration n for any temperature T when a_i and b_j have been determined from a fit to a set of experimental isotherms. This is essentially the Clausius-Clapeyron linear relationship between ln(p) and $1/T$ where the slope (second term in Equation 186) is the isosteric enthalpy of adsorption (Q_{st}) or:

Equation 187

$$Q_{st} = -R\sum_{i=0}^{m} a_i n^i$$

where R is the gas constant.

1.3.3.3 The Langmuir-Freundlich Equation

The Langmuir-Freundlich equation is as follows:

Equation 188

$$\left(\frac{n}{n_L}\right) = \left(\frac{kp^{1/m}}{1+kp^{1/m}}\right)$$

where n_L is the maximum amount adsorbed, p is the pressure, m and k are fitting constants.

As with the DA analysis, isotherm data can be fitted using one of the above three relationships between p and n above to develop isosteric ln$P$ vs. $1/T$ plots. From these plots, the isosteric heat of adsorption can be determined using the Clausius-Clapeyron equation.

A comparison of the three methods for describing hydrogen and deuterium adsorption on a MOF material has shown that the virial methods give more accurate heats of adsorption at low surface coverage (Figure 189). This is attributed to the fact that the Langmuir–Freundlich isotherm does not reduce to Henry's law at zero surface coverage.[258]

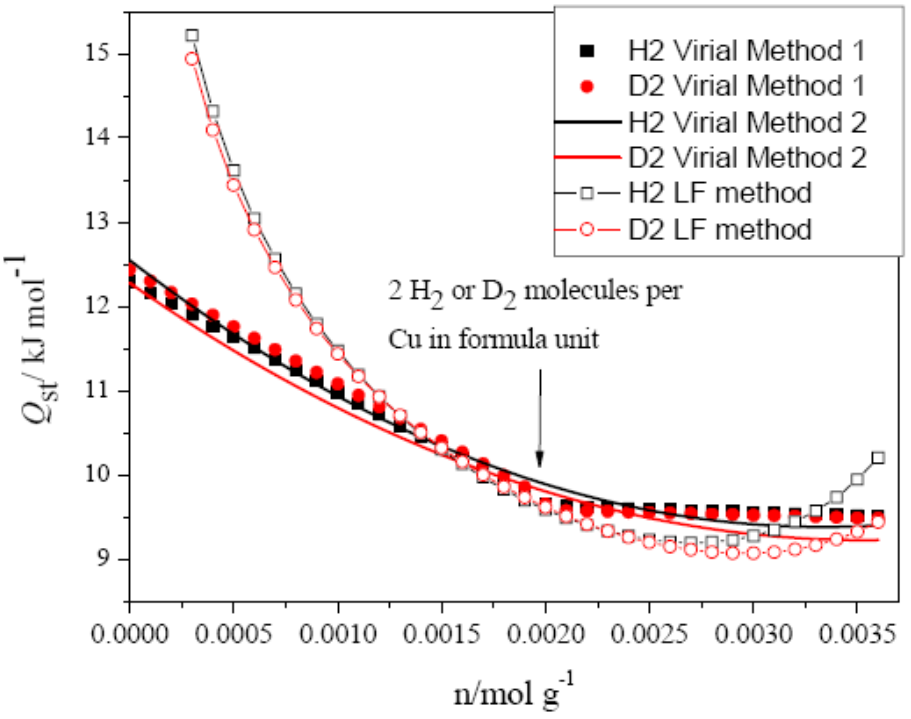

Figure 189. Comparison of isosteric enthalpies of adsorption (Q_{st}) calculated using virial methods and Langmuir-Freundlich methods for H_2 and D_2 adsorption on a MOF material.[258]

1.3.3.4 The Dubinin-Astakhov Model

The DR (Dubinin-Radushkevich) and DA (Dubinin-Astakhov) equations, originally found by Dubinin and Radushkevich[259] to be very good empirical fits to adsorption data in porous carbon and zeolites, were later derived by Dubinin based upon two assumptions. The first assumption made by Dubinin[260] was the "thermodynamic criterion" which is supported by many experimental observations. This criterion utilizes the concept of adsorption potential, A, and is given by

Equation 189

$$\left[\frac{\partial A}{\partial T}\right]_{\theta} = 0$$

where

Equation 190

$$A = \mathrm{R}T\ln\left(\frac{P_s}{P}\right)$$

Here P_s is the vapor pressure of the adsorbate that would be observed over the liquid phase that has a flat interface with the gas and P is the actual adsorbate pressure. The second assumption presented by Dubinin[260] was that the energy of adsorption between the adsorbate and the adsorbent surface follows a Weibull distribution curve. From this the generalized DA equation is derived, of which the DR equation is a special case. One form of the DA equation is:

Equation 191

$$\ln\left(\frac{n_A}{n_{Ao}}\right) = B\left(\frac{T}{\beta}\right)^k \ln^k\left(\frac{P_s}{P}\right)$$

In this equation k is a constant whose value can vary somewhat, usually from 1.5 to about 4. The special case with k equal to 2 is the DR equation. The parameter β is dependent upon the adsorbate; whereas, the energy term B is dependent upon the adsorbent. The subscribe A indicates the adsorbate. The n_{Ao} is the number of moles to completely fill the pores of the adsorbent. For this purpose, a corrected density of the liquid is used. This correction depends upon where in the isotherm the pore filling begins. Dubinin, Zhukovskaya and Murdmaa (DZM) presented a tabulation of the corrected densities.[261] It is also possible to calculate density from quantum mechanical based equations. [262] The external, non-porous area is assumed to be very small relative to the pore volume and may therefore be ignored.

At high enough coverage, adsorption on microporous adsorbents can usually be described by the Dubinin-Astakhov (DA) model.[263] The DA equation, when adapted for *excess adsorption* measurements[264], can be expressed as:

Equation 192

$$w = w_o \exp[-(A/E)^m] - w_g$$

The quantity w is the volume (cm^3/g) of the adsorbed phase in the microporous volume w_0 of the adsorbent, m is a structural heterogeneity parameter,[144] and E is a characteristic energy of the adsorption process which is dependent on the mean potential inside the pores.[265] The term w_g is an additional small correction to the standard DA isotherm to account for excess adsorption measurements. It can be expressed as $w_g=c\rho_g V_p$, where c is a constant and ρ_g is the gas-phase density in the porous volume V_p of the sample. The quantity A is the adsorption potential given by:

Equation 193

$$A = RT\ln(P_S / P)$$

where R is the universal gas constant, P_S is the saturation pressure of the adsorbate, and T is the absolute temperature. As with the generalized DA model, for excess adsorption when m=1 and m=2, the DA model reduces to the Freundlich and the Dubinin-Radushkevich models, respectively.[266]

As introduced above, the DA model is based on the concept of pore filling by a liquid for adsorption isotherms measured below the critical temperature of the adsorbate. Under these conditions the characteristic curves of w versus A are considered temperature invariant.[264] However, for the typical supercritical isotherms of hydrogen storage measurements, the saturation pressure *Ps* does not exist. In this case, the pseudo-saturation vapor has to be defined using an approach such as the one proposed by Amankwah and Schwarz.[144] For such an analysis, P_s is determined by introducing a new parameter γ, which expresses the pseudo-saturation pressure as a function of temperature according to:

Equation 194

$$P_S = (T / T_C)^{\gamma} P_C$$

where T_C and P_C are the critical temperature and pressure of the adsorbate. The parameter γ is specific to the adsorbent-adsorbate pair and can be determined from fitting the adsorption data. For $\gamma = 2$, Equation 194 reduces to the so-called Dubinin empirical equation.[264]

For hydrogen storage applications, determination of the adsorption enthalpy is critical the heat management design of the storage system. With physisorption materials the adsorption enthalpy reflects the strength of gas-solid interactions and can vary with the properties of the adsorbent.[267] It can usually be calculated from adsorption isotherms at constant w from the Clausius-Clapeyron expression:

Equation 195

$$\Delta H = -R \left[\partial \ln(P) / \partial (1/T) \right]_w$$

The use of Equation 195 in conjunction with the standard DA isotherm yields the following expression for the adsorption enthalpy:

Equation 196

$$\Delta H = E \ln(w_o/w)^{1/m} + \gamma RT$$

Equation 196 is a variant of other expressions[268,269] used for subcritical adsorption. Here the temperature dependence of the enthalpy is explicitly related to the parameter

γ. Physically, this parameter appears to be associated with the internal energy of the adsorbate in the pore. Note that the temperature-independent part of Equation 196 is:

Equation 197

$$\Delta H_o = E \ln(w_o/w)^{1/m}$$

1.3.3.5 The Modified Dubinin-Astakhov (MDA) Analytical Model

More recently, an advanced modification of the Dubinin-Astakhov model has been developed for hydrogen adsorption.[151] The Modified DA analytical model involves a five-parameter equation that correlates the experimentally measured surface excess with the state points (PCT isotherms). It is given by:

Equation 198

$$n_{ex} = n_{\max} \exp\left[-\left(\frac{RT}{\alpha + \beta T}\right)^2 \ln^2\left(\frac{P}{P_o}\right)\right] - V_a \rho_g$$

where, *T* and *P* are the temperature and the pressure, *R* is the universal gas constant, the parameter n_{max} is the limiting adsorption (maximum absolute adsorption value in mol kg^{-1}: per Equation 180) and the parameter P_0 is the pressure corresponding to the limiting adsorption (no longer the saturation pressure since it is applied in the supercritical region), the parameter V_a is the adsorption volume, ρ_g is the bulk density of the gas at *P* and *T*, and the parameters α and β are the enthalpic and entropic contributions of free energy of adsorption. All five parameters (α , β , P_0, n_{max}, *and* V_a) are variables that are fit iteratively to a set of *P, T, n* data. The model is fit to the experimental data using an iterative procedure. The Levenberg-Marquardt algorithm is used to search for the coefficient values that minimize standard error of estimate. This is a form of nonlinear, least-squares fitting.

The temperature dependent form of the free energy of adsorption given in the Equation 198 allows the model to accurately fit the experimental data collected over a wide range of temperatures using only these five parameters.

To use this method to determine the isosteric heats of adsorption, the above Modified Dubinin-Astakhov (MDA) analytical model is fit by iteration of the five parameter to experimentally measured surface excess adsorption isotherms. Using the best fit values of the five parameters, the absolute adsorption isotherms can then be generated from the modified absolute adsorption (MDA) model:

Equation 199

$$n_a = n_{\max} \exp\left[-\left[\frac{RT}{\alpha + \beta T}\right]^2 \ln^2\left(\frac{P_0}{P}\right)\right]$$

The isosteric heats at constant absolute adsorption are then calculated using the Clausius-Clapeyron equation applied to these calculated absolute adsorption isotherms.

Figure 190 shows the experimental surface excess hydrogen adsorption data on activated carbon Maxsorb® collected over a temperature range of 30-273 K (circles). The solid lines are the best fit to the data using Equation 198.
The parameters obtained for the best fit are: n_{max} = 14.24 wt%, α = 3120.3 J/mol, β = 17.922 J/ mol K, P_o = 1329 MPa and V_a = 1.4163 Lkg^{-1}.

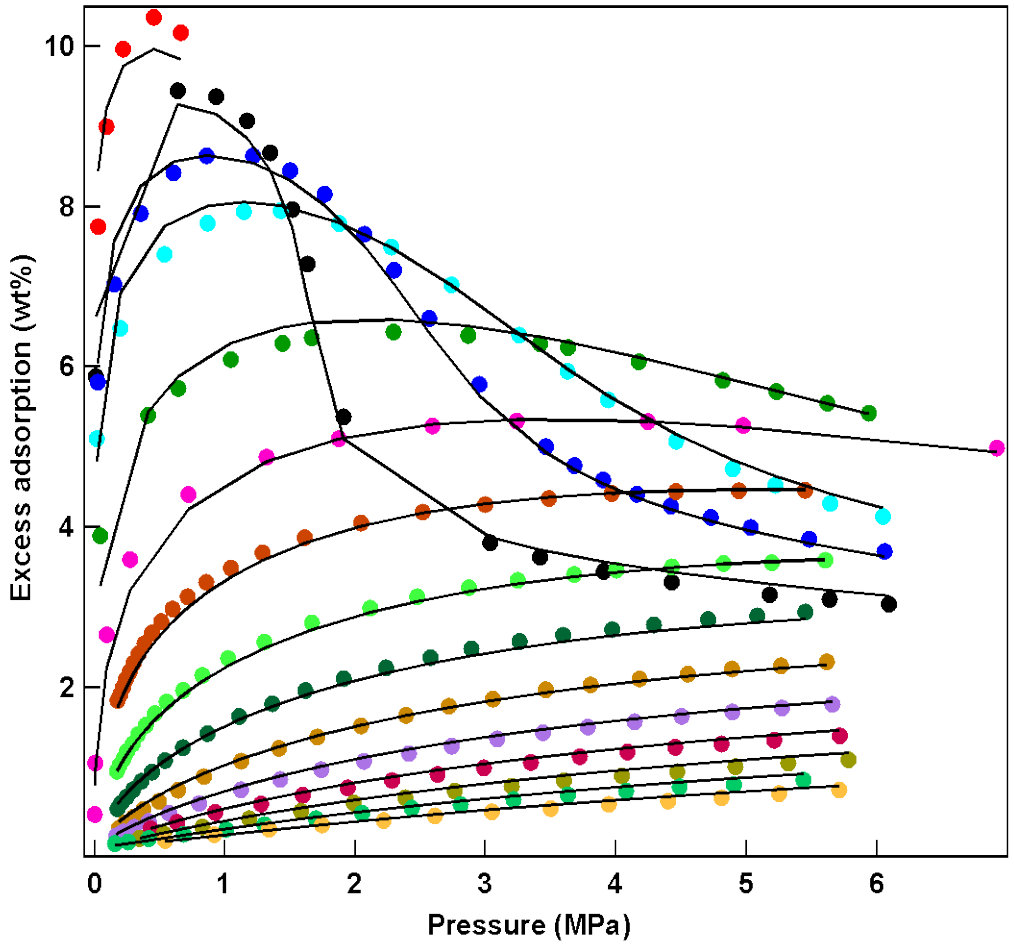

Figure 190. Experimental surface excess hydrogen adsorption data (circles) of the physisorption material Maxsorb® over a temperature range of 30 to 273 K. Solid lines are the best fit made using Equation 198.[270]

The absolute adsorptions corresponding to the above excess are now constructed using the Equation 199. These are shown in the Figure 191.

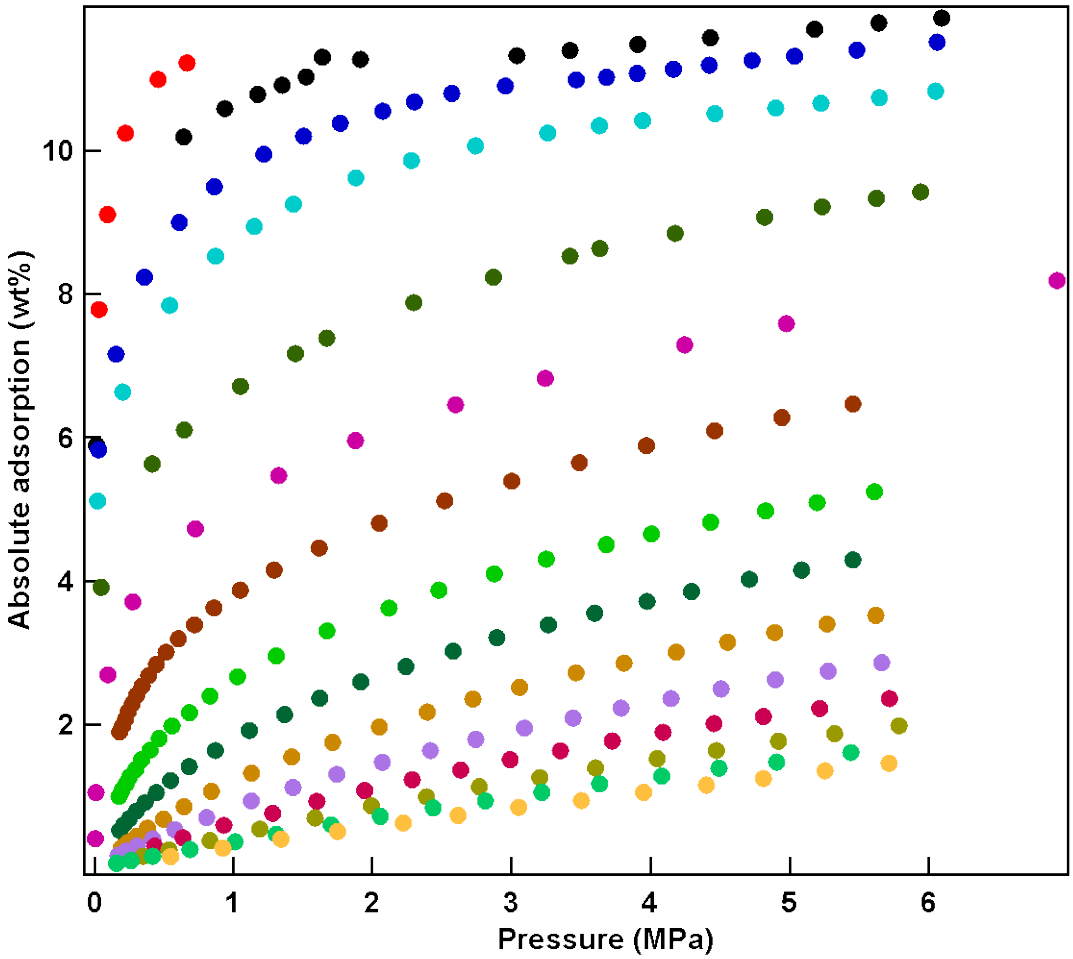

Figure 191. Absolute hydrogen adsorption results of Maxsorb® over a temperature range of 30 to 273 K constructed using Equation 199.[270]

Adsorption isosteres at constant absolute adsorptions are now made from the interpolated data in Figure 190 and are shown below in the Figure 192.

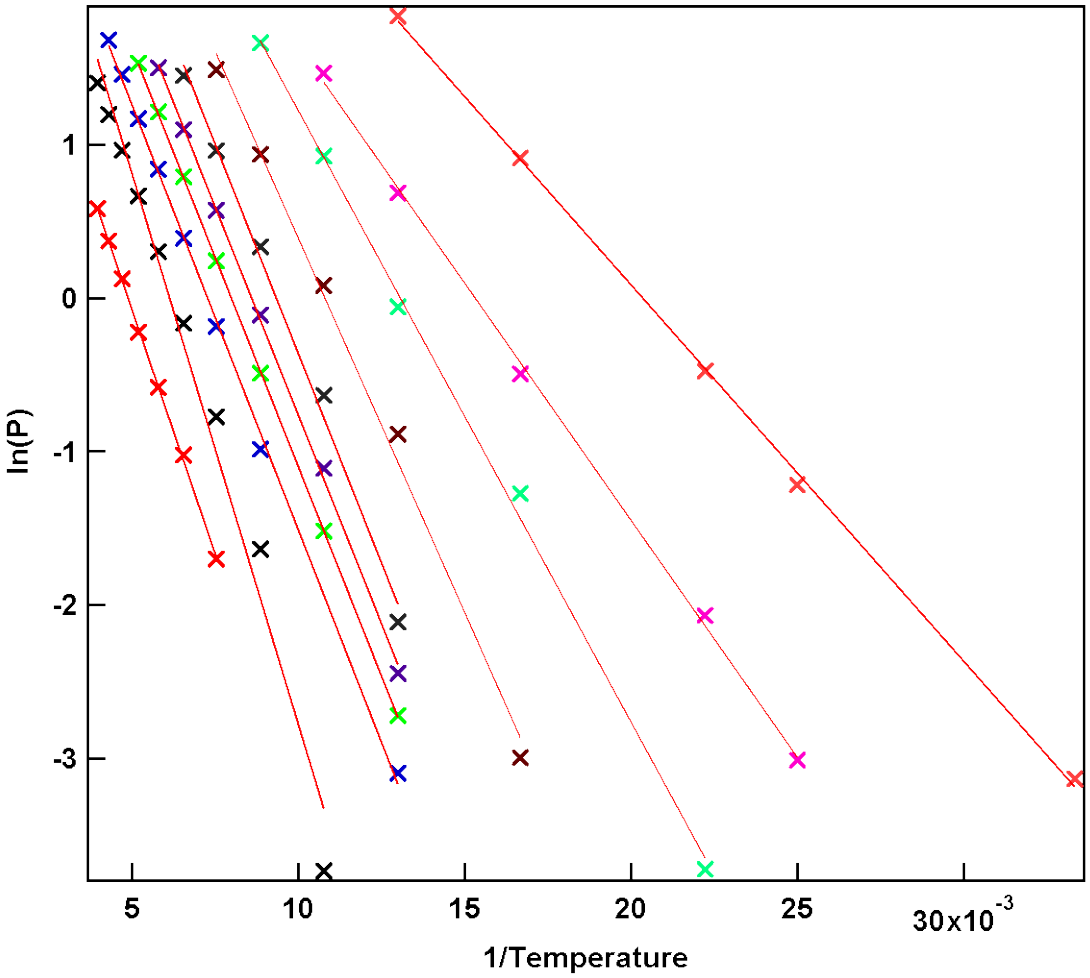

Figure 192. Adsorption isosteres at different absolute adsorptions.[270]

The slope of each adsorption isostere multiplied by R gives the isosteric heat at each coverage. Figure 193 (solid circles) presents the isosteric heats as function of absolute adsorption capacity.

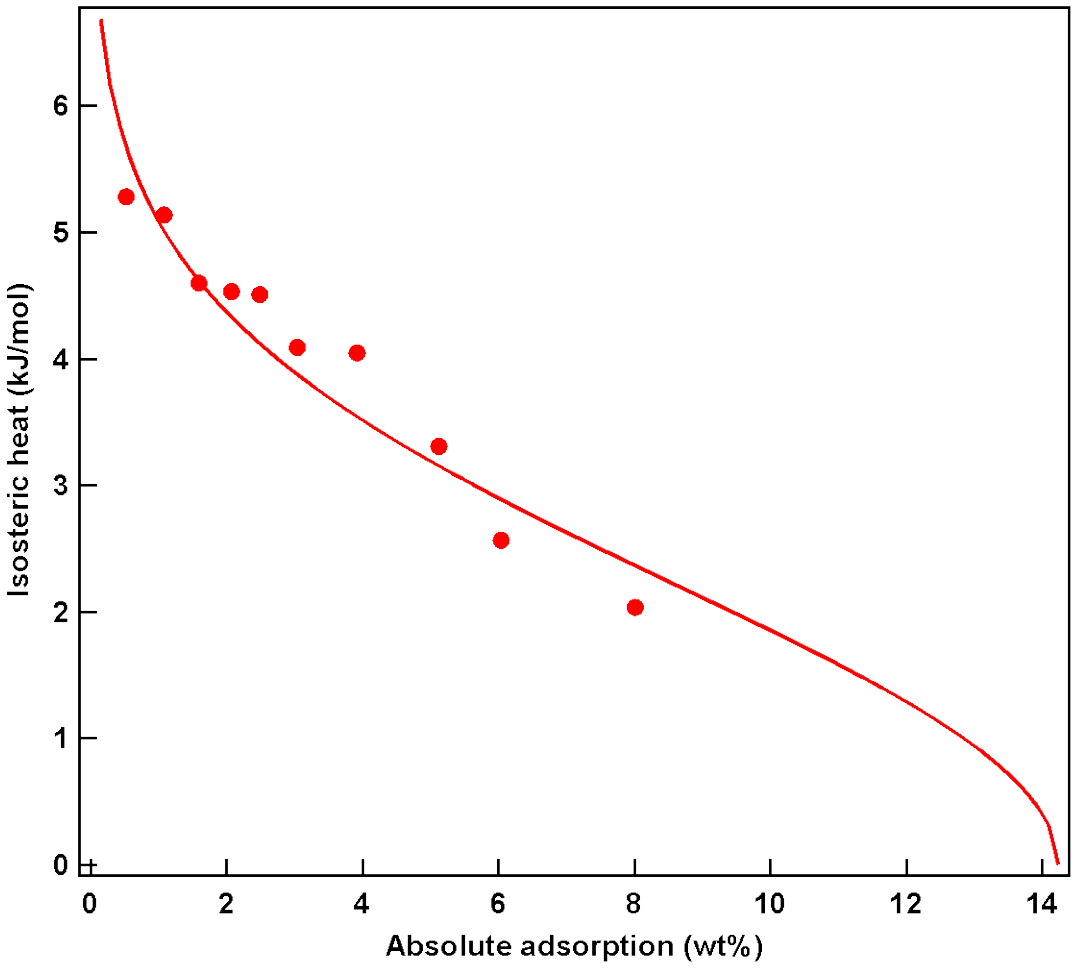

Figure 193. Solid symbols give the isosteric heat of adsorption obtained by using Clausius-Clapeyron equation on the absolute adsorption. Solid line gives the isosteric heat of adsorption calculated using the modified DA model.[270]

Finally, the isosteric heats of adsorption calculated from directly from the "excess capacity" isotherms (Figure 190) and those calculated from the derived "absolute capacity" isotherms using the MDA model are compared in Figure 194. The resulting heats of adsorption differ by as much as 20%. This difference may be quite significant when determining the overall heat transfer requirements of a physisorption hydrogen storage system.

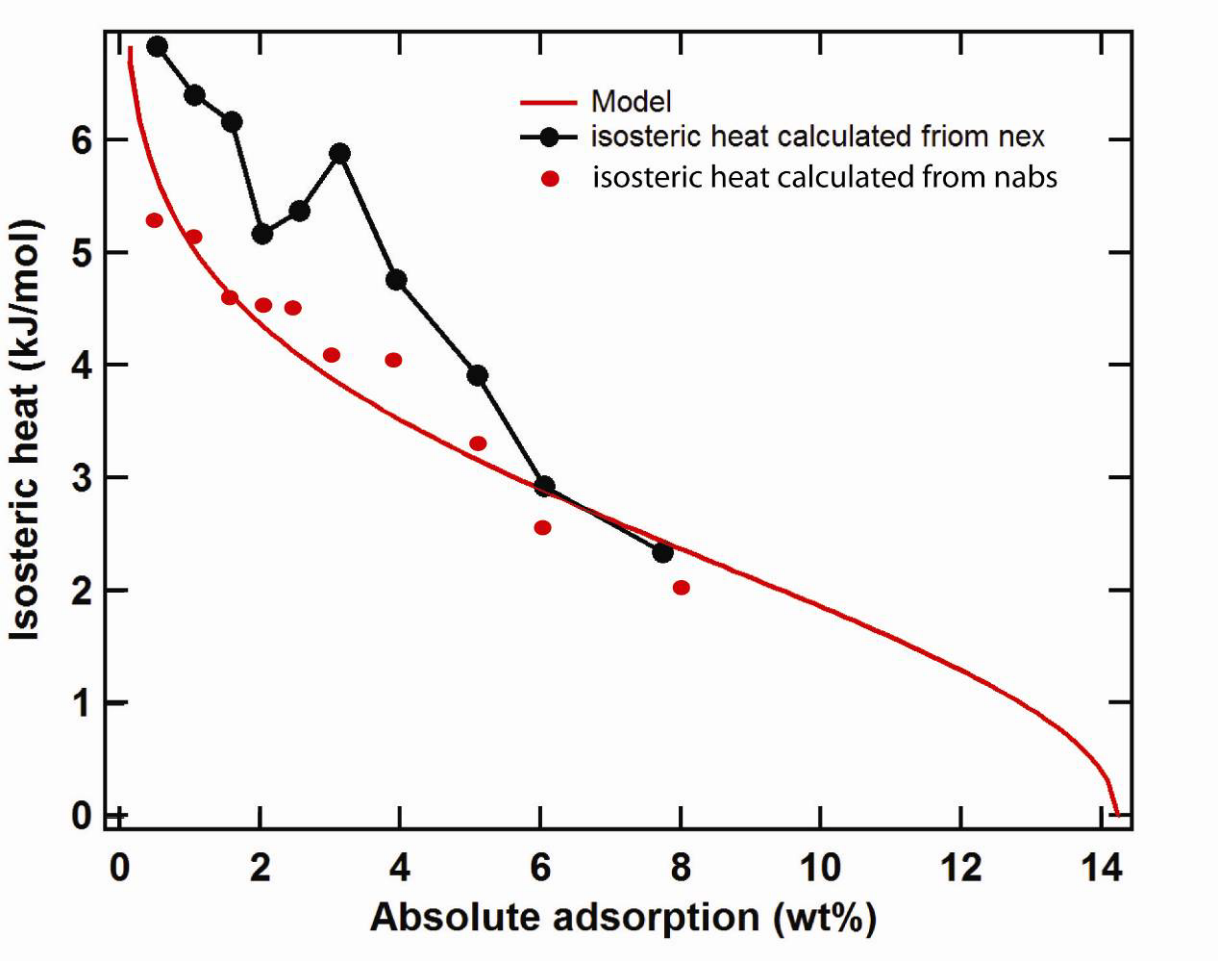

Figure 194. Solid symbols give the isosteric heat of adsorption obtained by using Clausius-Clapeyron equation on excess (black) and absolute (red) adsorption results. Solid red line gives the isosteric heat of adsorption calculated using the modified DA model.[270]

It should be noted that the determination of isosteric heat by applying Clausius-Clapeyron relation on the experimental data at higher coverage can have high uncertainty due to fewer isotherms available at higher coverages. Isosteric heat of adsorption can also be directly obtained by deriving Q_{st} from the Clausius-Clapeyron relation of the modified Dubinin-Astakhov (DA) analytical model. According to this model, isosteric heat is defined as:

Equation 200

$$Q_{st} = -\alpha\sqrt{-\ln\left(\frac{n_a}{n_{\max}}\right)}$$

The solid line in Figure 193, is the isosteric heat given by the Equation 200, where n_a is a continuous variable that varies from zero to n_{max}. At near-zero coverage, the isosteric heat determined by the DA model shows a weak divergence which is attributed to its logarithmic dependence on n_a. Thus the model does not accurately reproduce its dependence on n_a in Henry's law region.

The above modeling techniques for deriving "absolute" Isosteric Heats of Adsorption are presently being evaluated for there applicability to a wide range of hydrogen storage physisorption materials.[271]

1.3.4 Variable-Temperature Infrared Spectroscopy

Another method to obtain the isosteric heat of adsorption is based on variable-temperature infrared spectroscopy. Unperturbed H_2 is infrared inactive, but shows Raman bands at $\nu_{H\text{-}H}$ = 4161 and 4155 cm^{-1} for para- and ortho-hydrogen, respectively.[272] Association of H_2 molecules with the surface of a framework, however, polarizes the H-H bond, causing the vibrational transition to become infrared active with a characteristic IR absorption band appearing in the range of 4050–4110 cm^{-1}. The bathochromic shift of this transition is determined by the strength of the interaction between H_2 and a binding site, with stronger binding interactions resulting in a greater shift from the unperturbed system. Hydrogen bound at any available site within a given material can therefore be observed by infrared spectroscopy.[273] This can be used to monitor adsorption thermodynamics by following the variable temperature IR (VTIR) spectroscopic method.[275]

At any given temperature, the integrated intensity of the characteristic IR absorption band (of adsorbed hydrogen) is proportional to surface coverage, h, thus giving information on the activity of both the adsorbed species and the empty adsorbing sites; simultaneously, the equilibrium pressure gives the activity of the gas-phase. Hence, the corresponding adsorption equilibrium constant, K, can be determined, and the variation of K with temperature leads to the corresponding values of adsorption enthalpy and entropy. For deriving these values, integrated band intensity, A, temperature, T, and equilibrium pressure, p, determined simultaneously by using an appropriate IR cell, are considered to be related by the Langmuir-type equation (Equation 201):

Equation 201

$$\theta = A/A_{\mathrm{M}} = K(T)p/[1 + K(T)p]$$

where A_M stands for the integrated band intensity corresponding to full coverage (h = 1). By combining Equation 201 with the well known van 't Hoff Equation 202 leads to Eqn. 13 below:

Equation 202

$$K(T) = \exp[-\Delta H^0/RT]\exp[\Delta S^0/R]$$

Equation 203

$$\ln[A/(A_M - A)p] = (-\Delta H^0/RT) + (\Delta S^0/R)$$

By plotting the left-hand side of Equation 203 against reciprocal temperature, for data obtained over a relatively large temperature range, corresponding values of ΔH^0 and ΔS^0 can directly be derived. [275]

Zeolite	ν(H–H) (cm^{-1})	$-\Delta H^0$ (kJ mol^{-1})	$-\Delta S^{0,b}$ (J mol^{-1} K^{-1})	$-\Delta S^{0,c}$ (J mol^{-1} K^{-1})
(Mg,Na)–Y	4056	18	136	81
Ca–Y	4078	15	127	72
Mg–X	4066	11	103	48
Na–FER	4100	6.0	78	23
K–FER	4111	3.5	57	2
Li–ZSM–5	4092	6.5	90	35
Na–ZSM–5	4101	10.3	121	66

[a] ΔH^0 and ΔS^0 values are given per mole of molecular hydrogen.
[b] Referred to a standard state at 1 Torr (1.33 mbar).
[c] Referred to a standard state at 1 bar.

Table 13. Spectroscopic and thermodynamic data for hydrogen adsorbed on several zeolites. Error limits for ΔH^0 and ΔS^0 are ±1 $kJmol^{-1}$ and ±10 $Jmol^{-1}K^{-1}$, respectively.[275]

Variable-temperature infrared spectroscopy can be utilized to estimate the hydrogen adsorption enthalpies at very low hydrogen loadings which are usually associated with the strongest hydrogen-framework interactions. However, with increased hydrogen loading, where hydrogen adsorption enthalpies will decline abruptly mainly due to hydrogen-hydrogen interactions, variable-temperature infrared spectroscopy does not provide reliable information about the weak interactions.

1.3.5 Optimal Value of Adsorption Enthalpy

The optimal hydrogen adsorption enthalpy in porous materials can be calculated using Equation 204, which is based on the Langmuir-type adsorption model:

Equation 204

$$\Delta H^0_{opt} = T\Delta S^0 + [(RT/2)\ln(P_1P_2/P_0^2)]$$

This equation can give the optimum value of adsorption enthalpy (ΔH^0_{opt}) for maximum hydrogen delivery as a function of temperature (T) and adsorption entropy (ΔS^0), P_0 being the standard pressure value to which ΔS^0 is referred (1 bar), P_1 the hydrogen loading pressure and P_2 the exhaust delivery pressure. In other words, Equation 204 applies to hydrogen storage/delivery cycles between pressures P_1 and P_2 at a temperature T. Alternatively, the optimum operational temperature (as a function of standard adsorption enthalpy and entropy) is given by:

Equation 205

$$T_{opt} = \Delta H^0/[\Delta S^0 + (R/2)\ln(P_1P_2/P_0^2)]$$

Assuming P_1 = 30 bar and P_2 = 1.5 bar as being reasonable pressure values for the hydrogen storage-delivery cycle, and taking ΔS^0 = -66.5 J mol^{-1} K^{-1} as being a representative value of entropy change, Equation 204 yields ΔH^0_{opt} = -15.1 kJ mol^{-1} at 298 K. On the other hand, for an enthalpy change of ΔH^0 = 6.64 kJ mol^{-1}, typical of hydrogen adsorption on MOFs and other microporous materials, Equation 205 yields T_{opt} = 131 K when operating between 1.5 bar and 100 bar.[149] An example of the measured enthalpies of adsorption for some well know physisorption materials (AX21 and MOF-177) are shown in Figure 195.

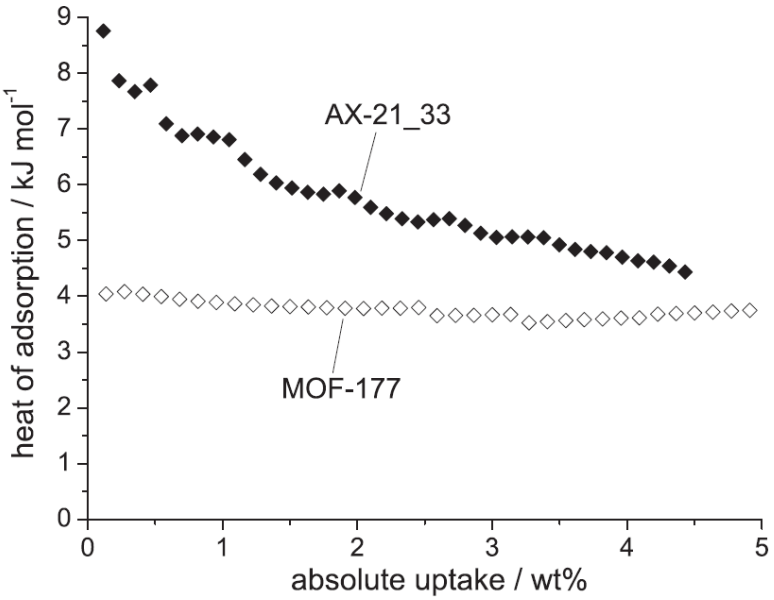

Figure 195. Heat of adsorption for AX-21_33 (closed symbols) and MOF-177 (open symbols).[274]

When one introduces the entropy-enthalpy correlation to the Langmuir adsorption model, a value of ΔH^0_{opt} in the range of -22 to -25 kJ mol^{-1} is needed for a material operating between 1.5 and 30 bar at 298 K.[275] Thus an optimal physisorption enthalpy falls into a range just a little lower than that of the classic hydride $LaNi_5H_6$ with an heat of formation of ΔH^0 = 30 kJ mol^{-1}. The ultimate goal then is to obtain high-hydrogen capacity physisorption materials with elevated adsorption enthalpies.

1.3.6 Recommended Best Practices for Presenting Isosteric Heats of Adsorption

It is the recommendation of this best practices document that:

1. **Two Isosteric Heats of Adsorption as a function of coverage be reported based on: a) calculations from the directly measured "excess capacity" isotherms, and b) calculations from derived "absolute capacity" isotherms.**
2. **All assumptions, models and details used for predicting the "absolute capacity" isotherms should be reasonable, make physical sense, and be clearly reported along with the results in any publication or presentation.**
3. **Calculations of Heats of Adsorption be based on a minimum of 5 different isotherms over a wide range of temperatures (preferably 77K to room temperature).**

1.4 Thermodynamics of Off-board Regenerable Hydride Materials

This section discusses the thermodynamics of chemically reacting systems for off-board regenerable chemical hydrides. Because off-board regenerable hydride materials are not reversible under typical on-board temperature and pressure conditions it is not possible to measure thermodynamic properties through equilibrium techniques such as van' t Hoff volumetric or gravimetric methods. Thus, the study of thermodynamic properties is generally limited to Calorimetric Methods such as bomb calorimetry, thermal gravimetric analysis (TGA) and differential scanning calorimetry (DSC). The details of making thermodynamic measurements using these techniques are presented below (section 2.2).

While the enthalpy of reaction (or heat of reaction) may be determined by calorimetry measurements, it can also be estimated indirectly from the difference in the know values of the enthalpies of formation of the reactants and products of the hydrogen delivery reaction.

In general, the enthalpy of reaction is the energy released or absorbed during a chemical transformation and is defined as the difference of the enthalpy of products ($H_{products}$) and the enthalpy of reactants ($H_{reactants}$). There are three constraints imposed on the definition of the enthalpy of reaction and they are:

Stoichiometric quantities are used
The reaction proceeds to completion
The reactants and products are at the same temperature and pressure

If the reaction does not follow these constraints, then the enthalpies associated with these deviations must be accounted for. Some useful information to keep in mind regarding the enthalpy of reaction is:

The standard enthalpy (heat) of reaction (denoted as ΔH_r°) is the heat of reaction when both the reactants and products are at a reference temperature and pressure, usually 25°C and 1 bar. If ΔH_r° is negative then the reaction is said to be exothermic at temperature T, and if ΔH_r° is positive then the reaction is said to be endothermic at temperature T. At low to moderate pressures, ΔH_r° is nearly independent of pressure.

The heat of reaction is an extensive property and its value depends on how the stoichiometric equation is written. For example, the heat of reaction for $A \rightarrow B$ is half of the heat of reaction for $2A \rightarrow 2B$. The heat of reaction depends on the phase (solid, liquid, or gas) of the reactants and products. For example the higher heating values

(HHV) and lower heating values (LHV) are two values that are dependent on the phase of product water:

Equation 206

$$CH_4(g) + 2O_2(g) \rightarrow CO_2(g) + 2H_2O(l): \quad \Delta H_r^\circ = -890.3 \ \frac{kJ}{mol}$$

$$CH_4(g) + 2O_2(g) \rightarrow CO_2(g) + 2H_2O(g): \quad \Delta H_r^\circ = -802.3 \ \frac{kJ}{mol}$$

The difference between the reactions is the phase of water in the products. Because enthalpy is a state function, the difference is the enthalpy change associated with the vaporization of two moles of water at 25°C. In other words, $2\Delta H_v^\circ(water@25^\circ C)$.

The internal energy of reaction can also be calculated if the reaction proceeds in a closed reaction vessel at constant volume. Analogous to the enthalpy of reaction, the internal energy of reaction is the difference between products and reactants ($U_{products} - U_{reactants}$) if stoichiometric quantities or reactants react completely at temperature T. The internal energy of reaction can be calculated from the enthalpy of reaction by the following relation:

Equation 207

$$\Delta U_r(T) = \Delta H_r(T) - RT\left(\sum_{\substack{gaseous \\ products}} v_i - \sum_{\substack{gaseous \\ reactants}} v_i\right)$$

where v_i are the stoichiometric coefficients.

To illustrate using the previous example of the (LHV) combustion of methane (bottom Equation 206):

Equation 208 $\Delta U_r(T) = \Delta H_r(T) - RT(2H_2O(g) + CO_2(g) - 2O_2(g))$

(or at 25°C) $\Delta U_{LHV\ CH4}(298) = -802.3-(0.008314*298) = -804.8\ kJ/mol$

Using this relation assumes ideal gas behavior and that the specific volumes of the liquid and solid reactants and products are negligibly small compared with those of the gases. If there are no gaseous reactants or products, then to a good approximation $\Delta U_r(T) \approx \Delta H_r(T)$.

Typically, heats of reaction can be calculated from tabulated values of enthalpies of formation. For example for a typical reaction say $aA + bB \rightarrow cC + dD$, the standard heat of reaction (calculated from the standard heats of formation) would be:

Equation 209 $$\Delta H_r^\circ = \left(\left(c\Delta H_f^\circ\right)_C + \left(d\Delta H_f^\circ\right)_D\right)_{products} - \left(\left(a\Delta H_f^\circ\right)_A + \left(b\Delta H_f^\circ\right)_B\right)_{reactants}$$

Or more generally as:

Equation 210 $$\Delta H_r^\circ = \sum_{products} v_i \left(\Delta H_f^\circ\right)_i - \sum_{reactatnts} v_i \left(\Delta H_f^\circ\right)_i$$

where i denotes the species and v_i denotes the stoichiometric coefficient for species i.

Another useful class of reaction enthalpies are the standard enthalpies (or heats) of combustion. The standard heat of combustion (denoted as ΔH_c°) of a material is the heat of reaction of that material with a stoichiometric amount of oxygen to yield specified products, of which the products and reactants are at the arbitrary, but yet conventional, reference state (i.e., 25°C and 1 bar). Standard heats of combustion values are tabulated for large number chemicals in sources such as Perry's Chemical Engineers' Handbook or in NIST Chemistry Webbook. Standard heats of reaction that involve only combustible products can be calculated from the standard heats of combustion. Mathematically this can be represented as:

Equation 211 $$\Delta H_r^\circ = \sum_{products} v_i \left(\Delta H_c^\circ\right)_i - \sum_{reactatnts} v_i \left(\Delta H_c^\circ\right)_i .$$

One of the principle applications of this equation is to determine the heats of formation for combustible substances whose formation reaction do not occur naturally or occur at very slow reaction rates. As an example, consider the formation reaction of pentane,

Equation 212 $$5C(s) + 6H_2(g) \rightarrow C_5H_{12}(l)$$

which cannot be carried out in the laboratory. However, all reactants and products can be combusted whereby the standard heats of combustion can be determined experimentally. Therefore, the standard heat of formation for pentane can be calculated as:

Equation 213 $$\left(\Delta H_f^\circ\right)_{C_5H_{12}(l)} = 5\left(\Delta H_c^\circ\right)_{C(s)} + 6\left(\Delta H_c^\circ\right)_{H_2(g)} - \left(\Delta H_c^\circ\right)_{C_5H_{12}(l)} .$$

Given the thermodynamic construct presented above, one can now tackle calorimetry for experimentally determining heats of reaction and heat capacities. In order to determine the heat capacities or heats of reaction, the first law of thermodynamics for the system under study must be employed; That is: $Q_V = \Delta U_V (closed\ system)$ or $Q_P = \Delta H_P (open\ system)$. The subscripts V and P are reminders that the processes occur under constant volume or constant pressure.

1.5 Hydrogen Storage System Energy Considerations

1.5.1 On-board Reversible Hydride Storage Systems

Metal hydrides are one example among a number of prospective hydrogen storage materials being investigated worldwide. Some metal hydrides are reversible at room temperature which dictates relatively high energies of formation of the hydride from hydrogen and constituent metals. However, the binding energy of hydrogen in metal hydrides covers a wide range from being unstable endothermic hydrides (alane) to highly stable exothermic hydrides (alkali metal and rare earth hydrides). This has a direct impact on whether a hydrogen storage material will be used only once on-board a vehicle and regenerated (chemical hydrides: alane, amino-boran, etc., or if the enthalpy of reaction is in the narrow range (10 to 40 kJ/molH_2) to allow on-board hydrogen recharging. Thus accurate information on thermodynamic stability of hydrides is absolutely crucial for practical applications.

The ideal enthalpy of formation to provide 1 bar of hydrogen at room temperature is about 35 kJmol^{-1} For a hydrogen fuel cell vehicle approximately 5 kg of hydrogen is needed to provide the same driving range as a standard gasoline powered vehicle. The amount of energy required to completely fill (or release) this amount of hydrogen is 87.5 MJ. Filling an ambient hydride system in 5 minutes with hydrogen would produce 292 kW of heat or enough heat to boil approximately 9 gallons of water.

With these materials, only thermodynamic considerations do not take into account the complexity of the design and efficiency of heat transfer to and from the storage system (Figure 196) or the efficiency of the balance of plant energy requirements of the complete on-board reversible hydride storage system (Figure 197).

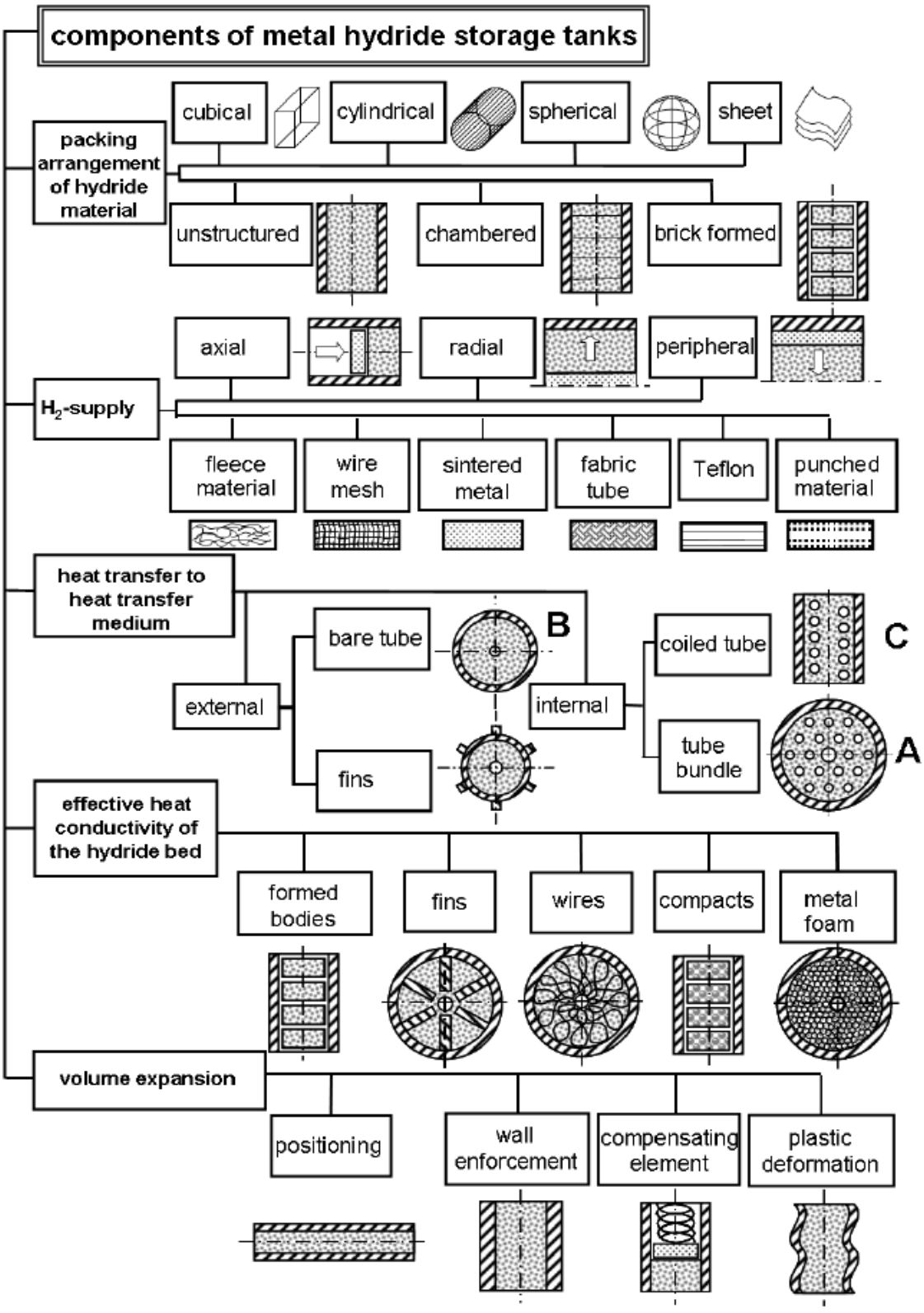

Figure 196. Design principles of metal hydride storage tanks.[276]

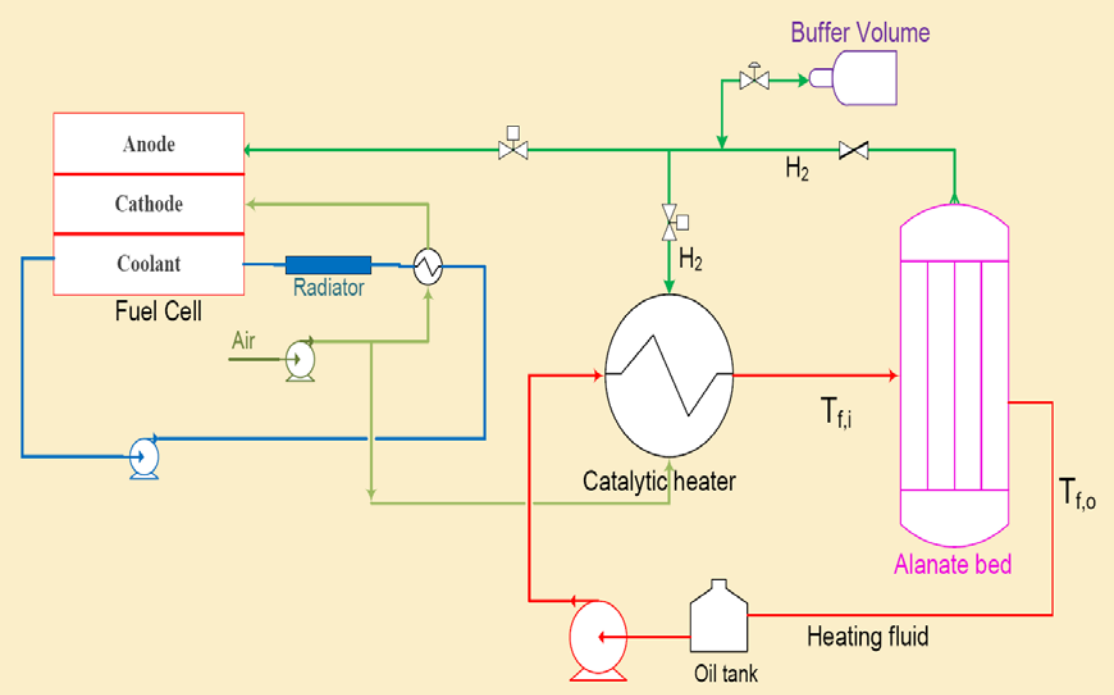

Figure 197. Schematic diagram showing some of the balance of plant components required for a hydride based hydrogen storage / fuel cell system.[277]

1.5.2 Off-board Regenerable Hydrides Storage Systems

The off-board regeneration of chemical hydrides is a key factor in the full analysis of practicality and cost effectiveness of these materials for use in storing hydrogen for vehicular applications. In the case of these exothermic hydrogen release systems, simply exposing spent material to gaseous hydrogen is not a practical method for regeneration of the hydrogen storage material. For materials such as ammonia borane,[278] lithium-aluminum-hydride,[279] and alane[280] a chemical process is required to re-hydrogenate the materials after hydrogen release.

Any discussion of chemical hydrogen storage regeneration must start with a quantitative description of the free energy of hydrogen release from the storage material. In this case we will employ ammonia borane ($H_3N–BH_3$ or AB) as an example as chemical regeneration in this system has been studied quite extensively. The dehydrogenation of AB (2-2.5 equiv H_2 released, generating polyborazylene) is exothermic by ca. -60 kJ/mol (Equation 214). While this is closer to thermoneutral than hydrolysis of AB (ΔH = ca. -950.4 kcal/mol), for example, the reaction is quite exergonic due to the entropy increase from the evolved H_2 gas. The reverse, endergonic reaction (Equation 215) requires a tremendous hydrogen pressure, on the order of 100,000 atm. This pressure is too great to be feasible on an industrial scale. Instead, several regeneration schemes that involve stepwise reactions of spent fuel with proton (H^+) and hydride (H^-) sources have been explored. Addition of H^+ and H^- has the same net result as direct H_2 addition, but these former reactions are mechanistically and thermodynamically feasible. Schemes of this sort are the best way to efficiently overcome the innate energy barrier in chemical hydrogen storage regeneration by separating the large thermodynamic and entropic barriers into achievable steps.

Equation 214 $\mathbf{AB \rightarrow 2\,H_2 + BNH_n}$

Equation 215 $\mathbf{BNH_n + 2\,H_2 \rightarrow AB}$

Another important concept is that the relative extent of dehydrogenation of AB, may impact the effectiveness of a given regeneration scheme. While AB has an ultimate H_2 capacity of 19 wt.% corresponding to storage of three molecules of H_2, in practice release of 2-2.5 equivalents of H_2 is an achievable, realistic goal. Complete release would result in the formation of boron nitride ($\Delta_f H^\circ$ = -477 kJ/mol) which is undesirable. Furthermore, BN is quite unreactive, requiring strong acids or strong oxidants for even partial digestion.[281] In general, a total of 13-16 wt.% hydrogen is realistically obtainable from ammonia borane. Thus, by design, the spent fuel in the reported regeneration schemes for ammonia borane refers to the material produced when 2-2.5 H_2 is released.

The published report for the regeneration of ammonia borane from spent fuel (Figure 198) shows the several chemical steps necessary for regeneration.

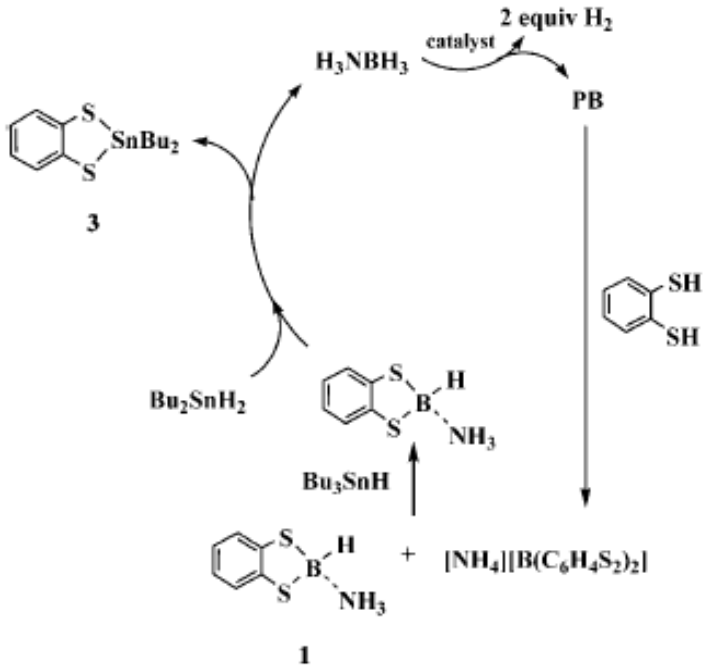

Figure 198. Demonstrated off-board regeneration scheme for spent ammonia borane[278].

The most important issue in the regeneration process is the overall energy efficiency. The publication of Figure 198 describes a method to estimate the optimum energetic efficiency for ammonia borane regeneration. Equation 216 has been developed on the basis of the energy of oxidation for one mole of H_2 to form H_2O (42 kJ).

Equation 216

$$\frac{(\text{Equiv.H}_2\text{ stored})(57.8)}{(\text{Equiv.H}_2\text{ used})(57.8)+\sum(\Delta H_{endo})-(\%\text{ heat recovery})\sum(-\Delta H_{exo})}=efficiency$$

Other methods for regeneration of exothermic hydrogen release materials such as electrochemical hydrogenation have been explored successfully. [282] The direct hydrogenation of aluminum to alane ordinarily requires over 10^5 bars of hydrogen pressure at room temperature but in solution direct electrochemical conversion of aluminum to alane is possible.

1.5.3 Physisorption storage systems

The system behaviors of hydrogen physisorption storage systems can be significantly influenced by the intrinsic thermal effects of adsorption (storage) being exothermic and desorption (release) endothermic. During filling under conditions in which the adsorption heat cannot be efficiently dissipated, the system heats up resulting in reduced storage capacity due to temperature increase. In a discharge process without energy supply for desorption, the system temperature will drop, and hence the adsorbent is able to retain a large amount of hydrogen gas. This will lead to an increase in the residual amount of hydrogen at the depletion pressure and decrease of the amount of hydrogen gas extracted from the system. Nevertheless, these issues could be resolved by equipping an adsorption vessel with multilayer vacuum super insulation.[20]

Figure 199 depicts a typical low-temperature adsorption vessel. The vessel is completely filled with adsorbent material and is insulated to minimize heat transfer with the environment. The purpose of the heat exchange device is to cool or heat the system.[283]

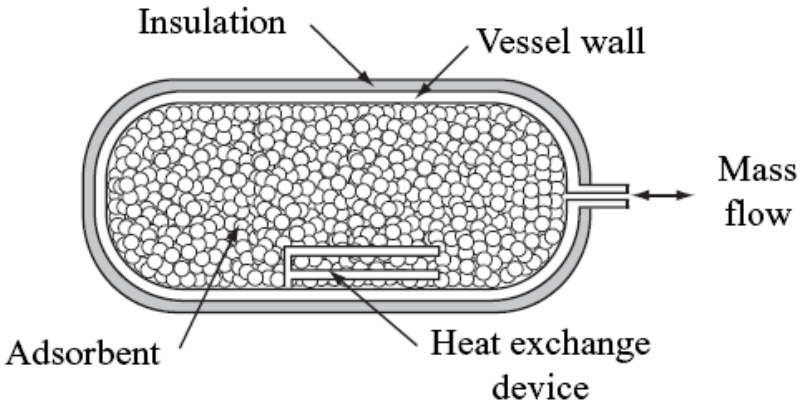

Figure 199. Typical cryogenic adsorption-based vessel.[283]

2 Experimental and Analysis Considerations

For reversible hydrogen storage materials (both reversible hydrides and physisorption materials) the energy release on hydrogen uptake and the energy required to release the stored hydrogen is one of the most important thermodynamic properties to be measured. For reversible hydrides it is generally the enthalpy and entropy of hydride formation that is of interest and for physisorption materials it is the isosteric heat of adsorption that one wants to ascertain. These properties are usually determined from PCT isotherm measurements. PCT measurements are typically made using either volumetric or gravimetric instruments. There are important practical and accuracy issues with both methods that must be fully understood in order to make high-quality measurements. These issues have been covered to a large extent in subsections 5.3 , 5.4 and 5.5 of the *Introduction* and subsections 2.3.1 , 2.3.2 and 2.3.3 of the *Capacity* section of this Best Practices document. In addition to the volumetric and gravimetric methods for making PCT measurements an overview is presented here in subsection 2.1.4 for the combinatorial method of making PCT / van 't Hoff measurements of enthalpy and entropy of hydride formation using Hydrogenography.

It is vitally important for physisorption measurements of any kind, that capacity data is properly labeled as either "excess", "absolute", or "total" capacity. And equally important that any assumptions made in determining the capacity values are clearly reported. The use of one or the other of these different means of calculating and reporting capacity will also impact the determination of the isosteric heat of adsorption and, therefore, should be clearly disclosed in all reporting thermodynamic results.

The basic result that is generated from both volumetric and gravimetric measurements is "excess" hydrogen capacity. From a best practice point of view and consistency in the field, the measured hydrogen "excess" capacity is what should be reported. Everything else, absolute and total capacity, is an estimate based on this physical measurement and will only be as valid as the assumptions made in making these estimate.

Other methods to measure thermodynamic properties and important considerations in using these methods are covered in subsections 2.2 – 2.6 of this Thermodynamics Section of the document.

2.1 PCT Measurements

Volumetric method and gravimetric method are the two primary methods for the determination of equilibrium sorption isotherms. In the volumetric method, the hydrogen sorption or uptake is measured by monitoring the drop in hydrogen pressure in a system of a fixed, known volume, with desorption being monitored by an increase in pressure. The volumetric method is also known as the Sievert's Method or Manometric Method. In the gravimetric method, the hydrogen uptake is measured by monitoring the weight of the sample following a step change in the hydrogen pressure. A series of isotherms measured at different temperatures can then be used to calculate certain thermodynamic properties of the hydrogen solid system.

2.1.1 Equilibrium PCT Measurements

Van 't Hoff plots are a commonly used method for determining the thermodynamics. It is critical for thermodynamic analysis that the measurement of a PCT isotherm is performed in such a way that the hydrogen gas, and hydrogen storage media have attained equilibrium before recording Peq or (for hydrides) the equilibrium plateau pressure. Achieving true equilibrium pressures is what separates out (and removes) any slow kinetics effects from the pressures that are used to create van 't Hoff plots and, ultimately, determine reaction enthalpies and entropies.

To be able to derive van 't Hoff plots accurately from PCT isotherms it is important that enough data points have been taken in each PCT isotherm to be able to clearly identify plateau pressures and distinguish phase transitions. In volumetric PCT measurements it is recommended that at least 30 but preferably as many as 100 steps in concentration (data points) be taken for each isotherm (with at least 5-10 data points per plateau). This is equally true of gravimetric measurements. However, the fact that gravimetric PCT measurements take steps in pressure rather than concentration means that it may be difficult to determine exact equilibrium pressures for materials with flat plateaus (complex hydrides for example). This is because a material may go from the unhydrided state to the completely hydrided state in one pressure step (as there is no limit on the amount of hydrogen to which the sample is exposed). The equilibrium pressure for a given sample temperature will be somewhere between the final pressures before and after the hydriding (or dehydriding) pressure step. In this case the accuracy of the equilibrium pressure is a function of the size of the pressure step that is taken rather than the accuracy of the measuring pressure transducer.

The plot of the van 't Hoff relationship of pressure and temperature is often used as a simple way to compare stability of hydrides. It is important to note however, that the

slope of the ln P versus 1/T remains only an estimation of the formation enthalpy of the hydride, even for the ideal case treated here.

For an idealized reversible system, the enthalpy of transformation, $\alpha \rightarrow \beta$, can be derived from Equation 162. The contribution of the heat of hydrogen solution (partial molar enthalpy of solution of hydrogen in the metal/compound) is not taken into account in this calculation and must be evaluated to obtain a reasonable estimation of the actual Heat of Hydride Formation. The contribution of the partial heat of solution to the total Heat of Hydride formation is impacted by:

a) the compositional extent of the solid solution (see for example Y-H_2 system shown in Figure 200 below),
b) the relative strength (energetics) of this partial enthalpy of solution and the integration of this value between n_H=0 up to the composition at the phase boundary n_H=a, and
c) in addition, accurate measurements of the enthalpies of solution and hydride transformation are highly dependent on the 'quality' of the pressure measurements (calibration of the pressure sensors...). This is particularly true in the low pressure range where a direct measurement of the heat evolved (absorbed) may be the preferred measurement technique.

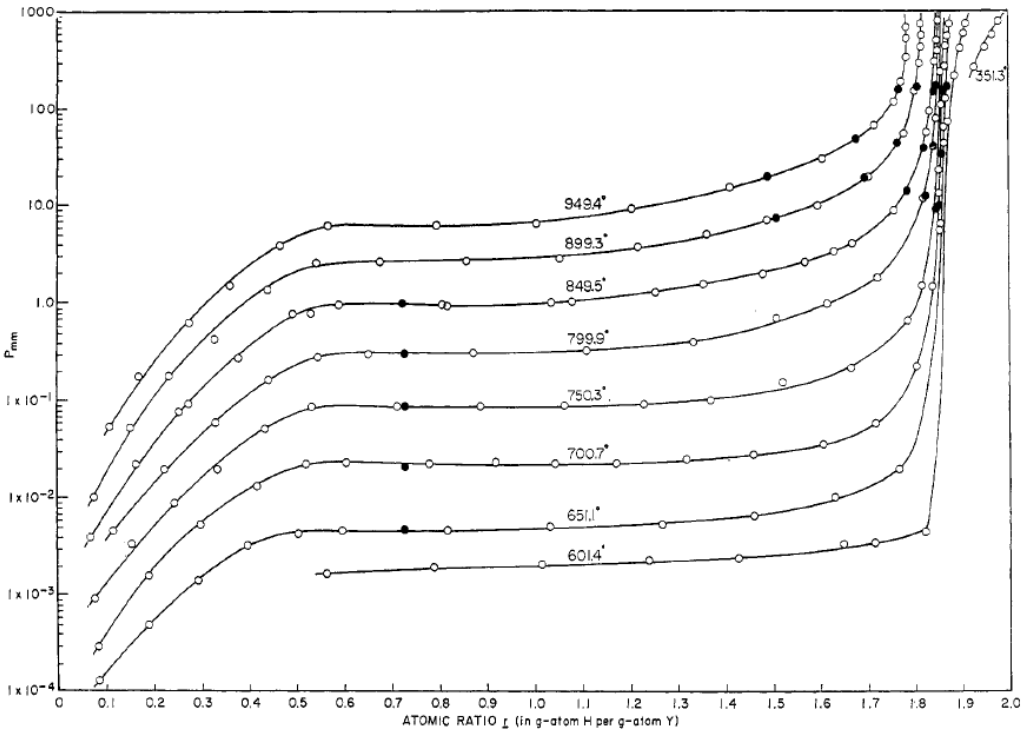

Figure 200. Experimental isotherms for the system yttrium-hydrogen (O, absorption points; ● desorption points) showing the wide compositional range of the solid solution phase.[284]

An important distinction between gravimetric and volumetric methods is that gravimetric instruments make PCT measurements by incremental changes in pressure, whereas volumetric instruments make PCT measurements by incremental changes in concentration. Thus, in gravimetric PCT measurements one has control over the y-axis (pressure) but essentially no control over concentration. For materials with relatively flat equilibrium plateaus (alanates, borohydride… essentially reversible chemical hydrides) an incremental increase in pressure from slightly below the plateau to just above the plateau will fully hydride the sample. The inverse is true for desorption. This is why gravimetric equilibrium PCT measurements on such materials often have no data points actually on the plateau. The plateau pressure can thus be inferred to be between the highest pressure of the sample in its unhydrided state and the lowest pressure in its hydrided state.

2.1.2 Volumetric Method

For routine hydrogen sorption measurements of porous materials, the volumetric method predates gravimetric method, primarily owing to the technological developments necessary for the latter, in terms of microbalance technology and the need for computer control. However, for volumetric method, it is important to accurately determine the sample skeleton volume (or skeletal density), which could cause large errors in the calculation of the heats of adsorption. In practice, He, which is assumed to have negligible adsorption on the substrate at room temperature and low pressure, is usually employed as the calibration gas and the volume difference between the measured volume of the sample cell before and after loading the sample into the cell at room temperature is the sample skeleton volume.[143]

The following are important issues that need to be addressed in making accurate volumetric measurements in particular for physisorption materials at low temperatures and high pressures.

2.1.2.1 Temperature Correction

The excess H_2 storage capacities in porous MOFs are often measured at cryogenic condition (77 K). The huge temperature difference between the gas reservoir and sample holder needs to be corrected based on the methods discussed above. In practice, it is necessary to soak the sample holder in liquid nitrogen bath for 30 min or longer to reach a thermal equilibrium. In addition, with simple Dewar systems, a deeper or larger flask is recommended because it can keep the temperature longer. An important consideration is that if the cryogenic liquid level in the Dewar changes significantly

during a measurement, the gas temperature (density) gradient will also change, causing a change in the "apparent volume" and thus errors in the measurements. Cryogenic systems that maintain a constant cryogenic temperature zone either through LN_2 refill or by cooling through Cryo-evaporation are more stable and will remove or significantly reduce this error.

When it comes to room temperature measurement, the environmental temperature fluctuation will also affect the results. It would is recommended to keep all components of the equipment (including sample holder) in a constant temperature environment.

2.1.2.2 Temperature Measurement

It is often the case with volumetric instruments that the thermocouple used to measure sample temperature is not in direct contact or, at least, in the middle of the sample. In many cases the thermocouple is in the furnace (or dewar, or cryostat) surrounding the sample holder. This is unlikely to give an accurate reading of the actual sample temperature because of heat leaks through the gas tubing, convection, etc. This problem becomes worse as the sample temperature is further from room temperature. Typically the measured temperature of the furnace is set using a calibration table or function to account for the difference in temperature at the point of measurement and the actual temperature of the sample. However, even a slight change in the position of the sample holder in the furnace (dewar) can cause a significant (as much as 10-20%) variation in the actual temperature of the sample. This, in turn, will cause large errors in the determination of heats of reaction by the van 't Hoff method. Bogdanovic et al. reported an error of $\pm$1.7 kJ/mol H_2, or 2.4%, based simply on an uncertainty of $\pm$ 0.5 ^{o}C in the sample temperature.[285]

The take home message is that temperature measurements that are not taken from within, or at least, in close proximity to the sample are probably unreliable and certainly will not be able to register temperature changes in the sample due to exothermic or endothermic reactions.

2.1.2.3 Free space measurement

One of the biggest problems encountered for high-pressure sorption measurements is the determination of the dead volume. Since porous MOFs are usually microporous, the helium uptake during the free space measurement is almost inevitable. In addition, there is often a large difference between the free space determined via adsorption vs. desorption. The difference of free space obtained can easily impose 10% error on the final result. In order to get an accurate result, the free space used for temperature correction to the adsorption isotherms should be obtained through adsorption data, and more than ten separate dead volume measurements should be carried out to get an accurate mean value.

2.1.2.4 Sample Quantity

The effect of sample quantity on the result is not straightforward. Small amounts of sample give less of an error on the dead volume determination, but pressure changes due to sorption are subsequently smaller, leading to larger errors in the final result. Larger quantities of sample give more accurate and reliable reading on the pressure change, but would also introduce more error on the dead volume determination. Generally, dead volume measurements using Helium at room temperature provides enough accuracy that the advantage of higher accuracy in the pressure change measurement is significantly more important. Thus, larger amounts of sample are almost always preferred.

2.1.2.5 Sample Handling

If the porous material has high H_2 storage capacity, it normally also means it will adsorb moisture in the air too. In order to prevent contamination from the air, all sample handling should be carried out in a glove box and then sealed before removal. Before measurement, samples should be degassed on the equipment at high temperature overnight to completely remove any adsorbed moisture.

2.1.2.6 Leak Checks

Hydrogen leaks in high pressure equipment not only affect the results, but can also be very dangerous regardless of the type of measurement equipment being used. All gas fittings and seals should be checked regularly (every measurement) to prevent gas leakage. One can easily identify a gas leakage during the free space determination. If there is huge difference between different runs, that typically means a gas leakage. In addition, a flammable gas detection system is very helpful during the H_2 measurement.

2.1.2.7 Full Isotherm Van 't Hoff Measurements

The classical method for determining the thermodynamics of hydride formation and decomposition as discussed in section 1.2.4 above is to make a series of PCT isotherm measurements at different temperatures. Then to create a van 't Hoff diagram by plotting the natural log of the plateau pressures vs. 1/sample temperature. This is illustrated in Figure 201 for a series of PCT desorption measurements on $LaNi_5$.

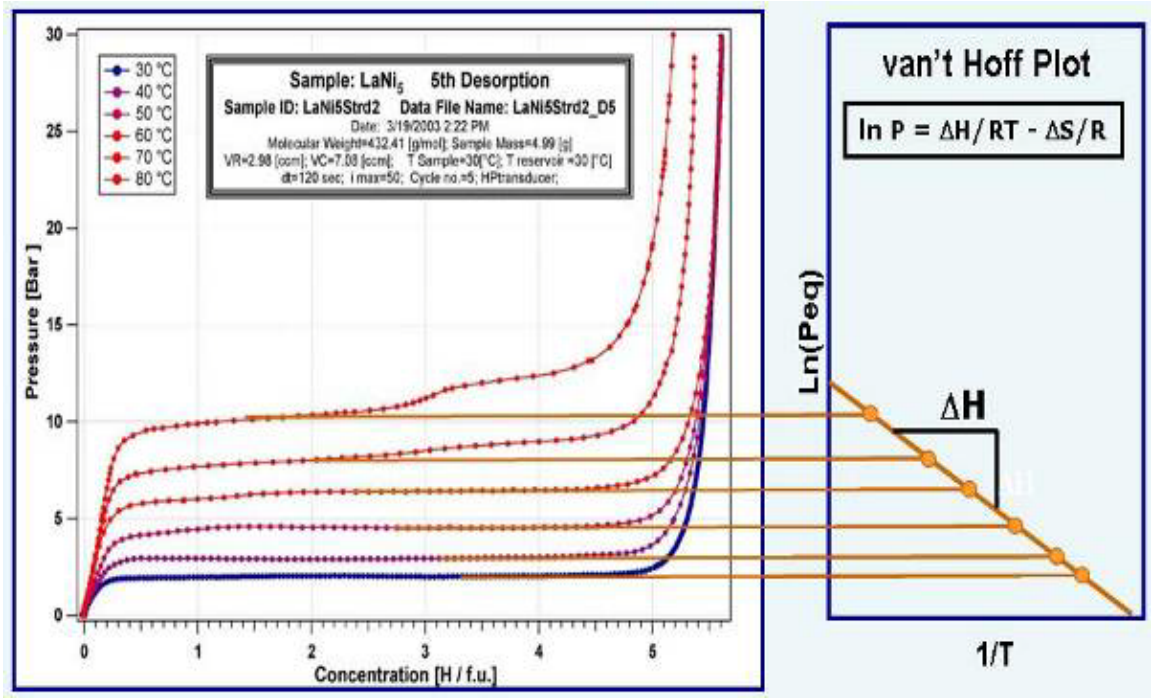

Figure 201. Standard method of making a Van 't Hoff plot from a series of desorption PCT measurements at different temperatures $LaNi_5$.

Using the volumetric measurement technique dosing takes place in increment concentration steps, unlike in the gravimetric technique where data is collected in incremental pressure steps and there may or may not be actual data points on the plateau depending on the intrinsic slope of the two-phase region (alloy and hydride). The volumetric measurement technique is advantageous for van 't Hoff analysis for two reasons. The first is that this method is very accurate in identifying plateau pressures at exact and consistent hydrogen concentrations. The second is that, at those concentrations the pressure time profile can be observed to ensure that the reaction has reached equilibrium. In fact, for materials with poor kinetics, it may be possible to use the pressure / time profile to extrapolate to a theoretical plateau pressure without waiting an unreasonable amount of time (more than a few days) to reach equilibrium for each gas dose.

As mentioned earlier, it is important to collect many data points along the PCT isotherm. One reason is that more than one hydride phase may be formed with very similar heats of formation. Large dosing steps, or the pressure stepping process in the case of gravimetric measurements are likely to miss these details. This is one reason why the volumetric method of having many concentration data points on a PCT plateau is advantageous. In such a case it is necessary to take very small steps in concentration and wait sufficiently long at each step to reach equilibrium. An example of this is shown in Figure 201 and detailed in Figure 202. PCT measurements (left) were made using very small steps in concentration (small volume doses and small pressure steps) on a $LaNi_5$

sample at different temperatures. The ability to collect many data points along the isotherm made it possible to observe the formation of a second meta-stable hydride phase (which has been identified as the gamma-phase by Ono[286] and others). This is important, because, had only a few (e.g. 10) data points been taken the step in the plateau pressure may not have been observed. The potential effect on the determination of the entropy and enthalpy of hydride formation are shown schematically in a simulated van 't Hoff plot on the right side of Figure 202. The difference in the equilibrium pressures between the two plateaus (orange vs. green) is significant and if incorrectly ascribed to one hydride or another (or in the case of only a few data points; averaged between the two) would lead to inaccuracies in the determination of the entropies and enthalpies of hydride formation.

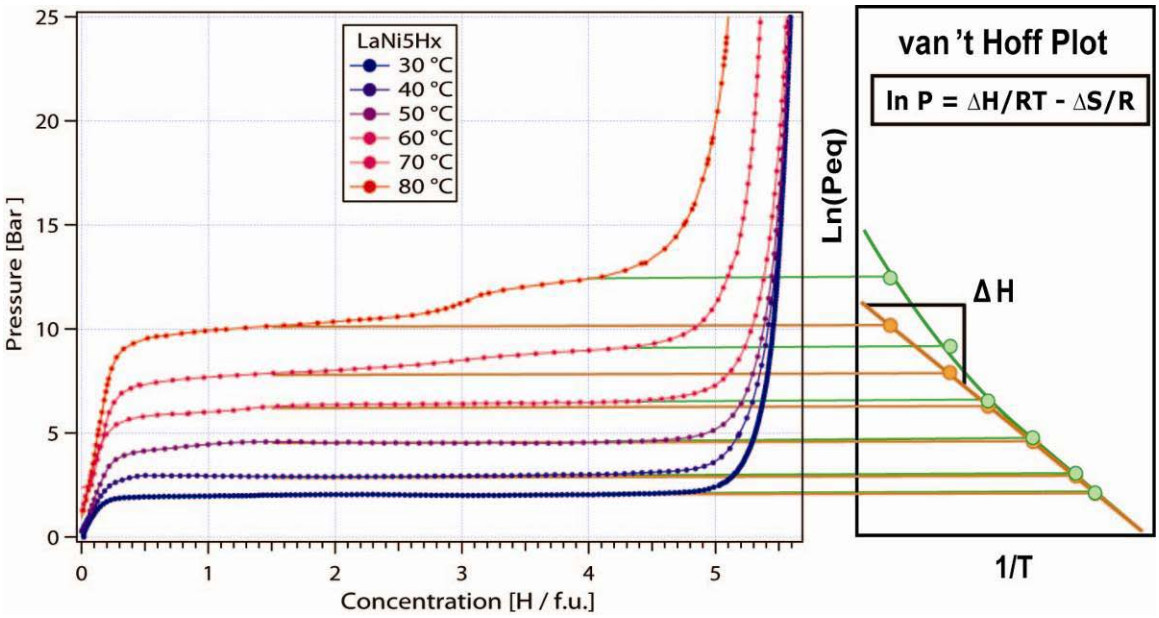

Figure 202. Illustration of detailed volumetric desorption PCT measurements at different temperatures for $LaNi_5$ (left) and different possible van 't Hoff plot derived from these isotherms (right).

2.1.2.8 Micro-Volumetric Full Isotherm Measurements

Occasionally samples are too small (1-100 of mg depending on H_2 capacity) to be measured on a standard volumetric instrument. This has been the circumstance for some thin film samples and materials that are difficult to synthesize in large quantities, as was the case in the early days of single wall carbon nanotubes.[214] In such cases a specialized micro-volumetric instrument was used to perform PCT measurements in much the same manner as a typical full sized volumetric instrument.

Figure 203 shows a series of PCT measurements of a thin-film sample of palladium/nickel (Pd deposited on thin Ni film and removed from the substrate) using a Sievert's-type instrument with a MicroDoser attachment.[287] Not only was the sample relatively small (91.3 mg), but palladium-hydride has a relatively low hydrogen content (0.6 wt.%). Thus, the PCT measurements involved extremely small quantities of gas. The number of data points along the PCT curves demonstrate the ability to dose the sample with very small quantities of hydrogen. This is a necessary prerequisite for being able to perform a "Direct van 't Hoff" measurement on this sample.

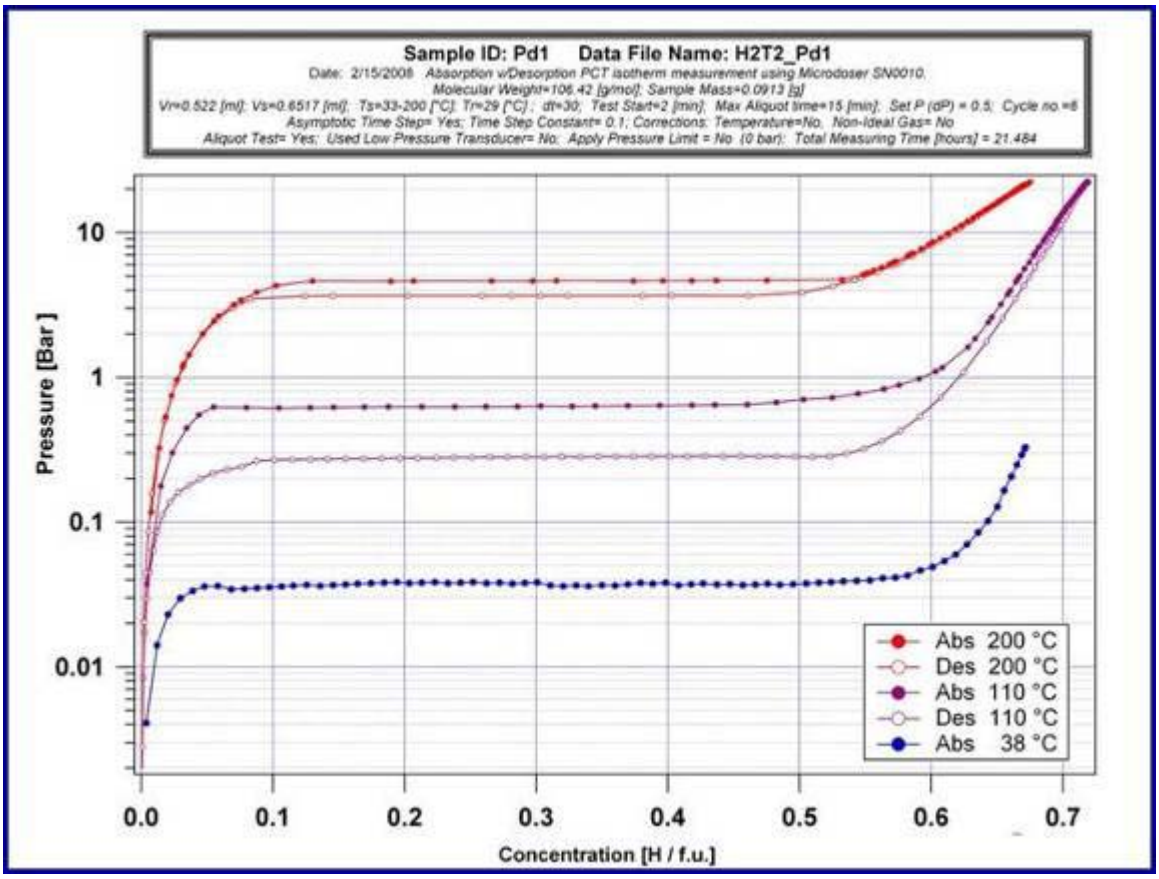

Figure 203. A series of absorption and desorption PCT measurements at 38°C, 110°C and 200°C on a thin-film Pd/Ni sample removed from the substrate.[287]

Focusing on these full PCT measurements for the moment, one can see that there is a clear hysteresis between absorption and desorption measurements. To understand whether this was a materials effect or an artifact of non-equilibrium measurements, it is necessary to look at the pressure-time data recorded during the automatic dosing process. For this experiment, the equipment allowed efficient exponential time data

collection an equilibrium test function to be performed to reduce the quantity of data collected and speed up the total isotherm collection time. The equilibrium test function required the instrument to only stay within a given dose until the approach to equilibrium test condition was met (i.e. rate of absorption or desorption falls below a selected value).

Figure 204 shows a portion of the pressure time sequence of doses collected in the beginning of the absorption PCT at 38°C. The data demonstrates that the absorption at each dose has reached a sufficiently steady pressure. This means that the sample's hydride phase can be considered to be in equilibrium with the gas phase at the final pressure reading of each dose (equilibrium pressure). It is this final pressure reading that corresponds to the plateau pressure in the corresponding PCT plot at the measured hydrogen concentration.

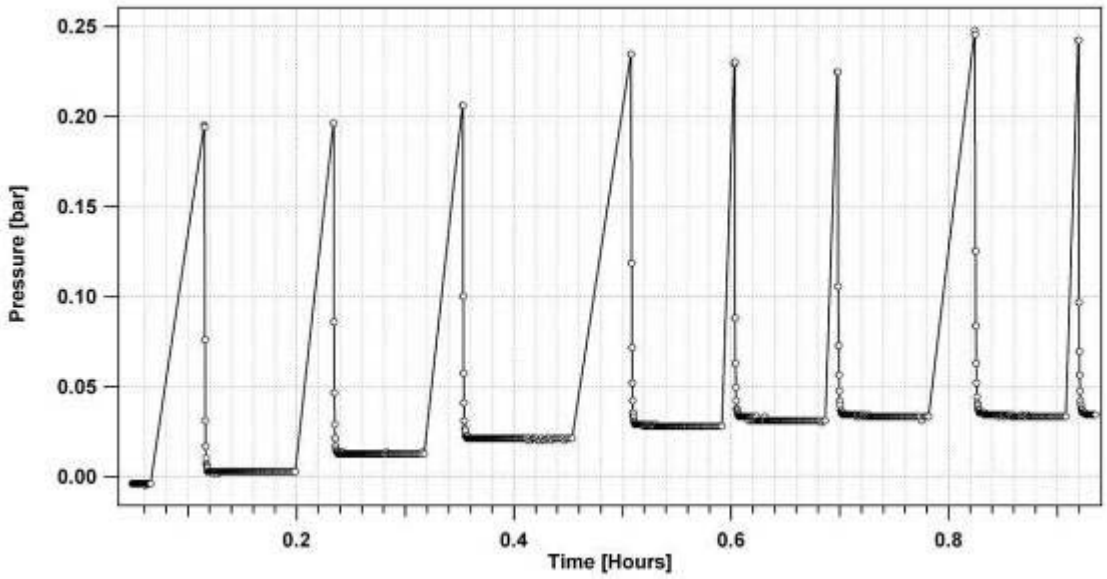

Figure 204. Portion of pressure vs. time data for a sequence of doses of hydrogen during an absorption PCT measurement at 38°C.

Figure 205 shows similar pressure vs. time data across the plateau region of the desorption PCT at 200°C. Note that data is collected very rapidly at the beginning of each dose. In some cases, the first data point of each dose is taken just as the dosing valve opens, before the gas pressures between the dosing reservoir and the sample volume have equalized. Thus, the actual reservoir pressure is observed at the beginning of many of the individual doses.

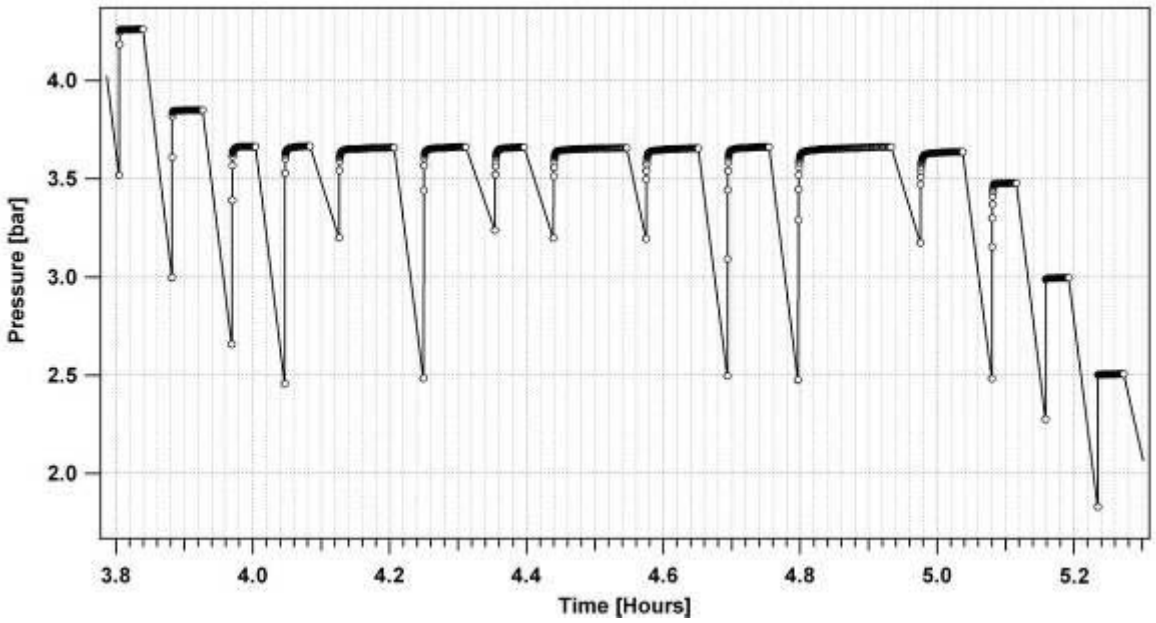

Figure 205. Pressure vs. time data for the plateau region of the desorption PCT measurement at 200°C.

The important point of these figures is to show that for every dose the instrument waited a sufficiently long time for the desorption to reach an equilibrium state. This is demonstrated more clearly by focusing in on an individual dose of Figure 205 (shown below in
Figure 206).

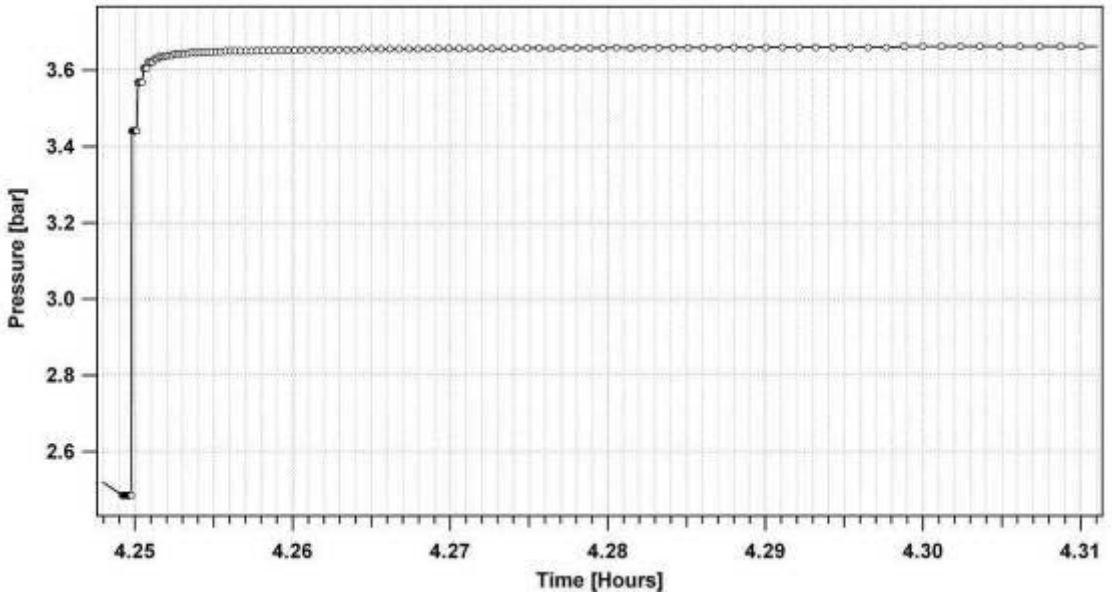

Figure 206. Pressure vs. time data of a single desorption dose in the PCT measurement at 200°C.

One can be certain then that the observed hysteresis is truly a material effect and not an artifact of the measurement process.

2.1.2.9 Direct Van 't Hoff Measurement Technique

The issue, however, is that even for materials with relatively good absorption and desorption kinetics (e.g. $LaNi_5$ in the example), collecting a series of PCT measurements may take from several days to weeks. Even worse, materials with moderate to poor kinetics may take many weeks to months to perform a proper series of equilibrium thermodynamic PCT measurement.

Fortunately, well designed volumetric equipment can allow one to perform what we term here a "Direct van 't Hoff" measurement. This method is efficient in that the measurement time can be reduced to less than a single PCT measurement. The technique is only accessible to volumetric measurement systems. However, there are important caveats and precise control over the experiment is absolutely necessary. The method is explained here using hydrogen desorption from $LaNi_5$ as an example.

Figure 207 shows a real-time desorption PCT measurement on $LaNi_5$ in which the automated desorption dosing (removing hydrogen in steps) is manually halted at a hydrogen concentration of about 3 H/f.u. This is done by changing the maximum time for the current dose from 25 minutes to infinity. Thus, the experiment is fixed at a point where the all quantities are known. That is, a known quantity of sample in a known volume, and a known total amount of hydrogen (in the gas + hydride phase) in the system. If the sample is large enough (~5 grams for $LaNi_5$) and the instrument volume small enough (~ 10 ml in this case) the gas pressure measured when equilibrium is achieved will be the plateau pressure for the sample in a narrow range of hydrogen concentrations at that particular sample temperature.

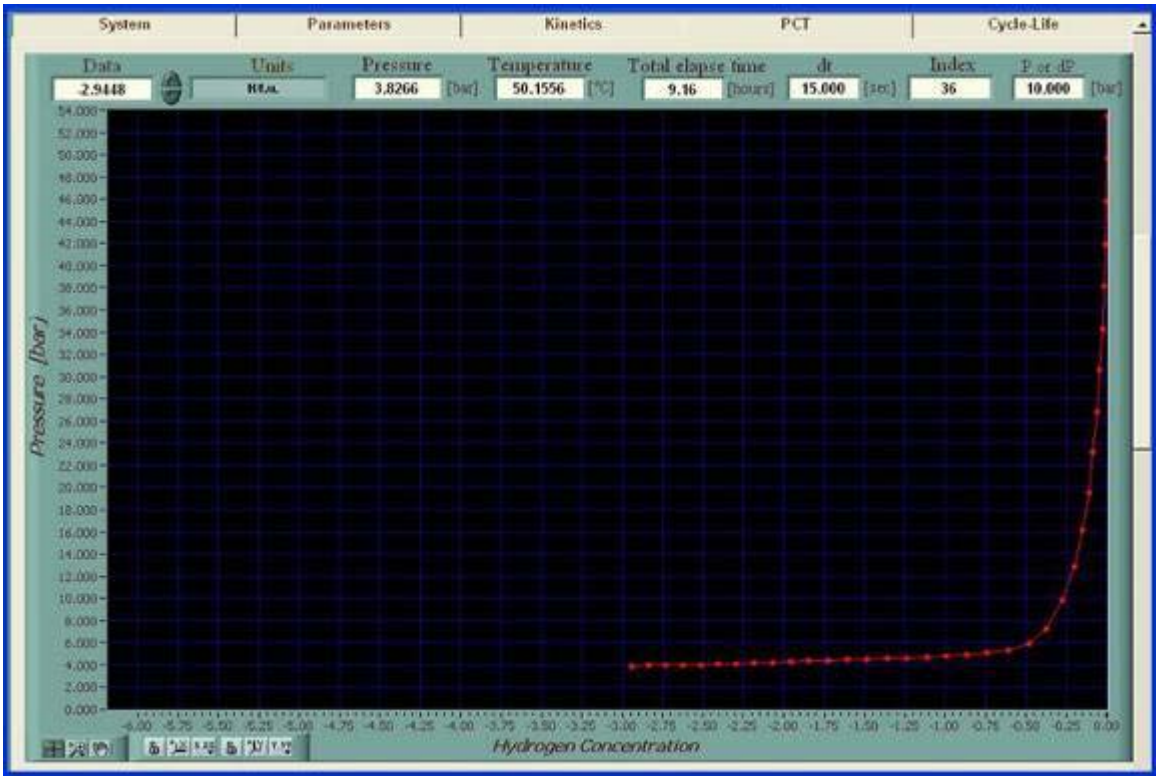

Figure 207. A desorption PCT measurement on $LaNi_5$ at 50°C in which dosing is stopped at a hydrogen concentration of 1/2 the total sample content (i.e. ½ $LaNi_5H_6$ or 3 H/f.u.).

The real-time pressure vs. time data used to produce the PCT plot of Figure 207 is shown in Figure 208. The dosing was manually stopped after approximately 9 hours into the run. At this point the individual dosing time limit was changed to infinity and the samples temperature was decreased to near room temperature. The sample temperature was then increase in steps of 10°C from 30°C to 80°C. At each step, the temperature was held constant until equilibrium was achieved and then increased to the next temperature. In this example a series of equilibrium pressures were collected at 6 temperatures over about a 2 hour period.

Figure 208. The pressure / time profile for the same desorption PCT on $LaNi_5$ in which dosing is stopped at 3 H/f.u. and the temperature of the sample is first reduced to room temperature then increased in steps of 10°C.

With the "Direct van 't Hoff" method, it is important to ensure that concentration does not change significantly during the temperature stepping. As the temperature is increased the sample will desorb hydrogen until the equilibrium pressure is attained. This means that the sample's hydrogen content will change. In-other-words, it is important to maintain a relatively constant concentration and to certainly avoid the sample falling off the plateau. Figure 209 shows a zoom in on the real-time measurement of hydrogen concentration (H/f.u.) vs. time plot during the temperature stepping process. In this case, the sample's hydrogen concentration change was only 0.3 H/f.u. which is about the space between two consecutive data points on the PCT curve. This example worked well because the sample was large (5 grams) and the total gas volume of the PCT instrument was small (approximately 10 ml). Smaller samples, sloping plateaus and larger gas volumes may lead to errors in the direct van 't Hoff measurement method.

Figure 209. The Concentration / time profile for the same desorption PCT on $LaNi_5$ zooming in on the portion of concentration change as the sample's temperature is increased in steps of 10°C.

The results of the "Direct van 't Hoff" data are shown in Figure 210 and are compared with data taken from the full series of PCT measurements at the same hydrogen concentration. The direct data is in agreement with the PCT data and actually shows significantly less standard deviation. A noteworthy point in this example is that the choice of "mid-plateau" was not ideal for $LaNi_5$, as it is at that concentration at which the gamma-phase hydride occurs. The PCT measurements themselves show the gamma-to-beta hydride phase transition. This may explain the deviations in the van 't Hoff results from the PCT data. It would have been better to perform separate "Direct van 't Hoff" measurements at 1.5 and 4 H/f.u. to accurately determine the enthalpy of formation (or decomposition) of the two different hydride phases. The important point is that the enthalpy of dehydriding $LaNi_5$ was determined in a simple measurement that took about 2 hours rather than several days. The dehydriding enthalpy was determined to be -29.68 kJ/mol H_2 which corresponds well with known literature values. The

average value from eight separate publications is 29.8 kJ/mol H_2, with values ranging from 28.5 to 30.8 kJ/mol H_2.[288]

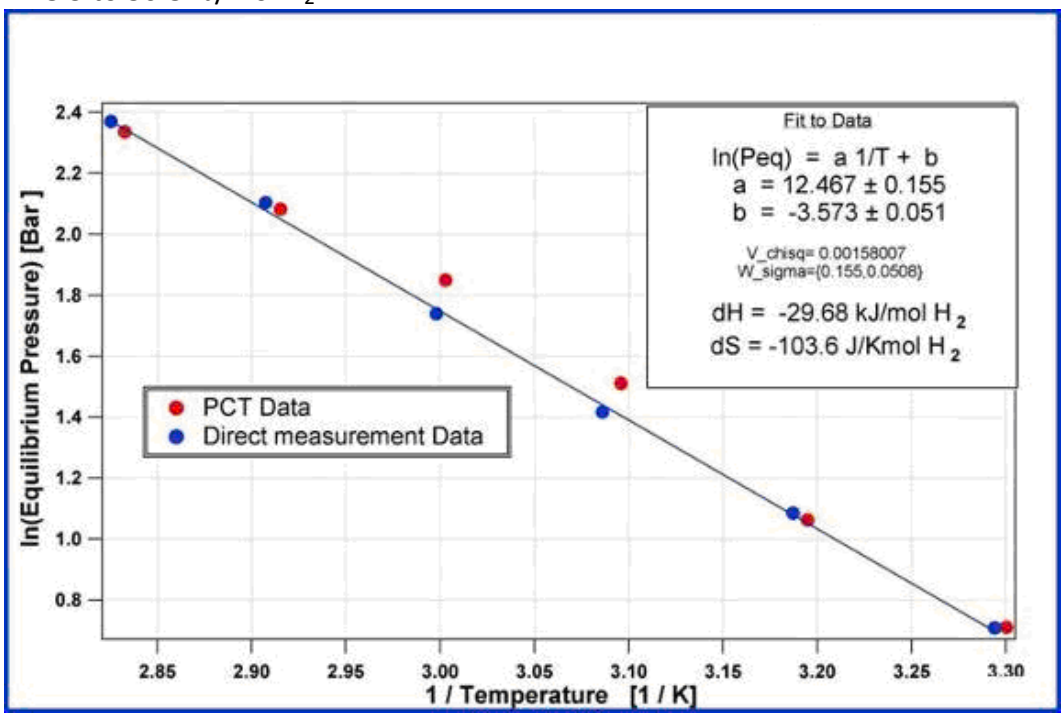

Figure 210. Van 't Hoff plot of equilibrium desorption plateau pressures from a series of PCT measurements (red) and a single "Direct van 't Hoff" measurement on $LaNi_5$ from 30°C to 80°C. The enthalpy and entropy of hydrogen desorption determined from the slope and intercept of the direct measured data are given in the inset of the figure.

Unknown, reversible hydrides will certainly require one or two full PCT measurements to determine what hydriding plateaus exist within a measurable pressure range. But once these are determined, rapid dosing to fixed concentration and direct van 't Hoff measurements can be performed to quickly and accurately determine enthalpies of hydride formation.

2.1.2.10 Micro-Volumetric Direct Van 't Hoff Measurements

While large sample sizes are preferred, sometimes samples are too small to be measured on a standard volumetric instrument. Thus, a micro-volumetric instrument as discussed above can be employed. It is also possible to make "Direct van 't Hoff" measurements on very small samples. The key factor is that the total free gas volume of the instrument should be equally small. This is demonstrated in the following example of the hydriding of a very small sample of Pd.

Because the free-gas volume of the commercial instrument used in this example (PCTPro-MicroDoser) is very small (~1.5 ml) it was possible to perform "Direct van ‘t Hoff" measurements on a Pd thin film sample. This is particularly advantageous when kinetics are so slow that full series of PCT isotherms would take an unacceptable amount of time to complete a standard van ‘t Hoff plot.

These micro-volumetric "Direct van ‘t Hoff" measurements were done by running a standard PCT measurement until the samples hydrogen concentration reached a desired value (in this case a little less than 0.3 H/M. At this point, the control parameters were changed to stay for an unlimited amount of time at the current dose, while the samples temperature was increased in steps. With each temperature increase, the sample desorbs hydrogen until a new equilibrium is achieved. The pressure and temperature were then recorded to create a van ‘t Hoff diagram.

The samples hydrogen concentration was monitored continuously. When the desorption pressure reached a point where the concentration is no longer near mid-plateau, the sample was then dosed with more hydrogen to return to a middle range concentration and the process was resumed. Figure 211 shows the pressure / concentration diagram of the measurement with the initial dosing to reach a concentration of 0.3 H/M. This was followed then by two separate series of doses at higher temperatures to return to mid-plateau concentrations. Note that accurate determinations of the hydrogen concentration in the sample can only be done while changing temperatures if there is temperature compensation in the concentration calculating algorithm.

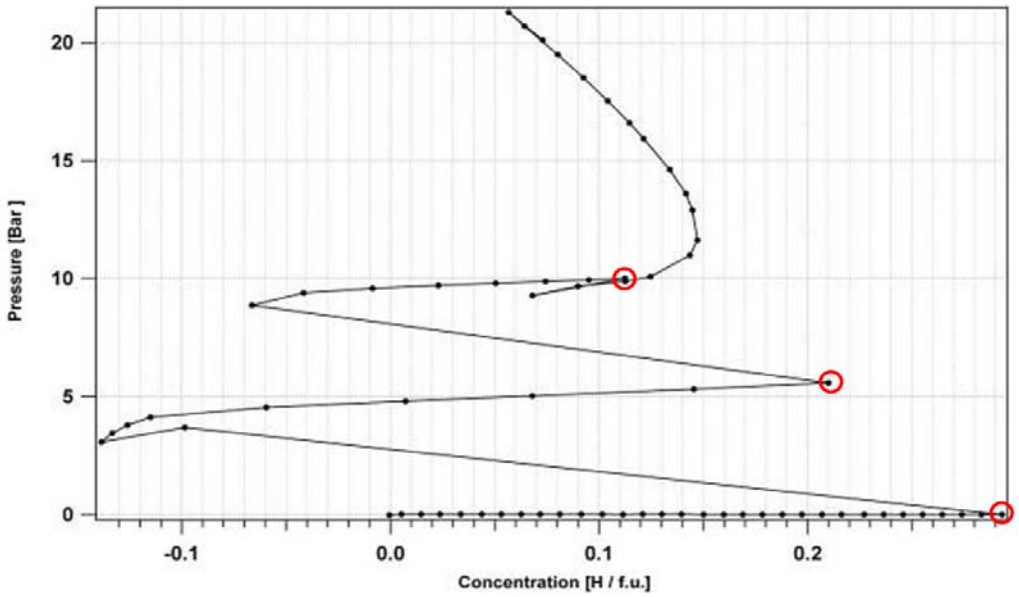

Figure 211. Pressure vs. concentration diagram of the “Direct van ‘t Hoff” measurement. The initial dosing reached a concentration of 0.3 H/M. This was followed by increasing the temperature in two steps with a separate series of

doses at each step to return to mid-plateau concentrations. "Direct van 't Hoff" measurements were taken at the points indicated by the red circles.

The temperature stepping process of the "Direct van 't Hoff" measurement and the associated changes in pressure (log scale) and concentration changes are presented in

Figure 212. Equilibrium temperatures and pressures were taken from this data to create the van 't Hoff plot of Figure 213. Long stretches of inactivity in the measurement were because the experiment was performed over a few days (with no changes made during the night). Clusters of doses can be observed at the beginning and end of the measurement as the sample's hydrogen content was modified to re-center the measurement to mid-plateau. With experience (and good kinetics), such a measurement to collect 10 or more equilibrium data points, would require about a day. This is a big advantage over the many days that would be needed to perform an equivalent series of equilibrium PCT measurements.

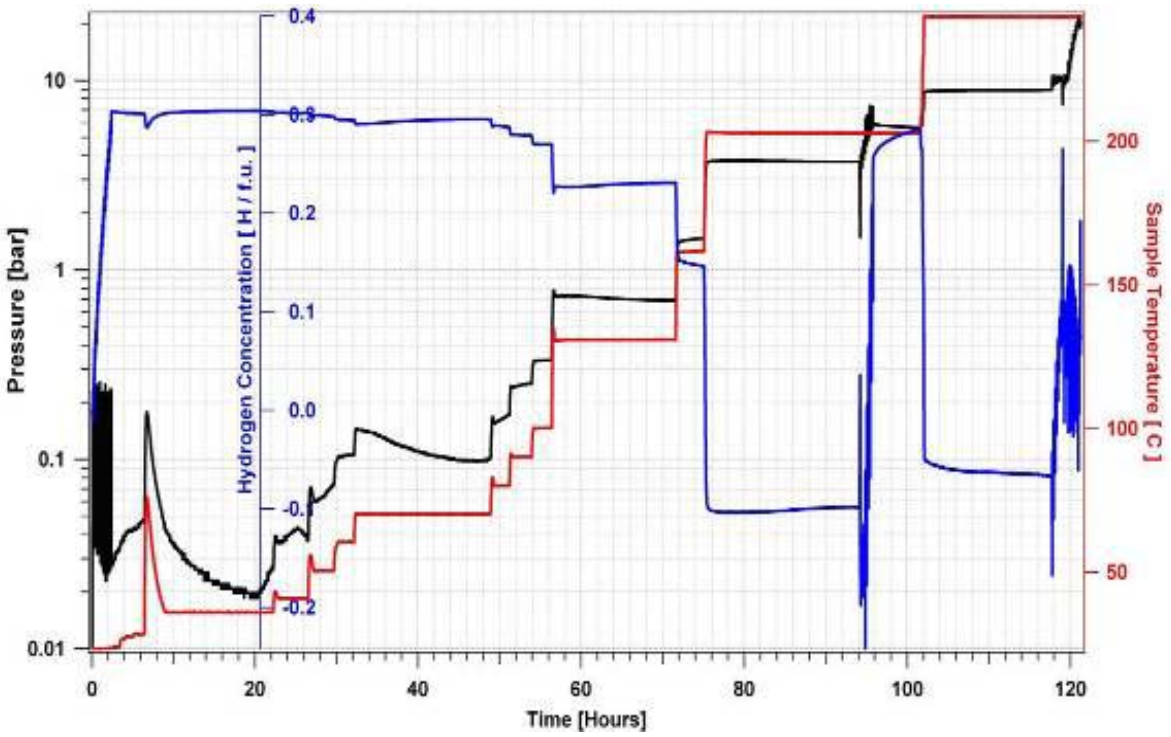

Figure 212. The temperature stepping process of the "Direct van 't Hoff" measurement on a Pd/Ni thin film sample with the associated changes in pressure (log scale) and concentration.

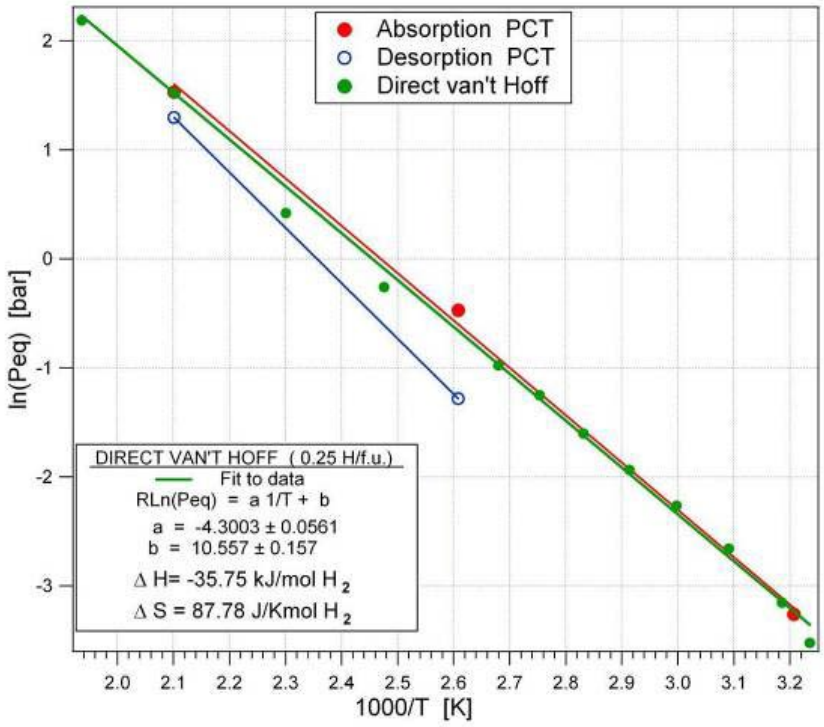

Figure 213. Van 't Hoff plot of equilibrium desorption plateau pressures from a series of PCT measurements (red: absorption, blue: desorption) and a single "Direct van 't Hoff" measurement on a 91 mg Pd/Ni thin film sample from 38°C to 250°C. The enthalpy and entropy of hydrogen desorption determined from the slope and intercept of the direct measured data are given in the inset of the figure.

Figure 213 shows the van 't Hoff data for both the absorption and desorption PCT measurements using plateau pressures at 0.3 H/M as well as the "Direct van 't Hoff" data. The difference in enthalpies of absorption and desorption (hysteresis) can be seen from the PCT data. The enthalpies of hydride formation have been calculated from the slope of the Direct van 't Hoff data (excluding two points, see explanation below) to be -35.75 kJ/mol H_2 and the entropy to be 87.78 J/K mol H_2. This is in approximate agreement with literature values for bulk palladium of the absorption enthalpy of the $\alpha \rightarrow \beta$ phase transition of -37.12 kJ/mol H_2 and the absorption entropy of approximately 91.0 J/K mol H_2.[289]

These measurements not only demonstrate advantages, but also point to a couple of important caveats in the method. While it is possible to do this direct measurement on such a small (low H content) sample, it is absolutely necessary to keep track of the sample's hydrogen concentration because the temperature changes cause relatively large concentration changes. In this case, dosing was used to re-adjust concentration to the mid-plateau point 2 times during the temperature stepping process.

It also shows another important point which still remains to be clarified. This is that for interstitial hydrides there is hysteresis in the plateau pressures between absorption and desorption. One would assume when the temperature is increased in steps in a "Direct van 't Hoff" measurement, that it is purely the desorption equilibrium that is being measured and when the temperature is decreased in steps it is absorption plateau pressures that are being measured. However, this is contrary to the present results which show that of the "Direct van 't Hoff" data points appears to align with the absorption PCT data. A notable exception is the two data points in the middle region of the plot. This deviation may be due to the hydrogen concentrations in the sample at these points being far from mid-plateau (i.e. having fallen off the plateau). Or it may be due to a change from absorption to the desorption equilibrium conditions.

To reiterate, the key to such measurements is to have the free gas volume of the instrument matched to the quantity of sample with as much material and as little gas volume (ideally none) as possible.

2.1.2.11 Physisorption Measurement Systems

Hydrogen physisorption measurements are often performed with a volumetric system involving successive gas expansions from a reference to a sample cell as shown in Figure 214. Schematic view of a volumetric system.[290]

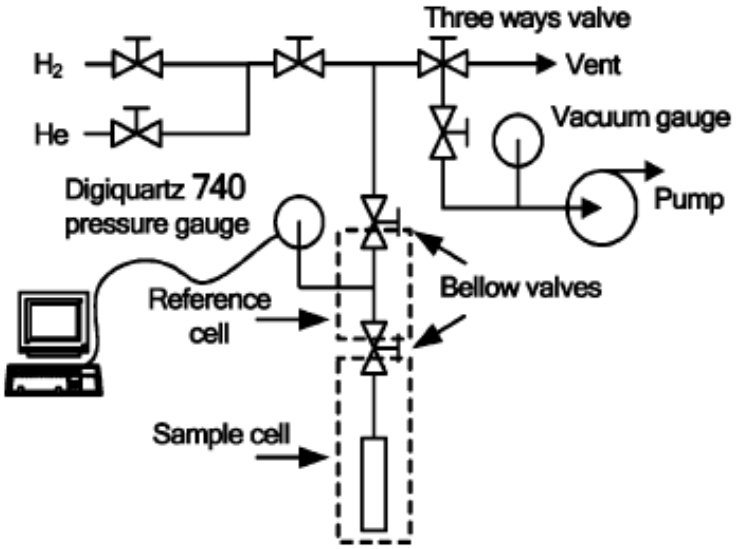

Figure 214. Schematic view of a volumetric system.[290]

The majority of physisorption storage measurements are carried out at low temperatures (typically 77K). Because of the extreme temperature differential between the reference cell and pressure transducers, temperature monitoring, control, and in particular, stability are very important in all temperature and pressure ranges of physisorption measurements. For low temperature measurements, one common setup is to place the sample cell inside a temperature controlled cryostat operated using liquid nitrogen (Figure 215). It is critical to understand that if a basic liquid Nitrogen (or Argon…) dewar is used to keep the sample at 77K, the liquid Nitrogen level must be kept constant (either by topping up the dewar or by moving the dewar). If not the temperature gradient will change with time and will typically have a significant affect on the results that is difficult if not impractical to correct. Because of this complication, a temperature controlled cryostat is often used instead of a dewar. A cryostat will also enable measurements at temperatures other than that of the cryogenic liquid.

An advanced system of control over the static (not changing in time) gas temperature gradient can be achieved by creating a quasi-discreet temperature change in the tubing between the cryogenic temperature of the sample cell and the elevated temperature (typically room temperature) of the gas dosing volumes. This is done by fixing a second temperature control system (also shown in Figure 215) on the gas tubing just above the sample cell. A small heating element allows heating on a small length of the tubing to keep the major part of the gas at, or near, room temperature with minimal perturbation of the cell's temperature. It also allows for a nearly discrete temperature change in the gas rather than an extended temperature gradient which is more difficult to compensate for in the gas law calculations of hydrogen mass balance.[21] The sample cell's controlled heating element enables the sample temperature to be controlled at temperatures above that of the cryogenic liquid (typically T> 77K). This enables adsorption and desorption isotherms to be collected at several sample temperatures which is required to determine the isosteric heats of adsorption. Clearly accurate measurements of the sample's temperature is essential for meaningful thermodynamic analysis.

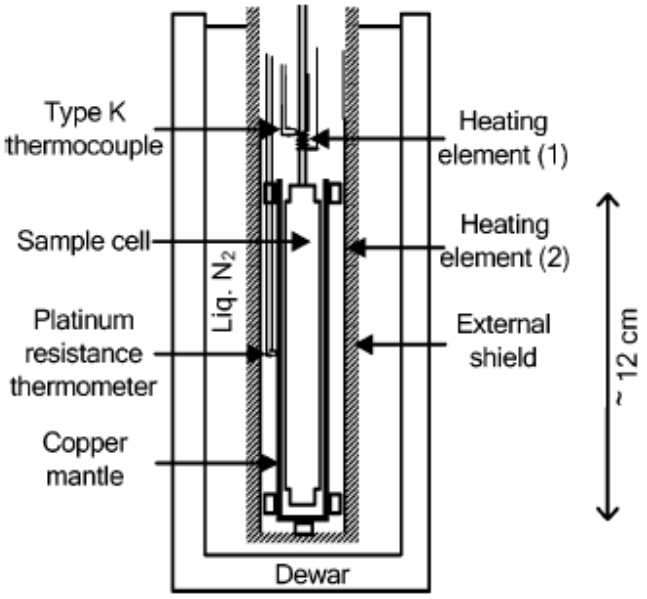

Figure 215. Schematic view of the cryostat (details).[290]

Measurements (Figure 216) of excess hydrogen adsorption isotherms at temperatures ranging from 83 to 273 K based on the above system has allowed the accurate determination of isosteric heats of adsorption of several microporous materials by applying the Dubinin-Astakhov (DA) model.[290]

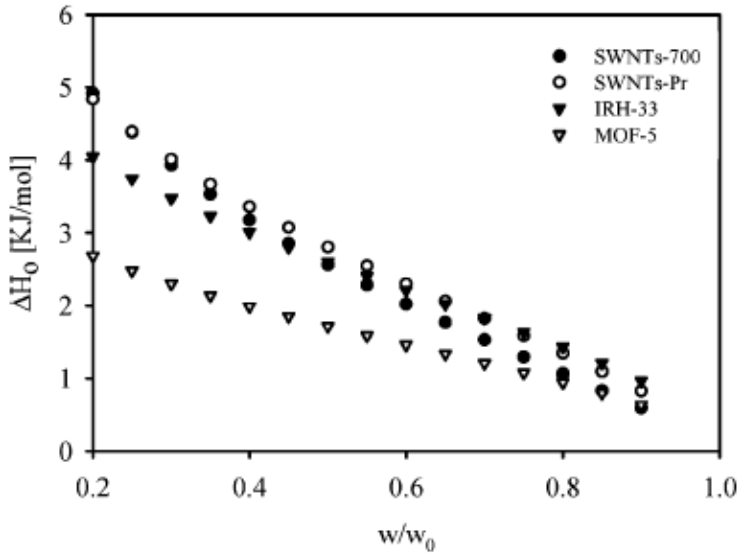

Figure 216. Adsorption enthalpy ΔH^0 plotted as function of fractional filling for different samples where w_0 is the maximum uptake at 77K.[290]

2.1.3 Gravimetric Method

The gravimetric method is often used to determine thermodynamic information indirectly through PCT measurements. The plateau pressures from multiple isotherms can be compiled into a van 't Hoff plot. As described in Section 1.2.4 , the van 't Hoff equation can be used together with a van 't Hoff plot to determine ΔH_f and ΔS_f for a reaction.

2.1.3.1 Hysteresis in Reversible Hydrides

However, these measurements are not always as straightforward as they may seem. As mentioned earlier, hysteresis can lead to a different ΔH for the sorption and desorption reactions, so it is important to specify whether absorption or desorption values are being reported. While some hysteresis may be an intrinsic property of the storage materials, it can also be due to not achieving equilibrium conditions. In particular, materials with large heats of formation will produce significant heat on adsorption heating the sample and cooling on desorption. Thus, for the measurement to achieve equilibrium, the sample must return to the set temperature by transferring heat. This can be difficult to achieve where the only thermal contact the sample has is with the large volume of gas as is the case in gravimetric measurements. While hysteresis effects can be reduced by allowing a longer time to reach equilibrium at each measurement point, some materials have such poor kinetics that this is impractical.

2.1.3.2 Temperature Measurements

Accurate sample temperature measurement is critical to correctly determine enthalpies of reaction (and isosteric heats of adsorption) using PCT measurements. This may be a significant issue with gravimetric measurements due to the difficulty of obtaining the exact sample temperature measurements. This is because, generally speaking there is no thermocouple in direct contact with the sample in most gravimetric systems. Note that this is also often the case with volumetric instruments that do not have a thermocouple in the middle of the sample as mentioned above.

Highly exothermic materials lead to even greater difficulty, since a typical sample temperature may fluctuate considerably during hydrogen uptake and release. In this case the equilibrium pressure will correspond to the sample temperature which may be far from the applied pressure. Thus, the assumed sample temperature and measured

pressure may not correspond well at all to the actual hydrogen uptake conditions actually being experienced by the sample itself. In volumetric instruments this can be remedied to some extent because the sample is generally in direct contact with the vessel walls allowing greater heat transfer. It should be noted that this factor is somewhat muted by the fact that powder samples typically have poor heat transfer properties. Possibilities to mitigate these effects through enhanced heat transfer methods are discussed in section 3.10 of the Kinetics chapter. However, with gravimetric measurements the samples are typically suspended in the gas, excluding the possibility of significant heat transfer, except through the gas itself.

2.1.3.3 Buoyancy

Buoyancy corrections have such a serious impact on the accuracy of gravimetric measurements that it is worth covering this issue again in this section (please refer to subsection 5.5.1 in the Introduction section as well). One common error is to introduce the adsorbate density in the corrections and quoting the uptake results as an excess uptake which it is not. There is also the risk of using an arbitrarily low adsorbate density and reporting an unrealistic uptake value. This has been dealt with in subsection 5.5.1 in the Introduction, but worth reemphasizing here.

Having another look at the buoyancy correction, the upward buoyancy force on the sample is equal to the weight of the fluid displaced by the sample. The degree of the buoyancy effect is proportional to the volume displaced by the sample and the density of the surrounding gas. The upward force due to buoyancy of the sample only is given by:

Equation 217

$$F_b = g\rho_H \Delta V = m_s g\left(\frac{\rho_H}{\rho_s}\right)$$

where m_s and ρ_s are the mass and density of the sample and ρ_H is the density of the hydrogen gas. For a symmetrical balance (see Equation 9) the buoyancy force will also include the mass m_t and density ρ_t of the tare which may include terms representing the mass and density of the sample holder (bucket, pan, beam, and the hang-down wires).

Equation 218

$$F_b = m_s g\left(\frac{\rho_H}{\rho_s}\right) - m_t g\left(\frac{\rho_H}{\rho_t}\right)$$

Or more explicitly:

Equation 219
$$F_b = m_s g\left(\frac{\rho_H}{\rho_s}\right) + m_{sp} g\left(\frac{\rho_H}{\rho_{sp}}\right) + m_{shd} g\left(\frac{\rho_H}{\rho_{shd}}\right) - m_{cw} g\left(\frac{\rho_H}{\rho_{sp}}\right) - m_{cwhd} g\left(\frac{\rho_H}{\rho_{cwhd}}\right)$$

Where the subscripts sp = sample pan, shd = sample hangdown wire, cw = counter weight, and cwhd = counter weight hang down wire. Any other components on the balance that is in the gas, such as sample holders, glass wool, etc. must also be included in the buoyancy correction (with an accurate knowledge of the weight and density of each). In addition any differences in the balance arm volume on the sample side versus the tare side must also be added in to this buoyancy correction. In the above equations, it has been assumed that the all components are at the same temperature and that the hydrogen gas density is the uniform throughout the instrument. At elevated pressures ρ is not only a function of pressure and temperature but must also include corrections for non-ideal gas behavior. This calculation is may be complicated by the fact that at sample temperatures far from room temperature there will most probably be a temperature gradient (and thus hydrogen gas density gradient) in the gas surrounding the components of the balance (pan, hang-down wires, balance beam). In a symmetrical microbalance instrument, it is generally assumed that both sides of the balance experience the same gradients and are zeroed accordingly. However, with very small samples, any minute difference in the instrumental buoyancy may present large apparent mass changes in the sample. With large temperature gradients the correction may include the fact that the material densities will change with temperature.

In addition in the presence of a temperature gradient there may be convective gas movement which also must be taken into account either by minimizing the effect through equipment design or by at least recognizing the contribution this has to decreased accuracy in the measurement (in particular of small-mass low density samples at cryogenic or elevated temperatures).

For asymmetric balances (spring balances or magnetic suspension balances), the influence of buoyancy on the sample and instrument components must be corrected computationally, taking into account that the buoyancy of the balance parts occurs at temperatures different from that of the sample. Thus, the upward force due to buoyancy on an asymmetric microbalance is

Equation 220
$$F_b = g\rho\Delta V = g\rho\left(P_s, T_s\right)\left(\frac{m_s}{\rho_s}\right) + g\rho\left(P, T_x\right)\left(\frac{m_B}{\rho_B}\right)$$

where $\rho(P_s,T_s)$ is the density of the hydrogen gas at the sample, $\rho(P,T_x)$ is the density of the hydrogen gas at various points along the components of the balance (P is constant, but T_x will vary), m_s and ρ_s are the mass and density of the sample and m_B and ρ_B are the mass and density of the balance components (bucket, pan, beam, and the hang-down wires).

When the density of the materials is ill-defined (e.g. for many microporous materials) helium displacement curves can be used to calculate the buoyancy effect. In this case, the essence of the buoyancy measurement lies in the extraction of the skeletal volume ($V_s=m_s/\rho_s$) from the helium displacement curve. This can be performed directly using a microbalance to determine the skeletal volume of the adsorbent. This measurement is quite straightforward when a sample is tested on a symmetrical *instrument* with no tare weight. This approach is basically the gravimetric [method] equivalent of the free (dead) space volume measurement in the volumetric [method]. In fact, there might be no need for separate pycnometry measurements although it can constitute as excellent verification.

Note that there is some concern that the helium may interact with some materials in a way that causes error in determining the skeletal volume and consequently may lead to errors in the quantity of hydrogen absorbed by such a sample. These interactions may be in the form of helium adsorption or it is possible that the helium pressure may affect the density of the material. While not common for most materials, this issue will have the strongest effect on low density, physisorption materials and may be exacerbated by small sample sizes.

2.1.3.4 Other Considerations

Other important issues to be considered when making gravimetric measurements are:

- The impact of impurities in the hydrogen gas
- Foaming or material loss of the sample
- Evolved gases (e.g. solvents, water, ammonia…) from the sample during bake out or desorption measurements
- Gas leaks out of (high pressure) or into (sub-ambient) into the instrument
- Sample temperature measurements
- Adequate heat transfer to or from the sample
- Airless transfer of the sample into the instrument
- Volume dilatation of the sample on heating or hydrogen absorption

These topics are covered in detail in 5.5 of the Introduction section. These are important considerations that should be well understood before making measurements.

2.1.3.5 Gravimetric Thermodynamic Measurements

One important distinction between gravimetric and volumetric measurements of PCT isotherms is that in the gravimetric method data is collected in incremental steps in pressure (slices along the pressure axis of the PCT plot) whereas in the volumetric method data is collected in incremental steps in concentration (slices along the concentration axis of the PCT plot). This has an important consequence for thermodynamics measurements. The classic van 't Hoff method determines enthalpies and entropy from a series of PCT isotherms. This method relies on using equilibrium pressure and temperature data at constant concentrations. The pressure and temperature data will be as accurate as the sensors that are used to measure them. However, concentration in a gravimetric measurement will be determined by the pressure step which is a function of the pressure control device, not the pressure measurement transducer. For most materials that have sloping isotherms this will not be a problem because Peq values (for a given temperature) can be adequately interpolated between data points at different (but close) concentrations. However, for hydrides with relatively flat plateaus it is generally not possible to collect data points on the isotherm (see Figure 18 and Figure 19). This means that the Peq will have to be estimated to be between the two endpoints of the isotherm and therefore the accuracy of the Peq value is dependent on the size of the gas dosing steps rather than on the accuracy of the pressure transducer. Obviously the thermodynamic results will be more accurate for measurement made with the smallest dosing steps the instrument can perform. However, very small pressure dosing steps may require substantially more data collection time.

2.1.4 Capacity and Thermodynamic Measurements

Most of the general considerations above have an impact on the of hydrogen storage capacity (for both volumetric and gravimetric type measurements). Errors in capacity measurements will have some effect on the determination of isosteric heats of formation of physisorption materials (see section 1.3) because the P-T relationship to determine enthalpy is calculated along isosteres (lines of constant concentration). These means that errors in concentration values that are pressure and temperature dependent will ultimately impact the calculation of enthalpy. For this reason it is important that concentration determinations are accurate even for isosteric heats of adsorption measurements.

The same consideration is true for hydrides that have sloping or multiple plateaus. Again, this is because the van 't Hoff analysis should be performed at a specific hydrogen concentration in the sample (usually center of a plateau). If the plateaus are sloping, for a given isotherm the equilibrium pressure Peq can vary significantly depending on the hydrogen concentration. Thus, any errors in concentration that are dependent on

pressure or temperature will produce incorrect isotherms. These errors will translate into an error in the van 't Hoff determination of enthalpy and entropy of hydride formation or decomposition.

2.1.5 Thermodynamic Measurements Using Hydrogenography

The "Hydrogenography" technique was invented at the VU University Amsterdam as described in the thesis of Robin Gremaud. It is now being further developed at the Delft University of Technology. Hydrogenography is an alternative to the conventional volumetric and gravimetric PCI methods used to study the thermodynamic properties of hydrogen storage materials. Unlike bulk techniques, Hydrogenography is applied on thin films of metal hydrides. It is an optical technique, based on the fact that metallic films change their optical properties upon hydrogen loading and unloading (Figure 217).[291]

Figure 217. Metal hydride thin film in the metallic (left) and in the hydrided (right) state during electrochemical loading.[292]

The Hydrogenography approach is similar in to the conventional Sievert's technique with the difference that the hydrogen concentration cannot be measured directly during the experiment. Instead, we monitor the change in the optical transmission of metal thin films while increasing and decreasing the hydrogen pressure during loading and unloading, respectively (Figure 218).[293]

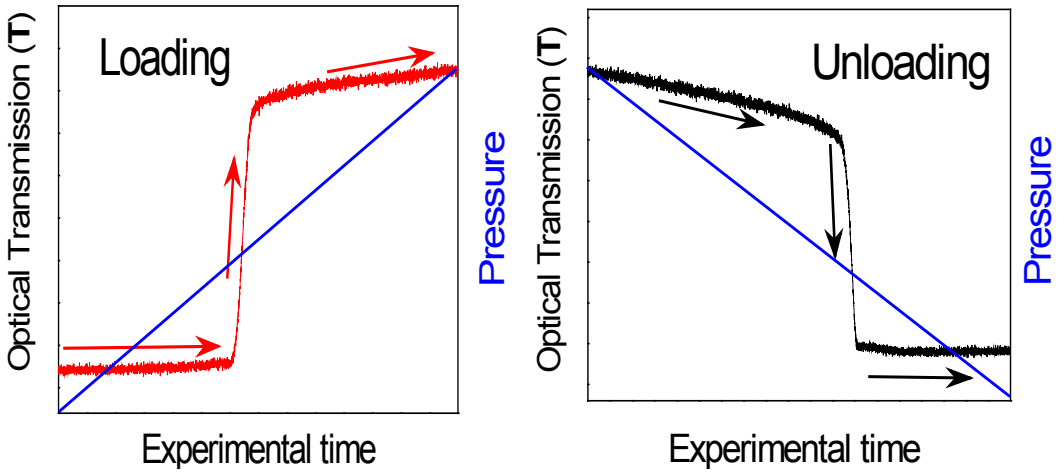

Figure 218. Optical transmission change in the metallic thin film during hydrogenation (left) and dehydrogenation (right).[293]

In this case an abrupt change in the transmission corresponds to the coexistence region or equilibrium plateau. Using the same experimental data in different coordinates, namely $P(H_2)$ vs. $\ln(T/T_o)$ we plot the so-called Pressure-Transmission-Isotherms (PTIs).[233] According to the Beer-Lambert law, the logarithm of the normalized optical transmission is proportional to the hydrogen concentration in the material in the two-phase region.[294,295,296] Note, that the method is not confined to materials showing a metal insulator transition on hydrogenation: materials such as Pd that show large enough optical changes in transmission on hydriding can be studied by Hydrogenography as long as the layer thickness is below 50 nm. This makes PTIs equivalent to the Pressure-Concentration-Isotherms (PCIs) obtained with standard volumetric or gravimetric methods, with the advantage that, due to the thin film geometry, the usual heat transfer and diffusion issues encountered during the recording of PCIs are minimized.

The optical transmission is used only as an indicator of the (de)/hydrogenation pressure. The determination of the absolute hydrogen concentration falls outside the scope of Hydrogenography. In the two-phase region, the hydrogen concentration can be derived from the optical transmission, when the limiting hydrogen concentration of the α and β phase are known and when there is an abrupt change in optical properties on forming a hydride (i.e. relatively flat plateau). To estimate the exact amount of hydrogen dissolved we use electrochemistry or nuclear resonance reaction methods (N-15).

Through the recording of pressure–transmission isotherms at several temperatures the van 't Hoff plot can be constructed and the corresponding thermodynamic parameters (ΔH, ΔS) of hydride formation and decomposition are derived.

A big advantage of Hydrogenography over the conventional methods is the possibility to measure a large number of chemical compositions simultaneously.[293,233] This combinatorial high-throughput technique is capable of exploring the thermodynamic behavior of about 10^3 samples by using large area gradient films with controlled chemical composition. These can be created by co-deposition of two, three or more metal constituents simultaneously with a spatially resolved gradient in the quantity of each component film that is deposited. Measurement of the PTIs over a wide temperature range allows for the parallel determination of the enthalpies and entropies of hydrogen (de)/absorption for all the compositions present in the deposited thin film. This enables the investigation of full metal-hydrogen binary, ternary or quaternary systems and allows the identification of the most suitable compositional region and/or alloy for practical application in a matter of days. This has been successfully probed with the ternary Mg-Ni-Ti system, where a thermodynamically favorable composition of $Mg_{0.69}Ti_{0.07}Ni_{0.29}$ with an enthalpy of hydride formation of -40 kJ/mol H_2 was found.[293] Each composition, represented as a spot on the Mg-Ti-Ni phase diagram (Figure 219) is determined either by measuring the thickness gradient of individual component films using Profilometry or by using Rutherford Backscattered Spectrometry (RBS) on the co-deposited thin film. For each spot the equilibrium pressure for hydrogenation is determined. In case the PTI yields a sloping plateau or a plateau with several steps we discard this data point. On the basis of the temperature dependence of the plateau pressures the map of the enthalpy of hydride formation is constructed, which allows for an easy detection of the most interesting thermodynamic region (Figure 219).

The thin films are often X-ray amorphous, which complicates the structural analysis of interesting areas such as the Mg_2Ni with 5% Ti. However, in this case, using DFT calculations lead to the conclusion that it consist of a mixture of TiNi and Mg_2Ni resulting in a doped Mg2NiH4 structure.[297] Recent EXAFS data confirm this analysis. An important note is, that while the enthalpy is around 40 kJ/mol [H_2], the plateau pressures are in the 1-10 mbar range (relatively stable). This is due to the fact that the entropy deviates substantially from the typical value of 130 J/mol K. In fact, comparing the enthalpy with the entropy map reveals an amazing correlation between the two, the origin of which is presently unresolved.

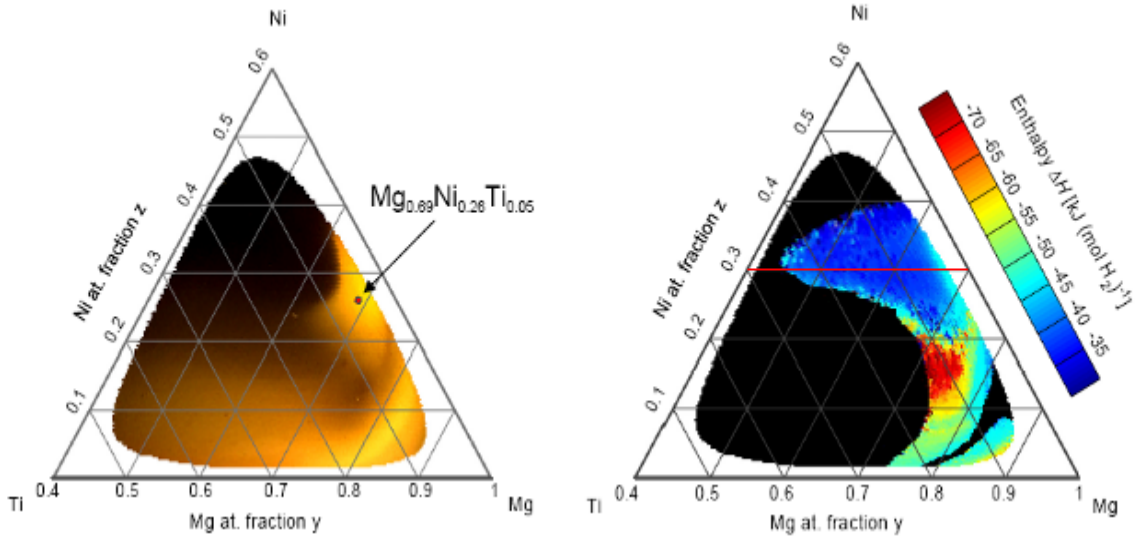

Figure 219. Ternary composition diagram (left) showing the final optical transmission state and the enthalpy map (right) of the Mg-Ni-Ti system, estimated using the optically determined hydrogenation plateaus. Black region on the right-hand picture represents chemical compositions that do not have a well defined plateau on the PTIs.[293]

As Hydrogenography is an optical technique, there are several requirements of the samples. First of all, thin films should be deposited on a transparent substrate, usually glass, sapphire or quartz to have no influence on the measured signal. Typically, sample sizes used in the Hydrogenography experiments ranges up to 3 inch diameter wafers. It is basically determined by the sample holder of the deposition system and the diameter of the sapphire windows of the gas cell.

Secondly, samples should have a measureable transmission in the as-deposited state, meaning that an initial optical transmission, T_o should be higher than the dark signal (signal with no illumination). To satisfy this demand the thickness of thin films is restricted to 50-100 nm.

Another important point is the optical contrast, i.e. the difference between optical transmission in the metallic and hydrided state, which represents the width of the plateau in the Pressure-Transmission-Isotherm. Hydrogenography is capable of monitoring the change in the optical transmission to the order of 0.5%-1% for the above mentioned thicknesses, which makes it possible to measure thin films remaining in the metallic state on hydrogenation such as Pd. For other materials, such as Mg, Y or Gd the optical contrast is not an issue as they experience a metal-to-semiconductor transition on hydrogen loading and their optical transmission changes substantially. In this case, however, the maximum optical transmission might be a problem as it can exceed the saturation level of the camera. To prevent the saturation a light filter should be used to decrease the light intensity.

As most metal hydrides are highly oxidizing materials, all films are covered with thin layer of Pd (10-20 nm) to protect them against oxidation. Additionally, this Pd layer serves as a catalyst for the dissociation of the H_2 molecule to atoms.

After deposition, fresh samples are either stored in a glove box to prevent from any possible contamination or directly transferred to the Hydrogenography setup, where the optical transmission is measured as a function of time, hydrogen pressure, or temperature.

A Hydrogenography setup is represented schematically in Figure 220. The main component is the (de)/hydrogenation gas cell, where the samples are placed. The whole cell is located in an oven with a temperature controller. The maximum temperature that cell components including transparent sapphire windows can withstand is limited to 573 K, which restricts the operation temperature range to 293 K - 573 K. The complete thermal equilibration of the setup is verified by comparing the output of two PT-100 resistors placed at different locations in the oven, one of them being in contact with the sample holder. A 150 W diffuse white light source (the projector) illuminates the sample from the substrate side, and a 3-channel (RGB) SONY XC-003 Charged-Coupled Device (CCD) camera continuously monitors the transmitted light as a function of hydrogen pressure. To avoid any disturbance from a stray light entering the setup, a blanket is used to cover the camera and vacuum cell. The 3-channel transmission intensities are added together, resulting in a 1.1 to 3.3 eV photon energy bandwidth. The use of a camera allows for the recording of the transmission for all compositions simultaneously.

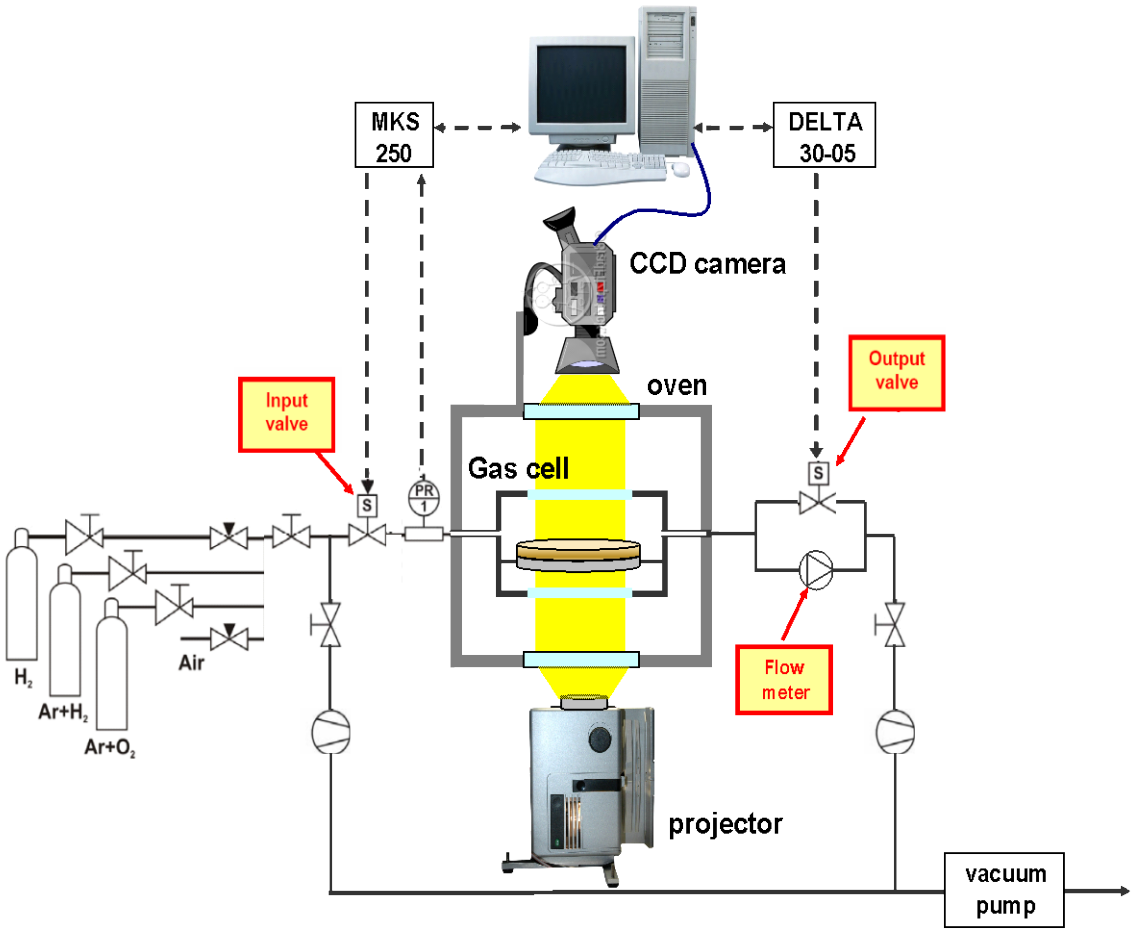

Figure 220. Schematic representation of the *Hydrogenography* setup.

Unlike the standard Sievert's setup, where the pressure-composition-isotherms are determined on a discrete or nearly static basis, i.e. point by point or aliquot by aliquot, Hydrogenography operates in a dynamic mode, meaning that a certain constant flow rate of a gas through the hydrogenation cell is maintained during the absorption and desorption reactions. The gas pressure in the cell is controlled by the inlet and the outlet electronic valves and a flow meter. The amount of gas entering the cell is regulated by a forward Proportional-Integral-Differential (PID) system that controls the opening of the input valve depending on the desired pressure and the reading of the actual pressure by the Baratron pressure gauge. The type of the electronic valve allows a pressure ramp up from vacuum to a maximum of 10 bar H_2, which is the maximum pressure that a typical single crystal sapphire windows of the gas cell with a UHV compatible metal-glass seal can withstand.

The output valve and the flow meter (Figure 220) control the pumping speed at the output of the cell to have a constant gas flow of 30 sccm. The opening of the output valve is regulated by the PC via a Delta 0-30 volt power supply. The flow meter, connected in parallel to the valve is used to set the gas flow. When the pressure in the cell is below 150 mbar, the pressure difference is insufficient to maintain a constant flow of 30 sccm and the pumping rate is controlled by the electronic valve only. At higher pressures the output valve is becomes essentially closed and the outlet flow from the cell to the vacuum pump is controlled solely through the flow meter.

A selection of bottles with $Ar+H_2$ mixtures and pure H_2, connected to the inlet of the gas cell in Figure 220 allows one to measure the hydrogenation behavior of the metal hydride samples over a wide pressure range between 10^{-6} bar *and* 10 bar. For desorption, a flow of an $Ar+O_2$ mixture or air is used to enhance the dehydrogenation of metal hydrides of metal hydrides with slow kinetic, such as Mg. Otherwise, unloading experiments are performed in vacuum.

Before an equilibrium measurement can be done, the thin films need to be cycled. Cycling is a common procedure for many metal hydride systems and consists of a few relatively fast loading/unloading cycles. This is needed to i) stabilize the system behavior by the release of stress and modification of the microstructure.[298] It is also important, ii) to optimize the signal to noise ratio of the light source and the camera with respect to the thickness (50-120 nm) and type of the sample (with or without a metal-to-semiconductor transition). The amount of cycles necessary to achieve a reproducible behavior strictly depends on the type of film, i.e. its interaction with the substrate and the stability of the film. The number of cycles needed does not usually exceed 20 cycles.[298] Optimization of the optical signal is needed to ensure that the optical transmissions of a film in the metallic state is higher than the limit of detection and lower than the saturation limit of the camera. If a too large optical change occurs, a gray filter is used to prevent the saturation of the CCD camera signal.

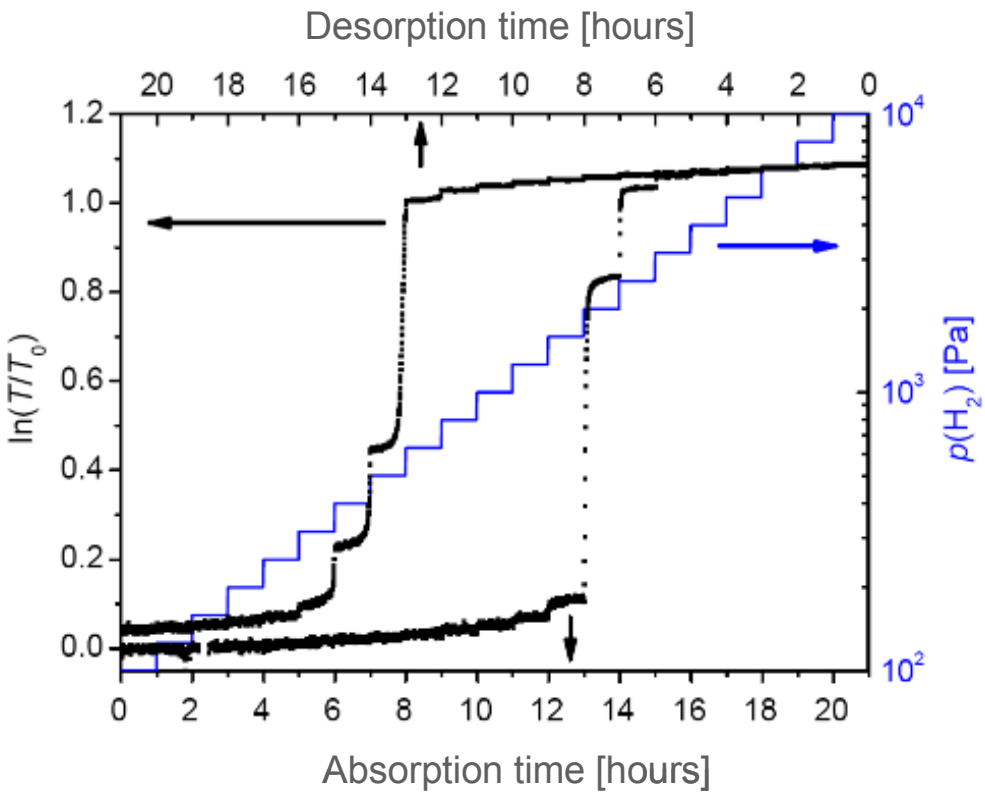

Figure 221. Transmission measurements (black line) of a 65 nm PdHx thin film as a function of hydrogen pressure during absorption and desorption step scans at 294 K after cycling. Each pressure step (blue line) is maintained one hour to ensure relaxation of the film and equilibrium with the hydrogen environment. The transmission T is normalized by the transmission in the as-deposited metallic state T_0.

After the cycling procedure, the equilibrium properties can be measured. There are two possible ways to record the pressure-transmission-isotherms, namely with a pressure-stepping mode or by continuous pressure ramping. A stepwise mode of pressure change is needed to check the kinetics of a hydride formation or desorption. This is done by measuring the optical signal ($\ln(T/T_0)$) as a function of time with each pressure step to ensure that equilibrium is reached within the fixed dosing time (Figure 221).[299] If equilibrium is not reached within the time limit of each separate step, the time to reach can be extrapolated for the entire measurement and a new PTI can be recorded for the second time with a more gradual increase or decrease of the hydrogen pressure. Thus the step scan measurement is generally used to determine the time constant needed to obtain a quasi-equilibrium measurement.

2.2 Calorimetry

Calorimetry is the science of measuring the heat of chemical (e.g., reactions) and physical transformations (e.g., mixing, melting, and vaporization, etc.). A calorimeter is the analytical tool used to measure the heat effects associated with the chemical and/or physical transformations. A calorimeter may be operated under constant volume (i.e., a closed system) or constant pressure (i.e., an open system). There are various types of calorimeters that are commercially available. Various types of calorimeters include Adiabatic calorimeters, Reaction calorimeters, Bomb calorimeters, Calvet calorimeters, Constant Pressure calorimeters, Differential Scanning calorimeters, and Isothermal Titration calorimeters. All of which are measuring heats of physical or chemical transformations under specified conditions (i.e., constant pressure or constant volume). The goal is not to cover every type of calorimeter on the market, but rather to discuss the general calorimetry concepts applied to constant volume and constant pressure.

2.2.1 Bomb Calorimetry: Measuring Heats of combustion

Constant volume calorimeters (often called bomb calorimeters) are typically used for measuring heats of combustion. A bomb calorimeter consists of a sample cup, stainless steel bomb (containing oxygen, sample, and ignition wires), heat transfer fluid (typically water), thermocouple, and a dewar. The bomb calorimeter is approximated as being adiabatic (i.e., no heat loss to the surroundings). The stainless steel bomb is immersed into the heat transfer fluid. The idea is to capture the heat generated from the reaction (or combustion) via the water bath. It should be noted that in the case of a slow reaction if the water bath is not in an insulated vessel (i.e. a situation where there is significant heat loss to the surroundings) the calorimeter can not be considered truly adiabatic and this may lead to errors in the results of the measurement. In order to accurately quantify the energy of combustion, the calorimeter requires calibration. Keep in mind that the calibration will include the water bath, sample cup, and the stainless steel bomb. There are two ways to calibrate the calorimeter, the first way is to introduce electrical energy into the system and record the temperature rise as a function of time and the second way is to perform a combustion experiment with a known compound. A typical standard is benzoic acid. The standard enthalpy of combustion of benzoic acid at 298.15°K is $\Delta H_c^0{}_{298.15}$ = -26.452 kJ/gram for the reaction below with reactants and products in their standard states for this temperature:

Equation 221 $\mathbf{C_6H_5CO_2H(s) + 15/2O_2(g) = 7CO_2(g) + 3H_20(l)}$

The mean heat capacity for the entire calorimeter system $\bar{C}_{P\ calorimeter}$ is determined by:

Equation 222

$$\left(\bar{C}_P\right)_{calorimeter} = \frac{Q_V\big|_{known}}{\left(\Delta T_{rise}\right)_{observed}} = \frac{\left(m_{Benzoic\ Acid}\right)\left(\Delta H_c\big|_{Benzoic\ Acid}\right)}{\left(\Delta T_{rise}\right)_{observed}}$$

Where Q_V is the known reaction heat generated for *m* grams of benzoic acid and ΔT_{rise} is the measure temperature change in the cell. In both cases the amount of energy deposited within the calorimeter is known. The calibration that results is either a mean heat capacity for the entire calorimeter system ($\bar{C}_{P\ calorimeter}$) or correlated to an equivalent amount of water (n_{water} with a known heat capacity of 75.327 J/molK).

Equation 223

$$n_{water} = \frac{Q_V\big|_{known}}{\left(C_P\right)_{water}\Delta T_{rise}\big|_{observed}} = \frac{P_{electrical}\cdot t}{\left(75.327\frac{J}{mol\cdot K}\right)\Delta T_{rise}\big|_{observed}} = \frac{\left(V\cdot I\right)_{electrical}\cdot t}{\left(75.327\frac{J}{mol\cdot K}\right)\Delta T_{rise}\big|_{observed}}$$

where $P_{electrical}$ is the Power, *t* is the heating time, *V* is the applied voltage, and I is the applied current.

2.2.2 Examples:

Good examples of calibrations and measurements using bomb calorimetry can be found at: http://www.science.uwaterloo.ca/~cchieh/cact/c120/calorimetry.html

These examples illustrate the utility of bomb calorimetry for determining heats of formation and heats of combustion.

It should be noted that the use of bomb calorimetry for such measurements often rely on a number of underlying assumptions. The assumptions include:

- *Adiabatic operation*
- *Ideal gas behavior*
- *Energy released from ignition source (e.g. nickel fuse wire) is negligible*
- *All reactions went to completion*
- *Reactions proceed without significant temperature rise, thus correlating the heat of combustion to standard conditions*

Bomb calorimetry is well suited for heats of combustion, but may not be suitable for reactions occurring at elevated temperatures. In such cases a differential scanning calorimeter (DSC) may be a better option. Details of the DSC measurement method can be found in the Introduction section 5.7 . A DSC operates by employing a reference (typically an empty crucible) that experiences identical processing conditions as that of the sample side. In typical DSC applications the crucibles can be closed or open (Figure 222). For example, there are high pressure crucibles that can be operated with pressures up to 500 bar. In addition, the DSC can be used to experimentally determine heat capacities under constant volume or constant pressure conditions.

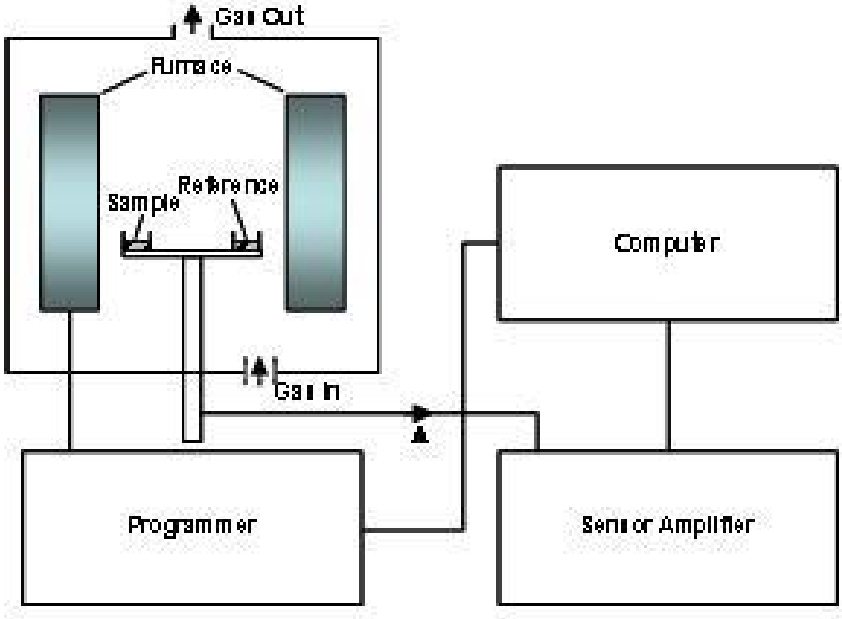

Figure 222. Diagram of a basic DSC instrument.[300]

An alternative technique, which shares much in common with DSC, is differential thermal analysis (DTA). In this technique it is the heat flow to the sample and reference that remains the same rather than the temperature. When the sample and reference are heated identically phase changes and other thermal processes cause a difference in temperature between the sample and reference. Both DSC and DTA provide similar information. Many modern commercial DTA are called heat flux DSC. A DTA curve can be used only as a *finger print* for identification purposes rather than enthalpy of reaction measurements. The usual application of this method are the determination of phase diagrams, heat change measurements, and decomposition in various atmospheres.

It is important to realize that the intensity of the heat flow signal is proportional to the temperature ramp (i.e. faster ramp rates, bigger peaks). Thus, the ramping rates may have a significant impact on the accuracy of the determination of reaction heats from the integration of the resulting peak data. **For best practice, regular calibration and calibration runs for different ramp rates, and different gas atmospheres are vital.**

It is equally important to understand that making measurements using an inert carrier gas, is equivalent to performing the reaction under a hydrogen partial pressure of close to 0 bar, i.e. equivalent to high vacuum. This may, in fact, change the chemical decomposition route or behavior as compared to how decomposition will occur in a real application, under a few bar of hydrogen pressure.

How can we use a DSC to measure the heats of reaction where the reaction takes place at an elevated temperature? In each of the examples above the reactions were simple combustion reactions. In many cases the reactions are not so straight forward to measure the heat effects. For example take the reaction of periclase (MgO) and quartz (SiO_2) to form forsterite (Mg_2SiO_4):

$$I: \quad 2MgO(c) + SiO_2(c) = Mg_2SiO_4(c) \qquad \Delta H^I = ?$$

Forsterite is a compound of interest in the geological community, the reaction of periclase and quartz to produce forsterite proceeds very slowly and cannot be measured directly. The Bureau of Mines was able to quantify the heat of reaction for this reaction by using Hess' Law and solution calorimetry as follows:

$$II: \quad SiO_2(c, 25^\circ C) + 6HF(soln, 73.7^\circ C) = H_2SiF_6(soln, 73.7^\circ C) + 2H_2O(soln, 73.7^\circ C)$$
$$\Delta H^{II} = -148.16 \frac{kJ}{mol}$$

$$III: \quad MgO(c, 25^\circ C) + 2HF(soln, 73.7^\circ C) = MgF_2(soln, 73.7^\circ C) + H_2O(soln, 73.7^\circ C)$$
$$\Delta H^{III} = -162.13 \frac{kJ}{mol}$$

$$IV: \quad Mg_2SiO_4(c, 25^\circ C) + 10HF(soln, 73.7^\circ C) = 2MgF_2(soln, 73.7^\circ C) + H_2SiF_6(soln, 73.7^\circ C) + 4H_2O(soln, 73.7^\circ C)$$
$$\Delta H^{IV} = -399.07 \frac{kJ}{mol}$$

Using Hess' Law the heat of reaction for ΔH^I can be computed as:

Equation 224

$$\Delta H^I = 2\Delta H^{III} + \Delta H^{II} - \Delta H^{IV} = -73.35 \frac{kJ}{mol}$$

Similar analysis may be pursued to evaluate the heat of reaction of hydrides with other compounds to release hydrogen. One example being the evaluation of the thermodynamic stability of the MgH_2/Si system:[301]

Equation 225

$$2MgH_2 + Si \rightarrow Mg_2Si + 2H_2.$$

The stability of the silicide (Mg_2Si) was observed to destabilize the corresponding hydrides. For Mg_2Si, the standard enthalpy of formation is –77.8 kJ/mol. Therefore, formation of Mg_2Si should reduce the standard enthalpy of dehydrogenation of MgH_2 from -75.3 kJ/mol for pure MgH_2 to -36.4 kJ/mol for MgH_2 + 1/2Si. Thus, destabilization of the hydride increases the equilibrium pressure or, equivalently, reduces the temperature necessary for a particular pressure such as 1 bar. While this system was not shown to be reversible, thermodynamic data for the silicide enabled an estimation of the equilibrium pressure of 1 bar hydrogen at ~20°C for this system.

In other cases, there may be difficulties that either complicate obtaining heats of reactions or prevent the isolation of the heat of reaction. When the product set is ill-defined, this complicates matters further. This is where creativity comes to bear in devising a scheme to deconvolute the ancillary heat effects from the sought after heat effect (e.g., heat of reaction). As an example consider the overall thermal decomposition of ammonia borane

Equation 226

$$NH_3BH_3(s) \xrightarrow{\Delta H_r^\circ} 2H_2(g) + \sum \left(P_i + P_j \right)$$

The product sets P_i and P_j are the result of the stepwise decomposition occurring at different temperatures. Unfortunately, the product sets are ill-defined and the quantification of the product sets is currently unknown. The thermodynamic cycle for the stepwise decomposition of ammonia borane can be generalized in the following diagram.

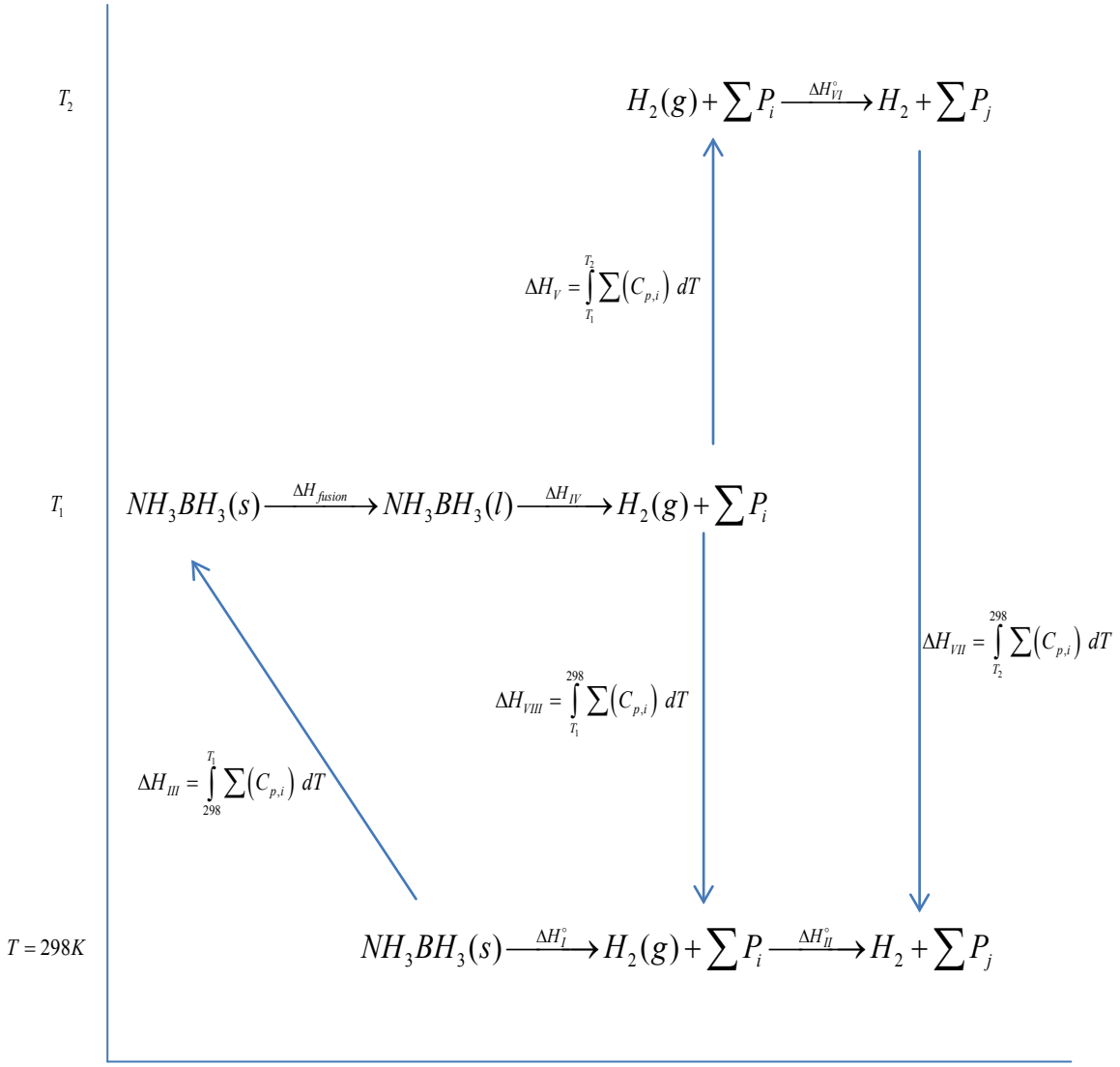

$$\Delta H^\circ_r = \Delta H^\circ_I + \Delta H^\circ_{II} = \left(\Delta H_{III} + \Delta H_{fusion} + \Delta H_{IV} + \Delta H_{VIII}\right)_{\Delta H^\circ_I} + \left(\Delta H_V - \Delta H_{VIII} + \Delta H_{VI} + \Delta H_{VII}\right)_{\Delta H^\circ_{II}}$$

Figure 223. Diagram detailing the major chemical and physical transformations of the decomposition of ammonia borane.

This is a rudimentary diagram showing the major chemical and physical transformations of the decomposition of ammonia borane. What is not shown are the side reactions producing ammonia, borazine, and diborane. Complicating matters further is the fact that upon melting, ammonia borane immediately decomposes (exothermically) to release one equivalent of hydrogen. The energy liberated causes a temperature rise of

the contents, thus promoting the second equivalent of hydrogen. Consequently, the chemical and physical transformations tend to overlap causing difficulties in deconvoluting the heat effects. One additional complication deserving attention is the non-stoichiometric release of hydrogen above two. In other words, the decomposition of ammonia borane is complicated and therefore non-trivial to obtain the heat effects experimentally without gross simplification.

2.2.3 Combined Calorimetry and Gas Sorption measurements

Combined calorimetry and volumetric gas sorption measurements have been performed on hydrides over the years and have important advantages over the use of only one or the other technique.[302] The following example shows how simultaneous calorimetry and gas sorption provide a direct measurement of the formation enthalpy in a single one hour sorption cycle versus the many hours, days, weeks or even months that may be required through equilibrium PCT measurements.

One way to obtain the energetics of H_2 binding is to directly measure the heat released during hydrogen absorption, however it is essential to quantify the exact uptake of hydrogen absorbed or desorbed to correctly determine the enthalpy of reaction. More typically, the energetics of hydrogen absorption and desorption are obtained by applying the van 't Hoff relationship between equilibrium hydrogen pressures and temperature. While very accurate, this can be a time-consuming process. An elegant solution is to determine thermodynamic properties directly through a combination of simultaneous gas sorption analysis and calorimetry measurements.[303]

By coupling a calorimeter to a Sievert's gas sorption analyzer one can measure directly the heat (enthalpy) of formation of a metal hydride and its hydrogen sorption properties simultaneously (Figure 224). The two instruments are ideally suited for the study of hydrogen storage materials allowing one to probe simultaneously the hydrogen sorption capacity, kinetics, and energetics of materials over a very wide range of temperature and pressure (from RT to 300 °C and vacuum to 200 bar).

Figure 224. PCTPro-2000 Sievert's apparatus coupled with a C80 calorimeter permitting simultaneous measurements of gas adsorption/desorption and heats of sorption.[303]

To use the instruments in a combined way requires only a stainless steel extension gas line to attach the calorimeter's sample vessel to the sample port of the volumetric gas sorption instrument. Before materials testing, the dead gas volume of the sample vessel (~6 ml) was determined by an automated helium gas dosing routine. Then, with the calorimeter held at 40°C, the combined instruments were tested by providing a dose of hydrogen at 11.2 bar into the empty sample vessel. The purpose of this test was to measure the background effect due purely to heating the gas as it is dosed into the sample vessel. The measurement showed that the background gas heating effect from this quantity of gas would not significantly impact the direct measurement of the enthalpy of hydride formation (0.5% of the expected ~30 kJ/mol H_2 for the $LaNi_5H_6$ formation). This is important as the heating of the gas that is absorbed by the sample may have a significant effect on the results. A simple solution to reduce this error is to preheat the gas to the temperature of the sample before it enters the calorimeter.

As an example of the combined measurements, an intermetallic compound $LaNi_5$ was chosen as a model hydrogen storage material to be tested due to its widespread use as a reference material in the field of hydrogen storage.[304] $LaNi_5$ forms a stoichiometric hydride $LaNi_5H_6$. A coarsely ground sample of $LaNi_5$ (4.377 gm) was loaded into the

calorimetry sealed gas vessel under air. A non-absorbing stainless steel rod of equal gas displacement volume as the $LaNi_5$ sample was placed in an identical sample holder in the reference cell. The sample vessel was purged of air, evacuated and heated to 40 °C. This was followed by an automated activation cycling procedure involving 30 cycles of sequential H_2 absorptions and desorptions (Figure 225).

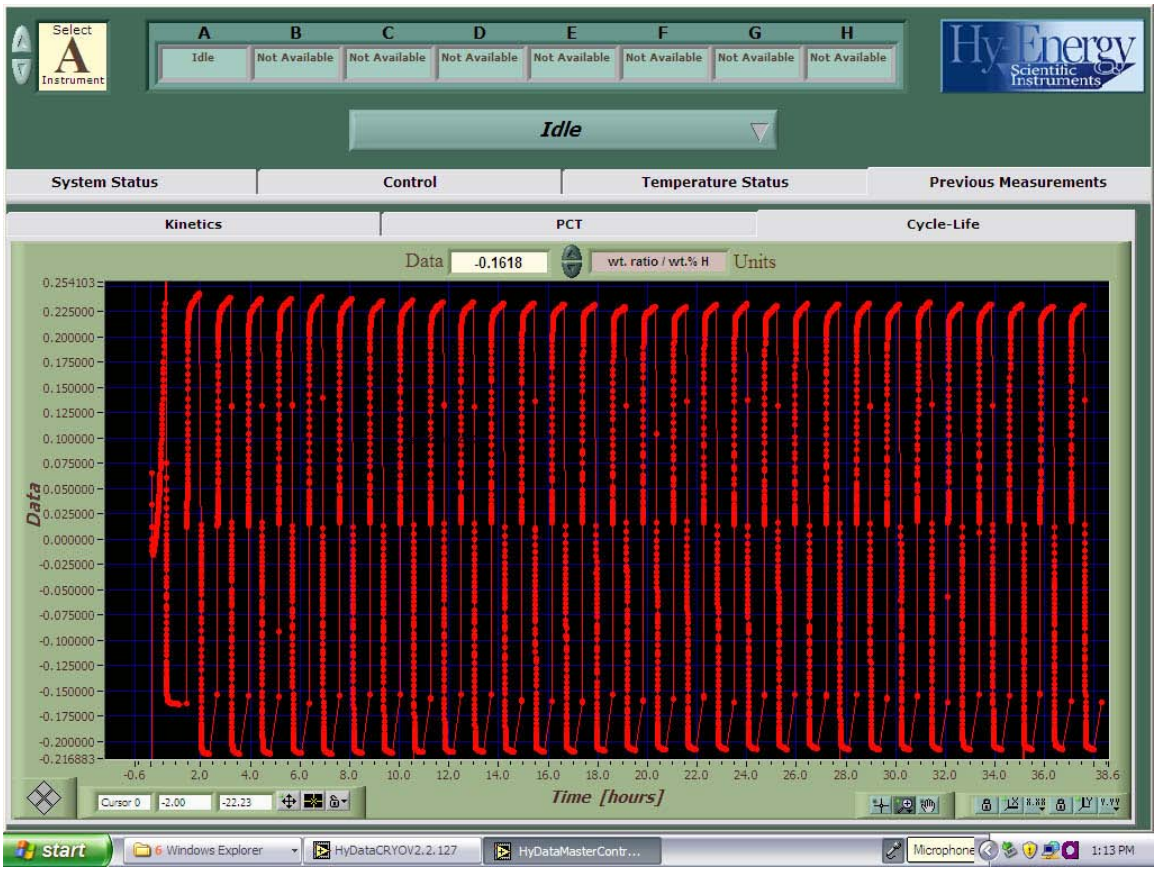

Figure 225. Cycling kinetics data showing activation of $LaNi_5$. Note lower initial capacity of the sample.[303]

The gas sorption cycling measurements showed reasonable absorption and desorption kinetics, as expected, but very low capacity. The first two cycles appeared to have a normal activation behavior, however, the sample was only partially hydrided. Further cycling did not increase the hydrogen content of the sample, and was steady but incomplete even after more than 30 cycles. The final reversible capacity was 0.23 wt. %, which is only 1/6 of the normal hydrogen storage capacity. This particular measurement stresses the important need for simultaneous gas sorption measurements combined with calorimetry. This is necessary to quantitatively determine the extent to which reactions reach completion and thereby accurately determine the enthalpy of reaction.

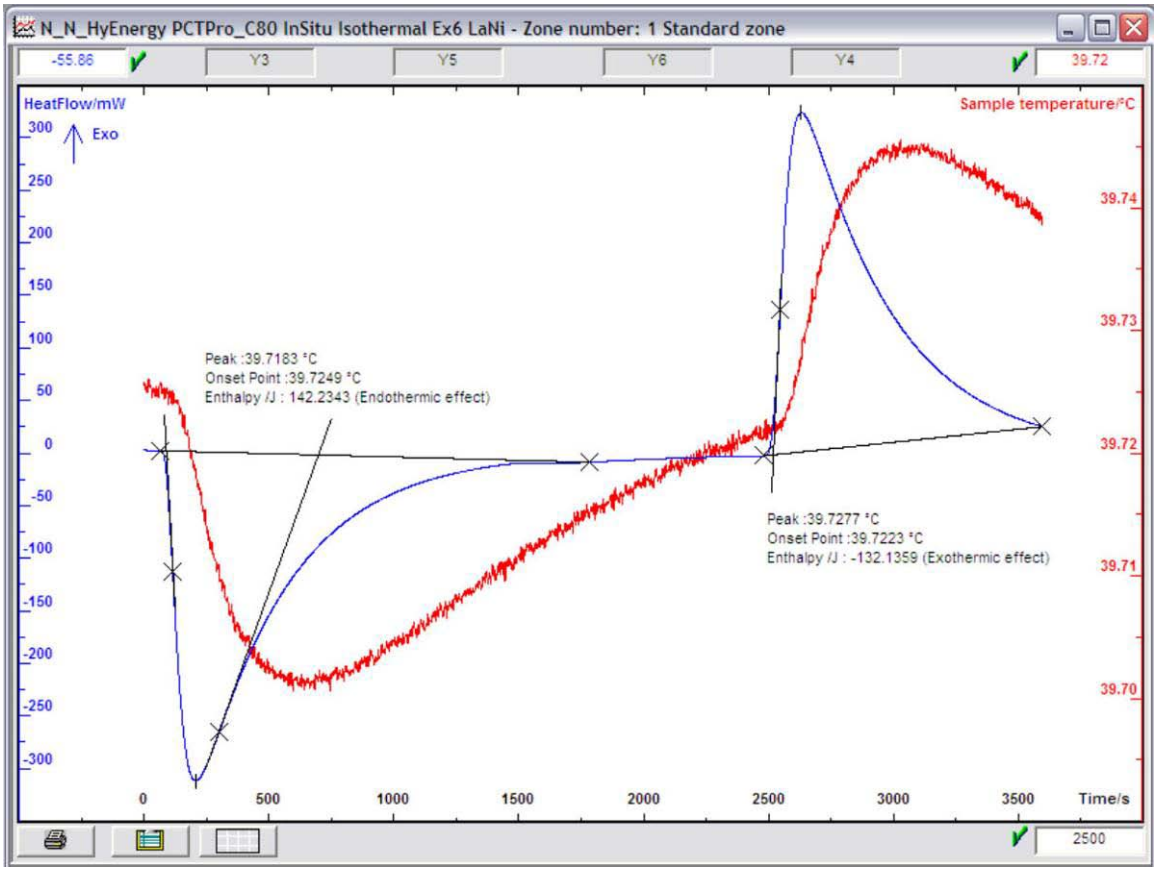

Figure 226. Calorimetric curves showing exothermic and endothermic peaks for hydrogen absorption and desorption cycles.[303]

The energy (enthalpy) of hydride formation was evaluated from in situ heat flow data from the calorimeter (Figure 226) during one of the absorption/desorption cycles (No. 20, Figure 225) performed by the volumetric gas dosing instrument. The individual absorption and desorption total heat released and taken up was calculated by integration of the corresponding exotherm and endotherm. These values were then divided by the total number of moles of absorbed and desorbed hydrogen measured by the volumetric gas sorption instrument to provide the true heat of hydride formation. Based on the number of moles of hydrogen absorbed (4.88×10^{-3} moles) the formation enthalpy was determined to be 29.2 kJ/mol H_2 for this sample of $LaNi_5H_6$. This is consistent with known literature values. The average value from eight separate publications is 29.8 kJ/mol H_2, with values ranging from 28.5 to 30.8 kJ/mol H_2.[288] Had only a calorimetric measurement been performed the assumption that the sample completely hydrided to the full 1.4 wt.% (all $LaNi_5H_6$) would have given a value for the enthalpy of formation that would be in error by a factor of 6 (i.e. 4.8 kJ/mol H_2).

Visual inspection of the sample used in these experiments, when removed from the sample holder after 30 cycles, showed that a large portion of the original intermetallic particles were still present mixed with a smaller portion of the fine gray metal-hydride powder confirming that the starting material sample did not fully react with hydrogen (Figure 227). Sieving and weighing of the fine powder (hydride sample) gave a mass percent conversion of only $1/6^{th}$ supporting the gas sorption measurement results. This phenomenon is most likely due to passivation of the surface by a thin oxide layer that prevents hydrogen dissociation and penetration into the metal to form a hydride. This example is not the exception, but rather points out the critical fact that gas-solid reactions of any kind cannot be assumed to proceed to completion except under ideal conditions.

Figure 227. After 32 cycles $LaNi_5$ sample still contains 5/6 of a course un-reacted material. [303]

The advantage of such simultaneous measurements is that they can provide a direct measurement of the formation enthalpy in a single short sorption cycle versus the many hours, days, weeks or even months that may be required through equilibrium PCT measurements. In addition, this integrated setup provided multiple property measurements (gas uptake capacity, kinetics and thermodynamics) in a single measurement on one sample. Ordinarily, these would be multiple measurements on more than one sample on several instruments with all the inherent questions about consistency of materials, conditions and reproducibility.

2.3 Calorimetry vs. Van 't Hoff Measurements

Calorimetry and van 't Hoff measurements can often give slightly different results for reversible hydrides. One of the main contributions to this effect is that calorimetry measures the total heat produced or consumed in going from an unhydrided to fully hydrided state (or vise versa) including the uptake of hydrogen as a solid solution in the host metal prior to and after forming the hydride. On-the-other-hand, the van 't Hoff method is typically only performed on the two phase plateau region and, thus, measures only the enthalpy of hydride formation (Figure 228).

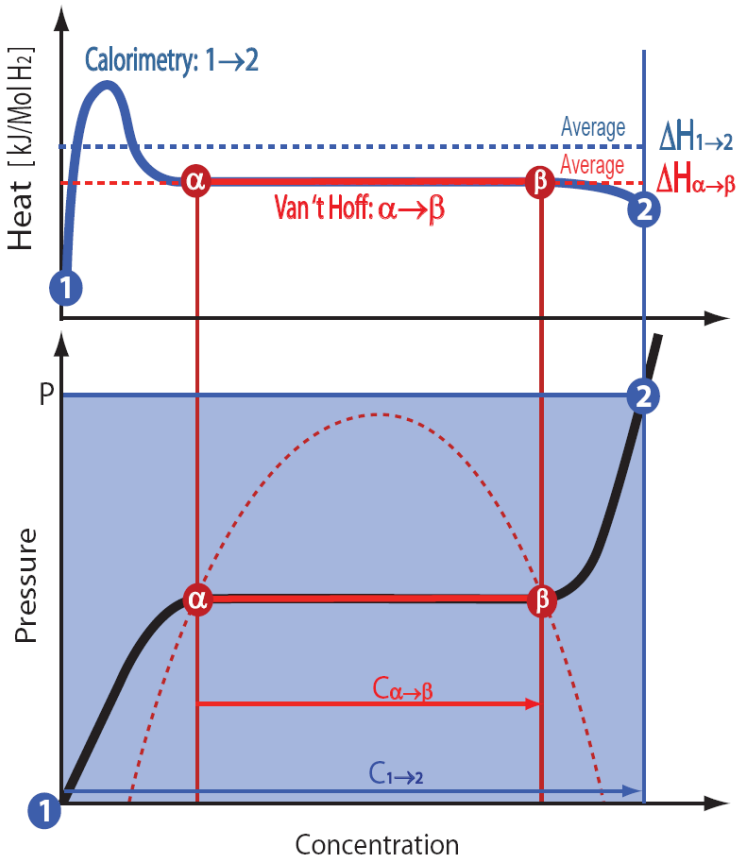

Figure 228. Isotherms and enthalpies corresponding to the formation ($\Delta H_{\beta\rightarrow\gamma}$), decomposition ($\Delta H_{\gamma\rightarrow\beta}$) of the nonstoichiometric γ-trihydride, and $ZrNiH_{3-\gamma}$ from the monohydride.

This was explained in detail in section 1.2.3 . To summarize: for an idealized reversible system, the enthalpy of transformation, from the hydrogen-metal solid solution (α-phase) to the hydride (β-phase), is given by the van 't Hoff relationship (and from Equation 159.

Equation 162). The contribution of the heat of hydrogen solution (partial molar enthalpy of solution of hydrogen in the metal/compound and hydride) is not taken into account in this calculation and must be evaluated to obtain a reasonable estimation of the actual total heat of hydride formation. This is particularly true with respect to determining the heat evolved or consumed in actual hydrogen storage applications.

An example of this is shown in Figure 229, in which calorimetry measurements (bottom) are carried out for individual doses of gas while simultaneously measuring a PCT isotherm (top) for the ZrNi-ternary hydride system.[305] Enthalpy of hydride formation is constant and identical for absorption and desorption only in the two-phase hydride formation region corresponding to the flat plateau portion of the PCT plots.

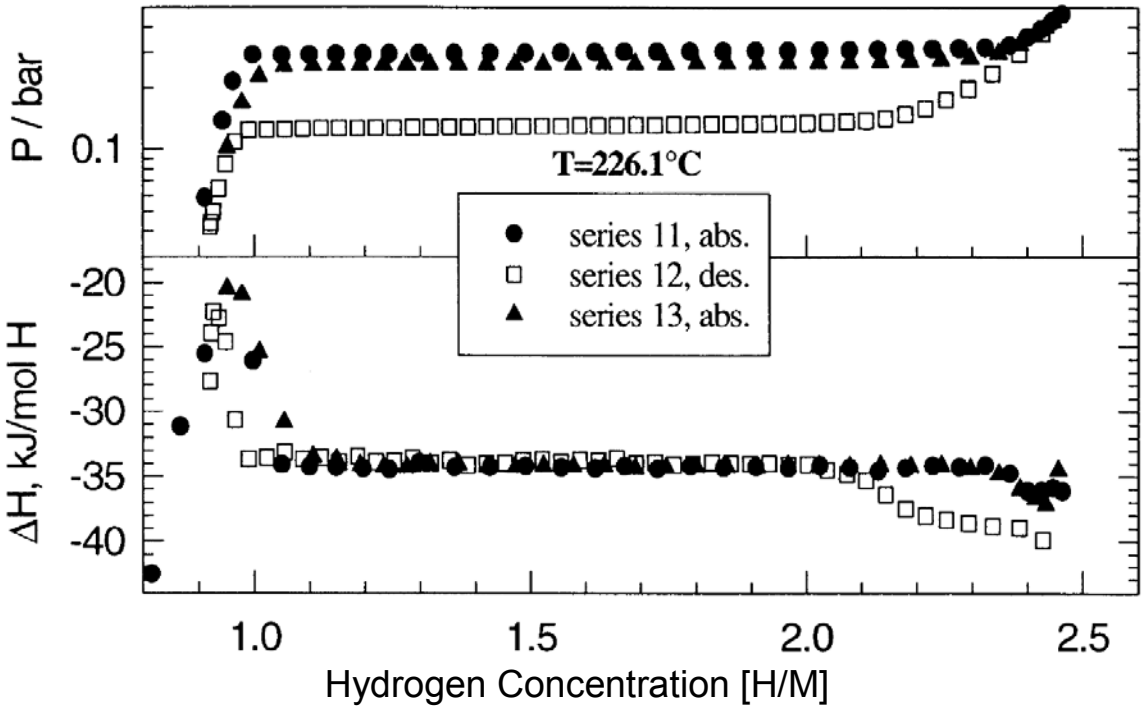

Figure 229. Isotherms and enthalpies corresponding to the formation ($\Delta H_{\beta\rightarrow\gamma}$), decomposition ($\Delta H_{\gamma\rightarrow\beta}$) of the nonstoichiometric γ trihydride, and $ZrNiH_{3-\gamma}$ from the monohydride.[305]

Ultimately, on a per mole H_2 basis, the thermodynamic data collected by both van 't Hoff and calorimetry in the two-phase region of hydride formation should be identical. This was discussed in some detail by Flanagan and coauthors with respect to hysteresis in metal hydrides.[184,306]

2.4 Heat Capacity Measurement

2.4.1 Continuous Heat Capacity Measurements

Determining heat capacity with a continuous mode calorimeter is simple and fast. Most calorimeters with a programmed temperature ramp (including DSC) are suitable for this type of measurement. In this method, the heat is added continuously, the temperature of the sample increases linearly and the slope of a temperature versus time plot is related to the specific heat. In an alternate method, the pulse method, heat is applied for a fixed time, and then (after waiting for thermal equilibrium) the temperature increase in the sample is measured. With continuous heating it is important to raise the temperature slowly so there is time for the sample to come to a uniform temperature.

There are two possibilities for the continuous C_p method:
Continuous C_p without reference
Continuous C_p with reference

C_p is calculated at each point (no filter is applied), obtaining N_t points of $C_p(T_i)$, where N_t is the number of acquisition points.

2.4.2 Continuous Heat Capacity Measurements without Reference

Precision determination of the C_p without reference requires two tests under the same experimental conditions:

The first test is carried out with two empty vessels without the sample (blank),
The second test is carried out with the vessels and the sample.

The difference between the two signals is proportional to the specific heat of the sample. This magnitude is converted directly into heat flow by the calibration curve of the DSC. This method supplies the determination directly for each temperature and does not use a reference sample (such as sapphire).

At each temperature T_i, the C_p of the sample satisfies the equation:

Equation 227

$$mC_p \frac{dT_i}{dt} = Q_i,$$

where Q_i is the heat flow consumed or released by the cell at point n_i. Hence:

Equation 228

$$C_p(T_i) = \frac{Q_{sample}(T_i) - Q_{blank}(T_i)}{Mass_{sample} \times \frac{dT(T_i)}{dt}}$$

The heat flow (*Q*) of the sample and blank are obtained during the acquisition. The mass is entered manually. For each point, it is necessary to calculate the heating rate $\frac{dT(t_i)}{dt}$ by calculating the derivative of the temperature. From $C_{P_{ref}}(T_i)$ calculated, it is possible to obtain the curves $C_{P_{ref}}(T)$ and $C_{P_{ref}}(t)$.

2.4.3 Continuous Heat Capacity Measurements with Reference

The precise determination of C_p with reference requires three tests performed under the same experimental conditions:

The first test is carried out with two empty vessels without the sample (blank),
The second test is carried out with vessels and the reference sample,
The third test is carried out with vessels and the sample.

This time the signals delivered by the calorimeter are expressed in V. At each temperature T_i, the C_p of the sample is given by the formula:

Equation 229

$$C_p(T_i) = \frac{Q_{sample}(T_i) - Q_{blank}(T_i)}{Q_{ref}(T_i) - Q_{blank}(T_i)} \cdot \frac{Mass_{ref}}{Mass_{sample}} \cdot C_{p,ref}(T_i)$$

Where Q_{sample} and Q_{blank} are the measured heat flow of the sample and blank respectively. The calorimetric signals of the sample, the reference and the blank are obtained during the acquisition. For each point, it is necessary to calculate the C_p of the reference from the coefficients of the function $C_{P_{ref}}(T)$. This enables an array of the $C_{P_{ref}}(T)$ containing the N_t values $C_{P_{ref}}(T)$ to be generated.

2.4.4 Heat Capacity Measurements by the Step Method

A method often used to obtain heat capacity by DSC is the continuous heating method. This mode permits evaluating the difference between two successive tests, with and without a sample. Determination of heat capacity can also be obtained by a second method. Between two temperature isotherms, the thermal effect corresponding to the sample being heated is integrated. This method allows the sample to reach thermal equilibrium after a temperature step; this gives the method greater precision.
Two methods can be used for the stepped C_p method:

C_p by Step without reference
C_p by Step with reference

The C_p is no longer calculated point by point but using increments of temperature. Before the acquisition, the initial and final temperatures are entered, as well as the intermediate steps (temperature and duration of steps) and the heating rates between each step. The steps are indexed j, the temperatureis constant and equal to T_j on each step. We therefore obtain a mean C_p on different parts of temperature [T_j ; T_{j+1}].

Equation 230

$$Q = \frac{dH}{dt}$$

where Q is the power dissipated or consumed by the work cell.
But : $\Delta H = mC_p\Delta T$
So between the temperatures T_j and T_{j+1} :

Equation 231

$$C_{p\_mean} = \frac{\int_{t_i}^{t_{i+1}} Q dt}{m\left(T_{j+1} - T_j\right)}$$

The integration is done using the trapezoidal method. ΔH corresponds to the area under the curve of the heat flow signal.

The determination of the integration limits t_j and t_{j+1} for each step is calculated as follows: D_j being the length of the step, t_j equals 80% of D_j. It means that if D_j equals 100 s and D_{j+1} equals 200 s, the integration will start 80 s after the beginning of the step D_j and will stop after 160 s of the step D_{j+1}. Thus, the entire signal (with the exception of the two extremities) is integrated and a maximum time is left to allow the signal to stabilize after the change of temperature.

2.4.5 Heat Capacity Measurements by the Step Method without Reference

Precise determination of the C_p by step without reference requires two tests to be performed under the same experimental conditions:

A first test with empty vessels without the sample (blank),
A second test with vessels and the sample.

The difference between the two signals is proportional to the sample's heat capacity. This magnitude is converted directly into heat flow by the calibration curve of the DSC. This method permits direct determination for any temperature and does not use a reference sample (such as sapphire).

C_p is given for each temperature interval by the formula:

Equation 232

$$Cp_{mean}\left(\frac{T_{j+1}+T_j}{2}\right)=\frac{\int_{t_i}^{t_{i+1}} Q_{sample}\cdot dt-\int_{t_i}^{t_{i+1}} Q_{blank}\cdot dt}{Mass_{sample}\cdot(T_{j+1}-T_j)}$$

The calorimetric signals of the sample and the blank are obtained during the acquisition. For each point, it is necessary to calculate the temperature variation between two consecutive steps.

2.4.6 Heat Capacity Measurements by the Step Method with Reference

The precise determination of the C_p by step with reference requires three tests to be performed under the same experimental conditions:

The first test is carried out with two empty vessels without the sample (blank),
The second test is carried out with vessels and the reference sample,
The third test is carried out with vessels and the sample.

The reference sample is a substance with a known C_p equation.

C_p is given for each temperature interval by the formula :

Equation 233

$$Cp_{mean}(\frac{T_j + T_{j+1}}{2}) = \frac{\int_{t_i}^{t_{i+1}} Q_{sample} \cdot dt - \int_{t_i}^{t_{i+1}} Q_{blank} \cdot dt}{\int_{t_i}^{t_{i+1}} Q_{ref} \cdot dt - \int_{t_i}^{t_{i+1}} Q_{blank} \cdot dt} \times \frac{Mass_{ref}}{Mass_{sample}} \cdot \frac{Cp_{ref}(T_{j+1}) - Cp_{ref}(T_j)}{2}$$

The calorimetric signals of the sample, the reference and the blank are obtained during the acquisition. For each point, it is necessary to calculate the C_p of the reference based on the coefficients of the function $C_{P_{ref}}(T)$ entered for the two temperatures T_j and T_{j+1}.

2.5 Thermal Gravimetry (TG) or Thermal Gravimetric Analysis (TGA)

Thermal gravimetry is a technique used to monitor the mass change as a function of precisely controlled temperature and environment (e.g., inert or reactive gas flows). The temperature program (or thermal treatment) includes both non-isothermal mass changes under prescribed heating rates and isothermal mass changes occurring as a function of time. Mass changes occur when volatile compounds are removed from the sample. Volatile compounds are generated via vapor pressure and reactions in solid phase producing gas phase products. There are also solid-solid reactions that can take place where no mass loss is observed. These changes can be observed by using differential thermal analysis (DTA) or differential scanning calorimetry (DSC).

Thermal gravimetric measurements are typically used for kinetic analyses of chemical reaction.

2.6 Temperature Programmed Desorption (TPD)

Temperature-Programmed Desorption (TPD) refers to a wide range of experimental methods that rely on temperature variation and generally include mass spectroscopy to investigate and quantify desorption reactions. The technique can be used for both reversible and irreversible processes, with the latter referred to as Temperature-Programmed Reaction Spectroscopy (TPRS). Details of the TPD measurement method can be found in the Introduction section 5.6 of this document.

The TPD experimental method was traditionally done to investigate adsorption processes (e.g. in heterogeneous catalysis). Hence, it has most often been used for physisorption of H_2 on porous materials. When done correctly the method can be used to determine the quantity of hydrogen desorbed following the application of a thermal ramp, and can provide useful thermodynamic information of hydrogen sorption on porous materials, as well as on-board and off-board rechargeable hydrides. However, quantitative analysis requires very accurate calibration of the mass spectrometer against known flow rates. It is also important to understand that TPD or any dynamic type measurement of measurement gives results that are a convolution of both thermodynamic and kinetic properties of the hydrogen storage material. This may lead to miss-interpretation of the results.

One example of the use of TPD to provide some insight into the nature of physisorption of hydrogen on a Ni-MOF material ($NaNi_3(OH)(SIP)_2$ [SIP=5-sulfoisophthalate]) is the recent study by Forster et al.[307] In this case, TPD experiments were carried out in a fixed-bed tubular reaction system equipped with a specially designed heater for control of the Ni-MOF sample temperature between 77 and 373 K and a thermal conductivity detector.[308] The experiments involved; first hydrogen adsorption at 80 K, followed by flushing the sample with nitrogen at the same temperature. Once the baseline of the integrator was stable, the TPD run was started with flowing nitrogen as a carrier gas at a heating rate of 5 K/min from 80 to 250 K.

Several observations strongly support the existence of accessible, coordinatively unsaturated Ni(II) sites within the pore system for this Ni-MOF compound following full dehydration.[307] First, there are four sites where water coordinates to NiO_6 octahedra per three crystallographically unique Ni(II) atoms. TPD measurements (Figure 230) showing that desorption of hydrogen occurs at temperatures between 140 and 160 K gave support to the presence of unsaturated metal binding sites for hydrogen in this material. The peak in the TPD curve exhibits pronounced structure, which persisted when the measurement was repeated at various ramping rates. This observation suggests that multiple, strong metal binding sites are responsible for the observed hydrogen retention. Moreover, virtually no TPD peaks are seen in samples that were dehydrated at temperatures less than 573 K, despite the fact that these samples also

have high measured surface areas. The most likely explanation for this observation is that the material becomes porous before the water molecules coordinating to active Ni(II) sites are removed, and that the coordinatively unsaturated Ni(II) sites then become accessible in the pore system once these water molecules are removed at higher dehydration temperatures.[307]

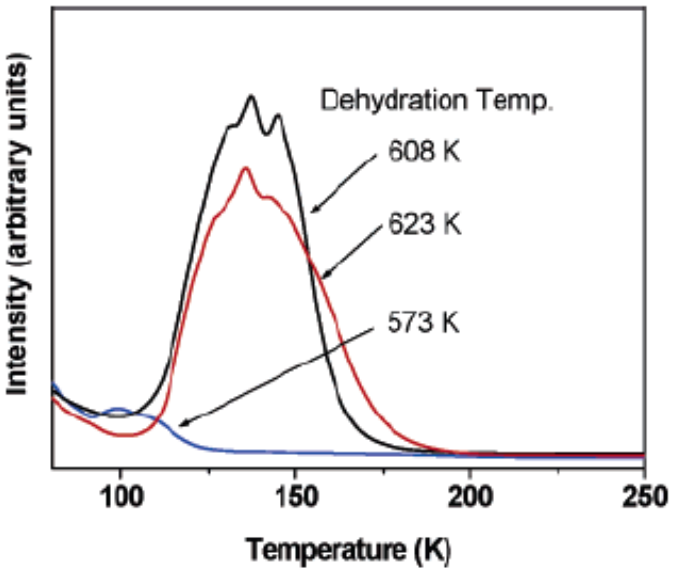

Figure 230. Low-temperature H_2-TPD profiles of Ni-MOF material depending on dehydration temperatures. Ramping rate: 5 K/min.[307]

TPD works well as a complementary tool to support the heats of adsorption measured by other methods.

NOTE: For all Temperature Programmed (ramping) methods in which heat is not measured, it is important that caution be exercised in ascribing different temperatures of hydrogen release between samples directly to changes in hydrogen binding energies. Data from such methods generally represent a convolution of thermodynamic and kinetic effects. Differences in kinetics of hydrogen release or uptake between samples will be observed as hydrogen or release at different temperatures. One simple way to help distinguish kinetic effects from thermodynamic properties is to run the same sample at different temperature ramping rates to see if there is significant change in hydrogen release or uptake temperatures. A significant change in temperatures would indicate that kinetics has a strong impact on the results. It is always advisable to double check thermodynamic properties using other additional methods such as van 't Hoff or calorimetry techniques.

3 Matching Experimental Setup to Measurement Goal

The three classes of measurements, system performance, materials development, and fundamental mechanisms, require slight variation in the approach to measurements.

Typically, system performance measurements will be focused on a scaled-up measurement that is large enough to accurately represent the behavior of the storage material at a full application level. Generally speaking this would be 100 gm to 1 kg of material. Such measurements will most likely concentrate on heat transfer during hydrogen uptake and release, local temperatures within the material test bed and rates of hydrogen sorption and desorption rather than measurements of the intrinsic thermodynamics of the material. However, the thermodynamic properties of the storage material is fundamental to performance at a scaled-up level, so it is important that the thermodynamic characteristics of the material are well determined before system performance measurements are undertaken.

Thermodynamics measurements from a materials discovery and development perspective will require careful measurements to ensure thermodynamic equilibrium and essentially identical measurement conditions to be able to accurately compare one material from another. An example being the subtle differences in isosteric heats of adsorption for different MOF materials.[309] In fact, in the field of metal hydride development for both gaseous hydrogen storage and nickel-metal-hydride batteries more than three decades of research have focused on the ability to make significant changes in thermodynamics (plateau pressures) of intermetallic hydrides AB_5, AB_2 etc. through small elemental substitutions for A or B elements. An early example of the dramatic effect on plateau pressures obtained through elemental substitution is given in Figure 231 below for the introduction of the elements M=Pd, Ag, Cu, Co, Fe, Cr, and Pt in place of nickel the intermetallic compound $LaNi_5$ ($LaNi_4M$).[310]

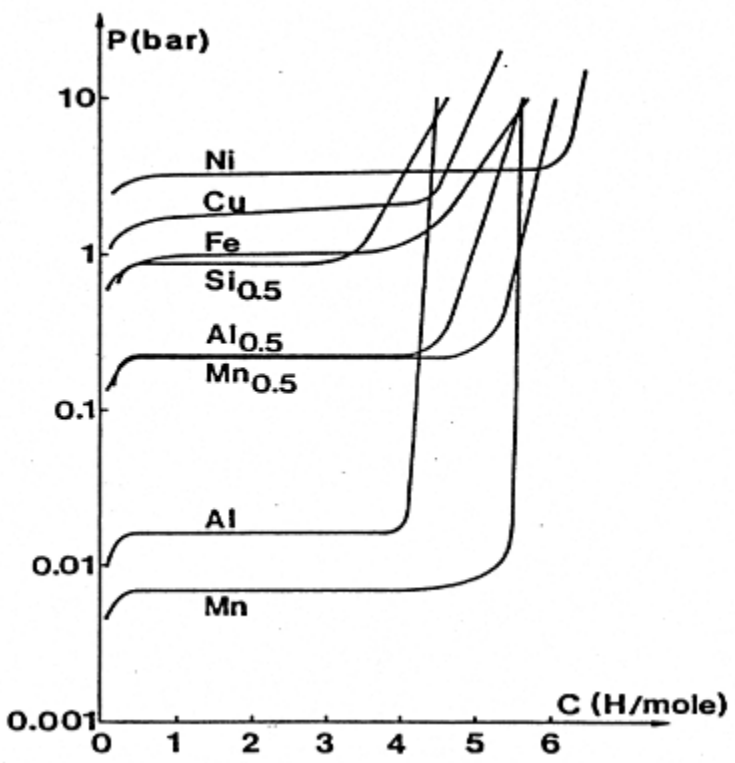

Figure 231. Hydrogen desorption PCT measurements at 40°C for the substitution of Ni in $LaNi_5$ by the elements M=Pd, Ag, Cu, Co, Fe, Cr: $LaNi_4M$ and Pt (5%).[310]

Studies of fundamental mechanisms of thermodynamics will require even more precision and care in measurements (highly uniform isothermal conditions and certainty of equilibrium) because changes in enthalpy and entropy of sorption may be very subtle. An example is the difficulty in confirming changes in both enthalpy and entropy of hydride formation at the nano-scale versus bulk material [311] and effects on thermodynamics of clamped versus free thin-film material.[323,324]

3.1 Experiments for Systems Performance

3.1.1 On-board Reversible Hydride Storage Systems

The determination of the enthalpy of hydride formation (ΔH) is critical for the optimal performance of scaled up applications.

Enthalpy determines:
energy consumption to release hydrogen, heat load during refill, the size of the heat transfer system, and for many systems, the temperature of hydrogen release may be above a fuel cell stack temperature.

Such were the findings of a collaborative project between General Motors and Sandia National Laboratories on scaled up testing of an alanate hydrogen storage system. Figure 232 shows the strong influence of ΔH (dH) on the ultimate efficiency of such a hydrogen storage system.[312]

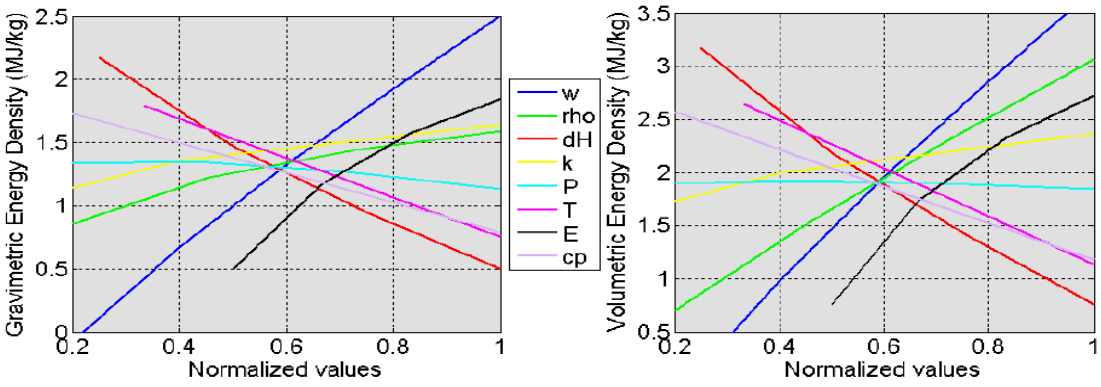

Property	Symbol	Units	Range
Effective capacity	w	kg H_2/kg hydride	0.02 – 0.10
Packing density	ρ_p	kg/L	0.5 – 2.0
Specific heat	c	J/kg*K	500 – 2750
Thermal conductivity	k	W/m*K	0.5 – 5.0
Pressure	P	bar	20 - 140
Temperature	T	°C	100 – 300
Enthalpy	ΔH	kJ/mol H_2	20 - 80

Figure 232. Sensitivity plots for gravimetric and volumetric energy density.[313]

There are many considerations to be taken into account when making thermodynamic measurement with the purpose of gaining materials performance information at a systems level. For example, under scaled-up materials measurements (representing system level performance) hydrogen storage materials are rarely operated under equilibrium conditions. The interplay between kinetics and thermodynamics therefore becomes even more important. For hydrides, large quantities of material (>10 grams) will produce (or consume on desorption) enough heat that a simple test cell may increase (or decrease) significantly in temperature. Therefore, isothermal conditions, typically used for van 't Hoff measurements, will not be maintained. This is important because it may be difficult to distinguish between pressure changes are related to the kinetics of approaching equilibrium or changes in the temperature (and thus equilibrium pressure) of the material. Also, large temperature changes, makes it very difficult to determine the final state of the material when equilibrium is eventually achieved. That is whether the final state is on the absorption or desorption isotherm or somewhere in-between.

An example of scale up measurements presented in an earlier section of this document demonstrates such a thermal excursion. In studies performed by Gary Sandrock on Ti-doped alanates, hydrogen absorption/desorption experiments were performed on a simple high-pressure cylindrical vessel shown in Figure 233.[120] The stainless steel reactor was loaded with about 100 g of bicatalyzed $NaAlH_4$ (78 g of $NaAlH_4$ and 22 g of $Ti(OBun)_4$ + $Zr(OPr)_4$). The reactor had internal thermocouples but no internal heat exchange structure. Absorption kinetics and capacity were measured volumetrically.

Figure 233. Scale up (100 g) reactor with end cap removed in Ar-glovebox to show catalyzed alanate.[121]

The higher than expected initial charging kinetics, combined with limited heat transfer, resulted in exothermic temperature excursions, as is common with hydrides. An example is shown in Figure 234 for the 4th hydrogen absorption. The fully dehydrided bed was heated to 155˚C and then charged with hydrogen at 172 bar. Within one minute, the exothermic hydriding reaction resulted in an internal temperature of 234 ˚C.

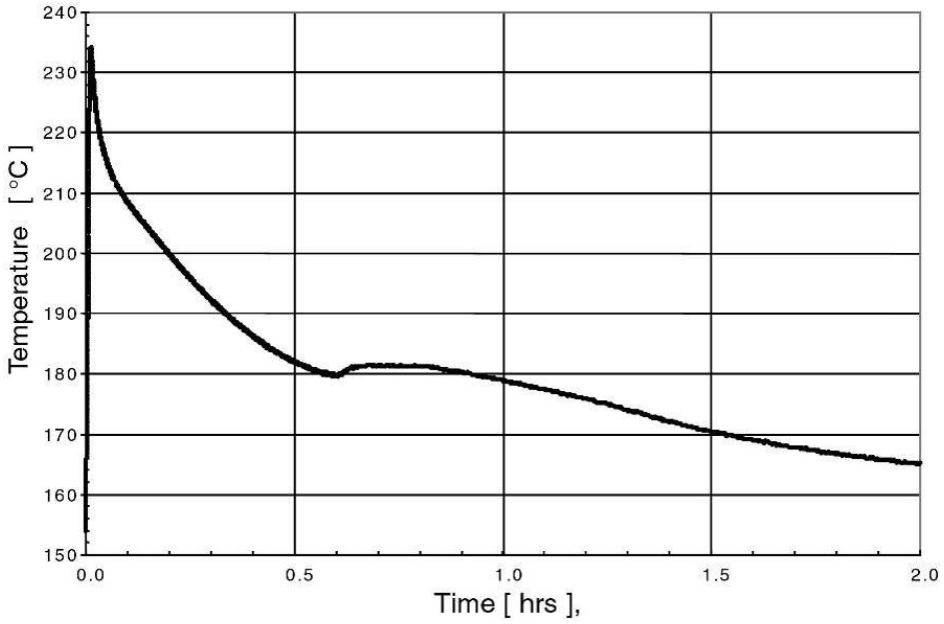

Figure 234. Exothermic temperature excursion during scale up bed charge half-cycle (P_i=174 bar, T_i=155˚C).[121]

This is essentially the van 't Hoff temperature for NaAlH4 at this applied pressure. However, the melting point of NaAlH4 is only 182˚C; thus, any NaAlH4 formed during the first 0.5 hr of Figure 234 would do so directly into the liquid phase. As one can see in the figure, a thermal arrest occurs at 182˚C due to solidification during cooling (about t = 0.6-0.8 hr). In the case of a scaled up system where sorption kinetics are much faster than heat transfer, an interesting possibility would be to perform such a thermal excursion measuring the pressure and temperature changes in time. If the system is truly in chemical equilibrium as the bed slowly cools, then plot of Ln(P) vs. 1/T at each time should produce the equilibrium van 't Hoff plot from which the enthalpy and entropy of hydriding could be determined. This approach (on a large scale) is similar to the "Direct van 't Hoff" method described in section 2.1.2.9 below. Note however, to stay within a relatively narrow hydrogen concentration range, the volume of gas in the system should be small with respect to the amount of material.

3.1.2 Off-board Regenerable Hydrides Storage Systems

Chemical hydrogen storage involves storing hydrogen in molecular chemical bonds where an on-board chemical reaction is used to release hydrogen. Currently, the resulting spent fuel may be regenerated off-board using chemical processing. In addition to the importance of on-board storage capacity and hydrogen release rates, the energy efficiency of the off-board regeneration of spent fuel is a key contributor to the overall energy efficiency of the fuel cycle.

With respect to on-board hydrogen delivery, critical materials properties governing the behavior of these materials are the (generally exothermic) heat of decomposition, the heat capacity and thermal conductivity of the materials. Also important is the pathway and activation energies associated with the kinetics of hydrogen release. Thus, one key to the success of off-board regenerable hydrides for vehicular hydrogen storage is the need to increase the rate and decrease the temperature of hydrogen release. For example, using ionic liquid/AB mixtures, very high rates of hydrogen release have been determined at temperatures between 100 and 120°C, where 8 wt.% hydrogen is released within two minutes at 120°C.[314]

As another example, using catalysts, release of hydrogen from AB may be accelerated. The University of Washington has demonstrated release of 5.8 wt.% hydrogen in three minutes at 25°C. Using heterogeneous catalysts Los Alamos National Laboratories researchers have demonstrated hydrogen release of 8 wt.% in 120 minutes at 70°C, or in 8 minutes at 110°C.[314]

By synthesizing metal-substituted derivatives of ammonia borane, a wide array of new metal amidoborane (M-AB) storage materials have been discovered and characterized by researchers at the Pacific Northwest National Laboratory (PNNL), LANL, and the University of Missouri. As one example, PNNL has shown that Li-AB releases 5 wt.% hydrogen in 2 minutes at 100°C. Li-AB also has a very high activation energy, a feature with positive implications for adequate storage lifetimes at 50-60°C.[314]

An overview of results from the US DOE Chemical Hydrogen Storage Center of Excellence (CHSCoE) is shown in Figure 235.

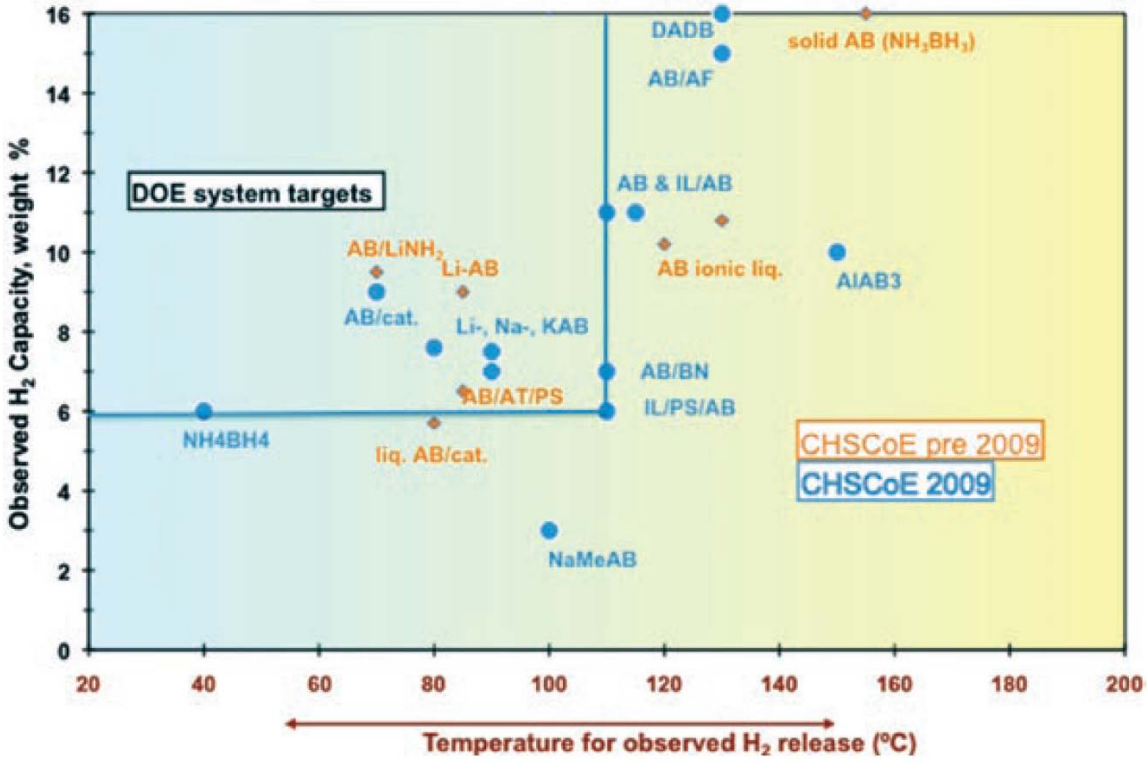

Figure 235. Synopsis of results for the release of hydrogen from a variety of materials as a function of temperature. [314]

3.1.3 Physisorption Storage Systems

The greatest challenge for physisorptive materials to be used for hydrogen storage is to increase the strength of the H_2 binding interaction.[95] Recently, Bhatia and Myers addressed this issue by employing the Langmuir equation to derive relationships between the operating pressures of a storage tank and the enthalpy of adsorption required for storage near room temperature.[149] Using P1 and P2 as the lower and upper bounds of the operating pressure and approximating the H_2 adsorption entropy as $\Delta S°ads \approx -8R$ (R=ideal gas constant), they derived Equation 234. They then used this equation to show that a microporous material operating between 1.5 and 30 bar at 298 K should have an average optimal adsorption enthalpy as $\Delta H°_{opt}$ of 15.1 $kJmol^{-1}$. Similarly, if P2 is increased to 100 bar, the required average adsorption enthalpy decreases to 13.6 $kJmol^{-1}$.

$$\Delta H^{\circ}_{\mathrm{opt}} = T\,\Delta S^{\circ}_{\mathrm{opt}} + \frac{R\,T}{2}\ln\left(\frac{P_1\,P_2}{P_0^2}\right)$$

Equation 234

In the same work, Bhatia and Myers derived Equation 235 which can be used to calculate the optimal operating temperature Topt of a hydrogen storage material for a given average enthalpy of adsorption ΔH°_{ads}. This relationship can be used to show that a microporous material with ΔH°_{opt} of 6 kJmol^{-1}, which is a typical value for current metal–organic frameworks and other microporous solids, can operate between 1.5 and 100 bar at an optimal temperature of 131 K.

$$T_{\mathrm{opt}} = \frac{\Delta H^{\circ}_{\mathrm{ads}}}{[\Delta S^{\circ}_{\mathrm{ads}} + (R/2)\ln(P_1\,P_2/P_0^2)]}$$

Equation 235

3.2 Experiments for Materials Development

3.2.1 On-board Reversible Hydride Storage Materials

The typical approach in hydrogen storage research to identify promising new materials based on high hydrogen capacity and then work to improve their kinetic and thermodynamic properties. For this reason, considerations for making accurate thermodynamic measurements are extremely important in experiments for materials development.

Work on modifying thermodynamic properties of classic intermetallic hydrides dates back several decades. In electrochemical application (Nickel Metal Hydride batteries) much of the work focused on improving the cyclability of the MH electrode against corrosion in the KOH electrolyte while maintaining hydriding plateaus below one atmosphere (to avoid hydrogen gas evolution on battery charging). In the field of metal hydrides for hydrogen gas storage, the focus was (and remains) the development of hydrogen storage materials with higher capacities and room temperature desorption above one atmosphere to release stored hydrogen without the need to introduce high-temperature heat. Figure 236 shows early measurements on the effect on plateau pressures of small modifications in the stoichiometry of $LaNi_5$.[310]

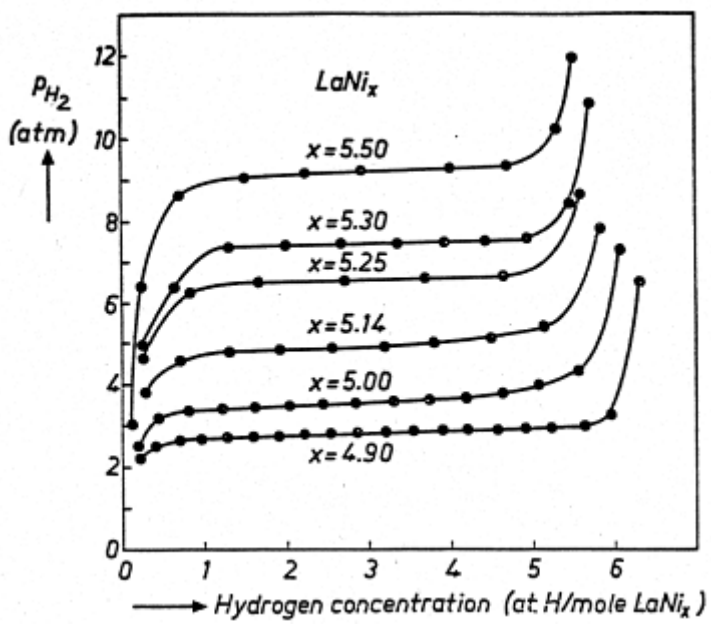

Figure 236. Hydrogen desorption PCT measurements at 40°C for the changes in the nickel content of $LaNi_5$. Alloys were annealed at 1400°C for approximately one week before testing.[310]

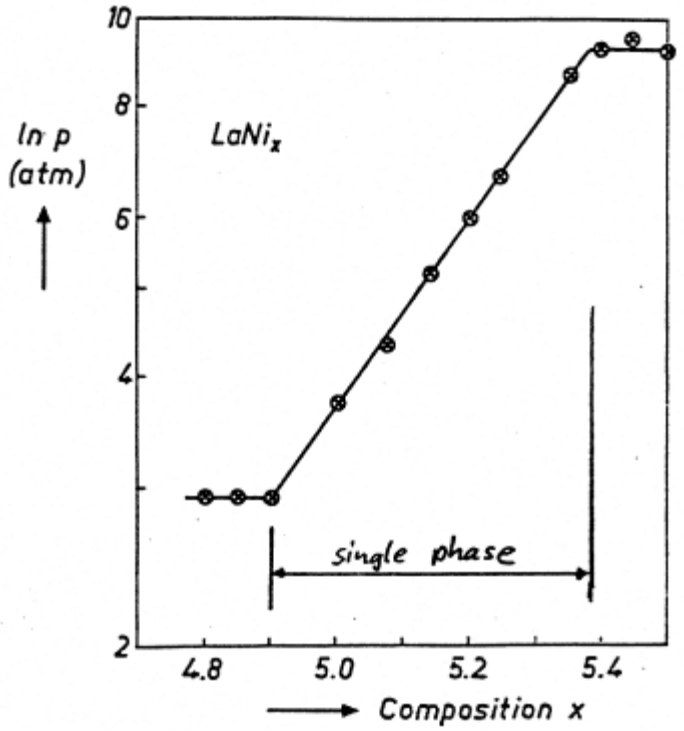

Figure 237. Hydrogen desorption plateau pressures at 40°C plotted as a function of nickel content in $LaNi_X$.[310]

Figure 237 plots the mid-plateau pressures of the same set of data as a function of nickel content.[310] The figure demonstrates that the alloy maintains a single phase $LaNi_X$ in the wide range of stoichiometry $4.9 < x < 5.4$. Increasing plateau pressures relate directly to the thermodynamics of hydride formation (i.e. a decrease in the enthalpy of reaction with increasing nickel content).

Intermetallic hydrides have always been attractive because of the simple ability to change thermodynamic properties (and kinetics) through elemental substitution (and the addition of catalytic additives). Unfortunately, while the intermetallic hydrides have high H/M ratios, they typically have low weight % hydrogen content because of being generally composed of high-Z elements. In this respect, much of the materials research for gaseous hydrogen storage has shifted over the last decade to low-Z hydrides. These are typically not alloys or intermetallic compounds, but rather reversible chemical hydrides and as such, generally much less amenable to property changes through elemental substitution. This has required new approaches to changing thermodynamic stabilities of such hydrides.

One approach has been to add second phase elements or compounds which destabilize the overall hydrided state or stabilize the overall dehydride state, reducing the overall enthalpy of reaction. Some examples of this are adding Ti to MgH_2[233] or mixing MgH_2 with $LiBH_4$.[315] This route has been effective in changing the thermodynamics of hydrogen storage material systems, but has introduced other challenges. Namely, multi-phase decomposition/recombination hydride materials often require the transport (diffusion or otherwise) of elements other than just hydrogen. While it is amazing that relatively rapid metal transport can occur at near room temperature conditions, the difference between host element transport in these systems and hydrogen mobility in intermetallic hydrides is significant. The impact on hydriding kinetics means that these systems must be operated at much higher temperatures, or novel approaches to improved kinetics must be developed.

With respect to accurate thermodynamic measurements on these new multi-phase hydride systems, one of the biggest difficulties is to separate kinetic effects from true thermodynamic properties. This is complicated when studying materials with slow kinetics (like alanates and borohydrides), where some amount of catalyst is often required to achieve equilibrium in a reasonable time period. The catalyst or additive itself may have an important effect on the thermodynamic stability of the hydrogen storage system.[316] Another approach is to measure samples at extreme temperatures and pressures and extrapolate the results to gain insights into performance under the desired system conditions. While the measurement conditions may be far from those required for practical applications, it is useful in identifying materials with attractive thermodynamic properties and to evaluate catalysts and other approaches to improve kinetics.

Vajo et. al. required both high temperatures and catalytic additives to determine the effect of ball milling MgH_2 with $LiBH_4$. They included 2-3 mol % $TiCl_3$ to improve the kinetics, but were still limited to temperatures above 315 ^{o}C. However, by taking multiple data points at high temperature and pressure, they were able to construct the van 't Hoff plot shown in Figure 238, which predicts thermodynamic performance across the entire range of interesting pressures and temperatures.[315] This type of extrapolation is often necessary in determining thermodynamic properties of materials with initially poor kinetics.

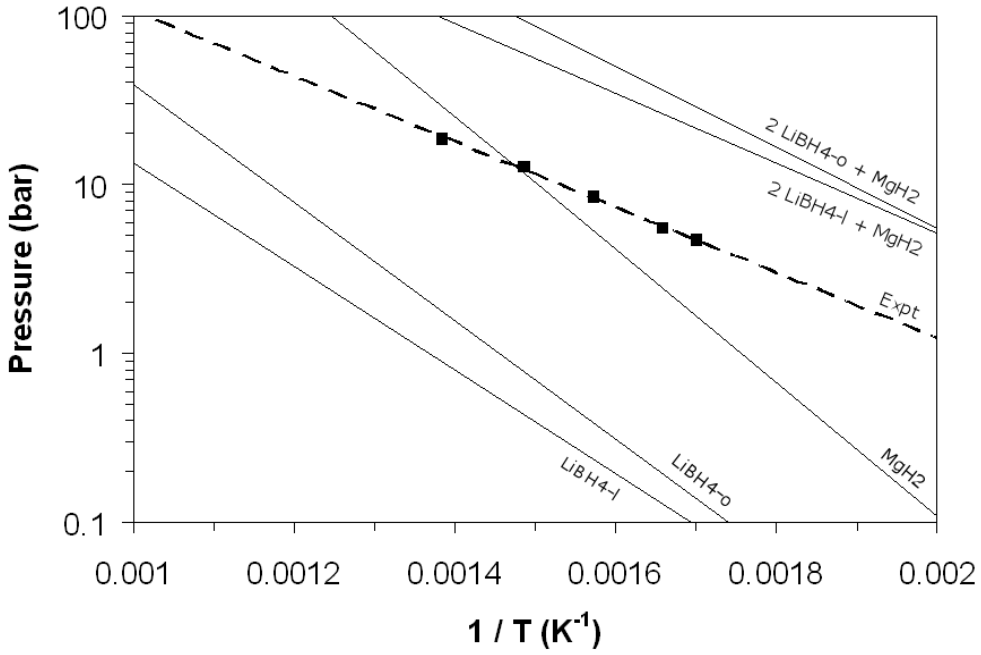

Figure 238. A van 't Hoff plot showing the expected equilibrium pressures for the dehydrogenation of $LiBH_4$ in both its orthorhombic and molten states (-o and -l suffix used to identify the respective state), MgH_2 and the destabilized system $LiBH_4$-MgH_2 with a 2:1 molar ratio. The experimental data reported by Vajo et al. (2005) are also plotted with a line of best fit for comparison.[317]

It is also important to note the method of preparation of samples, for example, catalysts or destabilizing elements are often added to storage materials through ball-milling. However, ball-milling is also a useful technique for reducing particle size and increasing strain in the material. As discussed in Section 4.1 , these physical effects can also impact the kinetic performance of a material and potentially also the thermodynamics. It is important to perform experiments in a way that the improvements from the different effects can be separated. For example, thin films deposited by sputtering can be effectively doped with a catalyst during deposition and then annealed to remove inhomogeneities in composition and grain structure.

3.2.2 Off-board Regenerable Hydride Storage Materials

Off-board regenerable hydrogen storage materials development has been aimed at modifying thermodynamics and improving control over the kinetics of exothermic reactions. There have been many approaches to improve hydrogen storage performance including the development of nanostructured materials. One option is to load a nanoporous scaffold with hydrogen storage materials to be able to produce nanoparticles of the storage material and to preserve these nanoscale dimensions. In one example, high-surface-area mesoporous silica was loaded with ammonia borane (AB) as a model system.[179] Mesoporous silica materials have an extremely high surface area and a highly ordered pore structure, which give them the appearance of nano-channeled silica scaffolds.[318] In the work of Gutowska et al. the mesoporous silica material SBA-15 was loaded with AB by the incipient wetness technique using a saturated methanolic solution of AB. Because of the porous nature of the silica scaffold, the internal channels of SBA-15 were filled by a capillary action upon exposure.

Isothermal calorimetry experiments using a Calvet calorimeter were used to quantify both the thermodynamics and kinetics for the release of the first equivalent of H_2 from neat AB and AB:SBA-15 (Figure 239).[179] Integration of the area under an isothermal calorimetry curve (Figure 239) provided the enthalpy of reaction for H_2 release (ΔH_{rxn}). The enthalpy for H_2 loss from neat AB (ΔH_{rxn} = -21 $\pm$ 1 kJ/mol). This value is in excellent agreement with the literature value for neat AB.[211] Wolf et al. used calorimetric instruments, coupled with gas-volumetric equipment, and thermogravimetric methods to investigate H_2 release from solid ammonia borane at isothermal temperatures in the range of 70-90 °C. They determined that the ammonia borane samples reacted uniformly and approximately one molar equivalent of H_2 was released. They also reported that the enthalpy of reaction, ΔH_{rxn}, of -21.7 ± 1.2 kJ/mol-NH_3BH_3, was nearly independent of temperature.

Note that isothermal calorimetry measurements to evaluate hydrogen release decomposition enthalpies require great care as outlined in the Introduction section 5.7 of this document. However, for irreversible off-board regenerable materials calorimetry measurements are more direct and a offer practical way to determine heats of decomposition.

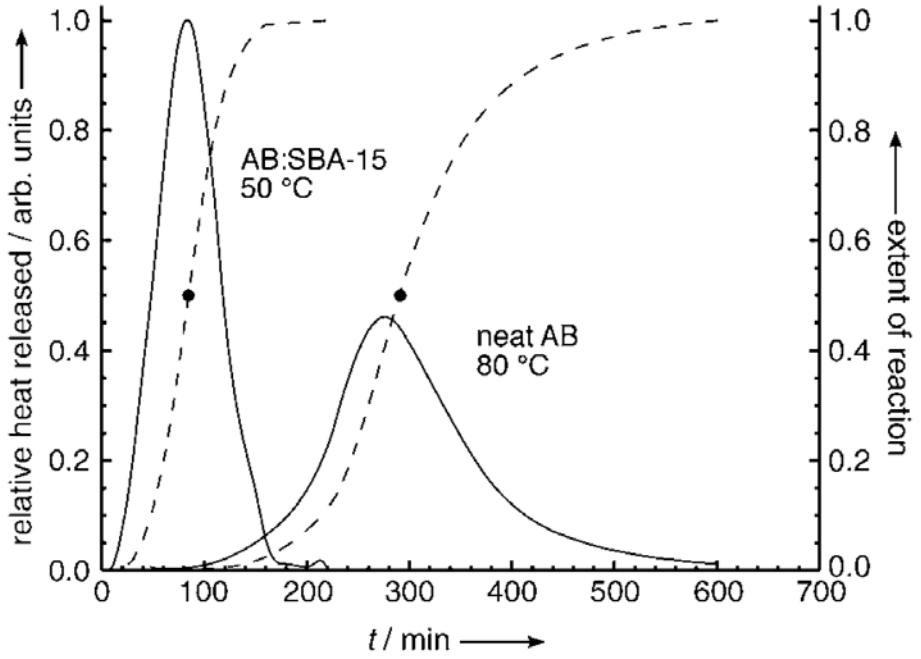

Figure 239. Scaled exotherms (solid lines) from isothermal calorimetry experiments that show the time-dependent release of H_2 from AB and AB:SBA-15 (1:1 wt/wt). [179]

In addition to these thermodynamic measurements Gutowska et al. related the exothermic heat released from neat AB measured by isothermal calorimetry to the extent of ammonia borane conversion (= integrated heat released up to elapsed time (t) per total heat released in complete reaction). This normalization resulted in a characteristic sigmoid-shaped fractional conversion curve for AB, similar to the results of evolved H_2 gas volume measurements.[215,211,319] An inherent assumption of this earlier work was that exactly one (1.0) equivalent of hydrogen was ultimately released in the reaction, based upon the reports of Wolf et al.[211]

Gutowska and co-workers then performed isothermal calorimetry measurements on neat AB in the range of 70-85°C and reported the time to half conversion ($t_{1/2}$) as a function of temperature (Figure 240).

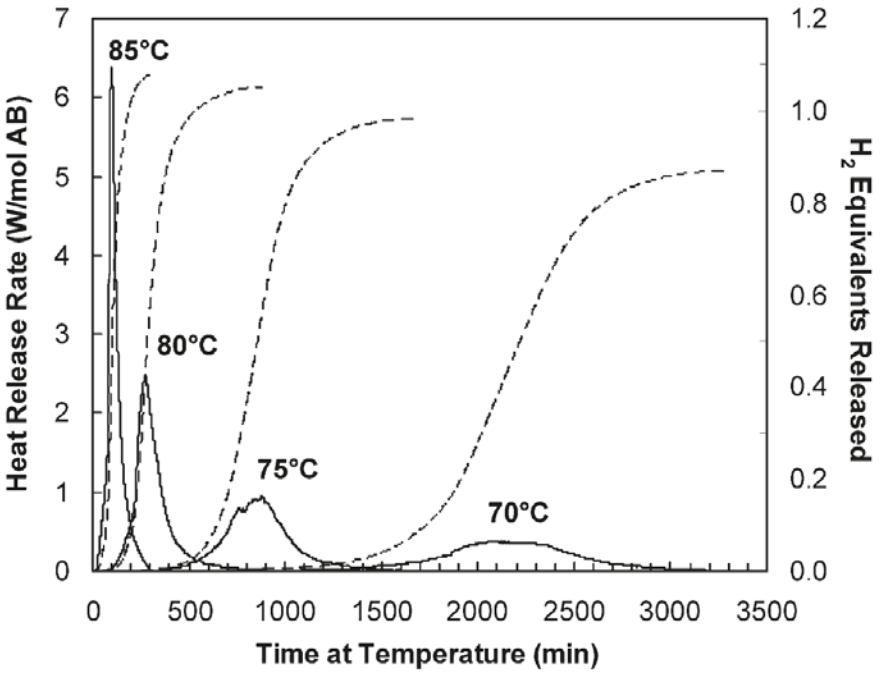

Figure 240. Calorimetric measured heat release normalized by the ammonia borane sample amount (solid lines) and the integrated equivalents of H_2 released (mol H_2/mol AB; dashed lines) assuming a constant heat of reaction of -21.7 kJ/mol AB. [320]

This calorimetry data was used recently to develop isothermal and adiabatic reactivity models to predict the stability of ammonia borane at 50-60°C, the extreme range of environmental temperatures for hydrogen storage materials in PEM fuel cell applications.[320] Results of the analysis show that solid ammonia borane is metastable in the 50-60°C range, having stability against appreciable reaction on the order of a week at 60°C and months at 50°C. One of the global model results are compared to the experimental ammonia borane conversion data in Figure 241.

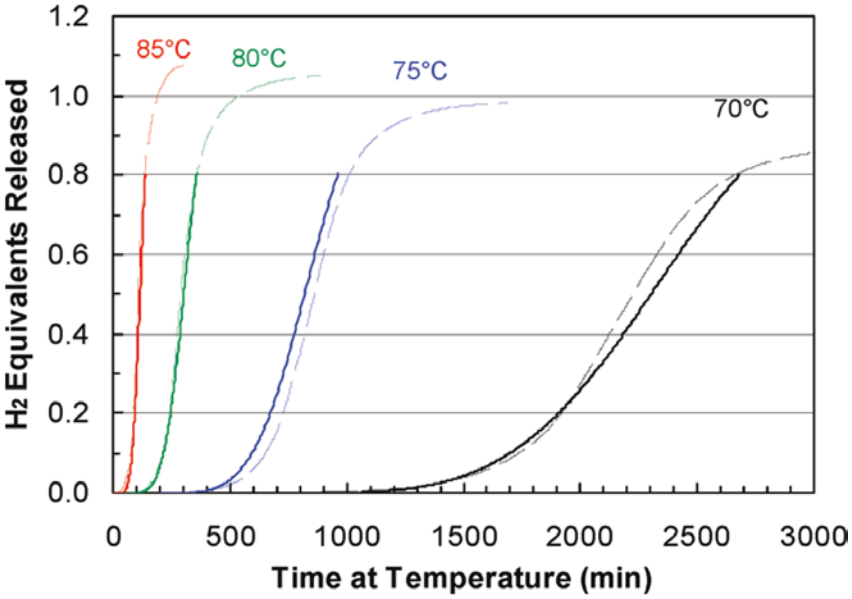

Figure 241. Global isothermal kinetic model results (solid lines) up to 0.80 H_2 equivalents released (the fit region) compared to the experimental data (dashed lines).[320]

3.2.3 Physisorption Storage Materials

In the development of new physisorption hydrogen storage materials it is critical to improve the understanding of the influence the structure and composition has on the thermodynamic properties of these materials. It is well-known that pore size below 10 nm has a significant influence on the heat of adsorption of hydrogen on porous materials.[256] By thermal desorption spectroscopy (TDS) of H_2 adsorbed in several metal-organic frameworks, it has been revealed that the hydrogen desorption temperatures are related to the pore sizes of these materials.[321] With the TDS technique, hydrogen is first adsorbed on the MOF at room temperature and then cooled down to 20 K, which could allow the removal of the free hydrogen molecules in the gas phase by applying a high vacuum (10^{-5} Pa), while retaining adsorbed H_2 molecules the surface of the framework. When increasing the temperature with a constant heating rate, the desorbed hydrogen molecules are detected with a mass spectrometer. Hydrogen adsorbed in cavities of different sizes possessing different energy, will be released at different temperatures. Hydrogen adsorbed in larger pores is released at lower temperatures while H_2 molecules more strongly adsorbed in smaller pores are desorbed at higher temperatures. Thus, measurements of the hydrogen desorption spectrum of different materials can be directly correlated with the size of the pores present in the framework (Figure 242).[321]

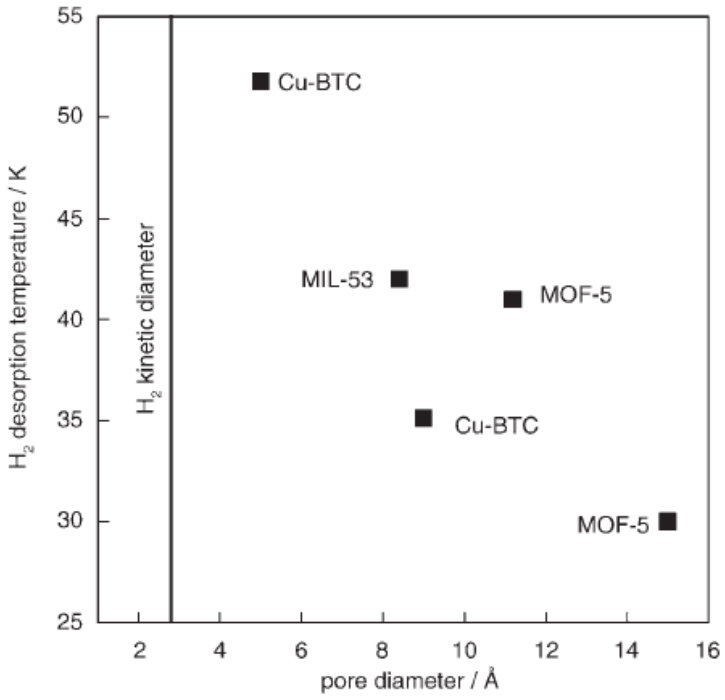

Figure 242. Thermal desorption temperatures of hydrogen in MOFs versus the diameter of their pores. [321]

This may indicate stronger binding in smaller pores. However, temperature programmed methods, it is important to note that caution should be exercised in ascribing higher temperatures of hydrogen release to stronger hydrogen binding. Kinetic effects can lead to a slower release of hydrogen which results in hydrogen coming off at higher temperatures.

Hydrogen adsorption measurements on porous materials over wide ranges of pressure and temperature can allow for the determination of the solid–gas interactions and provide significant insights on the state of the adsorbed hydrogen and the physical limits of these solid–gas systems.

The analysis of excess hydrogen adsorption isotherms measured over the 50–100 K and 0–40 bar ranges has revealed that the characteristic excess maximum was found to be displaced to lower pressures and to vary less as a function of temperature on MOF materials with shorter ligands (Figure 243). This can be explained, on the basis of enthalpy calculations, by an enhanced hydrogen affinity in smaller pores. The analysis was performed by modifying Clausius–Clapeyron equation with Dubinin–Astakhov (DA) model parameters (Equation 236). The equation represents the heat evolved as adsorption occurs over a range of filling temperatures and pressures corresponding to realistic operating conditions of a hydrogen storage system.

Equation 236

$$\Delta H = E(-\ln\theta)^{1/m} + \frac{\alpha TE}{m}(-\ln\theta)^{1/m-1} + \gamma RT$$

where E is a characteristic energy, m is a heterogeneity parameter, and θ is the fractional filling of the pores.

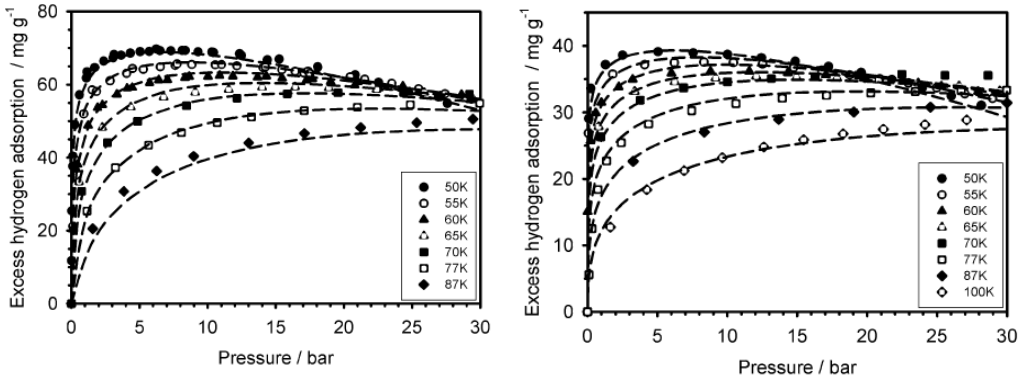

Figure 243. Excess hydrogen adsorption isotherms measured (data points) on the Cu_2(tptc) material (left) and Cu_2(bptc) material (right) over the 50–100 K range and modeled with the DA equation (dashed lines).[163]

In addition, it has also been found in this example, that the material with the shorter ligand has a reduced storage capacity. This can be explained, from measurements near saturation, by a reduction of both adsorbed phase density and volume (Figure 244). These results suggested that in view of the adsorption thermodynamic properties of the MOFs, a reduction in the framework weight may be needed to increase the gravimetric capacity of MOFs under the practical (P,T) operating conditions.**[163]**

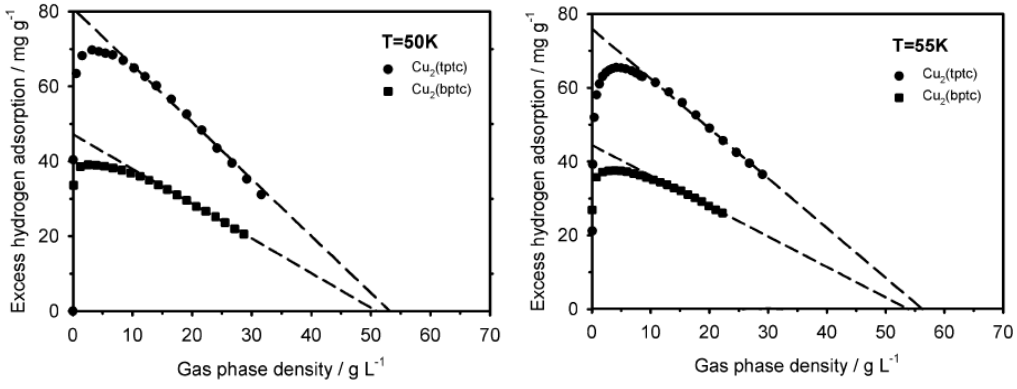

Figure 244. Plot of the measured excess hydrogen adsorption as a function of the gas density up to the near-saturation region at 50 K (left) and 55 K (right).

3.3 Experiments for Fundamental Studies

3.3.1 On-board Reversible Hydride Storage Materials

Understanding the fundamental thermodynamic properties, such as enthalpy of formation, of on-board reversible hydride storage systems is essential. Favorable thermodynamic properties are a key factor in identifying materials with the potential for on-board regeneration. It is therefore crucial that fundamental studies are performed carefully with a full understanding of the factors that influence the results, from broad concepts such as the interplay between kinetics and thermodynamics to specific issues such as unintentional annealing.

3.3.1.1 Annealing

The extreme conditions required in hydrogen storage testing can sometimes have unintended effects. For example, gravimetric measurements often include a bake-out procedure to establish the dry mass of a sample. Since this procedure involves heating the sample under vacuum, some annealing should be expected. Annealing conditions can have a significant effect on the plateau pressures measured during a PCT experiment. Figure 245 shows an example of isotherms at 473 K of ZrNi after various exposing the material to increasing annealing temperatures. The variation in plateau pressure is up to 10% with a 400 K difference in annealing temperature.[322] It is therefore important to track all steps in the measurement process and consider the potential effects when the sample is heated.

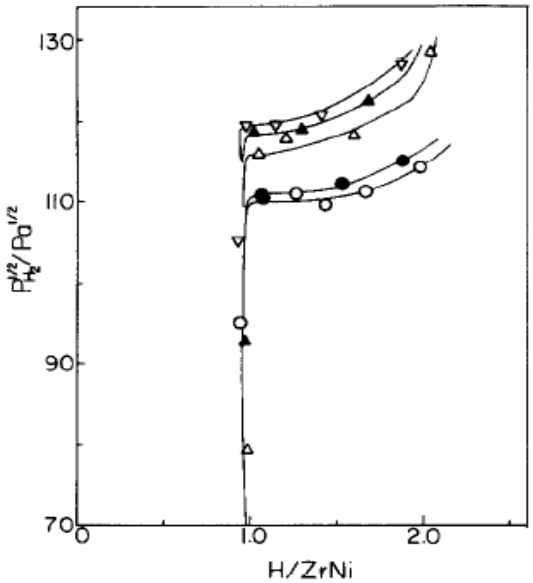

Figure 245. Isotherms for ZrNi at 473K for samples annealed at (○) 473 K, (●) 673 K, (△) 773 K, (▲) 873 K and (▽) 1000 K.

Activation cycling at elevated temperatures is also common for metal hydrides. For those who perform such activation processes on hydrides it should be noted that the activation process itself may induce the formation of a metastable phase of the hydride that is often observed as a second plateau at much higher pressures than normal in the initial PCT measurements. This plateau usually disappears with the first desorption. An example of this is shown for LaNi5 in Figure 246 where, after charging a sample at elevated temperatures (~100°C) and pressures (~100 bar), the following room temperature absorption PCT measurement exhibits a second higher pressure plateau that is not observed in the subsequent desorption.

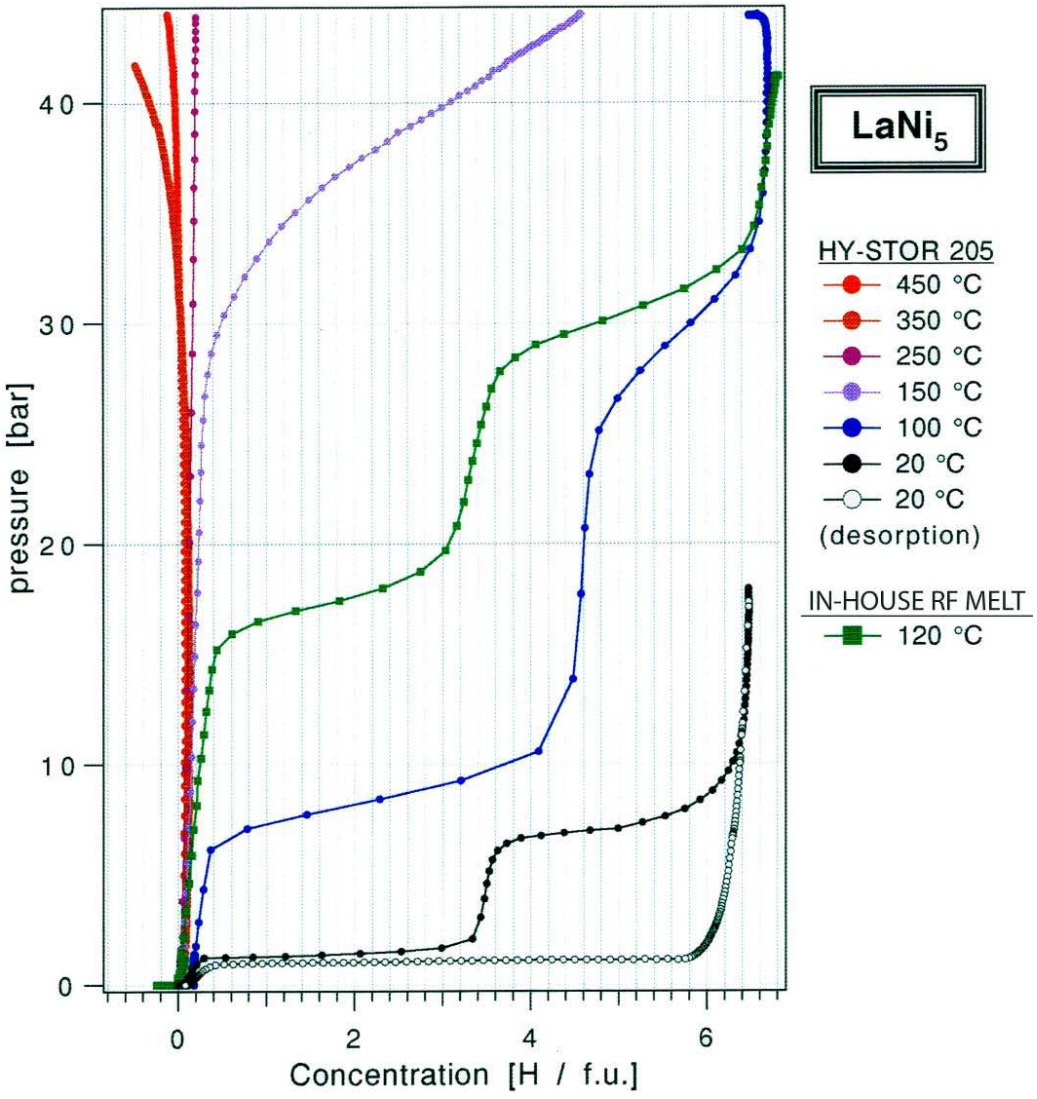

Figure 246. PCT measurements of $LaNi_5$ after heating under hydrogen.

3.3.1.2 Hydrogenography of Thin Films

A critical issue in Hydrogenography experiments is the impact of the substrate.[323, 324] The hydrogenation of metal hydrides is accompanied by a large volume expansions varying from 11% to as much as 35%. Bulk materials can expand isotropically in all three directions, whereas a rigid substrate does not allow the free expansion of the film parallel to the surface during hydrogen uptake. When hydrogen causes the host metal lattice to expand, adhesion forces act in the opposite direction to prevent the expansion of the film in the basal (x-y) directions. This creates considerable in-plane compressive stresses that can be on the order of several GPa (Figure 247).[325] These stresses may influence the equilibrium plateau pressures of metal hydride films and, consequently, alter the thermodynamics of the system as compared to the corresponding bulk materials.

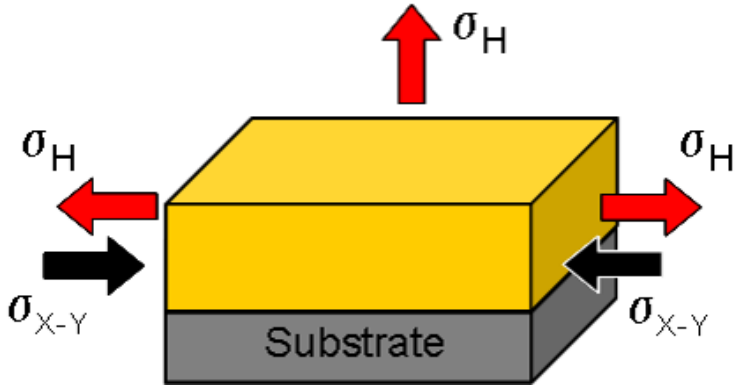

Figure 247. Schematic representation of the forces acting on a thin film during hydrogen absorption.

The influence of the clamping effect on the enthalpy and entropy of hydride formation and decomposition strictly depends on the way these stresses can be released. This, in turn, is governed by the film-substrate interaction energies. Both weak and strong film-substrate interactions have been observed. The former is characterized by an adhesion which is lower than the in-plane stresses, i.e. $\sigma_{\text{in-plane}} > \gamma$. In this case, the hydrogenation induced stresses are released by the formation of so-called buckles and a partial delamination of the thin film (Figure 248).[298] As a result, these films possess very similar thermodynamic data to that of bulk materials after they have undergone a complete activation procedure (Figure 249).

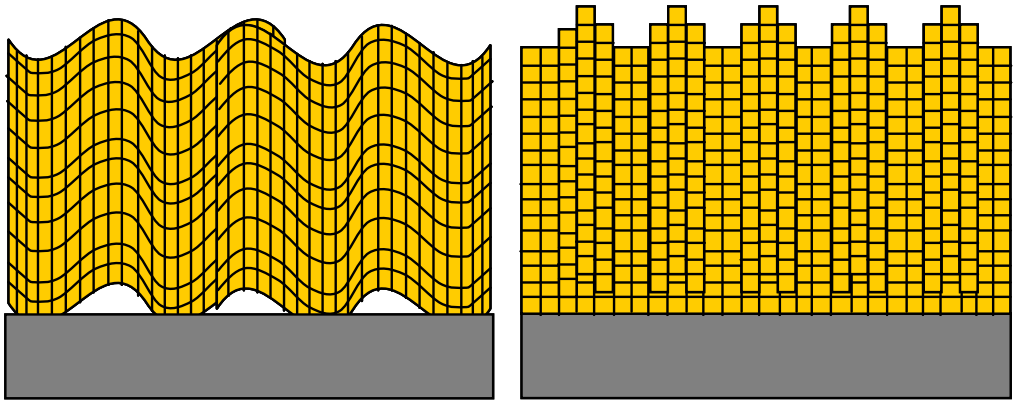

Figure 248. Schematic representation of stress release models in the metal hydride thin films with weak (left) and strong (right) adhesion to the substrate during (de)/hydrogenation.

A recent comparative study on buckled and free-standing Pd films by means of Hydrogenography and Sievert's volumetry confirms that buckling is a very effective stress release model, proving that delaminated films can be considered as nearly free and can be used to study hydrogenation behavior of the corresponding bulk materials.[323]

For strongly adhesive Pd thin films a completely different effect of the induced stress on the thermodynamic properties is found. Film-substrate interactions in these films are higher than the in-plane compressive stresses, $\sigma_{in\text{-}plane} < \gamma$. Thin films remain clamped during hydrogen absorption and desorption and the mechanical stress release occurs by means of rearrangement and pile up of the material (Figure 248). Consequently, the enthalpy of hydride formation and decomposition in the clamped Pd films is found to be lower and higher by 3 and 1 kJ/mol H2 respectively as compared to the buckled samples (Figure 249).[324]

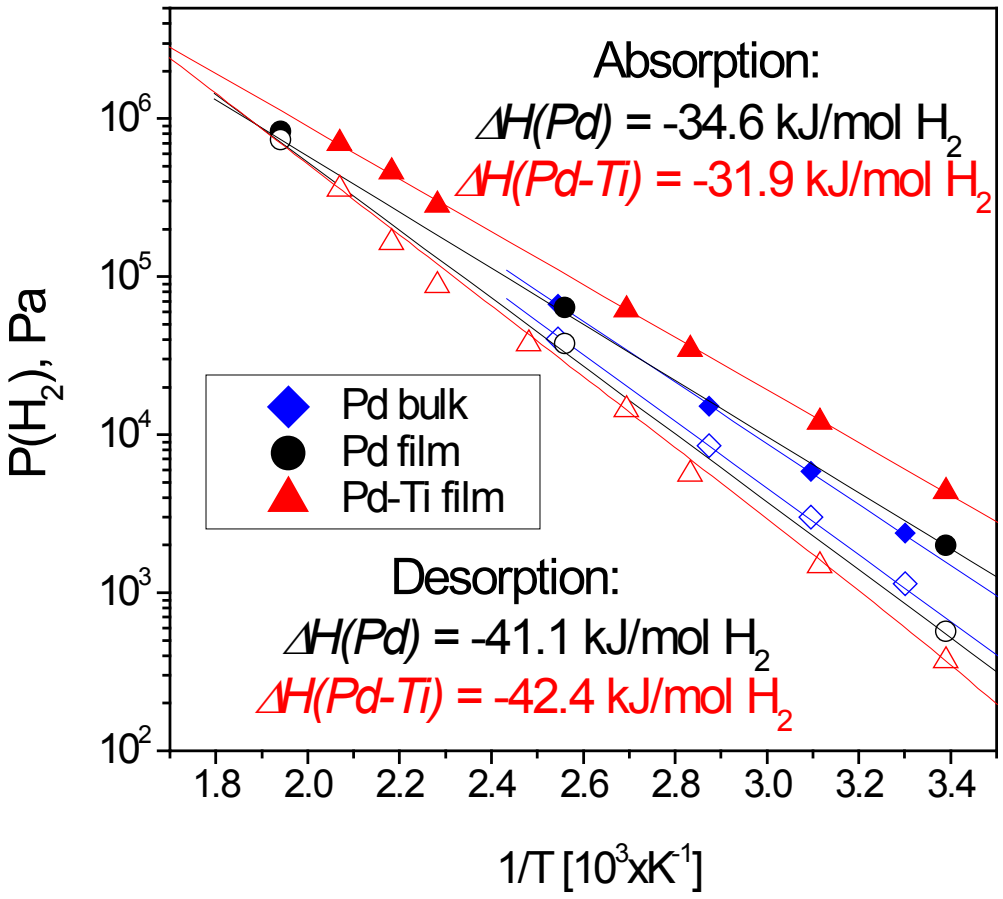

Figure 249. Van 't Hoff graph of the bulk Pd and clamped Pd films (red triangles) measured by the Hydrogenography; the enthalpy is calculated from regression analysis. Literature data on Pd films (black circles) and bulk Pd (blue diamonds) are presented for comparison. Filled and opened symbols represent absorption and desorption, respectively.

A simple model, based on the stress-strain analysis of the clamped and buckled Pd films upon hydrogen absorption and desorption unambiguously reveals that the change in thermodynamics correlate with the mechanical work done in the clamped hydride films.[324]

The effect on the thermodynamic properties of the clamped Pd films is still rather small and the Hydrogenography results are still relatively close to those of bulk. However, for other metal hydride thin films such effects can be misleading. The mechanical work depends on the volume expansion, the hydrogen concentration jump at the phase

transition, the molar volume, and the mechanical properties change during (de)/hydrogenation. A variation of some of these parameters can lead to a much larger impact of the stress energy on the thermodynamic properties of metal hydride thin films and all of these parameters should be taken into account during the analysis of the Hydrogenography data. For instance, the Mg_2Ni system possesses a 2 times larger volume expansion as compared to Pd, meaning that the hydrogen atoms will contribute more energy to expand the lattice. This will result in a higher chemical potential needed to drive the hydrogenation and dehydrogenation reactions, leading to an increase and a decrease of the absorption and desorption pressures, respectively. An increase of the mechanical work shifts the plateaus and lead to an 'incorrect' thermodynamic properties and a different hysteresis behavior if compared to bulk data. This problem, however, can be overcome by using a model that has been proposed where the bulk thermodynamic properties can be simply calculated back from the Hydrogenography results combined with a simple stress and strain analysis of the films.[324]

During the Hydrogenography experiments, additional attention should be paid to the kinetics of the (de)/hydrogenation reactions of the clamped metal hydride films. High stresses in these films might cause the kinetics to slow down, which will result in a sloping behavior of the pressure-transmission-isotherms. Therefore, it is very important to measure first the loading/unloading cycle (after the activation procedure) in a step scan mode to insure that equilibrium has been achieved between hydrogen in metal and in gas phase. With this, the time needed for the real equilibrium scan can be determined.

Alloying process between Pd-cap layer and a metal hydride film is another difficulty which can affect the Hydrogenography experiment and the data analysis. An inter-alloying process can change the chemical composition and the stability of the measured film; the experimental results, obtained in this kind of systems will not reflect the thermodynamic properties of the corresponding bulk materials. Alloying can also lead to a formation of a blocking layer, which is not permeable for hydrogen and result in a negligible hydrogen absorption by the sample. For this reason, to insure stability of the film, it is necessary to measure and compare several loading/unloading cycles.

No substantial alloying is expected during the Hydrogenography experiments below 363 K. However, as the diffusion of metal atoms is a temperature limited process, Hydrogenography experiments at elevated temperatures (>363 K) need to be conducted with an additional interlayer between Pd and the film to prevent inter-alloying from occurring. This interlayer should be chemically stable within the measurement temperature range.

3.3.2 Off-board Regenerable Hydrides Storage Materials

An excellent example of the use of thermodynamic measurements to gain a better understanding of the fundamental processes of the decomposition of the off-board regenerable hydrides was the study of Graetz and Reilly on different polymorphs of AlH_3.[238] In this case, the thermodynamics of the α, β and γ polymorphs of AlH_3 were determined using differential scanning calorimetry (DSC) and ex situ X-ray diffraction (XRD). The DSC instrument was a heat-flux configuration whereby energy released or absorbed is determined by measuring the heat flow between the sample and a reference crucible. The reaction enthalpies were determined by measuring the heat absorbed/ released during a temperature ramp between 35 ◦C and 300 ◦C at a rate of 10◦C/min. In this study it was assumed that the magnitude of the decomposition enthalpy is equivalent to the formation enthalpy. Although measurements were performed during the decomposition reaction, the values were reported as formation enthalpies (with a sign change) to be consistent with similar studies in the literature. Ex situ XRD samples received the same thermal treatment as the DSC samples, but were quenched in a room temperature water bath in a sealed vessel after reaching a given point in the thermal ramp. Results of the two separate measurements on the α-AlH_3 phase are shown in Figure 250. As expected, the diffraction pattern demonstrates that α-AlH_3 is completely transformed to Al metal (and H_2) during the temperature ramp.

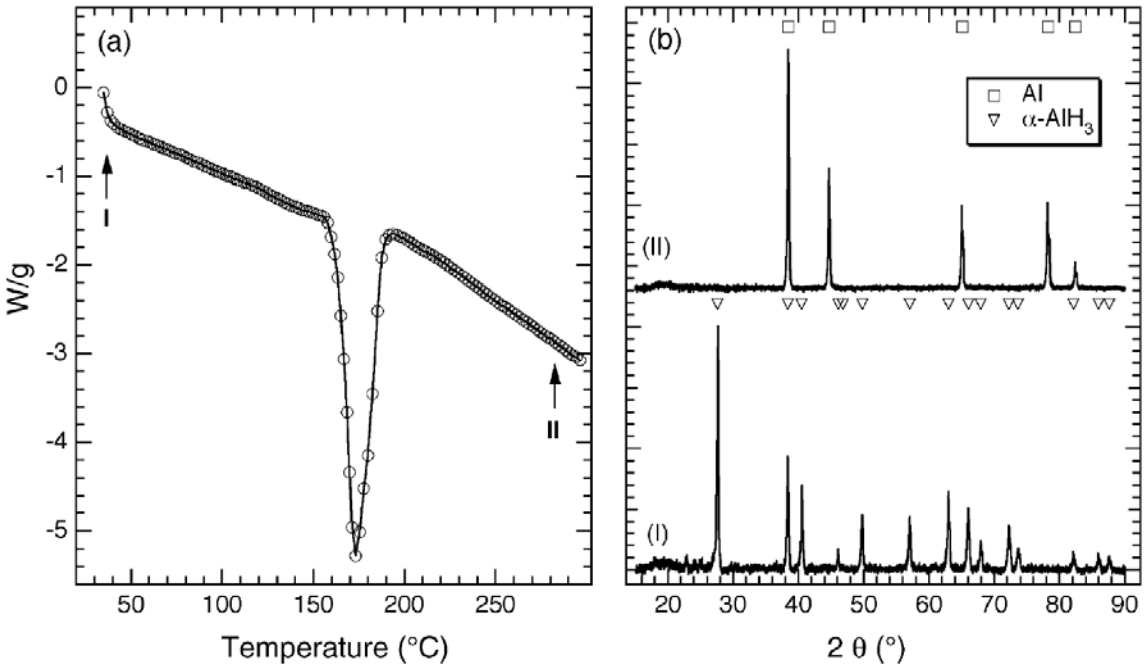

Figure 250. (a) Differential scanning calorimetry plot of α-AlH3 in the temperature range of 35–300 ◦C ramped at a rate of 10 ◦C/min; (b) ex situ diffraction patterns acquired at room temperature before thermal treatment (I) and after a temperature ramp to 300 ◦C (II).[238]

The Gibbs free energy of formation at room temperature (ΔG_{298K}) was calculated using the measured formation enthalpy and an entropy change (ΔS) was assumed to be equal to 130.7 J/mol K, which is the entropy associated with the transformation of hydrogen from a disordered gas to an ordered solid.

Similar measurements were performed on β-AlH_3 phase and γ-AlH_3 phase materials. The results demonstrate that at around 100 ◦C the decomposition of the β and γ polymorphs occurs by an initial phase transition to the α polymorph followed by decomposition of the α phase. The measured enthalpy of the $\beta \rightarrow \alpha$ transition is 1.5 ± 0.4 kJ/mol AlH_3. It was noted that the measured transition enthalpy may be slightly higher than the actual value due to contributions from some γ-phase impurity. A enthalpy of 2.8 ± 0.4 kJ/mol AlH_3 was found for the $\gamma \rightarrow \alpha$ transition. The transformation to the α-phase is exothermic and is therefore likely to occur spontaneously at room temperature. A formation enthalpy of approximately −10 kJ/mol AlH_3 was measured for α-AlH_3, which is in good agreement with previous experimental and calculated results.

The combined measurements of DSC and ex-situ X-ray diffraction point to the importance of knowing a) the constituent compositions of reactants and products, b) the reaction pathways, and c) ensuring that the reactions have gone to completion in order to use the measured heats to determine enthalpies of reaction.

3.3.3 Physisorption Storage Materials

The interaction energy of just a few kJ/mol between the frameworks and the dihydrogen molecules within porous materials, can be easily overwhelmed by the thermal energy of the hydrogen gas, thus resulting in very low hydrogen uptake at room temperature even under a high pressure.[326] The detailed understanding of the location of H_2 and the energetics of H_2-framework interactions within porous materials are of crucial importance for developing materials that can function near ambient temperatures.[273]

A useful experimental method for aiding in a molecular level understanding of hydrogen adsorption in porous materials is inelastic neutron scattering (INS) spectroscopy of the hindered rotational transitions of the adsorbed hydrogen molecules. The lowest transition hindered rotor energy level of the H_2 molecule is a rotational tunneling transition, which depends exponentially on the height of the barrier to rotation. It is for this reason that this technique is extremely sensitive to the chemical environment of adsorbed H_2 and can thereby provide detailed information about the various binding sites that the hydrogen molecules occupy and the approximate order in which these are filled. Because of the very large inelastic incoherent neutron scattering cross section for

hydrogen, vibrational modes not involving hydrogen are not normally observed, which greatly simplifies the analysis of the observed spectra. This technique has become invaluable to the understanding of the hydrogen adsorption characteristics of a variety of nanoporous substrates including zeolites and carbon nanostructures and has also been recently employed to investigate the details of hydrogen adsorption in porous MOFs.[327]

As an example, INS spectra of MOF-5, recorded at different temperatures for loadings of less than $8H_2$ per formula unit, exhibit two peaks centered at 10.3 and 12.1 meV (a lower value corresponds to a larger rotational barrier).[12] These peaks could be assigned to H_2 bound to the Zn_4O cluster unit and the BDC^{2-} linker, respectively. Higher H_2 loadings revealed a splitting of the 12.1 meV absorption band, indicating that multiple binding sites exist for which adsorbed H_2 molecules have similar rotational barriers. Variable-temperature INS studies on HKUST-1 revealed six different hydrogen adsorption sites. Vacant axial coordination sites of the Cu^{II} centers, where hydrogen possesses a large rotational barrier, were occupied first. This is consistent with the estimated binding energy of just 6^{-10} kJ mol^{-1}. The remaining sites are located near the benzene ring and carboxylate moieties of the ligand. The absorption peak in the INS spectra corresponding to hydrogen bound in the small pocket shifts to higher energy at high loadings, suggesting that hydrogen binding indeed provokes minor changes in the environment of this adsorption site (Figure 251).[328] These INS studies combined with powder neutron diffraction (PND) measurements on MOFs have consistently revealed that the metal centers have higher hydrogen binding energy than the organic linkers, which is very instructive for developing new MOF materials with higher adsorption enthalpies for near ambient hydrogen storage applications.

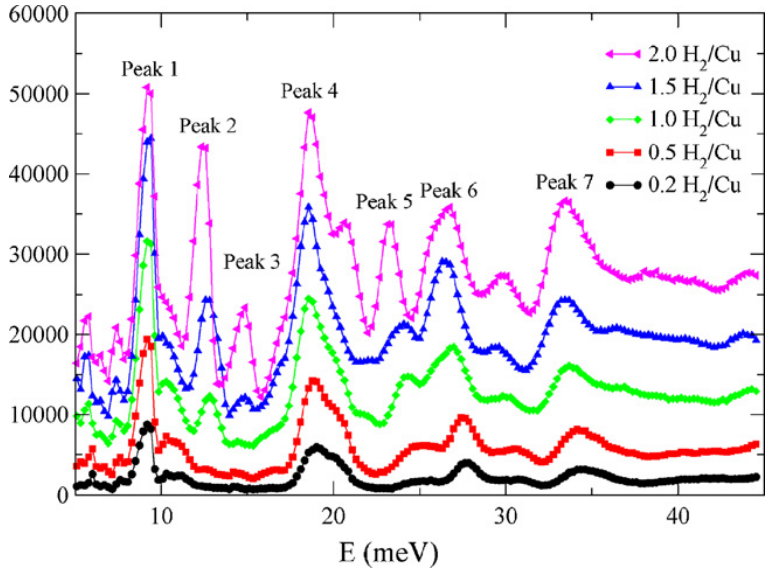

Figure 251. INS spectra of H_2 in HKUST-1 at 0.2, 0.5, 1.0, 1.5, 2.0 H_2:Cu. The background spectrum has been subtracted from the H_2 spectra.[328]

As mentioned in this Thermodynamics measurement section 1.3.4 variable-temperature spectroscopy can be a useful method to explore the site-specific interactions of hydrogen within a framework and the energetics of those binding events. The results of hydrogen uptake in MOF-5 using infrared spectroscopy revealed two transitions at 4112 and 4121 cm^{-1} at low pressures, which were assigned to para- and ortho-hydrogen coordinated at the same type of site within the framework.[171] As the H_2 pressure was increased, the two transitions became obscured by a broad absorption band centered at 4130 cm^{-1}. The binding energies determined for the low- and high-pressure sites were 7.4 and 3.5 kJ mol^{-1} H_2, respectively (Figure 252).[171]

The infrared studies on Ni_2(dhtp) demonstrated that H_2 was adsorbed at the coordinatively-unsaturated nickel(II) sites at a relatively high temperature of 180 K with a strong adsorption enthalpy of 13.5 kJ $mol^{-1}H_2$ (Figure 252) Two vibrational frequencies were observed at 4035 and 4028 cm^{-1}, corresponding to two distinct binding sites with the hydrogen molecule eclipsing an Ni-O bond, where the oxygen atom arises either from the carboxylate or alkoxide group. With the increase of H_2 loading, two new bands at ν_{H-H} = 4132 and 4120 cm^{-1} are observed, which originate from hydrogen bound to the aromatic linkers (Figure 252).[329]

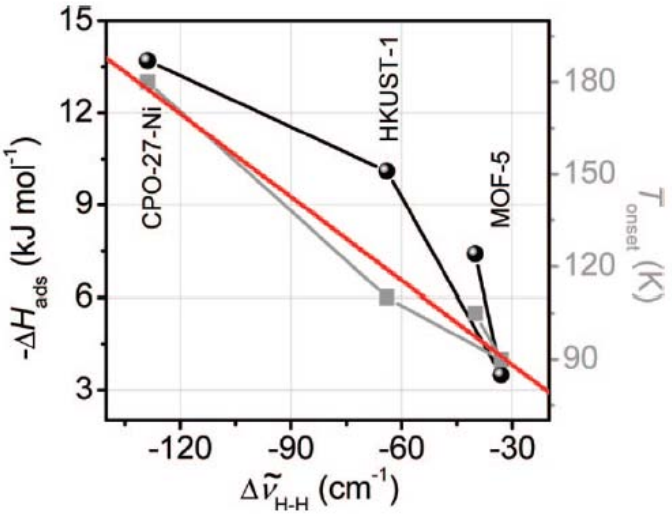

Figure 252. Dependence of the adsorption enthalpy (ΔH_{ads}, black circle) and of the temperature at which the H_2 complexes are observed (T onset, gray squares) on the corresponding shift of the H-H stretching frequency for the three MOFs under investigation. Para-H_2 has been used as reference. The red line corresponds to the linear regression of the T_{onset} data: y = mx + q where m = -0.90436 K cm and q = 61.15506 K (r^2 = 0.9694 and max. dev. = 8.57425). For CPO-27-Ni, the barycenter of the 4028 and 4035 cm^{-1} bands has been considered.[329]

4 Example Approaches to Improve Thermodynamics

4.1 Materials Improvements

4.1.1 Alloys with Destabilizing Elements

One common technique to reduce stability of a metal hydride such as LaH_2 is to combine it with another element with a lower affinity for hydrogen (such as Ni) to form an intermetallic hydride $LaNi_5H_6$ with and intermediate stability. This is known as the "Miedema's rule of inverse stability" This is described by a model for calculating the enthalpy of formation developed by Bouten and Miedema.[330] Their model states that an alloy of two transition metals, A and B, which forms a hydride, AB_nH_{2m}, will have an enthalpy of formation approximately given by:

Equation 237 $$\Delta H\left(AB_nH_{2m}\right) = \Delta H\left(AH_m\right) + \Delta H\left(B_nH_m\right) - \Delta H\left(AB_n\right)$$

Equation 237 is advantageous when $\Delta H(B_nH_m)$ is small or positive and $\Delta H(AB_n)$ is negative. It is derived from the assumption that A has a much stronger affinity for hydrogen, and therefore the A-B bond is broken and islands of AH_m surrounded by B are formed.

4.1.2 Mixtures of Destabilizing Hydrides

Recent work has shown that significant destabilization can also be achieved through the mixing of hydride materials. For example, in the experiments described in above, the decomposition reaction of $LiBH_4$ is given in Equation 238:

Equation 238 $$\mathbf{LiBH_4 \rightarrow LiH + B + 3/2H_2}$$

However, as described in Section 3.1.1 above, Vajo et al showed that it is possible to reduce the enthalpy of reaction by mixing MgH_2 with $LiBH_4$. The new reaction is given by:

Equation 239 $$\mathbf{2LiBH_4 + MgH_2 \rightarrow 2LiH + MgB_2 + 4H_2}$$

MgB_2 has a lower enthalpy than pure B, reducing the enthalpy of reaction by 25 kJ/mol H_2.[315]

Predicting mixtures that will result in optimally stabilized end states is not a simple process. Often complicated multistep reactions will replace the predicted one step reaction, indicating the need for care and experimentation to back up predictions. For example, it is tempting to try a similar destabilization of $Ca(BH_4)_2$ with MgH_2 as shown in Equation 240 and Equation 241:

Equation 240 $$\mathbf{Ca(BH_4)_2 \rightarrow CaH_2 + 2B + 3H_2}$$

Equation 241 $$\mathbf{Ca(BH_4)_2 + MgH_2 \rightarrow CaH_2 + MgB_2 + 4H_2}$$

However, careful consideration reveals that $Ca(BH_4)_2$ has a lower enthalpy of formation than MgH_2, and therefore will decompose before Equation 241 can take place. For this reason, Siegel et. al have set out some guidelines for choosing destabilizing mixtures. These can be summarized as: the enthalpy of reaction of the proposed mixing compound must be less than that of the original compound, if a hydride-forming element is included, the enthalpy of formation of the hydride must also be considered, and it is not generally possible in these systems (versus intermetallic alloys) to tune a reaction by altering the stoichiometry, as there is only one appropriate stoichiometry that will lead to the desired one step reaction.[331]

4.1.3 Size Effects

Nanoscale size effects are believed to influence the thermodynamic as well as the kinetic properties of hydrogen storage materials. These effects have been evaluated by theory, but are difficult to duplicate in experiments due to the extremely small sizes required, sometimes smaller than 2 nm before significant effects are predicted. There are multiple mechanisms by which nanoscale effects could change the thermodynamics, such as increasing the surface area and adding strain at grain boundaries.

4.1.3.1 Increased Surface Area

In a bulk material, the difference in surface energy between the hydrided and unhydrided states is negligible, since the surface area of the sample is relatively small. However, a sample composed of nanoparticles may have such a high surface area that it is necessary to include an analysis of the change in surface energy during the reaction. This has been done both by adding an extra term in the van 't Hoff equation (see Equation 242)[332] and Density Functional Theory (DFT) calculations.[333]

Equation 242

$$\ln\left(\frac{P_{eq}}{P_o}\right) = \frac{\Delta H_o + \frac{3V_M \Delta M \rightarrow M_{H2}}{r}}{RT} - \frac{\Delta S_o}{R}$$

In Equation 242, V_M is the molar volume of the metal phase, $\Delta M \rightarrow M_{H2}$ is the change in surface energy between the metal and the hydride phase and r is the average particle radius. For an increase in surface area to increase the equilibrium hydrogen pressure at a given temperature, $\Delta M \rightarrow M_{H2}$ must be positive. For example, for the Mg to MgH_2 transition, $\Delta M \rightarrow M_{H2}$ is 1.76 Jm^{-2}, which results in a predicted increase in the effective ΔH of more than 10% for spherical nanoparticles with an average radius less than 4 nm.[332] DFT calculations predict a similar change only for nanoparticles with a radius less than 2 nm.[333]

4.1.3.2 Grain Boundaries

Increased grain boundary area has been shown to enhance the kinetics of hydrogen storage materials, as discussed in section 4.2 of the kinetics chapter. When grain sizes reach the nanoscale, many theories predict that there can be some thermodynamic improvement as well. The strain present due to mismatched crystal orientation at the grain boundaries can lead to excess volume in the sample, which in turn creates excess energy in the material.[334] An alternative explanation is to treat the grain boundaries as an enhanced surface area and follow the same treatment outlined in section 4.1.3.1 above.[332] However, there is little experimental evidence to support these concepts so far.

4.1.4 Thermodynamic Improvements of On-board Reversible Hydride Materials

One focus in developing materials which may be recharged on-board a vehicle is to start with a high capacity material and work to improve its thermodynamic and kinetic properties. The most important thermodynamic property in these studies is usually the enthalpy of formation, since this has the most influence on obtaining favorable operating pressure and temperature conditions possible. The entropy of formation would appear to offer similar opportunities for improvement based on the van 't Hoff equation. However, since the change in entropy corresponds mostly to the shift from molecular hydrogen gas to hydrogen atoms dissolved in solid solution, there may be less room for improved performance through the modification of entropy.

The study of magnesium based hydrogen storage materials is a good example. Magnesium is appealing due to its low cost, abundance, and high capacity. However, the enthalpy of formation of MgH_2 is approximately -75 kJ/mol H_2, well above the ideal value of -30 kJ/mol H_2. Many efforts have focused on reducing the enthalpy of formation of MgH_2 and related compounds to a more practical level. Unfortunately, this has proved challenging as Mg forms stoichiometric complex hydrides when combined with other metals rather than alloy hydrides.

4.1.5 Thermodynamic Improvements of Off-board Regenerable Hydride Materials

One example of the efforts to improve the thermodynamics of off-board regenerable hydrogen storage materials is the recent work by Shih-Yuan Liu and co-workers at the University of Oregon.[335] Their work has focused on developing CBN (heterocycles containing carbon, boron, and nitrogen) hydrogen storage materials that are liquid-phase and have the potential to be reversibly regenerated using molecular hydrogen. In order to accomplish reversibility, neutrality in free energy of the hydrogen release process (i.e., ΔG ~0 kJ/mol) at the operating temperature is required. The dehydrogenation of ammonia-borane ($H_3N–BH_3$ or AB) is exergonic by -13 kcal/mol (–54.4 kJ/mol) at 298 K (Figure 253 (1)). In contrast to AB, the dehydrogenation of its isoelectronic organic counterpart, ethane ($CH_3–CH_3$), is endergonic (not spontaneous, in contrast with an exergonic process, absorbs energy from the surroundings) by +25 kcal/mol (–104.7 kJ/mol) (Figure 253 (2)). The coupling of endothermic dehydrogenation

from carbon-carbon with exothermic dehydrogenation from BN in a cyclic six-membered framework could lead to a reversible H_2 storage system. Indeed, high-level computational analysis indicates that the release of H_2 from CBN heterocycles (Figure 253 (3)) has favorable overall thermodynamics conducive to reversibility.[336]

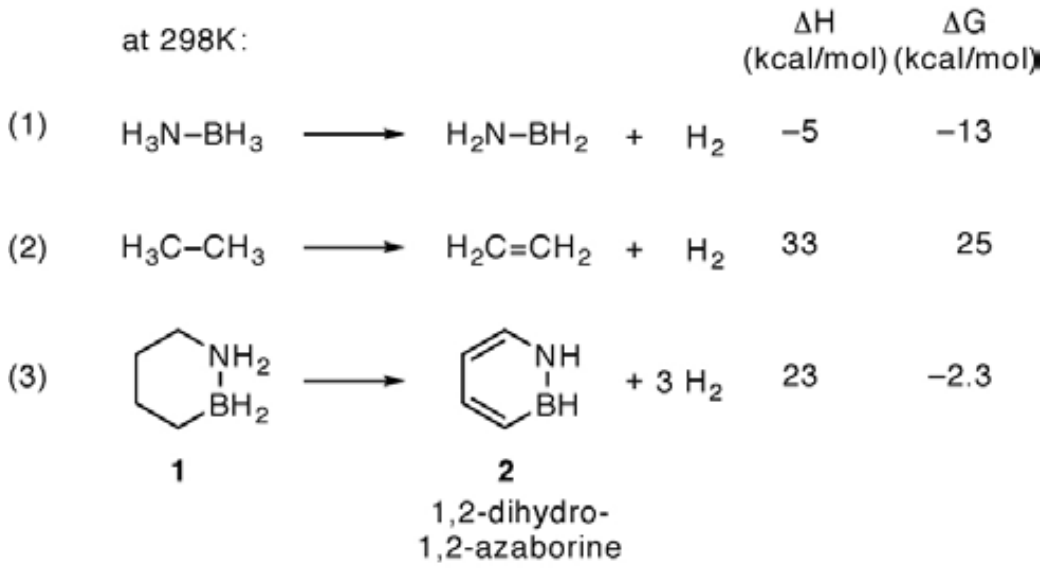

Figure 253. Thermodynamics of hydrogen release from (1) AB, (2) Ethane, and (3) potential CBN hydrogen storage materials.[335]

Theory was used to guide the researcher's initial target selection for synthesis. Figure 254 illustrates the calculated thermodynamic data for H2 desorption for seven proposed CBN materials. Materials (1), (3), and (7) were predicted to have the potential for reversibility (ΔG ~ 0 kcal/mol).[336]

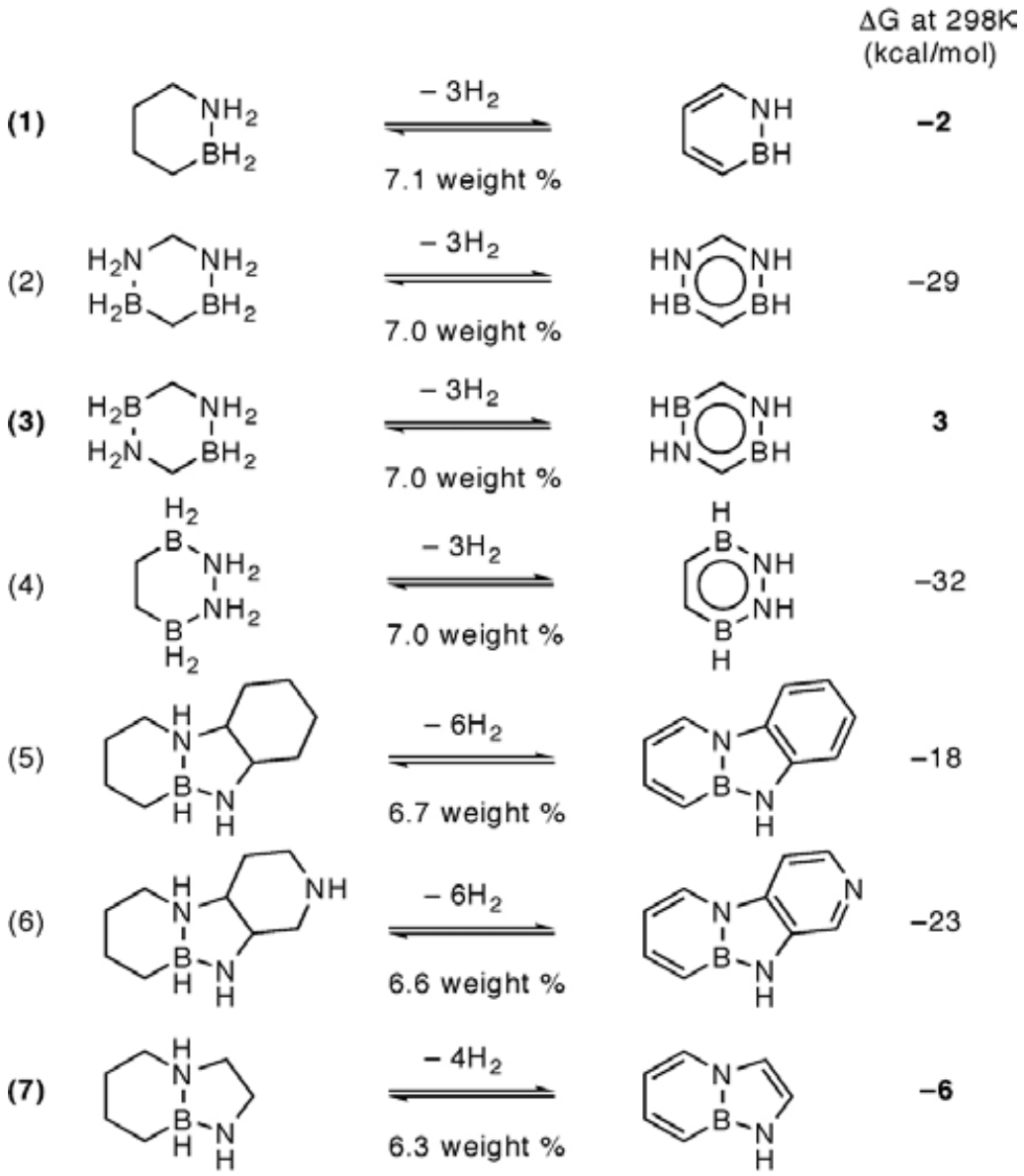

Figure 254. Calculated Thermodynamic Properties of CBN Heterocycles.[335]

Initial work accomplished the synthesis of representative model compounds on the proposed pathway from the fully charged to discharged material 1 in Figure 254.[335]

4.1.6 Thermodynamic Improvements of Physisorption Materials

Current major obstacle for hydrogen storage on physisorption materials lies in their low heats of adsorption. A desired binding energy of ca. 20 kJ/mol in the overall hydrogen loading range has been proposed for room temperature hydrogen storage. Introducing coordinatively unsaturated metal centers (UMCs) on the surfaces has been proved very attractive in enhancing the adsorption enthalpies particularly for MOF materials. A recent systematic investigation of hydrogen affinities of different UMCs in a series of isomorphous MOF structures revealed that open nickel centers possess the highest hydrogen binding energy compared to other first transition metals and magnesium (Figure 255).[337] Although high adsorption enthalpies up to 13.5 kJ/molH_2 have been achieved in some porous MOFs at very low hydrogen coverage, the adsorption enthalpies abruptly decline to 5–6 kJ/mol with the increase of hydrogen loadings and no significant improvement of hydrogen uptakes could be observed at room temperature under high pressure. In order to enhance the room temperature hydrogen storage capacities, it is believed that high concentrations of UMCs on the surfaces within porous MOFs must be generated, and this may require more rational design and some new synthetic methods in future development of porous MOFs.[326]

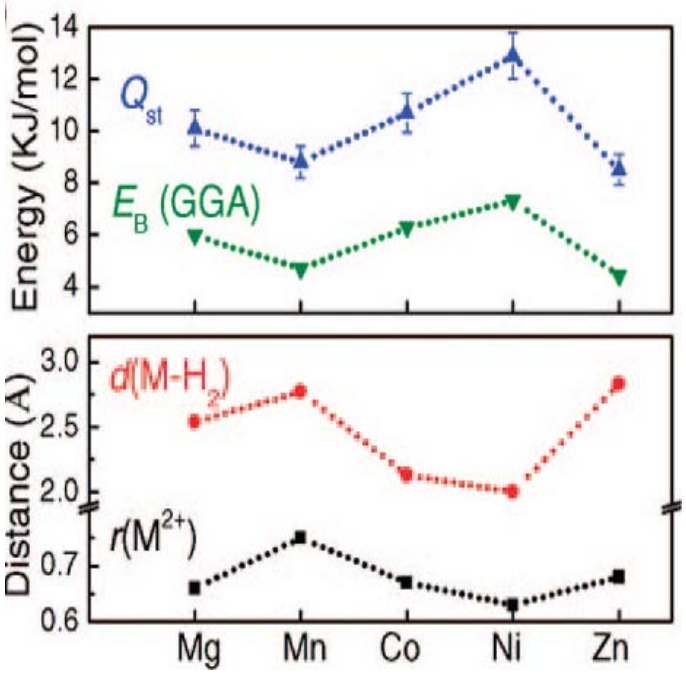

Figure 255. The empirical transition metal ion radius, the calculated M-H_2 distance, the experimental Q_{st} (along with error bar), and the calculated E_B(GGA) of M_2(dhtp).[337]

Section 5: Cycle-Life Measurements

Cycle-Life performance measurements are critical for evaluating the practical use of hydrogen storage materials in applications such as hydrogen powered automobiles where hundreds to thousands of cycles will be required. It is important that these measurements be performed accurately and with a thorough understanding of a) how measurements should be performed to best represent the conditions under which hydrogen storage materials will be used in life applications, b) what impact the experimental setup itself can have on the performance results, c) how to best gain insight from the measurements into what causes cycling performance degradation. In this section, we will focus on developing a better definition of how such tests should be performed, what parameters may impact the results, and what properties are e.g., capacity fade, or degradation in kinetics, are the most critical in performance evaluation.

This section will give a brief introduction to the basic concepts of Cycle-Life Measurements and then focus on the difficulties that can arise in making accurate measurements and interpreting the data.

5 Introduction and Definitions

The following is a brief introduction to the general concepts of Cycle-Life Measurements and some of the basic applications to hydrogen storage materials.

5.1 Basics of Cycle-Life Measurements

Cycle-Life Measurements is the study of performance of on-board reversible hydrogen storage materials as they may be used in real applications. Typically, the first step is to make basic measurements of the total reversible capacity of the material as hydrogen is charged and released from the material over several cycles. Following this, measurements may then focus on modifying the storage material itself to improve the ability to maintain capacity over many cycles. This may be supported by more

fundamental studies of what causes degradation of the material with cycling. An important metric of performance besides capacity is the rate of hydrogen uptake and release which is also likely to degrade with cycling. In the later stages, measurements are aimed at evaluating how storage materials perform when cycled under non-ideal conditions (temperature excursions, exposure to air, impurities in the hydrogen gas supply….). Finally, thorough testing of the materials and storage system at a scaled up level are necessary to be able to evaluate true application level performance. Each level of Cycle-Life testing may require its own unique experimental setup, procedures and special attention to details that may unexpectedly adversely impact the reliability of the measurements.

Cycle-Life measurements have been performed most extensively on reversible metal hydrides and to a much lesser extent on reversible physisorption hydrogen storage materials. For this reason the next chapter will focus on the Cycle-Life properties of reversible hydrides. While some of these hydrogen-materials interactions (such as decrepitation) are specific to hydrides, many similar issues may affect the cycling properties of physisorption materials. For example, hydrogen uptake is known to change the lattice dimensions in some MOFs. This may ultimately affect the long-term cycling performance of these materials. Another issue with hydrides to consider for physisorption materials is degradation or long-term cycling stability. For example, exposure to excessive temperature is known to cause degradation or complete decomposition of some MOFs. It may be that hydrogen cycling will lead to similar degradation behavior of these materials. Certainly, exposure to impurities in the hydrogen supply that has a strong impact on hydrides, are likely to affect hydrogen uptake of some physisorption materials (in particular those that contain active catalysts e.g. platinum in spill-over materials). However, little is know about the long-term effects on physisorption materials due to the presence of impurities.

Cycle-Life measurements in this chapter are specifically addressed within the context of on-board reversible hydrogen storage. Off-board regenerable materials necessarily involve the chemical reprocessing of spent materials and, as such, are outside the scope of Cycle-Life measurements covered in this document.

5.2 Cycle-Life Properties of On-board Reversible Hydrides

5.2.1 Introduction: Long-Term Stability of Metal Hydrides

Intermetallic metal hydrides, such as $LaNi_5$, have been of great interest for different applications that require numerous hydrogen absorption/desorption cycles, including

hydrogen storage, heat pumps, cryo-coolers, etc. The $LaNi_5$ intermetallic compounds have been studied because of their high hydrogen capacity in excess of 6 atoms per unit of $LaNi_5$ or 7.6×10^{22} atoms/cm^3, nearly twice as high as in liquid hydrogen and the fact that the alloy takes up and releases hydrogen near ambient temperature and pressure conditions. However, problems are encountered when repeated hydriding/dehydriding is performed on these, especially AB_5 alloys hydrides. In fact, even the alloy fabrication and preparation processes can have a very large effect on the hydrogen storage cyclability of all hydrogen storage materials. An example is shown below in Figure 256 of a comparative study of the cyclic life performance of different commercially available $LaNi_5$ samples.[338] This example shows that painstaking characterization of the material and of the process is mandatory for the use of hydrides in basic research as well as in their applications.[339]

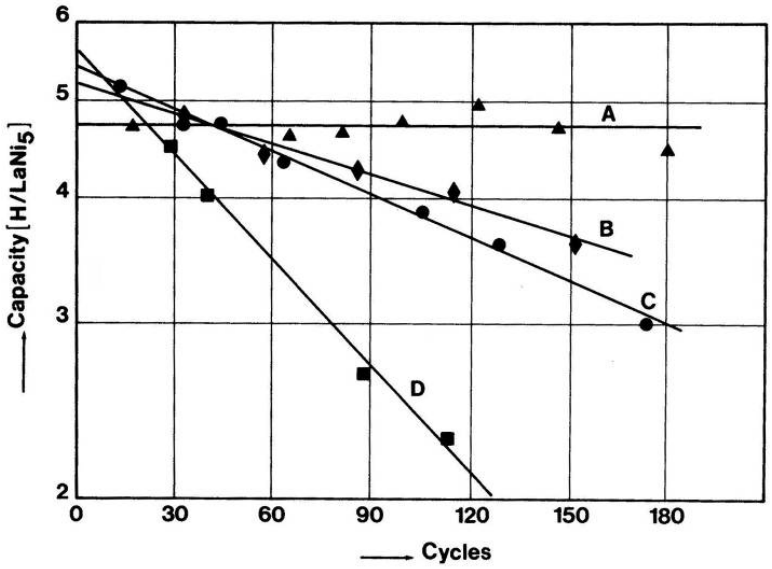

Figure 256. Hydrogen storage capacities of $LaNi_5$ samples from various suppliers during absorption cycling: (A) Research Chemicals sample, dry H_2; (B) Ergenics; (C) Research Chemicals; (D) Molycorp. Samples are cycled in 12 atm with about 10 Torr H_2O.[338]

One of the advantages of the intermetallics is that they are generally accessible to elemental substitution. In the case of $LaNi_5$, a series of isostructural pseudo-binary $La_{1-x}R_xNi_5$ and $LaNi_{5-x}M_x$ compounds can be obtained by replacing either the La or Ni in the crystal structure of the intermetallics.[340] By modifying the composition of these AB_5-based intermetallics, the pressures at which room temperature hydriding occurs can be

changed dramatically. This allows for the tailoring of sorption properties to meet the requirements of a variety of applications.

Again for applications including electrochemical (Nickel-Metal-Hydride batteries), a major problem is encountered when the materials are charged and discharged over many cycles. For $LaNi_5$ and other intermetallics, the ability to modify the elemental composition of the alloy has proven highly successful in improving the Cycle-Life performance of the materials. An example of this was demonstrated by Bowman et al. in a study of thermal hydrogen absorption-desorption capacities of tin-substituted $LaNi_5$.[341] Samples with only a minor amount of tin substituted for Ni dramatically improved the hydrogen Cycle-Life capacities of the materials. The study verified that partial Sn substitution produced alloys that were very resistant to intrinsic disproportionation (the decomposition of the alloy into more stable hydrides or alloys) of $LaNi_5$ into LaH_x and Ni metal (Figure 257).

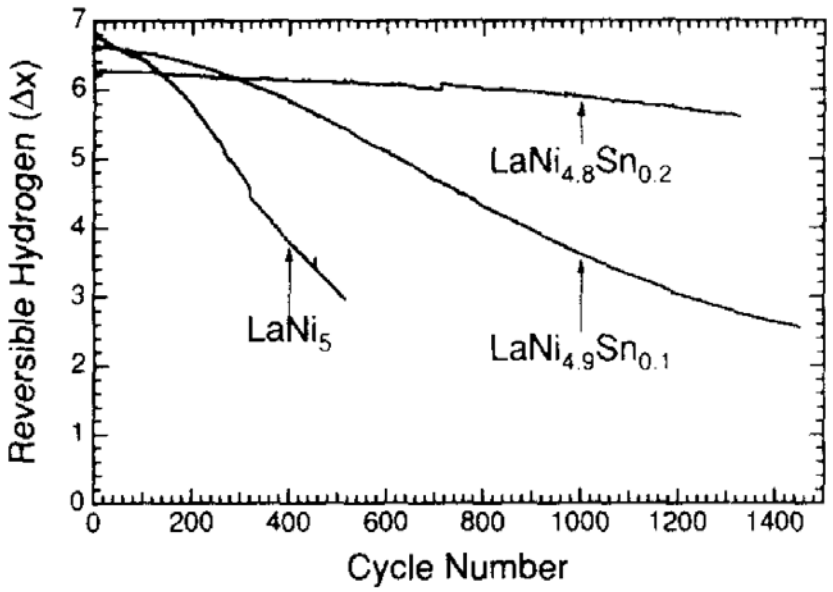

Figure 257. Hydrogen concentration changes Δx for $LaNi_{5-y}Sn_yH_x$ obtained from the maximum and minimum pressures for each cycle.[341]

In practical applications, the hydrogen storage materials are subjected to numerous hydrogen charge-discharge cycles. For hydrogen powered vehicles, the required target for the storage system has been set at an operational Cycle-Life (1/4 tank to Full Tank) of 1000 cycles (2010) and 1500 cycles by 2015.[155]

The physical, crystallographic, micro-structural, and thermodynamic behavior of the materials used to store hydrogen may change after only few or after many absorption-desorption cycles. In the case of metal hydrides, some factors that will impact the Cycle-Life behavior are: whether the hydride has one, two or more plateaus, volume expansion of the crystal lattice, maximum pressure exerted above the plateau pressures, maximum temperature of operation, kinetics, the purity of the hydrogen gas, alloy composition, defects in the lattice, and alloying elements added to stabilize starting material.

5.2.2 Decrepitation of Hydrides

The process of hydrogenation and dehydrogenation of a metal lattice usually causes lattice expansion and contraction. In general, the strain caused by the difference in lattice dimensions at the metal-to-hydride interface causes defects leading to crack formation. Through this process, most intermetallic alloys and compounds form fine powders on hydriding. This process is referred to as *Decrepitation.*

The starting materials to make hydrides are often coarse metal particles, each on the order of several mm in size. Each particle generally consists of a host of single crystal domains, or grains. Grain boundaries within the particle are typically on the scale of micrometers. Once molecular hydrogen comes in contact with the particle surface, dissociation occurs through a catalytic reaction and generates atomic hydrogen (H) interstitials which transport relatively fast through the grain boundaries (at low temperatures) and diffusing more slowly through the volume of the grain. Decrepitation takes place with each hydrogen absorption/desorption cycle. After repeated cycling, the particles disintegration into smaller and smaller particles.[342] This process is very common in hydrides of elemental metals as well as in intermetallic compounds or alloys. The degree of decrepitation depends on the number of cycles and the plastic behavior of the alloy or metal. In the case of $LaNi_5$, the particle slowly disintegrated to some minimum dimensions after which there is very little reduction in particle size. This may be due micro-plasticity exhibited in intermetallics, which are generally very brittle. Many of the elemental hydrides have metallic character and plastic deformation occurs during hydriding that accommodates the strain thus inhibiting significant decrepitation.

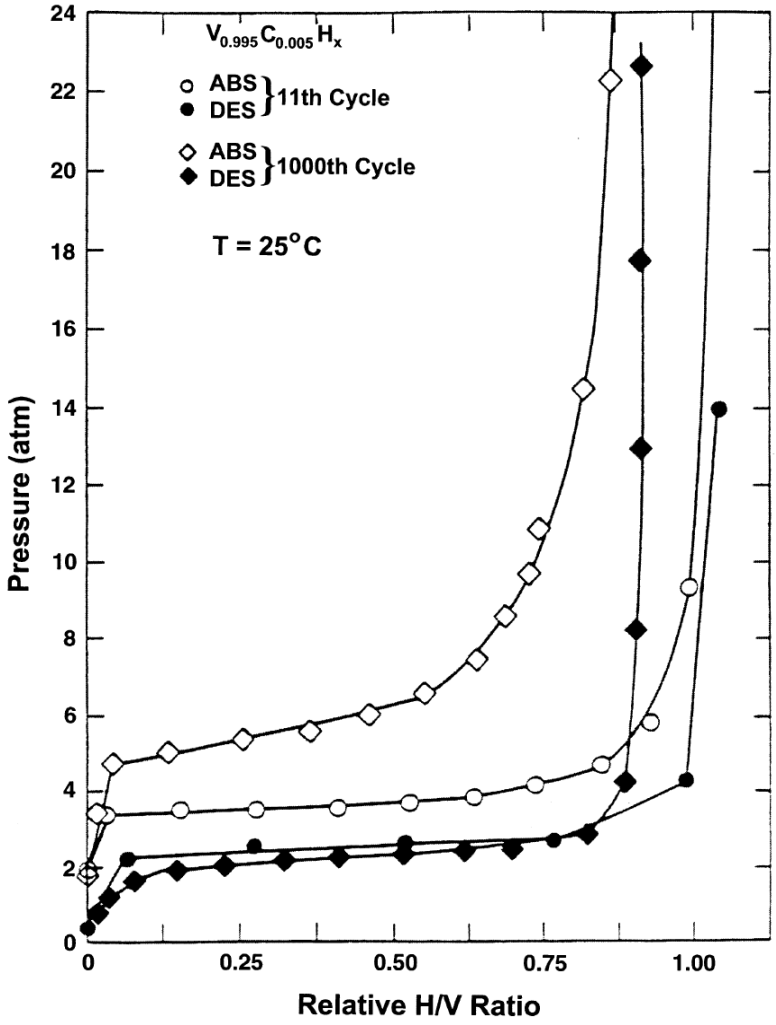

Figure 258. Reversible portions of the pressure–composition isotherms obtained at 298 K on thermal cycled $V_{0.995}C_{0.005}H_X$.[344]

A good example of this is the hydrides of vanadium and some vanadium alloys.[343,344] Although the VH ,V–C–H , and V–Zr–C–H systems cannot experience the intrinsic chemical disproportionation reactions that occur in $LaNi_5H_X$ [345] and other ternary hydrides, minor changes were observed in the isotherms for vanadium hydride and some vanadium-alloy hydrides after several hundred absorption–desorption cycles across the β–γ plateau region. Room temperature isotherm of $V_{0.995}C_{0.005}H_X$ taken after 11 and 1000 thermal cycles are shown above in Figure 258.

The morphology of decrepitated powers can affect packing, which in turn can lead to internal gas impedance and container deformation.[47] The morphology of the powders also affects heat transfer. Most hydride powders have poor heat transfer coefficients and require engineering for thermal enhancement (e.g., Al foam, internal fins, etc.). This is made worse by decrepitation leading to the loss of thermal contact with the heat transfer media. The end result is that the decrepitation that occurs with each hydriding cycle may have an important and unpredictable effect on the Cycle-Life properties of a hydrogen storage material.

The decrepitation process is something that should be taken into account in making Cycle-Life measurements. In general, decrepitation is one of several processes that take place in the first few to tens of cycles and is wrapped up in what is commonly called the *Activation* process. In Cycle-Life measurements, the material will likely show increased capacity in the first activation cycles before reaching a more steady-state cycling behavior (usually a slow loss in capacity). It was pointed out in prior chapters that it is important to make sure the sample is fully activated before ascribing long-term hydrogen storage properties to a material. This is equally true for Cycle-Life measurements and is best achieved by recording complete uptake and release data in the first 20 or so cycles.

5.2.3 Degradation by Disproportionation of Hydrides

Capacity loss with cycling in hydrides is often due to disproportionation (the decomposition of the alloy into more stable hydrides or alloys). Commonly the metal alloy or hydride will decompose at the surface and the element with a higher affinity for hydrogen or oxygen will form a stable hydride or oxide reducing the overall content of alloy able to store hydrogen. Whether through intrinsic instabilities or extrinsic reaction with impurities, the material will show a loss in capacity over extended hydrogen cycling.

An example of disproportionation during pressure cycling can be seen from the measurements performed by Goodell on the hydriding of $LaNi_5$, $CaNi_5$, and $LaNi_{4.7}Al_{0.3}$.[346] The results of those measurements are shown in Figure 259 (a). It can be seen that that the Al substituted alloy $LaNi_5Al_{0.3}$ shows virtually no degradation compared with $LaNi_5$ and certainly $CaNi_5$ which are known to disproportionate. This is possibly due to Al ordering in Ni sub-lattice reducing disproportionation.[347] Figure 259 (a) also shows that the hydriding properties are almost recovered by reproportionation through vacuum thermal treatment of the samples.

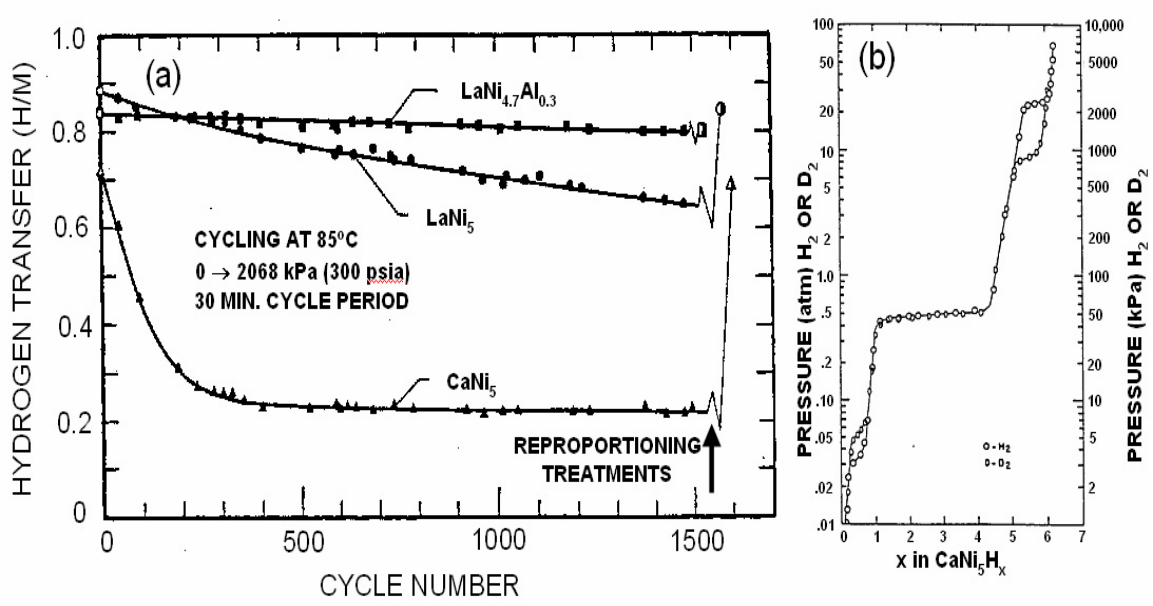

Figure 259. (a) Comparison of hydrogen capacity loss as function number of pressure cycles for $LaNi_{4.7}Al_{0.3}$, $LaNi_{5.2}$, and $CaNi_5$, before and after pressure cycling at 85°C between 0 and 2068 kPa (300psi).[346] This shows a significant loss in $CaNi_5$ but this loss is recovered after reproportionation. (b) A reference isotherm of $CaNi_5$ (taken at 25°C) showing three different plateaus due to the three distinct $CaNiH_x$ phase compositions.[348]

5.2.4 Gaseous Impurity Effects on Classic Hydrides

Four classic types of alloy-impurity interactions are described below, three of which are demonstrated in the data of Figure 260.[59]

Innocuous: (not shown in Figure 260) is observed as essentially no cyclic effect on rate or capacity, i.e., inert. Examples of innocuous impurities include N_2 and CH_4 interactions with AB_5 intermetallics at room temperature.

However, it should be noted that innocuous impurities at high levels (<1%) can exhibit what appears to be retardation during absorption. This is simple "inert gas blanketing" where the innocuous impurity gas simply collects and concentrates in the cracks and interparticle voids, resulting in a type of H_2 diffusion barrier. Inert gas blanketing is asymmetric and is not seen on desorption as the impurity gas is quickly swept away.

Poisoning: results in a severe and rapid loss of H-capacity with cycling. The impurity is able to virtually stop hydriding with only a monolayer of surface coverage, suggesting that dissociative chemisorption (H_2-dissociation into atomic hydrogen at the surface) is deactivated. Typical poisons include CO (near room temperature) and the S-containing gases (e.g., CH_3SH methyl mercaptan). Impurity tests on $LaNi_5$ and Fe-Ti alloy with H_2S and CH_3SH (shown in Figure 260a) and CO impurity gases exhibited a rapid loss of hydrogen capacity, and were considered to be the result of surface poisoning.[349]

Within a macroscopic bed, poisoning is very heterogeneous with the remaining un-poisoned material showing good kinetics. This can be seen in Figure 260a by the way the initial slope of the curves were not greatly affected by cycling. For practical purposes, it is important to know that poisoned alloys can usually be regenerated by heating and flushing with relatively pure H_2, albeit sometimes with difficulty.

Retardation: is characterized by losses of absorption/desorption reaction rates without significant loss in ultimate H-capacity. An example of the retardant effect shown in Figure 260b for ammonia NH_3. Although only the first 4 minutes of absorption are shown in Figure 260b, given enough time all the curves reach virtually full hydrogen capacity. Other retardants include CO_2 on the AB_5 alloys or CO at temperatures above 100°C.

Occasionally, retardation is followed by a recovery, as shown by the example of the short-term 0_2 impurity effects in Figure 260c. This behavior is known only for the AB_5 intermetallics and is associated with the development of a "self-restoring" surface composed of relatively transparent La_20_3 and/or $La(OH)_3$ and fine catalytic Ni particles.[350] The effects of retardation can generally be easily erased by switching back to high purity H_2.

Reaction: is the effect of bulk corrosion loss of alloy resulting in irreversible capacity loss. Tests of 1000 ppm level of oxygen impurity in hydrogen revealed significant loss in $LaNi_5$ capacity due to oxidation. Although 0_2 exposure exhibits a short-term retardation-recovery behavior (Figure 260c), its long term behavior is as a reactant by oxidizing the alloy (Figure 260d). The alloy damage caused by a reactant generally cannot be recovered without complete metallurgical reprocessing.

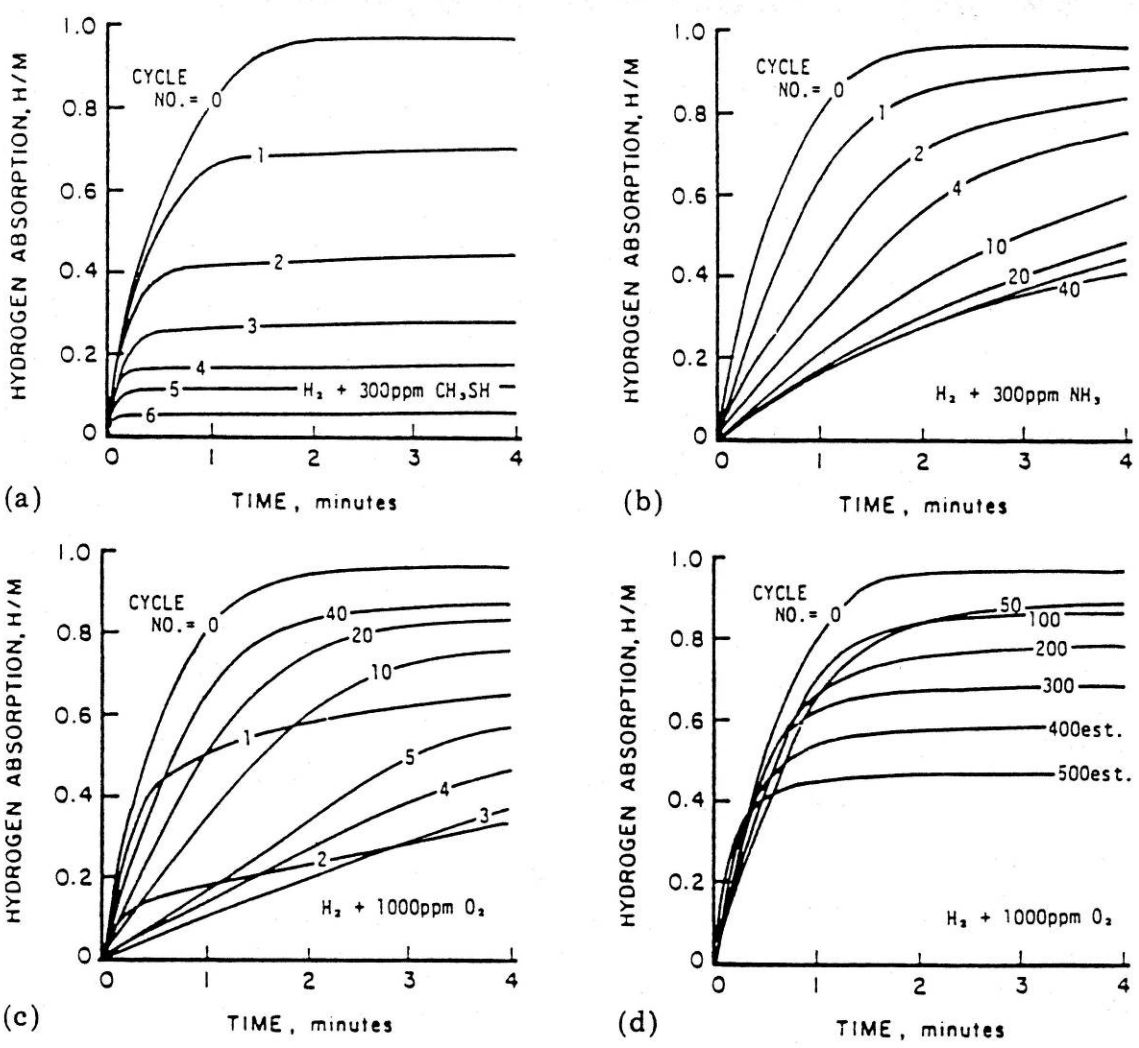

Figure 260. Effects of different types of impurity interactions with $LaNi_5$ on the absorption H/M vs. time profiles during repeated cycling. (a) Poisoning, (b) Retardation, (c) Retardation-Recovery, (d) Reaction. Curves measured at 25°C and 3.4 atm H_2 pressure.[59]

An empirical mathematical damage model for quantifying alloy-impurity effects was proposed and developed by Goodell.[351] Unfortunately, this model has not been evaluated or applied to other Cycle-Life degradation data by subsequent investigators.

Equation 243

$$\Delta\left[\frac{H}{M}\right] = \Delta\left[\frac{H}{M}\right]_0 \exp -\left[\frac{(NAqr\phi)}{[(C - C_o)/100]^{+m}}\right]$$

where $\Delta[H/M]_0$ = initial hydrogen transfer capacity, N is the number of cycles, C = impurity concentration, C_o = threshold concentration for damage, ϕ= is damage function given by hydridable metal atoms consumed/impurity atom, q = $\Delta[H/M]_0$ stoichiometric ratio for an intermetallic, r = number of active impurity atoms/impurity molecules, A= $(0.001)^{(1-m)}$, and m = concentration dependence. For example, for $LaNi_5$ and $TiFe_{0.85}Mn_{0.15}$ tests performed with CO at 25°C, showed ϕ=1733 (m=1) and 1320 (m=1) respectively, whereas, with NH_3 at 25°C showed ϕ=8.6 (m=0.5) and 12.6 (m=0.5), and O_2 at 25°C showed ϕ=1.4 (m=0.5) and 169 (m=1).

5.3 Cycle-Life Properties of Physisorption Storage Materials

Very few Cycle-Life measurements of hydrogen storage properties physisorption materials exist. The lack of data points out the need for more intensive work in this area; in particular with respect to long term cycling performance of physisorption materials in view of automotive applications. For this reason, issues that will certainly be germane to such measurements are outlined below.

1. Even though hydrogen storage in physisorption materials is through weak surface interactions of molecular hydrogen, it can not be assumed that performance degradation does not occur with hydrogen cycling for all physisorption materials.

2. Measurements can be difficult because typical 77K temperatures will have to be consistently maintained throughout hundreds of cycles.

3. However, kinetics are generally fast, therefore, pressure cycling can be done within a reasonable time. Thermal cycling may not be needed.

4. Because physisorption capacity measurements are susceptible to large errors (as described in the Capacity Section of this document), it is critical that any evaluation of long-term cycling performance be done using isotherms done under identical conditions at regular cycling intervals. It is unlikely to be sufficient to simply compare maximum uptake (or release) per cycle.

5. Impurities in the hydrogen supply are likely to impact Cycle-Life performance (e.g. MOFs that decompose with water contact). Yet some impurities (Air…) may condense out of the hydrogen supply at low temperatures before being exposed to the storage materials. Contamination issues should be evaluated with respect to how the materials will be used in an actual application.

6. Studies involving natural gas storage have shown that impurities in the gas accumulate in high surface area carbon adsorbents. However, this principally impacts low pressures capacities (<2 bar) which might not be utilized in hydrogen storage applications. Thus, the impact of contaminates should be investigated as a function of pressure as well as temperature.

7. Pressure cycling may induce some lattice changes in the materials (some MOFs for example). The impact of these changes, such as hydrogen gas trapping, or structural degradation with repeated cycling should be investigated. It is recommended to use simultaneous measurement techniques, when possible, to investigate structural changes with hydrogen content. An example would be in-situ X-ray Diffraction or neutron diffraction while performing hydrogen uptake and release isotherm measurement.

6 Cycle-Life Measurements Methods

This long-term performance behavior is often referred to as *degradation behavior.* Two general approaches have been taken with respect to the measurement of the long-term stability of hydrides. One approach (*Hydriding-dehydriding) Cycling Tests* evaluates the ability to maintain properties, such as hydrogen capacity operating temperature and/or pressure after numerous hydriding-dehydriding cycles. Another approach, *Aging Test,* has been to evaluate the hydride's performance after is maintained at very high pressure and temperatures for a long period of time. These may be further divided into: (1) *Intrinsic* and (2) *Extrinsic testing.* All intrinsic test involve using pure hydrogen, and extrinsic tests involve gaseous impurities (generally in ppm levels to simulate nominal hydrogen gas composition) mixed with hydrogen gas. The different types of degradation testing are laid out below in Figure 261.

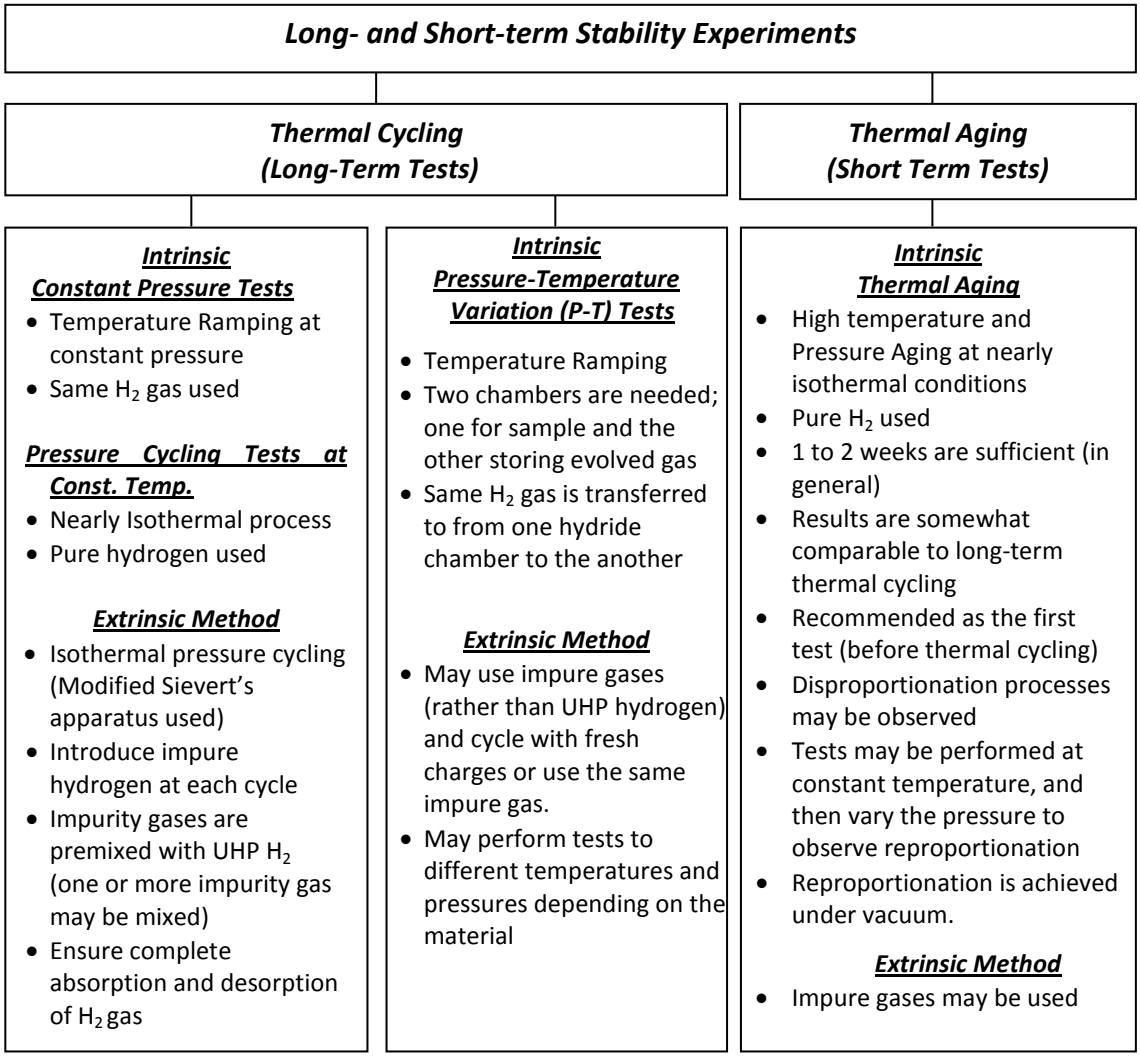

Figure 261. Chart of hydrogen storage materials stability testing methods.[352]

As shown above, cycling tests are comprised of: (a) *Thermal Cycling (constant pressure),* (b) *Pressure Cycling (constant temperature)* and (c) *Pressure-Temperature cycling,* referred to as *P-T cycling* in which both the pressure and temperature are varied, but the volume of hydrogen added to the samples is fixed. P-T tests are important, for example, in heat pump applications in which a certain volume of hydrogen gas is transferred from a high pressure hydride to a low pressure chamber, and back and forth. In cases where the fresh hydrogen needs to be recharged frequently, for example in hydrogen powered vehicles, (extrinsic) pressure cycling tests are used. In these tests one uses ultra high purity (UHP) hydrogen premixed with ppm levels of impurity gases that are generally be encountered in modern hydrogen refueling stations.

6.1 Pressure Cycling Tests

The most direct way to measure the Cycle-Life performance of hydrogen storage materials is to perform a series of full absorption and full desorption measurements with the material at one set temperature and with fixed charge and discharge pressures. For hydride systems with a plateau, the charge pressure would be set above the plateau and discharge pressure below the plateau. Such measurements can be made using either volumetric or gravimetric instruments. However, because the measurements may be performed over 10's, 100's or 1000's of cycles, instrument stability over very long periods of time is essential. For this reason, volumetric (manometric) instruments are typically used. At its most basic level, this involves a sample cell of known volume, and separate calibrated dosing volumes for absorption (smaller) and desorption (larger) with a dosing valve between the dosing volume and sample cell. The amount of hydrogen uptake or release of hydrogen is determined from the change of pressure measured upon exposing the sample to high pressure (absorption: smaller calibration volume) or low pressure (desorption: larger calibration volume).

This method has the advantage that fresh hydrogen gas is being used with each cycle, which most closely represents real world applications. However, while this relatively simple type of measurement provides a first look at the cyclic stability of reversible hydrogen storage materials, it does not necessarily simulate how a material will actually be used (for example in a hydrogen powered vehicle). Real world use in a vehicle will have many partial discharge and refills and the hydrogen release will most likely vary greatly with the demand and use of the vehicle. In other words, the material will experience dormant periods, then be heated for delivery of hydrogen with varying endothermic excursions from a steady state temperature. These delivery variations will take place over relatively long periods of time. Charging, and the associated exothermic release of heat combined with cooing are expected to occur in a matter of minutes on refilling. Real world conditions will certainly be very different than initial simplified Cycle-Life experiments based on a series of isothermal full absorption/desorption cycling measurements. The cycling conditions themselves are likely to have a very strong impact on the Cycle-Life characteristics of the material.

6.2 Pressure-Temperature Cycling Tests

Pressure-Temperature Cycle Tests are a step closer to actual application conditions. These tests are performed in the same manner as pressure cycling measurements but change the sample temperature as well as pressure on each absorption and desorption.

For absorption the charging pressure is increased and temperature decreased to conditions that would be found at a filling station. For desorption the pressure is lowered and temperature increased to onboard hydrogen delivery conditions. As with pressure cycling tests, fresh hydrogen is usually used with each cycle.

6.3 Thermal Cycling Tests

Pressure cycling, as described above, can be very time consuming and involves the consumption of large amounts of gas and potentially the change out of gas cylinders introducing the potential for unknown factors. For example, one assumes that all gas cylinders are of consistently high purity, but this is not guaranteed. Also, when a gas cylinder is removed and replaced with a new one, it is imperative that all lines, valves and pressure regulators that have been exposed to air in the process are evacuated if not at least thoroughly purged of air and impurities before continuing with the cycling experiments.

Pressure cycling also involves the functioning of mechanical devices (valves) with each cycle. While this is closer to real world applications, it may not necessarily be the most efficient or effective way to get preliminary performance data. For this reason, Cycle-Life performance is sometimes characterized by thermal cycling. The advantage of this method is in its simplicity and the (near) certainty that no gaseous impurities are introduced with the hydrogen for more than just the first charging.

The basic measurement apparatus involves one (known) volume at a known temperature connected to a sample cell of known volume and a pressure transducer to record pressure changes on absorption and desorption. The sample cell is then heated to release hydrogen and cooled to absorb hydrogen into and out of the calibration volume. The gas is never changed and there are not necessarily any dosing valve operated during the measurements. The sample is simply heated and cooled repetitively and the amount of hydrogen released and absorbed is measured with each cycle. Lambert et al. performed degradation tests on $LaNi_5$ samples micro-alloyed with different elements using such an apparatus.[353] A schematic of this apparatus is shown in Figure 262. One (heated) vessel was filled with the sample and the other was an attached vessel to receive or supply the volume of discharge or absorbed hydrogen. This device had two different calibrated reservoir vessels (75 and 500 cc). The larger vessel was used for samples with plateau pressure near 1 bar at room temperature the smaller vessel was used for sample with much higher plateau pressures. This allowed for a reasonably measureable pressure change on going from a fully hydrided to un-hydrided state on both low and high plateau pressure samples.

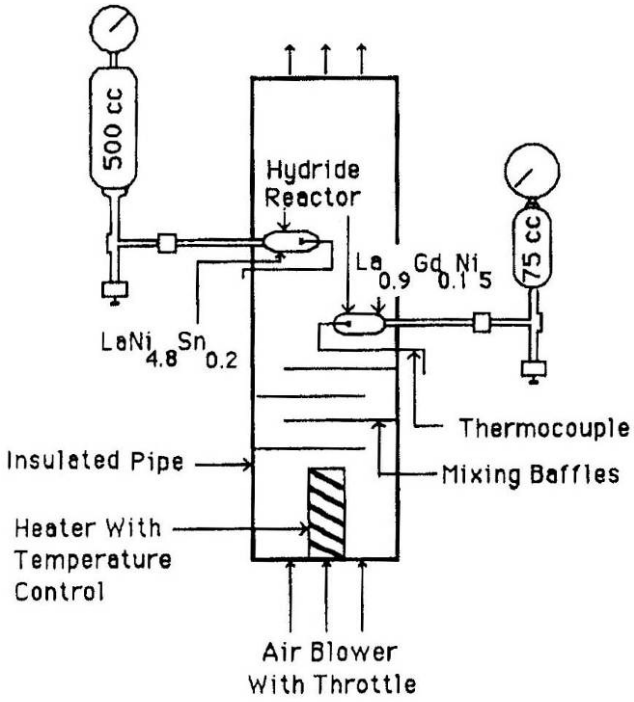

Figure 262. Thermal Cycling Apparatus: Heating cooling apparatus for long-term thermal cycling.[353]

Absent the effect of impurities, these tests are useful in examining the intrinsic degradation of the storage material due to hydrogen uptake and release as well as due to temperature changes and possibly induced thermal gradients.

6.4 Closed System vs. Fresh Gas Tests

The disadvantage of pure thermal cycling versus pressure, or pressure-temperature cycling is that in thermal cycling the same gas is always used so the effect of impurities that one finds in commercial hydrogen is not introduce in each cycle as it would be in many real applications. However, extensive closed cycling does correspond to the operation of hydrides in heat pumps and sorption cryocoolers, etc.[354] It also can be significantly different from actual applications in that the hydrogen pressure is the resulting equilibrium pressure rather than the applied pressures that would be found in

an actual application. In the case of hydrides the pressure essentially follows the van 't Hoff plot, so there is not the driving potential of a large over- or under- pressure applied to the materials. This in itself, may have a considerably different impact on internal stress, defect formation, and ultimately the Cycle-Life stability of hydrogen storage materials as compared to pressure, or pressure-temperature cycling tests.

The advantage of this method is the simplicity and reliability of the measurement system. It reduces the number of conditions, potential mechanical issues, and actual operations involve. These are usually fully automated measurements that can be performed for long periods of time without much operator intervention. An important aspect is that it also quickly supplies base-line information about a material's performance without the introduction of additional factors such as gas impurities. These measurements can then be compared with pressure, or pressure-temperature cycling results (with and without controlled impurities) to get a clearer picture of what has the strongest influence on a material's storage properties degradation.

6.5 Aging Testing

The long-term stability tests using the above cycling methods are generally very lengthy. To minimize the total experiment time and get a quick idea of property changes of hydrides one can use A*ging Tests*. These are typically short-duration tests. While in actual applications, charge/discharge cycling ideally takes place at near ambient conditions (although, perhaps up to 200°C and 100 bar H_2 pressure), in A*ging Tests*, experiments are generally performed at considerably higher pressures and temperatures to accelerate degradation processes.

Lambert et al. also performed thermal aging tests on substituted $LaNi_5$ samples.[353] About 12 grams of the intermetallic samples were ground and loaded into a sample holder. The samples were first subjected to 10 activation cycles on a standard Sievert's apparatus and then absorption and desorption PCT isotherms were taken at 25°C. The samples were then transferred to their thermal aging apparatus and heated to 180°C and a pressure of 193 bar. The samples were held in this condition for 256 hours and the pressure increase was monitored as an indication of the decrease in H/M content of the hydride. A desorption PCT was then measured after the sample had been cooled to 25°C. A schematic diagram of their apparatus is shown in Figure 263. A metal-hydride compressor with ultrapure hydrogen source was used to supply hydrogen pressures as high as 207 bar to the sample.

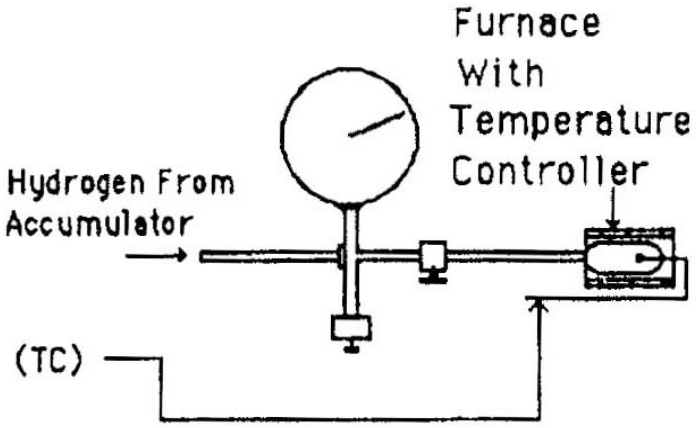

Figure 263. High pressure thermal aging apparatus.[353]

For hydrides, selection of the thermodynamic parameters for these tests depends on the nature of isotherms. It is recommended that the aging be performed in fully hydrided phase, above the plateau pressure. An age-testing pressure envelope is shown in Figure 264. A pressure concentration parabola is drawn to encompass initiation and completion of the two (α+β) phase region. In these aging tests the mid-plateau H/M is determined, and the pressure and temperature are maintained near the top of the parabola for faster response. The actual experimental conditions are generally, 10-25% lower pressures than the apex of the parabola, depending on the nature of the materials to be closer to the plateau pressure.

These tests may be classified as *Short-Duration tests*, conducted for 1 to 3 weeks to give a reasonable idea of the hydriding behavior of the alloy/compound. By comparison, detailed cycling tests may take several months. The situation will vary from alloy to alloy, especially if the alloy results in an amorphous hydride. In some important examples of such research, Aoki and Jai-Young Lee's group have reported detailed investigations of Laves-phase amorphous hydrides.[355,356,357,358] Note that it is a good practice to check the phase diagrams, if available, of the alloys being studied to be aware of any phase transitions of the parent metal/alloys, or hydride themselves that may occur under such aging conditions.

The idea of these *Short-Duration tests* is to stress the material/hydrogen sorption process in a way that extrapolates to the results that would be obtained by long-term cycling. The basic purpose is to observe if any, and to what degree, hydrogen-storage properties degradation has taken place. The process of aging is shown in Figure 264 in a schematic using a pressure-composition isotherm (left) and pressure vs. time schematic (right).

An absorption isotherm is obtained (after initial activation cycles), and the sample chamber is sealed at a temperature T_1(^oC) with β phase hydride at H/M =1. Then the sample temperature is quickly increased to a temperature,T_2, which is associated with a pressure increase (and likewise a loss of hydrogen capacity, the magnitude of which varies from alloy to alloy). After the sample achieves a temperature of T_2, the aging process starts as shown on the right in Figure 264. If the hydrogen pressure increases over time, then the H/M in the sample also decreases as a function of time. The capacity loss due to this aging process is an indicator of the degradation that might be expected from hydrogen absorption / desorption cycling of the same material.

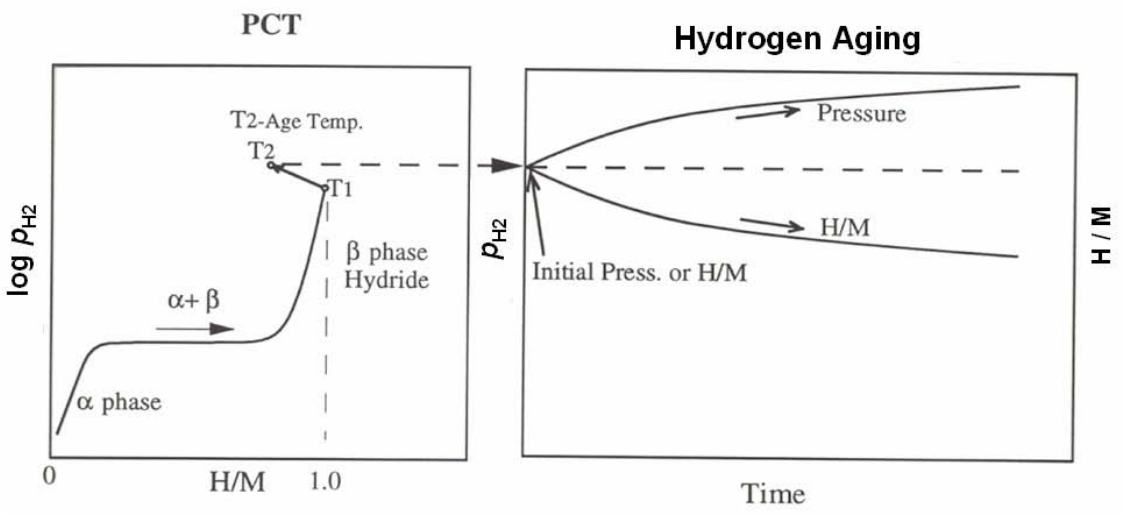

Figure 264. Thermal aging method is shown in the schematic. (Left) An isotherm is generated at a temperature T_1 until fully saturated in the β phase (above the plateau pressure). The sample holder is sealed and the sample heated to the aging temperature T_2. Once the temperature is stabilized, then sample is allowed to age for a certain period of time (Right). If there is disproportionation, then the pressure rises and H/M decreases as function of time.[352]

In general *aging* results are comparable with long-term cycling results. It is worth noting however, that isotherm results after aging tests are similar but not exactly the same as in long-term cycling tests for intermetallics, in particular for $LaNi_5$, an example of this is shown in the following section.[353] An important exception to the ability of aging tests to simulate the effects of cycling is in cases where there is compositional inhomogeneity of the starting alloys or the alloy was not properly annealed. Aging will produce different results as will later be demonstrated in the case of $LaNi_5$ micro-alloyed with Al.

In general, it is assumed that degradation due to disproportionation (the decomposition of the alloy into more stable hydrides or alloys) results from cycling alone. However, it is possible to achieve these results by simply subjecting the hydrides to static higher hydrogen pressures than the isotherm plateau pressure for a particular temperature.[359] This process is referred to as "*Thermal Aging*". Sandrock et al. showed the disproportionation of $LaNi_5H_6$ could be reversed through *Reproportionation Aging* (RPA) by holding the sample under *vacuum* for a certain period of time, and then cooling it down to room temperature. Isotherms of disproportionated and reproportionated hydrides show dramatic changes.[47] Changes in the slopes and H/M capacities allow some assessment of property changes under different conditions. They suggested that significant disproportionation occurs only if the pressure is significantly above that of the plateau pressure. In Figure 265, isotherms of $LaNi_5$ were taken after aging at 136, 61, 10, atm, and under vacuum at 180°C. It can be seen that high-pressure aging leads to sloping plateaus but when vacuum aged (annealed), one observed nearly flat plateau and properties are more or less recovered. It should also be noted that there are some reports of the restoration of hydriding properties by a different process involving cycling.[360]

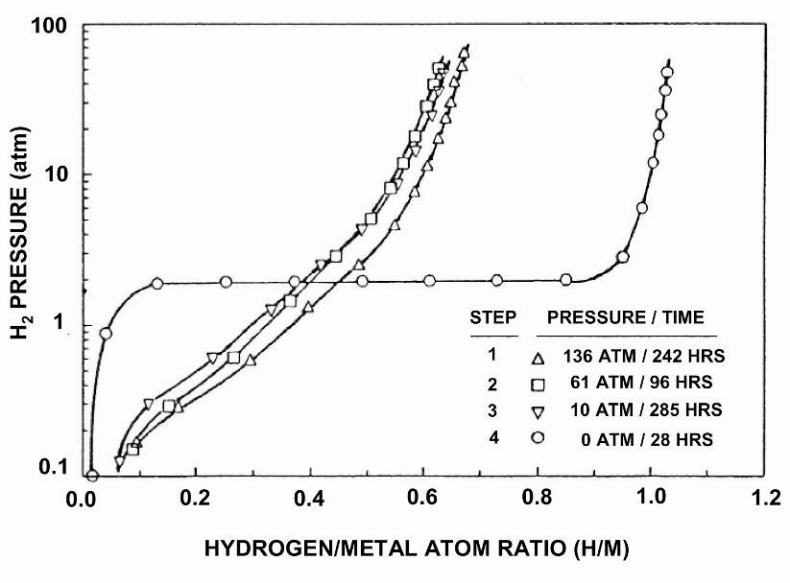

Figure 265. Isotherms of $LaNi_5$ taken at 25°C after subjecting to aging at high and low hydrogen pressures. Note that the isotherm for vacuum aged sample at 180°C is nearly (but not exactly) the same as the isotherm before aging indicating full reproportionation of the $LaNi_5$ hydride with a flat plateau after vacuum aging.[359]

In the past, cycling and aging tests were not optimized based on first using this aging/isotherm measurement approach. Pressures and temperatures were simply based on extreme conditions rather selecting the best settings based on such data to accelerate the aging process.

6.6 Intrinsic Testing of Intermetallic Hydrides (Thermal, Pressure and P-T Cycling Tests)

Intrinsic cycle testing of hydrides involves using the same gaseous hydrogen over and over again with every absorption/desorption cycle. Pure hydrogen is typically used, but it can be extended to industrial or laboratory hydrogen gas as long as the fresh gas is not added at every cycle. These types of degradation studies are carried out for alloys or intermetallic hydrides that are used for heat pumps and other applications, where the same hydrogen is recycled back and forth. Using this degradation method, one can examine the long-term intrinsic behavior of elemental, binary, ternary hydrides in the absence of any gas impurity effects.

For these tests to be valid, it is clear that the apparatus used must be completely free of leaks because the introduction of even ppm levels of impurities (air) nullifies the assumption of purely intrinsic properties. This means that all components must be able to withstand the pressure and temperature conditions of the cycle tests without leaking (i.e. through thermal expansion of seals) or out-gassing at elevated temperatures. For this reason metal-on-metal seals and hydrogen compatible metal components (i.e., constructed from 316L stainless steel) are highly recommended.

7 Matching Experimental Setup to the Measurement Purpose

The three classes of measurements, fundamental mechanisms, materials development, and system performance, require slight variation in the approach to measurements.

Studies to understand fundamental mechanisms impacting the Cycle-Life performance of materials will require extra precision and care in measurements. The main determinant is that no experimental artifact is introduced and miss-interpreted as a mechanistic effect. The advantage of the Cycle-Life measurements for fundamental studies is the repetitive nature of the cycling measurements and that generally only one sample is being studied at a time. The key to success, however, is that the cycling conditions must be identical with every cycle (absorption pressure, desorption pressure, temperature, purity of the gas, and the time or, better, the hydrogen content).

Cycle-Life Measurements from a materials discovery and development perspective will also require careful control to ensure absorption and desorption conditions are

appropriate and consistent with not only with every cycle, but also with every sample. It is essential that identical measurement conditions are always used to be able to accurately compare the long-term performance of one material from another. This includes identical temperature condition, sample sizes, identical gas purity. In addition, since more than just the cycling stability will change with modifications to a material (e.g. plateau pressure changes) it is very important to ensure that the cycling conditions are comparable between materials. For hydrides, this will most-likely require certainty of equilibrium pressures for all material and appropriate adjustments of charge and discharge pressures with respect to the equilibrium pressure.

Typically, system performance measurements will be focused on a scaled-up measurement that is large enough to accurately represent the behavior of the storage material at a full application level. Generally speaking this would be 100 gm to 1 kg of material. Such measurements will most likely concentrate on extrinsic changes in storage bed properties, rather than intrinsic Cycle-Life property changes of the storage materials. These include among other things changes with cycling of: heat transfer during hydrogen uptake and release, local temperatures within the material test bed, decrepitation and/or agglomeration of the materials, interlocking of grains and resulting forces generated with material expansion, gas channeling effects, special variations in hydrogen content, and ultimately the result of these effects on changes in capacity and rates of hydrogen sorption and desorption at a system level. Once again, initial studies designed to evaluate the impact of these issues should be performed with strictly consistent conditions with every cycle. Once system level effects are well characterized and then optimized, it would be appropriate to do system level cycling testing under variable conditions such as, for example, those found in representative vehicle drive cycle performance tests.

8 Experimental and Analysis Considerations

The typical approach in hydrogen storage research is to identify promising new materials based on high hydrogen capacity and then work to improve their kinetic and thermodynamic properties. In general, the last step has been to evaluate and improve the cyclability of the materials. Ultimately, a material with great hydrogen storage capacity, kinetics and thermodynamics may be of little use if these properties are not maintained over tens, hundreds or even thousands of cycles. For this reason, accurate Cycle-Life measurements are extremely important for the development of practical hydrogen storage materials. The following are some considerations and caveats that should be considered when making Cycle-Life measurements.

8.1 Pretreatment / Activation

Hydrogen storage materials, in particular, physisorption storage materials almost always require a pretreatment process to prepare the samples for optimal performance in Cycle-Life testing. For physisorption materials, this generally means baking out the sample at a specific temperature for a minimum of several hours to a day or more under moderately high vacuum. The bake-out procedure will depend on the material being studied. For example most carbon-based materials can withstand relatively high temperatures (300°C or more), however, some MOFs will decompose at these temperatures. Preliminary examination (e.g., XRD, IR, microscopy….) of samples before and after a bake out procedure is vital to ensure that the bake-out conditions are sufficient to remove residual contaminants and that the samples are not damaged by the bake-out conditions. Care must always be taken after performing a bake-out to not expose the sample to air or other contaminants, before preliminary examinations or cycling measurements.

Activation is the process of the initial cycling of a material to reach the point of steady-state hydrogen uptake and release behavior. It is important to properly activate samples to be able to study their long-term Cycle-Life performance. Activation is often required in hydride hydrogen storage materials.

For classic hydrides, the activation process involves the initial decrepitation and potentially surface segregation of the alloy and complete hydriding of all portions of the sample. It is sometimes necessary to heat the alloy to elevated temperatures (up to 100°C above the desired Cycle-Life measurement temperature) and expose the sample to hydrogen at high pressure. For example, depending on the preparation and degree of exposure to air $LaNi_5$ samples may will not completely hydride without performing a set of charge (100 bar) and discharge (rough vacuum) at 100°C.

Initial cycling may involve other mechanisms than decrepitation or surface segregation to completely activate hydrogen storage materials. An example of such an activation process in cycling measurements on Sodium Alanate ($NaAlH_4$) is shown in Figure 266.[361] In this interesting case of non-reactive (TiO_2) doping, the desorption rates were found to be comparable with direct doping of 1 mol% $TiCl_3$. The advantage of using nanoparticles TiO_2 is that there is no capacity loss due to the Na-halide reaction (forming NaCl and excess Al) found when doping with $TiCl_3$. The measurement points out the extreme effect of activation on the measured desorption capacity. Had the measurement been stopped after the first cycle or two, the material may have been disregarded as having very little hydrogen storage capacity. On-the-other-hand, had long-term cycling been

done without recording data in the first 20 cycles the activation process would have been overlooked. In this case, it is believed that the activation properties have something to do with increasing the dispersion or reduction of the TiO_2. Such knowledge is key in understanding the Ti-enhanced hydriding properties of the alanates and methods to improve introduction of the Ti-dopants into the materials.

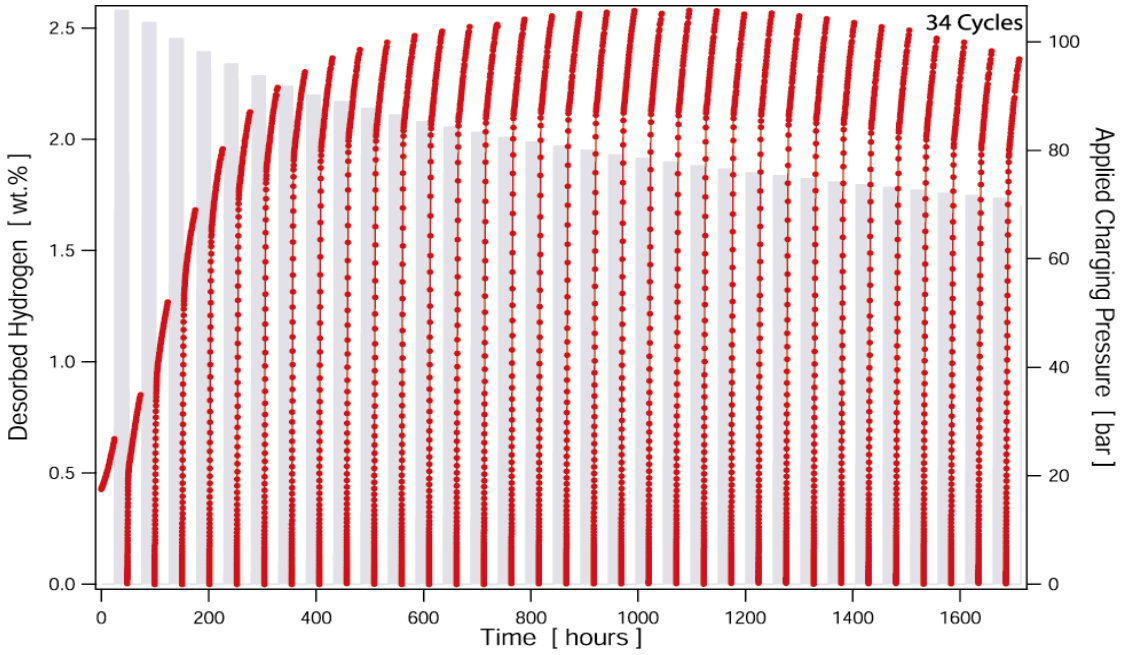

Figure 266. Hydrogen cycling of $NaAlH_4$ (NaH + Al starting material) doped with 10 mol% of TiO_2 nanoparticles. An activation process is observed in the first 20 cycles. Red: hydrogen desorption capacity, Gray: hydrogen charging pressure at each cycle.

8.2 Preferred Experimental Procedures

The following is a few suggestions about specific experimental considerations that are recommended to help improve the reliability of Cycle-Life measurements.

8.2.1 Pressure-Temperature Cycling

1. Before starting cycling one should measure isotherms to define the pressure and temperature range that are optimal for cycling.

2. In addition, from the time data of the isotherms or individual kinetics measurements, kinetic data should be extracted and reviewed particularly near the full capacity region. This will provide an idea of how many hours it takes to absorb or desorbs the hydrogen at a particular temperature. It is suggested that majority of the cycling should be performed at the temperature at which an optimized isotherm is obtained; that is the temperature at which a complete equilibrium isotherm can be collected in a reasonable amount of time for convenience. Such kinetic data should be taken as a reference to determine time and temperature for the cycling experiments.

3. In some case where the times are long for hydriding and dehydriding, it is suggested that one does partial hydriding. In this case, the results may not be indicative of the optimal performance of the material itself. However, when one considers the typical real-world application of hydrogen-powered transportation, a vehicle will be filled with hydrogen at a refilling station where the time to fill is limited. Therefore, such curtailed Cycle-Life results are still meaningful even when kinetics is slow. At issue is that if one attempts Cycle-Life measurements that go to near completion at each cycle the experimental time for a reasonably representative number of cycles will be prohibitively long and may take years to complete. So, one must balance an acceptable level of accuracy with practical measurement times. What is critical is that these issues and experimental conditions are well documented in the presentation of results.

4. The above consideration with respect to kinetic effects is overcome in large part by performing full (near equilibrium) isotherm measurements at several points during the Cycle-Life experiments. These complete isotherms will provide a lot more detailed and accurate performance properties of the materials than simple capacity versus cycle plots.

5. Another factor to take into account is the amount of material used for cycling; it should be small enough to avoid large thermal excursions such that even the materials with slow kinetics can be tailored for the simulation experiment. And large enough to provide accurate hydrogen uptake and release data. Depending on the density of the material; 1 to 10 gram sample sizes are recommended.

8.2.2 Thermal Aging

1. Thermal aging should be performed near the critical temperature that is obtained from isotherm data at various temperatures. This is perhaps the fastest method to perform aging experiments.
2. As with other types of cycling experiments, it is highly recommended to perform full (near equilibrium) isotherm measurements at several points during the thermal aging experiments (or at a minimum; before and after thermal aging). These complete isotherms will provide a lot more detailed and accurate performance properties of the materials than simple capacity versus cycle plots.
3. While it will be shown below that thermal aging is a good (and fast) substitute for certain metal hydrides, it may not be appropriate for other materials. Therefore, at least one set (but preferably several sets) of comparisons measurements (P-T cycling and thermal aging) should be done on a representative sample to ensure that thermal aging approach is appropriate.

8.3 Impact of Cycle Testing Parameters

When making Cycle-Life experiments, one has to choose a set of conditions or parameters within which the cycles will be performed. It is vital that the results are interpreted within the context of the conditions of the experiments. For example, in doing automated cycling test, a condition must be met that switches the measurement from absorption to desorption and again back to absorption portions of each cycle. Typically, the parameter that is used is time. That is an absorption will be performed for x number of minutes or hours and the subsequent desorption will be for y minutes or hours (not necessarily the same amount of time). Data should then be considered within the context of this parametric limit. Since the limit parameter is time, then it is important to evaluate time-dependent properties such as the rates of absorption or desorption. This is particularly true for materials that have slow kinetics and may or may not reach true equilibrium conditions within a fixed amount of time.

Reversible Li-amides provide a good example. With respect to amides for hydrogen storage, the initial publication on the reversible release and uptake of hydrogen involving Li-amide, -imide, -hydride, and -nitride (Equation 244) opened up a whole new class of light-weight materials for hydrogen storage.[362]

Equation 244 $\mathbf{LiNH_2 + 2LiH \Leftrightarrow Li_2NH + LiH + H_2 \Leftrightarrow Li_3N + 2H_2}$

PCT absorption and desorption isotherm Measurements on the first portion of the reaction (left part of Equation 244) were performed on these materials over several cycles ranging in temperatures between 120°C and 160°C.[363] These measurements demonstrated that these are still relatively high-temperature hydrides (Figure 267).

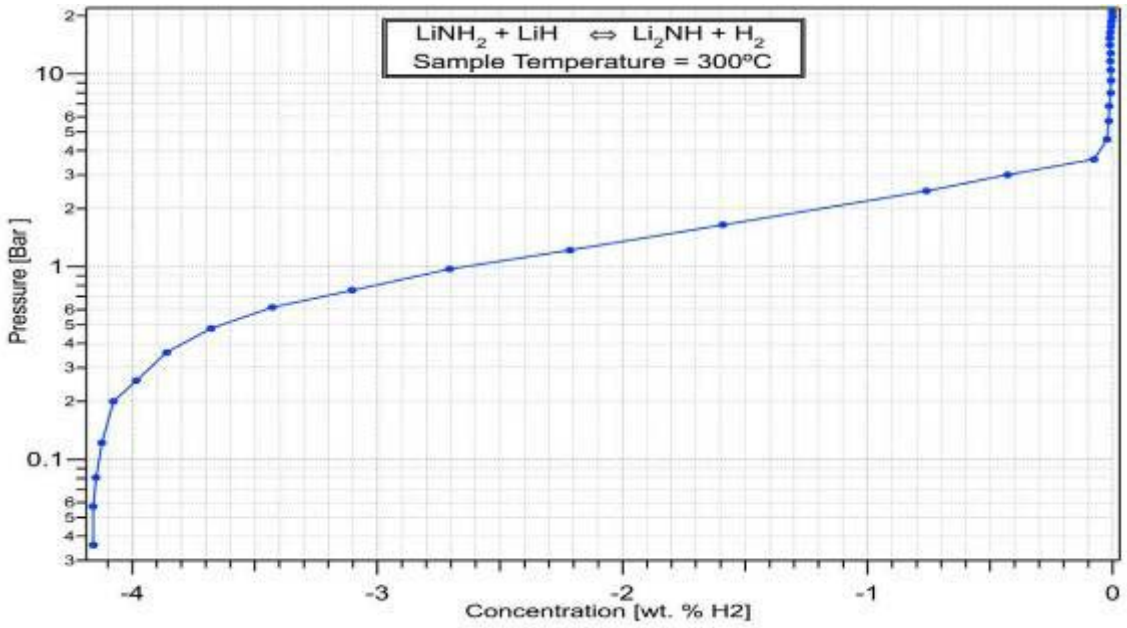

Figure 267. PCT measurement of 11th hydrogen desorption cycle of $LiNH_2$ with LiH after partial absorption.[363]

Pressure versus time data collected during PCT dosing measurements of these materials also showed that sorption kinetics are slow in these solid-phase reactions (Figure 268).

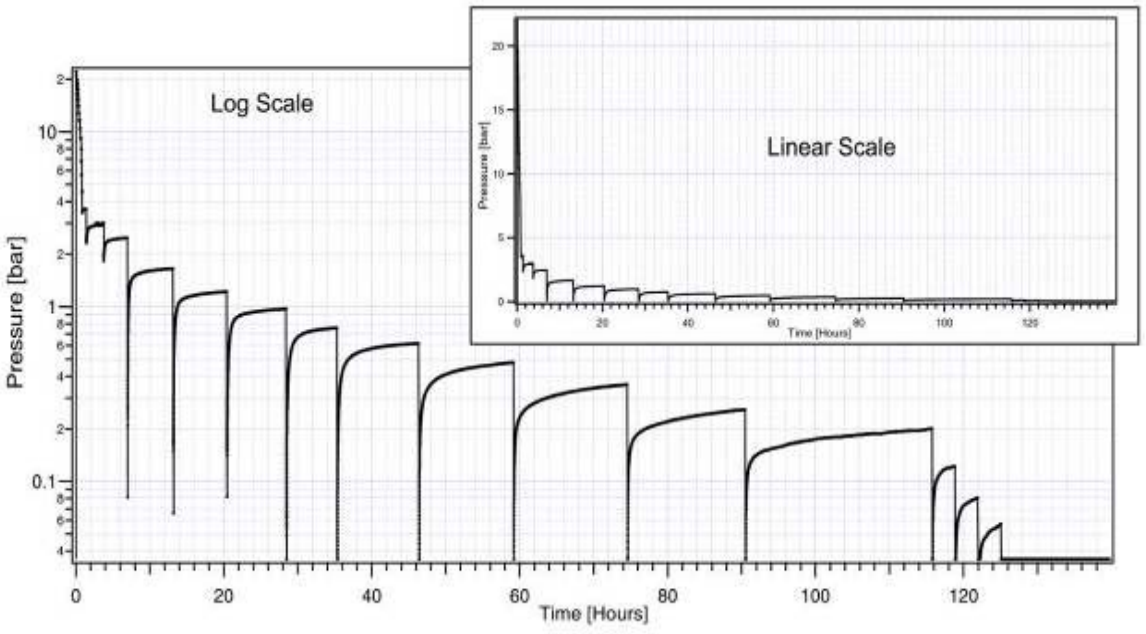

Figure 268. Approach to equilibrium during PCT measurements (previous figure) of hydrogen desorption from the reaction of $LiNH_2$ with LiH.[363]

The development of amides for hydrogen storage was followed by Li/Mg-based amides that were reversible at lower temperatures.[364,365] Advances on these materials focused not only on the fundamental processes involved in hydrogen uptake and release but also on practical investigations of the hydrogen storage properties of these materials. In particular, Cycle-Life measurements were carried out to determine the performance of these materials over long-term hydrogen cycling.[363] The starting material was $LiNH_2$ and MgH_2 mechanically milled together in a 2:1 ratio, in a tungsten-carbide vessel under argon for 2 hours. Complete hydrogen absorption and desorption measurements were made on an automated volumetric apparatus with the sample held at 200°C (Figure 269). Absorptions were at constant pressures of 83 and 103 bar. Desorptions were made to a calibrated 2 liter vessel at 0.5 bar. Only desorption concentrations were measured. Each individual desorption measurement lasted 15 hours. The absorption measurements were initially set to 30 hours then reduced to 15 hours. However, the capacity dropped off indicating that hydrogen absorption was not complete in the shorter time period, so the absorption times were again increased to 30 hours. The initial tests on Li-Mg-N-H system showed relatively stable cycling properties at 200°C: 0.1% capacity loss per cycle - estimate 500 cycles to 50% capacity loss.

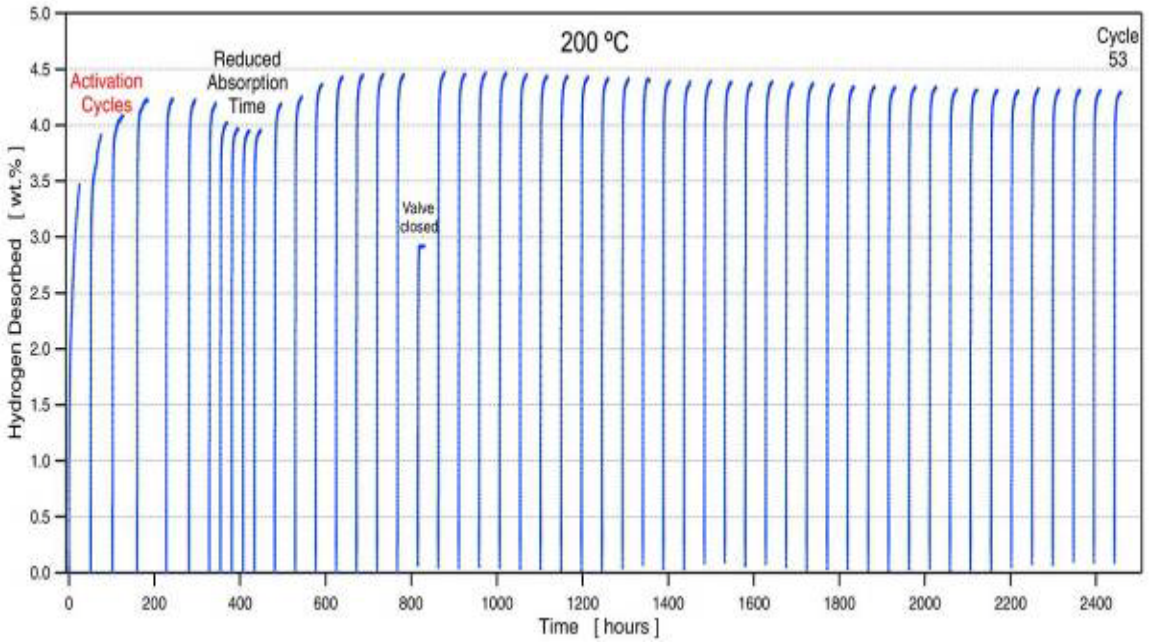

Figure 269. Reversible hydrogen desorption capacity with cycling of Li-Mg-N-H (charging constant pressure 69-83 bar, discharge to 0.5 bar, 200°C).[363]

An individual cycle shown in Figure 270 indicates the desorption kinetics were reasonable at 200°C for the first portion of the hydrogen release (1.5 hours for 4 wt.% hydrogen release). However, the kinetics taper off to a slower rate at later time.

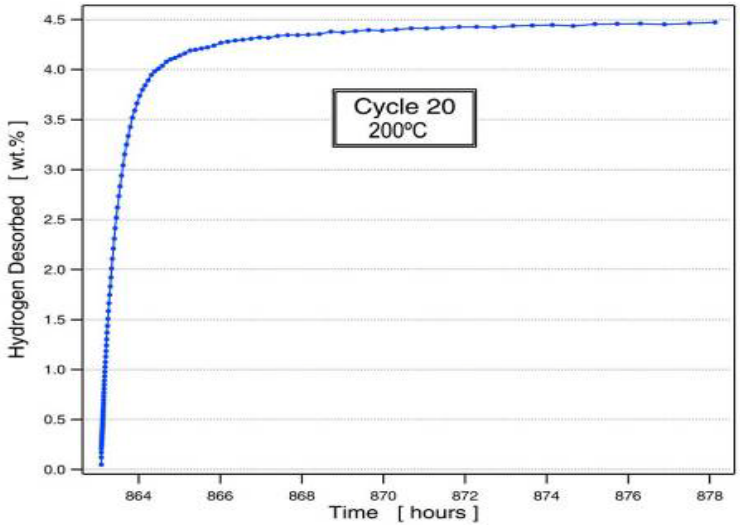

Figure 270. Hydrogen desorption cycle no. 20 for the Li-Mg-N-H system (charging constant pressure ~100 bar, discharge to 0.5 bar , 200°C).[363]

However, a comparison of average desorption rates for the Li-Mg-N-H system (Figure 271) show some degradation of desorption rates with cycling (10-15% over 53 cycles).

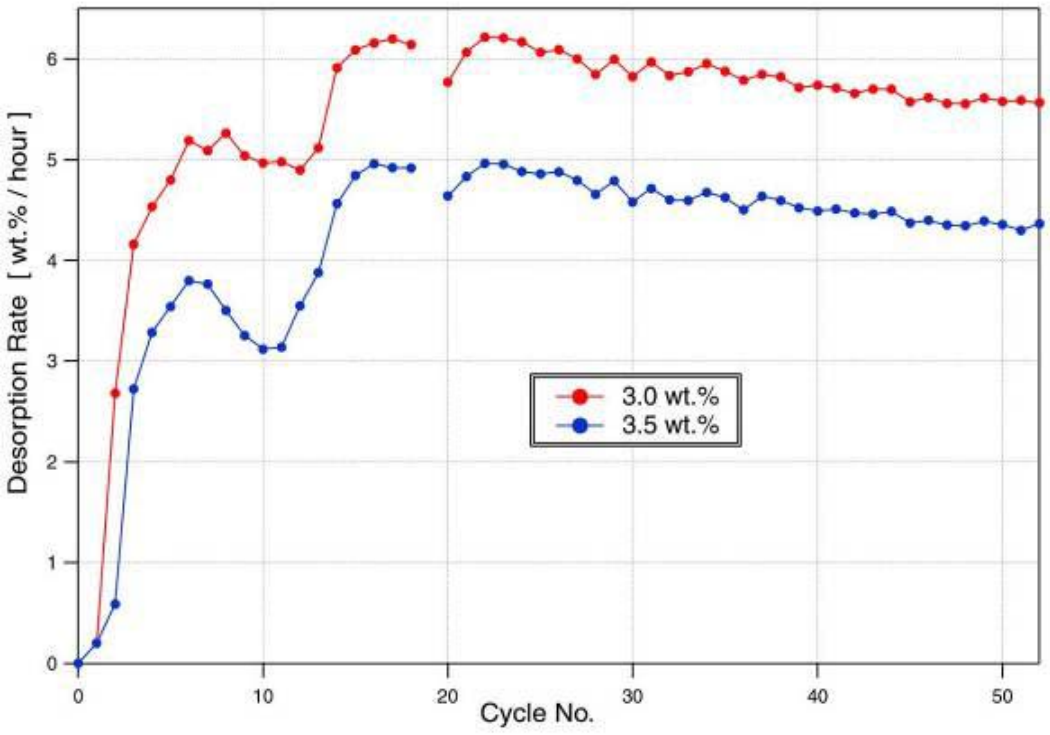

Figure 271. Average hydrogen desorption rate to 3.0 and 3.5 wt.% for the Li-Mg-N-H system (charging constant pressure ~100 bar, discharge to 0.5 bar , 200°C).[363]

It is probable that absorption rates were also declining with cycling. For this reason, it is important to understand that the capacity fade observed with fixed-time step cycling may in fact be due to degradation in the absorption and desorption rates rather than a degradation of the intrinsic hydrogen capacity of the material. That is, less and less hydrogen was able to be absorbed and desorbed within a fixed period of time.

More recent cycling measurements were carried out on the same type of material for 270 cycles.[366] The cycling process again used fixed-cycle time. The results (Figure 272) showed a similar drop in capacity (0.09% per cycle). However, only a third of this loss could be accounted for by the evolution of NH_3 (resulting in a loss of nitrogen and thus capacity from the system). Test of exposure of these materials to humid air also did not appear to have a significant impact on performance.

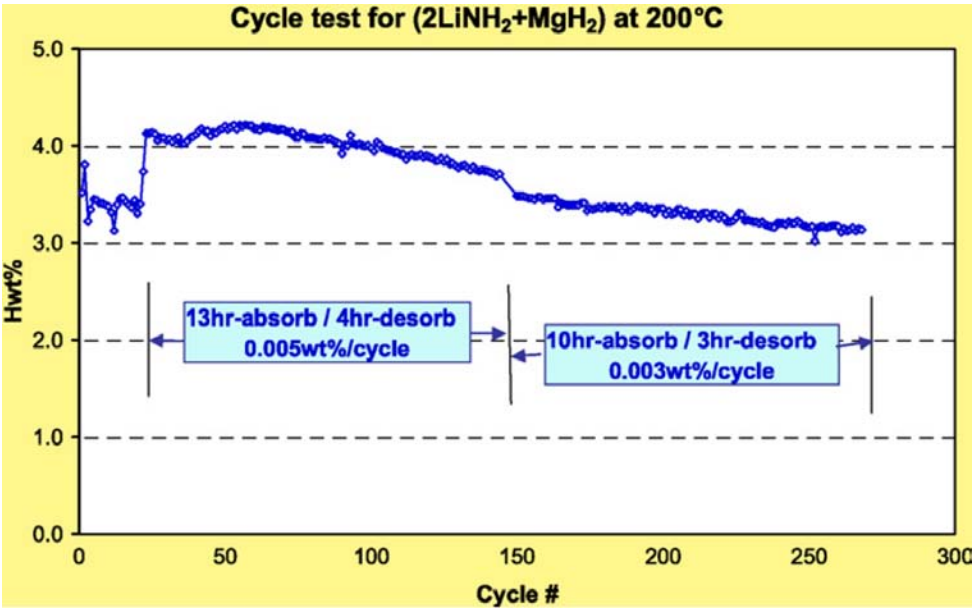

Figure 272. ($2LiNH_2 + MgH_2$) cycle test at 200 ◦C. The duration of sorption cycles and capacity loss for each cycle are marked.[366]

The results of this study appear to confirm the above observation that when sorption rates degrade with cycling, then a fixed-cycle time leads to a loss of capacity due to increasingly incomplete sorption rather than an intrinsic loss of materials storage capacity.

In Cycle-Life measurements, care should be taken to evaluate all of the measurement conditions to avoid ascribing such an artifact of the experimental parameter settings to

one material property (e.g. loss of capacity) when it may be due to another material property (reduction in kinetics).

The ideal situation in such cycling measurements would be to be able to wait until a true (or close to true) equilibrium condition is achieved in each cycle. But with materials such as these amides, that have relatively poor kinetics, such a measurement would take an unreasonably long amount of time.

A good approach would be to make a very long term absorption and desorption measurement near the beginning of cycling (cycle 10 or so) and at the completion of cycling and to compare the capacity and rates of these initial and final measurements.

Even better would be to perform a complete set of absorption and desorption PCT isotherm measurements near the beginning of cycling (cycle 10 or so) and at the completion of cycling. Then to compare plateau capacities (and shape) at the beginning and after many cycles.

9 Examples Cycle-Life Measurements

9.1 Examples of Intrinsic Cycling Measurements

9.1.1 Pressure Cycling of Classic Hydrides

$LaNi_5H_6$ is the classic example of a room-temperature ambient-pressure reversible hydride. Its discovery has lead to important commercial applications, most notably the billion-dollar Nickel-Metal-Hydride rechargeable battery industry. For this and other applications the cyclic stability of hydride is critical for commercial viability. For this reason, the Cycle-Life properties of $LaNi_5$ and alloys of this intermetallic compound have been some of the most extensively studied. In the following we present some representative cycling studies that have been performed on $LaNi_5$.

To start with, a classic example of a room temperature isotherm of $LaNi_5$ measured by Lundin and Lynch is shown in Figure 273(a).[367,368] They also obtained high temperature isotherms and derived the van 't Hoff Plots for both absorption and desorption Figure 273(b); both the absorption and desorption plots are shown. Also an inset of the crystal structure of $LaNi_5$ P6/mmm and the 5-site model of the $LaNi_5H_6$ are included in Figure 273(a), taken from Percheron-Guegan, Lartigue, and Achard.[369,370]

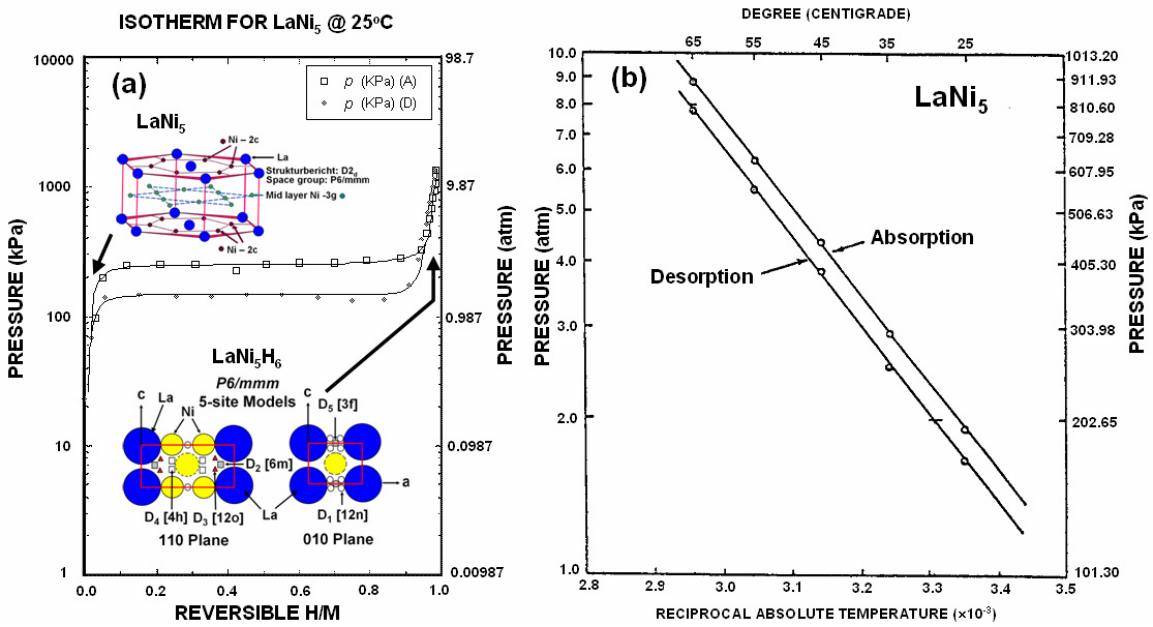

Figure 273. (a) Room temperature isotherm of the classic $LaNi_5$, (b) van 't Hoff plot of $LaNi_5$ obtained from the isotherms taken at many temperatures[367,368] (a-bottom) Hexagonal Structure of $LaNi_5H_6$.[369,370]

Various Cycle-Life tests on $LaNi_5$ intermetallic hydrides began in the 1980's and were typically volumetric pressure-cycling measurements. Cycling tests for durability of the were conducted by Cohen et al., in 1980, who reported 75% of the hydrides disproportioned to LaH_2 after 1500 cycles.[371,372] In 1983, Goodell and Rudman, reported loss of 27% after 1500 thermal cycles on $LaNi_5$, and they reported about 75% conversion to LaH_2 due to disproportionation in these intrinsic tests.[123] Also in 1983, Gamo et al. reported 60% loss of capacity after 3500 pressure cycles (with 99.9% purity hydrogen introduced every cycle).[373] Later, J.Y. Lee et al. showed a loss of 62% of the hydrogen capacity in $LaNi_5$ after 3500 cycles.[374] Unlike all of these other volumetric (manometric) measurements, in 1989, Benham and Ross performed Cycle-Life measurements on $LaNi_5$ using a gravimetric measurement method.[375] Uchida reported x-ray line profile analyses after 3300 hydriding/dehydriding on $LaNi_5$ hydride to study particles and other structural details. Josephy et al.[376] performed line broadening analyses on $LaNi_5$ hydrides that were cycled 45,000 times and reported little change in microstrain before and after cycling; they attributed the reported loss of capacity due extrinsic deterioration by oxygen of the particles.[377] This was followed by a study by Chandra and Lynch in 1989, on the detailed thermodynamic and structural tests on four different variants of $LaNi_{x-5}M_x$.[378]

9.1.2 Pressure Cycling of Physisorption Materials

The cycling durability of physisorption materials is equally important as that of hydrides, but few studies have been performed on these materials. In much the same vein as hydrides, physisorption materials might be subject to both intrinsic (structural degradation) and extrinsic (reduced capacity due to impurities in the hydrogen) effects. Possible long-term degradation requires extensive hydrogen cycling studies on physisorption materials under a variety of conditions, including exposure to impurities in the gas stream.

One example of physisorption P/T cycling is a set of high-pressure absorption/ desorption measurements performed at 77K on the MOF $Zn(bdc)(ted)_{0.5}$.[379] For cycle capacity, an adsorption/desorption isotherm was measured up to pressures of 40 bar. The highest capacity point (saturation) in the every adsorption isotherm was taken to represent each cycle. No out-gassing was conducted between the cycles. The initial hydrogen uptake value of this material was 4.00 wt.%. A separate measurement on the same material confirmed good reproducibility of the measurement with a capacity of 4.06 wt.%. No severe capacity drop was observed up to 30 cycles and 98% of initial capacity was maintained.

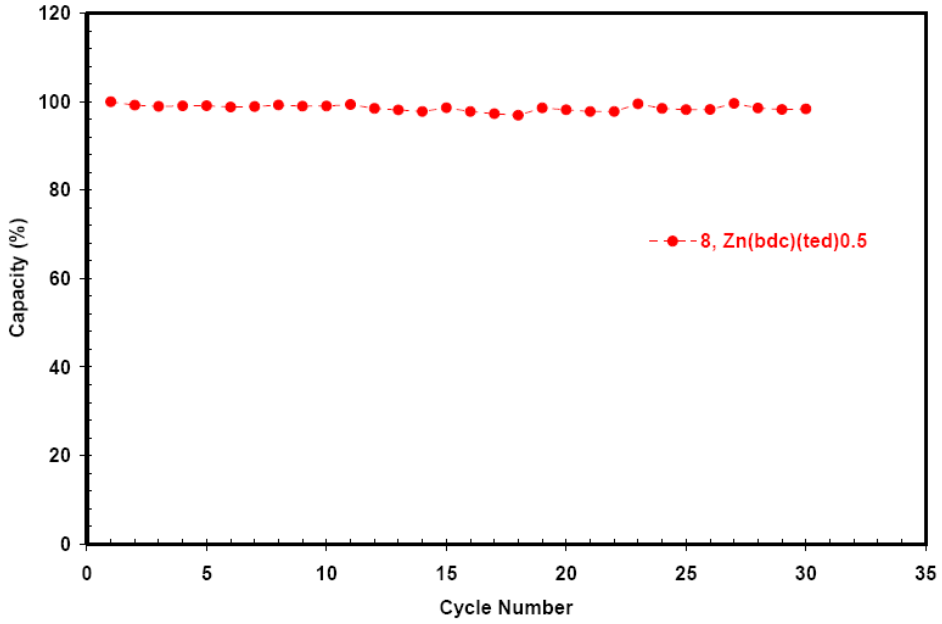

Figure 274. High pressure hydrogen physisorption capacity on MOF $Zn(bdc)(ted)_{0.5}$ at 77 K as a function of the number of adsorption/desorption cycles. Each cycle is a set of adsorption-desorption isotherm. Each point represent maximum uptake (% of full capacity) of the associated adsorption isotherm.[379]

9.1.3 Thermal Cycling of Classic Hydrides

One mechanism for the loss in capacity with cycling is the partial disproportionation of the intermetallic or alloy into its elemental components with each cycle. Disproportionation of intermetallics is indicated by the changes in the shape of the isotherms and associated loss in the hydrogen capacity. This phenomenon may be attributed to short range diffusion of the atoms, increased thermodynamic stability of one of the elemental species to form an elemental hydride, and dissociation of the non-hydride forming second atom as a metal. It is not always the case that binary intermetallic hydrides dissociate into elemental hydrides. Many variants of AB_5 and AB alloys that have been used for hydrogen storage applications over the years (mainly $LaNi_5$ and FeTi type hydrides) do exhibit a propensity for disproportionation. For example, at the start $LaNi_5+3H_2 \rightarrow LaNi_5H_6$, but after cycling (or also aging at high pressures), disproportionation may occur according to the equation: $LaNi_5H_6 \rightarrow LaH_2+ 5Ni +2H_2$.

In 1992, Lambert et al. performed degradation tests on $LaNi_5$ samples micro-alloyed with different elements.[353] In these experiments, Ni was substituted by In or Sn, or La was substituted by Gd. *P-T type intrinsic* thermal *cycling tests* were performed on $LaNi_{5.2}$, $LaNi_{4.8}In_{0.2}$, $LaNi_{4.8}Sn_{0.2}$ and $La_{0.9}Gd_{0.1}Ni_5$. A simple closed system device consisting of two vessels was used to make the measurements (See Figure 262 above). In these cycling tests the sample was heated from 24°C to 125°C, with corresponding nominal pressures of 1.6 and 5.03 atmospheres during the heating cycle and then the reverse upon cooling. Each complete cycle lasted one hour.

A typical *intrinsic P-T thermal cycle* obtained from $LaNi_{4.8}Sn_{0.2}$ hydride is presented in Figure 275. This dynamic plot of log pressure vs. inverse temperature (in time) has the same axis as a van 't Hoff plot and, therefore may be plotted against iso-concentration equilibrium van 't Hoff data if available.

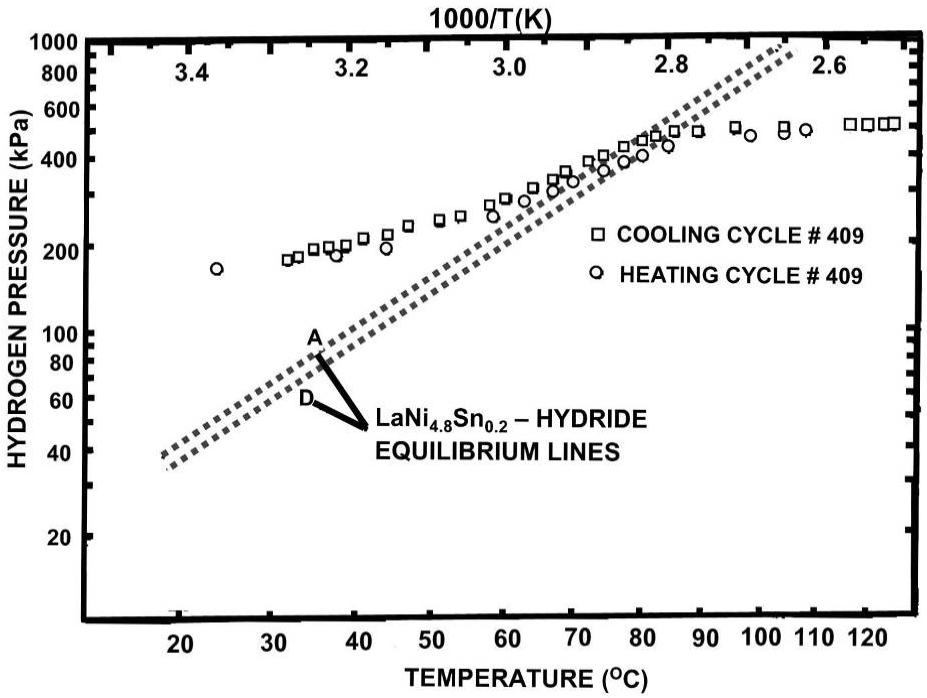

Figure 275. A typical cycle for $LaNi_{4.8}Sn_{0.2}$ by heating in closed system from room temperature to 125°C and cycled between saturated conditions to depleted conditions. This is shown as high pressures below equilibrium (saturated) and low pressures above equilibrium (depleted) where lines A and B are the absorption – desorption equilibrium pressures respectively.[353]

In this extensive study by Lambert et al., several thousand hydrogen sorption cycles were performed on several classic hydrides for prolonged time using the test method described in detail in their paper.[353] One example of these cycling measurements is shown in Figure 276 for an off-stoichiometric alloy ($LaNi_{5.2}$).[353] Isotherms were taken (by removing the sample from the cycling apparatus and then attaching it to the Sievert's apparatus. This was done after an initial 10 activation cycles, as well as after 1500 and 10000 P-T cycles. It can be seen that there is a significant loss of hydrogen capacity after many cycles and the plateau eventually exhibits a severe slope.

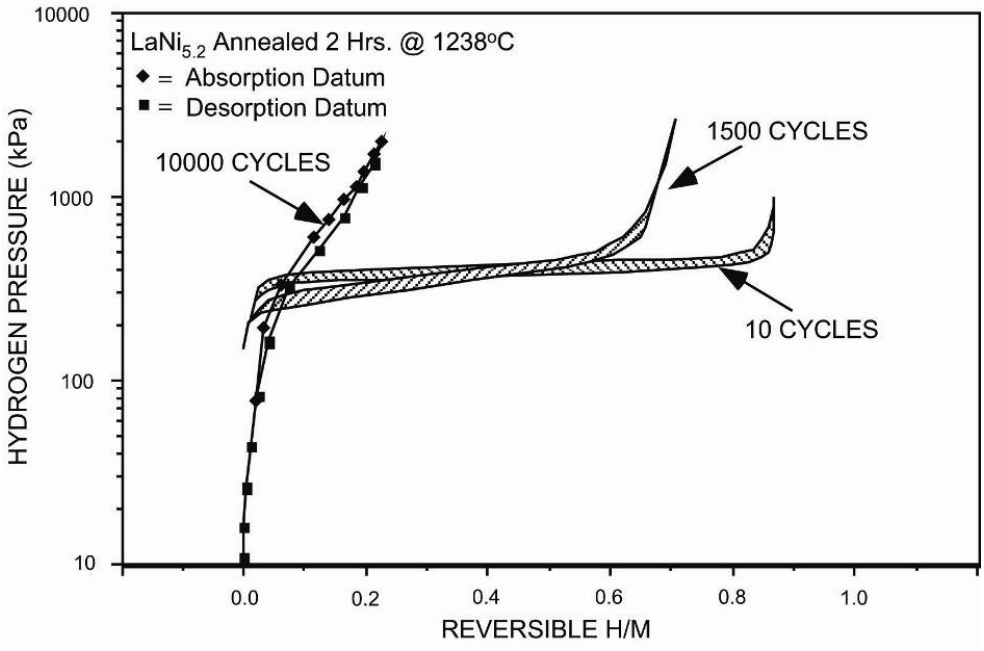

Figure 276. Isotherm of $LaNi_{5.2}$ taken at 25°C after intrinsic P-T cycling for 10 (activation), 1500, 10,000 times showing severe degradation of this hydride.[353]

By comparison, similar *intrinsically P-T* cycling measurements on a Sn-substituted alloy ($LaNi_{4.8}Sn_{0.2}$) showed very little loss in hydrogen capacity, even after 10,000 cycles. In addition, the pressure plateau does not develop a significant slope (Figure 277a). Whereas, a La-substituted alloy, $La_{0.9}Gd_{0.1}Ni_5$, showed a severe loss of capacity and sloping plateau after the same number of cycles (Figure 277b). Further details on x-ray diffraction patterns, domain size determination, microstrain, before and after thermal cycling for both the hydrides can be found in Lambert et al.[353] and Chandra et al.[378]

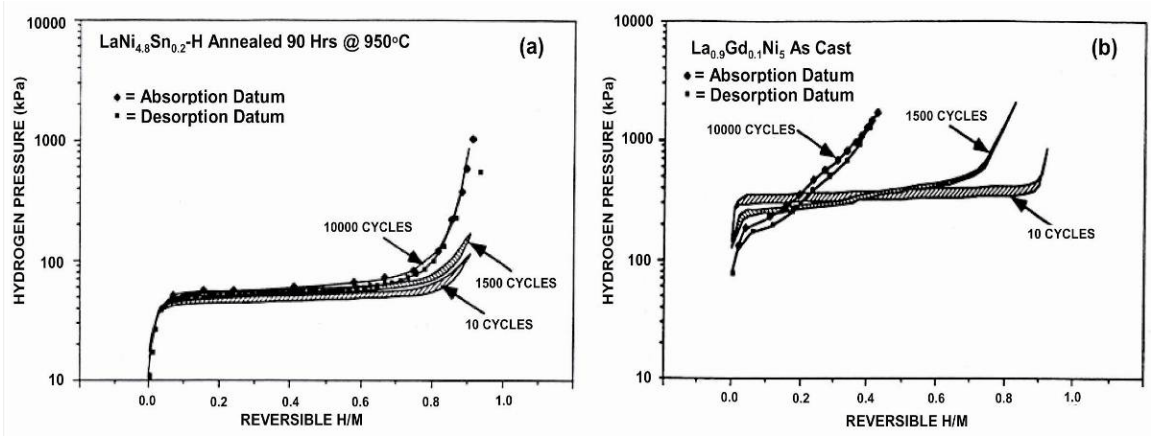

Figure 277. Isotherms of (a) $LaNi_{0.8}Sn_{0.2}$ and (b) $La_{0.9}Gd_{0.1}Ni_5$ taken at 25°C, before and after P-T intrinsic cycling for 1500 and 10,000 times showing virtually no loss in hydrogen capacity in the case of $LaNi_{0.8}Sn_{0.2}$, and extensive loss for $La_{0.9}Gd_{0.1}Ni_5$ after prolonged cycling.[353]

The dramatic degradation in storage properties was interpreted as being caused by the disproportionation of $La_{0.9}Gd_{0.1}Ni_5$ due to substitution of Gd for La. However, in the context of making Cycle-Life measurements, it should be noted that, in these experiments, the cycling pressure for $LaNi_{4.8}Sn_{0.2}$ was lower than those of the $La_{0.9}Gd_{0.1}Ni_5$. From an experimental point of view, it may be possible that higher maximum cycling pressures (as compared to $LaNi_{4.8}Sn_{0.2}$) may have actually had a strong impact on the stability of the alloy. Such effects have been demonstrated by Sandrock et al. as was shown earlier (see Figure 265).[359]

In contrast, Dantzer showed no loss of hydrogen capacity in $LaNi_5H_6$ after P-T intrinsic cycling between 25° and 80°C.[380] The take-home-message from these examples is that a detailed knowledge of long-term cycling and/or thermal aging behavior of hydrides is absolutely critical for the develop practical solid-state hydrogen storage systems.

9.1.4 Thermal Aging Tests on Classic Hydrides

The *"Aging Tests"* tests are relatively fast for AB_5 hydrides. They can be used to quickly give a rough idea of the changed thermodynamic properties that would be expected from long term cycling.

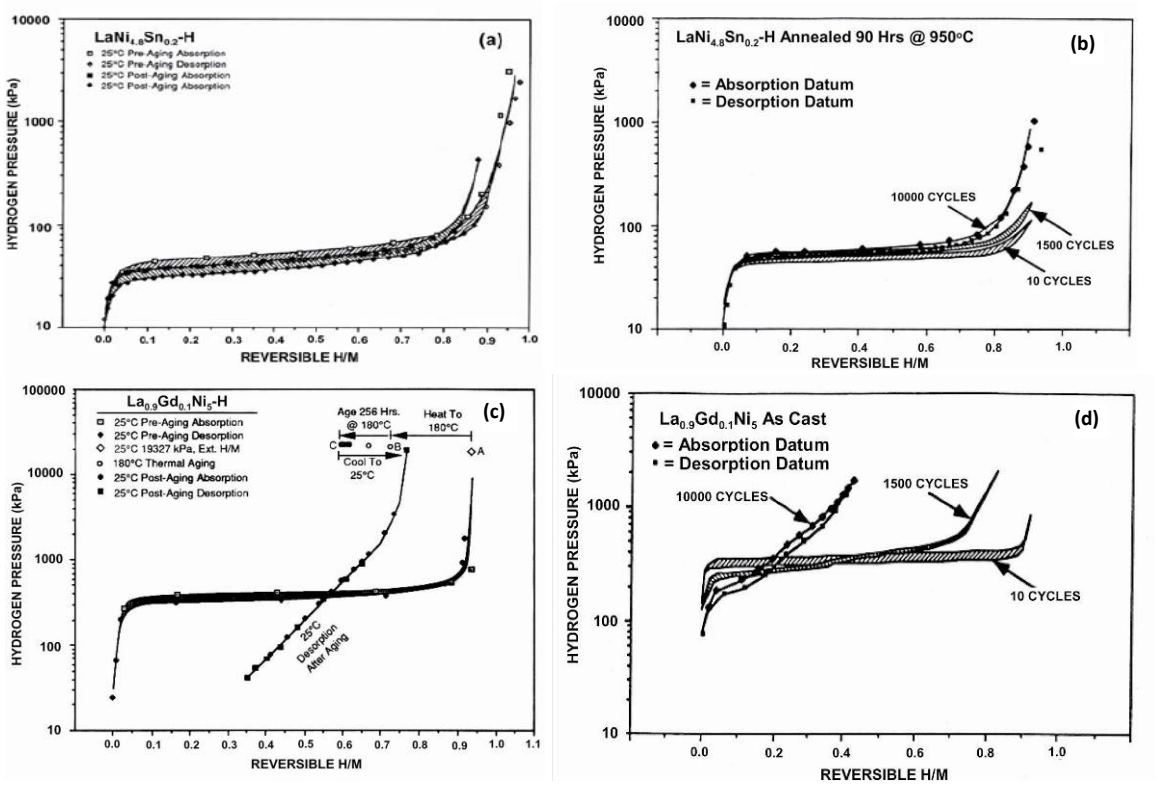

Figure 278. Comparison of $LaNi_{0.8}Sn_{0.2}$ isotherms after: (a) thermal cycling and (b) thermal aging (180°C at 29.6 atm) experiments. Comparison of $La_{0.9}Gd_{0.1}Ni_5$ isotherms after: (c) thermal cycling and (d) thermal aging (180°C at 190.7 atm) experiments. The time taken for cycling several months, where as time taken for aging is ~2 weeks), yet the results are nearly the same. Note that the cycling/aging apparatuses are different form the Sievert's apparatus used to obtain the isotherms.[353]

As an example, aging tests were performed on $LaNi_{4.8}Sn_{0.2,}$ using a sample from the same batch as used for the cycling results shown in Figure 277(a).[353] The thermal aging process was performed using the method and apparatus described above (section 6.5). Isotherms were taken at 25°C, before and after the intrinsic thermal aging process. The results, as shown in Figure 278(a) are similar to those of intrinsic P-T cycling Figure 278(b). Thermally aged $La_{0.9}Gd_{0.1}Ni_5$ hydride also exhibited somewhat similar isotherms to those obtained after intrinsic P-T cycling (Figure 278(c and d)).

9.2 Examples of Extrinsic Cycling Measurements

An example of an *extrinsic pressure cycling* measurement taken at the University of Nevada, Reno is shown in Figure 279(a). This figure shows 250 *extrinsic pressure cycles* (charging with fresh gas with each cycle) performed on a complex hydride (between $Li_2NH \Leftrightarrow LiNH_2$). The hydrogen gas was used was a special mixture of UHP hydrogen containing 100 ppm CH_4 impurity. Figure 279(b) shows one complete hydriding and dehydriding cycle. Hydrogen gas desorption occurred from point A to B performed by active vacuum pumping. The measurement included a check for complete transformation of the $LiNH_2$ phase to Li_2NH (shown in the expanded view of Figure 279 (c)). This was done by closing the vacuum and measuring any residual increase in the sample chamber pressure. If a certain level of residual pressure was reached, the sample was then pumped on for another fixed period of time. This process continued until pre-determined lower level of residual pressure was achieved. After this the next hydrogenation cycle began as shown in Figure 279 (b).

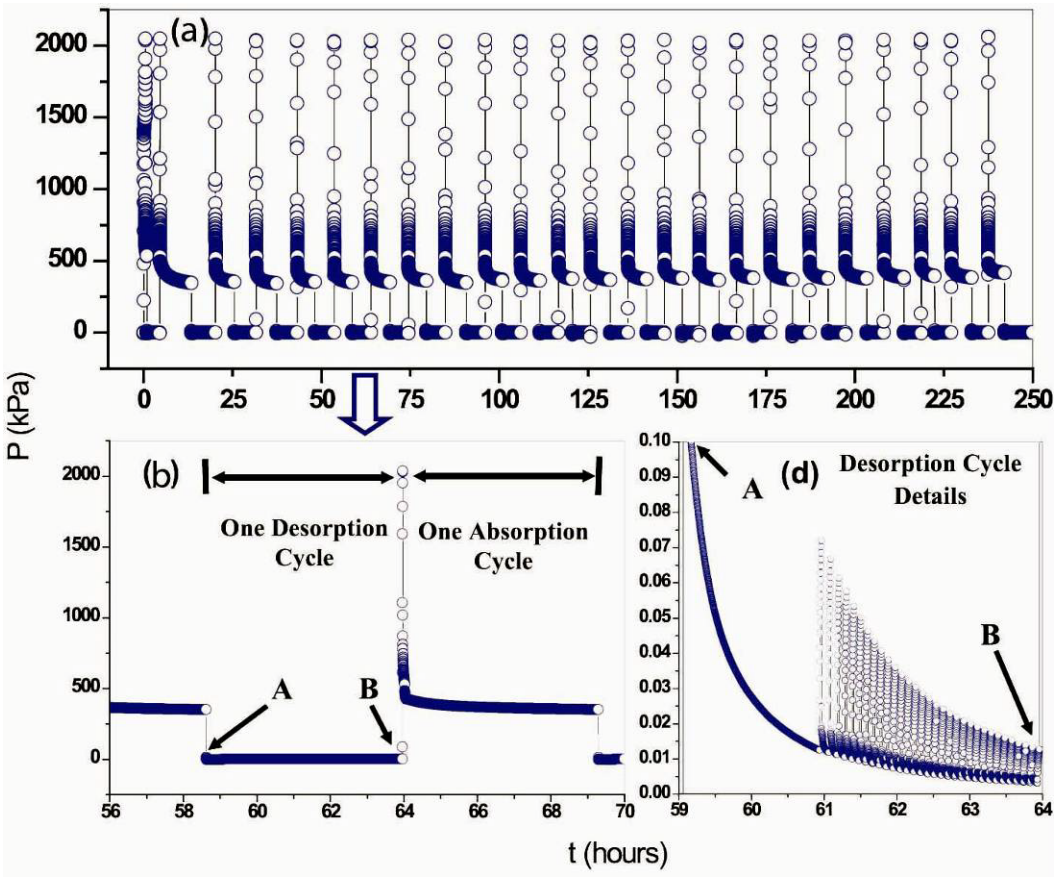

Figure 279. (a) Example plot of pressure cycling; partial view of the pressure vs. time is shown. (b) One dehydriding and one hydriding cycle is shown; (c) details of the dehydriding cycle from A to B.[381]

9.2.1 Pressure Cycling with Impurities on Classic Hydrides

There have been relatively few studies performed on extrinsic cycling of classic metal hydrides. A good example of early extrinsic testing on hydrides was reported by Sandrock and Goodell in 1984.[127] They described the effect of impurities on classic AB_5 and AB hydrides by the introduction of small amounts of gaseous CO, CO_2, CH_4, C_2H_4, N_2, NH_3, H_2S and CH_3SH (methyl mercaptan) in the hydrogen test gas. In their experiments, samples were prepared as thin (1.5 mm) compressed powder disks for better heat transfer. They first activated the alloy disk samples at room temperature using purified hydrogen. This was followed by extrinsic cycling of the samples with hydrogen containing pre-determined levels (parts per thousands) of an impurity. The majority of the impurity tests were performed at 25° and 85°C. It is important to mention that cycle time was 30 minutes in total with 15 minutes each for absorption and desorption. Some of the results for $LaNi_5$ are presented as hydrogen absorption vs. time at various cycles were presented earlier in Figure 260.

Alloy surface poisoning with gaseous impurities in hydrogen has profound effects on the hydriding properties and is highly dependent on the surface structure of the alloys or compounds.[382] Thus, s*urface poisoning* or contamination of metal hydrides is a very important research issue. Surface poisoning may be initiated with small amounts of impurities in hydrogen and is a rather complex problem. The resistance to degradation of surface properties due to impurities needs to be evaluated for different alloys.

Examples of surface contamination, with 300 ppm of H_2O, O_2, and CO in H_2 gas, on $Fe_{0.85}Mn_{0.15}Ti$ and $LaNi_5$ hydrides are shown in Figure 280.[382] Although the impurity quantities are small, they have profound effects on the surface catalytic properties and, by consequence, the long-term cycling performance. In $LaNi_5$ and Fe-Ti type hydrides, there is propensity to form La_2O_3, $La(OH)_3$ or TiO_x when trace levels of O_2 is adsorbed on the surface. The heat of formation of La_2O_3 is very high (-1277 kJ/mol) compared to that of TiO_2 (–913 kJ/mol). The most notable difference between the two alloys is that the O_2 and H_2O surface contaminated $Fe_{0.85}Mn_{0.15}Ti$ hydrides do not recover with cycling (Figure 280a) while the $LaNi_5$ hydride does recover after about 10 cycles (Figure 280b).

In contrast, carbon monoxide contamination is very severe both in the case of $LaNi_5$, and $Fe_{0.85}Mn_{0.15}Ti$ alloys (Figure 280). It has been postulated that for $LaNi_5$, CO gas reacts with the surface to form a $Ni(CO)_4$ layer.[383] To summarize, $LaNi_5$ is resistant to extrinsic impurities such as O_2 and H_2O, but not CO gas. The (Fe, Mn)Ti alloys, on the other hand, are generally not resistant any of these impurities and only slightly more resistant to CO poisoning than $LaNi_5$.

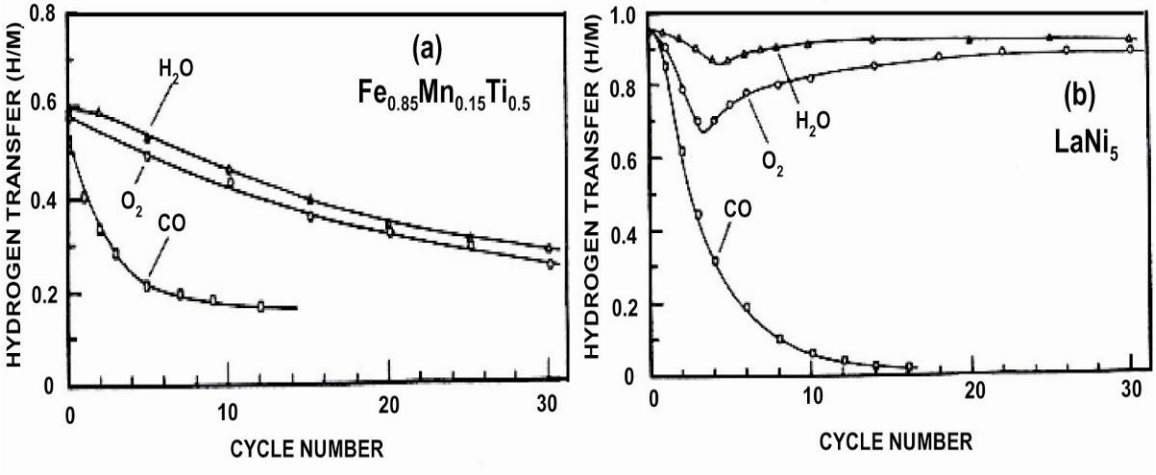

Figure 280. High temperature and Pressure isothermal cycling using impure hydrogen: Extrinsic cyclic response of (a) $Fe_{O.85}Mn_{0.15}Ti_{0.5}$ (hydrogen cycle at 25°C, 69 → 634 → 69 kPa) and (b) $LaNi_5$, (0.5 hour cycle at 25°C, 69 → 276 → 69 kPa).[382]

9.2.2 Pressure Cycling with Impurities on Complex Hydrides

Impurities in hydrogen are detrimental for prolonged cycling in PEM fuel cell application; especially hydrocarbons that lead to the formation of CO as well as ammonia and sulfur containing compounds. The impurities may originate from the hydrogen gas supply (and consequently damage storage materials as well the fuel cell), or the impurities may come from out gassing or decomposition of the hydrogen storage materials. In general, fresh charges of hydrogen (with ppm or ppb impurity) at every cycle will degradade the hydrides and eventual loss of hydrogen absorption capacity.

Sandrock et al. pointed out that the high levels of gaseous impurities were found in the complex hydride sodium alanate prepared through solvent methods and with the addition of organo-metallic Ti-dopants.[121,120] Sandrock reported Dry-$TiCl_3$ catalyzed Na-Al hydrides did not evolve any impurity gas during reactions.[121] Gross et al. reported that the hydrogen capacities were lowered to 3 wt. % using liquid catalysts (both absorption and desorption).[384] They also performed in-situ x-ray diffraction measurements and showed that the low hydrogen capacity was mainly due to inability to completely recharge to a composition of 100% $NaAlH_4$.[385] Most significantly, Gross et al. demonstrated that the alanates could be easily synthesized without any wet chemical processes or precursors from NaH, Al and $TiCl_3$.[386] The advantage, in this case, is that the hydrogen storage material is completely solvent free and will not outgas impurities with the stored hydrogen. An important distinction between the alanates and classic hydrides becomes apparent from these latter studies: Namely, that the hydrogen storage performance of these materials themselves is relatively impervious to the presence of impurities at levels that would generally render classic hydrides inoperable.

9.2.3 Pressure Cycling with Impurities on Imide/Amides

Li amide-imide pressure cycling data is presented here as an example of *Extrinsic Cycling* measurements (fresh hydrogen with controlled gaseous impurities). Chandra et al. examined the effect of long-term pressure cycling of the Li-N-H system using industrial hydrogen containing known concentrations of impurities (*Hydrogen min % (v/v) 99%, Water~32 ppm, O_2~10ppm, N_2~400 ppm, Total Hydrocarbons: 10 ppm, CO_2~10 ppm, CO~10 ppm, argon may be present, reads as oxygen)*.[387] In this study, the material was subjected to one hour hydriding-dehydriding cycles (30 minutes each) with maximum pressure of 2 bar fresh industrial hydrogen at every cycle and exposing the sample to vacuum for the desorption half cycle. The results of the measurements are shown in Figure 281. The left figure (a) presents isotherms of the hydriding transition between Li_2NH and $LiNH_2$ taken after the indicated number of cycles. A loss of 2.53 wt.% out of 5.6 wt.% stored hydrogen was observed after 1100 pressure cycles. It is noteworthy that the capacity drops to about 50% of its initial capacity after the first 500 cycles, followed by very little further loss in capacity out to 1100 cycles.

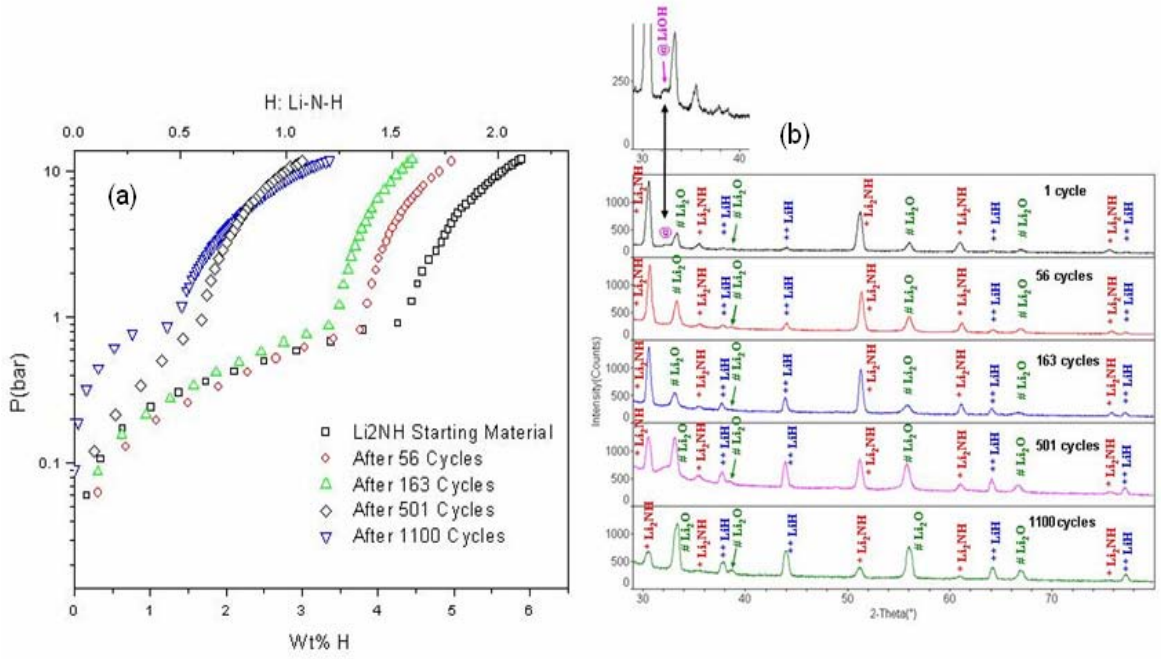

Figure 281. (a). Absorption isotherms of Li-amide obtained after non-equilibrium pressure cycling for 1, 56, 163, 501, 1100 times with impure hydrogen (ppm levels of O_2, H_2O and others). (b) Corresponding ex-situ X-ray diffraction taken from the sample after each isotherm was obtained in desorbed condition.[387]

X-ray diffraction measurement after the corresponding (isotherms (a)) desorption cycles are shown in Figure 281 (b). An analysis of the X-ray diffraction data demonstrated that, in desorbed state, the sample was composed mainly of Li_2NH, LiH, and Li_2O phases. The XRD results showed nearly complete transition from $LiNH_2 \rightarrow Li_2NH$ with the expected presence of LiH and, in addition, the impurity phase (Li_2O). After 1100 pressure cycles, the LiH phase increases from 11 wt% to 58 wt%, and the Li_2NH phase decreases from 82wt% to 13 wt%. The decrease in amount of Li_2NH can be observed in the Bragg peak at 30.5^o of the XRD patterns. The impurity Li_2O phase increased from 7 wt% to 29 wt% after 1100 cycles. These measurements clearly indicate that the decrease in the imide Li_2NH is due to the formation of Li_2O and stable LiH due to oxygen and water impurities in the hydrogen supply.

As a follow up, the same materials were investigated using the *Intrinsic* Thermal Aging method. A sample of Li_2NH was hydrided with 100ppm of CO in UHP hydrogen and held for approximately 240 hours at 12 bar and 325 ^oC. The isotherms obtained before and after aging did not show any significant change. As with the alanates, it appears that the behavior of these complex hydrides is quite different than those of the classic hydrides, as thermal aging with contaminants does not impact material performance and, in contrast, oxides (e.g. Li_2O) are not readily reduced back to the parent phases under reasonable thermodynamic conditions.[387]

10 Summary of Cycle-Life Measurements

Classification of testing methods for durability of alloys/intermetallic are presented, examples of intrinsic and extrinsic tests that include *Cycling and Aging* have been for AB_5/AB, and an elemental vanadium hydride. More recent results on extrinsic tests on light weight complex hydrides (imide-amide) that were cycled between Li_2NH / $LiNH_2$ phases are also reported. In general, there is reasonable amount of intrinsic data available, but extrinsic data is lacking; more research is need for the hydrides to be used in practical applications.

Summary

It is our intent that this overview of fundamental processes and measurement considerations will aid research and development of new and better hydrogen storage materials. In particular we hope to have clarified some of the recommended practices and caveats in performing high-quality experiments to measure the hydrogen sorption and desorption kinetics properties of advanced materials.

Acknowledgements

We gratefully acknowledge assistance and financial support from the U.S. Department of Energy Office of Energy Efficiency and Renewable Energy Hydrogen Storage Program. This work supported the President's Hydrogen Fuel and Advanced Energy Initiatives. The authors also acknowledge technical advice and contributions from many experts in the field including Dr. Philip Parilla and Dr. Thomas Gennett of the National Renewable Energy Laboratory in Golden CO, Dr. Carole Read of the U.S. Department of Energy, Dr. Gary Sandrock, Dr. George Thomas, and Dr. Robert Bowman Jr. consultants to the U.S. Department of Energy, Professor Gavin Walker of the University of Nottingham, United Kingdom, dr. Thomas Autrey of Pacific Northwest National Laboratory, Dr. Michael Miller of Southwest Research Institute in San Antonio TX, Dr. Anne Dailly, Dr. Frederick Pinkerton, Dr. Scott Jorgensen of General Motors GM R&D Center, Dr. Ole Martin Løvvik of the Institute for Energy Technology in Kjeller, Norway, Dr. Eric Poirier of General Motors/Optimal CAE Inc., Professor Channing Ahn of the California Institute of Technology in Pasadena CA, Dr. Kevin Ott, Dr. Anthony Burrell, and Dr. Troy Semelsberger of Los Alamos National Laboratory, Professor Richard Chahine and Dr. Renju Zacharia of the Université du Québec à Trois-Rivières, Canada, Andrea Sudik, Ford Motor Company, USA, Professor Klaus Yvon of the University of Geneva, Switzerland, Professor Sam Mao of the University of California Berkeley in Berkeley CA, and Dr. Nobuhiro Kuriyama and Dr. Tetsu Kiyobayashi of the National Institute of Advanced Industrial Science and Technology in Osaka, Japan.

Disclaimer

References

1 Walker, G.S. (editor), "Solid-state hydrogen storage: materials and chemistry", Woodhead Publishing Ltd, Cambridge, UK, (**2008**).

2 Barnes, R.G. (editor), "Hydrogen Storage Materials", Trans Tech Publications, (**1988**).

3 Schlapbach, L., and Züttel, A., "Hydrogen-storage materials for mobile applications", *Nature*, 414 (**2001**): 353-358.

4 Broom D.P., "Hydrogen Sorption Measurements on Potential Storage Materials", JRC Scientific and Technical Reports (**2008**), JRC 43223, EUR 23242 EN, ISBN 978-92-79-08345-7 ISSN 1018-5593 DOI: 10.2790/86100.

5 Wiberg, E., and Amberger, E., "Hydrides of the Elements of Main Groups", Z-ZV. Elsevier, Amsterdam, (**1971**) 2. D.A. Armitage.

6 Muller, W.M., Blackledge, J.P., Libowitz, G.G. editors., "Metal Hydrides", Academic Press, New York, (**1968**).

7 Dedieu, A., "Transition Metal Hydrides", Wiley-VCH (**1991**).

8 Stephens, F.H., Vincent Pons, V., and Baker, R.T., "Ammonia–borane: the hydrogen source par excellence?", *Dalton Trans.*, (**2007**), 2613–2626 DOI: 10.1039/b703053c.

9 Zidan, R., "Aluminum Hydride", in "Handbook of hydrogen storage: New Materials for Future Energy Storage", eds. Hirscher, M., Hirose, K., Weinheim : Wiley-VCH, (**2009**) p. 249.

10 Thomas, K.M., "Hydrogen adsorption and storage on porous materials", *Catalysis Today*, 120 (**2007**) p. 389–398.

11 Darkrim, F.L., Malbrunot, P., and Tartaglia, G.P., "Review of hydrogen storage by adsorption in carbon nanotubes", *Int. J. Hydrogen Energy* 27 (**2002**): 193-202.

12 Rosi, N.L., Eckert, J., Eddaoudi, M., Vodak, D.T., Kim, J., O'Keeffe, M., Yaghi, O.M., "Hydrogen Storage in Microporous Metal-Organic Frameworks", *Science*, 300 (**2003**) p. 1127–1129.

13 Eyring, H., Lin, S.H., Lin, S.M., "Basic Chemical Kinetics", Wiley (**1980**).

14 Espenson, J.J., "Chemical Kinetics and Reaction Mechanisms", McGraw-Hill (**1995**).

15 Masel, R.I., "Chemical Kinetics and Catalysis", Wiley, (**2001**).

16 Nicholas, J.E., "Chemical Kinetics", Wiley, (**1976**).

17 van den Berg, A.W.C. and Arean, C.O., "Materials for hydrogen storage: current research trends and perspectives", *Chemical Communications*, (**2008**) p. 668–681.

18 Schmitz, B., Muller, U., Trukhan, N., Schubert, M., Ferey, G., Hirscher, M., "Heat of Adsorption for Hydrogen in Microporous High-Surface-Area Materials", *Chem. Phys. Chem.*, 9 (**2008**) p. 2181–2184.

19 Perry, R.H. and Green, D.W., "Perry's Chemical Engineers", Handbook, McGraw-Hill (**1984**) ISBN 0-07-049479-7.

20 Roy, B.N., "Fundamentals of Classical and Statistical Thermodynamics", John (**2002**) Wiley & Sons, ISBN 0-470-84313-6.

21 Reif, F., "Chapter 5 – Simple applications of macroscopic thermodynamics", Fundamentals of Statistical and Thermal Physics, McGraw-Hill.(**1965**), ISBN 0070518009.

22 "The International System of Units (SI)", International Bureau of Weights and Measures (**2006**), The International System of Units (SI) (8th ed.), p. 116–119, ISBN 92-822-2213-6, http://www.bipm.org/utils/common/pdf/si_brochure_8_en.pdf .

23 10th CGPM (**1954**, Resolution 6, CR, 80), 11th CGPM (**1960**, Resolution 12, CR, 87), 13th CGPM (1967/68, Resolution 3, CR, 104 and Metrologia, **1968**, 4, 43), 14th CGPM (1971, Resolution 3, CR, 78 and Metrologia, **1972**, 8, 36).

24 IUPAC, Compendium of Chemical Terminology, 2nd ed. (the "Gold Book") (**1997**).

25 NIST "Appendix C – General Tables of Units of Measurement", Handbook 44 (**2009**), http://ts.nist.gov/WeightsAndMeasures/Publications/upload/AppendC-09-HB44-FINAL.pdf .

26 International Union of Pure and Applied Chemistry, http://old.iupac.org/index.html .

27 Everett, D.H., "Definitions, Terminology and Symbols in Colloid and Surface Chemistry", *Pure and Applied Chemistry*, 31.4 (**1972**) p. 579-638.

28 Everett, D.H., "Manual of Symbols and Terminology for Physicochemical Quantities and Units, Appendix II, Definitions, Terminology and Symbols in Colloid and Surface Chemistry PART I", Adopted by the IUPAC Council at Washington DC, USA, on 23 July **1971**, Prepared for Internet, (**2001**), L.K. KOOPAL http://old.iupac.org/reports/2001/colloid_2001/manual_of_s_and_t/ .

29 Keller, J. and Stuadt, R. "Gas Adsorption Equilibria" New York: Springer, (**2005**).

30 Zhou, L. "Progress and problems in hydrogen storage methods". *Renewable and Sustainable Energy Reviews*, (**2005**) 9, p. 395-408.

31 Poirier, E. and Dailly, A., "Investigation of the Hydrogen State in IRMOF-1 from Measurements and Modeling of Adsorption Isotherms at High Gas Densities", *J. Phys. Chem. C* (**2008**), 112, p.13047–13052.

32 Poirier, E., and Dailly, A., "Thermodynamics of hydrogen adsorption in MOF-177 at low temperatures: measurements and modeling", *Nanotechnology* (**2009**), 20, 204006.

33 Dubinin, M.M. and Astakhov, V.A., Izv. Akad. *Nauk SSSR Ser. Khim.* 1 (**1971**) p. 5–11 (translated from Russian).

34 Robell, A.J., Ballou, E.V., Boudart, M.J., "Surface Diffusion of Hydrogen on Carbon", Phys. Chem. , 68 (**1964**) p. 2748-2753.

35 Srinivas, S.T. and Rao, P.K., "Direct Observation of Hydrogen Spillover on Carbon-Supported Platinum and Its Influence on the Hydrogenation of Benzene", *J. Catal.*, 148 (**1994**) p. 470-477.

36 Conner, W.C. and Falconer, J.L., "Spillover in Heterogeneous Catalysis", *Chem. Rev.*, 95 (**1995**) p. 759-788.

37 Lueking, A.D. and Yang, R.T., "Hydrogen spillover to enhance hydrogen storage – study of the effect of carbon physicochemical properties", *Applied Catalysis A*, 265 (**2004**) p. 259-268.

38 Li, Y., Lachawiec, A., and Yang, R., "Hydrogen Storage by Spillover", University of Michigan Project ID: ST28, Presentation U.S. DOE Hydrogen Program Review (**2006**).

39 Yang, R.T., and Wang, Y., "Catalyzed Hydrogen Spillover for Hydrogen Storage", *J. Am. Chem. Soc.*, 131 (**2009**) p. 4224–4226.

40 Miller, M.A., Cheng-Yu Wang, C-Y., Grant N., and Merrill, G.N., "Experimental and Theoretical Investigation Into Hydrogen Storage via Spillover in IRMOF-8", *J. Phys. Chem. C*, 113 (**2009**) p. 3222–3231.

41 Saha, D. and Deng, S., "Hydrogen Adsorption on Ordered Mesoporous Carbons Doped with Pd, Pt, Ni, and Ru", *Langmuir* 25(21) (**2009**) p. 12550–12560.

42 Campesia,R., Cuevasa, F., Gadioub, R., Leroya, E., Hirscher, M., Vix-Guterlb, C., and Latroche, M., "Hydrogen storage properties of Pd nanoparticle/carbon template composites", *Carbon*, 46 (**2008**), p. 206-214.

43 Contescu,C.I., Brown,C.M., Liu,Y., Vinay,Y., Bhat,V., and Gallego, N.C., "Detection of Hydrogen Spillover in Palladium-Modified Activated Carbon Fibers during Hydrogen Adsorption", *J. Phys. Chem. C* 113 (**2009**) p. 5886–5890.

44 Stadie, N.P., Purewal, J.J., Ahn, C.C., and Fultz, B., "A Reevaluation of Hydrogen Spillover in Platinum Doped Superactivated Carbon", *J. Phys. Chem. C*, (**2009**) submitted.

45 Jain, P., Fonseca, D.A., Schaible, E., and Lueking, A.D., "Hydrogen uptake of platinum-doped graphite nanofibers and stochastic analysis of hydrogen spillover", *J. Phys. Chem C*, (**2007**) 111(4), p. 1788–1800.

46 Ghimbeu, C.M., Zlotea, C., Gadiou, R., Cuevas, F., Leroy, E., Latroche, M., and Vix-Guterla, C., "Understanding the mechanism of hydrogen uptake at low pressure in carbon/palladium nanostructured composites", *J. Mat. Chem*., (**2011**) doi: 10.1039/C1JM12939B.

47 Sandrock, G., "A panoramic overview of hydrogen storage alloys from a gas reaction point of view", *J. Alloys and Compounds*, 293-295 (**1999**) p. 877-888.

48 Mao, S.S., Chen, X., "Selected nano-technologies for renewable energy applications", *Int. J. Energy Research*, 31 (**2007**) p. 619-636.

49 Grochala, W. and Edwards, P.P., "Thermal Decomposition of the Non-Interstitial Hydrides for the Storage and Production of Hydrogen", *Chemical Reviews*, 104 (3) (**2004**) p. 1283-1316.

50 Wikipedia article titled "Hydride", http://en.wikipedia.org/wiki/Hydride, Please note that due to its open-source format, the exact text from the Wikipedia article may be different depending on when the article is accessed. The presented text was taken on August 17, 2009. The presented text has also been reviewed for accuracy.

51 Parent Hydride Names and Substitutive Nomenclature (Draft March **2004**) http://www.iupac.org/reports/provisional/abstract04/RB-prs310804/Chap6-3.04.pdf .

52 Wu, Y., "Hydrogen Storage via Sodium Borohydride", Millennium Cell Inc. Presentation at GCEP (The Global Climate and Energy Project) Hydrogen Workshop, Stanford University, April 14-15, (**2003**).

53 Kubas, G.J., Ryan, R.R., Swanson, B.I., Vergamini, P.J., and Wasserman, H.J., "Characterization of the first examples of isolable molecular hydrogen complexes, $M(CO)_3(PR_3)_2(H_2)$ (M = molybdenum or tungsten, R = Cy or isopropyl). Evidence for a side-on bonded dihydrogen ligand", *J. Am. Chem. Soc*, 106 (**1984**) p. 451.

54 Kubas, G.J., "Metal Dihydrogen and s-Bond Complexes— Structure, Theory, and Reactivity", Kluwer-Academic/Plenum Publishers, New York, (**2001**).

55 Wikipedia article "Dihydrogen complex", http://en.wikipedia.org/wiki/Dihydrogen_complex .

56 Rouquerol, F., Rouquerol, J., Sing, K.S.W., "Adsorption by powders and porous solids : principles, methodology, and applications", Academic Press (**1999**) London.

57 Gross, K.J. "Characterization of Advanced Hydrogen Storage Materials", MRS Spring Hydrogen Tutorial, (**2006**).

58 Dantzer, P., "Metal-Hydride Technology: A Critical Review", Topics in Applied Physics - Hydrogen in Metals III, 73 (**1997**) p. 279-340.

59 Sandrock, G.D., Murray, J.J., Post, M.L., and Taylor, J.B., "State-of-the-art Review of Hydrogen Storage in Reversible Metal Hydrides for Military Fuel Cell Applications", Final Report for ONR Contract N00014-97-M-0001, NTIS Order No. AD-A328 073/2INZ. (**1997**).

60 Gross, K.J., "Intermetallic Materials for Hydrogen Storage", PhD thesis. Institut de Physique, Université de Fribourg, (**1998**).

61 Gross, K.J., Measurement performed by author.

62 Bevington, P.R., "Data Reduction and Error Analysis for the Physical Sciences", McGraw-Hill book co. New York (**1969**).

63 NIST "Guidelines for Evaluating and Expressing the Uncertainty of NIST Measurement Results", Available at http://physics.nist.gov .

64 Wikipedia article "Propagation of uncertainty", http://en.wikipedia.org/wiki/Propagation_of_uncertainty .

65 Frieske, H. and Wicke, E., Ber. Brunsenges. *Physik. Chem.* 77, (**1973**) p. 50.

66 Frieske, H., Dissertation, Münster Germany (**1972**).

67 http://ts.nist.gov/WeightsAndMeasures/CalibrationProcedures.cfm .

68 http://ts.nist.gov/WeightsAndMeasures/Publications/techcritvolume.cfm .

69 Dailly, A., Ahn, C., Vajo, J., and Bowman, R. Jr., "Volumetric Analyses of Sieverts Apparatus Data", APS March Meeting, March 21–25, (**2005**), Los Angeles, CA.

70 Burns, G.W., and Scroger, M.G., "The Calibration of Thermocouples and Thermocouple Materials", NIST Special Publication 250-35, (**1989**). http://ts.nist.gov/MeasurementServices/Calibrations/upload/SP250-35.pdf .

71 The SP 250 series on NIST measurement services http://ts.nist.gov/MeasurementServices/Calibrations/sp250_series.cfm .

72 Goodell, P.D., and Sandrock, G.D., "Kinetic and Dynamic Aspects of Rechargeable Metal Hydrides", *J. Less-Common Metals*, 73 (**1980**) p.135-142.

73 Blach, T.P., and McGray, E., "Sieverts apparatus and methodology for accurate determination of hydrogen uptake by light-atom hosts", *J. Alloys and Compounds*, 446-447 (**2007**) p. 692-697.

74 Poirier, E., Chahine, R., Tessier, A., Bose, T.K., "Gravimetric and volumetric approaches adapted for hydrogen measurements with in situ conditioning on small sorbent samples", *Review of Scientific Instruments*, 76, (**2005**), 055101.

75 Blackman, J.M., Patrick, J.W., Snape, C.E., "An accurate volumetric differential pressure method for the determination of hydrogen storage capacity at high pressures in carbon materials", *Carbon*, 44 (**2006**) p.918-927.

76 Lemmon, E.W., Peskin, A.P., McLinden, M.O., Friend, D.G., NIST12 Thermodynamic and Transport Properties of Pure Fluids - NIST Standard Reference Database 23, Version 8.0, U.S. Sec. of Comm.: Washington DC (**2007**).

77 Bhadeshia, H.K.D.H., "Thermogravimetry", University of Cambridge, Materials Science and Metallurgy, (**2002**).

78 Nix, R.M., "An Introduction to Surface Chemistry: 5.6 Temperature-Programmed Desorption", School of Biological and Chemical Sciences, Queen Mary, University of London (**2003**). http://www.chem.qmul.ac.uk/surfaces/scc/scat5_6.htm .

79 Bhadeshia, H.K.D.H., "Differential Scanning Calorimetry", University of Cambridge, Materials Science and Metallurgy, (**2002**).

80 Bhadeshia H.K.D.H., "Thermal analyses techniques. Differential thermal analysis", University of Cambridge, Material Science and Metallurgy. www.msm.cam.ac.uk/phase-trans/**2002**/Thermal1.pdf .

81 Sircar, S., "Gibbsian Surface Excess for Gas Adsorption ─ Revisited", *Industrial & Engineering Chemistry Researc*h, 38 (**1999**) p. 3670-3682.

82 Sircar, S., "Measurement of Gibbsian Surface Excess", *AIChE Journal*, 47 (**2001**) p. 1169-1176.

83 Sircar, S., *International Adsorption Society*, (**2002**) p 377.

84 Haas, M.K, Zielinski, J.M., Dantsin, C.G., Coe, Pez, G.P., Cooper, A.C., "Focus Section: Tailoring singlewalled carbon nanotubes for hydrogen storage", *Journal of Materials Research* , 20 (**2005**) p. 3214-3223.

85 Lachawiec, A.J. Jr., DiRaimondo, T.T., Yanga, R.T., "A Robust Volumetric Apparatus and Method for Measuring High-Pressure Hydrogen Storage Properties of Nanostructured Materials", *Review of Scientific Instruments*, 79 (**2008**) 063906-12.

86 Malbrunot, P., Vidal, D., Vermesse, J., "Adsorbent Helium Density Measurement and Its Effect on Adsorption Isotherms at High Pressure", *Langmuir*, 13 (**1997**) p. 539-544.

87 Yang, R.T., "Adsorbents : fundamentals and applications", Wiley-Interscience: Hoboken, N.J., (**2003**).

88 Zlotea, C., Moretto, P., and Steriotis, T., "A Round Robin Characterization of the Hydrogen Sorption Properties of a Carbon Based Material", *Int. J. Hydrogen Energy*, 34 (7) (**2009**) p. 3044-3057.

89 Broom, D.P., "Hydrogen Storage Materials, The Characterisation of Their Storage Properties" Green Energy Technology series, Springer-Verlag (**2011**) London.

90 Wikipedia article titled "Chemical Kinetics",

http://en.wikipedia.org/wiki/Chemical_kinetics, Please note that due to its open-source format, the exact text from the Wikipedia article may be different depending on when the article is accessed. The presented text was taken on January 8, **2008**. The presented text has also been reviewed for accuracy.

91 Panchenkov, G.M., G.M., and Lebedev, V.P., "Chemical Kinetics and Catalysis", Moscow (**1974**).

92 Whitten, K.W., Davis, R.E., Peck, M.L., "General Chemistry with Qualitative Analysis", 5th Ed. Saunders College Publishing, (**1996**).

93 Wang, X.L., and Suda, S., "Reaction Kinetics of Hydrogen-Metal hydride systems", *Int. J. Hydrogen Energy*, 15 (**1990**) p.569-577.

94 Rudman, P.S., "Hydriding and Dehydriding Kinetics", *J. Less-Common Metals*, 89 (**1983**) p. 93-110.

95 Long, J.R. and Dincă, M., "Hydrogen Storage in Microporous Metal–Organic Frameworks with Exposed Metal Sites", *Angew. Chem. Int. Ed.*, 47 (**2008**) p. 6766-6779.

96 Whitaker, S., "Advances in Theory of Fluid Motion in Porous Media", *Industrial and Engineering Chemistry*, 61.12 (**1969**) p. 14-28.

97 Bear, J., "Dynamics of Fluids in Porous Media", Dover Books on Physics and Chemistry (**1998**).

98 Ingham, D.B., and Pop, I., "Transport Phenomena in Porous Media", ISBN-13 p. 978-0-08-042843-7, Pergamon Imprint (**2002**).

99 Fukai, Y., "The Metal-Hydrogen System, Basic Bulk Properties", 1st ed., Springer-Verlag: Berlin, Heidelberg (**1993**).

100 Lauhon, L.J., Wallis, T.M., and Ho, W., "Vibrational Excitation and Quantum Tunneling of Single Hydrogen Atoms Observed by STM", American Physical Society, Annual March Meeting, March 12 - 16, (**2001**) Seattle, Washington Meeting ID: MAR01, abstract #L13.003.

101 Jensen, C.M., Sun, D., Raman, S.S., Murphy, K., Niemczura, W.P., Kumashiro, K.K., Eberhard, M., Wang, Z., and Gu, X-Q, "Catalytically Enhanced Systems for Hydrogen storage", Proceedings of the US DOE Hydrogen Program Review, NREL/CP-610-32405 (**2002**).

102 Anton, D.L., "Hydrogen desorption kinetics in transition metal modified NaAlH4", *J. Alloys and Compounds*, 400 (**2003**) p. 356-357.

103 Schlapbach, L., Anderson, I., Burger, J.P., In Material Science and Technology, Buschow, K.H.J. Ed., VCH mbH: Weinheim and New York, (**1993**), Vol. 3b, chap.12, p. 270.

104 Schlapbach, L., Meli, F., Züttel, A., In Intermetallic Compounds, Westbrook, J.H., Fleischer, R.L., Eds., John Wiley & Sons, Vol. 2, Practice (**1994**) p. 475-483.

105 Schlapbach, L., "Magnetic properties of $LaNi_5$ and their variation with hydrogen absorption and desorption", *J. Phys. F.*, 10 (**1980**) p. 2477.

106 Yoshida, M., and Akiba, E., "Hydrogen absorbing properties of ScM_2 Laves phase alloys (M = Fe, Co and Ni)", *J. Alloys and Compounds*, 226 (**1995**) p. 75-80.

107 Gérard, N., and Ono, S., In Hydrogen in Intermetallic Compounds II, Schlapbach, L., Ed., Springer-Verlag: Berlin, Vol. 67 (**1992**) p. 165-195.

108 Stander, C., and Zeit, M., "Kinetics of Formation of Magnesium Hydride from Magnesium and Hydrogen", *Phys. Chem. Neue Folge*, 104 (**1977**) p. 229.

109 Kaviany, M., 'Principles of Heat Transfer in Porous Media", 2nd ed. (**1995**) Corr. 2nd printing, (**1999**), XXII. ISBN: 978-0-387-94550-7.

110 Vafai, K., and Tien, C.L., "Boundary and Inertia Effects on Flow and Heat-Transfer in Porous Media", *Int. J.Heat and Mass Transfer*, 24 (2) (**1981**) p. 195-203.

111 Oi, T., Maki, K., and Sakaki, Y., "Heat transfer characteristics of the metal hydride vessel based on the plate-fin type heat exchanger", *J. Power Sources*, 125, (**2004**) p. 52-61.

112 Sharp, J.H., Brindley, G.W., and Narahari, A., "Numerical Data for Some Commonly Used Solid State Reaction Equations", *J. Am. Ceram. Soc.*, 49 (**1966**) p. 379.

113 Valensi, G., "Kinetics of oxidation of metallic spherules and powders", *Compt. Rend.*, 202 (**1936**) p. 309.

114 Jander, W.Z., "Reaktione im festen Zustande bei hoheren Temperaturen", *Anorg. Allgem. Chem.*, 163 (**1927**) p. 1.

115 Avrami, M.J., "Kinetics of phase change I-III", *Chem. Phys.*7, 8, 9 (**1939,40,41**) pp. 1103,212,177.

116 Erofe'ev, B.V., "Generalized. equation of chemical kinetics and its application in reactions", *Compt. Rend. Acad. Sci. URSS*, 52 (**1946**) p. 511.

117 Wang, X.L., and Suda, S., "Kinetics of the hydriding–dehydriding. Reactions of the hydrogen–metal hydride systems", *Int. J. Hydrogen Energy*, 17 (**1992**) p. 139.

118 Gross, K.J., Measurement performed by author.

119 Dedrick, D., "Engineering Properties of Complex Hydrides for System Optimization", ASM Materials Solutions Conference, (**2004**).

120 Sandrock, G., Gross, K., Thomas, G., Jensen, C., Meeker, D., Takara, S., "Engineering considerations in the use of catalyzed sodium alanates for hydrogen storage", *J. Alloys and Compounds*, 330-332 (**2002**) p. 696-701.

121 Gross, K.J., Thomas, G.J., and Sandrock, G., "Hydride Development for Hydrogen Storage", Proceedings of the Hydrogen Program Review Meeting, Sandia National Laboratories, (**2000**).

122 Gross, K.J., Thomas, G.J., Majzoub, E., and Sandrock, G., "Light-weight Hydride Development", Proceedings of the Hydrogen Program Review Meeting, Sandia National Laboratories, (**2001**).

123 Goodell, P.D., and Rudman, P.S., "Hydriding and Dehydriding Rates of the $LaNi_5$-H System", *J. Less-Common Metals*, 89 (**1983**) p. 117-125.

124 Bogdanovic, B., and Sandrock, G., "Catalyzed Complex Hydrides", *MRS Fall Bulletin* (**2002**).

125 Sandrock, G.D., Gross, K., Thomas, G., "Effect of Ti-catalyst content on the reversible hydrogen storage properties of the sodium alanates", *J. Alloys and Compounds*, 339 (**2002**) p. 299–308.

126 Gross, K.J., Thomas, G.J., Mazjoub, E., and Sandrock, G., "The effects of titanium precursors on hydriding properties of alanates", *J. Alloys and Compounds*, 356-357 (**2003**) p. 423-428.

127 Sandrock, G.D., and Goodell, P.D., "Cyclic Life of Metal Hydrides with Impure Hydrogen: Overview and Engineering Considerations", *J. Less-Common Metals*, 104 (**1984**) p. 159-173.

128 Luo, W., and Gross, K.J., "A kinetics model of hydrogen absorption and desorption in Ti-doped NaAlH4", *J. Alloys and Compounds*, 385, 28 (**2004**) p. 224-231.

129 Supper, W., Groll, M., and Mayer, U., "Reaction Kinetics in Metal Hydrides Reaction Beds with Improved Heat and Mass Transfer", *J. Less-Common Metals*, 104 (**1984**) p. 279-286.

130 Bogdanovic, B., and Schwickardi, M., "Ti-doped Alkali Metal Aluminum Hydrides as Potential Novel Reversible Hydrogen Storage Materials", *J. Alloys and Compounds*, 253-254 (**1997**) p. 1-9.

131 Richard, M.-A., Cossement, D., Chandonia, P.-A., Chahine, R., Mori, D., and Hirose, K., "Preliminary evaluation of the performance of an adsorption-based hydrogen storage system", submitted **2008**, AIChE Journal.

132 Bogdanovic, B., Brand, R.A., Marjanivic, A., Schwickardi, M., and Tolle, J., "Metal-doped sodium aluminium hydrides as potential new hydrogen storage materials", *J. Alloys and Compounds*, 302 (**2000**) p. 36.

133 Cooper, A.C., Fowler, D.E., Scott, A.R., Abdourazak, A.H., Cheng H.S., and Bagzis, L.D., "Hydrogen Storage and Delivery B Reversible Hydrogenation of Liquid-Phase Hydrogen Carriers", Prepr. Pap., *Am. Chem. Soc., Div. Fuel Chem*, 50 (1), (**2005**) p. 271.

134 Gibbs, J.W., "The Collected Works of J.W.Gibbs", (**1928**) Longmans and Green, New York.

135 Benard, P. and Chahine R., "Modeling of adsorption storage of hydrogen on activated carbons", *Int. J. Hydrogen Energy* 26 (**2001**) p. 849–855.

136 Ridha F.N., "A study on high-pressure adsorption and desorption of methane, ethane, propane and their mixtures on porous adsorbents", Ph.D. Thesis **2006**,

Faculty of Chemical and Natural Resources Engineering, Universiti Teknologi Malaysia.

137 Adamson, A.W., "Physical Chemistry of Surfaces", 5th ed. New York. (**1990**), John Wiley and Sons, Inc.

138 Ross, S., and Morrison, L.D., "Colloidal Systems and Interfaces", New York (**1988**), John Wiley and Sons, Inc.

139 Gregg, S.J., and Sing, K.S.W., "Adsorption, Surface Area and Porosity", London (**1982**), Academic Press, Inc.

140 Hampel, C.A., and Hawley, G.G., "Glossary of Chemical Terms", 2nd ed., New York (**1982**), Van Nostrand Reinhold Company.

141 Do, D.D., "Adsorption Analysis: Equilibria and Kinetics", Singapore (**1998**), Imperial College Press.

142 Robens, E., Keller, J.U., Massen, C.H., and Staudt, R., "Sources of Error in Sorption and Density Measurements", *J. of Thermal Analysis and Calorimetry*, 55 (**1999**) p. 383-387.

143 Zhou, W., Wu, H., Hartman, M.R., Yildirim, T., "Hydrogen and Methane Adsorption in Metal-Organic Frameworks: A High-Pressure Volumetric Study", *J. Phys. Chem. C*, 111 (**2007**) p. 16131-16137.

144 Amankwah, K.A.G. and Schwarz, J.A., "A modified approach for estimating pseudo-vapor pressures in the application of the Dubinin-Astakhov equation", *Carbon*, 33 (**1995**) p. 1313-1319.

145 Poirier E., Chahine, R., Benard, P., Dorval-Douville, G., Lafi, L., and Chandonia, P.A., "Storage of hydrogen on single-walled carbon nanotubes and other carbon structures", *Applied Physics A*, 78 (**2004**) p. 961-967.

146 Chahine, R., and Bose, T.K., "Characterization and optimization of adsorbents for hydrogen storage", Hydrogen Energy Progress XI, Proceedings of the 11th World Hydrogen Energy Conference, Stuttgart, Germany, 23-28 June, Vol.2, (**1996**) p. 1259-1263.

147 Furukawa H., Miller, M., and Yaghi, O.M., "Independent verification of the saturation hydrogen uptake in MOF-177 and establishment of a benchmark for hydrogen adsorption in metal-organic frameworks", *J. Mat. Chem.* 17 (**2007**) p. 3197-3204.

148 Dinca M., Dailly, A., Liu, Y., Brown, C.M., Neumann, D.A., and Long, J.R., "Hydrogen Storage in a Microporous Metal-Organic Framework with Exposed Mn^{2+} Coordination Sites", *J. Am. Chem. Soc.,* 128 (**2006**) p. 16876-16883.

149 Bhatia, SK, and Myers, AL, "Optimum Conditions for Adsorptive Storage", *Langmuir*, 22 (**2006**) p. 1688-1700.

150 Reviewer comments, Richard M.-A., Cossement, D., Chandonia, P.-A., Chahine, R., Mori, D., Hirose, K., "Preliminary evaluation of the performance of an adsorption-based hydrogen storage system", *AiChE,* 55 (**2009**), p. 2985-2996.

151 Richard M-A, Benard, P., and Chahine, R., "Gas adsorption process in activated carbon over a wide temperature range above the critical point - Part 1: Modified Dubinin-Astakhov model", *Adsorption*, 15 (**2009**) p. 43-51.

152 Ivanov, E.J., Konstanchuk, I.G., Stepanov, A.A., Jie, Y., Pezat, M., and Darriet, B., "The Ternary System Mg-Co-H", *Inorg. Chem.*, 28 (**1989**) 613-615.

153 "Targets for on-board Hydrogen Storage Systems", United States Department of Energy – Energy Efficiency and Renewable Energy, (**2007**). http://www1.eere.energy.gov/hydrogenandfuelcells/storage/current_technology.html .

154 Read, C., Thomas, G., Ordaz, G., and Satyapal, S., "U.S. Department of Energy's System Targets for On-Board Vehicular Hydrogen Storage", *Material Matters* (**2007**), vol 2, issue 2, p. 3-4.

155 "DOE Targets for On-Board Hydrogen Storage Systems for Light-Duty Vehicles Current R&D Focus is on 2015 Targets with Potential to Meet Ultimate Targets", DOE, EERE publication, (revision Feb, **2009**) http://www1.eere.energy.gov/hydrogenandfuelcells/storage/pdfs/targets_onboard_hydro_storage.pdf .

156 Satyapal, S., "Current State of the Art", Figures by DOE: Thomas, G., (**2007**), Sandrock, G., (**2008**) Presentation "Hydrogen Storage", 2008 DOE Hydrogen Program Merit Review and Peer Evaluation Meeting June 9, **2008**.

157 Dillon A.C. and Heben M.J., "Hydrogen storage using carbon adsorbents: past, present and future", *Applied Physics A*, 72 (**2001**) p. 133-142.

158 Kojima, Y., Suzuki, K.-I., Fukumoto, K., Kawai, Y., Kimbara, M., Nakanishi, H., and Matsumoto, S., "Development of 10 kW-scale hydrogen generator using chemical hydride", *J. Power Sources*, 125 (**2004**) p. 22-26.

159 Ströbel R., Garche, J., Moseley, P.T., Jörissen, L., Wolf, G., "Hydrogen Storage by Carbon Materials", J. Power Sources 159 (**2006**) p. 781-801.

160 Okambawa R., Benaddi, H., St-Arnaud, J.-M., and Bose, T.K., "Gas-solid interaction and the virial description of the adsorption of methane on steam-activated carbon", *Langmuir*, 16 (**2000**) p. 1163-1166.

161 Zhou, X.B., Xiao, B., Fletcher, A.J., and Thomas, K.M., "Hydrogen Adsorption on Functionalized Nanoporous Activated Carbons", *J. Phys. Chem. B*, 109 (**2005**) p. 8880-8888.

162 Xiong Z, Yong, C.K., Wu, G.T., Chen, P., Shaw, W., Karkamkar, A., Autrey, T., Jones, M.O., Johnson, S.R., Edwards, P.P., and David, W.I.F., "High-capacity hydrogen

storage in lithium and sodium amidoboranes", *Nature Materials*, 7(2) (**2008**) p. 138-141.

163 Poirier, E., and Dailly, A., "Thermodynamic study of the adsorbed hydrogen phase in Cu-based metal-organic frameworks at cryogenic temperatures", *Energy Environ. Sci.*, 2 (**2009**) p. 420–425, Reproduced by permission of The Royal Society of Chemistry.

164 Gross K.J., Sandrock, G., and Thomas, G.J., "Dynamic in situ X-ray Diffraction of Catalyzed Alanates", *J. Alloys and Compounds*, 330 (**2002**) p. 691-695.

165 Giannasi A., Bowron, D.T., Celli, M., Sauvajot, J.L., and Zoppi, M., "Structure and purity of single walled carbon nanotube samples", *Carbon*, 45 (**2007**) p. 943–951.

166 Witham C., Hightower, A., Fultz, B., Ratnakumar, B.V., and Bowman, R.C. Jr., "Electrochemical Properties of $LaNi_{5-X}Ge_X$ Alloys in Ni-MH Batteries", *J. Electrochem. Soc.*, 144 (11) (**1997**).

167 Bojon J.P., Hilleret, N., and Weiss, K., "Origin of possible contamination introduced by a turbomolecular pumping system", *Vacuum*, 53 (**1999**) p. 247-251.

168 O'Hanlon, J., "A User's Guide to Vacuum Technology", Wiley-Interscience (**2003**).

169 Li, M. and Dylla H.F., "Model for the outgassing of water from metal surfaces", *J. Vac. Sci. Technol. A*, 11 (**1993**) p. 1702.

170 Welham, N.J. and Williams, J.S., "Extended milling of graphite and activated carbon", *Carbon* (**1998**) p. 1309-1315.

171 Bordiga, S., Vitillo, J.G., Ricchiardi, G., Regli, L., Cocina, D., Zecchina, A., Arstad, B., Bjrgen, M., Hafizovic, J., Lillerud, K.P., "Interaction of Hydrogen with MOF-5", *J. Phys. Chem. B*, 109 (**2005**) p. 18237–18242.

172 de la Casa-Lillo M.A., Lamari-Darkrim, F., Cazorla-Amoros, D., and Linares-Solano, A., "Hydrogen storage in activated carbons and activated carbon fibers", *J. Phys. Chem. B*, 106 (**2002**) p. 10930-10934.

173 Agostino R.G., Caruso, T., Chiarello, G., Cupolilo, A., Pacile, D., Filosa, R., Formoso, V., Colavita, E., and Papagno, L., "Thermal annealing and hydrogen exposure effects on cluster-assembled nanostructured carbon films embedded with transition metal nanoparticles", *Phys. Rev. B*, 68 (**2003**) p. 035413.

174 Kajiura, H., Tsutsui, S., Kadono, K., Kakuta, M., Ata, M., and Murakami, Y., "Hydrogen storage capacity of commercially available carbon materials at room temperature", *Appl. Phys. Let.*, 82 (**2003**) p. 1105.

175 Mueller, U., Schubert, M., Teich, F., Puetter, H., Schierle-Arndt, K., and Pastré., J., "Metal-organic frameworks—prospective industrial applications", *J. Mat. Chem.*, 16 (**2006**) p. 626-636.

176 Aiello, R., Sharp, J.H., Matthews, M.A., "Production of hydrogen from chemical hydrides via hydrolysis with steam", *Int. J. Hydrogen Energy* 24 (12) (**1999**) p. 1123–1130.

177 Gross, K.J., "Advanced Methods and Challenges in Characterizing Hydrogen Storage Materials", poster presentation MH2008, International Symposium on Metal-Hydrogen Systems, Reykjavik, (**2008**).

178 Karkamkar, A., Stowe, A.C., Hess, N.J., and Autrey, T., "Kinetic and Thermodynamic Investigations of Ammonia Borane on Various Mesoporous Scaffolds,", (**2006**) presented at the Fall 2006 ACS Meeting, San Francisco, CA.

179 Gutowska, A., Li, L., Shin, Y., Wang, C.M., Li, X.S., Linehan, J.C., Smith, R.S., Kay, B.D., Schmid, B., Shaw, W., Gutowski, M., and Autrey, T., "Nanoscaffold Mediates Hydrogen Release and the Reactivity of Ammonia Borane", *Angew. Chem. Int. Ed.*, 44 (**2005**) p. 3578 –3582.

180 Gross, K.J., Measurement performed by author.

181 Li, Y. and Yang, R.T. "Hydrogen Storage in Metal–Organic Frameworks by Bridged Hydrogen Spillover", *J. Am. Chem. Soc.*, 128 (**2006**) p. 8136–8137.

182 Miller, M. and Page, R., "National Testing Laboratory for Solid-State Hydrogen Storage Technologies, Southwest Research Institute", (**2008**) FY 2007 Annual Progress Report, USDOE Hydrogen Program.

183 Ubbelohde, A.R., "Hysteresis in Pd-H system", Some Properties of the Metallic State. I. Metallic Hydrogen and Its Alloys, *Proc. R. Soc. London, Ser. A*, 159 (**1937**) 295.

184 Flanagan, T.B., and Clewley, J.D., "Hysteresis in Metal Hydrides", *J. of Less-Common Metals*, 83 (**1982**) p. 127-141.

185 Young, K., Ouchi, T., and Fetcenko, M.A., "Pressure-composition-temperature hysteresis in C14 Laves phase alloys", *J. Alloys and Compounds*, 480 (**2009**) p. 428-433.

186 Cerny R., Joubert, J.-M., Latroche, M., Percheron-Guégan, A., and Yvon, K., "Anisotropic diffraction peak broadening and dislocation substructure in hydrogen-cycled $LaNi_5$ and substitutional derivatives", *J. Appl. Cryst.* 33, (**2000**) p. 997-1005.

187 Joubert J.-M., Latroche, M., Cerny, R., Bowman, R.C. Jr., Percheron-Guégan, A., and Yvon, K., "Crystallographic study of $LaNi_{5-x}Sn_x$ compounds and their hydrides", *J. Alloys and Compounds*, 293-295 (**1999**) p. 124-129.

188 Joubert J.-M., Latroche, M., Cerny, R., Percheron- Guégan, A., and Yvon, K., "Hydrogen cycling induced degradation in $LaNi_5$-type materials", *J. Alloys and Compounds*, 330-332 (**2002**) p. 208-214.

189 Gross, K.J., Chartouni, D., Leroy, E., Zuettel, A., and Schlapbach, L., "Mechanically milled Mg composites for hydrogen storage: the relationship between morphology and kinetics", *J. Alloys and Compounds*, 269 (**1998**) p. 259-270.

190 Gremaud, R., Broedersz, C.P., Borgschulte, A., van Setten, M.J., Schreuders, H., Slaman, M., Dam, B., and Griessen, R., "Hydrogenography of $Mg_yNi_{1-y}H_x$ gradient thin Films: Interplay between thermodynamics and kinetics of Hydrogenation", *Acta Materialia* 58, (**2010**) p. 658-668.

191 Sandrock, G.D., "The Metallurgy and Production of Rechargeable Hydrides", Hydrides for Energy Storage, Andresen, A.F. and Maeland, A.J., Eds., Pergamon Press, Oxford (**1978**) p. 353-393.

192 De Benedetto, S., Carewska, M., Cento, C., Gislon, P., Pasquali, M., Scaccia, S., and Prosini, P.P., "Effect of milling and doping on decomposition of NH_3BH_3 complex", *Thermochimica Acta*, 441 (**2006**) p. 184–190.

193 "Hydrogen Properties", College of the Desert, Hydrogen Fuel Cell Engines and Related Technologies: Rev 0, December (**2001**) http://www1.eere.energy.gov/hydrogenandfuelcells/tech_validation/pdfs/fcm01r0.pdf .

194 Staudt, R., Sailer, G., Tomalla, M., and Keller, J.U., "A note on Gravimetric Measurements of Gas Adsorption Equilibria", *Ber. Bunsenges. Phys. Chem.*, 97 (**1993**) p. 98.

195 Dreisbach, F., Loesch, H.W., and Harting, P., "Highest Pressure Adsorption Equilibria Data: Measurement with Magnetic Suspension Balance and Analysis with a New Adsorbent/Adsorbate-Volume", *Adsorption*, 8 (**2002**) p. 95-109.

196 Robens, E., Sandstede, G., Walter, G., and Wurzbacher G., "Fluctuations of the weight indicated by a microbalance in the pressure range between 1 and 103 torr with the sample at a lower temperature than the beam", in: C.H. Massen and H.J. van Beckum (Eds.): Vacuum Microbalance Techniques Vol. 7, Plenum, New York 70, p. 195.

197 Massen, C.H., Robens, E., Poulis, J.A., and Gast, T., "Disturbances in weighing – Part I A survey of work presented at the preceding VMT conferences", *Thermochim. Acta*, 82 (**1984**) p. 43.

198 Robens, E., Poulis, J.A., Massen, C.H., and Unger, K.K., "Determination of the amount adsorbed from the gas phase in porous solid", In: M. Ben Chanaa (Ed.): Proceedings of the XXVIth International Conference on Vacuum Microbalance Techniques, Marrakesh (Morocco), (**1995**).

199 Macedonia, M.D., Moore, D.D., and Maginn, E.J., "Adsorption Studies of Methane, Ethane, and Argon in the Zeolite Mordenite: Molecular Simulations and Experiments", *Langmuir* 16 (**2000**) p. 3823-3834.

200 Lopez-Peinado, A., Rivera-Utrill, J., and Lopez-Gonzalez, J.D., "Porous Texture Characterization of Coals and Chars", *Adsorption Sci. and Technol.* 2 (**1985**) p. 31.

201 Grebner, M., "Synthese und Eigenshaften von Dodecasil 1H als vielseitige Wirtsmatrix", Dissertation, Mainz, (**1994**).

202 Kuwabara, H., Suzuki, T., and Kaneko, K., "Ultramicropores in microporous carbon fibers evidenced by helium adsorption at 4.2 K", *J. Chem. Soc. Faraday Trans.*, 87 (**1991**) p. 1915.

203 Lemmon, E.W., and Huber, M.L., "Revised Standardized Equation for Hydrogen Gas Densities for Fuel Consumption Applications", *J. Research NIST* 113 6 (**2008**) p. 341-350.

204 Ginoux, L. and Bonnctain, L., "Some problems about gas adsorption isotherm measurements by automated procedures in manometric devices", In: F. Rodriguez-Reinoso, Rouquerol, J., Sing, K.S.W., and Unger K.K., (Eds.): "Characterization of Porous Solids II" Elsevier, Amsterdam, (**1991**) p. 189.

205 Fuller, E.L., Poulis, J., Czanderna, A.W., and Robens, E., "Volumetric and gravimetric methods of determining monolayer capacities", *Thermochim. Acta*, 29 (**1979**) p. 315.

206 Yang R.T., Li, Y., Lachawiec, A.J., and Wang, L., "Hydrogen Storage by Spillover", DOE Hydrogen Program Review (**2008**).

207 Baumann J., Baitalow, F., and Wolf, G., "Thermal decomposition of polymeric aminoborane $(H_2BNH_2)_X$ under hydrogen release", *Thermochimica Acta*, 430 (**2005**) p. 9–14.

208 Baitalow F., Baumann, J., Wolf, G., Jaenicke-Roessler, K., and Leitner, G., "Thermal decomposition of B–N–H compounds investigated by using combined thermoanalytical methods", *Thermochim. Acta* 391 (**2002**) p. 159–168.

209 Fernández, J.F. and Sánchez, C.R., "Simultaneous TDS–DSC measurements in magnesium hydride", *J. Alloys and Compounds* 356–357 (**2003**) p. 348–352.

210 Zidan, R.A., Takara, S., Hee, A.G., and Jensen, C.M., "Hydrogen cycling behavior of zirconium and titanium–zirconium-doped sodium aluminum hydride", *J. Alloys and Compounds* 285 (**1999**) p. 119–122.

211 Wolf, G., Baumann, J., Baitalow, F., Hoffmann, F.P., "Calorimetric process monitoring of thermal decomposition of B–N–H compounds", *Thermochim. Acta* 343 (**2000**) p. 19-25.

212 Gross, K.J., Measurements performed by author.

213 Chotard, J-N, Sheptyakov, D., and Yvon, K., "Hydrogen induced site depopulation in the $LaMgNi_4$-hydrogen system", Z. Kristallogr. 223 (**2008**) p. 690–696.

214 Lee, Y.-W., Clemens, B.M., Gross, K.J., "Novel Sieverts' type volumetric measurements of hydrogen storage properties for very small sample quantities", *J. Alloys and Compounds* 452 (**2008**) p. 410-413.

215 Zheng F, Rassat, S.D., Helderandt, D.J., Caldwell, D.D., Aardahl, C.L., Autrey, T., Linehan, J.C., and Rappé, K.G., "Automated gas burette system for evolved hydrogen measurements", *Review of Scientific Instruments* 79(8):Article no: 084103 (**2008**).

216 Pez, G.P., Scott, A.R., Cooper, A.C., and Cheng, H., "Hydrogen Storage By Reversible Hydrogenation Of Pi Conjugated Substrates", US Patent 7101530, (**2006**).

217 Pez, G.P., Scott, A.R., Cooper, A.C., Cheng, H., Wilhelm, F.C., and Abdourazak, A.H., "Hydrogen storage by reversible hydrogenation of pi-conjugated substrates", US Patent 7351395, (**2008**).

218 Crabtree, R.H., "Hydrogen storage in liquid organic heterocycles", *Energy and Environ. Sci*. (**2008**), 134.

219 Marwitz, A.J.V., Matus, M.H., Zakharov, L.N., Dixon, D.A., and Liu, S-Y., "A Hybrid Organic/Inorganic Benzene", *Angew. Chem. Int. Ed.*, 48 (**2009**) p. 973 –977.

220 Marwitz, A.J.V., Abbey, E.R., Jenkins, J.T., Zakharov, L.N., Liu, S.-Y., "Diversity through Isosterism: The Case of Boron-Substituted 1,2-Dihydro-1,2-azaborines", *Org. Lett.* , 9 (**2007**) p. 4905-4908.

221 Abbey, E.R., Zakharov, L.N., Liu, S.-Y., "Crystal Clear Structural Evidence for Electron Delocalization in 1,2-Dihydro-1,2-azaborines", *J. Am. Chem. Soc.* 130 (23) (**2008**) p. 7250-7252.

222 Campbell, P.G., Parab, K., Abbey, E.R., Marwitz, A., Liu, S-Y., "Hydrogen storage by CBN heterocycle materials", 238th ACS National Meeting, Washington, DC, United States, August 16-20, (**2009**), FUEL-297.

223 Antek G., Wong-Foy, Matzger, A.J., and Yaghi, O.M., "Exceptional H_2 Saturation Uptake in Microporous Metal-Organic Frameworks", *J. Am. Chem. Soc.*, 128, (**2006**) p. 3494-3495.

224 Lin, X., Jia, J., Zhao, X., Thomas, M., Blake, A.J., Walker, G.S., Champness, N.R., Hubberstey, P., and Schroeder, M., "High H_2 Adsorption by Coordination-Framework Materials", *Angew. Chem., Int. Ed.* 45, (**2006**) p. 7358-7364.

225 Kaye, S.S., Dailly, A., Yaghi, O.M., and Long, J.R., "Impact of Preparation and Handling on the Hydrogen Storage properties of Zn_4O (1,4-benzenedicarboxylate)$_3$ (MOF-5)", *J. Am. Chem. Soc.* 129, (**2007**) p. 14176-14177.

226 Pradhan, B.K., Harutyunyan, A.R., and Stojkovic, D., Grossman, J.C., Zhang, P., Cole, M.W., Crespi, V., Goto, H., Fujiwara, J., and Eklung, P.C., "Large cryogenic storage of hydrogen in carbon nanotubes at low pressures" *J. Mater. Res.*, Vol. 17 (9), (**2002**) p. 2209-2216.

227 Adamson, A.W., "Chapter 4 – Chemical thermodynamics. The First Law of Thermodynamics", A textbook of Physical Chemistry, 1st ed. (**1973**) Academic press. LCCN, p. 720-328.

228 Castellan, G.W., "Chapter 7 – Energy and the First Law of Thermodynamics, Thermochemistry", Physical Chemistry (2nd ed.). Addison-Wesley. (**1971**) ISBN 0201009129.

229 Image created by Hankwang, "Joule-Thomson coefficients for various gases at 1.013 bar",http://en.wikipedia.org/wiki/Joule%E2%80%93Thomson_effect, (5 May **2010**) data source http://webbook.nist.gov/chemistry/fluid/ *

230 Wicke, E., Brodowsky, "Hydrogen In Hydrogen in Metals I", Alefeld, G., and Volkl, J., Eds., Springer: Berlin, Vol. 1 (**1978**), p. 73.

231 Dantzer, P., "Properties of intermetallic compounds suitable for hydrogen storage applications", *Mat. Sci and Eng. A* 329-331 (**2002**) p. 313-320.

232 Züttel, A., Borgschulte, A., Schlapbach, L., Ed. Hydrogen as a Future Energy Carrier. Weinheim: Wiley-VCH, **2008**.

233 Gremaud, R., Broedersz, C.P., Borsa, D.M., Borgschulte, A., Mauron, P., Screuders, H., Rector, J.H., Dam, B., and Griessen, R., "Hydrogenography: An Optical Combinatorial Method to Find New Light-Weight Hydrogen-Storage Materials", *Adv. Mater.* 19 (**2007**) p. 2813-2817.

234 Chen, P. and Zhu, M., "Recent progress in hydrogen storage", *Mater. Today*, 11 (**2008**), p. 36–43.

235 Matsunaga, T., Buchter, F., Mauron, P., Bielman, M., Nakamori, Y., Orimo, S., Ohba, N., Miwa, K., Towata, S., Züttel, A., "Hydrogen Storage Properties of Mg(BH4)2", *J. Alloys and Compounds* 459 (**2008**) p. 583–588.

236 Chase, M.W., Jr. (Ed.), "NIST-JANAF Themochemical Tables", fourth ed., *J. Phys. Chem. Ref. Data, Monograph*, 9, (**1998**).

237 Baranowski, B., and Tkacz, M., "The equilibrium between solid aluminum hydride and gaseous hydrogen", *Z. Phys. Chem. Neue Folge*, 135 (**1983**) p. 27.

238 Graetz, J. and Reilly, J.J., "Thermodynamics of the α, β and γ polymorphs of AlH_3", *J. Alloys and Compounds,* 424 (**2006**) p. 262–265.

239 Kirchheim, R., Kieninger, W., Huang, X.Y., Filipek, S.M., Rush, J., Udovic, T., "Hydrogen in amorphous Ni-Zr and Ni-Ti alloys", *J. Less-Common Metals* 172-174 (**1991**) p. 880-889.

240 Kirchheim, R., Sommer, F., Schluckebier, G., "Hydrogen in amorphous metals—I", *Acta Metall.*, 30 (**1982**) p. 1059.

241 Jaggy, F., Kieninger, W., Kirchheim, R., "Distribution of site energies in amorphous NiTi and NiZr alloys", *Z. Phys. Chem. Neue Folge*, 163 (**1989**) p. 431.

242 Kirchheim, R., "Hydrogen solubility and diffusion in defective and amorphous metals", *Prog. Mater. Sci.*, 32 (**1988**) p. 261-325.

243 Zhukov, A., and Karlsson, R., "Statistical aspects of Van 't Hoff analysis: a simulation study", *J. Mol. Recognit.* 20 (**2007**) p. 379-385.

244 Choi, H.J. and Dincă, M., "Broadly Hysteretic H_2 Adsorption in the Microporous Metal-Organic Framework Co(1,4-benzenedipyrazolate)", *J. Am. Chem. Soc.,* 130. (**2008**), p. 7848-7850.

245 Westlake, D.G., "Generalized model for hydrogen embrittlement", *Trans. Am. Soc. Met.* 62 (**1969**) p. 1000.

246 Paton, N.E., Hickman, B.S., Leslie, D.H., "Behavior of hydrogen in alpha.-phase titanium-aluminum alloys", *Metall. Trans.,* 2 (**1971**) p. 2791.

247 Birnbaum, H.K., Grossbeck, M.L., Amano, M., "Hydride precipitation in Nb and some properties of NbH", *J. Less-Common Metals,* 49 (**1976**) 357.

248 Gahr, S. and Birnbaum, H.K., "Hydrogen embrittlement of niobium Ill. High temperature behavior", *Acta Metall.,* 26 (**1978**) p. 1781.

249 Schober, T., "The niobium-hydrogen system – an electron microscope study. I. Room temperature results", *Phys. Status Solidi*, A 29 (**1975**) p. 395.

250 Jamieson, H.C., Weatherly, G.C., Manchester, F.D., "The β α phase transformation in palladium-hydrogen alloys", *J. Less-Common Metals,* 50 (1976) p. 85-102.

251 Barrett, C., Tetelman, A., Nix, W., "The Principles of Engineering Materials", Prentice Hall (**1973**).

252 Berube, V., Chen, G., Dresselhaus, M.S., "Temperature dependence of the enthalpy of formation of metal hydrides characterized by an excess volume", *Int. J. Hydrogen Energy* 33 (**2008**) p. 4122-4131.

253 Thomas, K.M., "Adsorption and desorption of hydrogen on metal–organic framework materials for storage applications: comparison with other nanoporous materials", *Dalton Trans.*, (**2009**) p. 1487–1505.

254 Daniels, F., Williams, J.W., Bender, P., Alberty, R.A., Cornwell, C.D., "Experimental Physical Chemistry", McGraw-Hill: New York, (**1962**).

255 Private communications with Dr. Renju Zacharia and Professor Richard Chahine, Université du Québec à Trois-Rivières, Canada.

256 Collins, D.J., and Zhou, H.-C., "Hydrogen storage in metal-organic frameworks", *J. Mater. Chem.,* 17 (**2007**) p. 3154-3160.

257 Pfeifer, P., Wexler, C., Suppes, G., Hawthorne, F., Jalisatgi, S., Lee, M., D., Robertson, Buckley, P., Clement, J., "Multiply Surface-Functionalized Nanoporous

Carbon for Vehicular Hydrogen Storage", Presentation STO19, (**2010**) DOE Hydrogen Program Annual Merit Review, June 7-11, **2010**, Washington, DC.

258 Chen, B., Zhao, X., Putkham, A., Hong, K., Lobkovsky, E.B., Hurtado, E.J., Fletcher, A.J., Thomas, K.M., "Surface Interactions and Quantum Kinetic Molecular Sieving for H_2 and D_2 Adsorption on a Mixed Metal-Organic Framework Material", *J. Am. Chem. Soc.*, 130 (**2008**) p. 6411-6423.

259 Dubinin, M.M., and Radushkevich, L.V., "The equation of the characteristic curve of activated charcoal", *Doklady Akad. Nauk S.S.S.R.*, 55, (**1947**) p. 327.

260 Dubinin, M.M., in Cadenhead, D.A., Danielli, J.F., and Rosenberg, M.D. (Eds), "Physical Adsorption of Gases and Vapors in Micropores, Progress in Surface and Membrane Science", Vol. 9, Academic Press, New York, (**1975**), ISBN 0-12-571809-8, p 1.

261 Dubinin, M.M., Zhukovskaya, E.G., and Murdmaa, K.O., *Ivza. Acad. Nauk SSSR, Ser. Khim.,* (**1966**) p. 620.

262 Condon, J.B., "Equivalency of the Dubinin–Polanyi equations and the QM based sorption isotherm equation. A. Mathematical derivation", *Microporous and Mesoporous Materials*, 38 (**2000**) p. 359-376.

263 Poirier, E., Chahine, R., Bénard, P., Lafi, L., Dorval-Douville, G., and Chandonia, P.A., "Hydrogen Adsorption Measurements and Modeling on Metal-Organic Frameworks and Single-Walled Carbon Nanotubes", *Langmuir*, 22 (**2006**) p. 8784-8789.

264 Czerny, A.M., Bénard, P., Chahine, R., "Adsorption of Nitrogen on Granular Activated Carbon: Experiment and Modeling", *Langmuir*, 21 (**2005**) p. 2871-2875.

265 Chen, S.G., Yang, R.T., "Theoretical Basis for the Potential Theory Adsorption Isotherms. The Dubinin-Radushkevich and Dubinin-Astakhov Equations", *Langmuir*, 10 (**1994**) p. 4244-4249.

266 Walton, K.S. and LeVan, M.D., "Adsorbed-Phase Heat Capacities: Thermodynamically Consistent Values Determined from Temperature-Dependent Equilibrium Models", *Ind. Eng. Chem. Res.*, 44, (**2005**) p. 178-182.

267 Jagiello, J., Bandosz, T.J., Schwarz, "Research Article Characterization of Microporous Carbons Using Adsorption at Near Ambient Temperatures", J.A., *Langmuir*, 12, (**1996**) p. 2837-2842.

268 Ramirez, D., Qi, S., Rood, M.J., and Hay, K.J., "Equilibrium and Heat of Adsorption for Organic Vapors and Activated Carbons", *EnViron. Sci. Technol.* , 39, (**2005**) p. 5864-5871.

269 Bhatia, S.K. and Shethna, H.K., "Modified Pore Filling Isotherm with Application in Determination of Pore Size", *Langmuir*, 10, (**1994**) p. 3230-3243.

270 Figure provided by Dr. Renju Zacharia, Université du Québec à Trois-Rivières, Canada.

271 Personal communications with: Dr. Renju Zacharia and Professor Richard Chahine, Université du Québec à Trois-Rivières, Canada, Andrea Sudik and Justin Purewal, Ford Motor Company, USA, Philip Parilla and Lin Simpson National Renewable Energy Laboratory, USA.

272 Zecchina, A., Arean, C.O., Palomino, G.T., Geobaldo, F., Lamberti,C., Spoto, G., Bordiga, S., "The vibrational spectroscopy of H_2, N_2, CO and NO adsorbed on the titanosilicate molecular sieve ETS-10", *Phys. Chem. Chem. Phys.*, 1 (**1999**) p. 1649–1657.

273 Murray, L.J., Dinca, M., Long, J.R., "Hydrogen storage in metal–organic frameworks", *Chem. Soc. Rev.*, 38 (**2009**) p. 1294–1314.

274 Schlichtenmayer, M., Streppel, B., Hirscher, M., "Hydrogen physisorption in high SSA microporous materials e A comparison between AX-21_33 and MOF-177 at cryogenic conditions", *Int. J. Hydrogen Energy*, 36 (**2011**) p. 586 -591.

275 Garrone, E., Bonelli, B., Arean, C.O., "Enthalpy–entropy correlation for hydrogen adsorption on zeolites", *Chem. Phys. Lett.*, 456 (**2008**) p. 68–70.

276 Ranong, C.N., Höhne, M., Franzen, J., Hapke, J., Fieg, G., Dornheim, M., Eigen, N., Bellosta von Colbe, J.M., Metz, O., "Concept, Design and Manufacture of a Prototype Hydrogen Storage Tank Based on Sodium Alanate", The extended version of an oral presentation on the ProcessNet Annual Meeting (ProcessNet-Jahrestagung) (October 7-9, **2008**) Karlsruhe, Germany.

277 Kumar, D., General Motors Company, "System Design and Media Structuring for On-Board hydrogen Storage Technologies", DOE Annual Merit Review Presentation, (June 8, **2010**) , Project ID: ST009.

278 Davis, B.L., Dixon, D.A., Garner, E.B., Gordon, J.C., Matus, M.H., Scott, B., Stephens, F.H., "Efficient Regeneration of Partially Spent Ammonia Borane Fuel", *Angewandte Chemie, International Edition,* 48(37), (**2009**), p. 6812-6816.

279 McGrady, G.S., Jensen, C.M., "Method of preparation of titanium-doped lithium aluminum hydride for high performance hydrogen storage", From PCT Int. Appl. (**2010**), WO 2010080541.

280 Graetz, J.A., Reilly, J.J., Wegrzyn, J.E., "Regeneration of aluminum hydride", From U.S. Pat. Appl. Publ. (**2009**), US 20090291045.

281 See for example: (a) Mann, S., Geilenberg, D., Broekaert, J.A.C., and Jansen, M., "Digestion Methods for Advanced Ceramic Materials and Subsequent Determination of Silicon and Boron by Inductively Coupled Plasma Atomic Emission Spectrometry", *J. Anal. Atom. Spectrom.* (**1997**), 12, p. 975-979. (b) Hui, W.C., "Secret of formulating a selective etching or cleaning solution for boron nitride (BN) thin film", *Proc. SPIE*, 5276 (**2004**) p. 143-153.

282 Zidan, R., Garcia-Diaz, B.L., Fewox, C.S., Stowe, A.C., Gray, J.R., Harter, A.G. "Aluminium hydride: a reversible material for hydrogen storage", *Chemical Communications* (Cambridge, United Kingdom), 25 (**2009**) p. 3717-3719.

283 Paggiaro, R., Bénardb, P., and Polifke, W., "Cryo-adsorptive hydrogen storage on activated carbon. I: Thermodynamic analysis of adsorption vessels and comparison with liquid and compressed gas hydrogen storage", *Int. J. Hydrogen Energy,* 35 (2) (**2010**) p. 638-647.

284 Yannopoulos, L.N., Edwards, R.K., Wahlbeck, P.G., "The Thermodynamics of the Yttrium-Hydrogen System", *J. Phys. Chem.* 69, 8 (**1965**) p. 2511-2515.

285 Bogdanovic, B., Bohmhammel, K., Christ, B., Reiser, A., Schlichte, K., Vehlen, R., Wolf, U., "Thermodynamic investigation of the magnesium-hydrogen system", *J. Alloys and Compounds,* 282 (**1999**) p. 84-92.

286 Ono, S., Normur, K., Akiba, E., Uruno, H., "Phase transformations of the $LaNi_5$-H_2 system", *J. Less-Common Metal,s* 113 (**1985**) p. 113.

287 Collaboration with Pivak, Y., Schreuders, H., Dam, B., and Griessen, R., Vrije Universiteit Amsterdam, The Netherlands.

288 Sandrock, G., Hydride Materials Data Base: http://hydpark.ca.sandia.gov/MaterialsFrame.html.

289 Evans, M.J.B., and Everett, D.H., "Thermodynamics of the solution of hydrogen and deuterium in palladium", *J. Less-Common Metals,* 49 (**1976**) p. 123.

290 Poirier, E., Chahine, R., Benard, P., Lafi, L., Dorval-Douville, G., Chandonia, P.A., "Hydrogen Adsorption Measurements and Modeling on Metal-Organic Frameworks and Single-Walled Carbon Nanotubes", *Langmuir,* 22 (**2006**) p. 8784-8789.

291 Huiberts, J.N., Griessen, R., Rector, J.H., Wijngaarden, R.J., Dekker, J.P., de Groot, D.G., and Koeman, N.J., "Yttrium and lanthanum hydride films with switchable optical properties", *Nature,* 380 (**1996**) p. 231.

292 Griessen, R., and van der Sluis, P., "Schaltbare Spiegel aus Metallhydriden", *Phys. Blaetter,* 53 (**1997**) p. 1207.

293 Dam, B., Gremaud, R., Broedersz, Ch., Griessen, R., "Combinatorial thin film methods for the search of new light-weight metal-hydrides", *Scripta Materialia,* 56 (**2007**) p. 853.

294 Borgschulte, A., Westerwaal, R.J., Rector, J.H., Dam, B., Griessen, R., Schoenes, J., "The effect of the Strong Metal-Support Interaction on hydrogen sorption kinetics of Pd-capped switchable mirrors", *Phys Rev B,* 70 (**2004**) p. 155414.

295 Lohstroh, W., Westerwaal, R.J., van Mechelen, J.L.M., Chacon, C., Johansson, E., Dam, B., and Griessen, R., "Structural and optical properties of Mg2NiHx switchable mirrors upon hydrogen loading", *Phys Rev B* 70 (**2004**) p. 165411.

296 Borsa, D.M., Gremaud, R., Baldi, A., Schreuders, H., Rector, J.H., Kooi, B., Vermeulen, P., Notten, P.H.L., Dam, B., Griessen, R., "Structural, optical, and electrical properties of MgyTi1−yHx thin films", *Phys Rev B,* 75 (**2007**) p. 205408.

297 Broedersz, C.P., Gremaud, R., Dam, B., Griessen, R., and Lovvik, O.M., "Highly destabilized Mg-Ti-Ni-H system investigated by density functional theory and Hydrogenography", *Phys. Rev., B* 77 (**2008**) p. 024204.

298 Gremaud, R., Gonzalez-Silveira, M., Pivak, Y., Slaman, M., Schreuders, H., Dam, B., Griessen, R., "Hydrogenography of PdHx thin films: Influence of H-induced stress relaxation processes", *Acta Materialia,* 57 (**2009**) p. 1209.

299 Gremaud, R., Slaman, M., Schreuders, H., Dam, B., Griessen, R., "An optical method to determine the thermodynamics of hydrogen absorption and desorption in metals", *Appl. Phys. Lett.,* 91 (**2007**) p. 231916.

300 http://www.nrcan.gc.ca/mms-smm/expl-expl/cerl-lcre/dsc-dsc-eng.htm .

301 Vajo, J.J., Ahn, C.C., Bowman, R.C., and Fultz, B., "Altering Hydrogen Storage Properties by Hydride Destabilization through Alloy Formation: LiH and MgH_2 Destabilized with Si", *J. Phys. Chem. B*, 108 (37), (**2004**), p 13977–13983.

302 Dantzer, P., and Millet, P., "Advances in hydride phase growth: Automatic high precision calorimeter volumetric devices, for thermodynamic and kinetics analyses", *Review of Sci. Inst.*, Vol 71, 1 (**2000**) p. 142.

303 Levchenko, A.A., Etherington, G., and Gross, K., "Simultaneous calorimetric and gas sorption measurements provide vital information for developing future hydrogen storage materials", *Inter. Gases & Instrument.* Vol. 3, Issue 3, (**2009**).

304 Zhang, D.X., Wang, X.L., and Wang, G.S., "Recovery of Efficacy-Lost $LaNi_5$ by Chemical Preparation Method", *Z. Phys. Chem. Neue Folge*, 164, (**1989**) p. 1441.

305 Dantzer, P., Millet, P., and Flanagan, T.B., "Thermodynamic Characterization of Hydride Phase Growth in ZrNi-H_2", *Metallurgical and Materials Trans. A*, Vol 33A (**2001**) p. 29.

306 Flanagan, T.B., Clewley, J.D., Kuji, T., Park, C.N., and Everett, D.H., "Isobaric and isothermal hysteresis in metal hydrides and oxides", *J. Chem. Soc. Faraday Trans.*, vol. 82 (**1986**) p. 2589-2604.

307 Forster, P.M., Eckert, J., Heiken, B.D., Parise, J.B., Yoon, J.W., Jhung, S.H., Chang, J.-S., Cheetham, A.K., "Adsorption of Molecular Hydrogen on Coordinatively Unsaturated Ni(II) Sites in a Nanoporous Hybrid Material", *J. Am. Chem. Soc.,* 128 (**2006**) p. 16846-16850.

308 Jhung, S.H., Kim, H.K., Yoon, J.W., Chang, J.S., "Low-Temperature Adsorption of Hydrogen on Nanoporous Aluminophosphates: Effect of Pore Size", *J. Phys. Chem. B*, 110, (**2006**) p. 9371–9374.

309 Wang, X-S, Ma, S., Rauch, K., Simmons, J.M., Yuan, D., Wang, X., Yildirim, T., Cole, W.C., López, J.J., de Meijere, A., and Zhou, H.C., "Metal−Organic Frameworks Based on Double-Bond-Coupled Di-Isophthalate Linkers with High Hydrogen and Methane Uptakes", *Chem. Mater.,* (**2008**), 20, p. 3145–3152.

310 Van Mal, H.H., "Stability of Ternary Hydrides and Some Applications", *Philips Res. Peps. Suppl.,* 2 (**1976**) p. 1.

311 Pundt, A., and Kirchheim, R., "Metal-Hydrogen-Systems: Microstructural Aspects", *Ann. Rev. Mat. Res.,* 36 (**2006**) p. 555-608.

312 Jorgensen, S., Johnson, T., Kumar, S., Moen, C., "Design, Build, and Test of Full-scale, Modular, Solid-state Hydrogen-storage Tanks", Presentation IPHE meeting on hydrogen storage, Moscow, Russian Federation, October 27, (**2009**).

313 Johnson, T., Dedrick, D., & Jorgensen, S., "Effects of metal hydride properties on the performance of hydrogen storage systems", *Proceedings of the Materials Science and Technology Conference and Exhibition, MS&T* (**2007**) p. 484-504.

314 Ott, K.C., "IV.B.1a 2009 Overview - DOE Chemical Hydrogen Storage Center of Excellence (CHSCoE)", FY 2009 Annual Progress Report US DOE Hydrogen Program, http://hydrogendoedev.nrel.gov/pdfs/progress09/iv_b_1a_ott.pdf .

315 Vajo, J.J., Skeith, S.L., Mertens, F., "Reversible Storage of Hydrogen in Destabilized $LiBH_4$", *J. Phys Chem. B,* 109 (**2005**) p. 3719-3722.

316 Streukens, G., Bogdanovic., B., Felderhoff, M., and Schüth, F., "Dependence of dissociation pressure upon doping level of Ti-doped sodium alanate—a possibility for ''thermodynamic tailoring'' of the system", *Phys. Chem. Chem. Phys.*, 8, (**2006**) p. 2889–2892.

317 Walker, G.S., Figure 17.3 Chapter 17., "Multicomponent Hydrogen Storage Systems", Solid-state hydrogen storage: materials and chemistry, Ed. G S Walker, (**2008**) Woodhead Publishing Ltd, Cambridge, UK, p. 485.

318 Zhao, D., Feng, J., Huo, Q., Melosh, N., Fredrickson, G.H., Chmelka, B.F., Stucky, G.D., "Triblock Copolymer Syntheses of Mesoporous Silica with Periodic 50 to 300 Angstrom Pores", *Science*, 279 (**1998**) p. 548 – 552.

319 Heldebrant, D.J., Karkamkar, A., Hess, N.,J., Bowden, M., Rassat, S., Zheng, F., Rappe, K., and Autrey, T., "The Effects of Chemical Additives on the Induction Phase in Solid-State Thermal Decomposition of Ammonia Borane", *Chem. Mater.* , 20, (2008) p. 5332–5336.

320 Rassat, S.D., Aardahl, C.L., Autrey, T., and Scott Smith, R., "Thermal Stability of Ammonia Borane: A Case Study for Exothermic Hydrogen Storage Materials", Figures reprinted with permission from *American Chemical Society, Energy Fuels*, 24, (2010) p. 2596–2606.

321 Panella, B., Hones, K., Muller, U., Trukhan, N., Schubert, M., Putter, H., Hirscher, M., "Desorption Studies of Hydrogen in Metal–Organic Frameworks", *Angew. Chem. Int. Ed.,* 47 (**2008**) p. 2138 –2142.

322 Luo, W., Hones, K., Muller, U., Trukhan, N., Schubert, M., Putter, H., Hirscher, M., "Thermodynamic Characterization of the ZrNi-H System by Reaction Calorimetry and PCT Measurements", *J. Less-Common Metals,* 162 (**1990**) p. 251-266.

323 Pivak, Y., Gremaud, R., Gross, K., Gonzalez-Silveira, M., Walton, A., Book, D., Schreuders, H., Dam, B., Griessen, R., "Effect of the substrate on the thermodynamic properties of PdHx films studied by Hydrogenography", *Scripta Materialia*, 60(5) (**2009**) p. 348.

324 Pivak, Y., Schreuders, H., Slaman, M., Griessen, R., Dam, B., in preparation.

325 Ludwig, A., Caoa, J., Savana, A., and Ehmann, M., "High-throughput characterization of hydrogen storage materials using thin films on micromachined Si substrates", *J. Alloys and Compounds*, 446–447 (**2007**) p. 516.

326 Ma, S., and Zhou, H.-C., "Gas storage in porous metal–organic frameworks for clean energy applications", *Chem. Commun.*, 46 (**2010**) p. 44–53.

327 Ma, S., Eckert, J., Forster, P.M., Yoon, J.W., Hwang, Y.K., Chang, J.-S., Collier, C.D., Parise, J.B., Zhou, H.-C., "Further Investigation of the Effect of Framework Catenation on Hydrogen Uptake in Metal-Organic Frameworks", *J. Am. Chem. Soc.*, 130 (**2008**) p. 15896-15902.

328 Liu, Y., Brown, C.M., Neumann, D.A., Peterson, V.K., Kepert, C.J., "Inelastic neutron scattering of H_2 adsorbed in HKUST-1", *J. Alloys and Compounds,* 46–447 (**2007**) p. 385–388.

329 Vitillo, J.G., Regli, L., Chavan, S., Ricchiardi,G., Spoto, G., Dietzel, P.D.C., Bordiga, S., Zecchina, A., "Role of Exposed Metal Sites in Hydrogen Storage in MOFs", *J. Am. Chem. Soc.*, 130 (**2008**) p. 8386–8396.

330 Miedema, A.R., "The electronegativity parameter for transition metals: Heat of formation and charge transfer in alloys", *J. Less-Common Metals,* 32 (**1973**) p. 117.

331 Siegel, D., Wolverton, C., Ozolins, V., "Thermodynamic guidelines for the prediction of hydrogen storage reactions and their application to destabilized hydride mixtures", *Phys. Rev. B,* 76 (**2007**) p. 134102.

332 Berube, V., Radtke, G., Dresselhaus, M., Chen, G., "Size effects on the hydrogen storage properties of nanostructured metal hydrides: A review", *Int. J. Energy Res.*, 31 (**2007**) p. 637-663.

333 Wagemans, R.W.P., Van Lenthe, J.H., De Jongh, P.E., Van Dillen, A.J., De Jong, K.P., "Hydrogen storage in magnesium clusters: quantum chemical study", *J. Am. Chem. Soc.*, 127 47 (**2005**) p. 16675-16680.

334 Wolf, D., "Correlation between the energy and structure of grain boundaries in b.c.c. metals. I. Symmetrical boundaries on the (110) and (100) planes", *Philosophical Magazine*, *B*, 59 6 (**1989**) p. 667-680.

335 Liu,S.-Y., "Hydrogen Storage by Novel CBN Heterocycle Materials", FY 2009 Annual Progress Report, DOE Hydrogen Program.

336 Liu, S.-Y., "1,2-Dihydro-1,2-Azaborine: An Organometallic Benzene", IMEBoron XIII International Boron Conference, Platja d'Aro, Spain, September **2008**.

337 Zhou, W., Wu, H., Yildirim, T., "Enhanced H_2 Adsorption in Isostructural Metal-Organic Frameworks with Open Metal Sites: Strong Dependence of the Binding Strength on Metal Ions", *J. Am. Chem. Soc.*, 130 (**2008**) p. 15268–15269.

338 Holleck, G.L., Driscoll, J.R., Paul, B.E., "The use of $LaNi_5H_x$-type hydrides in Ni--- H_2 batteries: Benefits and problems", *J. Less-Common Metals*, 74, (**1980**) p. 379.

339 Pecheron-Guégan, A. and Welter, J.-M., "Preparation of Intermetallics and Hydrides", in L. Schlapbach editor, "Hydrogen in Intermetallic Compounds I", Topics in Applied Physics, Vol. 63, (**1988**), Springer-Verlag, Berlin, Heidelberg, New York, London, Paris, Tokyo.

340 van Vucht, J.H.N., Kuijpers, F.A., and Bruning, H.C.A.M., "Reversible Room Temperature Absorption of Large Quantities of Hydrogen by Intermetallic Compounds", *Philips Research Reports*, 25 (**1970**).

341 Bowman, R.C., Jr., Luo, C.H., Ahn, C.C., Witham, C.K., and Fultz, B., "The effect of tin on the degradation of $LaNi_{5-y}Sn_y$ metal hydride during thermal cycling", *J. Alloys and Compounds*, 217 (**1995**) p. 185–192.

342 Schlapbach, L., ed. "Hydrogen in Intermetallic Compounds II: Surface and Dynamic Properties, Applications", Topics in Applied Physics. (**1992**) Springer: Berlin.

343 Bowman, Jr., R.C., Lynch, F.E., Marmaro, R.W., Luo, C.H., Fultz, B., Cantrell, J.S., and Chandra, "Effects of thermal cycling on the physical properties of VHx", *Z. Physk. Chem.* , 181 (**1993**) p. 269-273.

344 Cantrell, J.S. and Bowman, Jr., R.C., "Phase composition and the effect of thermal cycling for VH_x, $V_{0.995C0.005}H_X$, and$V_{0.975}Zr_{0.020}C_{0.005}H_X$" *J. Alloys and Compounds*, 293-295 (**1999**) p. 156-160.

345 Marmaro, R.W., Lynch, F.E., Chandra, D., "Investigation of Long Term Stability in Metal Hydrides", NAS9-18175 report by HCl, 12410 North Dumont Way, Littletown, CO 80125 November, (**1991**).

346 Goodell, P.D., "Stability of Rechargeable Hydriding Alloys during Extended Cycling", *J. Less-Common Metals*, 99(1) (**1984**) p. 1-14.

347 Kim, G.H. and Lee., J.Y., "The Changes of Hydrogenation Properties Induced by Thermal Cycling in $MMNi_{4.5}Al_{0.5}$ and $MMNi_{4.15}Fe_{0.85}$", *J. Less-Common Metals*, 132(1) (**1987**) p. 123-132.

348 Sandrock, G.D., Murray, J.J., Post, M.L., and Taylor, J.B., "Hydrides and Deuterides of $CaNi_5$", *Materials Res. Bull.*, 17 (**1982**), p. 887-894.

349 Huston, E.L., "Development of a Commercial Metal Hydride Process for Hydrogen Recovery", Rept BNL 35440. (**1984**), Brookhaven National Laboratory: Upton, NY.

350 Schlapbach, L., Seilera, A., Stuckia, F., and Siegmanna, H.C., "Surface effects and the formation of metal hydrides", *J. Less-Common Metals*, 73 (**1980**) p. 145-160.

351 Goodell, P.D., Sandrock, G.D., and Bogdanski, R.R., "Development of a Commercial Metal Hydride Process for Hydrogen Recovery: Cyclic Hydrogen Transfer and Adsorption/Poisoning Tests of AB- and AB5-Type Hydriding Alloys", (**1982**) Contract Rep. BNL 509926-S, Brookhaven National Laboratory.

352 Chandra, D., "Intermetallics for hydrogen storage", in the book "Solid-state hydrogen storage, Materials and chemistry", edited by Gavin Walker, (**2008**) Woodhead Publishing Limited, Cambridge England, CRC Press, p. 327. Reproduction by permission of Woodhead Publishing Limited. This figure appears in Chapter 12, Intermetallics for hydrogen storage, in Solid-state hydrogen storage: materials and chemistry, ISBN 978 1 84569 270 4.

353 Lambert, S.W., Chandra, D., Cathey, W.N., Lynch, F., E., and Bowman, Jr., R., C., "Investigation of hydriding properties of $LaNi_{4.8}Sn_{0.2}$, $LaNi_{4.27}Sn_{0.24}$ and $La_{0.9}Gd_{0.1}Ni_5$ after thermal cycling and aging", *J. Alloys and Compounds*., 187 (**1992**), p. 113-135.

354 Bowman, Jr., R.C., "Development of Metal Hydride Beds for Sorption Cryocoolers in Space Applications", *J. Alloys Compounds*, 356-357 (**2003**), p. 789-793.

355 Aoki, K., Yanagitani, A., and Masumoto., T., "Crystalline to Amorphous Transformation in Laves Phase $GdFe_2$ Induced by Hydrogen Absorption", *Applied Physics Letters*, 52(25) (**1988**), p. 2122-2123.

356 Ahn, S.T., Kim, Y.G., and Lee., J.Y., "Formation of the Amorphous Phase in Zr_2Al by Hydrogen Absorption and the Effects of Titanium Substitution on the Amorphization Behavior", *J. Alloys and Compounds*, 186(1) (**1992**) p. 45-52.

357 Aoki, K., Yamamoto, T., and Masumoto, T., "Hydrogen Induced Amorphization in RNi_2 Laves Phases", *Scripta Metallurgica*, 21(1) (**1987**) p. 27-31.

358 Kim, Y.G. and Lee., J.Y., "Hydrogen-Induced Transformation to an Amorphous State in the Laves Phases $Ce(Ru, M)_2$ (M Equivalent- to Fe, Co, Ni)", *J. Alloys and Compounds*, 191(2) (**1993**) p. 243-249.

359 Sandrock, G.D., Goodell, P.D., Huston, E.L., and Golben, P.M., "On the Disproportionation of Intermetallic Hydrides", *Z. Für Phys. Chem. Neue Folge*, 164 (**1989**), p. 1285-1290.

360 Cohen, R.L. and West K.W., "Intrinsic Cycling Degradation in $LaNi_5$ and Annealing Procedures for Re-forming the Material", *J. Less-Common Metals,* 95(1) (**1983**) p. 17-23.

361 Gross, K.J., "Hydride Development for Hydrogen Storage", presentation DOE Hydrogen and Fuel Cells Annual Merit Review, Berkeley, CA May 19-22, (**2003**).

362 Chen, P., Xiong, Z.T., Luo, J.Z., Lin, J.Y., Tan, K.L., "Interaction of hydrogen with metal nitrides and imides", *Nature*, 420 (**2002**) p. 302-304.

363 Gross, K.J., Luo, W., Rönnebro, E., and Spangler, S., "Sorption Properties of Novel Hydrogen Storage Materials", Presentation, MH2004 Symposium on Metal-Hydrogen Systems, Fundamentals and Applications Krakow, Poland. 5–10 September (**2004**).

364 Luo, W. and Sickafoose, S., "($LiNH_2$-MgH_2): A Viable Hydrogen Storage System", *J. Alloys and Compounds*, 381 (**2006**) p. 284.

365 Nakamori, Y. and Orimo., "Li-N based Hydrogen Storage Materials", *S. Mat. Sci. and Eng. B*, 108 (**2004**) p.48.

366 Luo, W., Wang, J., Stewart, K., Clift, M., Gross, K., "Li–Mg–N–H: Recent investigations and development", *J. Alloys and Compounds*, 446–447 (**2007**) p. 336–341.

367 Lundin, C.E. and Lynch, F.E., "Solid State Hydrogen Storage Materials for Application to Energy Needs", (**1975**) First Annual Technical Report, AFOSR Contract F44620-74-C-0020, University of Denver.

368 Lundin, C.E. and Lynch, F.E., "Modification of Hydriding Properties of AB5 Type Hexagonal Alloys through Manganese Substitution", *proceedings of The International Conference on Alternate Energy Sources*, Veziroglu, T.N., Editor. (**1978**): University of Miami.

369 Percheron-Guegan, A., Lartigue, C., and Achard, J.C., "Correlations between the structural properties, the stability and the hydrogen content of substituted $LaNi_5$ compounds", *J. Less-Common Metals*, 109(2) (**1985**) p. 287-309.

370 Percheron-Guegan, A. and Lartigue, C., "Hydrogen Locations in $LaNi_5$ and Related Hydrides", *Materials Science Forum*, 31 (**1988**) p. 125.

371 Cohen, R.L., West, K.W., and Wernick, J.H., "Degradation of $LaNi_5$ by Temperature Induced Cycling", *J. Less-Common Metals*, 73(2) (**1980**) p. 273-279.

372 Cohen, R.L., West, K.W., and Wernick, J.H., "Degradation of $LaNi_5$ Hydrogen Sorption Material by Cycling", *J. Less-Common Metals*, 70(2) (**1980**) p. 229-241.

373 Gamo, T., Moriwaki, Y., Yanagihara, N., and Iwaki, T., "Life Properties of Ti-Mn Alloy Hydrides and their Hydrogen Purification Effect", *J. Less-Common Metals*, 89(2) (**1983**) p. 495-504.

374 Park, J.M. and Lee, J.Y., "The Intrinsic Degradation Phenomena of $LaNi_5$ and $LaNi_{4.7}Al_{0.3}$ by Temperature Induced Hydrogen Absorption-Desorption Cycling", *Materials Research Bulletin*, 22(4) (**1987**) p. 455-465.

375 Benham, M.J. and Ross, D.K., "Experimental Determination of Absorption-Desorption Isotherms by Computer-Controlled Gravimetric Analysis", *Z. Fuer Phys. Chem. Neue Folge*, 163 (**1989**) p. 25-32.

376 Uchida, H., Terao, K., and Huang, Y.C., "Current Problems in the Development and Application of Hydrogen Storage Materials", *Z. Fuer Phys. Chem. Neue Folge*, 164 (**1989**) p. 1275-1284.

377 Josephy, Y., Bershadsky, E., and Ron, M., "Investigation of $LaNi_5$ upon Prolonged Cycling", in International Symposium on Metal-Hydrogen Systems, Sept. 2-7 (**1990**). Banff, Alberta, Canada.

378 Chandra, D. and Lynch, F.E., Rare Earths Proceeding, Bautista, R.G. and Wong, M.M., Editors. TMS Publication. , (**1989**) p. 83-98.

379 Jeongyong, L., "Synthesis and gas sorption study of microporous metal organic frameworks for hydrogen and methane storage", Ph.D. Thesis (**2007**), Rutgers, the State University of New Jersey, New Brunswick.

380 Dantzer, P., "Static, Dynamic and Cycling Studies on Hydrogen in the Intermetallics $LaNi_5$ and $LaNi_{4.77}Al_{0.22}$", *J. Less-Common Metals*, 131 (**1987**) p. 349-363.

381 Lamb, J. and Chandra, D., University of Nevada, Reno (**2008**).

382 Sandrock, G.D. and Goodell, P.D., "Surface Poisoning of $LaNi_5$, FeTi and (Fe, Mn)Ti by O2, CO and H_2O", *J. Less-Common Metals*, 73(1) (**1980**) p. 161-168.

383 Snape, E. and Lynch, F.E., "Metal-Hydrides Make Hydrogen Accessible-II", *Chemtech*, 10(12) (**1980**) p. 768-773.

384 Gross, K.J., Thomas, G.J., and Jensen, C.M., "Catalyzed alanates for hydrogen storage", *J. Alloys and Compounds*, 330-332 (**2002**) p. 683-690.

385 Gross, K.J., Sandrock, G., and Thomas, G.J., "Dynamic in situ X-ray diffraction of catalyzed alanates", *J. Alloys and Compounds*, 330-332 (**2002**) p. 691-695.

386 Gross, K.J. and Majzoub, E., "Direct synthesis of catalyzed hydride compounds", September 21, (**2004**), U.S. Patent No. 6,793,909.

387 Chandra, D., Chien, W. and Lamb, J., "Effect of Gaseous Impurities on Long-Term Thermal Cycling", Final Report (**2007**), US DOE Hydrogen Program. p. 91-99.